eNergetics 2020

Proceedings of the

6^{th} Virtual International Conference on Science, Technology and Management in Energy

Editors:
Stajić, Z. and Velimirović, L. Z.

Publishers:
Research and Development Center "ALFATEC", Niš, Serbia
Complex System Research Center, Niš, Serbia

Serbia, Niš, December 14-15, 2020

Editors
Stajić, Z.
Velimirović, L. Z.

eNergetics 2020

6th Virtual International Conference on Science, Technology and Management in Energy

Proceedings

Publishers
Research and Development Center “ALFATEC”, Niš, Serbia
Complex System Research Centre, Niš, Serbia

Serbia, Niš, December 14-15, 2020

Proceedings of the
6th Virtual International Conference
on Science Technology and Management in Energy

Serbia, Niš, December 14-15, 2020

Editors:
Prof. Dr. Zoran Stajić and Dr. Lazar Z. Velimirović

Technical Editor:
Dr. Petar Vranić

Published by:
Research and Development Center “ALFATEC”, Niš, Serbia, and
Complex System Research Centre, Niš, Serbia

Printed by:
Copy House, Niš, Serbia

Number of copies printed: 100
The publishing year: 2021

Printing of this edition has been financially supported by
Serbian Ministry of Education, Science and Technological Development

ISBN 978-86-80616-07-0

CIP - Каталогизација у публикацији - Народна библиотека Србије, Београд

620.9(082)(0.034.2)

VIRTUAL International Conference on Science Technology and Management in Energy (6 ; 2020 ; Niš)
Energetics 2020 [Elektronski izvor] : proceedings / 6th Virtual International Conference on Science Technology and Management in Energy, Serbia, Niš, December 14-15, 2020 ; editors Stajić Z.[Zoran], Velimirović, L.[Lazar] Z. - Niš : Research and Development Centar "Alfatec" : Complex System Research Centre, 2021 (Niš : Copy House). - 1 elektronski optički disk (DVD) ; 12 cm

Sistemski zahtevi: Nisu navedeni. - Nasl. sa naslovne strane dokumenta. -
Tiraž 100. - Bibliografija uz svaki rad.

ISBN 978-86-80616-07-0 (RDCA)

а) Енергетика - Зборници

COBISS.SR-ID 34021385

eNergetics 2020

6th Virtual International Conference on Science Technology and Management in Energy

Organizer:
Research and Development Center “ALFATEC”

Co-organizers:
- Mathematical Institute of the Serbian Academy of Sciences and Arts
- Faculty of Technical Sciences, UKLO University St. Climent Ohridski
- Complex System Research Centre
- Academy of Sciences and Arts of the Republika Srpska
- Faculty of Mining and Geology, University of Belgrade

Supported by:
Serbian Ministry of Education, Science and Technological Development

Program Committee

Chair:

Prof. Dr. Zoran Stajić

Faculty of Electronic Engineering, Serbia

Members:

Dr. Lazar Velimirović

Mathematical Institute of the Serbian Academy of Sciences and Arts, Serbia

Prof. Dr. Aleksandar Janjić

Faculty of Electronic Engineering, Serbia

Prof. Dr. Gorazd Stumberger

Faculty of Electrical Engineering and Computer Science, Slovenia

Prof. Dr. Detelin Markov

Faculty of Power Engineering and Power Machines, Bulgaria

Prof. Dr. Marko Serafimov

Faculty of Mechanical Engineering, Macedonia

Prof. Dr. Mileta Janjić

Faculty of Mechanical Engineering, Montenegro

Prof. Dr. Miomir Stanković

Faculty of Occupational Safety, Serbia

Prof. Dr. Enver Agić

Public Enterprise Electric Utility of Bosnia and Herzegovina, BiH

Prof. Dr. Niko Majdandžić

Faculty of Mechanical Engineering, Croatia

Prof. Dr. Serkan Abbasoglu

Cyprus International University, Turkey

Prof. Dr. Bojan Srđević

Faculty of Agriculture, Serbia

Prof. Dr. K. Lenin

PVP Siddhartha Institute of Technology, India

Prof. Dr. Abdelhak Djoudi

National Polytechnic School, Algeria

Prof. Dr. Elson Avallone

Federal Institute of Education, Science and Technology of São Paulo, Brazil

Prof. Dr. Zdravko Milovanović

Faculty of Mechanical Engineering, Bosnia and Herzegovina

Prof. Dr. Miloš Jelić

Research and Development Center Alfatec, Serbia

Prof. Dr. Zoran Markov

Faculty of Mechanical Engineering, Macedonia

Dr. Saša Milić

Institute Nikola Tesla, Serbia

Prof. Dr. Krsto Miljanović

Agromediterranean Faculty, Bosnia and Herzegovina

Prof. Dr. Krum Todorov

Faculty of Power Engineering and Power Machines, Bulgaria

Prof. Dr. Dragoljub Mirjanić

Academy of Sciences and Arts of Republic of Srpska, Bosnia and Herzegovina

Prof. Dr. Tomislav Pavlović

Faculty of Sciences and Mathematics, Serbia

Prof. Dr. Ninoslav Sojadinović

Faculty of Electronic Engineering, Serbia

Prof. Dr. Howard Njoku

University of Nigeria, Nigeria

Prof. Dr. Zoran Gligorić

Faculty of Mining and Geology, Serbia

Prof. Dr. Reza Hamidi

Arkansas Tech University, USA

Prof. Dr. Goran Janaćković

Faculty of Occupational Safety, Serbia

Prof. Dr. Wassila Issaadi

Faculty of Technology, University of Bejaia, Algeria

Prof. Dr. Monica Carvalho

Federal University of Paraíba, Brazil

Prof. Dr. Prahaladh Paniyil

Clemson University, USA

Prof. Dr. Sandra Patricia Castaño Solis

ETS Universidad Politécnica de Madrid, Spain

Prof. Dr. Arunava Chatterjee

Meghnad Saha Institute of Technology, India

Prof. Dr. Vesna Karović Maričić

Faculty of mining and geology, Serbia

Organizing Committee

Chair:

Prof. Dr. Miomir Stanković

Faculty of Occupational Safety, Serbia

Members:

Prof. Dr. Zoran Stajić

Faculty of Electronic Engineering, Serbia

Dr. Lazar Velimirović

Mathematical Institute of the Serbian Academy of Sciences and Arts, Serbia

Dr. Petar Vranić

Mathematical Institute of the Serbian Academy of Science and Arts, Serbia

M.Sc. Ljubiša Stajić

Research and Development Center “ALFATEC”, Serbia

M.Sc. Radmila Janković

Mathematical Institute of the Serbian Academy of Science and Arts, Serbia

M.Sc. Jelena Velimirović

Mathematical Institute of the Serbian Academy of Sciences and Arts, Serbia

M.Sc. Biserka Mijucić

Research and Development Center “ALFATEC”, Serbia

M.Sc. Ivana Veličkovska

Mathematical Institute of the Serbian Academy of Sciences and Arts, Serbia

Table of Contents

Real Power Loss Reduction by Culicinae Optimization Algorithm

Lenin Kanagasabai

Prasad V. Potluri Siddhartha Institute of Technology, Department of EEE, Kanuru, Vijayawada, Andhra Pradesh – 5200007, gklenin@gmail.com

Abstract—**In this paper Culicinae Optimization Algorithm (COA) is projected to solve optimal reactive power problem. Proposed COA approach is based on the natural behaviour of Culicinae. Culicinae are holometabolous in environment and their phases of life are egg, larva, pupa, and adult. Predictably adult Culicinae go away from the water but in early life phases of Culicinae i.e., egg, larval, and pupal stages are aquatic. Fitness values of each Culicinae will be computed and among that best fitness will be chosen. In the exploration space Culicinae are arbitrarily distributed. In standard IEEE 30 and 57 bus test systems proposed Culicinae Optimization Algorithm (COA) has been evaluated. Simulation study shows that the COA reduced the power loss efficiently and control variables are within limits.**

Keywords – optimal reactive power, transmission loss, culicinae optimization algorithm

I. INTRODUCTION

Reactive power problem plays an important role in secure and economic operations of power system. Numerous types of methods Newton method, linear programming, interior point methods, successive quadratic programming method [1-5] have been utilized to solve the optimal reactive power problem. However many scientific difficulties are found while solving problem due to an assortment of constraints. Evolutionary techniques such as moth-flame optimization technique, particle swarm optimization, Ant Lion Optimizer [6-17] are applied to solve the reactive power problem. This paper proposes Culicinae Optimization Algorithm (COA) to solve optimal reactive power problem. Proposed COA approach is based on the natural behaviour of Culicinae. Fitness values of every Culicinae will be calculated and among that most excellent fitness will be selected. In the search space Culicinae are illogically dispersed. Then the computation of the optimal location of the Culicinae is done. Distance between the most excellent Culicinae and other Culicinae is calculated. In the solution space Culicinae will move capriciously to find out the optimum point. After few cycles to that revealed optimum points more Culicinae will be mesmerized. In standard IEEE 30 and 57 bus test systems proposed Culicinae Optimization Algorithm (COA) has been evaluated. Simulation study shows that the projected Culicinae Optimization Algorithm (COA) reduced the power loss efficiently.

II. PROBLEM FORMULATION

True power loss reduction is main objective of the problem:

$$F = P_L = \sum_{k \in Nbr} g_k (V_i^2 + V_j^2 - 2 V_i V_j \cos\theta_{ij}), \quad (1)$$

$$F = P_L + \omega_v \times Voltage\_Deviation, \quad (2)$$

$$Voltage\_Deviation = \sum_{i=1}^{Npq} |V_i - 1|. \quad (3)$$

Constraint (Equality):

$$P_G = P_D + P_L. \quad (4)$$

Constraints (Inequality):

$$P_{gslack}^{\min} \le P_{gslack} \le P_{gslack}^{\max}, \quad (5)$$

$$Q_{gi}^{\min} \le Q_{gi} \le Q_{gi}^{\max}, i \in N_g, \quad (6)$$

$$V_i^{\min} \le V_i \le V_i^{\max}, i \in N_B, \quad (7)$$

$$T_i^{\min} \le T_i \le T_i^{\max}, i \in N_T, \quad (8)$$

$$Q_c^{\min} \le Q_c \le Q_C^{\max}, \mathrm{i} \in \mathrm{N}_C \ . \qquad (9)$$

III. Culicinae Optimization Algorithm

In this work Culicinae optimization algorithm has been designed and defined to solve the problem. Natural actions of culicinae have been imitated to formulate the algorithm. Culicinae possess long and slender, legs with proboscis mouth for nourishing the blood. In Culicinae females are blood feeders and necessitate of elevated class protein food prior to lay eggs. Since Culicinae are well modified to discover the hosts and female Culicinae can move rapidly from one blood to a different one. Once infuse their saliva, it instills pathogens which has been picked up from other hosts and thus proficiently stretch the disease form one to another. Culicinae are holometabolous in nature and their stages of life are egg, larva, pupa, and adult. Naturally Adult Culicinae departs from the water but in early life stages of Culicinae i.e., egg, larval, and pupal stages are aquatic in nature.

In the procedure of the designing the optimization algorithm at first problem is defined by:

$$Min_c\, f(C), C \in c_n, n = 1,2,3,...,N \ , \qquad (10)$$

where $f(C)$ is the objective function, c is decision, c_n is the probable values of the decision variables, N is the number of decision variables.

Upper and lower bound of the values are defined by:

$$Lower\_Bound\_c_n \le c_n \le Upper\_Bound\_c_n \ , \qquad (11)$$

$$c_n \in \{c_1, c_2, c_3, ..., c_n\} \ . \qquad (12)$$

Then the fitness values of each Culicinae will be computed and among that best fitness will be chosen. In the exploration space Culicinae are arbitrarily distributed. Then the computation of the optimal location of the Culicinae is done as follows:

$$SmellY_i c_n = \frac{1}{DYc_{ni}} * \log(fitness(c_n)) + Q \ , \qquad (13)$$

$$Q = 0 \le Q \le 0.50 \ . \qquad (14)$$

Distance between the best Culicinae and other Culicinae is computed. In the solution space Culicinae will move arbitrarily to determine the optimum point. After few cycles to that discovered optimum points more Culicinae will be fascinated. Computation of the smell in the solution space is done by:

$$D(Y_i c_n) = \sqrt{\sum_{i=1}^{n} (c_n(Y_i) - c_n(c_n))} \ . \qquad (15)$$

Afterwards the position of each Culicinae will be updated. Naturally based on the density of smell each Culicinae will move towards to the optimal point which is based on the attained value and it defined as:

$$SmellY_i c_n = \frac{1}{\sqrt{T_{Yn} - c_n + (\mathrm{R}_{Yn} - \mathrm{cR}_n)_2}} \times \times \log(fitness(\mathrm{c}_n)) + Q \ . \qquad (16)$$

If there is no change in the optimal point after little iteration then it will be considered as convergence has been reached. End criterion has been defined as follows:

$$c_{new} = c_{old} + smellY_i c_n * |c_{Yn} - c_n| \ , \qquad (17)$$

$$R_{new} = R_{old} + smellY_i c_n * |R_{Yn} - R_n| \ . \qquad (18)$$

Start

Based on the number of variables Culicinae population are initialized

Primary locations of the Culicinae are engendered

For i=1

Total Number of Culicinae is evaluated

Fitness of each Culicinae in the population is computed

For iteration

If there is no change in the optimal condition in iterations then stop

Update the solutions

Output the best solutions

End

IV. SIMULATION STUDY

Culicinae Optimization Algorithm (COA) has been tested in standard IEEE 30 Bus system [18]. Table I shows the constraints of control variables, Table II shows the limits of reactive power generators and comparison results are presented in Table III. Fig. 1 gives the Comparison of parameters. Real power reduction has been achieved. Percentage of power loss reduction also improved.

Table III shows the power loss comparison with other standard techniques – modified particle swarm optimization, particle swarm optimization, Evolutionary programming, and self- adaptive real coded genetic algorithm.

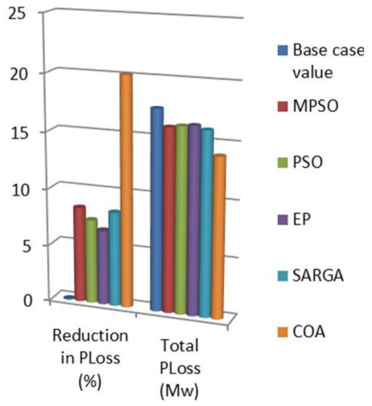

Figure 1. Comparison of parameters

TABLE I. CONSTRAINT VALUES OF THE CONTROL VARIABLES.

	Parameter	Minimum value (PU)	Maximum value (PU)
IEEE 30 Bus	Generator Voltage	0.95	1.1
	Transformer Tap	0.9	1.1
	VAR Source	0	0.20

TABLE II. CONSTRAINS VALUES OF THE REACTIVE POWER GENERATORS.

	Bus	Value of Q Minimum (PU)	Value of Q Maximum (PU)
IEEE 30 Bus	1	0	10
	2	-40	50
	5	-40	40
	8	-10	40
	11	-6	24
	13	-6	24

TABLE III. SIMULATION RESULTS OF IEEE −30 SYSTEM.

Parameter	Base case value	MPSO [19]	PSO [22]	EP [21]	SARGA [21]	COA
VG−1	1.060	1.101	1.100	NR*	NR*	1.012
VG−2	1.045	1.086	1.072	1.097	1.094	1.034
VG−5	1.010	1.047	1.038	1.049	1.053	1.018
VG−8	1.010	1.057	1.048	1.033	1.059	1.019
VG−12	1.082	1.048	1.058	1.092	1.099	1.022
VG-13	1.071	1.068	1.080	1.091	1.099	1.031
Tap-11	0.978	0.983	0.987	1.01	0.99	0.945
Tap-12	0.969	1.023	1.015	1.03	1.03	0.913
Tap-15	0.932	1.020	1.020	1.07	0.98	0.902
Tap-36	0.968	0.988	1.012	0.99	0.96	0.913
QC-10	0.19	0.077	0.077	0.19	0.19	0.090
QC-24	0.043	0.119	0.128	0.04	0.04	0.104
PG (MW)	300.9	299.54	299.54	NR*	NR*	298.22
QG (MVAR)	133.9	130.83	130.94	NR*	NR*	130.10
Reduction in Power Loss (%)	0	8.4	7.4	6.6	8.3	20.16
Total Power Loss (MW)	17.55	16.07	16.25	16.38	16.09	14.011

NR* - Not reported.

Proposed Culicinae Optimization Algorithm (COA) has been tested, in IEEE 57 Bus system. Table IV shows the constraints of control variables, Table V shows the limits of reactive

TABLE IV. CONSTRAINTS OF CONTROL VARIABLES.

	Parameter	Minimum value (PU)	Maximum value (PU)
IEEE 57 Bus	Generator Voltage	0.95	1.1
	Transformer Tap	0.9	1.1
	VAR Source	0	0.20

TABLE V. CONSTRAINS OF REACTIVE POWER GENERATORS.

	Bus	Q Minimum (PU)	Q Maximum (PU)
IEEE 57 Bus	1	-140	200
	2	-17	50
	3	-10	60
	6	-8	25
	8	-140	200
	9	-3	9
	12	-150	155

TABLE VI. SIMULATION RESULTS OF IEEE −57 SYSTEM.

Parameters	Base case	MPSO [19]	PSO [22]	CGA [20]	AGA [20]	COA
VG 1	1.040	1.093	1.083	0.968	1.027	1.015
VG 2	1.010	1.086	1.071	1.049	1.011	1.014
VG 3	0.985	1.056	1.055	1.056	1.033	1.023
VG 6	0.980	1.038	1.036	0.987	1.001	1.014
VG 8	1.005	1.066	1.059	1.022	1.051	1.025
VG 9	0.980	1.054	1.048	0.991	1.051	1.024
VG 12	1.015	1.054	1.046	1.004	1.057	1.033
Tap 19	0.970	0.975	0.987	0.920	1.030	0.912
Tap 20	0.978	0.982	0.983	0.920	1.020	0.914
Tap 31	1.043	0.975	0.981	0.970	1.060	0.905
Tap 35	1.000	1.025	1.003	NR*	NR*	1.003
Tap 36	1.000	1.002	0.985	NR*	NR*	1.011
Tap 37	1.043	1.007	1.009	0.900	0.990	1.013
Tap 41	0.967	0.994	1.007	0.910	1.100	0.912
Tap 46	0.975	1.013	1.018	1.100	0.980	1.024
Tap 54	0.955	0.988	0.986	0.940	1.010	0.936
Tap 58	0.955	0.979	0.992	0.950	1.080	0.924
Tap 59	0.900	0.983	0.990	1.030	0.940	0.943
Tap 65	0.930	1.015	0.997	1.090	0.950	1.052
Tap 66	0.895	0.975	0.984	0.900	1.050	0.911
Tap 71	0.958	1.020	0.990	0.900	0.950	1.023
Tap 73	0.958	1.001	0.988	1.000	1.010	1.022
Tap 76	0.980	0.979	0.980	0.960	0.940	0.931
Tap 80	0.940	1.002	1.017	1.000	1.000	1.010
QC 18	0.1	0.179	0.131	0.084	0.016	0.131
QC 25	0.059	0.176	0.144	0.008	0.015	0.140
QC 53	0.063	0.141	0.162	0.053	0.038	0.103
PG (MW)	1278.6	1274.4	1274.8	1276	1275	1272.20
QC (Mvar)	321.08	272.27	276.58	309.1	304.4	272.30
Reduction in Power Loss (%)	0	15.4	14.1	9.2	11.6	23.95
Total Power Loss (MW)	27.8	23.51	23.86	25.24	24.56	21.141

NR* - Not reported.

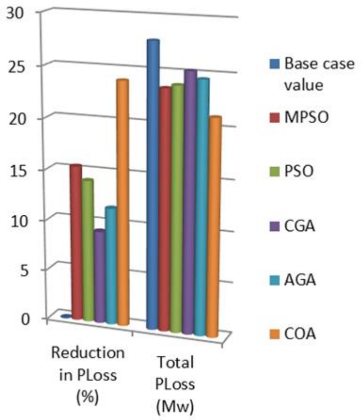

Figure 2. Comparison of values

power generators and comparison results are presented in Table VI. Fig. 2 indicates the comparison of values.

Table VI shows the power loss comparison with other standard techniques- modified particle swarm optimization, particle swarm optimization, canonical genetic algorithm, adaptive genetic algorithm. Percentage of the power loss reduction has been achieved.

V. CONCLUSION

In this work optimal reactive power problem has been solved by Culicinae Optimization Algorithm (COA) in efficient mode. Computation of the optimal location of the Culicinae has been done. Distance between the most excellent Culicinae and other Culicinae is calculated. Position of each Culicinae will be updated. Naturally based on the density of smell each Culicinae will move towards to the optimal point which is based on the attained value. After few number of iteration there is no change in the optimal point and it considered as convergence has been reached. Proposed Culicinae Optimization Algorithm (COA) has been tested in standard IEEE 30 and 57 bus test system and simulation results show the projected algorithm reduced the real power loss considerably. 20.16 % and 23.95 % reduction of real power loss have been attained.

REFERENCES

[1] Lee, K. Y., Park, Y. M., & Ortiz, J. L. (1984, May). Fuel-cost minimisation for both real-and reactive-power dispatches. In *IEE proceedings C (generation, transmission and distribution) 131*(3), 85-93.

[2] Deeb, N. I., & Shahidehpour, S. M. (1988). An efficient technique for reactive power dispatch using a revised linear programming approach. *Electric power systems research, 15*(2), 121-134.

[3] Bjelogrlic, M., Calovic, M. S., Ristanovic, P., & Babic, B. S. (1990). Application of Newton's optimal power flow in voltage/reactive power control. *IEEE Transactions on Power Systems, 5*(4), 1447-1454.

[4] Granville, S. (1994). Optimal reactive dispatch through interior point methods. *IEEE Transactions on power systems, 9*(1), 136-146.

[5] Grudinin, N. (1998). Reactive power optimization using successive quadratic programming method. *IEEE Transactions on Power Systems, 13*(4), 1219-1225.

[6] De Sousa, V. A., Baptista, E. C., & Da Costa, G. R. M. (2012). Optimal reactive power flow via the modified barrier Lagrangian function approach. *Electric power systems research, 84*(1), 159-164.

[7] Li, Y., Li, X., & Li, Z. (2017). Reactive power optimization using hybrid CABC-DE algorithm. *Electric power components and systems, 45*(9), 980-989.

[8] Mouassa, S., Bouktir, T., & Salhi, A. (2017). Ant lion optimizer for solving optimal reactive power dispatch problem in power systems. *Engineering science and technology, an international journal, 20*(3), 885-895.

[9] Ding, J., Zhang, Q., & Ma, Y. (2018, May). Optimal reactive power dispatch based on the CS-PSO algorithm. In *2018 13th IEEE Conference on Industrial Electronics and Applications (ICIEA)* (pp. 1172-1176). IEEE.

[10] Abaci, K., & Yamaçli, V. (2017). Optimal reactive-power dispatch using differential search algorithm. *Electrical Engineering, 99*(1), 213-225.

[11] Ding, J., Zhang, Q., & Ma, Y. (2018, May). Optimal reactive power dispatch based on the CS-PSO algorithm. In *2018 13th IEEE Conference on Industrial Electronics and Applications (ICIEA)* (pp. 1172-1176). IEEE.

[12] Nguyen, T. T., Vo, D. N., Van Tran, H., & Van Dai, L. (2019). Optimal dispatch of reactive power using modified stochastic fractal search algorithm. *Complexity*, 2019.

[13] ben oualid Medani, K., Sayah, S., & Bekrar, A. (2018). Whale optimization algorithm based optimal reactive power dispatch: A case study of the Algerian power system. *Electric Power Systems Research, 163*, 696-705.

[14] Hussain, A. N., Abdullah, A.A., & Neda, O.M. (2019). Optimal Capacitor Sizing for Reactive Power Optimization by Using a New Hybrid Algorithm Based on Merging of Chaotic Strategy with PSO Algorithm. *Journal of Engineering and Applied Sciences, 14*, 2112-2123.

[15] Abaci, K., & Yamaçli, V. (2017). Optimal reactive-power dispatch using differential search algorithm. *Electrical Engineering, 99*(1), 213-225.

[16] Polprasert, J., Ongsakul, W., & Dieu, V. N. (2016). Optimal reactive power dispatch using improved pseudo-gradient search particle swarm optimization. *Electric Power Components and Systems, 44*(5), 518-532.

[17] Basu, M. (2016). Quasi-oppositional differential evolution for optimal reactive power dispatch.

International journal of electrical power & energy systems, 78, 29-40.

[18] IEEE (1993). *The IEEE-test systems*. Available at: http://www.ee.washington.edu/trsearch/pstca/.

[19] Hussain, A. N., Abdullah, A. A., & Neda, O. M. (2018). Modified particle swarm optimization for solution of reactive power dispatch. *Research journal of applied sciences, engineering and technology, 15*(8), 316-327.

[20] Dai, C., Chen, W., Zhu, Y., & Zhang, X. (2009). Seeker optimization algorithm for optimal reactive power dispatch. *IEEE Transactions on power systems, 24*(3), 1218-1231.

[21] Subbaraj, P., & Rajnarayanan, P. N. (2009). Optimal reactive power dispatch using self-adaptive real coded genetic algorithm. *Electric Power Systems Research, 79*(2), 374-381.

[22] Pandya, S., & Roy, R. (2015, March). Particle swarm optimization based optimal reactive power dispatch. In *2015 IEEE International Conference on Electrical, Computer and Communication Technologies (ICECCT)* (pp. 1-5). IEEE.

A Review on The Panorama of Combined Heating, Cooling, and Power in Brazil

Karollyne Marques de Lima[1], Danielle Bandeira de Mello Delgado[2,3], Monica Carvalho[4]

[1]Graduate Program in Renewable Energy, Federal University of Paraíba, João Pessoa, Brazil, karollyne@cear.ufpb.br
[2]Federal Institute of Education, Science and Technology of Bahia, Paulo Afonso, Brazil,
[3]Graduate Program in Mechanical Engineering, Federal University of Paraíba, João Pessoa, Brazil, danielle.delgado@ifba.edu.br
[4] Department of Renewable Energy Engineering, Federal University of Paraíba, João Pessoa, Brazil, monica@cear.ufpb.br

Abstract—**Combined heating, cooling, and power (CHCP) systems are distributed power generation models that have several advantages over conventional, centralized power generation. A review of the panorama of CHCP in Brazil is presented herein, based on experimental and analytical studies. The focus of this research is to map and point out, through bibliographic research, the potential for CHCP in Brazil, according to the application and fuel employed. A bibliographic search was carried out on scientific papers and works published in scientific journals (databases: Periodicos Capes and Google Scholar) in the period 2010 – 2020. As a result, few studies were found on the subject. Despite the advantages of CHCP over conventional energy systems, there are barriers in Brazil for the technical feasibility of CHCP, such as the high capital costs, lack of subsidies, and tax incentives.**

Keywords – trigeneration, CHCP, distributed generation, polygeneration

I. INTRODUCTION

Energy is fundamental for the development of society and in recent decades, the need for the development of low carbon technologies has emerged, aimed at reducing environmental impacts and improving sustainability aspects. A sustainable energy system can be treated as a development of the distributed generation (DG, also referred to as decentralized energy) concept [1], which is geographically distributed over the area that is serviced and close to the consumer [2]. Within the electric power system, DG presents numerous technical and environmental advantages, both for the final consumer and for society, with the main advantages related to decreased costs with energy transmission and distribution. The term trigeneration is often employed to refer to the combined production of three energy services[1] – therefore, the terms "combined heating, cooling, and power" (CHCP) and "trigeneration" are used interchangeably. The concepts of combined production of energy services (e.g., polygeneration, cogeneration, and trigeneration) are directly related to DG.

Electricity, heating, and cooling are the three main components responsible for energy demands in residential, commercial and public buildings worldwide [4]. Integrated energy systems, such as CHCP, benefit from the energy integration of the processes in their equipment, extracting the maximum thermodynamic potential from the consumed resources [5]. The combined production of energy services yields an efficient use of resources (which requires a detailed study of the generation/consumption rate [6]), along with reliability and continuity in energy supply, with considerable improvements regarding autonomous systems [7].

CHCP systems can be applied to industrial processes and different buildings [8], and the

[1]Additional equivalent term: "combined cooling, heating, and power" (CCHP). More comprehensive terms include polygeneration and integrated energy systems (IES) [3].

ISBN: 978-86-80616-07-0

key aspect in the operation of these combined energy systems, in the absence of environmental constraints, is to satisfy the energy demands of the consumer center with minimal cost. CHCP systems can employ different prime movers, such as alternative engines, gas turbines, microturbines, steam turbines, and Stirling engines, for example. Although some of the technologies are well-established and commercially available, such as internal combustion engines, gas turbines, and absorption cooling [9], there are other promising technologies to be considered (e.g., organic Rankine systems, fuel cells and liquid desiccant cooling).

CHCP (and its variations) has been successfully employed by the industrial sector to realize primary energy savings, increase energy efficiency, reduce product costs and associated environmental impacts – and these advantages can be extended to residential [10] and tertiary sector applications [11].

Fig. 1 shows a general scheme for a CHCP system, fundamentally based on the coupling of a cogeneration module (prime mover) to an absorption chiller that produces cooling from the harnessed heat. Storage tanks can be inserted between the heating and cooling units and the final user.

There is no data on combined heat and power (CHP) or CHCP within the Brazilian energy matrix, but according to the Brazilian Association of Cogeneration Energy Industry [12], there was 18.5 GW of CHP installed in Brazil up to October 2019 (approximately 11% of the national generation park). Most of the energy systems used sugarcane biomass as fuel, followed by natural gas [13]. Fig. 2 shows the progression in the development of the cogeneration market in Brazil.

The objective of this study is to carry out a systematic literature review, to identify studies that addressed CHCP systems in Brazil, listing the sectors involved and fuels used, presenting a panorama of studies that have been developed over the past ten years. The overarching aim is to verify the feasibility of implementing these systems, and what are the most favorable conditions.

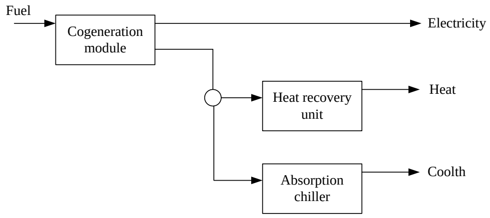

Figure 1. General scheme of a combined heating, cooling, and power system.

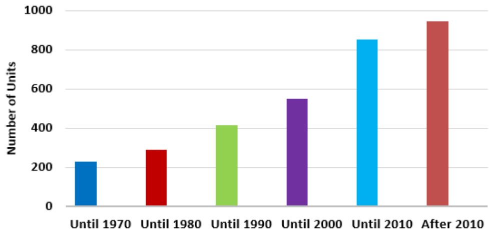

Figure 2. Cogeneration units in operation.

II. Methodology

A bibliographic research is presented herein, focusing on research papers and studies (MSc. and PhD. Theses) published between 2010 and 2020. The databases consulted were *Periódicos CAPES* and Google Scholar, using the descriptors: Trigeneration, CHCP, Brazil, Combined heating, cooling and power, as well as their synonyms and equivalents in Portuguese, in various combinations. Databases of Brazilian associations were also consulted: Energy Research Company (EPE), Association of the Energy Cogeneration Industry (COGEN), and Ministry of Mines and Energy (MME).

Experimental and simulation studies were included, which aimed to evaluate the performance of CHCP systems in Brazil, considering the fuels used in the plants and the sectors or locations of application.

Results derived from books, proceedings, conference abstracts and other forms of information disclosure were excluded from the analysis. In the case duplicate similar publications were identified, as in the case of conference proceedings published in a scientific journal, only the latter is mentioned. This took into account the importance of finding all the studies published on the subject and that, besides fulfilling the inclusion criteria, presented high methodological quality.

The first step of the review consisted of reading the titles and abstracts of all documents identified in the searches (manual and in databases), selecting only those that focused on the subject and type of study. Duplicated studies were removed. The second step of the review encompassed the full reading of the documents, with extraction of relevant data. Manual search was also carried out by reading the references listed in the studies, for possible inclusion of other studies that were not identified initially in the electronic search.

III. Results

The initial search retrieved nine papers from *Periódicos CAPES* and nine from Google Scholar. The studies were then screened by reading the titles and abstracts, and all 18 publications were considered relevant to the research scope established, fulfilling the inclusion and exclusion criteria. The studies were published between 2010 and 2020, with 10 experimental studies and eight simulations. There were five MSc. theses, one PhD. thesis, and 12 research papers. Regarding the geographic location of studies, nine were carried out in the Southeast region, four were carried out considering the Northeast region, one considered the South region, one considered the North region, one did not specify its location within Brazil, and two did not specify neither the consumer center or the location.

Next, a brief explanation of each study, including the description of the studied system, methodology, and main results is presented, in alphabetical order.

A. *Experimental Studies*

Reference [8] carried out energy, exergy, and exergoeconomic evaluations for a micro-trigeneration system designed to meet electricity and cooling demands of a university building, while heat was directed to an on-site biodiesel plant. The most sensitive components to exergoeconomic improvements were the steam generator and the heat exchanger of the absorber. Margins for improvement were identified regarding the heat transfer area in the generator, utilization of new materials, substitution of the refrigerant, and variations in the thickness and geometry of the heat exchanger.

Reference [14] carried out energy and economic analyses for a natural gas CHCP system installed in an ice cream factory, with unspecified location in Brazil. An internal combustion engine (ICE) was available for the production of electricity, a recovery boiler for the production steam, and an absorption chiller for refrigeration purposes. The best economic result was obtained for the third scenario investigated, with the ICE and recovery boiler only, with net present value (NPV) of $ 269,390.40, a 26.32% internal rate of return (IRR), and a 3.4 year simple payback.

Reference [15] tested three configurations of an energy system, designed to meet the electricity and cooling demands of a university building, while heat is harnessed to drive a pilot-scale biodiesel plant, at the Federal University of Paraíba (Northeast Brazil). Energy results for two CHP-based arrangements and one CHCP-based arrangement are presented. The CHCP-based arrangement could meet the heat demands of the biodiesel plant, despite the 15 m distance between equipment.

Reference [16] presented an optimization of the energy supply for a research center located in Jundiaí (Southeast Brazil). The energy demands were electricity, steam and chilled water, and the objective was to minimize the operation costs of the system. The facility already has a trigeneration system and the result of the optimization defined its operation, establishing when or how to use the contracted demand. The optimization used the generalized reduced gradient (GRG) method.

Reference [17] applied first and second laws of thermodynamics to analyze the quantity and quality of energy of a small trigeneration system, not connected to the grid, using Liquefied Petroleum Gas as fuel. The energy system is located at the State University of São Paulo (Southeast Brazil). Exergy flows were calculated, leading to the identification of where and why losses and irreversibilities occur, detecting the subsystems that presented lower thermodynamic performance.

Reference [18] developed a thermoeconomic analysis for a trigeneration system installed in a soluble coffee industry, located in Paraná (South Brazil). The objective was to identify margins for improvement in the economic and energy performance of the system. Optimization of energy consumption was carried out with Pinch analysis. The results demonstrated that the addition of a 4.5 MW turbo generator was technically and economically viable, resulting in lower product costs (heat, cooling and power), with a payback time of 14.5 months. There was a significant reduction in the cost of electricity (70%) with trigeneration.

Reference [19] presented energy and exergy analysis of a high-efficiency engine trigeneration system for a hospital located in Southeast Brazil. Software COGMCI was employed to simulate the system as an integrated thermal system, analyzing the hourly operation of the production of electricity and thermal flows (steam, hot water, chilled water).The results indicated energy utilization factors between 58% and 77% and exergy efficiencies between 35 and 41%, and analysis of the primary energy savings showed that the trigeneration system is more advantageous than the best technology used in centralized thermal plants.

Reference [20] tested two configurations of trigeneration systems: one is based on a 30 kW natural gas powered microturbine, and the other uses a 26 kW natural gas powered internal combustion engine coupled to an electrical generator. Tests were carried out in a laboratory located in Southeast Brazil. The exhaust gases from both configurations were directed to a 17.6 kW absorption chiller and a heat recovery boiler, for the production of chilled and hot water, respectively. Energy utilization factors, primary energy savings, and heat rates were obtained for both configurations, yielding 56.3%, 15.1% and 3.9 for the microturbine configuration, and 43.7%, 44.2%, and 3.6 for the engine.

Reference [21] presented an evaluation of different trigeneration systems (based on steam turbines, gas turbines, combined cycle - including a tetra-combined system), designed to meet the energy demands of three different applications: a dairy industry, a hospital, and a beverage industry. The configurations were optimized using the Genetic Algorithm method. The results showed that the hybrid absorption/ejecto compression refrigeration system was a good alternative to produce refrigeration, as the coefficient of performance and the exergy efficiency were higher than for the single-effect absorption refrigeration system.

Reference [22] reported on a trigeneration system projected, mounted, and tested at the University of São Paulo (Southeast Brazil). The trigeneration system combines a microturbine, a heat recovery boiler, and an ammonia-water absorption chiller. Theoretical results and experimental data were compared, and it was verified that the exhaust gases could supply the total absorption chiller with sufficient margins to attend the hot water demand of the heat recovery boiler.

Table I shows the summary of the panorama of the studies covered, highlighting the object of study and the fuel used for experimental studies.

B. Modeling and Simulation Studies

Reference [23] proposed a trigeneration system to meet the energy demands of a resort hotel, located in Piauí (Northeast Brazil). The energy utilization factor of the trigeneration system was 81.6%, against 21% of the conventional solution.

Reference [24] addressed thermal integration in the synthesis of polygeneration systems for buildings, and carried out a MILP-based optimization with Pinch analysis for the energy supply and conversion system of a hospital located in the Southeastern region of Brazil. A trigeneration system was suggested, with natural gas cogeneration modules and boilers, and the installed cooling capacity of the optimal solution corresponded to 60% absorption chillers and 40% of mechanical chillers (only to cover peak demands).

Reference [25] analyzed and compared four configurations of trigeneration systems, based on mathematical models derived from energy and exergy balances and CO_2 emissions. The trigeneration configurations included vapor compression chillers, absorption chillers, a combination of the two previous cycles, and incorporation of an organic Rankine cycle. It was observed that the energy, exergy, and CO_2-based efficiencies depended on the energy demands. All trigeneration configurations operated more efficiently than the separate production of energy services.

TABLE I. PANORAMA OF EXPERIMENTAL STUDIES.

Reference	Type of Study	Study Object	Fuel
Marques et al. (2020)	Energy, exergy, and exergoeconomic assessments	University laboratory + adjacent biodiesel production plant (Northeast Brazil)	Natural gas
Alcântara et al. (2019)	Economic and energy analysis	Ice cream industry (Brazil)	Natural gas
Cavalcante et al. (2017)	Energy analysis of three configurations	University laboratory (Northeast Brazil)	Natural gas
Pérez et al. (2015)	Energy and exergy analysis	Laboratory setup (Southeast Brazil)	Liquefied petroleum gas
Lovati (2015)	Optimization of operation (exergoeconomics)	Research center (Southeast Brazil)	Natural gas/Diesel oil
Silva (2015)	Thermoeconomic analysis and optimization of process utility consumption(pinch analysis)	Soluble coffee industry (South Brazil)	Coffee and woodchip biomass
Espirito Santo (2014)	Performance simulation and evaluation	Hospital (Southeast Brazil)	Natural gas
Rocha et al. (2012)	Energy analysis of two configurations	Laboratory setup (Southeast Brazil)	Natural gas
Jaramillo (2011)	Optimization of configurations (Genetic algorithm)	Dairy industry, hospital, and beverage industry (Southeast Brazil)	Natural gas
Preter et al. (2010)	Energy analysis: theoretical *vs.* experimental results	Laboratory setup (Southeast Brazil)	Natural gas

Reference [26] simulated the feasibility of a trigeneration project, employing technical and economic analyses. The trigeneration system produces electricity for internal consumption and exports to the grid, chilled water for air conditioning purposes, and steam for the industrial process. The energy system included a natural gas microturbine and engine, with heat recovery units, and an absorption chiller. Six different scenarios were formulated, based on different operation strategies of the energy system and economic conditions, and the economic feasibility depended strongly on the electric and thermal demands.

Reference [27] evaluated the technical feasibility of operating a natural gas trigeneration system, based on a concentrated solar system within an integrated solar combined cycle. The consumer center is a hospital located in Northeast Brazil (Bahia), with requires electricity, cooling, and heat. The system was designed considering thermal parity, to meet the energy demands of the hottest day of the year. Although the simulations were carried out for only three days (lowest and highest temperatures, and cloudy day), it can ensure autonomous operation on any day of the year.

Reference [28] presented analyses for natural gas trigeneration systems designed for four different buildings in Southeastern Brazil (Minas Gerais): a hospital, a residential building, a university building, and a hotel. Analysis utilized net present value, grid dependence index, payback time, levelized cost of energy, and primary energy ratio. For the hospital and hotel, economic viabilities were exactly on the breakpoints; for the residential building, the best financial benefit was obtained; and for the university building, unfortunately the system resulted as non-viable.

Reference [29] optimized the operation of a trigeneration system that met the energy demands of a Southeast Brazil hospital. The resulting system was compared with the traditional system, evaluated via equivalent annual cost, internal rate of return, and payback. Results were very positive for the trigeneration system, and margins for improvement of its economic feasibility include a reformulation of the natural gas market in Brazil.

Reference [30] discussed guidelines on how well-established methodologies for environmental and thermoeconomic analysis should be taken into account to access the feasibility of CHCP plants in the Brazilian Amazon. The analysis considered a thermoelectric power plant located in Manaus, powered by diesel engines. Two approaches were suggested: the first focused on the optimization of exergy, economic, and environmental internal costs of the CHCP plant, and the second optimizes the economic and environmental relationships of the plant with the technosphere and environmental surroundings by a Pareto optimal approach. The former is simpler to implement, as it employs conventional computational software, and the latter is computationally intensive, demanding mathematical background and more sophisticated computer software.

Table II shows the summary of the panorama of the studies covered, highlighting the study object and fuel used, for modeling and simulation studies. From the information consolidated in Tabs. I and II it is observed that for experimental and theoretical (modeling and simulations of study cases) studies, trigeneration is adequate for some typical types of loads, such as in hospitals and hotels, due to the diversification of energy demands. Regarding the fuels employed, natural gas was widely employed, even when less carbon intensive options were considered, due to its efficiency and lower cost.

As mentioned by [8], studies on trigeneration schemes help confirm and evidence the benefits that can be realized, helping expand distributed generation strategies. The authors also remark that the consideration of trigeneration leads to a diversification of discussions on the energy matrix, and micro-trigeneration (under 50 kWe) is highlighted for the tertiary sector (“the best way for decentralized power, cooling, and heating” [31]). Environmental concerns have also motivated research on trigeneration systems, as verified herein.

The progressive development of the cogeneration market in Brazil gives an indication of the potential of trigeneration, with application in the industrial, commercial and services sectors. However, the implementation of trigeneration in the Brazilian energy matrix requires the overcoming of a series of technical, financial and political barriers. Factors that hinder the dissemination of trigeneration, which deserve special attention, include: high capital costs, lack of government support, and more favorable tax incentives. Investments must be made into research and development, regarding

TABLE II. PANORAMA OF MODELING AND SIMULATION STUDIES.

Reference	**Type of Study**	**Study Object**	**Fuel**
Leite (2019)	Exergoeconomic assessment	Resort hotel (Northeast Brazil)	Diesel
Pina et al. (2018)	MILP-based optimization with Pinch analysis	Hospital (Southeast Brazil)	Natural gas
Givisiez et al. (2018)	Economic analysis (energy tariffs): trigeneration *vs.* conventional system	Hospital (Southeast Brazil)	Natural gas
Givisiez (2018)	Economic analysis: trigeneration *vs.* conventional system	Hospital, residential building, university building, and hotel (Southeast Brazil)	Natural gas
Ochoa et al. (2017)	Technical and economic feasibility	Unspecified consumer center and location	Natural gas
Silva (2017)	Thermodynamic and environmental analysis	Unspecified consumer center and location	Diesel oil/ Biodiesel
Malagueta et al. (2014)	Technical feasibility based on thermal parity	Hospital (Northeast Brazil)	Natural gas
Cruz et al. (2011)	Feasibility analysis	Thermoelectric power plant (North Brazil)	Diesel oil

the components and operation of small and large-scale trigeneration plants.

Finally, despite the significant health-related impacts of the COVID-19 crisis, the energy sector is also suffering adverse effects that slowdown energy transitions [32]. It is expected that governments will have to enforce stimulus plans to alleviate the economic damages, which should include energy efficiency measures. Trigeneration can play an important role, as mentioned by [33], motivating economic competitiveness and providing more affordable energy while also reducing environmental impacts.

IV. Conclusion

This review study demonstrate how trigeneration systems have been explored so far in Brazil, considering the period 2010-2020. Few Brazilian studies were identified on trigeneration. Experimental studies are concentrated in research, teaching and development institutes.

The configurations of the trigeneration systems varied according to their different applications, which included hospitals, industrial facilities, and residential and university buildings. The majority of studies utilized natural gas as the main fuel.

Although the Brazilian energy matrix is predominantly renewable and Brazilian energy policies favor advances in the use of biomass, wind and solar photovoltaic energy, these resources are still underexploited and were not expressive in the results herein obtained.

It is important to disseminate the diversification of the available resources and stimulate not only the adoption of a lower cost solution, but also include concepts of energy efficiency and environmental friendliness.

References

[1] Rong, A., & Lahdelma, R.. (2016). Role of polygeneration in sustainable energy system development challenges and opportunities from optimization viewpoints. *Renewable and Sustainable Energy Reviews, 53*, 363-372.

[2] Vera, D., Jurado, F., Torreglosa, J. P., & Ortega, M. (2018). Biomass Gasification for Power Generation Applications: A Modeling, Economic, and Experimental Study. *Advances in Renewable Energies and Power Technologies*, 87-121.

[3] Gluesenkamp, K., & Radermacher, R. (2011). Heat-activated cooling technologies for small and micro combined heat and power (CHP) applications. *Small and Micro Combined Heat and Power (CHP) Systems*, 262-306, Woodhead Publishing.

[4] Al Moussawi, H., Fardoun, F., & Louahlia, H. (2016). Review of tri-generation Technologies: Design evaluation, optimization, decision-making, and selection approach. *Energy Conversion and Management, 120*, 157-196.

[5] Carvalho, M., Lozano, M. A., & Serra, L. M. (2012). Multicriteria synthesis of trigeneration systems considering economic and environmental aspects. *Applied Energy, 91*, 245-254.

[6] Romero, A., Millar, D., Carvalho, M., & Abrahão, R. (2020). 100% renewable fueled mine. *Energy*, 117964.

[7] Delgado, D. B. M., Carvalho, M., Coelho Junior, L. M., & Chacartegui, R. (2018). Analysis of Biomass-fired Boilers in a Polygeneration System for a *Hospital. Frontiers in Management Research, 2*(1), 1-13.

[8] Marques, A. S., Carvalho, M., Lourenço, A.B., & Santos, C. A. C. (2020). Energy, exergy, and exergoeconomic evaluations of a micro-trigeneration system. *Journal of the Brazilian Society of Mechanical Sciences and Engineering, 42*(324), 324.

[9] Bagade, S., Mahesh, S., & Mahajan, S. R. (2019). Trigeneration Systems: A Review. *International Journal of Research in Advent Technology, 7*(5), 38-43.

[10] Pina, E. A., Lozano, M. A., Ramos, J. C., & Serra, L. M. (2020). Tackling thermal integration in the synthesis of polygeneration systems for buildings. *Applied Energy, 269*, 115115.

[11] Carvalho, B. C. T., Melo, C. T. M., Romero, A. J., Khanmohammadi, S., & Carvalho, M. (2019). Multicriteria optimization of renewable-based polygeneration system for tertiary sector buildings. *Environmental Engineering & Management Journal (EEMJ), 18*(11).

[12] COGEN. (2020a). *Cogeneration Units in operation.* Available at: http://www.cogen.com.br/siscogen/indicadores-de-gestao/unidades-de-cogeracao-em-operacao. Acess in February 28, 2020. (In Portuguese)

[13] COGEN. (2020b). *Cogeneration has 18.5 GW installed in the country, most of which is biomass.* Available at: http://www.cogen.com.br/principais-noticias/cogeracao-tem-18-5-gw-instalados-no-pais-com-maior-parte-de-biomassa. Access in February 28, 2020. (In Portuguese)

[14] Alcântara, S. C. S., Ochoa, A. A. V., da Costa, J. A. P., Michima, P. S. A., & Silva, H. C. N. (2019). Natural gas based trigeneration system proposal to an ice cream factory: An energetic and economic assessment. *Energy Conversion and Management, 197*, 1-14.

[15] Cavalcante, A. W. A., dos Santos, C. A. C., & Ochoa A. A. V. (2017). Thermodynamic analysis of an energy high performance systems. *IEEE Latin America Transactions, 15*(3), 454-461.

[16] Lovati,C. V. (2015). Operational optimization of a trigeneration system to meet variable demands. Dissertation (Master in Mechanical Engineering), Espírito Santo: Federal University of Espirito Santo. (In Portuguese)

[17] Pérez, N. P., Sadamitsu, M. T., Silveira, J. L., Antunes, J. S., Tuna, C. E., Valle, A. E., & Silva, N. F. (2015). Energetic and exergetic analysis of a new compact trigeneration system run with liquefied pretroleum gas. *Energy, 90*, 1411-1419.

[18] Silva, A. C. C., (2015). Thermoeconomic analysis of a trigeneration system in a food industry. Dissertation (Master in Mechanical Engineering), Maringá: State University of Maringá. (In Portuguese)

[19] Espirito Santo, D. B. (2014). An energy and exergy analysis of a high-efficiency engine trigeneration system for a hospital: A case study methodology based on annual energy demand profiles. *Energy and Buildings, 76*, 185-198.

[20] Rocha, M. S., Andreos, R., & Simões-Moreira, J. R. (2012). Performance tests of two small trigeneration plants. *Applied Thermal Engineering, 41*, 84-91.

[21] Burbano Jaramillo, J. C. (2011). Exergoeconomic optimization of a tetra-combined trigeneration system. Thesis (Doctorate in Mechanical Engineering), São Paulo: Polytechnic School of the University of São Paulo. (In Portuguese)

[22] Preter, F. C., Simões-Moreria, J. R., Rocha, M. S., & Andreos, R. (2010). Evaluation of a trigeneration system using microturbine, ammonia-water absorption chiller, and a heat recovery boiler. In *13th Brazilian Congress of Thermal Sciences and Engineering.*

[23] Leite, A. L. F. (2019). Exergoeconomic analysis of a system of trigeration in the tertiary sector: a case study in a resort. Dissertation (Master in Mechanical Engineering), João Pessoa: Federal University of Paraíba. (In Portuguese)

[24] Pina, E. A., Lozano, M. A., & Serra, L. M. (2018). Opportunities for the Integration of Solar Thermal Heat, Photovoltaics and Biomass in a Brazilian Hospital. In *Proceedings of the EuroSun*. 2018, (pp. 10-13).

[25] Silva, V. H. M. M. (2017). Thermodynamic and environmental analysis of trigeneration systems according to their architecture and energy demands. Dissertation (Master in Mechanical Engineering), Rio de Janeiro: Pontifical Catholic University of Rio de Janeiro. (In Portuguese)

[26] Ochoa, A. A., Costa, J. A., Diniz, H. H., Assumpção, L., Carvalho, V., & Franco, S. S. (2017). Financial analysis of an energy trigeneration plant (Electricity, Cold and Heat). *CIENTEC Magazine, 9*(2), 112-125. (In Portuguese)

[27] Malagueta, D. C., Szklo, A. S., & Dutra, R. M. (2014). Parametric analysis of a CSP-ISCC trigeneration plant for a hospital in Bom Jesus da Lapa. In *Recife: V Brazilian Congress of Solar Energy*. (In Portuguese)

[28] Givisiez, A. G. (2018). Technical and economical evaluation of combined cooling, heat and power technology: A Brazilian study case considering different consumers. Dissertation (Master in Electrical Engineering), Juiz de Fora: Federal University of Juiz de Fora.

[29] Givisiez, A. G., de Oliveira, L. W., Dias, B. H., & Forbes, M. Z. (2018). Optimal operation and economical analysis of a trigeneration system. In *Simpósio Brasileiro de Sistema Elétricos (SBSE).*

[30] Cruz, R. W., Serra, L. M., & Lozano, M. A. (2011). Thermoeconomic and environmental guidelines for trigeneration projects in the Brazilian Amazon. In *ECOS 2011 – 24th International Conference on Efficiency, Cost, Optimization, Simulation and Environmental Impact of Energy Systems*, (pp. 3171-3182), Serbia.

[31] Easow, R., & Mulley, P. (2010). Micro-Trigeneration: The best way for decentralized power, cooling and heating. In *2010 IEEE Conference on Innovative Technologies for an Efficient and Reliable Electricity Supply* (pp. 459-466).

[32] Carvalho, C., Delgado, D. B. M., Lima, K. M., Cancela, M. C., Siqueira, C. A. S., & Souza, D. L. B. (2020). Effects of the covid-19 pandemic on the Brazilian electricity consumption patterns, International Journal of Energy Research, in press.

[33] Cavalcanti, E. J. C., Carvalho M., & Silva, D. R. S. (2020). Energy, exergy and exergoenvironmental analyses of a sugarcane bagasse power cogeneration system, *Energy Conversion and Management*, (in press).

PV Production Forecast From Reduced Data Sets

Bratislav Trojić[1], Aleksandar Janjić[2], Uroš Ilić[3], Vladislav Lazić[4]

[1,2,3,4]Faculty of Electronic Engineering, Nis, Serbia, bratislav.trojic@gmail.com[1]; aleksandar.janjic@elfak.ni.ac.rs[2]; urosilic@elfak.rs[3]; vladislav.lazic@gmail.com[4]

Abstract—**Production forecast from solar power plants is a complex task, requiring sophisticated mathematical tools and accurate measurements of input parameters. However approximate models are sufficient for certain applications, such as the forecast of total hourly energy for needs of the electrical market. This paper shows new and contemporary methods for forecasting, such as implementation of machine learning. In this paper the next hour solar prediction is predicted on the basis of the reduced set of data, using standard multiple linear regression models. The method is illustrated on real solar power plant.**

Keywords – forecast, machine learning, PV, decision tree, power plant

I. INTRODUCTION

The renewable energy sources have been used more frequently across the world in recent years. One of the critical challenges in transition on renewable energy sources like solar energy, is an issue of variability and reliability for such energy resources [1-4].

Real problem also arises in energy economy and the variable nature of these resources requires big changes that will be able to cope with that. These changes are necessary for operators in power productions, utility companies and the most for independent service operators (ISOs), especially if is considered high market penetration rates. Even though that the solar energy is the most widespread available power resource, implementation is still difficult because of its sensitivity to weather conditions. That difficulties have a great impact on market prices because the process of production is not so likely predictable.

The variability directly affects both capital and operational costs, also contributing to lower capacity factors. Because of that, various algorithms are used at the ISOs to forecast solar production in the most accurate way possible. Forecasting the amount of energy produced by a PV plant is indispensable to allow an optimal integration. Any kind of accurate forecast gives a positive effect on energy markets. Short-term, intra-hour forecasts are relevant for dispatching, regulatory and load following purposes, but the intra-day (especially in 1–6 h ahead horizon) forecasts are critical for power system operators that handle multiple load zones, and trade outside of their territory. So, in order to characterize the viability of solar production in a given location, detailed variability and forecastability studies become imperative [5].

Like mentioned, deviations between forecast and actual energy affect both ISOs and market agents. The former has to readjust the operation of some power plants in the energy mix to offset such unexpected changes, while the latter face penalties derived from the readjustment. The precise way in which these situations are resolved is country and system-specific. There are a limited number of studies that address the economic implications of solar power forecast accuracy, which can be approached from two perspectives, grid operation and market bidding [6].

Market participants make their decisions based on those forecasts for relevant objects like wind and solar power. A misplanning leads automatically to either an oversupply or undersupply on the market. This will be adjusted by intraday or balancing markets. Thus, if there is oversupply at a certain hour we expect lower prices in the intraday market than in the day-ahead market. Obviously, for the undersupply the situation is vice versa [7].

There are many scientific papers in this area and different forecasting approaches have been used to achieve the desired goals. The traditional

ISBN: 978-86-80616-07-0

prediction of PV energy production is based on the classical approach of time series forecasting of solar energy and weather conditions, which are used to calculate the electrical energy of PV systems [1]. One of the methods of prediction that has been used recently very often, is the use of Machine Learning for these purposes [2-4]. In scientific papers that are using Machine Learning for prediction, a couple of algorithms stand out that have proven to be the most suitable. Most of the works use Artificial Neural Networks (ANN) [8-9] and Support Vector Machine [10-11], but some of them use other algorithms like Decision Tree [12-13]. Also, many papers clearly indicate large impact of production forecast on the market and the prices on the stock exchanges [6,7,14].

In this work, the 1-h averaged data for the PV power solar plant output collected for two years are used to develop and train forecasting model for predicting the power output 1 h-ahead of time, based on the information about previous hour. The goal is to develop machine learning regression algorithm which will perform fast and easy prediction for real needs market agents and ISOs. Here will not be considered the main weather factors, but are taken only effect of these weather conditions [5]. The main goal is to make an initial algorithm that will perform a fast and accurate enough prediction for an hour in advance. In essence, we apply forecasting model on operational data set to evaluate the performance of non-exogenous methodologies, thus creating a baseline for developing more sophisticated models.

II. Data Analysis

This work uses data collected from three photovoltaic solar power plants which are located in Romania. The time period spans two years period i.e. from January 2017 to December 2018. The data points collected from the power plant site correspond to the hourly average of power output. Although many work papers are dealing with weather characteristics like solar irradiance, cloud cover, wind speed, these are not considered in this study. The main objective is to assess performance of endogenous methodologies in the forecasting of the power output with no external weather influence on forecast model [5].

Our analysis consists of extracting data from three different PV systems and preparing train and test data which were used for training models and after testing that models.

The power output data set is plotted in Fig. 1. Here we can see annual trend of electricity production from solar panels for each of the power plants and for each year. It can be seen that the power plants are not of the same nominal power, which gives diversity of the data.

The gaps visible in Fig. 1 correspond to periods in which the power plant was not operating at full capacity due to malfunction or probably weather condition.

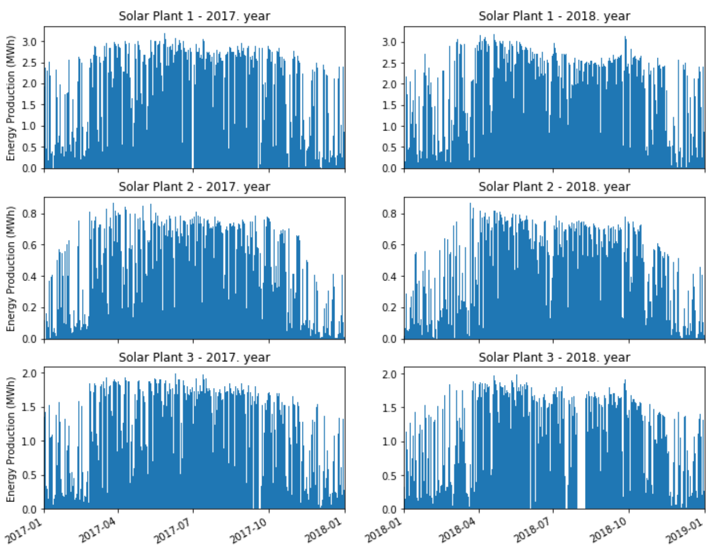

Figure 1. Energy Production data used for processing.

Fig. 2 shows us production of PV plant on daily basis for random tree days in June 2017 year for the same solar plant.

In this figure, it can be seen that some days have irregular curve of power production. The reason for this is most likely the weather conditions. Since we did not take in account the weather conditions, this model will show us accuracy in prediction these irregular curves of power production, although we do not observe the real reason for why this happens but only look at the consequences.

III. Training Prediction Model

For model training, machine learning algorithm is used with decision tree regression. The model of machine learning algorithm and preprocessing of data was developed in programming language Python 3.7.

In Regression Tree each node or leaf represents a numeric value. In our case we have three features based on which we are building an algorithm, so here, we are using multiple regression. When we talk about multiple regression, we are talking about large decision tree with large number of branches. Because of that it is very important for machine learning algorithm to manage that tree through its characteristics like depth of the tree, split samples of leaves etc. This is important to manage accuracy of the model and potential overfitting or underfitting. For these reasons, machine learning algorithm of decision tree was fine tuned for his hyperparameters.

A. *Data Preprocessing*

Before training any machine learning model, it is important to adjust gathered data for proper input in algorithm. It is important to determine the variables on which basis the regression algorithm can perform prediction. In this paper were used the main methods for data preprocessing like feature selection and normalization:

1) The *feature selection* was performed according to the principal of endogenous methodology, as mentioned in section II. The idea is to determine the prediction for the next hour of the day, based on the information about the hour before. Analyzing figures in section II, it was concluded that the main factor, in addition to the value of energy produced for the previous hour, is the date. Specifically, information about the time of the day and month in the year noticeably affects training algorithm.
2) To avoid dependence on the choice of measurement units and to make possible comparing selected features, it is necessary to do *normalization*. This involves transforming the data to fall within a smaller or common range [10].

Normally in a machine learning process, data was divided into training and test sets; the training set is then used to train the model and the test set is used to evaluate the performance of a model.

B. *Tuning Hyperparameters*

We'll still build our tree recursively, making splits on the data as we go, but we need a new method for determining the optimal split.

It often happens overfitting model to the data, which is often detrimental to the model's performance when is introduced to a new data. To prevent this overfitting, one thing that could be done is define some parameter which ends the recursive splitting process. As mentioned earlier, this may be a parameter such as *maximum tree depth* or *minimum number of samples (leaves)* required in a split. Controlling these model hyperparameters is the easiest way to counteract overfitting.

Also, it could be simply performed a significance test when considering a new split in the data, and if the split does not supply statistically significant information (obtained via a significance test), then any further splits will not be performed on a given node.

Fig. 3 shows us the behavior of one most important accuracy parameter of trained model in

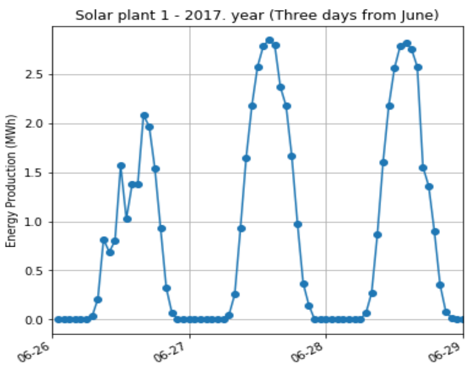

Figure 2. Data for the first solar plant 26.07.-29.07.2017.

relation to the main parameters of the algorithm. These parameters of decision tree algorithm are max depth and minimum samples leaf. Tuning hyperparameters is performed in the manner shown in the Fig. 3. Here it was observed accuracy (R-squared) of the trained model for each values of the mentioned parameters. This method led to the conclusion that the model with highest R-squared is one with decision tree which has max depth 10, and minimum samples leaf 16. We can see that this is branched tree with 10 conditions in depth and minimum 16 leaves on the last conditions.

C. Feature Importance

Feature importance is information that gives us a better picture of how production forecast comes to the seen results. By analyzing the trained decision tree model, we obtain the information shown in the following figure.

Fig. 4 shows us, how much each feature has an impact on the prediction process for default and for tuned decision tree algorithms. It is clear that the most important information is about the produced energy of hour before. The feature about time of the day, affects forecast relatively little, but still significantly for accuracy. The least important feature is about the month that has very little impact. Furthermore, here we can see that by tuning decision tree algorithm we reduced the impact of that feature. This is important information, which can be an indicator for some future research.

With such developed algorithm, various evaluation analyzes were applied to check accuracy and precision.

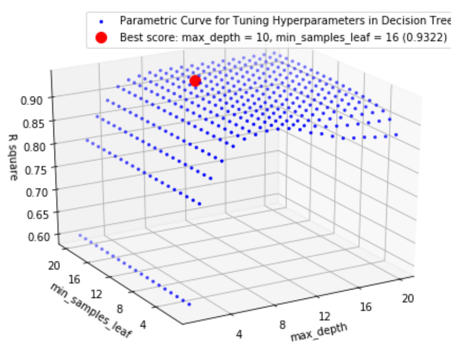

Figure 3. How accuracy of the algorithm depends on the two main parameters of decision tree.

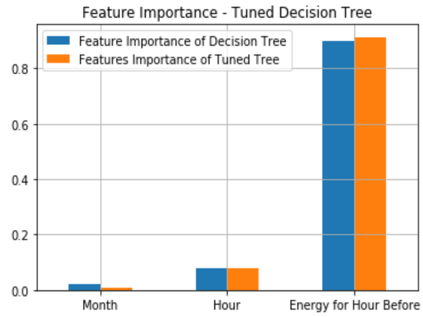

Figure 4. Feature importance for default and Tuned decision tree algorithms.

IV. Algorithm Evaluation

In this chapter, it is presented the evaluation of the trained model by applying the model to the test data i.e. data extracted from the entire data set before training. The chapter is practically divided into several parts. First is about accuracy metrics of the model, then applying cross-validation. After that we observe results of the trained model with proper visualization, while in the last part, the trained decision tree algorithm is compared with the Linear Regression and Support Vector Machine algorithm. Based on all this, a better analysis of the advantages and disadvantages of our algorithm is given.

A. Regression Accuracy Metrics

The predictive model's error rate can be evaluated by applying several accuracy metrics in machine learning and statistics. The basic concept of accuracy evaluation in regression analysis is that comparing the original target with the predicted one. The *MSE*, *MAE*, *RMSE*, and *R-Squared* are mainly used metrics to evaluate model performance in regression analysis [9-14].

1) *MAE* (Mean absolute error) represents the difference between the original and predicted values extracted by averaged the absolute difference over the data set. There is also *MAPE*, which represents percentage of *MAE*.

$$MAE = \frac{1}{N}\sum_{i=1}^{N}\left|y_i - \hat{y}\right| . \qquad (1)$$

2) *MSE* (Mean Squared Error) represents the difference between the original and predicted values extracted by squared the average difference over the data set:

$$MSE = \frac{1}{N}\sum_{i=1}^{N}\left(y_i - \hat{y}\right)^2 \ . \qquad (2)$$

3) *RMSE* (Root Mean Squared Error) is the error rate by the square root of MSE:

$$RMSE = \sqrt{MSE} \ . \qquad (3)$$

4) *R-squared* (Coefficient of determination) represents the coefficient of how well the values fit compared to the original values. The value from 0 to 1 interpreted as percentages. The higher the value is, the better the model is:

$$R^2 = 1 - \frac{\sum_{i=1}^{N}\left(y_i - \hat{y}\right)^2}{\sum_{i=1}^{N}\left(y_i - \bar{y}\right)^2} \ , \qquad (4)$$

where $\hat{y}$ is predicted value of y, $\bar{y}$ is mean value of y and the N is the total number of samples.

Calculating these evaluation parameters, we obtained the results for our trained model (Tuned Decision Tree) (Table I).

B. *Cross-validation*

To validate the stability of the machine learning model, cross-validation was done. Validation ensures that the model picks up the right (relevant) patterns from the dataset. Essentially, the goal of validation techniques is to make sure machine learning models have a low bias-variance factor.

Like solution for checking if overfitting or underfitting occurs, five-folds cross-validation was done. In Fig. 5 we can see results of every fold individually. It can also be seen that there are no unexpected jumps for *R-squared* from the range smaller than *0.91*. This gives us a picture of the suitability of the algorithm in terms bias and variance of data.

TABLE I. EVALUATION RESULTS

Parameters	**Tuned DT**
MAE	0.0267567
MSE	0.0038582
RMSE	0.0621144
R-squared	0.92362

C. *Results of Test Data*

Then we applied our trained algorithm to the test data. In the next pictures will be shown some days predicted by hour and error rates.

In Fig. 6, it is shown comparison of actual and predicted data of some random medium sunny August day, with green line marked error rate. Here can be noticed that error rate of prediction for every sample of that day is relatively low, even within a 5 percent margin.

In Fig. 7, the same thing is shown, but for some random May day. This is a depiction of

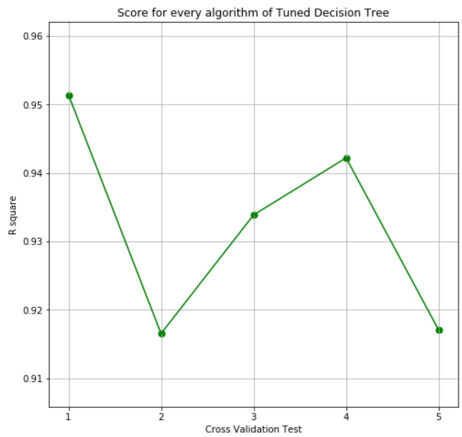

Figure 5. Cross-validation of tuned decision tree model.

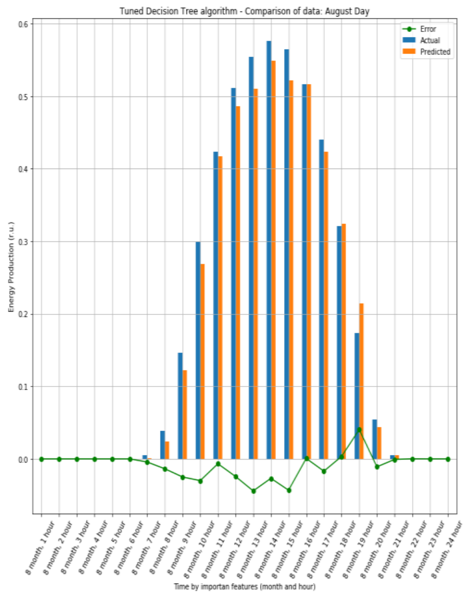

Figure 6. Forecast of production for one August day.

very sunny day. We can also see here, that the error rate is low with exception of one hour.

In Fig. 8, we can see something different. This is an example of some very cloudy February day. Here can be noticed that production forecast didn't do so accurately prediction. This is to be expected because actual value of data falls below the actual margin of error.

Essentially, prediction for sunny days is relatively good and accurate, also and for less sunny days. There are real problems that happens with predictions of cloudy days. The error in such cases is large in relation to the produced power, but the positive thing is that in such cases the error in relation to the nominal power is not so large. But this is certainly something to be dealt with in future works.

D. Comparison of Algorithms

From the collected data, in addition to tuned decision tree, two more regression models were developed. Those were Linear Regression (LR) and Support Vector Machine (SVM). They were developed in order to compare and analyze accuracy of all three algorithms.

Fig. 9 presents the forecasting results of three different models. From this comparison, it can be seen that the performance of the proposed method with Tuned Decision Tree (TDT) is superior to the two others, with LR or SVM. Both LR and SVM have shown a tendency to have large errors in the hours of the day when there is no production.

In summary, the determined accuracy metrics of all tree models is shown in Table II.

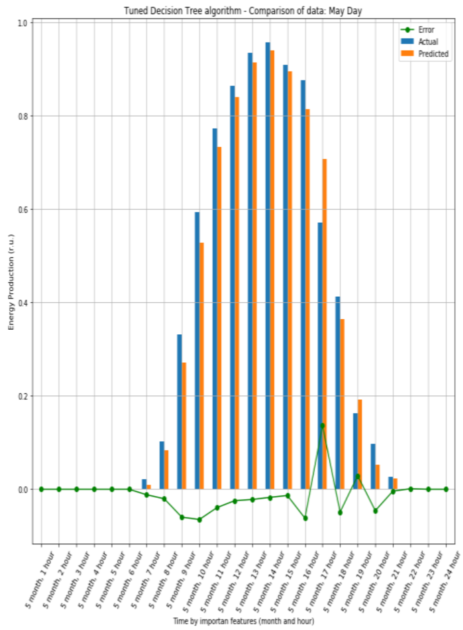

Figure 7. Forecast of production for one May day.

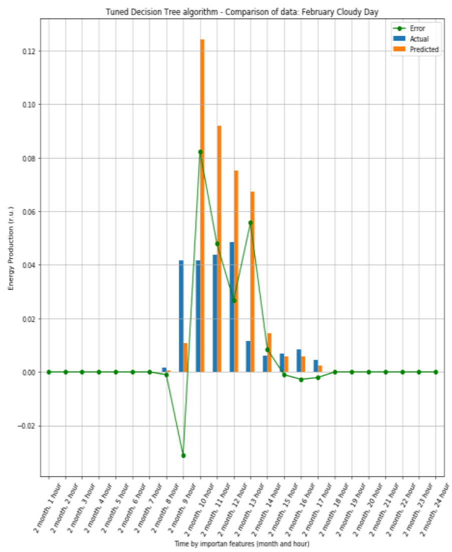

Figure 8. Forecast of production for one very cloudy February day.

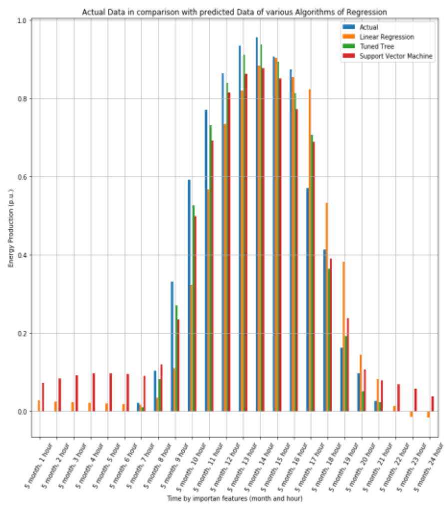

Figure 9. Forecast of production for three different algorithms of one May day.

TABLE II. COMPARISON OF ACCURACY MATRICS

Param.	LR	SVM	TDT
MAE	0.0503	0.0722	***0.0267***
MSE	0.0073	0.0055	***0.0038***
RMSE	0.0854	0.0853	***0.0621***
R-sq.	0.8556	0.8560	***0.9236***

It can be concluded that the tuned decision tree model proved to be better in all metric parameters.

V. CONCLUSION

In this study, the feasibility of utilizing decision tree method regression to predict the hourly output from a PV system was evaluated. For this purpose, a PV solar plants installed in Romania was used as a case study. The present method for solar power forecasting has been developed from scratch and the capability of tuned decision tree model for predicting the PV production has been verified with a better prediction accuracy of the other models. To appraise the model's prediction performance, accuracy metrics such as *MAE*, *MSE*, *RMSE* and *R-squared* were used. The paper also proposed using decision tree methods to provide insight into the analysis of the importance of each input feature. The presented analysis will allow researchers and industry practitioners to gain better understanding of developed forecast. The developed machine learning models can be applied to predict one-hour-ahead PV power generation based on endogenous parameters like date time information and previous hour values of photovoltaic power output. No exogenous data such as solar irradiance telemetry was used in the forecasting models, which essentially means that the solar panels themselves are the only "sensors" used to generate input data in this work. The models are developed for stand-alone PV system; however, they could be used to predict PV power output in grid-connected systems. Primarily, the purpose of the work is ability to quickly and easily predict an hour ahead for the needs of the market and market agents.

Future studies will also focus on assessing the performance of machine learning methods in other time-scales and for different types of features. Traditionally, solar power forecast accuracy is expressed in terms of classic metrics, and it is widely accepted that a smaller error is always better. Nevertheless, this does not always hold when actual market conditions are considered. Deviations between scheduled and actual production result in penalties that apply to market agents who participate in the imbalance electric system. Thus, to completely understand model performance, market conditions must be taken into account.

ACKNOWLEDGMENT

This work was supported by Ministry of Science and Technological Development, Republic of Serbia (Project number: III 44006).

REFERENCES

[1] Bacher, P., Madsen, H., & Nielsen, H. A. (2009). Online short-term solar power forecasting. *Solar energy*, *83*(10), 1772-1783.

[2] Li, Z., Rahman, S. M., Vega, R., & Dong, B. (2016). A hierarchical approach using machine learning methods in solar photovoltaic energy production forecasting. *Energies, 9*(1), 55.

[3] Mellit, A. (2008). Artificial Intelligence technique for modelling and forecasting of solar radiation data: a review. *International Journal of Artificial intelligence and soft computing, 1*(1), 52-76.

[4] Sharma, N., Sharma, P., Irwin, D., & Shenoy, P. (2011, October). Predicting solar generation from weather forecasts using machine learning. In *2011 IEEE international conference on smart grid communications (SmartGridComm)* (pp. 528-533). IEEE.

[5] Pedro, H. T., & Coimbra, C. F. (2012). Assessment of forecasting techniques for solar power production with no exogenous inputs. *Solar Energy, 86*(7), 2017-2028.

[6] Antonanzas, J., Pozo-Vázquez, D., Fernandez-Jimenez, L. A., & Martinez-de-Pison, F. J. (2017). The value of day-ahead forecasting for photovoltaics in the Spanish electricity market. *Solar Energy, 158*, 140-146.

[7] Ziel, F. (2017, June). Modeling the impact of wind and solar power forecasting errors on intraday electricity prices. In *2017 14th International Conference on the European Energy Market (EEM)* (pp. 1-5). IEEE.

[8] Dumitru, C. D., Gligor, A., & Enachescu, C. (2016). Solar photovoltaic energy production forecast using neural networks. *Procedia Technology, 22,* 808-815.

[9] Chen, C., Duan, S., Cai, T., & Liu, B. (2011). Online 24-h solar power forecasting based on weather type classification using artificial neural network. *Solar energy, 85(*11), 2856-2870.

[10] De Leone, R., Pietrini, M., & Giovannelli, A. (2015). Photovoltaic energy production forecast using support vector regression. *Neural Computing and Applications, 26(*8), 1955-1962.

[11] da Silva Fonseca, J. G., Oozeki, T., Takashima, T., Koshimizu, G., Uchida, Y., & Ogimoto, K. (2011, June). Photovoltaic power production forecasts with support vector regression: A study on the forecast horizon. In *2011 37th IEEE photovoltaic specialists conference* (pp. 002579-002583). IEEE.

[12] Wang, J., Li, P., Ran, R., Che, Y., & Zhou, Y. (2018). A short-term photovoltaic power prediction model based on the gradient boost decision tree. *Applied Sciences, 8*(5), 689.

[13] Ahmad, M. W., Reynolds, J., & Rezgui, Y. (2018). Predictive modelling for solar thermal energy systems: A comparison of support vector regression, random forest, extra trees and regression trees. *Journal of cleaner production, 203*, 810-821.

[14] Kaur, A., Nonnenmacher, L., Pedro, H. T., & Coimbra, C. F. (2016). Benefits of solar forecasting for energy imbalance markets. *Renewable energy, 86,* 819-830.

The Utilization of Waste Materials from Biofuel Production by Lactic Acid Bacteria Isolated from Traditional Milk Products

Jovan Ćirić[1,2], Nataša Joković[3], Nikola Stanković[3], Marko Živković[2], Đorđe Lazarević[2]

[1]Faculty of Technology, University of Niš, Leskovac, Serbia, joca.ciric@gmail.com
[2]Faculty of Electronic Engineering, University of Niš, Niš, Serbia
[3]Faculty of Sciences and Mathematics, University of Niš, Niš, Serbia

Abstract—**The production of ecological renewable fuel is a topic that attracts the attention of a large number of researches in the last few decades. Biodiesel is one of the most studied. Also, a lot of researches are focused on the use of waste glycerol as a by-product in biodiesel production. It was confirmed that waste glycerol can be a valuable raw material for the production of valuable products, even microbial metabolites. The majority of lactic acid bacteria members can assimilate glycerol and produce lactic acid by using it. There is published research about the conversion of waste glycerol to lactic acid and some of them confirmed that certain strains of *Enterococcus faecalis* can produce lactic acid on waste glycerol media. The results of studying the possibility of microbial conversion of waste glycerol as a by-product obtained in biodiesel production, by lactic acid bacteria isolated from traditional milk products, to produce lactic acid as a valuable product are presented in this paper.**

Keywords – biodiesel, waste glycerol, Enterococcus faecalis

I. INTRODUCTION

The use of alternative energy sources is becoming more and more important because of well-known facts that fossil fuel reserves are not limitless, whereby their use provokes the emission of harmful gases whose accumulation leads to environmental contamination and global warming [1]. Biodiesel is one of the most popular and most studied alternative fuels. During the production of biodiesel from a different kind of raw material (vegetable oil, waste oils, animal fat, algal oil), glycerol is generated as a by-product [2]. Approximately, waste glycerol represents 10 % of the starting compounds for biodiesel production [3]. While the biodiesel production exponentially increased in the recent years, the amounts of waste glycerol also increased which caused a rapid decrease of its price, 0.27-0.41 USD/kg for the pharmaceutical grade (99.9 %) and 0.09– 0.20 USD/kg for the technical grade (80 %) [2]. It is expected that the global production of waste glycerol in 2020 will be 41.9 billion kilograms [4]. Consequently, economic valorization and efficient waste glycerol management are exceptionally important for the sustainability of commercial biodiesel production. It resorts to the production of value-added products and, in this way, waste glycerol will be considered as a desirable by-product, not as a waste product with a disposal cost.

Waste glycerol obtained in biodiesel production is impure and, except glycerol, it usually contains a lot of impurities such as water, methanol, soaps, catalysts, salts and non-glycerol organic matter (free fatty acids). For further use, it is necessary to purify it but the conventional purification techniques are sometimes complicated and very expensive thus, the valorization of waste glycerol as obtained has become very important [2]. Microbial conversion and application of waste glycerol in industrial fermentations is a very popular way of

ISBN: 978-86-80616-07-0

use in recent years and it can become one of the cheapest natural substrates with great potential.

A lot of microorganisms can assimilate and convert glycerol into valuable products such as organic acids, alcohols, polymers, polysaccharides and antibiotics [5-7]. Also, much research confirmed that various strains of lactic acid bacteria can successfully convert glycerol to lactic acid [8-10]. Some strains of lactic acid bacteria *Enterococcus faecalis* can produce lactic acid on media with pure and waste glycerol obtained in biodiesel production [8-12]. Some researches confirmed that the metabolically-engineered *E. faecalis* can efficiently convert waste glycerol to lactic acid [9-10].

II. EXPERIMENTAL

In this study, strain *Enterococcus faecalis* MK3-10A was used in performed fermentations. The studied strain was isolated from fermented milk spread (kaymak) [13,14].

E. faecalis MK3-10A were cultivated in 300 ml of MRS (de Man, Rogosa, Sharpe) broth without carbon source (10 g/l peptone; 10 g/l meat extract; 5 g/l yeast extract; 2 g/l K_2HPO_4; 5 g/l CH_3COONa; 2.5 g/l $MgSO_4$ x 7 H_2O; 0.2 g/l $MnSO_4$ x 7 H_2O; pH 6.4). Pure glycerol (Sigma Aldrich) and waste glycerol were added afterward (15 g/l). Waste glycerol from sunflower oil and rapeseed oil-based biodiesel production was obtained in the Laboratory for Chemical engineering of Faculty of Technology in Leskovac, University of Niš. Therefore, in this study are used MRS medium with pure glycerol as a carbon source (PG medium) and media with waste glycerol obtained in sunflower oil-based biodiesel production (SfOG medium) and rapeseed oil-based biodiesel production (RsOG medium).

Under the aseptic conditions, liquid samples (10 ml) were sampled after every 2 h of fermentation. Microbial growth was measured spectrophotometrically (λ = 620 nm, Cole Parmer 2100 UV/VIS spectrophotometer) [11]. The concentrations of glycerol and produced lactic acid were determined using an HPLC method (Agilent 1100 Series chromatograph, Aminex HPX-87H column).

All experiments were performed in triplicate. Results for microbial growth, glycerol consumption, and product concentration were used for calculation of consumption rate glycerol Δ_{glyc} (mg/ml/d) and production rate yield of lactic acid $Y_{P/S}^{LA}$ (mg/ml/d) [15] and the percentile of consumption was calculated in the relation between the decrease of carbon source with the starting concentration.

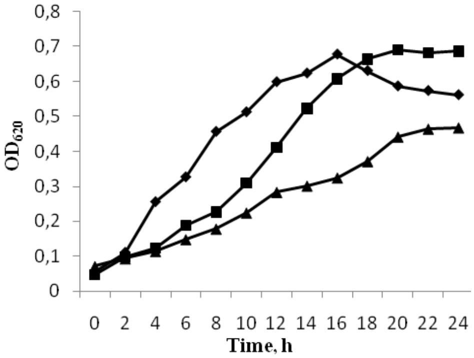

Figure 1. Changes of the optical density (biomass) during the fermentation of *E. faecalis* MK3-10A in the PG (♦) SfOG (■) and RsOG medium (▲)

III. RESULTS AND DISCUSSION

The results of the study of utilization of waste glycerol obtained in biodiesel production by lactic acid bacteria *E. faecalis* MK3-10A are shown in Table I and Figs. 1-3.

It was noticed that *E. faecalis* MK3-10A showed relatively good and constant growth on glycerol media with pure glycerol and SfOG media, while on the RsOG medium microbial growth was a bit different, it was weaker (Fig. 1). The maximum biomass growth was achieved on the SfOG medium (OD_{620}^{max}=0.642) and the slightly lower on the PG medium (OD_{620}^{max} =0.622). On PG medium the sustained growth (lag phase) was noticed in the first 2 h of fermentation and other media, it was noticed in

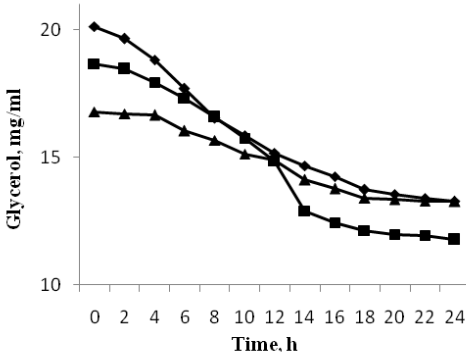

Figure 2. Changes of the concentrations of glycerol during the fermentation of *E. faecalis* MK3-10A in the PG (♦) SfOG (■) and RsOG medium (▲).

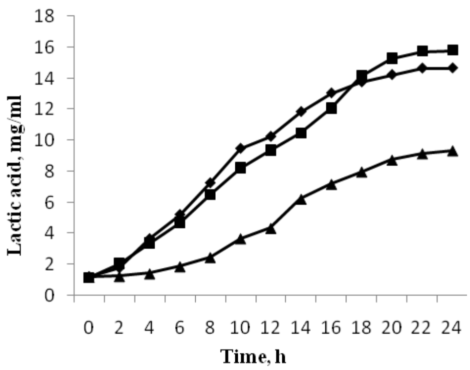

Figure 3. Changes of the lactic acid concentrations during the fermentation of *E. faecalis* MK3-10A in the PG (♦) SfOG (■) and RsOG medium (▲)

the first 4 h of fermentation. This was followed by an exponential growth phase which lasts up to 16 h (PG medium), 20 h (SfOG medium) and 22 h (RsOG medium).

The increase in biomass resulted in the decrease (consumption) of glycerol (Fig. 2). The highest glycerol consumption rate of 6.96 mg/ml/day was achieved during the fermentation process on the SfOG medium while 37 % of the total available amount of glycerol was consumed (Table I). Compared to the PG medium, where 34% of glycerol was consumed, glycerol consumption rate on SfOG medium was 7% higher. During the fermentation of RsOG medium, the achieved consumption of 21% was the lower (3.60 mg/ml/day) similar to it was the case with microbial growth. In all three fermentation media, the concentration of glycerol decreased constantly until the 16 h of fermentation (Fig. 2). It can be concluded that the growth of *E. faecalis* MK3-10A was the effect of glycerol consumption as the sole carbon source.

Lactic acid production followed the microbial growth and glycerol consumption (Fig. 3) which is under the definition of primary metabolism and production of primary metabolites [16]. In all studied media it can be noticed that lactic acid concentration increased until 20 h of fermentation. The maximum lactic acid concentration (15.78 mg/ml) and production rate yield (14.64 mg/ml/day) was obtained on SfOG medium (Table I) which was 8% and 9% higher than was obtained on PG medium. Same as it were cases with growth and glycerol consumption, the lowest lactic acid concentration and production rate yield were obtained on RsOG medium (9.34 mg/ml and 8.16 mg/ml/day, respectively). This can be explained by the harmful and inhibitory effects of impurities contained in waste glycerol from rapeseed oil-based biodiesel production.

The lactic acid bacteria *E.faecalis* MK3-10A did not use all available amounts of glycerol. The production of lactic acid inhibited bacterial growth and it is known that lactic acid in a concentration higher than 1-2% can inhibit further microbial growth [16-18].

There are no published results about the production of lactic acid by growing lactic acid bacteria on waste glycerol obtained in sunflower and rapeseed oil-based biodiesel production so it was difficult to make a comparison. There are some published study results of bioconversion soybean waste glycerol to lactic acid [8,12, 19,20] but not by *E. faecalis*. For example, *R. oryzae* NRRL 395 produced 48 mg/ml of lactic acid (3.7 g/g glycerol) and reached the 0.7 g/g glycerol of biomass on medium with waste glycerol obtained in soybean oil-based biodiesel production with the starting concentration of

TABLE I. THE EFFECT OF PURE AND WASTE GLYCEROL ON THE MICROBIAL GROWTH (ΔOD_{620}^{MAX}), THE CONSUMPTION RATE OF GLYCEROL (Δ_{GLYC}), AND THE RELATIVE CONSUMPTION CARBON SOURCES (%), AS WELL AS THE ACHIEVED MAXIMUM LACTIC ACID CONCENTRATION (C_{MAX}^{LA}) AND PRODUCTION RATE YIELD ($Y_{P/S}^{LA}$)

Characteristics of bioprocess								
Carbon source (Glycerol)	(ΔOD_{620}^{max})		Δ_{glic}			C_{max}^{LA}		$Y_{P/S}^{MK}$
	-		(mg/ml/day)		(%)	mg/ml		(mg/ml/day)
PG	0.622	±0,021	6.48	±0,33	34	14.65	±0,43	13.44
SfOG	0.642	±0,026	6.96	±0,24	37	15.78	±0,51	14.64
RsOG	0.396	±0,017	3.60	±0,36	21	9.34	±0,11	8.16

PG - Pure glycerol
SfOG -Waste glycerol obtained in sunflower oil-based biodiesel production.
RsOG -Waste glycerol obtained in rapeseed oil-based biodiesel production.

75 g/l [12]. It was reported that *E. coli* AC-521 isolated strain showed good productivity of lactic acid (85.8 g/L and a molar yield of 0.90) by using soybean waste glycerol [19]. Also, *E. coli* LA20 engineered strain produced 56 g/L of L-lactate by using waste glycerol [20].

IV. Conclusions

In this performed fermentations, the strain *E. faecalis* MK3-10A showed the best growth and lactic acid production (15.78 mg/ml or 14.64 mg/ml/day, respectively) on media containing glycerol obtained in sunflower oil-based biodiesel production. Therefore, this waste glycerol has a great potential as a low price carbon source for the further research of lactic acid production on the laboratory and semi-industrial level.

In general, this could be a very perspective possibility of microbiological treatment of waste material that obtained in the production of green fuels.

Acknowledgment

This work has been funded by the Ministry of Education, Science and Technological Development of the Republic of Serbia (Projects III 45001 and III 44006).

References

[1] Danilović, B., Avramović, J., Ćirić, J., Savić, D., & Veljković, V. (2014). Production of biodiesel from microalgae. *Chem. Ind., 68*(2), 213-232.

[2] Konstantinović, S. S., Danilović, B. R., Ćirić, J. T., Ilić, S. B., Savić, D. S., & Veljković, V. B. (2016). Valorization of crude glycerol from biodiesel production. Chemical Industry and *Chemical Engineering Quarterly, 22*(4), 461-489.

[3] Hu, S., Luo, X., Wan, C., & Li, Y. (2012). Characterization of crude glycerol from biodiesel plants. *Journal of agricultural and food chemistry, 60*(23), 5915-5921.

[4] Nanda, M. R., Yuan, Z., Qin, W., Ghaziaskar, H. S., Poirier, M. A., & Xu, C. C. (2014). Thermodynamic and kinetic studies of a catalytic process to convert glycerol into solketal as an oxygenated fuel additive. *Fuel, 117,* 470-477.

[5] Garlapati, V. K., Shankar, U., & Budhiraja, A. (2016). Bioconversion technologies of crude glycerol to value added industrial products. *Biotechnology Reports, 9,* 9-14.

[6] Wilkens, E., Ringel, A. K., Hortig, D., Willke, T., & Vorlop, K. D. (2012). High-level production of 1, 3-propanediol from crude glycerol by Clostridium butyricum AKR102a. *Applied microbiology and biotechnology, 93*(3), 1057-1063.

[7] Ćirić, J. T., Konstantinović, S. S., Ilić, S. B., Gojgić-Cvijović, G., Savic, D. S., & Veljković, V. B. (2016). The impact of isatin derivatives on antibiotic production by Streptomyces hygroscopicus CH-7. *Chem. Ind., 70*(2), 123-128.

[8] Choubisa, B., Patel, H., Patel, M., & Dholakiya, B. (2012). Microbial production of lactic acid by using crude glycerol from biodiesel. *J. Microbiol. Biotech. Res, 2*(1), 90-93.

[9] Doi, Y. (2015). L-lactate production from biodiesel-derived crude glycerol by metabolically engineered Enterococcus faecalis: cytotoxic evaluation of biodiesel waste and development of a glycerol-inducible gene expression system. *Applied and Environmental Microbiology, 81*(6), 2082-2089.

[10] Murakami, N., Oba, M., Iwamoto, M., Tashiro, Y., Noguchi, T., Bonkohara, K., Abdel-Rahman, M.A., Zendo, T., Shimoda, M., Sakai, K., & Sonomoto, K. (2016). L-Lactic acid production from glycerol coupled with acetic acid metabolism by Enterococcus faecalis without carbon loss. *Journal of bioscience and bioengineering, 121*(1), 89-95.

[11] Ćirić, J., Joković, N., Ilić, S., Konstantinović, S., Savić, D., & Veljković, V. (2020). Production of lactic acid by Enterococcus faecalis on waste glycerol from biodiesel production. *Chemical Industry and Chemical Engineering Quarterly, 26*(2), 151-156.

[12] Vodnar, D. C., Dulf, F. V., Pop, O. L., & Socaciu, C. (2013). L (+)-lactic acid production by pellet-form Rhizopus oryzae NRRL 395 on biodiesel crude glycerol. *Microbial cell factories, 12*(1), 1-9.

[13] Joković, N. (2010). Doctoral dissertation, Faculty of Biology, University of Belgrade, Belgrade, Serbia (in Serbian).

[14] Jokovic, N., Nikolic, M., Begovic, J., Jovcic, B., Savic, D., & Topisirovic, L. (2008). A survey of the lactic acid bacteria isolated from Serbian artisanal dairy product kajmak. *International journal of food microbiology, 127*(3), 305-311.

[15] Nielsen, J., Villadsen, J., & Liden, G. (2003). *Bioreaction engineering principles*. New York: Kluwer Academic/Plenum Publishers.

[16] Gopal, P. K. (2003). *Encyclopedia of Dairy Sciences*, Vol. 3; Lactobacillus spp. *Lactobacillus acidophilus*, (pp.1484-1488.).

[17] Cenci, G., Rossi, J., Trotta, F., & Caldini, G. (2002). Lactic acid bacteria isolated from dairy products inhibit genotoxic effect of 4-nitroquinoline-1-oxide in SOS-chromotest. *Systematic and applied microbiology, 25*(4), 483-490.

[18] Gilliland, S. E. (2003). Probiotics. In *Encyclopedia of Food Science and Nutrition, 8ed,* Elsevier. London.

[19] Mazumdar, S., Blankschien, M. D., Clomburg, J. M., & Gonzalez, R. (2013). Efficient synthesis of L-lactic acid from glycerol by metabolically engineered Escherichia coli. *Microbial cell factories, 12*(1), 1-11.

[20] Hong, A. A., Cheng, K. K., Peng, F., Zhou, S., Sun, Y., Liu, C. M., & Liu, D. H. (2009). Strain isolation and optimization of process parameters for bioconversion of glycerol to lactic acid. *Journal of Chemical Technology & Biotechnology, 84*(10), 1576-1581.

Influence of Charges on the Price of Electricity - The Case of a Public Company “Elektroprivreda BiH” Sarajevo

Enver Agić[1], Suad Halilčević[2], Bakir Agić[3]

[1]University of Business Engineering and Management, 78000 Banja Luka, Bosnia and Herzegovina, enveragic99@gmail.com

[2,3]Faculty of Electrical Engineering, University of Tuzla, 75000 Tuzla, Bosnia and Herzegovina, suad.halilcevic@untz.ba[2]; bakir.agic@outlook.com[3]

Abstract—**This paper gives an overview of the impact of charges on the price of electricity in the public company “Elektroprivreda Bosne i Hercegovine”d.d. Sarajevo (JP EPBiH). The introductory part gives an overview of the fees that have been introduced recently by various levels of government in the Federation of Bosnia and Herzegovina and of course amounts to all these fees. It is particularly indicative that in the course of time, more and more fees are present that this company must cover its business, those that are not "recognized" through the tariff procedure. The open market certainly works towards the efficient operation of this company, because the cost-reduction, more efficient operation of the plant, the survival of the market is questioned in the future.**

Keywords – electricity, price of electricity, fees, influence of fees on the price, tariff procedure

I. Introduction

The subject of this research are fees introduced after 01/07/2011, considering that FERK tariff rates that started applying from listed date which were determined during the third tariff procedure.

Through the third tariff procedure the expenses of fees which were loading the operating costs were recognized, which is consistent with methodology that FERK uses for determination of the tariff rates and prices where FERK is in charge. The recognition of the expenses of fees is done in the tariff procedures or in the procedure of determination of price of purchasing electricity from a public supplier [1].

The fees which were introduced after 01/07/2011, as well as existing fees which were edited on some way, that have impact on the financial result of this organization, the price of electricity:

- Pollution charge - federal level
- Canton charge - special effect on HNK
- Forest use fee - canton charge
- Fee for setup of underground and over ground network and road use fee
- Other.

II. Pollution Charge

Pollution charge is paid in accordance with the environmental protection law of Federation of Bosnia and Herzegovina (FBiH) from 2003 that was edited and supplemented in 2010. Billing and payment of pollution charge started with “Regulation on types of charges for air pollutants”, by which the obligation of payment of pollution charge in TPP Kakanj and TPP Tuzla was introduced [1].

The regulation was introduced by Government of FBiH in October 2011, having in mind the capacities and planned volume of production in TPP Tuzla and TPP Kakanj in next couple of years and previous achievement in 2013, it is for certain that the yearly expenses are approximately going to be around 5.5 and 6.5 million KM (1€=1.95KM), using current regulation and depending on volume of production in blocks and TPPs, the coal quality, technology, etc.

In time of implementation of the third tariff procedure, the Regulation on types of charges for air pollutants was not existing, so the recognition on the basis of fee has not been requested by JP EPBiH, and this expense has not been calculated in tariff rates.

At the end of 2012, FERK determined the purchase price of electricity from public supplier JP EPBiH for qualified buyers on 110 kV and 35 kV voltage. During the determination of the price, FERK recognized part of new expenses to JP EPBiH incurred by payment of the pollution charge, so the pollution fee of 0.7 million KM was recognized.

III. Canton Charge – Special Effect on HNK

Assembly of the Herzegovina - Neretva Canton adopted the law on waters of Canton in session on 28/06/2013. The canton fee which is of special impact for this canton, especially for subjects that use the general goods without paying the concession fee and that also perform activities on territory of HNK, was introduced by this law [1].

With normal hydrology (70% of inflow probability), i.e., yearly production in HPP on Neretva river of approximately 1400 GWh would cost JP EPBiH around 7 million KM every year, while for the second semester of 2013 the cost was 2.85 million KM. This would directly hit the business result of JP EPBiH.

JP EPBiH is not billing and paying the fee that is introduced by this law, because it considers that the costs are unjustifiably increasing on the basis on the use of hydro-accumulation objects.

From the stated reasons, JP EPBiH referred to relevant institutions (Legislative - legal commission of the FBiH Parlament government office for legislation and compliance with European Union regulations, etc.) to dispute the obligation of paying the fee. Also, JP EPBiH sent the constitutional review initiative of the law on waters of Herzegovina - Neretva Canton to the Federal Ministry of Energy, Mining and Industry.

At the end of October 2013, the Government of Federation of Bosnia and Herzegovina adopted the information about introduction of this fee and came to a conclusion in which it is recommended to coordinate the given law with federal law to the Government of Herzegovina - Neretva Canton. The prime minister of the Government of FBiH was authorized to start the procedure at Constitutional Court FBiH, in order to assess the constitutionality of the decision of 74th clause of the Cantonal law on waters, if in 30 days the Government of HNK Canton don't accept the recommendation. Because of the political order of BiH, this is not yet done!

IV. Forest Use Fee – Canton Charge

According to the decisions of the FBiH Constitutional Court, which repealed the FBiH law on forests and the decree of the FBiH government, the obligation to pay 0.7 percent of the total annual income of the EPBiH in the name of compensation for the use of public forest functions ceased [1].

After federal regulations were repealed, a large number of cantons adopted cantonal regulations, which introduced the fees for forests of the same or similar name.

These are new regulations, where the introduced fees will reflect on the costs and financial result of JP EPBiH, the annual cost for 2013 was 300k - 350k KM.

V. Fee for Setup of Underground and Overground Network

Lately, all electricity distribution branches have had the problem of determining fees for the use of construction land for the installation of underground and over ground electricity networks and utility fees by municipalities in enormously high amounts.

Since the above may significantly affect the business results of JP EPBiH, a number of legally permitted actions have been taken in order to challenge the acts on the basis of which these fees are determined, as well as the amount of these fees, determined by individual decisions.

Fees that have been determined so far and that are paid or disputed by some of the legally permitted procedures, do not have a significant impact on the business of JP EPBiH [1].

However, if all local communities, on whose territory JP EPBiH performs distribution activity and has its own network, introduce this type of fee, it is estimated that the total amount of fees would be 50 million KM.

A very broad interpretation of the term public area by local communities also contributes to this assessment.

VI. Road Use Fee

JP EPBiH allocates significant funds for land use in the road belt. To consider this issue, it is important that on 05.09.2013. The Law on Electricity in the FBiH ("Official Gazette of the FBiH", No. 66/13) came into force, which stipulates in Article 73, paragraph 3 that "an electric power entity performing its activity as a public service has the right to place its installations in public areas as well as in the road zone of road infrastructure free of charge in accordance with technical and other regulations with the obligation to obtain the consent of the institutions responsible for the management of public areas” [1].

According to the mentioned legal provision, JP EPBiH as a company that performs electricity distribution as a public service is not obliged to pay fees in case of installation in public areas and in the road zone, but only to obtain the consent of the competent institutions for their installation.

Pursuant to the aforementioned provision of the Law, JP EPBiH disputes the payment of fees in case of installation in public areas and in the road zone, but this dispute results in non-issuance of consent of competent authorities and inability to build electricity plants necessary for electricity distribution and supply.

In order to avoid additional obligations, JP EPBiH sent an initiative to the relevant ministry for authentic interpretation of the relevant provision of the Law on Electricity in FBiH.

An initiative for the adjustment of regulations in FBiH is being prepared, taking into account the fact that the Law on Electricity in FBiH, the Law on Roads of the Federation of BiH and the Law on Principles of Local Self-Government of FBiH are not adjusted when it comes to paying fees.

VII. Other Fees

In addition to the aforementioned fees, which were recently introduced, JP EPBiH pays other fees, where several types of water management fees are especially emphasized, which with the normal hydrological situation are up to 18.1 million KM per year, then liabilities for employee benefits, which are up to over 61 million KM. annually.

At the same time, increasing costs and liabilities arise due to the introduction of fees that are the responsibility of local levels of government (city and municipality).

The fee for water protection in TPP Tuzla was increased in 2012 from 1108.75 thousand KM to 1586.26 thousand KM. This represents an increase in the cost of compensation from 477.5 thousand KM, which is not included in the existing tariffs, nor in the price of the service of the public supplier JP EPBiH [2].

VIII. Conclusion

After the end of the 3rd tariff procedure, regulations were adopted which introduced new types of fees and which have a significant impact on the operating costs of JP EPBiH. The burden of new fees can be estimated in the coming years at 13-14 million KM of costs per year, with the amount that in practice will depend primarily on the volume and structure of production in hydropower and thermal power plants.

TABLE I. Fees in million KM*.

Fees	Recognized in the price of electricity	Paid, not recognized in the price of electricity	Disputed, not paid and not in tariff
Pollution charge	0.70	6.50	
Water management fees and water protection fees	18.10	0.50	2.90
Other fees (utilities, road belt, employee payroll taxes)	62.00		50

*1€ = 1.95 KM

Apart from a part (10-15%) of the costs of the air pollution fee, these fees are not recognized through the prices of electricity at the expense of the tariff and qualified customers of JP EPBiH.

The above estimate does not include cantonal fees for the installation of overhead and underground networks and fees for the use of the road belt, which are estimated at 50 million KM.

JP EPBiH regularly calculates and settles fees that are not disputable, and it is the amount of 7 million KM at the annual level.

Other liabilities are disputed and depending on the outcome of proceedings and disputes could be charged to operating costs and financial results of JP EPBiH in the coming period. Fees that are recognized through the tariff procedure, fees that are not recognized in the tariff procedure, and are paid because they are disputable and fees that are not recognized in the tariff procedure and are disputable, are given in the Table I.

REFERENCES

[1] Materials from the work of the Supervisory Board Public company "Elektroprivreda BiH" d.d. Sarajevo (2013). 33 Sessions, "Information on the impact of fees of all levels of government on the business of JP "Elektroprivreda BiH" d.d. Sarajevo", 19.12.2013. (pp. 1-4).

[2] Public company "Elektroprivreda BiH" d.d. Sarajevo. (2013). Three-year business plan, 2011-2014. (p. 278).

The Influence of Solar Radiation on Degraded and Undegraded Photovoltaic Panels

Samir Tabet[1], Razika Ihaddadene[2], Belhi Guerrira[3], Nabila Ihaddadene[4], Kh. Bekhouche[5], Y. Adila[6]

[1,2,4]Department of Mechanical Engineering, Med Boudiaf University, M'sila, Algeria, samir.tabet@univ-msila.dz[1]; razika.ihaddadene@univ-msila.dz[2]; nabila.ihaddadene@univ-msila.dz[4]
[3,6]Laboratory of Mechanical Engineering (LGM), University Mohamed Khider of Biskra, Algeria, b.guerira@univ-biskra.dz[3]; yazidinay@gmail.com[6]
[5]LMSM Laboratory, University Mohamed Khider of Biskra, Algeria, k.bekhouche@univ-biskra.dz

Abstract—**Photovoltaic modules performance can be degraded due to several factors such as temperature, humidity, irradiation, site dependent dust and mechanical shock. This article presents a comparative study of two panels of type ALPV85-125M-36, the first non-degraded taken as a reference and the second degraded comes from the micro photovoltaic power plant located in Biskra (Algeria). This later was degraded for 6 years in arid climate in this region. This comparison was made under real conditions and using a new method the evaluation of the power generated by photovoltaic panels as linear function of solar radiation. The experimental test was performed for the two panels for one day in the same real conditions (temperature, solar radiations, wind speed and direction and humidity). The results indicated that the power generated by the panels (none degraded and degraded) was affected by the received solar radiation. This effect was quantified by the following equations; P_{ND}=0.011G-0.186 (R^2=0.89), P_D=0.001G+0.065 (R^2=0. 93). The degradation rate of the slope of the power evolution according to solar radiations was 90.91% after 6 years in the climatic conditions of this region of this type of panel.**

Keywords - photovoltaic panel, degradation, solar irradiation

I. Introduction

Renewable energy has taken special attention because of its applications in recent decades. It is presented as a solution to overcome the energy crisis and alleviate the environmental pollution caused by the combustion of fossil fuels. Among the many renewable energy sources (solar, wind, hydro, geothermal and biomass), the solar energy is considered a promising energy source for industrial, municipal and agricultural production [1]. It is characterized by its availability worldwide and it is respectful of the environment.

Solar photovoltaic is one of the applications of solar energy for the production of electricity under the photovoltaic effect (directly converts solar radiation into electricity). Photovoltaic devices are simple in design requiring very little maintenance. They are robust and capable of delivering a wide range of power. Their field of application is vast and varied; in remote buildings, solar home systems, water pumping, communications, satellites and space vehicles, and even in megawatt power plants [2]. According to the International Energy Agency (IEA) report, renewable power capacity is set to expand by 50% between 2019 and 2024, led by solar PV. Solar PV is thought to account for ~60% of the expected growth [3].

Algeria has one of the largest solar fields in the world; the duration of insolation over almost the entire national territory exceeds 2,000 hours annually and reaches 3,900 hours (highlands and Sahara). As a result, the national renewable energy potential being strongly dominated by solar energy, Algeria considers this energy as an opportunity and a lever for economic and social development, in particular through the establishment of industries that create wealth and jobs [4].

The performance of photovoltaic modules can be degraded due to several factors namely; temperature, humidity, irradiation, dust which are site dependent and mechanical shock. This degradation results in the progressive damage to the characteristics of a component or of a system which can modify its ability to operate within the limits of the acceptability criteria and which is caused by the operating conditions. The PV systems performance is directly related to environmental conditions among which, in the first rank solar irradiance and spectrum, and ambient temperature [5-7].

Generally, the comparison between degraded and non degraded panels is performed by comparing the maximum power produced (given by the manufacturer and measured) at the test conditions (STC; irradiance 1000 W/m² and temperature 25°C). In this study, another comparison of the two panels under the same real conditions was performed. The aim of this work is to study the influence of solar radiation on degraded and non degraded panels. The degraded panel provided by the micro station of the University of Mohammed Khieder of Biskra (Algeria). This region is characterized by an arid climate.

This paper is divided into three parts as follows; the first one is devoted to the description of the material and method (the photovoltaic micro-power plant, the experimental set up) used, followed by results and discussion then a conclusion will ends this work.

Figure 1. Overview of the photovoltaic micro-plant.

II. MATERIAL AND METHOD

A. The Photovoltaic Micro-Power Plant

The photovoltaic micro-power plant of the University of Biskra is illustrated in Fig. 1. This region is located about 470 km south-east of Algiers at an altitude of 124 m, latitude of 34°.52 '(N) and longitude of 5° 45' (E) [8]. The PV micro-power plant presents a photovoltaic system connected to the laboratory networks This small photovoltaic plant with a capacity of 3400 watts was installed in 2013 to generate electricity for the university . It is composed of a PV field made up of 40 solar modules, five inverters (INGECON Sun), two cabinets, one upstream, the other downstream with security and metering elements and a data acquisition unit controlled by a PC. The photovoltaic field of this micro-plant is made up of 40 photovoltaic *modules of the type AL PV85-25M-36 based on* monocrystalline silicon. The assembly and connection of the generator modules (voltage and current) are conditioned by the electrical parameters of the DC / AC converter. Thus, there are 10 solar panels composed of 4 modules each. These panels are grouped into two parallel branches of 5 panels in series.

B. Experimental Set Up

Two panels of ALPV85-125M-36 type are used in this study. The first one comes from the photovoltaic micro-power plant of the University of Biskra (Algeria) which has undergone natural degradation in this region (6 years). The second one is a new identical photovoltaic panel (not degraded), it is taken as a reference. The two panels are illustrated in Fig. 2. Each panel is composed of 36 monocrystalline silicon cells connected in series. They can provide under standard test conditions (STC) a maximum power of 85W, a current of 4.64 A under a voltage of 18.3V. The electrical characteristics are noted in Table I. These two PV panels were mounted on the same support in the south direction and tilted at 36.8°.

In order to compare the two PV panels degraded and non degraded, an experiment was carried out on April 18, 2020 at the University

Figure 2. The used PV panels : (a) None degraded, (b) Degraded.

of Biskra. The two panels are placed in the same place following the same direction and the same inclination to have the same operating conditions for the experiment (temperature, solar radiation, wind speed, humidity).

All the values of ambient temperature, panel temperature, solar radiation, wind speed, relative humidity, current intensity, voltage throughout the day (from 6:00 a.m to 6:00 p.m) with a step of five ten minutes were collected. The global solar radiation was measured using a pyranometer. The ambient temperature is carried out with Pt100 sensor. Two voltage and current sensors are used to calculate the power.

III. Results and Discussion

The comparison of the two photovoltaic panels (non-degraded and degraded) during this study is based on solar radiation effect on the power generated by these panels.

TABLE I. THE ELECTRICAL PARAMETERS OF THE USED PV PANELS.

Parameters	Values
Nominal power	85 W
Short-circuit current (Isc)	5.33 A
Open circuit voltage (Voc)	21.83 V
Maximum Power current (Imax)	4.93 A
Maximum Power tension (Vmax)	17.27 V
Cells number (N)	36
Temperature coefficient of Isc	+0,069%/C°
Temperature coefficient of Voc	-0,39%/C°
Temperature coefficient of Pmp	-0,46%/C°

A. Solar Radiation Evolution

The solar radiation evolution during this day from 6:30 a.m. to 6:00 p.m. with a step of 15 minutes is illustrated in Fig. 3. It should be noted that the solar radiations during this day vary according to the hour; they have a minimum value of 1.5 W/m² noted at 6 h 30 min and a maximum value of 360 W/m² register at 13h 30 min. This day was not a clear sky, it is a cloudy sky.

B. Evaluation of the Non Degraded Power Panel

The non-degraded module power evolution is illustrated in Fig. 3. This power exhibits fluctuations, it has a minimum value of 0.01 W noted at 6h 30min and a maximum value of 4.96 W recorded at 13h 30min. It is noted that this power follows the same pace as the solar radiation.

In order to see the effect of solar radiation on the power of the non-degraded panel, the evolution of this power as a function of the solar radiation received on this panel as noted in Fig. 4. As noted the non degraded PV panel power increase with the increase of the solar radiation value. It presents a linear relationship with the solar radiation received by this panel, it can be presented mathematically as:

$$P_{ND} = 0.011 \times G - 0.186\,, \tag{1}$$

where P_{ND} and G are the non degraded panel power and the solar radiation received on the surface of the panel respectively. This linear relation presents a good coefficient of determination (R^2) of 0.89.

C. Evaluation of the Degraded Power Panel

Likewise, this change exhibits fluctuations, it has a minimum value of 0 W noted at 6h 30min and a maximum value of 0.83 W recorded at 13h 30min. It follows the same patterns as the solar radiation received. It increases with the increase of solar radiation as noted in Fig. 5. This relationship between them can be expressed as a linear function as noted by the following Eq.:

$$P_D = 0.011 \times G + 0.065\,, \tag{2}$$

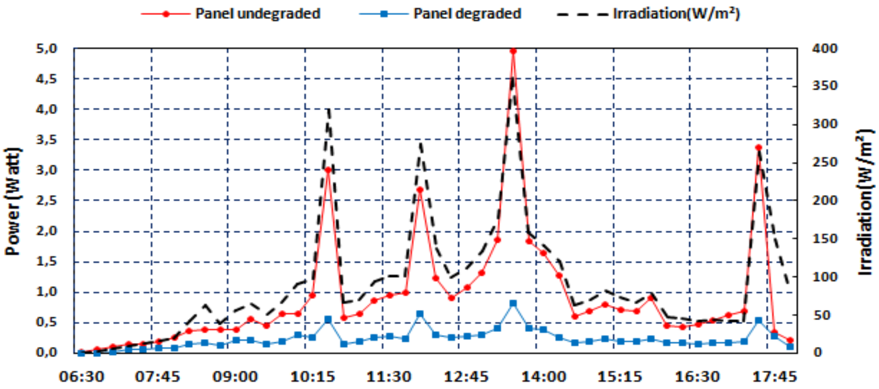

Figure 3. Panels Power (degraded, non degraded) and solar radiation evolution during the day 18/05/2020.

where P_D is the non degraded panel power and the solar radiation received on the surface of the panel.

Similarly, the evaluation of the degraded panel power over the day was done as illustrated in Fig. 3 This linear relation presents a good coefficient of determination (R^2) of 0.93 more than that noted in the non degraded power panel. Which means that the degraded paned is more affected by the solar radiation more than the non degraded panel.

It is noted that the power generated by the two panels (non-degrade and degraded) are function on radiations and time. The power supplied by the degraded panel is lower than that supplied by the non-degraded panel during the entire study day as illustrated in Fig. 3. This power difference between the non-degraded and the degraded panels (loss power) is proportional to the solar radiation; it takes low values for low solar radiation values and large values for high solar radiation values. For example, at 1:30 p.m., the power recorded by the non-degraded panel was 4.96 W and 0.83 W for the degraded panel. The power values of the two panels (non degraded and degraded) are similar at the beginning and at the end of the day.

This linear behavior of the evolution of the power generated by the photovoltaic panel as a function of solar radiations was also observed by [9] on degraded panels (2 years) monocrystalline silicon and aSi. The same behavior was observed for the evolution of the daily power according to solar radiations of the degraded panels for the months July-December of the year 2011-2012 [10].

The comparison between power generated evolution of the by the two photovoltaic panels (none degraded and degraded) according to solar radiations is illustrated in Fig. 6. Following a linear regression as indicated above, the slope of the line ($P = f(G)$) of the non-degraded panel is greater than that of the non-degraded panel. This signifies that the

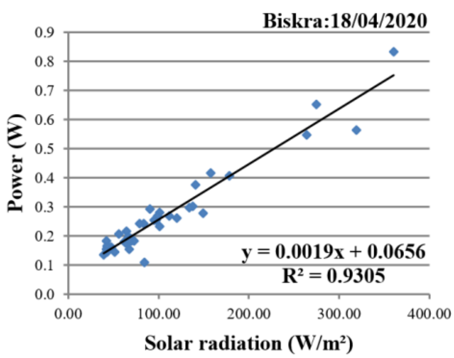

Figure 4. Non-degraded panel power evolution as function of received solar radiation.

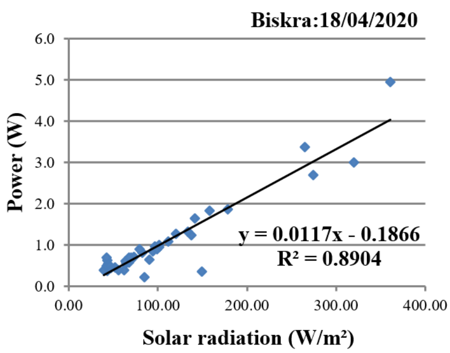

Figure 5. Degraded panel power evolution as function of received solar radiation.

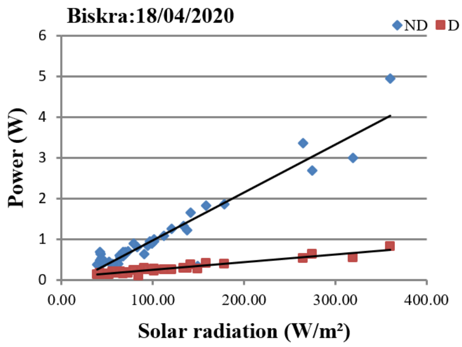

Figure 6. Non-degraded and degraded panels power evolution as function of received solar radiation.

slope varies with the degradation, it decreases with the degradation.

The slope of the power evolution as a function of solar radiation for the non-degraded panel was 0.011 W/(W/m²). After 6 years of degradation in an arid climate in Biskra region, this slope has become 0.001 W/(W/m²) with a degradation rate of 90.91%.

This degradation is attributed to climatic conditions (solar radiation, wind speed, ambient temperature and humidity) effect on photovoltaic panels. This study was carried out during a single day, it should be generalized for one year r more with other types of PV panels and other climatic conditions, which will be the subject of another work.

IV. Conclusion

A comparative study of two panels (ALPV85-125M-36) degraded and none degraded was performed in this study. A new panel noted as none degraded and a degraded panel for 6 years in the micro photovoltaic power plan of Biskra as degraded. A new method of comparison was performed; the comparison of the generated power as linear relation to the solar radiation of the two panels (none degraded and degraded).The two panels were tested for one day(18/05/2020) in the same real conditions and the power generated and solar radiation received by those panels were registered every 15 minutes.

The non-degraded panel power evolution exhibits fluctuations as the solar radiation fluctuations; it follows the same pace as the solar radiation. The non degraded PV panel power increase with the increase of the solar radiation value. This evaluation can be presents as a linear relationship; it can be presented mathematically as:

$$P_{ND} = 0.011 \times G - 0.186 \ . \qquad (3)$$

The degraded panel power also follows the same pattern as the solar radiation received. It decreases with the decrease of solar radiation. The degraded panel power evolution can be expressed as a linear function of the solar radiation as:

$$P_D = 0.011 \times G + 0.065 \ . \qquad (4)$$

The degraded power evolution presents a good coefficient of determination (R^2) of 0.93 more than the none degraded power evolution (0.89). Which means that the degraded paned is more affected by the solar radiation more than the non degraded panel.

The comparison between power generated evolution of the by the two photovoltaic panels (non-degraded and degraded) according to solar radiations revels that the non-degraded panel slope is greater than that of the degraded panel. This signifies that the slope varies with the degradation, it decreases with the degradation. The rate of degradation of the slope of the power evolution line as a function of solar radiation was 90.91%. This degradation is attributed to climatic conditions (solar radiation, wind speed, ambient temperature and humidity) effect on photovoltaic panels.

References

[1] Jamil, B., & Bellos, E. (2019). Development of empirical models for estimation of global solar radiation exergy in India. *Journal of Cleaner Production*, *207*, 1-16.

[2] Parida, B., Iniyan, S., & Goic, R. (2011). A review of solar photovoltaic technologies. *Renewable and sustainable energy reviews*, *15*(3), 1625-1636.

[3] International Energy Agency (2020). *Renewables 2019.* Available at: https://www.iea.org/reports/renewables-2019.

[4] Ihaddadene, R., Jed, M.E.H, Ihaddadene, N., & Hneini, M. (October, 2019). Performance Analysis of a Photovoltaic Array(15.936 MWc) at Ain Skhouna PV Power Station (Saida, Algeria). In *5th Jubilee Virtual International Conference on Science, Technology and Management in Energy Proceedings*.

[5] Aarich, N., Raoufi, M., Bennouna, A., & Erraissi, N. (2018). Outdoor comparison of rooftop grid-connected photovoltaic technologies in Marrakech (Morocco). *Energy and Buildings*, *173*, 138-149.

[6] Jed, M. E. H., Ihaddadene, R., Ihaddadene, N., Sidi, C. E. E., & Bah, M. E. (2020). Performance analysis

of 954,809 kWp PV array of Sheikh Zayed solar power plant (Nouakchott, Mauritania). *Renewable Energy Focus, 32*, 45-54.

[7] de Azevedo Dias, C. L., Branco, D. A. C., Arouca, M. C., & Legey, L. F. L. (2017). Performance estimation of photovoltaic technologies in Brazil. *Renewable Energy, 114,* 367-375.

[8] Wikipedia. *Wilaya de Biskra*. Available at: https://fr.wikipedia.org/wiki/Wilaya_de_Biskra

[9] Cotfas, D. T., & Cotfas, P. A. (2019). Comparative Study of Two Commercial Photovoltaic Panels under Natural Sunlight Conditions. *International Journal of Photoenergy*, 2019.

[10] Kichou, S., Abaslioglu, E., Silvestre, S., Nofuentes, G., Torres-Ramírez, M., & Chouder, A. (2016). Study of degradation and evaluation of model parameters of micromorph silicon photovoltaic modules under outdoor long term exposure in Jaén, Spain. *Energy conversion and management, 120,* 109-119.

Numerical Analysis of the Road Traffic Intensity Influence on The Urban Heat Island Characteristics, Case of Belgrade City, Serbia

Ivan Lazović

„VINČA" Institute of Nuclear Sciences - National Institute of the Republic of Serbia, University of Belgrade, Belgrade, Serbia, ivan.lazovic@vinca.rs

Abstract—**High levels of air pollutants and high outdoor temperatures during the summer period in large cities depend on many parameters. The main causes of high pollution in urban areas is increased traffic intensity and reduced natural ventilation. A large number of input parameters are required for the calculation of air temperature, relative humidity, wind speed, and direction in a complex urban environment using computational fluid dynamics (CFD) simulations. These parameters can be largely obtained by experimental measurements. However, in certain cases, additional calculations or simulations are necessary to determine input parameters values. Road traffic emissions mostly depend on real-time traffic intensity. Input parameters for the CFD simulation and the levels of air pollutants from traffic are obtained by traffic contamination modeling using the COOPERT method. Numerical CFD simulations and in-situ measurements of the outdoor temperature and CO_2 concentration distributions were performed for the case of the complex urban geometry of Belgrade city center in the framework of this study. The numerical model has been validated by the measurement data. Based on the obtained results, it is noted that both ambient air temperature and CO_2 concentration are higher near the streets characterized by intensive traffic and at the locations predominately composed of multiblock residential buildings compared with other parts of the city.**

Keywords - urban heat island, road traffic, computational fluid dynamics

I. INTRODUCTION

A large fraction of the world's population lives in cities. Most cities around the world face undesirable thermal impacts due to the fast decline in natural land surfaces [1,2]. Rapid urbanization in cities and an increase in their population are key drivers of global environmental change [3]. Although these processes influence global - scale climate changes, rather significant effects can be seen in the impact on local microclimate conditions, at individual cities scale.

The urban heat island (UHI) effect in cities is one of the most important issues concerning thermal pollution in urban areas [4,5]. Oke [6] in his paper presented a comprehensive review of earlier observational studies on the characteristics, causes, and effects of UHI. Their relative importance was determined in numerous follow-up studies focused on: trapping of short and long-wave radiation in between buildings, decrease in long-wave radiative heat losses due to reduced sky-view factors, increase in storage of sensible heat in the construction materials, anthropogenic heat release from the combustion of fossil fuels (domestic heating, traffic), reduction of potential for evaporation, which implies that energy is converted into sensible rather than latent heat, and reduction of convective heat removal due to the reduction of wind speed.

It is a well-known fact that local temperatures are influenced by a complex interplay between different effects: wind speed, wind direction, evaporation and rain, atmosphere pollution with three-atomic pollutant gases (CO_2, NO_X, SO_X, and H_2O), and particulate matter air pollution.

Reference [7] classified 20 air temperature measurement stations, for 22 months. The urban heat island effect had higher maximum values for 5-6°C in the city center compared with the corresponding rural area. These locations were characterized by the presence of large areas covered by asphalt layers and by high traffic intensity.

Motor vehicles are a major source of air pollution with a significant impact on the urban environment. About 80% of the total population in Europe lives in urban areas where the largest contribution to air pollution increase comes from traffic, and especially social transport [8]. The emission of exhaust gases from urban traffic is one of the main factors that determine the level of air pollution in urban areas. The exhaust gases lead to the increased convective and radiation heat transfer, which occurs between the air and the earth's surface and consequently leads to an increase in temperature in urban areas. The main air pollutants emitted by motor vehicles include CO_2, CO, hydrocarbons, NOx, particulate matter (PM), benzene, formaldehyde, acetaldehyde, 1,3-butadiene, O_3, nitrates, and inorganic and organic acids.

CFD based numerical model suggested in the framework of this study was used to perform case study simulations of air temperature and CO_2 distributions in Belgrade city, Serbia. The numerical model has been validated by experimental measurement data.

The atmosphere above the urban area is a semi-transparent medium, and the effective atmospheric emissivity is related to the concentration of the three atomic gasses [9]. It is widely accepted that the increase in CO_2 amount emitted to the atmosphere is the main reason for the increase in outside temperature in urban environments. It is assumed, for this study, that the prevailing source of CO_2 emissions in the observed urban environment of Belgrade city is the urban traffic. Numerical simulations were performed to obtain values of CO_2 pollution for locations where it was not possible to conduct an experimental measurement campaign. This study is focused on the investigation of the influence of road traffic intensity on the urban heat island characteristics, mainly on outdoor temperature, using measurement data and numerical simulations.

II. Experimental Investigation

The study site in this research work is part of the city center in Belgrade, Serbia, Fig. 1. The following air and urban characteristics were measured at this location: air temperature, relative humidity, wind velocity and direction, the surface temperature of the buildings' facades, grass, roads, and global solar radiation, number of vehicles per category, road length, and average vehicles speed. The local meteorological mast has been installed on the roof of The College of Textile – Design Technology and Management-DTM (44º48'37''N, 20º28'42''E). The measured local meteorological data have been continuously monitored every 10 minutes.

The COPERT software was used to calculate emissions of the most important harmful substances emitted from different categories of vehicles based on their traffic flow data. The software calculates values of CO_2, VOC, NO_x, CO, and PM on the street and intersection levels are obtained based on entered data. The COPERT Street level [10] was designed to calculate hourly emissions, so the activity data should be entered for each hour of the day and every traffic link. The measurement of the number of vehicles was performed at seven crossroads and streets that intersect at that crossroads at selected urban locations, Fig. 2. The selected vehicles are categorized into one of 7 groups: 1) bicycles, 2) motorcycles, 3) passenger vehicles, 4) vans, 5) buses, 6) easy trucks, and 7) heavy-duty trucks.

The model assumes that the prevailing source contributing to the increase of CO_2 concentration is the urban traffic. Three different categories of road capacity were identified based on the current street network of the studied urban area: 1) street crossing (red color); 2) heavy traffic loaded streets (cyan color) and 3) moderate traffic loaded streets (blue color), Fig. 3.

Figure 1. Urban structure of the Belgrade Center.

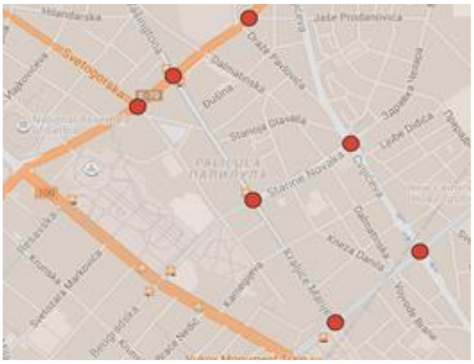

Figure 2. Location of measurement number of vehicles per category.

Figure 3. Street network of Belgrade Center.

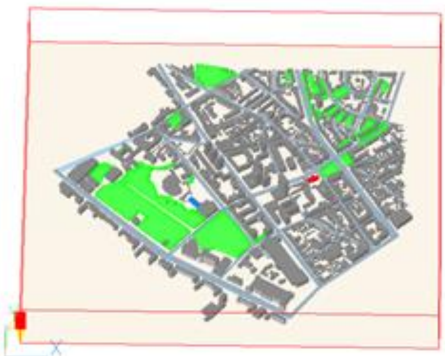

Figure 4. 3D solid model of Belgrade Center.

III. CFD SIMULATIONS

The 3D model of the selected urban area is presented in Fig. 4. Green infrastructure (parks) is marked in green, the buildings and other tall objects are marked in dark grey, the roads are marked in light grey, the swimming pool is blue, and the location where the local meteorological measurements were made is marked in red. Meteorological input data for numerical simulations were obtained from experimental measurements performed with the meteorological mast placed on the school building. Numerical simulations were performed by PHOENICS computer code [11].

A. Solver Outline

Comprehensive CFD code CHAM Phoenics was used for all numerical simulations in the selected urban area of Belgrade, Serbia. A computational grid was constructed dividing the geometrical domain in a finite number of control volumes. The conservation equations mass, momentum, heat (temperature), turbulent quantities (turbulent kinetic energy, k, and it's dissipation, ε), and CO_2 mass fraction written in the general form with the dependent variable denoted by *Φ* give the following system of partial differential Eq. (PDEs):

$$\frac{\partial}{\partial x_i}(\rho U_j \Phi) - \frac{\partial}{\partial x_i}\left(\Gamma_\Phi \frac{\partial_\Phi}{\partial x_i}\right) = S_\Phi , \qquad (1)$$

where:

ρ - Air density,

U_j - Wind velocity components (*j=1, 2, 3*),

Φ - General depended variable (summarized in Table I).

Γ_Φ - Diffusion coefficient of variable Φ (summarized in Table I).

S_Φ - Source terms of variable *Φ* (summarized in the Table I).

The notation of the symbols in Table I is g_i – pressure, g_i - gravitational acceleration, T_{ref} - reference air temperature and σ - Stefan-Boltzmann constant, and ε_a - effective atmospheric emissivity.

B. Computational Domain and Computational Grid Generation

The required condition for good positioning of numerical boundaries is to enable sufficient distance from the domain of the interest. This distance has to be large enough to enable fully developed flow inside the computational domain. The main domain dimensions are 1536 m in x-direction, 1425 m in y-direction, and 200 m in z-direction, Fig. 5.

TABLE I. SUMMARIZED TERMS IN EQUATION (1).

Equation:	Φ	Γ_{Φ}	S_{Φ}
Continuity	1	0	0
Momentum	U_j	μ_{eff}	$-\partial p/\partial x_j + +\rho g_i (T_a - T_{ref})$
Energy	T	γ_{eff}	$\varepsilon_a \sigma (T_{rad}^4 - T_a^4)$
Species	Y_{CO_2}	γ_{CO_2}	0
Turbulence kinetic energy	k	ν_t/σ_k	$P_k + G_k - \varepsilon$
Dissipation rate of turbulence	ε	ν_t/σ_ε	$(\varepsilon/k)(C_{\varepsilon 1} P_k + +C_{\varepsilon 3} G_k + C_{\varepsilon 2}\varepsilon)$
Radiant temperature	T_{rad}	γ_{rad}	$-\varepsilon_a \sigma (T_{rad}^4 - T_a^4)$

$$\mu_{eff} = \mu_{mol} + \mu_t; \quad \gamma_{eff} = \gamma_{mol} + \gamma_t$$

$$\mu_t = \frac{C_\mu \rho k^2}{\varepsilon}; \quad P_k = \nu_t (\partial_k U_i + \partial_i U_k)\partial_k U_i;$$

$$G_b = \nu_t \beta g_i \partial_i T$$

$$(\sigma_k, \sigma_\varepsilon, C_{\varepsilon 1}, C_{\varepsilon 2}, C_\mu, C_{\varepsilon 3}) = = (1.0, 1.314, 1.44, 1.92, 0.09, varies)$$

$$\gamma_{rad} = (16/3)\sigma T_{rad}^3 \{1/(\varepsilon_a + s_a + 1/X_{gap})\},$$

$$\varepsilon_a = \varepsilon_a(H_2O) + \varepsilon_a(O_3) + \varepsilon_a(overlap) + \varepsilon_a(CO_2)$$

C. Grid Independence Study

The five different computational meshes were constructed to investigate the solution dependence of mesh finesses. Course grid consisting of 430000 finite volumes, a less coarse grid consisting of 1232622 finite volumes, a medium grid consisting of 2167500 finite volumes, a fine grid consisting of 3244032 control volumes, and a very fine grid consisting of 7161165 finite volumes. The first case (with air inlet positioned on east domain boundary) was used to test solution-grid dependence. The case was calculated on all five meshes, and change in air temperature magnitude in vertical x = constant plane. Calculated velocity magnitude values stopped changing more than 5% switching from medium to very fine mesh.

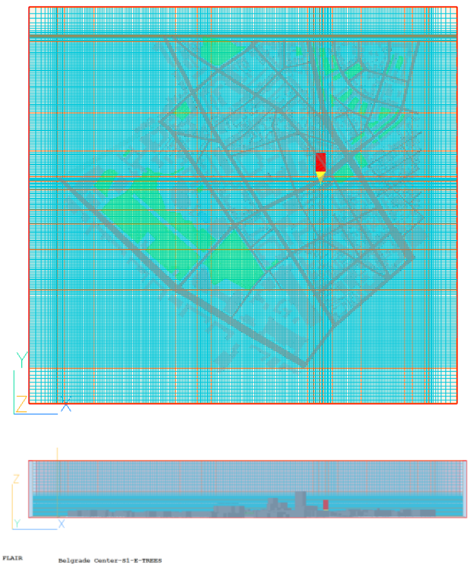

Figure 5. Finite volume grid of the computational domain.

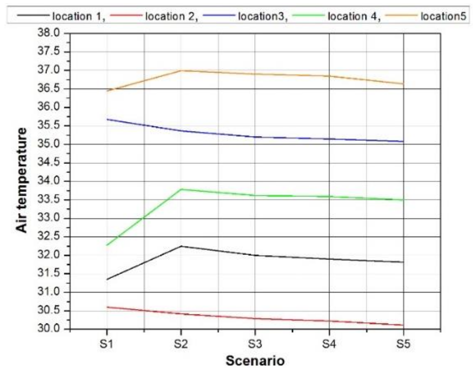

Figure 6. Finite volume grid of the computational domain.

Thus, the solution was adopted as grid-independent, Fig. 6. Based on this, the medium mesh was adopted for all numerical simulations performed in the scope of this work.

Model validation was done comparing the air temperature for five selected locations in the city area at a height of 1.85 meters (corresponding to human height). The selected city locations are: location 1-school building (44°48'37.4"N 20°28'42.3"E), location 2-park (44°48'30.9"N 20°28'12.4"E), location 3-city market (44°48'41.7"N 20°28'20.8"E), location 4-high traffic street near the park (44°48'36.5"N 20°27'58.9"E), location 5-crossroads with high traffic flow (44°48'34.1"N 20°28'31.2"E).

TABLE II. INPUT ATMOSPHERIC PARAMETERS FOR CFD SIMULATIONS.

Time	**8:00-9:00**	**14:00-15:00**	**18:00-19:00**
Air temperature [ºC]	35.9	40.8	37.6
Relative humidity [%]	33.1	21.4	25.4
Atmosphere pressure [hPa]	1000.1	1000.3	999.8
Wind velocity (at 10 meters a.g.l.) [m/s]	1.1	2.8	3.1
Wind direction [degree]	300	330	322
Global solar radiation [W/m^2]	410	794	217

IV. RESULTS AND DISCUSSION

Numerical simulations were performed for the warmest day in the measurement period using the suggested CFD based model. Input data of atmospheric parameters are taken from the measurement database based on time of day, as shown in Table II.

TABLE III. RESULTS OF NUMERICAL SIMULATION POLLUTANTS DEPENDING ON THE INTENSITY OF TRAFFIC.

Measurement location	***Pollutant [g]***	**8:00-9:00**	**14:00-15:00**	**18:00-19:00**
Crossroads 1-Cvijićeva-Zdravka Čelara-Starine Novaka	CO_2	245339	228025	184396
	CO	411.1	424.9	325.3
	NO_X	452.7	390.6	327.7
	PM	8.3	7.4	5.9
	VOC	87.1	102.7	71.0
Street 1-Zdravka Čelara	CO_2	119007	116064	91670
	CO	199.4	216.3	161.7
	NO_X	219.6	198.8	162.9
	PM	4.0	3.8	3.0
	VOC	42.3	52.3	35.3
Street 2-Cvijićeva (from Bul. Despota Stefana to the Crossroads 1)	CO_2	140705	145184	106457
	CO	222.7	254.5	183.1
	NO_X	267.8	269.2	190.9
	PM	4.8	5.0	3.4
	VOC	41.9	60.1	39.1
Street 3-Cvijićeva (from Crossroads 2 to the Ruzveltova)	CO_2	117740	122731	101448
	CO	193.7	219.3	174.9
	NO_X	229.6	230.8	189.3
	PM	4.2	4.3	3.4
	VOC	41.4	51.4	39.4
Street 4-Starine Novaka	CO_2	101432	100455	80049
	CO	167.7	186.0	144.5
	NO_X	190.3	181.0	145.2
	PM	3.4	3.4	2.6
	VOC	32.3	46.8	33.0
Crossroads 2-27 Marta-Starine Novaka	CO_2	176695	219759	171030
	CO	287.9	405.0	314.7
	NO_X	337.3	411.5	315.5
	PM	6.0	7.7	5.7
	VOC	49.4	105.1	74.7
Street 5-Kraljice Marije	CO_2	83443	98119	86187
	CO	138.6	188.9	170.9
	NO_X	165.7	185.8	161.5
	PM	3.0	3.5	3.0
	VOC	26.5	51.2	46.0
Street 6-Beogradska	CO_2	117344	141862	107948
	CO	191.2	261.4	198.6
	NO_X	224.0	265.6	199.2
	PM	4.0	5.0	3.6
	VOC	32.8	67.8	47.1
Street 7-27. Marta	CO_2	48171	60530	47939
	CO	75.5	106.0	87.1
	NO_X	92.0	112.1	87.4
	PM	1.6	2.1	1.6
	VOC	12.3	24.6	19.6
Crossroads 3-27 Marta-Takovska	CO_2	47817	57625	46630
	CO	70.3	91.8	83.0
	NO_X	91.4	104.8	83.4
	PM	1.6	1.9	1.5
	VOC	10.3	16.5	16.8
Street 8-Takovska (from Crossroads 3 to the Jaša Prodanović st)	CO_2	100075	107483	97840
	CO	152.6	163.8	157.9
	NO_X	192.3	201.6	180..7
	PM	3.5	3.6	3..1
	VOC	23.7	27.0	26.1
Street 9-Takovska (od raskrsnice 3 do Svetogorske)	CO_2	61684	64949	55867
	CO	89.2	103.9	95.8
	NO_X	120.7	125.4	100.8
	PM	2.1	2.3	1.8
	VOC	12.8	21.1	19.5
Street 10-Džordža Vašingtona	CO_2	95635	115250	93260
	CO	140.6	183.6	166.0
	NO_X	182.7	209.6	166.8
	PM	3.3	3.7	3.0
	VOC	20.6	32.9	33.6
Crossroads 4-Takovska-Svetogorska	CO_2	197061	198724	180215
	CO	280.7	319.1	297.3
	NO_X	394.4	405.9	328.0
	PM	6.9	7.4	5.8
	VOC	39.6	72.6	61.1
Street 11-Majora Ilića	CO_2	25632	30173	27050
	CO	36.5	48.4	44.6
	NO_X	51.3	61.6	49.2
	PM	0.9	1.1	0.9
	VOC	5.1	11.0	9.2
Street 12-Takovska (from Crossroads 4 to the Bul. kralja Aleksandra)	CO_2	211752	212250	187840
	CO	301.7	340.8	309.9
	NO_X	423.8	433.5	341.8
	PM	7.4	7.9	6.0
	VOC	42.5	77.5	63.7
Crossroads 5-Ruzveltova-Cvijićeva	CO_2	296152	272975	229387
	CO	481.5	476.5	390.2
	NO_X	596.9	537.5	439.3
	PM	11.0	10.0	7.9
	VOC	103.6	109.8	89.4
Street 13-Ruzveltova	CO_2	82280	71229	61653
	CO	136.9	137.4	122.2
	NO_X	167.7	138.0	117.6
	PM	3.1	2.6	2.2
	VOC	28.9	36.8	33.9

The mean surface temperatures of trees, grass, building facades and roofs, pavements, streets, and water used as input parameters are given below:

- The temperature of trees: 26˚C
- The temperature of grass: 27˚C
- The temperature of building façades and roofs: 37˚C
- The temperature of pavements and streets: 37˚C

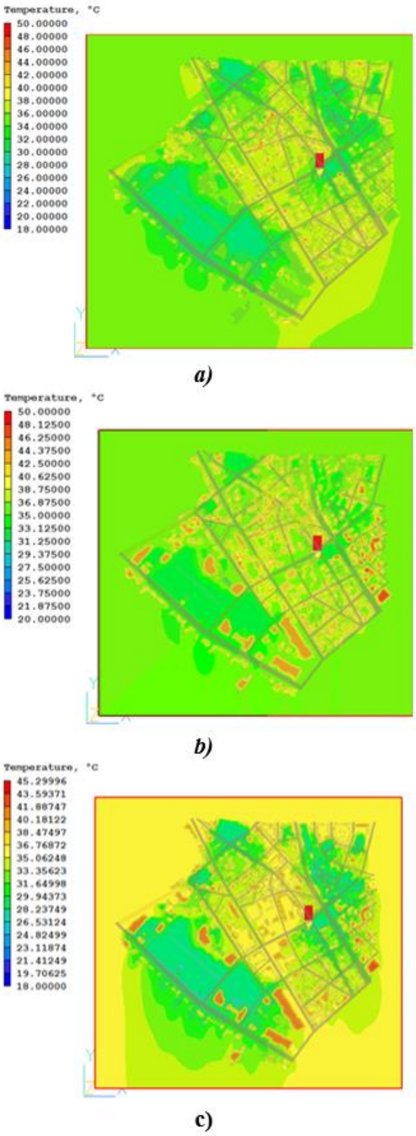

Figure 7. Ambient air temperature at a height of 1.8 m a) morning, 08-09h b) afternoon, 14-15h and c) evening, 18-19h manager duties.

- The temperature of the water surface: 18˚C.

The average values of air pollutants, based on the number of vehicles, obtained by numerical simulation using computer software COPERT are shown in Table III. Air pollutant values are presented for crossroads and streets in which road traffic intensity was measured. The highest concentrations of CO_2, CO, NOx, and PM were observed at Crossroad 5 during the morning and afternoon. This can be explained by the fact that this is a crossroad of two streets with high traffic intensity at this time of the day due to a large number of people driving back from work. Intensive traffic is considered to be the main cause of high air pollution. The highest concentration of VOCs was observed in the same location during afternoon hours. This is caused by an increase in temperature during the day, which leads to the evaporation of organic matter. On the other hand, the lowest concentrations of air pollutants were observed in Street 11, which corresponds to the low traffic intensity in this street. Generally, the concentrations of CO_2, CO, PM, and NOx are highest during the morning and afternoon at all locations due to high traffic intensity, which is the prevailing source of air pollution. VOC concentration increases as daily temperature raises, reaching the maximum in the afternoon hours.

The following conclusions can be drawn based on the obtained results: the highest measured and numerically calculated values of air temperature were obtained in the afternoon. The biggest difference in air temperature between high-temperature locations and other parts of the city environment is determined in the evening, after sunset Fig. 7. This difference is the smallest in the afternoon. Ambient temperature is lower at locations with green areas and parks, and it is higher in the areas near the streets characterized by the high traffic intensity. Higher ambient temperature is also characteristic for areas with dense multiblock buildings and asphalt-covered surfaces. To sum it up, ambient temperature is higher for 1.5-3°C near the streets than in other parts of the selected urban area.

CO_2 concentration distribution in the horizontal plane at a height of 1.85 m above ground level obtained by numerical simulations are presented in Fig. 8. It can be seen that CO_2 concentrations are significantly higher near the

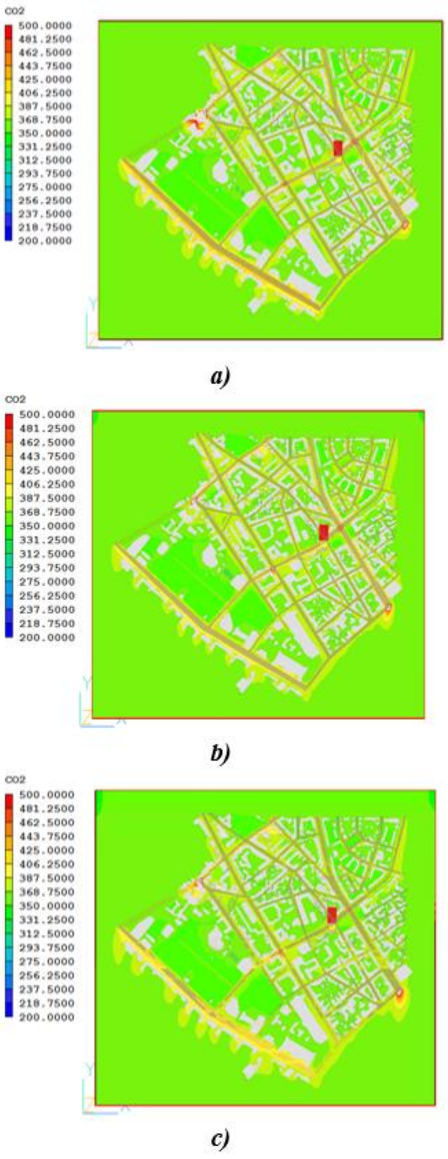

Figure 8. CO_2 concentrations at a height of 1.8 m a) morning, 08-09h b) afternoon, 14-15h and c) evening, 18-19h.

road compared with the other parts of the domain. Since CO_2 is heavier than air (the molecular mass of carbon dioxide is 44 g mol^{-1}, while air is 28 g mol^{-1}) it prevents generated heat from rising back from the Erath surface to the atmosphere and leads to the greenhouse effect. This global effect predominantly influences the increase in the air temperature in the above-defined urban zones. The greenhouse effect leads to air temperatures higher for several degrees in the near roads' zones compared with the other parts of the city.

V. CONCLUSION

Detailed three-dimensional simulations of air temperature and CO_2 concentration distributions were performed for the Belgrade city center, Serbia to determine possible dependence of air temperature increase from the road traffic intensity.

- CFD simulations were performed for three different parts of the day;
- Ambient temperature is 1.5-3 °C higher in the areas near the streets with high traffic intensity;
- CO_2 and NOx air pollutants are more affected by the increase in the air temperature in the city area compared with other air pollutants;
- This study showed that CFD simulations can be successfully utilized to predict outdoor air temperature in complex urban areas;
- This type of research can be significantly used in the planning and design of urban environments, as well as of smaller complexes within the larger urban environment;
- It is planned to further develop the current CFD model to include other important effects, such as the influence of other gaseous species with the greenhouse effect and health-hazardous components;
- The performed work offers a workflow that can be successfully used to develop and/or investigate different scenarios for energy consumption and outdoor thermal comfort.

ACKNOWLEDGMENT

This work was funded by the Grant of the Ministry of Education, Science and Technological Development of Republic of Serbia.

REFERENCES

[1] Oke, T. R. (2002). *Boundary layer climates*. Routledge.

[2] Santamouris, M. (2013). *Energy and climate in the urban built environment*. Routledge.

[3] Khan, A., & Chatterjee, S. (2016). Numerical simulation of urban heat island intensity under urban–suburban surface and reference site in Kolkata, India. *Modeling Earth Systems and Environment*, *2*(2), 71.

[4] Mirzaei, P. A. (2015). Recent challenges in modeling of urban heat island. *Sustainable cities and society*, *19*, 200-206.

[5] Wu, H., Wang, T., Riemer, N., Chen, P., Li, M., & Li, S. (2017). Urban heat island impacted by fine particles in Nanjing, China. *Scientific reports*, *7*(1), 1-11.

[6] Oke, T. R. (1995). The heat island of the urban boundary layer: characteristics, causes and effects. In *Wind climate in cities* (pp. 81-107). Springer, Dordrecht.

[7] Livada, I., Santamouris, M., Niachou, K., Papanikolaou, N., & Mihalakakou, G. (2002). Determination of places in the great Athens area where the heat island effect is observed. *Theoretical and Applied Climatology*, *71*(3), 219-230.

[8] Colvile, R. N., Hutchinson, E. J., Mindell, J. S., & Warren, R. F. (2001). The transport sector as a source of air pollution. *Atmospheric environment*, *35*(9), 1537-1565.

[9] Stevanović, Ž., Lazović, I., & Đurović-Petrović, M. (2014, November). Numerical Simulation of Heat Island Phenomena Related to Traffic Pollution of Urban Atmospheric Layer. In *the 1st Environment and Natural Resources International Conference – ENRIC*, 86-93.

[10] Emisia. (2020). Available at: www.emisia.com.

[11] Concentration, Heat & Momentum Limited (CHAM). (2020). Available at: www.cham.co.uk.

Mobile Applications and Services for Next-Generation Energy Management in Smart Cities

Nenad Petrović[1], Vasja Roblek[2], Valentina Nejković[3]

[1,3]University of Niš, Faculty of Electronic Engineering, Niš, Serbia,
nenad.petrovic@elfak.ni.ac.rs[1]; valentina.nejkovic@elfak.ni.ac.rs[3]
[2]Faculty of Organisation Studies, Novo Mesto, Slovenia, vasja.roblek@gmx.com

Abstract—**Energy-efficiency is one of crucial aspects of sustainability within smart city ecosystems. In this paper, a novel approach to development of mobile applications for energy management leveraging highly automated development environment AppSheet and web-based augmented reality is presented. As proof-of-concept, two case studies are presented: energy-efficient smart home consumer device management and computing infrastructure management in Fog computing architectures.**

Keywords – AppSheet, augmented reality, energy management, fog computing, smart city, mobile applications

I. INTRODUCTION

Smart cities can be defined as a city that uses technology to serve people. It is structurally designed as a citizen-centric ecosystem based on numerous technological solutions and applications that aim to transform traditional urban infrastructure and services. It is going for an interoperable communication system that connects citizens and businesses. The communication systems enable private and public activities through a service such as energy distribution, transport, street lighting, waste management, etc., thus helping to optimize the use of resources and promote harmonious and sustainable development [1,2].

Smart cities are often defined uncritically as a sustainable way of urban development. As cities become increasingly complex as their characteristics are linked to the internet, theories lag behind their understanding [3]. Since it is assumed that a larger number of citizens and things will be connected with the help of the Internet of Things (IoT) and the so-called Internet of the Future, the complexity of urban systems will increase over time [4]. Historical insights show that as societies become more complex, energy consumption tends to increase [5,6]. It is also considered easier for cities to increase the use of renewable energies and to improve the efficiency of all energy systems [7]. The city offers its inhabitants shelter and provides high levels of living comfort and easy access to education, health, energy, water and food. Planning in the smart city must be based on the assumption that it is an economic city where we spend the least energy and resources on an activity without significantly reducing the comfort or safety of the population [8,9]. However, we would not need smart cities at all if we had resources for at least three more such planets and if we did not have problems with climate change.

The concept of a smart city is based on environmental protection, advanced information technology, clean mobility, a sustainable economy and, above all, an improved quality of life for citizens. For these reasons, the city is equipped with an infrastructure that provides it with data on energy consumption, water and air quality and waste management at every step. Since a cleaner urban environment is closely linked to improving the health of citizens, there is no doubt about why it is worth investing in this modern infrastructure [10,11]. Moreover, smart energy and economy, while increasing raw material efficiency, are the most tangible indicators against global warming [12].

The main objective is to improve the quality of well-being of citizens in urban environments for different target groups in order to create a sustainable, green and economically viable system that integrates social development policies. This area is highly inclusive as the quality of urban life is influenced by all the areas as mentioned above as well as by the products of other strategic development innovation partnerships [13,14].

With the growing phenomenon of informatization, the Smart City ecosystem is increasingly shifting to the cyber-physical environment, the central part of which is the urban data management platform, which can also be called the Smart City's brain [15]. The goal of the cyber-physical infrastructure is so also to create an analytical platform for planning, monitoring and managing the Smart city ecosystem with the following sets [16]:

a) Monitoring, planning, management of the harvested environment, includes monitoring systems, planning of existing and necessary capacities of economic and social infrastructure to determine the existing and to achieve a higher quality of urban life, development of criteria and measures that can be used to measure/define/improve the quality of urban life and their personalization, land policy and land management for the development of various activities, Systems for data and information acquisition (sensors, measurement devices), information-based systems and concepts for space exploitation, interconnection with other sectors (health mobility), integration platforms as entry windows to relevant data, products and services, planning, services and tools for digital privacy management, development and tracking of green effects infrastructures, environmental monitoring systems, etc.

b) Integration of participatory methods, systems and platforms in monitoring the quality of urban housing: participatory reporting for the development of urban centers, for participatory methods perception and planning of public services according to the concept of the "Citizen's Observatory", participatory urban planning.

c) Information-based systems and services for different target groups: older people, vulnerable groups, self-sufficiency and nutrition.

d) Business development with a focus on cradle to cradle design - the transition from linear to circular economy, digital transaction management and closing services according to eIDAS, robotics in architecture, treatment of green spaces, introduction of green infrastructure, multilingual platforms.

The platform collects, analyses and share information from the human environment. IoT, sensors, large amounts of data and intelligent devices and buildings play an important role, as they represent an increasingly important urban deck of the smart city ecosystem [17,18]. The so-called smart building is a building in which electrical devices can be remotely controlled from anywhere in real-time using a smart device. Such a technologically urban solution is important to ensure heating, security, economy and comfort. Applications of smart devices play an important role in this context [19-21].

In the case of IoT is going for the concept of connecting at least two devices with built-in sensors that can collect and send data via the Internet or another protocol that share theirs with other devices [22]. In the last few years, IoT has also become important in the field of energy management. The development has contributed to the emergence of the IoT-based energy management system, which plays an important role in building intelligent urban projects. Its role is to enable new energy-related value-added services and to facilitate the integration of different energy sources in an intelligent way, and to enable automatic control of operations [23].

In a smart urban environment, IoT-based energy management systems have emerged in the fields of smart building and the smart power grid. Their importance lies in enabling energy efficiency measures in buildings based on generally lower energy demand [24].

We focus on the role of intelligent applications that can be defined for the areas as mentioned above [24]: 1) Smart building - Applications can provide access to input data (energy consumption, temperature, humidity) and control of energy devices according to the requirements of a given situation and operating conditions 2) Smart grid - The smart grid enables consumers to make better choices in terms of power supply and access to information while allowing consumers to participate in optimizing energy system operation.

With the advent of IoT, there has been a link between the building sector and integrated intelligent information and communication solutions, which has influenced the growing importance of an effective energy management system, whose role is to support energy decision making not only in buildings but also at the neighborhood and city level. In the building sector, IoT-based systems are being implemented that enable the interactive operation of energy management systems in buildings. Intelligent applications that enable the management and control of energy devices, data analysis, and the behavior of residents concerning energy consumption, the creation of energy consumption plans and the personalization of information on energy consumption by end-users play an important role in this context [25].

The main purpose of this paper is to show the importance and functioning of energy management mobile applications for smart cities. Applications to control electricity consumption are thus becoming increasingly important. The concept of the paper aims at a holistic view and analysis of mobile applications and services for next-generation energy management in smart cities. Two case studies of mobile applications are presented: energy management application for smart home and energy-efficient infrastructure management in Fog computing. The proposed solutions incorporate innovative use cases (energy trading, remote infrastructure control) with state-of-the-art technology, such as augmented reality (AR) for user interfaces and block-chain technology relying on affordable IoT and smartphone devices.

II. Background and Related Work

A. AppSheet

For more than a decade, mobile applications are covering various aspects of our everyday life – from health to business and transportation. When it comes to smart cities, data-driven mobile applications play an important role in information exchange for their citizens. Therefore, different organizations need to deliver their applications and services, regardless of the mobile hardware and operating system. However, the development of distinct native mobile applications for various platforms is costly, time-consuming and requires expertise. For that reason, in recent years, the development of cross-platform mobile applications is becoming a trend. While most of them still require solid programming expertise, AppSheet [26] is one of the solutions that enables creation of complex mobile applications with wide compatibility, with just basic programming knowledge. This way, even domain experts can create mobile applications, while still putting the main focus on the problem they need to solve rather than the application development itself.

AppSheet is an online platform and development environment for rapid creation and deployment of multiplatform mobile applications, relying on cloud data sources, such as spreadsheets (Microsoft Excel and Google Sheets) and databases (Microsoft SQL Server, MySQL, Postgre SQL and others). It uses intuitive graphical environment for application design and development, while high-level declarative language is leveraged for formula definition and behavior, which consists of pre-defined actions triggered in a particular context. The available actions include view transition, sending HTTP request, accessing external website, sending an e-mail or SMS, making a call and others that aim to enable business logic implementation. Originally, AppSheet was created as Praveen Seshardi’s home project in 2014, but quickly drew attention of big companies which later invested into its development. Finally, it was acquired by Google in January 2020 and officially became a part of Google Cloud services, which led to tighter integration with other Google Services (such as Google Sheets). AppSheet is free to use for prototyping purposes and personal use, for up to 10 beta/test users. For large scale, commercial applications monthly fees are paid. Furthermore, advanced machine learning and AI-related features are available even in free version of AppSheet, such as voice commands, predictive models and optical character recognition (OCR). In this paper, predictive models and voice commands are used. The predicted values can be either numeric (regression), yes/no or enumeration (for classification). Predictive models can be trained with at least 25 data rows, while the training is done in just few seconds. On the other side, voice commands are automatically embedded within application and enable easy navigation through app views. However, active internet connection and client app downloaded from the corresponding store (Google Play or Apple App Store) are required in order to use all features of applications created in AppSheet, as they rely on cloud infrastructure, but some data is cached in background during app usage to enable offline view as well.

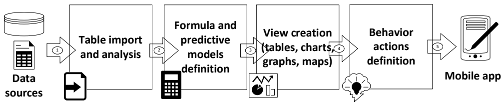

Figure 1. Mobile app creation steps using AppSheet: 1-Data source selection (databases or spreadsheets) 2-Data type settings 3-Selection of desired functions, input and output variables 4-Visualization style selection 5-Selecting the desired actions from the pre-defined list, setting action conditions and parameters.

In Fig. 1, an overview of mobile app creation workflow using AppSheet is given. First, AppSheet analyzes the structure of the selected data sources in order to automatically generate views and user interface enabling basic operations (select, edit, delete, and insert new entry). Moreover, the users can manually change the proposed data types for the columns of imported data. After that, it is possible to write formulas which calculate values of new columns using the existing ones or train predictive models. These calculated values can be added to the data view. Furthermore, it is possible to customize the generated views by selecting the desired visualization method or sorting, grouping and aggregating data. Finally, the application behavior is defined in order to enable transition between different views and embed business logic.

AppSheet mainly aims business use cases, such as customer relationship, personal logs/reports, inventory and project management. However, in scientific literature, many interesting case studies leveraging AppSheet for different purposes have been proposed so far. In [27], AppSheet-based mobile application was used for tree identification and monitoring within urban area. Furthermore, in [28], AppSheet was used together with Apps Script and YouTube API for personalized fitness trainer app implementation. On the other side, in [29], a waste management application was presented. Finally, in [30], two case studies related to adoption of AppSheet in COVID-19 pandemic were presented: indoor safety monitoring (social distancing, temperature and mask check) and critical resource overview and planning (PCR tests, hospital places, medical personnel availability).

B. AR.js

When it comes to augmented reality applications and services on smartphone devices, web is becoming a promising platform in recent years [31]. In this paper, we adopt AR.js for development of marker-based augmented reality user interfaces that enable more convenient energy consumer monitoring and control.

AR.js is an open-source, lightweight JavaScript library for development of augmented reality applications run in web browser [32]. It has broad compatibility including traditional PCs, tablets and smartphones. Moreover, it provides quite good performance on mobile devices without high hardware demands [32]. Furthermore, the development of AR applications based on this library is intuitive and straightforward, giving the ability to develop fully functional AR apps in just several lines of HTML and JavaScript code [33]. The main features of this library include pre-defined set of markers (numeric and QR), handling of device position and location, 3D object loading and animation. In [33], AR.js was approved as effective solution for various types of AR-based user interfaces, such as coordination of devices in robotic testbed, music loop sampler for stage performance and household devices control.

C. Data-Driven Framework for Energy-Efficient Smart Cities

For the first case study presented in this paper, we rely on data-driven framework aiming energy-efficiency in smart cities presented in [34]. It covers several aspects highly relevant for energy management: 1) consumer device monitoring based on affordable IoT devices – Raspberry Pi and smartphones 2) energy consumption prediction 3) anomaly detection 4) relay protection also based on Arduino Uno 5) energy trading based on block-chain technology targeting smart grid prosumers.

The smart home energy management mobile application presented makes leverages most of the capabilities offered by the framework from [34], but relies on its own prediction module provided by AppSheet platform for energy consumption prediction and anomaly detection.

The energy trading mechanism is based on linear optimization model for optimal energy allocation with respect to demand constraints aiming the minimization of overall costs, given as:

$$minimize \sum_{i,j \in SmartHomes} e[i,j]\left(\frac{tc[i,j]}{gc[i]} + dc[i,j]\right) \quad (1)$$

In Eq. 1, $e[i,j]$ refers to the amount of energy that will be sent from $smart\_home[i]$ to $smart\_home[j]$ within a smart grid as a result of energy trading, while it is zero if trading is not performed. Trading price offered by $smart\_home[i]$ to $smart\_home[j]$ is denoted as $tc[i,j]$. Moreover, $gc[i]$ stands for the cost of energy generation at $smart\_home[i]$ for given amount of energy $e[i,j]$. Finally, $dc[i,j]$ refers to the cost of energy distribution from $smart\_home[i]$ to $smart\_home[j]$.

However, for each $smart\_home[i]$ which sends energy during the exchange, the following constraint has to be satisfied:

$$\begin{gathered} te[i] + \sum_{j \in SmartHomes} e[j,i] - \\ -e[i,j] \geq d[i], i \in SmartHomes \end{gathered} . \quad (2)$$

In Eq. 2, $te[i]$ refers to the total amount of energy produced by $smart\_home[i]$, $e[i,j]$ is the energy sent to $smart\_home[j]$, $e[j,i]$ is energy received from $smart\_home[j]$, while $ed[i]$ is the overall energy within $smart\_home[i]$. In other words, this constraint means that each smart home participating in trading should be still able to satisfy its own demand once the trade is done.

D. SMADA-Fog

Fog computing refers to architectures that leverage the devices within the Edge of the network for processing as much as possible in order to overcome latency and data privacy-related issues [35]. It represents one of key-enablers for many smart city scenarios and use cases [36]. For that reason, energy-efficiency of Fog computing is one of crucial factors, when it comes to smart city sustainability. On the other side, from perspective of organizations involved into smart city government or which provide services, considering the fact that Edge servers (both traditional desktop computers or IoT devices) reside inside the boundaries (either physical or jurisdictional) of the organization, energy-efficiency is also highly relevant for overall infrastructure cost reduction.

SMADA-Fog [37] is a semantic-enabled, model-driven framework for modelling, simulation, deployment and adaptivity of services within Fog computing architectures. It relies on Docker [38] technology for deployment of services packed as Docker containers to wide variety of devices, from traditional servers and laptops to low-power IoT devices, such as Raspberry Pi. Moreover, as one of auxiliary tools, it relies on linear optimization model for optimal allocation of services to devices, aiming to achieve the best possible performance, while preserving the energy efficiency (minimum energy consumption):

$$\begin{gathered} maximize \sum_{i \in Services, j \in Devices} allocation[i,j] \times \\ \times \frac{performance[i,j]}{consumption[i,j]} \end{gathered} . \quad (3)$$

In Eq. 3, $allocation[i,j]$ is a binary value which denotes that $service[i]$ is deployed on $device[j]$ in case of value “1”. Moreover, $performance[i,j]$ is the measure describing how good the performance of $service[i]$ on $device[j]$ (greater value means better performance). Finally, $consumption[i,j]$ represents the value of energy consumed by $device[j]$ while running $service[i]$. Moreover, $device[j]$ has to satisfy several constraints, related to execution location (Edge or Cloud), memory, storage and demand requirements of $service[i]$ (more details in [37]).

In this paper, SMADA-Fog’s features related to optimal service allocation to the available devices and Docker-based mechanisms for their deployment are leveraged within the second case study.

III. Case Studies

A. System Architecture Overview

In this subsection, a generalized system architecture overview behind the case study applications will be given. It is illustrated in Fig. 2.

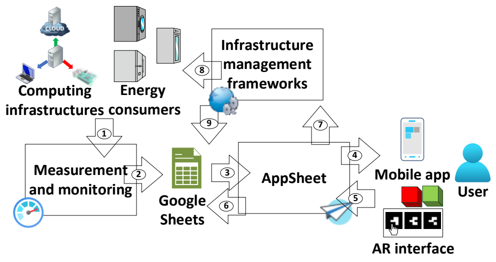

Figure 2. Generalized case study architecture overview: 1-Electric signals 2-Measured data 3-Importing spreadsheets to AppSheet 4-Rendering mobile application 5-User input (via mobile app or AR interface) 6-Insert data into spreadsheet 7-Calling external services 8-Consumer device control 9-Insert results into spreadsheet.

First, the measurement of electric signals coming from energy consumer devices is performed relying on smart meters based on smartphones and IoT devices. The measured values are inserted into Google Sheets document. After that, the spreadsheet is processed by AppSheet platform in order to visualize the data within the mobile application. The user is able to issue commands and take actions related to energy management either directly via mobile app or using augmented reality interface (such as switching devices on/off). During these actions, external services for energy management and low-level consumer device-related operations (such as relay protection system based on Arduino Uno [34] or Docker commands for container management [37]) are triggered via mobile app. Moreover, the external energy management frameworks include optimization procedures, such as optimal energy trading between smart grid prosumers [34], Docker container allocation [37] and, on the other side, block-chain-based energy trade mechanism [34]. Finally, the results of external energy management services execution are written back into Google Sheets, so the updated data is visible to the user.

B. *Energy Management for Smart Home*

The purpose of this mobile application is to provide easy household consumer device monitoring and energy management relying on [34]. The app has three main screens: 1) *Consumers* (Fig. 3a) – showing the list of household devices consuming electricity 2) *Consumption* (Fig. 3b) – which shows the energy prediction for different devices daily 3) *Trading* (Fig. 3c) – provides interface for accepting/rejecting energy trade offers or making new proposals.

For each of the consumer devices, it is possible to see its type (such as air conditioner, washing machine, heater etc.), status – on/off, current energy consumption, location – such as living room, bedroom, consumption prediction for current day and setting the time when to turn off the device automatically. The consumers can be turned on/off remotely using switching system based on Arduino Uno [34]. However, the devices are turned off automatically in case of anomalies relying on relay protection system also using Arduino Uno devices.

Moreover, an AR user interface for easier device management and monitoring is also included. Paper barcode markers are put near the consumer devices which are used by AR application to show 3D cubes serving as buttons. When marker is detected, the information about anomalies, consumption prediction and current consumption appears beside the cube. After that, by placing hands over marker, user can access the corresponding device details screen. In Fig. 4, a screenshot of AR application is shown.

Anomaly detection and consumption prediction are implemented using AppSheet's prediction module. For anomaly detection, the measurements of voltage and frequency of electric signal coming from IoT smart meters are used to classify whether anomalies are present

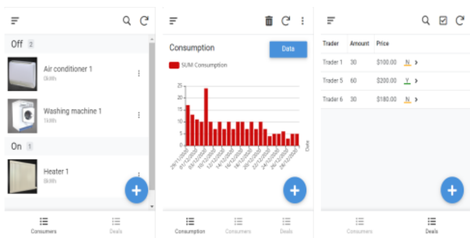

Figure 3. Main screens of energy management mobile application for smart home: a) Consumers b) Consumption 3) Trading.

Figure 4. AR interface mobile application for smart home energy management case study.

for given device or no. On the other side, historical data of device energy consumption together with daily temperature are used to forecast the daily load.

C. *Energy-Efficient Infrastructure Management in Fog Computing*

This mobile application enables convenient remote management of computing infrastructures relying on SMADA-Fog [37]. There are three main screens in the application: 1) *Devices* (Fig. 5a) – contains the list of available devices 2) *Services* (Fig. 5b) – the list of running and stopped services 3) *Mapping* (Fig. 5c) – allocation of services to desired devices.

For each of devices, the following parameters have can be set: identifier – which represents its unique name, architecture – either x86 or ARM for low-power IoT devices, status – turned on or off, IP address, number of working hours, unit consumption, total energy consumption (calculated in AppSheet as product of previous two), maximum load capacity (number of user) and current number of users. Apart from that, by clicking on the desired device, it is also possible to see the list of deployed services and navigate to their management page. Here, user can turn on or off the device remotely by activating the trigger which send call to the external infrastructure management service which responsible for device-level command execution. A detailed device view is shown in Fig. 6a.

In a similar way, it is possible to manage the services using the detailed view, as shown in Fig. 6b. For each of the services, it is necessary to set its unique name, device – identifier of a device where service is deployed, execution location – Cloud or Edge (when it comes to sensitive data storage), status – running, stopped, overloaded (too many users) or failed, load – current number of users demanding the service, number of instances, capacity – how many users can be serviced (depending on the device where the service is deployed and number of instances). By clicking the "Deploy" button, the desired service is deployed to the target device relying on SMADA-Fog framework [37] which constructs corresponding Docker commands. The *Mapping* screen shows the table describing how services are assigned to the devices.

Moreover, there are two more views within the application related to prediction – *Demand* as shown in Fig. 6c and *Consumption*. They leverage AppSheet's prediction module to forecast the number of users that will demand the service in next days, and energy consumption for each of the devices, based on historical data.

Regarding the AR-related capabilities, each device contains a set of barcode markers allocated, while beside each of them appears 3D cube of different color when camera of smartphone running AR interface application is pointed. By putting hands over cube, different command can be activated, such as opening the device detail view (redirection to screen shown in Fig. 6a) or directly showing the device's status, load or energy consumption, as shown for Raspberry Pi in Fig. 7.

However, in case when device is turned off, overloaded or fails, SMADA-Fog executes the optimization procedure to perform the re-deployment of services with respect to the previously described optimization model considering energy-efficiency.

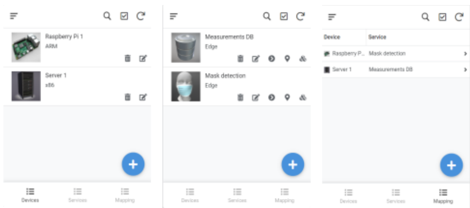

Figure 5. Main screens of Fog computing infrastructure management mobile application: a) Devices b) Services 3) Mapping.

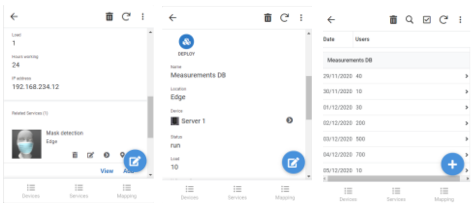

Figure 6. Additional screens of Fog computing infrastructure management mobile application a) Device details b) Service details 3) Demand predictions.

Figure 7. AR interface application for computing infrastructure management case study.

IV. EVALUATION AND RESULTS

Several aspects of evaluation were considered: the development process speed-up compared to traditional mobile app creation approach based on estimations from [39]; time necessary for new app version delivery; AppSheet’s prediction module accuracy in both case studies; application response time in case of complex scenarios involving linear optimization, such as energy trading and container re-deployment when device fails. For the first case study, the scenario with 3 smart homes participating in energy trading was considered. On the other side, for the second case study, the scenario with 4 Fog nodes (three Raspberry Pis and one traditional x86-based server) was evaluated.

During the evaluation, the following devices were used: a laptop equipped with Intel i7 7700-HQ quad-core CPU running at 2.80GHz with 16GB of DDR4 RAM and 1TB HDD acting as server running energy management framework and SMADA-Fog components, two Raspberry Pi 2 devices and 1 Raspberry Pi 3 device acting like Fog nodes. As app clients, two smartphones with different operating systems were used: iPhone 6s Plus smartphone (dual-core, 2GB of RAM) as representative of iOS devices and Xiaomi Redmi Note 7 (octa-core, 3GB of RAM) which is an Android smartphone. As active internet connection was required to run the case study applications, 4G mobile network with 50Mbps download/upload speed was used.

In Table I, the results achieved during the evaluation for case studies 1 and 2 are given. According to the achieved results, the proposed approach of mobile application generation using AppSheet based on Google Sheets as data sources is highly beneficial, as it dramatically speeds up the mobile application development compared to cross-platform solutions, based on estimations from [40]. Moreover, it enables rapid delivery of updates and new features, in just few seconds, without any additional installation, as apps are accessed via AppSheet client. Furthermore, the AppSheet’s consumption prediction model in the first case study achieved accuracy around 91% for anomaly detection (model M1), 88% for energy consumption prediction (M2) and 93% for service demand forecast (M3). The first two modules created in AppSheet show just slightly wore results than [34], which is acceptable, as model training is done in just few clicks using AppSheet, while, on the other side, in [34], customized deep learning neural networks were developed based on TensorFlow in Python programming language, which demands specialized knowledge, much more time and effort. Finally, regarding the service response time, it can be noticed that is about twice longer in the first case study, as it also included generation of smart contracts for energy exchange and blockchain transaction, apart from prediction, linear optimization and command generation.

V. CONCLUSION

Energy-efficiency is one of crucial aspects for smart city sustainability. On the other side, mobile applications play an important role in complex smart city ecosystem. In this paper, two innovative case studies related to energy management within smart cities are presented, developed adopting novel approach to multiplatform mobile application development with much less code, relying on intuitive AppSheet platform. According to the achieved results, the development time of the presented applications was much shorter than in case of traditional cross-platform frameworks (such as Xamarin), the same holds for new version delivery, while AppSheet’s prediction module shows satisfactory performance. Such approach to multiplatform application development is not only beneficial as it can save time and money, but also gives the ability to persons without programming specialization (such as domain experts) to develop complex domain-specific mobile applications.

TABLE I. EVALUATION RESULTS.

<table>
<tr><th rowspan="2">Aspect</th><th colspan="3">Value</th></tr>
<tr><th colspan="2">Case 1</th><th>Case 2</th></tr>
<tr><td>Development speed-up [times]</td><td colspan="2">14 times</td><td>10 times</td></tr>
<tr><td rowspan="2">Delivery time [s]</td><td colspan="2">iPhone 6s Plus</td><td>Xiaomi Redmi Note 7</td></tr>
<tr><td colspan="2">5.03</td><td>4.21</td></tr>
<tr><td rowspan="2">Prediction accuracy [%]</td><td>M1</td><td>M2</td><td>M3</td></tr>
<tr><td>91</td><td>88</td><td>93</td></tr>
<tr><td rowspan="2">Service response [s]</td><td colspan="2">3 traders
1 exchange</td><td>4 nodes
2 containers</td></tr>
<tr><td colspan="2">10.23</td><td>5.81</td></tr>
</table>

ACKNOWLEDGMENT

This work has been supported by the Ministry of Education, Science and Technological Development of the Republic of Serbia.

REFERENCES

[1] Nitoslawski, S. A., Galle, N. J., Van Den Bosch, C. K., & Steenberg, J. W. (2019). Smarter ecosystems for smarter cities? A review of trends, technologies, and turning points for smart urban forestry. *Sustainable Cities and Society*, *51*, 101770.

[2] Komninos, N., Kakderi, C., Panori, A., & Tsarchopoulos, P. (2019). Smart city planning from an evolutionary perspective. *Journal of Urban Technology*, *26*(2), 3-20.

[3] Colding, J., Colding, M., & Barthel, S. (2020). The smart city model: A new panacea for urban sustainability or unmanageable complexity?. *Environment and Planning B: Urban Analytics and City Science*, *47*(1), 179-187.

[4] Roblek, V., Meško, M., Bach, M. P., Thorpe, O., & Šprajc, P. (2020). The interaction between internet, sustainable development, and emergence of society 5.0. *Data*, *5*(3), 80.

[5] Lee, J., & Yang, J. S. (2019). Global energy transitions and political systems. *Renewable and Sustainable Energy Reviews*, *115*, 109370.

[6] Carréon, J. R., & Worrell, E. (2018). Urban energy systems within the transition to sustainable development. A research agenda for urban metabolism. *Resources, Conservation and Recycling*, *132*, 258-266.

[7] Dincer, I., & Acar, C. (2017). Smart energy systems for a sustainable future. *Applied Energy*, *194*, 225-235.

[8] Nižetić, S., Šolić, P., González-de, D. L. D. I., & Patrono, L. (2020). Internet of Things (IoT): Opportunities, issues and challenges towards a smart and sustainable future. *Journal of Cleaner Production*, *274*, 122877.

[9] Sánchez-Corcuera, R., et al. (2019). Smart cities survey: Technologies, application domains and challenges for the cities of the future. *International Journal of Distributed Sensor Networks*, *15*(6), 1550147719853984.

[10] Bibri, S. E., & Krogstie, J. (2020). The emerging data–driven smart city and its innovative applied solutions for sustainability: the cases of London and Barcelona. *Energy Informatics*, *3*(1), 1-42.

[11] Turgel, I., Bozhko, L., Ulyanova, E., & Khabdullin, A. (2019). Implementation of the Smart City Technology for Environmental Protection Management of Cities: The Experience of Russia and Kazakhstan. *Environmental and Climate Technologies*, *23*(2), 148-165.

[12] van Niekerk, A. J. (2020). Inclusive Economic Sustainability: SDGs and Global Inequality. *Sustainability*, *12*(13), 5427.

[13] Macke, J., Sarate, J. A. R., & de Atayde Moschen, S. (2019). Smart sustainable cities evaluation and sense of community. *Journal of Cleaner production*, *239*, 118103.

[14] Kutty, A. A., Abdella, G. M., Kucukvar, M., Onat, N. C., & Bulu, M. (2020). A system thinking approach for harmonizing smart and sustainable city initiatives with United Nations sustainable development goals. *Sustainable Development*, *28*(5), 1347-1365.

[15] Roblek, V., & Meško, M. (2020, June). Smart city knowledge management: Holistic review and the analysis of the urban knowledge management. In *The 21st Annual International Conference on Digital Government Research* (pp. 52-60).

[16] Cassandras, C. G. (2016). Smart cities as cyber-physical social systems. *Engineering*, *2*(2), 156-158.

[17] Alsamhi, S. H., Ma, O., Ansari, M. S., & Almalki, F. A. (2019). Survey on collaborative smart drones and internet of things for improving smartness of smart cities. *Ieee Access*, *7*, 128125-128152.

[18] Shu, L., Mukherjee, M., Pecht, M., Crespi, N., & Han, S. N. (2017). Challenges and research issues of data management in IoT for large-scale petrochemical plants. *IEEE Systems Journal*, *12*(3), 2509-2523.

[19] Khajenasiri, I., Estebsari, A., Verhelst, M., & Gielen, G. (2017). A review on Internet of Things solutions for intelligent energy control in buildings for smart city applications. *Energy Procedia*, *111*, 770-779.

[20] Borgia, E. (2014). The Internet of Things vision: Key features, applications and open issues. *Computer Communications*, *54*, 1-31.

[21] Del Rio, D. D. F., Sovacool, B. K., Bergman, N., & Makuch, K. E. (2020). Critically reviewing smart home technology applications and business models in Europe. *Energy Policy*, *144*, 111631.

[22] Hassan, W. H. (2019). Current research on Internet of Things (IoT) security: A survey. *Computer networks*, *148*, 283-294.

[23] Liu, Y., Yang, C., Jiang, L., Xie, S., & Zhang, Y. (2019). Intelligent edge computing for IoT-based energy management in smart cities. IEEE Network, 33(2), 111-117.

[24] Minoli, D., Sohraby, K., & Occhiogrosso, B. (2017). IoT considerations, requirements, and architectures for smart buildings—Energy optimization and next-generation building management systems. *IEEE Internet of Things Journal*, *4*(1), 269-283.

[25] Marinakis, V., & Doukas, H. (2018). An advanced IoT-based system for intelligent energy management in buildings. *Sensors*, *18*(2), 610.

[26] *AppSheet.* Available at: https://www.appsheet.com/.

[27] Martins, L., Macedo, F., & Saraiva, S. (2018). IDTREE: a mobile app for the management of urban trees. *Revista de Ciências Agrárias*, *41*(Especial), 31-38.

[28] Radenković, M., Petrović, N., & Nejković, V. (2020). Razvoj podacima-vođenih multiplatformskih mobilnih aplikacija korišćenjem AppSheet i Apps Script na osnovu Google Sheet tabela u oblasti zdravlja. In *IEEESTEC – 13th Student Projects Conference*, 1-4.

[29] Arumugam, S. K., Muhamad, R., & Yahya, K. (2020, May). Mapping of construction waste for eco-costs per value ratio (EVR) index using Google My Maps in Shah Alam, Malaysia. In *IOP Conference Series:*

Materials Science and Engineering (Vol. 849, No. 1, p. 012046).

[30] Petrović, N., Radenković, M., & Nejković, V. (2020). Data-Driven Mobile Applications Based on AppSheet as Support in COVID-19 Crisis. In *IcETRAN 2020* (pp. 1-6).

[31] Qiao, X., Ren, P., Dustdar, S., Liu, L., Ma, H., & Chen, J. (2019). Web AR: A promising future for mobile augmented reality—State of the art, challenges, and insights. *Proceedings of the IEEE*, *107*(4), 651-666.

[32] J. Etienne. *Creating Augmented Reality with AR.js and A-Frame*. Available at: https://aframe.io/blog/arjs/.

[33] Đorđević, L., Petrović, N., & Tošić, M. (2020). An ontology-based framework for automated code generation of Web AR applications. *Telfor Journal*, *12*(1), 67-72.

[34] Petrović, N., & Kocić, Đ. (2020). Data-driven framework for energy-efficient smart cities. *Serbian Journal of Electrical Engineering*, *17*(1), 41-63.

[35] Bermbach, D., et al. (2017, November). A research perspective on fog computing. In *International Conference on Service-Oriented Computing* (pp. 198-210). Springer, Cham.

[36] Dong, Y., Guo, S., Liu, J., & Yang, Y. (2019). Energy-efficient fair cooperation fog computing in mobile edge networks for smart city. *IEEE Internet of Things Journal*, *6*(5), 7543-7554.

[37] Petrovic, N., & Tosic, M. (2020). SMADA-Fog: Semantic model driven approach to deployment and adaptivity in Fog Computing. *Simulation Modelling Practice and Theory*, *101*, 102033.

[38] Docker. Available at: https://www.docker.com/.

[39] Delia, L., Galdamez, N., Thomas, P., Corbalan, L., & Pesado, P. (2015, May). Multi-platform mobile application development analysis. In *2015 IEEE 9th International Conference on Research Challenges in Information Science (RCIS)* (pp. 181-186). IEEE.

Thermal Performance Evaluation of a Flat-Plate Hybrid Photovoltaic-Tharmal Air Collector in South-East Nigeria

Howard O. Njoku[1], Julius M. Dzah[2], Mkpamdi N. Eke[3], Valentine O. Ekechukwu[4], Gabriel Takyi[5]

[1]Applied Renewable and Sustainable Energy Research Group, Department of Mechanical Engineering, University of Nigeria, Nsukka. 410001, Nigeria, howard.njoku@unn.edu.ng
[2,3,4]University of Nigeria, Nsukka, Nsukka, Nigeria, julius.dzah.fs59264@unn.edu.ng[2]; eke.mkpamdi@unn.edu.ng[3]; ovekechukwu@yahoo.com[4]
[5]Kwame Nkrumah University of Science and Technology, Kumasi, Ghana, gabrieltakyi@yahoo.co.uk

Abstract—**This study focuses on thermal performance evaluation of a hybrid PVT air collector under real outdoor conditions at the University of Nigeria, Nsukka, South-East Nigeria. Three scenarios (I, II and III) of forced convection were considered. The thermal efficiency, heat gain with insolation for each of the scenarios had similar trends from the results obtained. The maximum thermal efficiencies and the useful heat gains of the three scenarios were 59% and 1.75W for scenario I, 43% and 0.214W for scenario II, and 42.5% and 0.20W for scenario III at maximum insolation of 950, 980 and 955 W/m^2 respectively. The thermal cumulative efficiencies of the cases were 0.5, 0.29 and 0.18 for scenario I, II and III respectively. The Scenario I, which had the greatest forced convection produced the highest cumulative thermal efficiency. Thermal images for the absorber also showed the surface temperature distribution of the collector for a typical sunny day. It can be concluded from the results that, higher forced convection produces higher thermal performance of a hybrid PVT air collector.**

Keywords – hybrid PVT air collector, thermal efficiency, insolation, infrared, thermal image

I. Introduction

The Sun is the central resource for generating all kinds of renewable energies and it controls the climatic conditions of the earth. Renewable energy technologies are considered as clean sources of energy. They are sustainable based on current and future environmental safety concerns arising from the use of fossil fuel sources. The quest to generate and utilize energy from clean sources is of a global concern since the world has recognized that greenhouse gases are key contributors to the devastating global warming with its effects that threatens the safety and existence of life on earth. In order to alleviate the effect of the aforementioned situation, the Sustainable Development Goal (SDG) 7 stated that every country must ensure access to affordable, reliable, sustainable and modern energy for all. Between 1990 and 2010, the number of people globally with access to electricity has increased by 1.7 billion [1].

This paper aimed at energy-efficient technologies that uses solar energy resource to achieve the UN guidelines on agenda 2030 [2].

Solar energy is one of the most abundant renewable energy resources for economic growth and sustainability. It can be harnessed and utilized with two major types of technologies namely photovoltaic technology and solar thermal technology [3, 4]. The hybrid PVT system combines utilization of both technologies for electricity and heat generation as shown in Fig. 1.

II. DESCRIPTION OF PVT COLLECTOR

PVT collectors are hybrid technologies that combine both PV components and solar thermal components into a single unit such that the system not only makes use of solar energy by converting it to electrical energy, but also makes use of the excess thermal energy [5,6]. The flat-plate hybrid solar PVT collector consist of the PV cells that produces electricity, heat transfer fluid (which is usually water and/or air, and other existing fluid options such as air or nano-fluid), channels for fluid passage in and out of the system, absorber or collector, glazing, fans (optional) and thermal insulation to minimize the heat loss . Removing heat from PV cells also has the benefit of reducing thermal cycles and stresses [7]. Flat plate PVT collectors designed can be such that the PV component serves as the thermal absorber or in other cases, may just be a part of the hybrid flat plate PVT collector. Reference [8] showed the internal view of a typical flat plate PVT collector as shown in Fig. 2. PVT collectors make better economic use of the available space as compared with separate modules of PV and solar thermal collectors lying side-by-side to each other aside the fact that PVT collectors have a higher aesthetic appearance than separate systems.

There are many literature surveys on the application of PVT systems. Heat generated from PVT system is usually used for domestic hot water (DHW) production, drying or space heating. A PVT collector may have of a PV module (5% to 20% efficiency) and a heat removal device such as thermo-electric coolers [9]. The rationale for the emergence of PVT collectors was mainly to regulate and reduce the temperature of solar PV cells so that cell performance does not experience much loss due to high temperature.

The increase in temperature of PV cells leads to about 0.4% to 0.5% reduction of the electrical output of both the mono-crystalline and poly-crystalline cells per a degree rise in temperature [10-12] while for the amorphous silicon based cells a reduction of about 0.25% per degree rise in temperature will be experienced [13]. To maximize heat transfer in a PVT system and ameliorate its overall performance, the metal fins was employed at the back wall of the air duct [14]. Reference [15] experimented a novel hybrid PVT system with graphite, the efficiency of the system increased up to 7.2%. Using theoretical models of PVT systems, simultaneous cost reduction and energy conversion efficiency enhancement became feasible [16]. Based on the exergo-environmental analyses of glazed and unglazed hybrid PVT tiles, annual carbon dioxide emission reduction on the basis of overall thermal energy gain of glazed and unglazed hybrid PVT tile air collectors is higher by 27.7% and 62.3%, respectively [17].

Many new collector designs appeared on the commercial market over the past five years. There is need for standard tests to provide distinctive operating features of collectors. Information on how a collector absorbs energy, how it loses heat, the effects of angle of incidence of solar radiation, the significant heat capacity effects and the performance of the PV component hence the need for this study the features of an already existing PVT air collector constructed by [18].

III. AIR COLLECTOR PVT CONFIGURATION

PVT air collector is simply a flat- plate solar air heater with photovoltaic cells pasted on the black absorber plate [19]. PVT air cooling

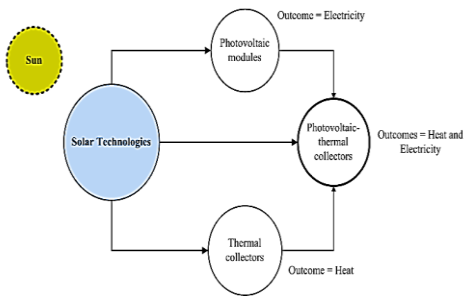

Figure 1. Concept of a PVT hybrid collector outputs.

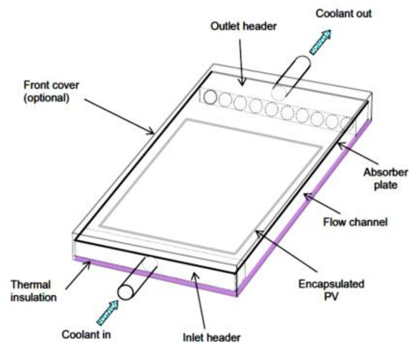

Figure 2. Internal Features of a Traditional PVT Collector [8].

design offers a simpler and economical solution to PV cooling than that of PVT water cooling. PVT air collectors have an important advantage over PVT liquid collectors, as the latter need thermal collecting materials attached to conventional PV modules [20]. Air can be heated to different temperature levels through forced or natural flow. Air-cooling, whether forced or natural flow, presents a less expensive and simple method of PV cooling and solar pre-heated air could be utilized in buildings for space heating in temperate zones as stated by [21,22]. However, PVT air system configurations have limited thermal performance due to low density, small volumetric heat capacity and low thermal conductivity of air. Air cooling configurations of solar PVT collectors can be further classified into forced convection and natural convection techniques. There are also different classes of PVT air collectors distinguished according to the air flow pattern and channel, presence or absence of glazing and the type of pass. PVT air designs have also been proved to be cheaper to construct compared to PVT water designs according to [23]. Reference [24] designed and evaluated the performance of single pass and double pass PVT air cooling systems for air heating under different conditions of flow rate, packing factor, collector length and duct depth. Their investigation showed 24-28% thermal efficiency and 30-35% combined efficiency for single pass, whereas the double pass PVT air heating system had 32-34% thermal efficiency and 40-45% combined efficiency. Reference [25] worked on various concepts of combined PVT collectors. With their approach to obtain maximum yield, they could not state categorically whether the yield of a complicated design would be substantially higher than the yield of a simple design. They considered and evaluated nine different designs and concluded that PV-on-sheet-and-tube design in a solar heating system was only 2% worse but was easier to manufacture and hence was said to be a good alternative. Reference [26] studied parameters affecting the performance of PVT systems such as glazed versus unglazed PVT collectors, optimum mass flow rate, packing factor, design configuration and types. They also analyzed absorber plate parameters including tube spacing, tube diameter and fin thickness. Reference [27] performed computer simulations with a view to improving the solar radiation absorptance and alleviate the high infrared emittance of flat plate PVT/air collector model. The simulation revealed that PVT/air collectors are generally less efficient than the liquid ones due to low PV cell packing factor, high IR emittance, low solar radiation absorptance and poor absorber-to-air heat transfer coefficient. Reference [28] made acomparative study for two different configurations of PV modules; where Module A was an isolated PV module and Module B, a PV module placed on a steel roof to investigate the effect of air-cooled natural and forced convection on temperature and efficiency of the different modules. It was shown that Modules B in both cases experienced higher temperatures. Module A showed lower temperatures for all forced fluid velocities. They concluded that forced convection produced about 7ºC lower temperatures for each aspect ratio considered and that had 3-5% gain in efficiency over natural convection in both cases. Reference [29] performed an experiment on different PVT system glazing configurations as follows; uncovered, single sheet covering and double sheet covering. It was seen at the end of the experiment that the uncovered sheet and tube collectors had the worst performance due to the large amount of heat losses. On the other hand, the electrical efficiency of sheet and tube collectors with double covering (glazing) recorded the worst performance due to the presence of the second cover which contributes to larger amount of optical losses. Fig. 3 shows the cross sectional views of different air pass configurations with different numbers of glazing.

IV. MATERIALS AND METHOD

The material for the experiment include fans, measuring devices such multi-channel thermometer, infrared thermal imager, multimeter, hotwire anemometer and solarimeter. The experimental method adopted was testing collector thermal performances under three scenarios (Scenario 1, II and III) of

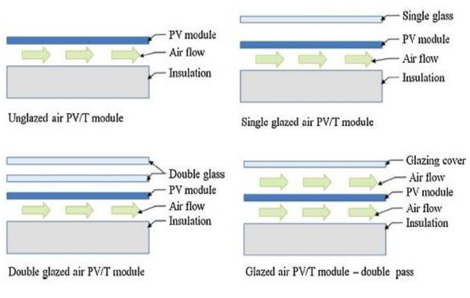

Figure 3. Different configurations of air pass with different configuration of glazing studied by [29].

Figure 4. Test procedure for experimental characterization of the PVT air collector.

forced convection based on the number of fans operated in each scenario. Test procedure is shown at Fig. 4.

For scenario 1, the efficiencies of collector were determined when all six fans were in operation. In the case of scenario II, efficiencies were determined when four fans were in operation and two disconnected. This was done to investigate the effects of reducing the number of operating fans by two. Scenario III was determination of collector efficiencies with two fans operating and four fans disconnected from the power source.

Data collected for the experiments were between 10:00 hrs to 15:00 hrs. These data permitted the characterization of a collector's parameters to indicate how the collector absorbs and loses energy to the surroundings. The PVT system used for the experiment was the work done by [22] at University of Nigeria, Nsukka. The test procedure for the experiment is shown in Fig. 5.

A. *Model Equations for the PVT System*

The actual useful energy gain from the collector is given as:

$$Q_u = \dot{m}C_p(T_s - T_1)\,. \tag{1}$$

The useful energy gain if whole collector were at the fluid inlet temperture is given by:

$$Q_u = A_c F_R\left[G_T(\tau\alpha) - U_L(T_i - T_0)\right]\,. \tag{2}$$

The quantity that relates the actual useful energy gain of a collector to the useful gain if whole collector were at the fluid inlet temperture. This quantity is the heat removal factor which can be calculated from Eqs. (1) and (2) as:

$$F_R = \frac{\dot{m}C_p(T_s - T_1)}{A_c\left[G_T(\tau\alpha) - U_L(T_i - T_0)\right]}. \tag{3}$$

The thermal efficiency of the collector is calculated from Eq. (4):

$$\eta_{th,c} = \frac{\dot{m}C_p(T_{out} - T_{in})}{A_C G_T}\,. \tag{4}$$

The cumulative thermal efficiency of collector of the of collector is given by:

$$\eta_{cumth,c} = \frac{\sum_{i=1}^{m}(Q_u)_i}{A_C\sum_{j=1}^{m}(G_T)_j}\,. \tag{5}$$

V. Results and Discussion

The result of experiments conducted on the system for all the scenarios were presented in Fig. 7, Fig. 8. and Fig. 9. For scenario I shown

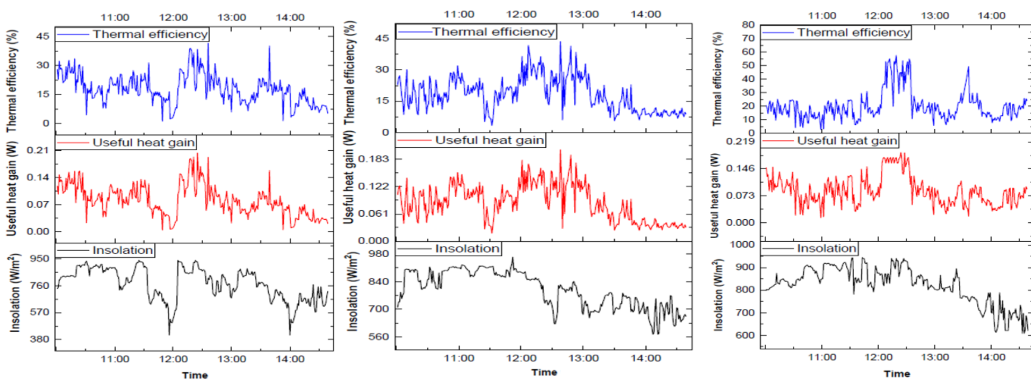

Figure 5. Thermal efficiency, useful heat gain and insolation for Scenario I, II and III.

in Fig. 5a, the thermal efficiencies of the system fluctuated within the range of 5% to 27% from 10 am to about 12 noon when it attained its peak at 58%. It continued varying at values close to the peak value for almost an hour when the thermal efficiency began to drop again in an unsteady manner. The useful heat gain plotted in the same figure had a similar shape as the thermal efficiency. The useful heat gain varied unsteadily within the range of 0.008 to 0.13W from 10 am to 12 noon. As with the thermal efficiency, the useful heat gain rose sharply to peak value of 0.18W at 12.15 pm and remained constant until 12.32 pm when it drop to lower values.

For Scenario II, the plot of thermal efficiency and useful heat against as a function of time are shown in Fig. 5b. The plot had similar profile. The thermal efficiency varied between 5% and 40% until mid-day with the minimum thermal efficiency recorded at around 11:30 am. Thermal efficiency was highest at values ranging from 30% to 42% between the hours of 12 noon until about 13:00 hours and then reduced to efficiency values between 7% and 20% around 13:40 hours. For the rest of the period between 13:40 hours to 14:40 hours, there was an unsteady variation closely around 13% thermal efficiency. The rate of useful heat gain also varied unsteadily between 0.03 and 0.14 W until midday. However, the minimum rate of useful heat gain was observed to occur at 11:30 am. The highest useful heat gain values of 0.122 to 0.19 W were recorded between the hours of 12 noon until about 13:00 and then reduced to values ranging between 0.3 and 0.82 W and remained in that range until 13:40 hours. The rest of the useful heat gain values varied unsteadily within a small range of 0.05 and 0.06 W from 13:40 to 14:40 hours. Insolation variation was unsteady throughout the period. Unlike the two preceding observations, solar variation did not portray very similar variation under this scenario. Insolation was relatively high 700 and 980 W/m^2 between the hours of 10:00 am to 12:20 pm. The highest and lower insolations were observed 11:50 am and 12:30 pm respectively. It was also observed that the period between the highest and lower insolation under this scenario coincided with the period where both thermal efficiency and useful heat gain were relatively high. After 13:00 hours, the insolation dropped gradually in an unsteady manner until it hit its minimum values at 14.10 hours.

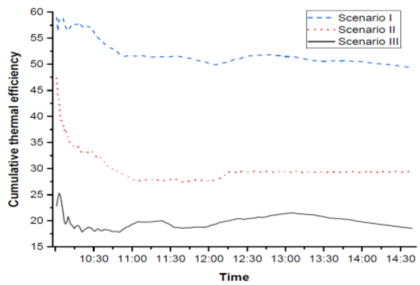

Figure 6. Cumulative thermal efficiencies against time for the three scenarios.

As for scenario III shown in Fig. 6, the plot had similar trend to the two previous scenarios. Unlike the two previous scenarios, thermal efficiency and useful heat gain exhibited more similarity than with insolation. Thermal efficiency and useful heat gain varied unsteadily throughout the period in the range 6% to 42% and 0.01 W to 0.21 W respectively. It showed very low values of 6% and 0.01 W of thermal efficiency and useful at an insolation level of 390 W/m^2 between the 11:30 am and 12:00 noon. These lowest conditions reoccurred at around 14:00 hours. On the other hand, the highest efficiencies and useful heat gain were 42% and 0.21 W respectively which occurred at 12:30 hours at insolation of 950 W/m^{2}The instantaneous thermal efficiencies cannot be used to clearly depict performances of air collector under different scenarios considered in this study. However, the cumulative thermal efficiency (CTEF) was used to differentiate between how various forced convection scenarios affect the thermal efficiency. Fig. 6 shows the cumulative thermal efficiency plots for all three scenarios with Scenario I having the highest value of 0.5. It is followed by scenario II and III with CTEF of 0.29 and 0.18 respectively.

VI. THERMAL CHARACTERIZATION

The instantaneous efficiencies of the collector obtained from eqn (4) were plotted against the reduced temperature parameter $(T_{av}-T_{amb})/G_T$, for the three scenarios of forced convection and shown in Fig. 7, Fig. 8 and Fig. 9. The thermal test data conversion was developed by researchers as model that can be used to predict thermal performances of thermal systems. The intercept on y-axis gives the value of value of factor FR(τα) and slope of the lines represent the value of FRUL. From the scatter plots, the FR(τα) and FRUL for the three

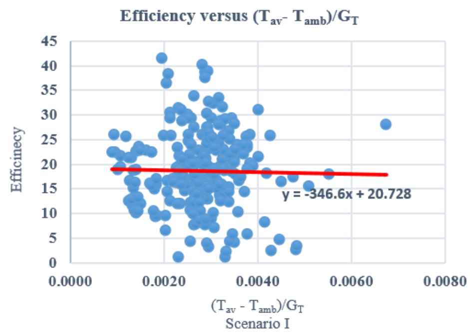

Figure 7. Thermal efficiency against reduced temperature parameter for Scenario I.

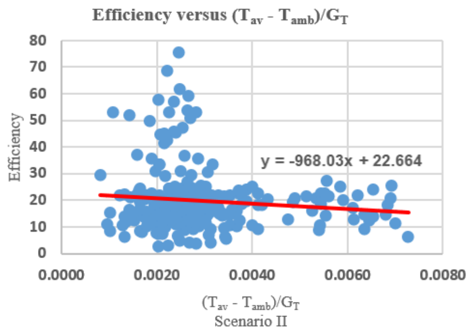

Figure 8. Thermal efficiency against reduced temperature parameter for Scenario II.

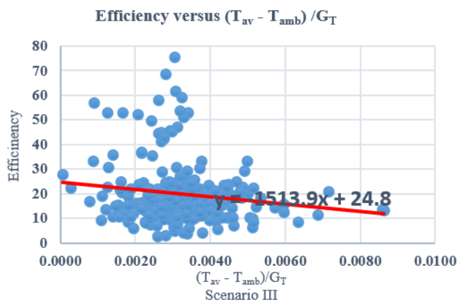

Figure 9. Thermal efficiency against reduced temperature parameter for Scenario III.

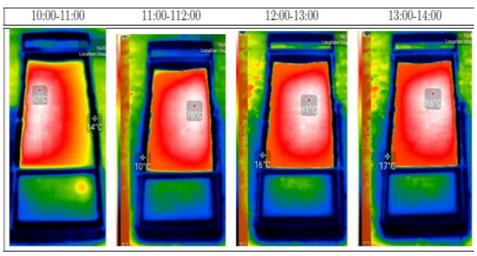

Figure 10. Infrared thermal images of collector on during experiment showing surface temperature across the collector.

scenarios have been shown on the equations of the lines of best fit. Further extension of the lines on either side will lead to intercept on Y and X axes. The intercept of the line on the y-axis is called as optical efficiency or maximum efficiency point. Scenarios I, II and III had optical efficiencies of 0.21, 0.23 and 0.25 respectively.

From the scatter plot, it is evident that Scenario III had the highest optical efficiency (at the y-intercept where heat losses are zero), followed by Scenario II and then lastly by Scenario I. These results were gotten from real outdoor conditions and might have been affected by the climate conditions on the day of experiment.

The gradient of the equation which represents the parameter of heat loss from the hybrid PVT air collector. The overall heat loss coefficient UL represents the heat loss from the collector in the form of convection, conduction and radiation. UL is a function of temperature and wind speed, with dependence as the number of covers increase (which is constant in this experiment). Even though Scenario III had the highest optical efficiency, it also had the highest heat loss coefficient among the three scenarios, followed by Scenario II and Scenario I respectively. This implies that Scenario III lost heat at a much faster rate than scenario II and I. Scenario I having the least heat lost may be as a result of it having the highest form of forced convection (mass ow rate) which in turn caused the collector the make use of the useful heat faster than in the other scenarios whose mass flow rate were not as high as that of Scenario I.

VII. IR Thermal Images of an Operating PVT on a Typical Sunny Day

Thermal images for the absorber were also take from the start of the experiment on a typical sunny day (Fig. 10). This infrared analysis was not done for the separate scenarios under consideration. Between 10:00 to 11:00 at insolution level of 672 W/m^2, the collector temperature was 67^{o}C. From 11:00 to 12:00, insolation level increased gradually but unsteadily within smaller margins of between 660 W/m2 to 730 W/m^2, resulting in accumulation of heat on the PV cell. From 12:00 - 13:00, the radiation level continued to increase but unsteadily between 700 and 840 W/m2 resulting in a peak temperature recording of 91^{0}C during the experiment. The observed absorber temperature increase is not only a factor of level of radiation but also the accumulation of temperature and warm surrounding. The absorber temperature from the time period of 13:00-14:00 recorded an absorber temperature of 86 ^{o}C. Furthermore, the absorber temperature variation could also be affected by prevailing wind conditions. The other smaller temperatures record at the edge of the absorber shows the temperature of the insulating material that was exposed to radiation. It was expected to record the least temperature in all cases since neither absorb nor conduct heat.

Acknowledgment

My sincere acknowledgments to my two supervisors and my sponsors DAAD for their contributions that led to the success of this research project.

I shall not forget to appreciate my colleagues; Jacob, Evans, Andrew, Stephen and Emmanuel who were always available to assist me in different forms while I was undertaking this research.

References

[1] The United Nations Development Programme (UNDP). (2015). *Sustainable Development Goals*.

[2] United Nations. (2015). *Transforming the world: the 2030 agenda for sustainable development*. United Nations, New York,.

[3] Renewable Energy Policy Network for 21st Century. (2017). *Renewables 2017 Global Status Report*. REN21 Secretariate, Paris.

[4] International Energy Agency. (2019). *World Energy Outlook 2019*. IEA Publications.

[5] Duffie, J. A., & Beckman, W. A. (2013). *Solar engineering of thermal processes*. John Wiley & Sons.

[6] Imenes, A. G., & Mills, D. R. (2004). Spectral beam splitting technology for increased conversion efficiency in solar concentrating systems: a review. *Solar Energy Materials and Solar Cells*, *84*(1-4), 19-69.

[7] Zaraket, J., Aillerie, M., & Salame, C. (2017). Capacitance evolution of PV solar modules under thermal stress. *Energy Procedia*, *119*, 702-708.

[8] Dubey, S., & Tiwari, G. N. (2008). Thermal modeling of a combined system of photovoltaic thermal (PV/T) solar water heater. *Solar Energy*, *82*(7), 602-612.

[9] Aste, N., Chiesa, G., & Verri, F. (2008). Design, development and performance monitoring of a photovoltaic-thermal (PVT) air collector. *Renewable Energy*, *33*(5), 914-927.

[10] Zhang, X., Zhao, X., Smith, S., Xu, J., & Yu, X. (2012). Review of R&D progress and practical application of the solar photovoltaic/thermal (PV/T) technologies. *Renewable and Sustainable Energy Reviews*, *16*(1), 599-617.

[11] Michael, J. J., Iniyan, S., & Goic, R. (2015). Flat plate solar photovoltaic–thermal (PV/T) systems: a reference guide. *Renewable and Sustainable Energy Reviews*, *51*, 62-88.

[12] Wang, R. Z., & Zhai, X. Q. (2010). Development of solar thermal technologies in China. *Energy*, *35*(11), 4407-4416.

[13] Shah, A., Torres, P., Tscharner, R., Wyrsch, N., & Keppner, H. (1999). Photovoltaic technology: the case for thin-film solar cells. *Science*, *285*(5428), 692-698.

[14] Tonui, J. K., & Tripanagnostopoulos, Y. (2007). Improved PV/T solar collectors with heat extraction by forced or natural air circulation. *Renewable Energy*, *32*(4), 623-637.

[15] Liang, R., Zhang, J., Ma, L., & Li, Y. (2015). Performance evaluation of new type hybrid photovoltaic/thermal solar collector by experimental study. *Applied Thermal Engineering*, *75*, 487-492.

[16] de Keizer, C., de Jong, M., Mendes, T., Katiyar, M., Folkerts, W., Rindt, C., & Zondag, H. (2016). Evaluating the thermal and electrical performance of several uncovered PVT collectors with a field test. *Energy Procedia*, *91*, 20-26.

[17] Agrawal, S., & Tiwari, G. N. (2013). Overall energy, exergy and carbon credit analysis by different type of hybrid photovoltaic thermal air collectors. *Energy Conversion and Management*, *65*, 628-636.

[18] Ezegwui, C. C. (2018). *Development and evaluation of a PVT solar air collector*. Department of Mechanical Engineering, University of Nigeria, Nsukka.

[19] Hegazy, A. A. (2000). Comparative study of the performances of four photovoltaic/thermal solar air collectors. *Energy Conversion and Management*, *41*(8), 861-881.

[20] Kim, J. H., Park, S. H., & Kim, J. T. (2014). Experimental performance of a photovoltaic-thermal air collector. *Energy Procedia*, *48*, 888-894.

[21] Chow, T. T. (2010). A review on photovoltaic/thermal hybrid solar technology. *Applied Energy*, *87*(2), 365-379.

[22] Tonui, J. K., & Tripanagnostopoulos, Y. (2007). Improved PV/T solar collectors with heat extraction by forced or natural air circulation. *Renewable Energy*, *32*(4), 623-637.

[23] Tripanagnostopoulos, Y., Nousia, T. H., Souliotis, M., & Yianoulis, P. (2002). Hybrid photovoltaic/thermal solar systems. *Solar Energy*, *72*(3), 217-234.

[24] Sopian, K., Yigit, K. S., Liu, H. T., Kakac, S., & Veziroglu, T. N. (1996). Performance analysis of photovoltaic thermal air heaters. *Energy Conversion and Management*, *37*(11), 1657-1670.

[25] Zondag, H. A., De Vries, D. W., Van Helden, W. G. J., Van Zolingen, R. J. C., & Van Steenhoven, A. A. (2003). The yield of different combined PV-thermal collector designs. *Solar Energy*, *74*(3), 253-269.

[26] Riffat, S. B., & Cuce, E. (2011). A review on hybrid photovoltaic/thermal collectors and systems. *International Journal of Low-Carbon Technologies*, *6*(3), 212-241.

[27] Sarhaddi, F., Farahat, S., Ajam, H., Behzadmehr, A. M. I. N., & Adeli, M. M. (2010). An improved thermal and electrical model for a solar photovoltaic thermal (PV/T) air collector. *Applied Energy*, *87*(7), 2328-2339.

[28] Mazón-Hernández, R., García-Cascales, J. R., Vera-García, F., Káiser, A. S., & Zamora, B. (2013). Improving the electrical parameters of a photovoltaic panel by means of an induced or forced air stream. *International Journal of Photoenergy*, *2013*.

[29] Zondag, H. A. (2008). Flat-plate PV-Thermal collectors and systems: A review. *Renewable and Sustainable Energy Reviews*, *12*(4), 891-959.

Greenhouse Gas Analysis of Energy Transition in Breweries

Daniel de Paula Diniz[1], Monica Carvalho[2]

[1]Graduate Program in Mechanical Engineering, Federal University of Paraiba, João Pessoa, Brazil, danieldiniz@cear.ufpb.br

[2]Department of Renewable Energy Engineering, Federal University of Paraiba, João Pessoa, Brasil, monica@cear.ufpb.br

Abstract—**In Brazil, the use of solar thermal energy in industrial processes is still incipient compared to other countries. Within the industrial branches that require process heat, the food and beverage industries stand out, especially breweries, with processes demanding high levels of energy and long execution times. This study compared two commonly used energy sources for heat generation in breweries, diesel and electricity, with the heat generated by solar thermal collectors. The Life Cycle Assessment (LCA) methodology was employed to quantify the emissions of greenhouse gases (GHG), using SimaPro v.9.0.0.49 software and the Ecoinvent database. The environmental impact assessment method selected was the IPCC 2013 GWP 100y, which groups the GHG emissions in terms of kg CO_2-eq. The study included fixed emissions associated with equipment, the lifetime, and the operational emissions associated with energy flows. Considering the annual operation of a brewery, it was verified that the partial replacement of traditional sources by solar thermal energy proved to be very effective, representing -770 kg CO_2-eq and -629 kg CO_2-eq for every 20% of diesel and electricity replaced, respectively.**

Keywords – sustainability, life cycle assessment, carbon footprint, industry, solar thermal

I. Introduction

With population growth, technological development, and improvement in the living conditions of society, global energy demand has grown considerably and this has had negative impacts on the environment as most of this energy derives from fossil fuels [1]. This highlights the need for improvement and application of technologies that use reliable and preferably renewable energy sources, becoming necessary to ensure the supply of future energy demands and minimize environmental impacts.

Solar energy technologies have been increasingly employed as an alternative to reduce the environmental impacts associated with climate change and dependence on fossil fuels – however, in Brazil, despite the considerable solar potential, solar technology encouragement is still incipient [2]. Solar energy technologies have been demonstrated to mitigate climate change through reducing energy-related emissions [3], and can be divided into photovoltaic solar technologies and solar thermal technologies.

Solar thermal applications include heating water or air, drying, distillation, and cooking, to name a few. These heated fluids can in turn be used for power generation or refrigeration purposes. Among these, solar water heating systems have the highest potential of application because they can be used for a broad variety of purposes [4].

Solar energy applications in the Brazilian industrial sector are important to contribute to the sustainable development of the country. Brazil has been privileged with solar irradiation and the widespread adoption of solar technologies can contribute to the reduction of greenhouse gas emissions [5]. Extracting the maximum thermodynamic potential of resources is an important energy efficiency strategy, and is essential in energy transition, as mentioned by [6], who reported a detailed study on landfill biogas utilization, and [7], who used industrial biosolid for the fertilization of elephant grass for energy purposes.

The global advancement of solar thermal energy technologies for industrial process heat and its future prospects has been reviewed by [8],

ISBN: 978-86-80616-07-0

who mentioned that about 32–35% of the entire global energy is consumed in the industrial sectors. In Brazil, the industrial sector consumes approximately 33% of all energy produced in the country - only 20% is related to electricity while the other 80% originates from other sources (renewable and from fossil fuels) [1]. Most of the energy consumed by Brazilian industries is associated with process heat generation [9]. From an environmental point of view, the industrial sector also appears as one of the major villains when analyzing the total anthropogenic emissions associated with the Brazilian energy matrix: the industrial sector accounts for approximately 19% of total emissions (435.8 Mt CO_2-eq), second only to the transportation sector, which is responsible for 45.8% [10].

Reference [8] have reported that 30% of industrial heat energy consumption is under 150°C, 22% is at intermediate temperatures between 150°C and 400°C, and the remaining 48% at high temperatures above 400°C. More specifically, in the food and beverage industry, there are low and medium temperature thermal processes that can benefit from the use of well-established solar energy technologies to meet these demands [11].

The production (and consumption) of food (including beverages) is one of the major determinants of global environmental degradation, as mentioned by [12]. The Life Cycle Assessment (LCA) is a consolidated methodology, recommended by international institutions (e.g., European Commission and the United Nations Environment Programme) to quantify the potential environmental impacts throughout the life cycle of a product, service or activity [12]. LCA can be applied to help tackle huge global environmental challenges, such as the necessary improvements of global environmental performance (climate, biodiversity, water, toxics, etc.), and is an important tool supporting economy and society to identify ways how to operate within planetary boundaries, aiding in the decision-making process and leading to substantial absolute environmental improvements, with important lessons learnt.

Recent studies have employed LCA to assess beer production: [13] used LCA to evaluate the environmental balance of the UK biogas sector (where brewery waste was used for biogas production), [14] analyzed the life cycle environmental impacts and costs of beer production and consumption in the UK, while [15] and [16] applied LCA to assess Italian and Romanian beer production, respectively.

Reference [17] used LCA to investigate how to minimize the cradle-to-grave beer carbon footprints related to the brewery size and primary packaging materials, and [18] reported an overview of sustainability challenges in beer production, and the carbon footprint associated with the production of hops. The study by [19] developed LCAs for pure malt beer and pure barley beer produced in Denmark, noting that for every tone of malt replaced by barley, 174 kg CO_2-eq was avoided. Reference [20] developed an LCA for the beer production process in Greece, bottled in 0.5 L green glass bottles, resulting in 392.46 g CO_2-eq/bottle. Reference [21] studied the production process of a lager brewery in Italy (1,880,000 L per year), and concluded that beer consumption in barrels was less polluting than in glass bottles.

Reference [22] evaluated the artisanal beer production in Belgium, considering a 20L steel barrel and 0.5L brown glass bottles, concluding that the barrel produces more emissions. Packaging was the factor that affected carbon emissions the most. Reference [23] applied LCA to a microbrewery in Chile, where the functional unit was a 0.33 L bottle of beer. Emissions associated with ale, bock, lager and weizen were 585, 605, 572 and 593 g CO_2-eq per bottle, where most emissions were associated with glass bottle production (35%), transport/distribution (26 %) and malt production (17%).

Reference [24] assessed the costs and environmental impacts associated with beer production and consumption in the United Kingdom, noting that, depending on the type of packaging, the production of 1 L of beer could emit between 510–842 g CO_2-eq. Reference [25] developed LCAs for Ale (High Fermentation) and Lager beers, remarking that fermentation temperatures should be as high as possible (within the limits that allow classification as a lager) to minimize the environmental impacts of lager production. The case study reported by [26] found that an Italian microbrewery emitted 58.2 t CO_2-eq / year to produce 579.5 hL, equivalent to approximately 1 kg CO_2-eq per liter. Reference [27] estimated the carbon emissions of lager packaged in 0.33 L and 0.66 L glass bottles, 0.33 L aluminum cans, and 30 L steel barrels, which were 570, 670, 740, 690 and 250 kg CO_2-eq/L, respectively.

The objective of the study presented herein is to apply the LCA methodology to quantify the greenhouse gas (GHG) emissions associated with providing process heat to a brewery located in Northeast Brazil. Utilization of electricity (electric grid) and diesel is compared with solar thermal energy. The hypothesis is that even a partial replacement of traditional thermal energy sources presents environmental advantages.

II. METHODOLOGY

The LCA methodology can quantify the potential environmental impacts associated with a product, process or service throughout its life cycle (or part of it) [28,29]. The life cycle can include raw material extraction, processing, manufacturing, transportation, use, maintenance, and final disposal. The LCA is internationally validated and consolidated, being standardized by the International Organization for Standardization (ISO) in ISO 14040 [30] and ISO 14044 [31] standards. In Brazil, these standards were translated by the Brazilian Association of Technical Standards (ABNT) [32,33].

LCA has four interrelated steps [32,33]: i) definition of the object and scope, where the boundaries of the analysis and the purpose of the study are defined, as well as the functional unit; ii) construction of the inventory, which is a quantified survey of data on all inputs (materials, energy and resources) and outputs (products, by-products, emissions) associated with the functional unit; iii) identification and assessment in terms of potential environmental impacts that can be associated with inventory data (in other words, this step applies an environmental impact assessment method to express results), and finally iv) interpretation of results .

Simapro 9.0.0.49 [34] software with the Ecoinvent database [35] was used for the development of Life Cycle Assessment (LCA). The environmental impact assessment method selected was IPCC 2013 GWP 100y [36], which groups GHGs emitted over a 100-year horizon, expressing the results in terms of a common metric, kg CO_2-eq. The functional unit considered herein was the consumption of 1 kWh of process heat.

For electricity consumption, the methodology of Ref. [37] was used to quantify GHG emissions associated with the consumption of 1 kWh of electricity in Brazil. The most recent data available are for 2019: hydroelectric 66.67%, natural gas 9.28%, oil 1.55%, coal 1.62%, nuclear 2.79%, biomass 8.25%, wind 9.15%, solar 0.69%. Data were obtained from the Daily Preliminary Operation Report (IPDO) of the National System Operator [10] and from the Generation Information Bank of the Brazilian Electricity Regulatory Agency (ANEEL). An electric boiler with 90% efficiency was considered.

For diesel, the process considered the utilization of heavy fuel oil, in an industrial furnace, considering a 95% efficiency in this boiler.

For the use of solar collectors, the process considered a solar collector system, with copper flat plate collectors, for hot water, which has an efficiency of 85%.

The heat demand of [38] was utilized herein: for a microbrewery (type “C”) that consumes 950 L of water daily, for approximately 44.23 kWh/day of heat is required.

III. RESULTS AND DISCUSSION

After introducing the processes specified in Simapro [34] using the Ecoinvent database [35], the IPCC 2013 GWP 100y [36] method was selected to express the environmental impact. Initially, GHG emissions associated with the consumption of 1 kWh of the electricity from the grid were calculated. Table I shows the composition of emissions, which total 0.227 kg CO2-eq per kWh consumed from the grid (low voltage).

TABLE I. GHG EMISSIONS ASSOCIATED WITH THE CONSUMPTION OF 1 KWH OF THE BRAZILIAN GRID IN 2019, AT LOW VOLTAGE [OWN SOURCE].

Source of Energy	**Emissions (kg CO_2-eq)**
Hydro	0.06020
Biomass	0.01770
Natural Gas	0.06460
Oil	0.02050
Coal	0.04030
Nuclear	0.00042
Wind	0.00169
Solar	0.00067
Losses, Transmission, Distribution	0.22700
TOTAL	0.22700

TABLE II. GHG EMISSIONS ASSOCIATED WITH THE SUPPLY OF 1KWH OF HEAT [OWN SOURCE].

Power Supply	**GHG Emissions ($kg\ CO_2$-eq/kWh_{th})**
Solar Collectors	0.0144
Diesel	0.3490
Eletricity	0.2760

Considering the efficiencies associated with each heat production process, the results for obtaining 1 kWhth of process heat are presented in Table II.

Table II shows that the utilization of electricity emits almost 21% less GHG emissions to the atmosphere than diesel, and solar collectors emit 96% less than diesel. The environmental advantage of solar collectors over electricity from the Brazilian electric grid for the production of heat yields 94% less emissions. Of the GHG emissions associated with heat production via solar collectors, it was found that 69.1% of the emissions (0.00995 kg CO_2-eq) were associated with the manufacture of the collectors themselves and the remainder associated with the energy consumption for their installation (Fig. 1).

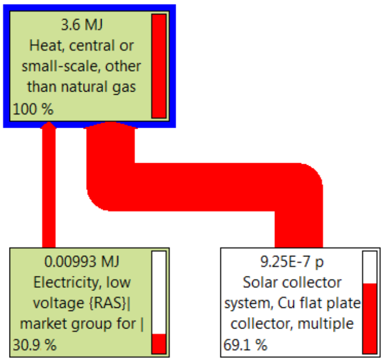

Figure 1. Percentage composition of emissions associated with 1 kWh of heat produced by a solar collector system.

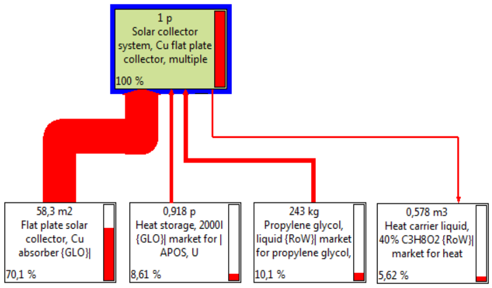

Figure 2. Percentage composition of emissions associated with the manufacture of copper solar collectors.

Fig. 1 is a sankey diagram, which shows the contribution of each process to the overall carbon emissions. The thickness of the connecting ribbons is proportional to the contribution, and the right side bars indicate the contribution to the environmental load. While a red color means a negative (adverse) environmental load, green means an avoided (positive) environmental load, in fact an environmental benefit. The cutoff of Fig. 1 is 2%, which means that although all constituent processes are included in the calculations, for clarity purposes the figure only shows those that contribute up to 2% to the result.

Regarding the manufacture process of the solar collector system, Fig. 2 shows that 70.1% of the emissions are associated with the production of the collector (copper), with smaller participation of the storage tank, and working fluids. The cutoff point is also 2%.

Concerning the emissions associated with obtaining heat from the diesel boiler, the LCA revealed that the manufacturing stage of the equipment is insignificant when compared to the amount of emissions associated with oil combustion. Fig. 3 shows the percentage composition of emissions associated with obtaining 1 kWh of process heat via diesel oil.

The cutoff point of Fig. 3 was also 2%. The carbon emissions associated with equipment are insignificant and do not even appear in the figure. The combustion stage is responsible for 87.1% of emissions: this is verified upon inspection of Fig. 3, which shows that up to the point where heavy fuel oil is available on the market, the cumulative emissions contribute to only 12.9% of final emissions.

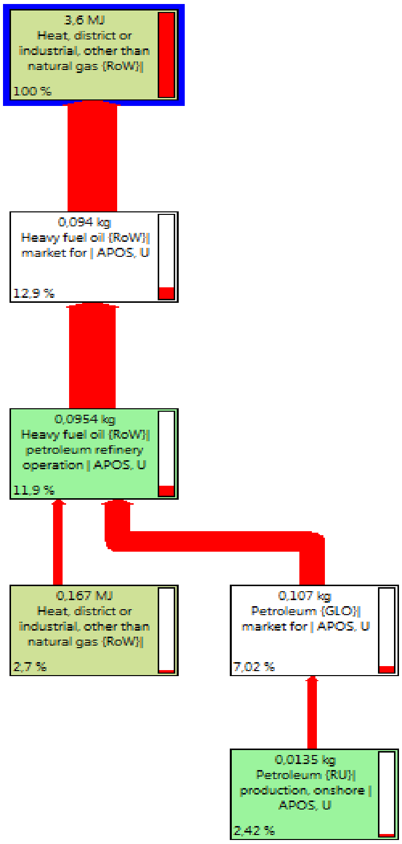

Figure 3. Composition of emissions associated with obtaining 1 kWh of heat via boiler diesel oil.

The is the main difference between employing fossil fuels and renewable resources is that in the first category, environmental impacts are strongly associated with their combustion, and in the second category, the environmental impacts associated with the operation and maintenance steps are minimal.

Considering that the annual heat demand for the microbrewery is 11,500 kWh (operating 252 days per year), Table III presents the results of GHG emissions associated with progressive thermal energy substitutions, based on this microbrewery.

With the total replacement of the energy source, using solar collectors for water heating, the microbrewery analyzed by [38] emits to the atmosphere 165 kg CO_2-eq/year, much lower than if only diesel used to feed the heat generator boiler (4013 kg CO_2-eq/year) or electricity (3174 kg CO_2-eq/year). These are the *Business As Usual scenarios.*

TABLE III. GHG EMISSIONS ASSOCIATED WITH THE SUPPLY OF 11,500 KWH_{TH} TO A MICROBREWERY [OWN SOURCE].

Partial replacement by solar energy ($kg\ CO_2$-eq)		
	Diesel + Solar	**Eletricity + Solar**
0% (Reference case)	4013	3174
20%	3243	2572
40%	2474	1970
60%	1704	1368
80%	935	767
100%	165	165

In a more realistic case, partial substitution is already quite effective, representing -770 kg CO_2-eq/year for every 20% diesel replaced and -602 kg CO_2-eq/year for electricity replaced. There is an important potential for climate change mitigation associated with energy substitution.

This climate change mitigation potential has already been observed in other studies. The work of [39] evaluated the carbon footprint associated with the production of two cake flavors, revealing the complexity of LCA and its richness of detail. Reference [40] performed experiments to compare the carbon footprints associated with the production of electricity via syngas and diesel, demonstrating the environmental advantages of biomass gas. Reference [41] studied the process of ice cream pasteurization and quantified the GHG emissions associated with the traditional use of LPG, suggesting the use of solar thermal energy as a form of reduction. Even without obtaining a totally positive result, [42] demonstrated the LCA calculations for a photovoltaic tile and compared results with a photovoltaic conventional system. LCA can helps identify the hot spots and thus directs efforts to improvements. Reference [43] studied the production process of sugarcane and confirmed, through an LCA, the emissions avoided when generating bioelectricity with sugarcane bagasse. Reference [44] studied the production process of a red ceramic industry, detailing its stages and environmental impacts associated with the use of different energy resources. Reference [45] verified four possibilities of final destination for urban pruning waste from João Pessoa, confirming that electricity generation is the most advantageous from an environmental perspective. Photovoltaic solar energy was compared with the electricity supplied to the Brazilian grid by [46] and [47], demonstrating the environmental benefits of using renewable energy.

Analysis of the results obtained herein confirm the hypothesis that even a partial replacement of traditional thermal energy sources presents numerous environmental advantages, with significant potential for climate change mitigation associated with the energy substitution of the heat source used in beer production processes.

IV. Conclusions

The use of LCA concepts can inform the environmental benefit associated with energy source substitution, demonstrating that the introduction of solar thermal energy is an environmentally viable alternative, from the viewpoint of GHG emissions.

With total replacement of the energy source for heat production, the use of solar collectors for water heating emitted 165 kg CO_2-eq/year, much lower than if only diesel was used to power the hot water boiler (4,013 kg CO_2-eq/year) or electricity (3,174 kg CO_2-eq/year). In a more realistic case, partial substitution is already quite effective, representing -770 kg CO_2-eq/year for every 20% of diesel replaced and -602 kg CO_2-eq/year for electricity.

The results obtained in this work, added to future research in other sectors, can help reduce the negative effects of industrial activities. Applying similar research to different industries could mitigate the intensification of the greenhouse effect, as all GHG emissions are emitted into the atmosphere and the global sum of avoided emissions could be high, opening the path to establish a low carbon economy.

Acknowledgment

The authors wish to acknowledge the support from the National Council for Scientific and Technological Development (CNPq) project 307394/2018-2. The authors also wish to thank the Coordination for the Improvement of Higher Education Personnel (CAPES) for the MSc. scholarship.

References

[1] EPE – Empresa de Pesquisa Energética. (2018). *Análise da eficiência energética em segmentos industriais selecionados – alimentos e bebidas*. Available at: http://www.epe.gov.br/pt/publicacoes-dados-abertos/publicacoes/projeto-de-assistencia-tecnica-dos-setores-de-energia-e-mineral-projeto-meta.

[2] Ferreira, A., Kunh, S. S., Fagnani, K. C., De Souza, T. A., Tonezer, C., Dos Santos, G. R., & Coimbra-Araújo, C. H. (2018). Economic overview of the use and production of photovoltaic solar energy in brazil. *Renewable and Sustainable Energy Reviews*, *81*, 181-191.

[3] Shahsavari, A., & Akbari, M. (2018). Potential of solar energy in developing countries for reducing energy-related emissions. *Renewable and Sustainable Energy Reviews*, *90*, 275-291.

[4] Barbosa, R. R., & Carvalho, M. (2018). Dimensionamento de um sistema de aquecimento solar de água para aplicações industriais. *Engevista*, *20*(2), 214-238.

[5] Kabir, E., Kumar, P., Kumar, S., Adelodun, A. A., & Kim, K. H. (2018). Solar energy: Potential and future prospects. *Renewable and Sustainable Energy Reviews*, *82*, 894-900.

[6] Nascimento, D. P., Menezes, V. L., Carvalho, M., & Chacartegui, R. (2019). Energy analysis of products and processes in a sanitary landfill. *IET Renewable Power Generation*, *13*(7), 1063-1075.

[7] Neves, T. I., Uyeda, C. A., Carvalho, M., & Abrahão, R. (2018). Environmental evaluation of the life cycle of elephant grass fertilization—Cenchrus purpureus (Schumach.) Morrone—using chemical fertilization and biosolids. *Environmental monitoring and assessment*, *190*(1), 30.

[8] Kumar, L., Hasanuzzaman, M., & Rahim, N. A. (2019). Global advancement of solar thermal energy technologies for industrial process heat and its future prospects: A review. *Energy Conversion and Management*, *195*, 885-908.

[9] Silva, J. A. C. (2014). *Potenciais aplicações de tecnologias solares em processos industriais como fonte de energia: uma revisão bibliográfica*. Escola de Engenharia de Lorena. Universidade de São Paulo.

[10] ONS - Operador Nacional do Sistema Elétrico, *IPDO Informativo Preliminar Diário de Operação*. Available at: http://www.ons.org.br/paginas/conhecimento/acervo-digital/documentos-e-publicacoes?categoria=IPDO.

[11] H. Schweiger. (2001). *Poship–the potential of solar heat for industrial processes*. Final Report. EU-Project No NNE-1999, 308.

[12] Cucurachi, S., Scherer, L., Guinée, J., & Tukker, A. (2019). Life cycle assessment of food systems. *One Earth*, *1*(3), 292-297.

[13] Styles, D., Dominguez, E. M., & Chadwick, D. (2016). Environmental balance of the UK biogas sector: An evaluation by consequential life cycle assessment. *Science of the Total Environment*, *560*, 241-253.

[14] Amienyo, D., & Azapagic, A. (2016). Life cycle environmental impacts and costs of beer production and consumption in the UK. *The International Journal of Life Cycle Assessment*, *21*(4), 492-509.

[15] De Marco, I., Miranda, S., Riemma, S., & Iannone, R. (2016). Life cycle assessment of ale and lager beers production. *Chemical Engineering Transactions*, *49*, 337-342.

[16] Ghinea, C., & Leahu, A. (2017). Life cycle environmental impacts of Romanian beer production. In *International Multidisciplinary Scientific GeoConference: SGEM*, *17*, (pp. 115-122).

[17] Cimini, A., & Moresi, M. (2018). Mitigation measures to minimize the cradle-to-grave beer carbon footprint as related to the brewery size and primary packaging materials. *Journal of Food Engineering*, *236*, 1-8.

[18] Hauser, D. G., & Shellhammer, T. H. (2019). An Overview of Sustainability Challenges in Beer Production, and the Carbon Footprint of Hops Production. *Master Brew. Assoc. Am*, *56*(4).

[19] Kløverpris, J. H. (2009). *Comparative life cycle assessment of malt-based beer and 100% barley beer*. Novozymes A/S.

[20] Koroneos, C., Roumbas, G., Gabari, Z., Papagiannidou, E., & Moussiopoulos, N. (2005). Life cycle assessment of beer production in Greece. *Journal of Cleaner Production*, *13*(4), 433-439.

[21] Cordella, M., Tugnoli, A., Spadoni, G., Santarelli, F., & Zangrando, T. (2008). LCA of an Italian lager beer. *The International Journal of Life Cycle Assessment*, *13*(2), 133-139.

[22] Melon, R., Wergifosse, V., Renzoni, R., & Léonard, A. (2012, November). Life Cycle Assessment of an artisanal Belgian blond beer. In *Proceedings of the 2nd International Conference on life cycle approaches*.

[23] Munoz, E., Riquelme, C., & Cardenas, J. P. (2012, November). Carbon Footprint of beer—Analysis of a small scale processing plant in Chile. In *Proceedings of the 2nd LCA Conference*, Lille, France.

[24] Amienyo, D., & Azapagic, A. (2016). Life cycle environmental impacts and costs of beer production and consumption in the UK. *The International Journal of Life Cycle Assessment*, *21*(4), 492-509.

[25] De Marco, I., Miranda, S., Riemma, S., & Iannone, R. (2016). Life cycle assessment of ale and lager beers production. *Chemical Engineering Transactions*, *49*, 337-342.

[26] Masotti, P., Campisi, B., & Bogoni, P. (2016). Carbon footprint evaluation of an Italian micro-brewery. *Procedia Environmental Science, Engineering and Management*, *3*(3), 119-127.

[27] Cimini, A., & Moresi, M. (2016). Carbon footprint of a pale lager packed in different formats: assessment and sensitivity analysis based on transparent data. *Journal of Cleaner Production*, *112*, 4196-4213.

[28] Guinée, J. B. (2001). *Life Cycle Assessment: An operational guide to the ISO Standards; LCA in Perspective; Guide; Operational Annex to Guide*. Centre for Environmental Science, Leiden University, The Netherlands.

[29] Guinée, J. B. (2002). *Handbook on life cycle assessment: operational guide to the ISO standards*. Kluwer Academic Publishers, Boston.

[30] International Organization for Standardization – ISO. (2006). ISO 14040:2006: Environmental management - Life cycle assessment - Principles and framework, Genebra.

[31] International Organization for Standardization – ISO. (2006). ISO 14044:2006: Environmental management - Life cycle assessment - Requirements and guidelines, Genebra.

[32] ABNT - Associação Brasileira de Normas Técnicas. (2009). Gestão Ambiental – Avaliação do Ciclo de Vida - Princípios e estrutura: NBR ISO 14040, Rio de Janeiro, versão corrigida 2014a.

[33] ABNT - Associação brasileira de Normas TécnicaS. (2009). Gestão ambiental - Avaliação do ciclo de vida - Requisitos e orientações: NBR ISO 14044, Rio de Janeiro, ABNT – versão corrigida 2014b.

[34] PRÉ Consultants, SimaPro. (2019). Available at: http://www.simapro.nl.

[35] ECOINVENT. (2018). *Database*. Available at: http://www.ecoinvent.ch.

[36] IPCC. (2013). *Revised supplementary methods and good practice guidance arising from the Kyoto protocol*. Available at: http://www.ipcc-nggip.iges.or.jp/public/kpsg/.

[37] Carvalho, M., & Delgado, D. (2017). Potential of photovoltaic solar energy to reduce the carbon footprint of the Brazilian electricity matrix. *LALCA: Revista Latino-Americana em Avaliação do Ciclo de Vida*, *1*(1), 64-85.

[38] Sousa, M. N., Geremia, A. R., & Rodrigues, L. J. (2018). Análise da viabilidade econômica e dimensionamento de sistemas de aquecimento solar de água para o processo de mosturação de cerveja. In *Congresso Brasileiro de Energia Solar, Anais do ABENS*.

[39] Diniz, D. P., & Carvalho, M. (2019). Pegada de carbono associada a produção de bolos. *Revista em Agronegócio e Meio Ambiente*.

[40] de Melo, F. M., Silvestre, A., & Carvalho, M. (2019). Carbon footprints associated with electricity generation from biomass syngas and diesel. *Environmental Engineering & Management Journal (EEMJ)*, *18*(7).

[41] Melquíades, T. F., Carvalho, M., Araújo, Y. R. V., & Junior, L. M. C., (2019). Pegada de carbono associada ao processo de pasteurização de sorvetes. *Revista em Agronegócio e Meio Ambiente*, *12*(2), 609-629.

[42] Carvalho, M., Menezes, V. L., Gomes, K. C., & Pinheiro, R. (2019). Carbon footprint associated with a mono-Si cell photovoltaic ceramic roof tile system. *Environmental Progress & Sustainable Energy*, *38*(4), 13120.

[43] Carvalho, M., Segundo, V. B. D. S., Medeiros, M. G. D., Santos, N. A. D., & Junior, L. M. C. (2019). Carbon footprint of the generation of bioelectricity from sugarcane bagasse in a sugar and ethanol industry. *International Journal of Global Warming*, *17*(3), 235-251.

[44] Abrahao, R., & Carvalho, M. (2017). Environmental impacts of the red ceramics industry in Northeast Brazil. *International Journal of Emerging Research in Management & Technology*, *6*, 310-317.

[45] Araújo, Y. R. V., de Góis, M. L., Junior, L. M. C., & Carvalho, M. (2018). Carbon footprint associated with four disposal scenarios for urban pruning waste. *Environmental Science and Pollution Research*, *25*(2), 1863-1868.

[46] de Souza Grilo, M. M., Fortes, A. F. C., de Souza, R. P. G., Silva, J. A. M., & Carvalho, M. (2018). Carbon footprints for the supply of electricity to a heat pump: Solar energy vs. electric grid. *Journal of Renewable and Sustainable Energy*, *10*(2), 023701.

[47] Delgado, D., Carvalho, M., Junior, L. M. C., Abrahão, R., & Chacartegui, R. (2018). Photovoltaic solar energy in the economic optimisation of energy supply and conversion. *IET Renewable Power Generation*, *12*(11), 1263-1268.

Energy Efficiency and the Role of Energy Managers

Jelena Malenović-Nikolić

Faculty of Occupational safety in Niš, Niš, Serbia, malenovicfznr@gmail.com

Abstract—**The level of energy efficiency, as a measure of rational use of energy resources, can reveal considerable inconsistencies in the use of available energy-generating products, whether they come from alternative or traditional sources. The implementation of energy efficiency measures and the completion of prescribed tasks by energy managers can greatly influence the level of energy efficiency of local public administrations.**

Keywords – energy management system, tasks of energy managers, local self-government units

I. INTRODUCTION

Energy efficiency is a term that primarily refers to the application of more efficient ways of utilizing energy, accompanied by the prescribed measures of energy efficiency. The concept can also include energy conservation measures, but only as a goal of rational use, without necessitating a diminished comfort of living. A major goal of energy efficiency is to reduce the energy losses through the use of modern technology. The management of energy efficiency, as a part of energy flow management in local self-government units, is an important step in the analysis of the real-world situation. If a problem is identified in the operation of the energy management system, it can indicate a lack of preparedness of local self-government representatives to find the ways to save money by increasing the level of energy efficiency. The positive aspects of using an energy management system also include the environmental effects, because reduced consumption of energy resources helps reduce pollutant emissions. Local self-government units are attempting to reduce energy consumption, although they use measures that are not the result of the systems approach and the analysis, but priorities chosen according to the opinions of individuals.

Energy costs are covered by the budget, which is why there is a common tendency to only reduce the cost, while entirely disregarding energy efficiency.

II. ENERGY MANAGEMENT SYSTEM

Adherence to the energy efficiency principles [1] also depends on the level of social responsibility, economic development, and the standard of living. Scientific and technological innovations provide a good foundation for a more efficient consumption of energy resources as well as final energy. Higher energy efficiency offers environmental benefits, as well, such as reduced environmental thermal stress and lower pollutant concentrations. Other, but by no means less important, goals include improving energy security, meeting the energy needs, and achieving long-term financial savings.

Adherence to the principles of energy efficiency and sustainable energy development of a country indicates to what extent the energy strategies are implemented. The implementation of the energy policy is a large issue in case the energy strategies include proposals that are not feasible before a set deadline. It is very difficult for developing countries to pursue energy strategies that involve maximizing the economic benefits while maintaining a high energy efficiency level, controlling the energy consumption, providing secure energy distribution, and preserving environmental quality.

Enforcement of the relevant legislation [2] and financial support in the form of subsidies, donations, and loans, accompanied by developed strategic and operational plans, can yield good results.

The management of energy development, from the phase of planning the level of energy efficiency, through the organization phase, to the implementation of concrete measures and the control of the performed activities, is a task to be handled by the energy management. Concrete energy efficiency measures can increase the savings in the municipal budget when they are implemented in public institutions, such as administrative buildings, social, healthcare, and cultural institutions, public utility companies, and local community offices.

The energy management system comprises processes and activities that are planned to be implemented in the public sector. Energy efficiency evaluation is performed based on the energy consumption data in public buildings (Fig. 1), which fall under the jurisdiction of the local self-government. The energy management system undertakes activities to raise awareness about energy efficiency at the local level under the supervision of an authorized energy consultant. The energy manager (Fig. 2) prepares the data for proposing the energy efficiency measures, which are based on the reconstruction, repair, additional construction, and insulation of a building. The Law on Efficient Energy [2] Use stipulates that the energy managers coordinate the design of an energy savings program [3], because they are licensed to prepare and work on the energy efficiency study [4] and to submit the annual report on the level of energy efficiency improvement [5].

Energy managers are tasked with preparing data for energy efficiency plans and with participating in the design of such plans.

They are mandated to participate in the design of local energy efficiency plans, to submit reports, and to participate in the review, repair, additional construction, or insulation of buildings within the given deadlines.

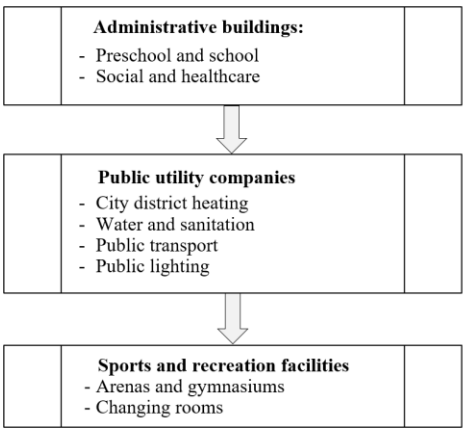

Figure 1. Public buildings.

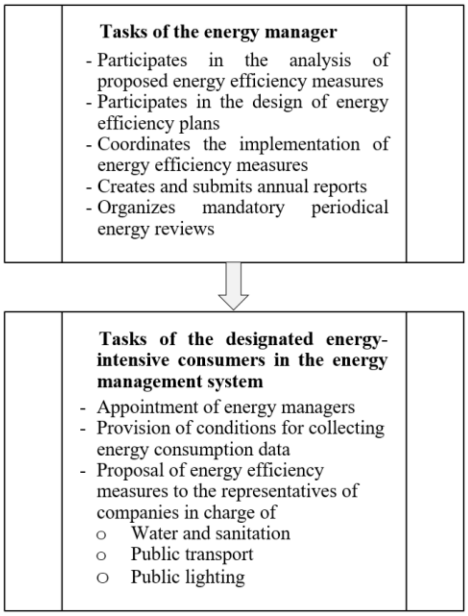

Figure 2. Energy management system tasks [6].

The Energy Efficiency Program is the plan that prescribes the energy efficiency measures and the manner of their implementation and financing. It is adopted on a three-year basis and is aimed at offering a way to save a minimum of 3% of the total energy consumption. The Energy Efficiency Program of a local self-government relies on the enforcement of the Law on Efficient Energy Use, the Methodology of Recommended Savings, defined in accordance with the European Commission recommendations, and the Act on Annual Energy Savings Goals of the designated energy-intensive consumers in the energy management system.

The core elements of the Energy Efficiency Program improvement [3,7] include the Plan for Energy-Related Building Repair and Maintenance, the Plan for Public Utility System Improvement, and the Plan of Renewable Energy Use. The Program should also include the designation of the entity to perform the proposed operational activities, the deadlines and expected results, the review of previous results, and the allocation of the necessary financial assets.

The proposal of energy efficiency measures is mostly based on the guidelines provided in the National Energy Efficiency Action Plan of the Republic of Serbia (Fig. 3), although the measures can be created separately according to the same principles. The proposal of energy

Energy efficiency measures:
- Replacement of light sources in public lighting
- Replacement or installation of the lighting system in new or existing residential buildings
- Replacement or improvement of the existing or installation of a new lighting system or lighting components in new or existing commercial or public service buildings
- Reconstruction of thermal insulation in specific portions of the building envelope (walls, roofs, ceilings, foundations, and the like) and/or window replacement in existing residential, commercial, and public service buildings
- Reconstruction of the building envelope and heating system in existing residential, commercial, and public service buildings
- Replacement of heating installations in existing residential, commercial, and public service buildings
- Introduction of new building codes for new residential, commercial, and public service buildings
- Replacement or installation of new water heating equipment in existing residential, commercial, and public service buildings
- Connection to the district heating system of new or existing residential, commercial, and public service buildings
- Replacement or installation of air conditioning devices with the power rating lower than 12 kW in new and existing residential, commercial, and public service buildings
- Installation of a solar system for the domestic water heating in new and existing residential, commercial, and public service buildings
- Primary energy savings from cogeneration facilities
- Motor pool vehicle replacement

Figure 3. Energy efficiency measures [6,10]

efficiency measures within the Program [8,9] should be explained in detail, which requires not only the name of the measure, but also the label, category, time frame, aim, target group, and the level of implementation (national, regional, or local).

The part of the Program dealing with the implementation of the measures should include all the required activities as well as the source of financing, measure implementation costs, and the names of the designated institutions to supervise the implementation of the energy efficiency measures.

III. THE ROLE OF ENERGY MANAGERS IN THE IMPLEMENTATION OF ENERGY EFFICIENCY MEASURES

The energy management system, as the basis of energy flow management, is an organized management system within which energy managers perform their legally defined duties.

One of the primary goals of this system is to help provide the highest possible level of energy efficiency and the foundation for a more favourable designation of energy indicator values. The structure, complexity, and scope of the energy management system depend on the level at which it is established (national, regional, local, company, or individual building). The basic elements of this system, which are also parts of the organizational system, are shown in Fig. 4.

Energy managers have to facilitate a high level of cooperation, which is why they need to possess good communication skills in addition to their technical expertise.

As active participants in energy management, energy managers perform important tasks, which are based on good communication, energy consumption control, annual reports of the savings achieved, analysis of energy use and consumption, choice of priorities for implementing the prescribed energy efficiency measures, participation in the application of energy efficiency principles, use of instruments that monitor heat and power consumption,

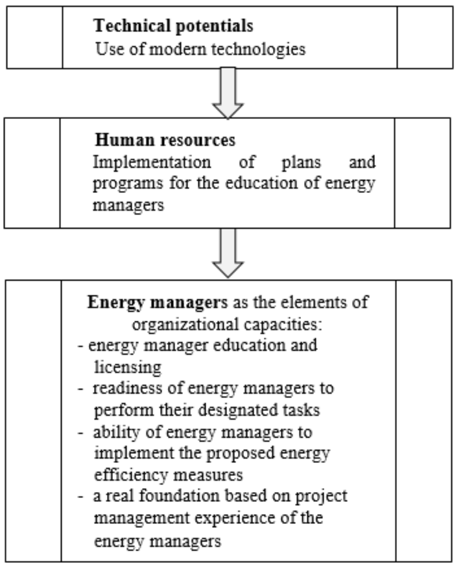

Figure 4. Organizational capacities.

proposals for energy optimization of technical devices, and application of local legislative acts relevant for energy efficiency improvement.

Energy managers have to cooperate with their colleagues who perform relevant tasks for energy efficiency. Therefore, these tasks require a high level of professional communication, acknowledgement of other professional opinions, and adherence to the prescribed procedures.

Inspections of public buildings and the implementation of energy efficiency measures require that energy managers cooperate with municipality presidents or mayors, sectoral heads, directors of public institutions, energy distributors and suppliers, public utility representatives, members of the media, but also with furnace operators and caretakers. Regular communication with stakeholder representatives requires energy managers to be able to handle a variety of professional situations, to show understanding when discussing technical issues with the less educated employees, and to show respect towards other individuals, regardless of their job or task. Professional communication also requires regular meetings, which should address the provision of data necessary for the creation of annual reports and the determination of energy efficiency levels. The reports also indicate how much work and effort energy managers put in to complete the planned tasks. Experience from practice has shown that there are cases in local self-governments where energy managers, although equipped with the required technical knowledge, show a lack of cooperation and motivation and fail to meet the deadlines or to use the prescribed data processing methods.

If the energy savings are at least 1% compared to the previous year, it is an indicator that the law was successfully implemented and that the subjects of the energy management system conscientiously performed their duties in energy policy implementation.

The results presented in the annual reports show among other things if the energy manager succeeded at organizing work activities and coordinating the formed team. The annual report is a control instrument for evaluating the work of the energy manager. Energy managers must also pay attention to the complaints and suggestions in order to improve the functioning of the energy management system. Energy managers collect and analyse internal complaints from co-workers and the energy management system users or external complaints from citizens and then make the necessary corrections, propose corrective measures, or correct their own actions if pertinent and deemed justified.

Basic IT literacy is a requirement for energy managers, as they have to create reports using the designated software and the Energy Management Information System (EMIS – or ISEM in Serbian) databases in municipalities.

Energy managers can also correct the energy inefficient behaviour of public building users. Such corrective actions can involve the education of the technical staff, the use of models reliant upon the exchange of experience, and a higher motivation to reduce energy provision costs, pollutant emissions and the burden on the local budget.

The results of energy managers’ work could greatly contribute to energy savings, which would be achieved through changing user behaviour (e.g. ventilation methods or indoor temperature levels), determining the causes of overconsumption (electrical devices), and using low-cost saving measures (lighting replacement, water valve fixture repairs), while maintaining the level of comfort.

An important role of energy mangers (Fig. 5) in improving energy efficiency is to communicate with the management representatives of public institutions and discuss the average consumption over the previous several years, the projected consumption for buildings of a specific category, and the implementation of recommended energy efficiency measures. Other ways to considerably improve the energy efficiency include motivating administrative workers in the various institutions, e.g. using the model where the institution gets to keep up to 50% of the financial savings or the model where different institutions are encouraged to compete among themselves on which of them will achieve the highest savings. Important activities of energy managers (Fig. 6) can include participating in the city/municipal decision making regarding energy efficiency, making recommendations for rational energy use, recognizing oversights in the implementation of energy efficiency measures, and periodically monitoring the functioning of technical systems (Fig. 7). Periodical account control is another important activity of energy managers, which is aimed at revealing potential inconsistencies and errors by the energy distributors or utility companies that supply

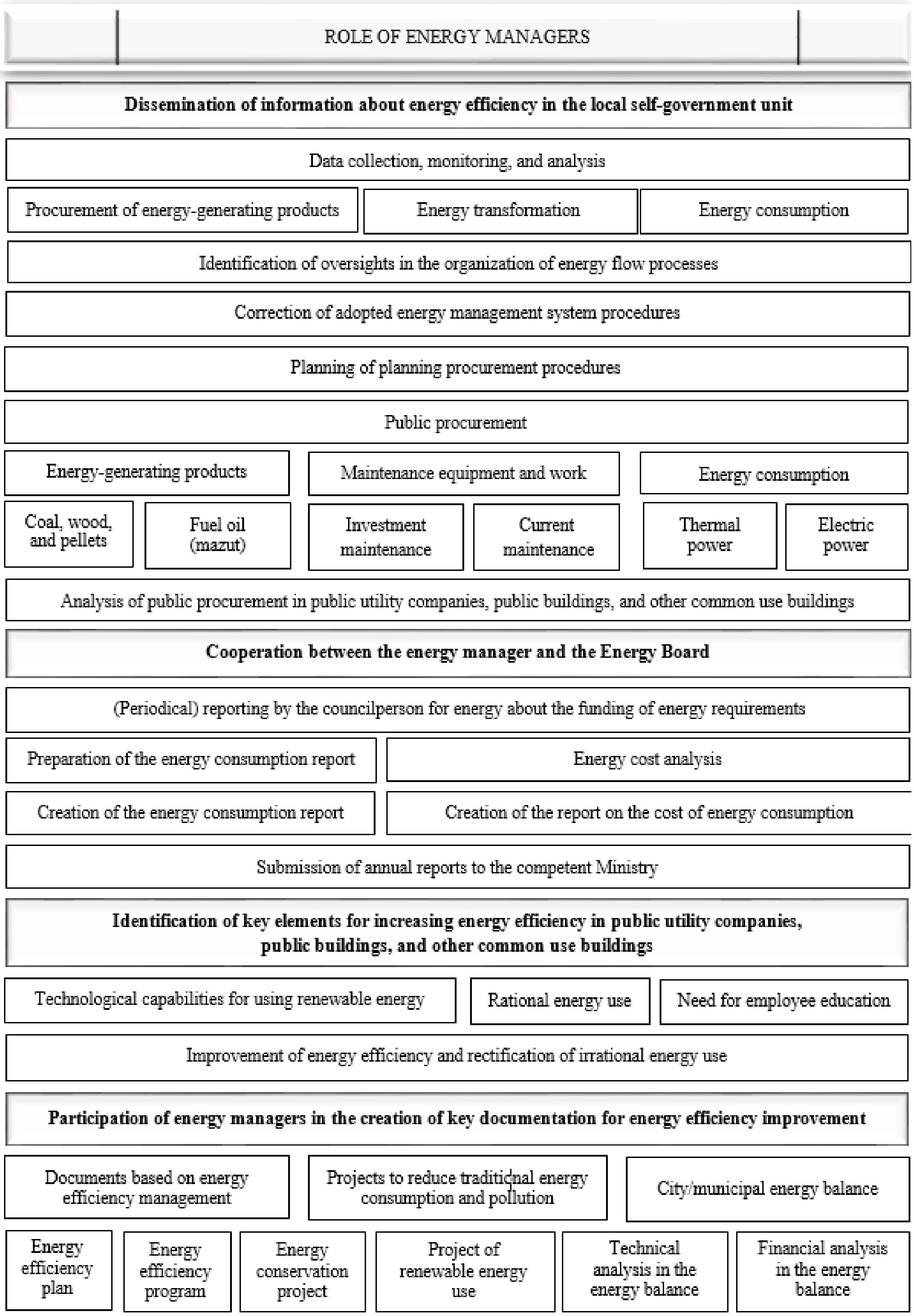

Figure 5. Role of energy managers.

energy or water. By having all the accounts inputted into the information system, energy managers gain a clear insight into the situation, which allows them to report the established inconsistencies and attempt to rectify the oversights or at least notify other system users if the intervention would fall outside their purview. The report on a completed account control forms the basis of action plans and proposals for corrective measures in order to maintain an uninterrupted operation of the management system. The role of energy managers in the management system of local public self-governments entails a high level of responsibility. It is necessary to make a careful selection of employees with adequate professional skills and personal traits before sending them to complete their training and obtain their energy manager licence.

Systematization of work activities for the energy manager position

- Collects and analyses data on the methods of energy use and the quantity of used energy;
- Prepares the Energy Efficiency Program on the planned energy savings methods and goals for a period of no fewer than three years;
- Prepares the Energy Efficiency Plan including measures and activities for its implementation for the duration of one year;
- Proposes measures that will contribute to energy efficiency;
- Determines the criteria for the public call for co-financing of the energy efficiency measures for the municipal administration
- Participates in the selection of subsidy recipients, monitors the implementation of approved projects, and writes reports on the application process

Figure 6. Energy manager work activities [6,11].

Energy manager duties:

- Develops energy efficiency programs and projects at eh municipal level;
- Implements energy efficiency programs and projects;
- Regularly visits and inspects buildings at the municipal/city/company level
- Controls energy consumption once a month
- Improves and assesses the technical equipment of buildings
- Specifies the needs for building repairs
- Implements the proposed measures
- Writes the annual energy consumption report

Figure 7. Energy manager duties.

The size of a city/municipality and the number of public buildings influence the complexity of energy manager tasks, which is why it is crucial to consider the extent of the work to be performed.

According to the job systematization (Fig. 7) within the Rulebook on Job Organization and Systematization in the Municipal Administration, the Municipal Attorney's Office, the Professional Services, and Special Municipal Organizations, the energy manager duties are assigned to the job of a Consultant, who also handles agricultural and rural development affairs.

IV. ENERGY EFFICIENCY OF LOCAL PUBLIC SELF-GOVERNMENT BUILDINGS

The energy efficiency programs of local public self-governments comprise the data on heat and electricity consumption per user and per one square meter, which can then be used in comparative analyses. The purpose of such methods is to establish the energy efficiency level in specific cities/municipalities so as to present a realistic picture of how the energy efficiency measures are being implemented. The results of electricity consumption of public lighting provide additional insight into the investment in improving the energy efficiency of public lighting. The present analysis includes the local self-government units given in Figs. 8, 9 and 10. The comparison of heat consumption shows that public buildings consume the most heat per one square meter in Varvarin and Velika Plana [7,9], whereas Kragujevac consumes the most heating energy per user.

The comparison of the presented results shows that the city of Kragujevac [8], which is also the biggest consumer of electricity, has the highest consumption per 1 square meter in terms of public buildings. Interestingly, the municipality of Nova Varoš [7] has the highest electricity consumption per user even though it has the lowest consumption per one square meter. The comparison of public lighting electricity consumption shows that Kragujevac and Bečej consume the most electricity per luminary, while Bečej and Varvarin [9] are the biggest consumers per user.

The overall comparison of the results indicates that the energy efficiency issues in

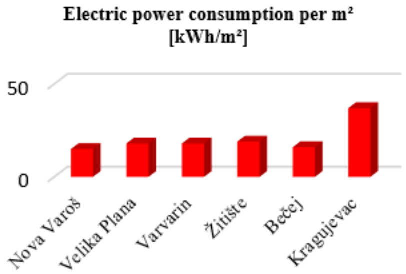

Figure 8. Electric power consumption.

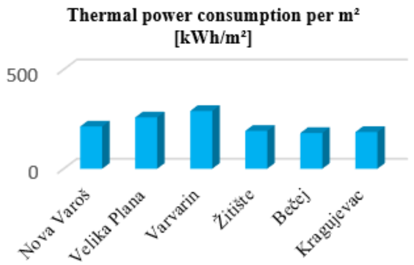

Figure 9. Electric power consumption.

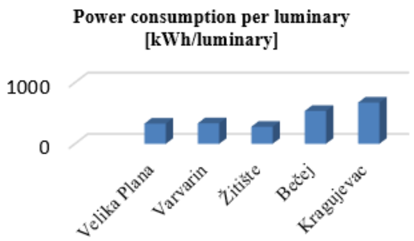

Figure 10. Electric power consumption.

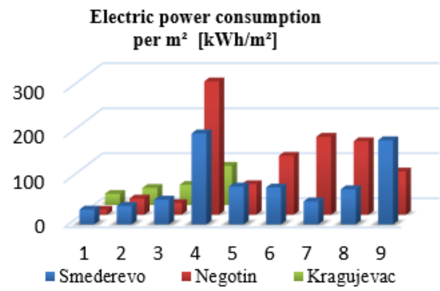

Figure 11. Electric power consumption.

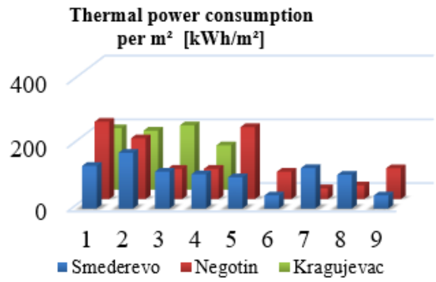

Figure 12. Thermal power consumption.

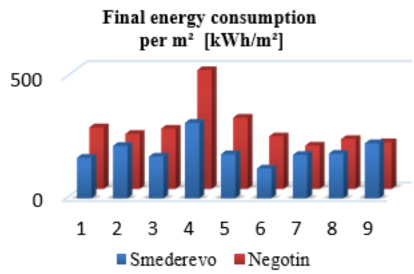

Figure 13. Electric power consumption for public lighting.

Kragujevac should be prioritized with regard to public lighting electricity consumption per luminary, electricity consumption per one square meter, and heat consumption per user.

A more detailed analysis of energy consumption by type of building (Figs. 11, 12 and 13), including primary schools (1), kindergartens (2), secondary schools (3), healthcare institutions (4), social institutions (5), cultural institutions (6), sports facilities (7), public administration institutions (8), and public utility institutions (9), was conducted for the cities of Smederevo, Negotin, and Kragujevac [8,10,11].

The energy consumption analysis by type of building provides a clearer picture of energy efficiency in the Serbian public sector, as it unequivocally reveals considerable inconsistencies. The data for Negotin [11] indicate large electricity consumption in healthcare institutions and large heat consumption in primary schools and social institutions. In Kragujevac, there is significant heat consumption in primary and secondary schools. Big electricity consumers in Smederevo [10] include public utility buildings and healthcare institutions. Energy efficiency programs usually do not contain any data related to building type that could greatly facilitate the energy managers' ability to identify problems, determine the causes of inconsistencies, and try to eliminate them.

The role of energy managers should therefore be defined as clearly as possible, because the issues to be resolved are only accumulating, especially considering the fact that the energy efficiency in local self-government units is considerably below the European average.

The state of the environment warrants the implementation of the energy efficiency measures that would encompass the reconstruction and insulation of public buildings. The energy efficiency program should essentially pave the way for more efficient energy use. The proposal for how to implement the measures and how to finance them should be made in consultation with the energy manager if one has been appointed.

V. Conclusion

In terms of energy efficiency, the state of the public sector suggests that more effort is required to monitor and control energy consumption. Energy managers play a vital role in determining the causes of excessive energy consumption, which is why the task should be entrusted to responsible and professionally highly skilled employees. Energy managers should also possess ample previous experience; it is recommended that employees who were previously involved in thermal power, electric power, or water and sanitation system maintenance be prioritized for energy manager training. IT is also desirable for energy managers to possess broader knowledge in the fields of project management, business communication, public administration, as well as the knowledge of one or more foreign languages.

Adherence to the principles of energy efficiency as well as the introduction of the energy management system can result in considerable energy savings if the energy managers opt for the systems approach to solving the current energy consumption problems. Energy managers are also crucial for the achievement of the set objectives and energy efficiency, but proper adherence to the laws also depends on the skills and commitment of the individual employees entrusted with completing the relevant tasks.

Acknowledgment

This research was funded by the Ministry of Education, Science and Technological Development of the Republic of Serbia.

References

[1] Energy Law. (2018). Official Gazette of the Republic of Serbia, no. 145/2014, 95/2018.

[2] Law on Efficient Use of Energy. (2013). Official Gazette of the Republic of Serbia, no. 25/2013.

[3] Rulebook on the conditions for the appointment of energy managers in the bodies of local self-government units. (2018). Official Gazette of the Republic of Serbia, no. 65/2018.

[4] Rulebook on the conditions for the appointment of energy managers in companies whose predominant activity is in the trade and services sector, state administration bodies, other bodies of the Republic of Serbia, bodies of the Autonomous Province and institutions. (2017). Official Gazette of the Republic of Serbia, no. 85/2017.

[5] Energy Sector Development Strategy of the Republic of Serbia by 2025 with projections until 2030. (2015). Official Gazette of the Republic of Serbia, no. 101/2015.

[6] Rulebook on the manner of implementation and content of the training program for energy managers, costs of attending the training, as well as detailed conditions, program and manner of taking the exam for energy managers. (2015). Official Gazette of the Republic of Serbia, no. 12/2015.

[7] Energy Efficiency plan for Nova Varoš. (2015). Official Gazette of the Republic of Serbia, no. 06-17/45/2015-02.

[8] Energy Efficiency plan for the cities of Kragujevac. (2018). Official Gazette of the Republic of Serbia.

[9] Ministry of Construction, Transport and Infrastructure. (2017). Local Energy Efficiency Action Plan for Pirot, Sokobanja, Vrbas, Vršac, Velika Plana, Varvarin, Žitište, Bečej, Nova Varoš i Krafujevac.

[10] Energy Efficiency plan for Smederevo. (2019). Beohidro DOO, Aurora.

[11] Energy Efficiency plan for Negotin. (2020). Aurora.

Reliability and Resilience of Power Supply Systems in Healthcare Infrastructure

Pablo Garrido-Píriz[1], Manuel Botejara-Antúnez[2], Gonzalo Sánchez-Barroso[3], Jaime González-Domínguez[4], Justo García Sanz-Calcedo[5]

[1,2,3,4,5]University of Extremadura, Graphical Expression Department, Badajoz, Spain
jgsanz@unex.es[5]

Abstract—**Power supply systems play a capital role in facilities which need any sort of electrical power. This importance is even major in basic pillars such as healthcare infrastructures, where the consequences of a blackout are bound to be severe. These infrastructures not only need to resist the blackout and work in normal conditions via auxiliary systems but also should be able to recover their normal operation state as soon as possible. Several terms have been pointed out as key parameters to refer to the management of power supply systems in literature with this regard. There is a compromise between investments and guaranteeing a continuous performance, by implementing redundancies or oversizing devices. A different perspective is addressed in this study, introducing the concept of resilience in these systems. In this study, power supply systems in health infrastructure have been assessed through resilience, regarding the possibility of unfavourable scenarios to happen and their capacity to return back to the original and steady state.**

Keywords – power supply system, adequacy, resilience, healthcare infrastructure

I. INTRODUCTION

Health infrastructure is a pillar of modern societies, where specialized medical services are provided to a significant amount of people. These infrastructures are especially vulnerable if they are stricken by a catastrophic scenario, so protocols are needed to be implemented [1]. These protocols where power supply systems are involved may include design conditions such as oversizing, but the most common way to address this problem is by installing redundant and parallel elements [2,3].

The consequences of a blackout in health infrastructures can be critical if there is not an auxiliary facility to provide the demanded electricity by the hospital. That is why this kind of infrastructures need to be equipped with auxiliary power supply elements to ensure a continuous electricity supply, in order to prevent the infrastructure from economic, social and even human losses [4]. There are multiple cases where a short power supply discontinuity in critical areas can mean the difference between a patient's life or death.

Questions that arise from the study of the performance level when a disruptive scenario occurs may be analysed through several perspectives. Classical approaches entail risk assessment, project management and predictive maintenance techniques [5]. Ref. [6] provides a detailed analysis pointing out the features of a normal operation, the understanding of a disruption and the way the system fails.

The main concept regarding the correct performance of power supply systems during a continuous period of time is their reliability, which can be defined as the probability of a system to perform correctly during a certain period of time [7]. That being said, resilience has outstood in recent literature as a parameter to integrate protection, prevention and prophylactic measures. The original definition of resilience involves the capacity of a generic material to return to its original state after the application of external forces. In this view, the resilience of a system can be understood as its capacity to return to a steady state after a disruptive scenario [8]. This definition can be extrapolated to power supply facilities, where the most typical worst-case scenario refers to power blackouts or power outages. Nonetheless, there are other scenarios that can also be assessed to evaluate the resilience of a power supply system, such as continuous power supply surges or overcurrent conditions [9-11]. Protection elements are proven to meet the expectations of disruption according to their regulations, so they can become handy to assess the design conditions and to accomplish a resilient facility.

The objective of this study is to provide a holistic review of the current studies regarding reliability of power systems, including important design considerations.

II. METHODOLOGY

The resilience term is implemented as a new perspective addressment, and remarkable items which may affect the decision-making processes are listed out.

Special conditions of power supply systems in medical infrastructures are also pointed out, marking the similarities and orientation dictated by the healthcare infrastructure guidelines, which are bound to be stricter than the standard regulations. As the characterization of available guidelines depends on heterogeneous factors such as geographical conditions, quality of equipment or size of the health infrastructure, the approach that has been made involves general and common aspects, leaving space for singular modifications that may arise.

Considering this, an overview about power systems performance is carried out through a resilience point of view, comparing the existing data and resources with the new trends tied to the concept of resilience. In this line, significant coincidences and contrasts are intended to be found out.

III. RESULTS

The concept which has been assessed to evaluate the performance of a power system during a disruption period is the resilience. The more resilience the system has the quicker it gets to its normal and steady operation. According to the existing literature on the evaluation of problems recorded in power supply elements, several relevant items have been found and contrasted with the concept of resilience. The main concepts that have been extracted are reliability, adequacy, security and investments.

A. Reliability

Regarding reliability techniques, several assumptions have to be considered. Disruption states in power supply elements can be studied through a stochastic perspective, that is, the result of the output is the result of a combination between deterministic and random variables. In other words, the disruption of a power supply system is not fully predictable.

Classic trends regarding calculating reliability indices such as probability indices to measure the risk or assurance under specified conditions of configurations, load, time and timespan [12,13]. Other indices are frequency, duration and expectation indices which characterize the failure or capacity deficiency. The main objective is to obtain the expected performance loss of the system.

L refers to the density function of an annual peak load, $L_{\min}$ and $L_{\max}$ are the peaks of this function, C_j is the greatest value of capacity that is insufficient to meet the load, $P_C(C)$ is the probability density function for capacity

TABLE I. VARIABLES TO ASSESS PERFORMANCE LOSS, ADAPTED FROM [12].

Name	Variable	
Probability of not meeting the annual peak load	***P (Capacity Deficiency)***	
Formula		
$P=\int_{L_{\min}}^{L_{\max}} P_L(L)P_C(C_j)dL$. (1)		
Name	**Variable**	
Expected Energy Curtailment	***E (Capacity Deficiency)***	
Formula		
$E=\sum_{i=1}^{N} L\int_{L_{i\min}}^{L_{i\max}} \frac{8760}{N}(L-C)P_{Li}(L)P_{Ci}(C)dCdL$ (2)		
Name	**Variable**	**Formula**
Expected Loss of Load	***XLOL***	*E/P*

without a disruption, and $P_L(C)$ is the probability density function corresponding to the loads over a certain period of time. Both stationary and peak states can be observed if the facility is measured over a significant period of time (i.e. a year) (Table I).

Posterior studies state an approach which include deviations, calculations in singular buses, optimization models by using Monte Carlo simulations, a solution model and an interruption cost calculation, although the latter is slightly vague [14].

Where PNS_{ij} is the amount of not served demand at the bus "*i*", considering state "*j*". N is the number of simulated states (Table II). The expected energy deficit can be showed in annual terms.

Incidentally, adequacy can be defined as the ability of a system to supply the load under any circumstances. The strong relationship between adequacy and reliability is linked to redundancy criteria. Consequently, this concept is associated to static conditions, where no disturbances are involved, and as resilience is linked to these scenarios its contribution is neglectable if calculated through a classical approach. However, recent models regarding to resilience introduce the contribution of dynamic resilience [15] and can be extrapolated to this issue. This variable allows to quantify the ability to return to the original state implementing the variation of adequacy over time. Considering an oversized facility, the ability of the power supply system can be monitored by determining the number of available power supply systems, including redundant ones [16].

Reliability associated with adequacy can be calculated as:

TABLE II. POWER LOSS, ADAPTED FROM [14]

Name	Variable
Expected Power Not Supplied at bus *i*	***EPNS$_i$***
Formula	
$EPNS_i = \dfrac{\sum_{j=1}^{N} PNS_{ij}}{N}$. (3)	

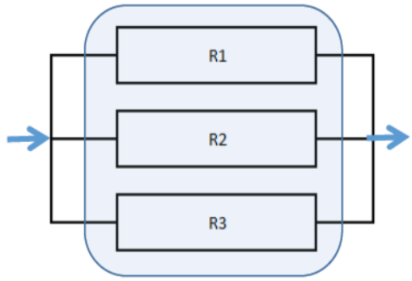

Figure 1. Parallel system diagram.

$$R(t) = 1 - \prod_{i=1}^{n} (1 - R_i(t)) \,, \tag{4}$$

where $F(t) = \prod_{i=1}^{n} F_i(t)$ and $R_i(t) = 1 - F_i(t)$ for each box, being *R* the reliability and *F* the probability of failure (Fig. 1).

On this line, resilience can be applied by integrating both the probability failure distribution function and the redundancy of the system. The main objective is to assess the reliability of the system, checking whether the power supply system would provide energy to the health infrastructure under unfavourable conditions or not.

B. *Availability*

The availability of a system can be defined as the ratio between the time where the facility produces energy and the whole period of time. It is a concept which is closely linked to reliability, since availability points out the actual power supply systems that can be used, while reliability focuses on the effectivity of power supply, no matter the source. This definition is particularly interesting regarding health infrastructure, as they usually are large facilities with auxiliary power systems to supply demanded energy in case of emergency.

Reference [17] provide a deep and exhaustive study about the factors that are involved regarding availability of subsequent subsystems, as well as other factors such as failure, transition and repair rate. The study is focused on a building cooling, heating and power facility (BHCP) and evaluates the sources of the power supply (Fig. 2). This is interesting from the point of view of a healthcare infrastructure, as the power that is supplied comes from both the grid and, if necessary, an auxiliary power system. Heating and cooling needs can be addressed as a different issue. At any rate, resilience can be considered with this regard as long as the system is bound to be studied through a recovery perspective. In this line, study presented in [18] fits in, as a serious disruption scenario is considered: an earthquake. Although at a larger scale, an analysis of the network vulnerability and a serviceability assessment of the system can be carried out, where losses in functionality, structure failures and the consequences of a loss of power is also evaluated. Typical parameters considered in these studies involve probability distributions and serviceability ratios.

In order to assess the availability of a power supply system in a health infrastructure, and to accomplish a compound of decision-making programs, protocols and risk management strategies, it is important to consider the records of the incidents, as well as their duration and severity.

In this view, alterations beyond set voltage limits and frequency limits which can affect the availability of the systems are to be supervised.

Renewable power supply systems have been implemented in modern buildings during recent years, and they can play an important role when it comes to satisfying energy demands. Wind turbines, solar power -photovoltaic and thermal where appropriate- can contribute to the health infrastructure energy demands. However, these sources often lack availability, as they have intermittent operation. Therefore, they can be pointed out as good auxiliary items when they are operative but establishing a baseline upon them could result in severe disruptions if power supply is not guaranteed. To accomplish a resilient power supply system based on renewable energy, new trends have been focused on storing energy excesses to compensate their inherent intermittency [19,20].

C. Security

From a different point of view, security stands as the main parameter of power supply facilities when it comes to the safety of both the facility and the people who may be at a potential risk. Security can be described as the ability of the system to respond to some disturbances that arise within that system.

It is interesting to evaluate the records of previous incidents, as well as the correspondent time of no-performance and if any damage and costs had to be considered. In this line, risk assessment and safety protocols are always to be in mind and applied if necessary. Regarding maintenance, risk-preparedness, emergency states and restoration activities, European guidelines are perfectly usable [21]. Apart from the features of the elements that make the facility up, the boundary conditions which the facility is subject to can also be considered. In this line, additional requirements and auxiliary power supply systems management have to be taken into account. National, regional or local

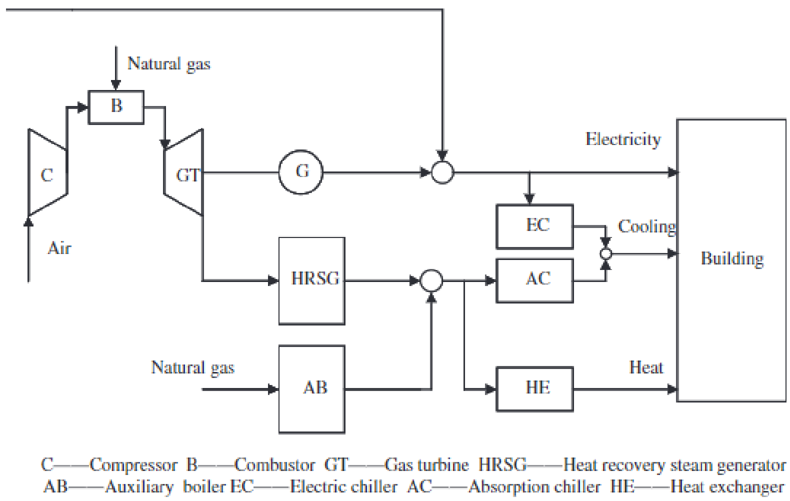

Figure 2. Multiple power supply systems for BHCP [17].

guidelines and regulations related to health infrastructures are also applicable.

New trends regarding safety management include terms as robustness, resilience, performance variability linked to outcomes and prophylaxis [22]. Although these concepts are referred to health and clinic issues, security can be addressed through resilience, constantly supervising safety issues while the system recovers its normal operation. Dynamic resilience may be useful to determine the capability and speed of recovery within the power supply systems in a health infrastructure during a disruption state.

D. Costs

Investments in equipment is one of the keys when it comes to design, optimization and operation. Not only can that, but costs of operation be significantly high if design conditions are not optimal. There is a counterpoint between costs and other "positive" parameters such as reliability, availability and resilience. There are several questions to be considered with this regard: "how much does it cost?", "is it worth?", "who is responsible within the different organization levels?" and "can costs be reduced without significantly decreasing quality?" [13]. Regarding this, it is interesting to assess reliability and investment costs curve and its marginal variations (Fig. 3).

Regarding direct costs, optimization analysis based on reliability costs can be carried out. Minimization of total costs is tied to finding the optimal value for both utility and consumer costs. This idea can be extrapolated to maintenance, repair and equipment renovation [13] (Fig. 4).

IV. Discussion

The utility of considering these alterations is useful because it helps to identify weak areas where modifications and reinforcements are needed. Additionally, chronological trends as

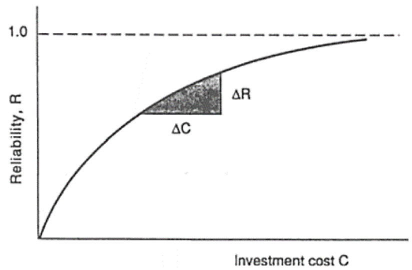

Figure 3. Marginal costs and reliability [13].

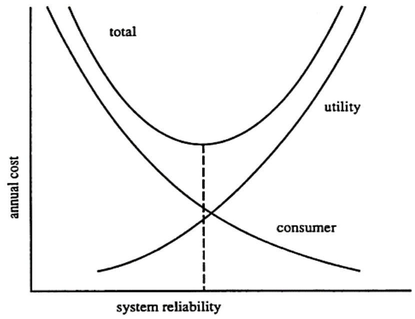

Figure 4. Overall costs vs. system reliability.

well as other statistical studies are also considered regarding reliability performance. Taking this into account, indices can be implemented for future reliability assessment. Given that resilience analysis is a complementary tool and it captures the idea of returning to a normal and steady operation ratio after a disruption scenario, a scoring system and a new framework can be deduced in this regard. This idea comes from semi-quantitative elements to assess the resilience of a generic system [23]. In healthcare infrastructures, it is typical to find questionnaires filled up by an expert panel to identify key factors to select and evaluate the weaker elements from the overall facility [24,25].

In addition to this, previous predictions can be modelled, proposing a comparison between actual models and previous results, where the actual operating experience is compared to the feedback cumulative results via the previously mentioned indices and statistical approaches. The response of the system can be observed and addressed through control processes, project management techniques and risk assessment tools. If any element of the system is bound to be modified, response changes can also be monitored. Furthermore, system malfunctions in this respect may be assessed through resilience assessment techniques, considering the applicability of qualitative models, semi-quantitative models and quantitative models [23] (Fig. 5). If any of the elements that define the facility is bound to fail and consequently would reduce the performance of the power supply system, scoring systems tied to resilience can be extracted and implemented, establishing a classification depending on whether the system is able to return to normal operation quickly or not. Failures in the system supply are tied to stochastic models, as they cannot be measured deterministically [13]. However, building a

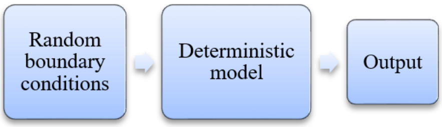

Figure 5. Assessment diagram.

deterministic model where input values are randomized may seem a reasonable option.

The modus operandi associated with the assessment of resilience involves analytical techniques. These ones refer to mathematical models, reliability indices evaluation based on numerical solutions and similar approaches, such as Markov diagrams or dynamic fault trees. The output of these models are normally expectation indices, which are able to orientate protocols and decision-making strategies [26].

Besides, simulation methods are also considered. In this group it can be found that probabilities, dependent events, behaviours and queueing operations are quite common. They can be simulated over a long period of time, providing detailed descriptions and a holistic understanding of the facility [27].

V. CONCLUSION

A review on the major parameters tied to power supply in healthcare systems has been carried out. Classical approaches have been considered and described, as main features, techniques and tools have been outlined. Afterwards, recent standpoints and studies have been extracted, in order to contrast them with previous models.

Resilience has been introduced as one of the trendiest concepts with transversal meanings, since it can be applied to various fields. In this study, power supply systems in health infrastructure have been assessed through resilience, regarding the possibility of unfavourable scenarios to happen and the capacity to return back to the original and steady state. Different applicable techniques have been pointed out, and relationships and contributions within classical and new concepts have been addressed.

ACKNOWLEDGMENT

The authors acknowledge the European Regional Development Fund and the Regional Ministry of Economy and Infrastructure for supporting this research. This study has been carried out through the research project GR-18029 linked to the VI Regional Plan for Research, Technological Development and Innovation of the Government of Extremadura 2017-2020.

REFERENCES

[1] Roccaforte, J., & Cushman. J. (2007). Disaster Preparedness, Triage and Surge Capacity for Hospital Definitive Care Areas: Optimizing Outcomes when Demands Exceed Resources. *Anesthesiology Clinics, 25*, 161-177.

[2] Djunaedy, E., Van den Wymelenberg, K., Acker, B., & Thimmana, H. (2011). Oversizing of HVAC system: Signatures and penalties. *Energy and Buildings, 43*, 468-475.

[3] Aghababian, R., Lewis, C. P., Gans, L., & Curley, F. J. (1994). Disasters Within Hospitals. *Annals of Emergency Medcine, 23*(4), 771-777.

[4] Zhong, S., Clark, M., Hou, X., Zang, Y., & Fitzgerald, G. (2014). Validation of a Framework for Measuring Hospital Disaster Resilience using Factor Analysis. *Environmental research and Public Health,* (11), 6335-6353.

[5] Sánchez-Barroso, G., & G. Sanz-Calcedo, J. (2019). Application of Predictive Maintenance in Hospital Heating, Ventilation and Air Conditioning Facilities. *Emerging Science Journal, 3*(5), 337-343.

[6] Dinh, L. T., Pasman, H., Gao, X., & Mannan, M. S. (2012). Resilience engineering of industrial processes: Principles and contributing factors. *Journal of Loss Prevention in the process Industries, 25*(2), 233-241.

[7] Billinton, R., & Allan, R. (1984). Power-system reliability in perspective, *Electronics and Power, 30*(3), 231-236.

[8] Zhong, S., Clark, M., Hou, X., Zang, Y., & Fitzgerald, G. (2014). Development of key indicators of hospital resilience: a modified Delphi study. *Journal of Health Services Research & Policy,* DOI: 10.1177/1355819614561537.

[9] Francis, R. A., Falconi, S. M., Nateghi, R., & Guikema, S. D. (2011). Probabilistic life cycle analysis model for evaluating electric power infrastructure risk mitigation investments, *Climatic change,* (106), 31-55.

[10] Urdaneta, A., Nadira, R., & Perez Jimenez, L. (1988). Optimal coordination of direction overcurrent relays in interconnected power systems. *IEEE Transactions on Power Delivery, 3*(3), 903-911.

[11] Amin, M. (2005). Energy Infrastructure Defense Systems. *Proceedings of the IEEE, 93*(5), 861-875.

[12] P. S. E. Committee. (1978). Reliability Indices for Use in Bulk Power Supply Adequacy Evaluation. *IEEE Transactions on Power Apparatus and Systems, 1&2 PAS-97*(4), 1097-1103.

[13] Billinton, R., & Allan, R. N. (1984). *Reliability Evaluation of Power Systems*. Pitman Books Limited.

[14] Ríos, S. M., V., Vidal P., & Kiguel, D. L. (1998). Bus-based reliability indices and associated costs in

the bulk power system. *IEEE Transactions on Power systems, 13*(3).

[15] Rose, A. (2007). Economic resilience to natural and man-made disasters: Multidisciplinary origins and contextual dimensions. *Environmental Hazards, 7*(4), 383-398.

[16] Cantabria University, Maintenance and Reliability General Theory, Open Course Ware.

[17] Wang, J., Fu, C., Yang, K., Zhang, X.-T., Shi, G.-H., & Zhai, J. (2013). Reliability and availability analysis of redundant BCHP (building cooling, heating and power) system. *Energy, 61*, 531-540.

[18] Adachi, T., & Ellingwood, B. R. (2008). Serviceability of earthquake-damaged water systems: effects of electrical power availability and power backup systems on system vulnerability. *Reliability Engineering and System Safety,* (93), 78-88.

[19] Su, W., Wang, J., & Roh, J. (2014). Stochastic Energy Scheduling in Microgrids With Intermittent Renewable Eergy Resources. *IEEE Transactions on Smart Grid, 5*(4), 1876-1883.

[20] Yekini Suberu, M., Wazir Mustafa, M., & Nouruddeen, B. (2014). Energy storage systems for renewable energy power sector integration and mitigation of intermittency. *Renewable and Sustainable Energy Reviews, 35*, 499-514.

[21] European Union, 2017. Commission regulation (EU) 2017/2197 - Establishing a network code on electricity emergency and restoration. EUR-LEX, 24 11 2017. [En línea]. Available at: https://eur-lex.europa.eu/legalcontent/EN/TXT/?uri=CELEX:32017R2196.

[22] Smith, A., & Plunkett, E. (2018). People, systems and safety: resilience and excellence in healthcare practice. *Anaesthesia, 74*(4), 508-517.

[23] Hosseini, S., Barker, K., & Ramirez-Marquez, J. (2016). A review of definitions and measures of system resilience. *Reliability Engineering and System Safety, 145*, 47-61.

[24] Heidaranlu, E., Ebadi, A., Khankeh, H. R., & Ardalan, A. (2015). Hospital Disaster Preparedness Tools: A Systematic Review. *PLOS Currents, 7*.

[25] *World Health Organization, Hospital Safety Index - Evaluation Forms 2nd Edition.* Available at*:* https://www.who.int/hac/techguidance/preparedness/hospital_safety_index_forms.pdf: WHO Library Cataloguing-in-Publication Data, 2015.

[26] Durga Rao, K., Gopika, V., Sanyasi Rao, V., Kushwaha, H., Verma, A., & Srividya, A. (2009). Dynamic fault tree analysis using Monte Carlo simulation in probabilistic sAfety assessment. *Reliability Engineering and System Safety, 94*, 872-883.

[27] Panteli, M., Pickering, C., Wilkinson, S., Dawson, R., & Mancarella, P. (2017). Power System Resilience to Extreme Weather: Fragility Modeling, Probabilistic Impact Assessment and Adaptation Measures. *IEEE Transactions on Power Systems, 32*(5), 3747-3757.

Influence of Supercapacitor Size on Battery Life and Selection of Optimal Parameter for Control Strategies in Hybrid Energy Storage System

Uroš Ilić[1], Vladislav Lazić[2], Bratislav Trojić[3]

[1,2,3]Faculty of Electronic Engineering, Nis, Serbia, urosilic@elfak.rs[1]; vladislav.lazic@gmail.com[2]; bratislav.trojic@gmail.com[3]

Abstract—**Hybrid energy storage systems are designed to overcome the shortcomings in the use of energy from renewable energy sources. The most efficient hybrid energy storage system, when we talk about solar energy, is the one that consists of a battery and a supercapacitor. Various topologies and control strategies have been developed to increase the efficiency of this system. This paper, in addition to considering the impact of supercapacitor size on battery life, also considers selection of parameters in the control strategy for energy allocation in a hybrid system. At the end of the paper, the simulation results obtained for different system parameters are presented.**

Keywords – battery, supercapacitor, lifespan, optimal parameters

I. INTRODUCTION

Electricity produced from renewable energy sources each year recorded an increase in production. According to a report by the International Renewable Energy Agency (IRENA) [1], in 2018, 6586 TWh of electricity was produced from renewable energy sources. In this production, energy from solar sources recorded an increase of 6.1% compared to the previous year, and compared to 2014 even 28%. The trend of increasing production will continue in the coming years.

The problem with renewable energy sources exists with the efficiency in monitoring the required amount of electricity, on the one hand due to frequent load fluctuations, and on the other due to frequent changes in the amount of energy produced from renewable energy sources. Therefore, it is necessary to store the energy and that is the most critical part of the system and represents the focus of considerable scientific research. The nature of the energy obtained from the sun is intermittent which causes frequent oscillations in the energy produced. A battery exposed to this process has a reduced lifespan [2], so the investment becomes unprofitable. Therefore, hybrid systems have been developed that mitigate the effects of the nature of solar energy.

There are different types of hybrid energy storage systems (HESS), and various topologies. As regards to different hybrid systems, the most commonly used are the battery/supercapacitor (SC), battery / superconducting magnetic storage system (SMES) and hydrogen storage system (HSS)/ battery HESS [3]. The most common hybrid energy storage system is battery/SC and it occurs in several topologies. Passive HESS is described in [4]. In this topology, HESS is directly connected to the DC link. In the case of a semi-active topology [5] there is one bidirectional DC/DC converter which is connected to the supercapacitor and which serves to satisfy the peak power and the high dynamic power demand. The topology with the best performance is the one that has two bidirectional converters, one of which is connected to the battery bank and the other to the SC bank. This topology enables wide application of control strategies and provides the highest level of flexibility in their application [6].

ISBN-978-86-80616-07-0

In this paper, in addition to the influence of the size of the supercapacitor on the battery life, the influence of the control strategy parameters on the battery life is considered as an additional parameter. This approach is a new one in relation to the work discussed in the literature.

The paper is organized as follows: Section II describes the structure of simulation system and control strategies. Section III shows the most significant results of the performed simulations. Finally, the conclusions and future works are described in Section IV.

II. Structure of Simulation System

A. System Configuration

The simulation system consists of photovoltaic energy system (PVES) which have solar PV arrays, a maximum power point tracking (MPPT) controller, DC/DC Boost converter, DC link, hybrid energy storage system (HESS) and changeable DC load. The hybrid energy storage system consist of lithium-Ion battery bank, supercapacitor bank, and a bi-directional DC/DC converter associated with each bank. Solar PV arrays, HESS and changeable load are connected on DC link.

Fig. 1 shows the schematic diagram of the simulated system.

B. Control of Photovoltaic Energy System (PVES)

The solar PV arrays contain 4 parallel strings and 2 series connections of Waaree Energies WU-120 solar cell. The output power of solar PV array depends on solar irradiation and cell temperature. The change in irradiation and temperature over time during the simulation is given in Fig. 2.

The photovoltaic (PV) array provides power to the unidirectional boost converter that is controlled by the Perturb and Observe (P&O) MPPT algorithm. Also, The Incremental

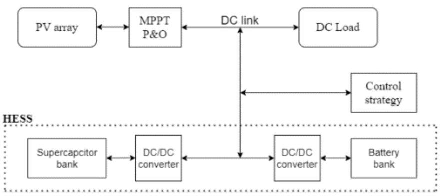

Figure 1. Schematic diagram of a simulated system.

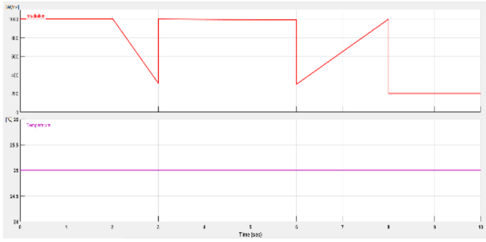

Figure 2. Irradiation and temperature diagram.

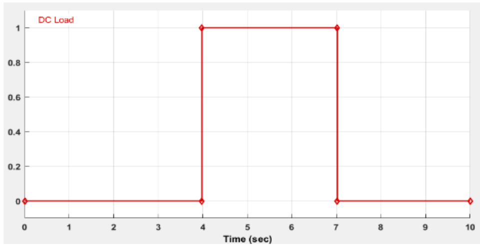

Figure 3. Change of DC load.

Conductance (IC) MPPT algorithm is often used in practice. Both algorithms have some drawbacks but are good enough to extract the maximum power from PVES [7].

On the other side, the power delivered by the system is defined by a DC load that is variable and has two levels. The change in load over time is shown in Fig. 3.

C. Control of HESS

According to the previously explained structure, HESS consists of a battery bank and a supercapacitor bank connected via bi-directional converters to a dc link. As HESS is used to control the power injection in grid. It is necessary to use DC/DC buck/boost converters here because DC/DC converter acts as a boost converter during HESS discharge mode and as a buck converter during HESS charge mode.

The applied power allocation strategy between the battery energy storage system (BESS) and the supercapacitor energy storage system (SESS) is described in detail in [8]. Power distribution according to the proposed strategy is based on the use of low pass filters (LPF). LPF divides the total current reference into low-frequency and high-frequency components. The low-frequency component is a reference to the battery current that is compared to the actual battery current and then the difference is passed to the PI controller, which further defines the duty ratio which is given to the pulse width modulation (PWM) generator to generate switching pulses corresponding to the battery bi-directional controller. The applied strategy differs from the others in the way of calculating the current reference for SESS. Battery error current ($I_{B_{err}}$) is added to high frequency component ($I_{HFC_{ref}}$). Due to the slow dynamics, the battery cannot follow the reference at the moment, so uncompensated power occurs in Eq. (1). In this regard, the current reference of the supercapacitor is calculated according to Eq. (2):

$$P_{B\_uncomp} = (I_{HFC_{ref}} + I_{B_{err}}) * V_B \ , \qquad (1)$$

$$I_{S\_ref} = \frac{P_{B\_uncomp}}{Vs} = (I_{HFC_{ref}} + I_{B_{err}}) * \frac{V_B}{Vs} \ . \qquad (2)$$

V_S represents the SC voltage, while V_B is the battery voltage. This reference supercapacitor current is compared with the actual SC current and the error is given to the PI controller. The PI controller generates the duty ratio, which is given to the PWM generator to generate switching pulses corresponding to SESS bi-directional converter.

Fig. 4 presents the HESS management scheme.

The parameters of the PI controllers used in the simulation are shown in Table I, and are defined as in [9].

The system is set up to simulate the intermittent nature of solar energy through variable irradiance, with a constant cell temperature. Also, load fluctuations are simulated by changing the load level as explained earlier. The parameters of the supercapacitor and the parameters of the control strategy were changed through 4 cases as shown in the next chapter.

TABLE I. PARAMETARS OF PI CONTROLERS.

PI controllers	Parameters	
	Proportional	Integral
PI 1	1.477	3077
PI 2	0.043	0.65
PI 3	0.45	14800

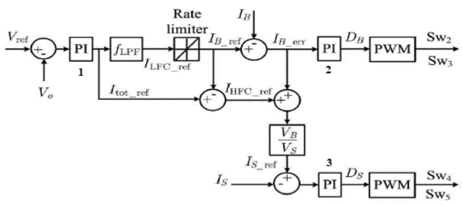

Figure 4. Control scheme of HESS [8].

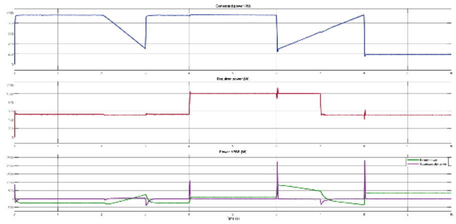

Figure 5. Simulation results for power flow in case 1.

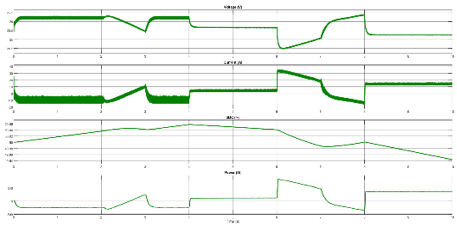

Figure 6. Simulation results for battery bank in case 1.

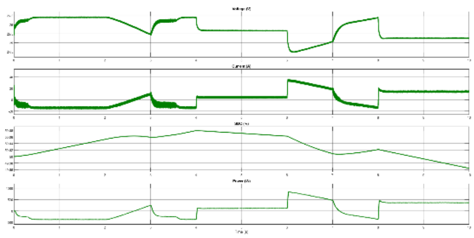

Figure 7. Simulation results for battery bank in case 2.

III. SIMULATION RESULTS

The parameters of the elements of the Hybrid Energy Storage System (HESS) used in the simulation are: battery bank 14Ah, 24V and supercapacitor bank 30F, 32V. The simulation lasts 10s, because the goal was to monitor the output parameters of the system (primarily batteries as the most sensitive part) on a small sample of time, with frequent changes in energy production and consumption. The initial value of the time constant low pass filter was taken as T = 0.05.

Fig. 5 shows a diagram of power flows through the elements of the system. In this example from case 1 it can be clearly seen how the elements of the HESS behave in relation to the produced and required energy.

The simulation results for the battery bank for case 1 are shown in Fig. 6. The diagram shows the values of voltage, current, battery charge (SOC) and power during the simulation. It is possible to notice that depending on the change of production and consumption, the battery bank adds energy to the system or charges its capacities in order to maintain a constant supply of energy.

Hybrid energy storage systems are designed to provide a longer life of the battery bank with the help of a supercapsitor bank due to the ability of the supercapacitor to charge and discharge quickly. In order to show the influence of the size of the supercapacitor bank on the observed parameters of the battery bank, several simulations were done with different sizes of the supercapacitor bank, and the characteristic one is shown in Fig. 7 marked as case 2. The size of the supercapasitor bank, in this case, is 1500 F.

The values of current in the moments of change (peaks) are lower by 10% and therefore there is a significant impact on the state of charge (SOC) of the battery, which would be 5% more charged in an hour of simulated activity than in the first case. Also, in the period of 0-3 seconds and 3-4 seconds, the oscillations of the current are reduced.

As mentioned earlier, in the filtration based control strategy the low pass filter serves to allocate power between the battery bank and the supercapacitor bank. The value of the time constant of the low pass filter crucially affects how much energy will flow through the battery and which through the supercapsulator Increasing the value of this parameter reduces the amount of energy that passes through the battery, and this allows the use of a battery that has a smaller capacity, without affecting the conditions in the system.

Fig. 8 and Fig. 9 show diagrams with system parameters from case 1 but with changed time constants of the low pass filter. First, case 3 is shown where the time constant is

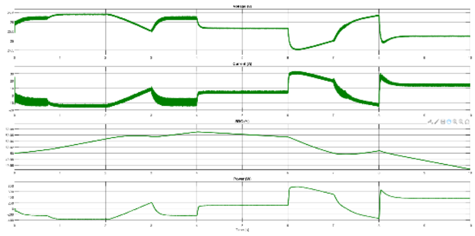

Figure 8. Simulation results for battery bank in case 3.

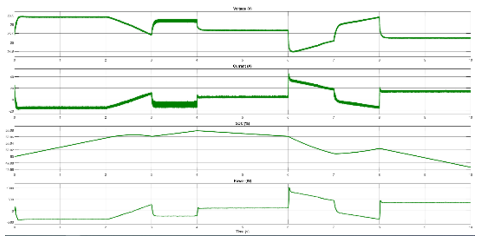

Figure 9. Simulation results for battery bank in case 4.

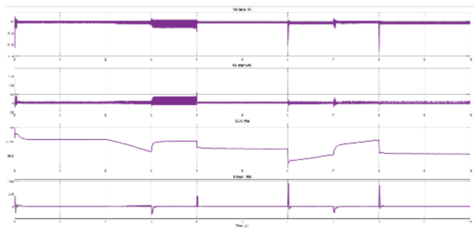

Figure 10. Simulation results for supercapasitor bank in case 4.

T = 0.1 (increase), then case 4 and T = 0.015 (decrease).

An increase in the time constant contributes to a decrease in the oscillation of the current in the initial period and there is a decrease in the value of the current in moments of sudden changes (peaks) of the current.

The time constant set in this way provides better conditions than in case 1, but not in relation to case 2.

In the diagram shown in Fig. 9, it can be seen that in case 4 (T = 0.015) there are no large current oscillations in the initial period, as well as that the SOC is at the level as in case 2. The downside of this parameter setting is the current values in the peaks, which are higher than in the case of 2 and up to 20 percent. This is due to the reduction of the time constant of the low pass filter, which results in more of the energy passing through the battery bank.

According to the theory, the supercapasitor bank takes on a large amount of energy in moments of sudden changes so that the battery does not suffer large stresses that reduce its lifespan. Fig. 10 shows a diagram of a supercapacitor bank for case 3, which shows the engagement of a supercapacitor in moments of sudden changes. In these moments, the power flowing through the supercapacitor is large, while in other time periods, the power is equal to zero. In other simulated cases, the difference is only in the amount of power that the SC takes on.

IV. Conclusion

Using the optimal size of battery and supercapacitor, as well as the optimal system parameters contributes to making the investment in the renewable energy systems more profitable. As shown in the simulations, increasing the capacity of the supercapacitor significantly improves the conditions in the battery bank, but due to the high price of the supercapacitor there are profitability limits up to which it is profitable to increase the size of the supercapacitor. The time constant of the low pass filter allows the allocation of power between battery and supercapacitor, which contributes to increasing the battery life, but only within certain limits. Often, the price of the system is more important to consumers than the length of service life, so it is necessary to develop optimization methods to determine the optimal parameters of the system taking into account a large number of economic and technical parameters. Such parameters would enable the development of a better management strategy, and by including algorithms for forecasting production and consumption, it is possible to achieve a high degree of efficiency and longevity of renewable energy systems.

Acknowledgment

This work was supported by the Ministry of Education, Science and Technological Development, Republic of Serbia (Project number: III 44006).

References

[1] IRENA. (2019). *Internacional Renewable Energy Agency Report*.

[2] Wang, G., Ciobotaru, M., & Agelidis, V. G. (2014). Power smoothing of large solar PV plant using hybrid energy storage. *IEEE Transactions on Sustainable Energy*, *5*(3), 834-842.

[3] Chong, L. W., Wong, Y. W., Rajkumar, R. K., Rajkumar, R. K., & Isa, D. (2016). Hybrid energy storage systems and control strategies for stand-alone renewable energy power systems. *Renewable and sustainable energy reviews*, *66*, 174-189.

[4] Ma, T., Yang, H., & Lu, L. (2015). Development of hybrid battery–supercapacitor energy storage for remote area renewable energy systems. *Applied Energy*, *153*, 56-62.

[5] Song, Z., Hofmann, H., Li, J., Han, X., Zhang, X., & Ouyang, M. (2015). A comparison study of different semi-active hybrid energy storage system topologies for electric vehicles. *Journal of Power Sources*, *274*, 400-411.

[6] Kuperman, A., & Aharon, I. (2011). Battery–ultracapacitor hybrids for pulsed current loads: A review. *Renewable and Sustainable Energy Reviews*, *15*(2), 981-992.

[7] Atallah, A. M., Abdelaziz, A. Y., & Jumaah, R. S. (2014). Implementation of perturb and observe MPPT of PV system with direct control method using buck and buck-boost converters. *Emerging Trends in Electrical, Electronics & Instrumentation Engineering: An international Journal (EEIEJ)*, *1*(1), 31-44.

[8] Kollimalla, S. K., Mishra, M. K., & Narasamma, N. L. (2014). Design and analysis of novel control strategy for battery and supercapacitor storage system. *IEEE Transactions on Sustainable Energy*, *5*(4), 1137-1144.

[9] Lotfi, R. (2018*). Energy management for Stand-alone Photovoltaic Battery-Supercapacitor Hybrid Storage System*. Available at: http://www.matworks.com

Shunt Compensation for Voltage Stability by Continuation Power Flow: Case of Electric Community of Benin Power Grid

Yao Bokovi[1], Comlanvi Adjamagbo[2], Adekunlé Akim Salami[3], Ayité Séna Akoda Ajavon[4]

[1,2,3,4]Department of Electrical Engineering, Laboratory of Research in Engineering Sciences (LARSI), High National School of Engineers (ENSI), Regional Center of Excellence for the Control of Electricity (CERME), University of Lome (UL), Lome, Togo, bokoviyao@gmail.com[1]; adjamagbonicolas@yahoo.fr[2]; akim_salami@yahoo.fr[3]; asajavon@yahoo.fr[4]

Abstract—**The study presented in this paper is the shunt compensation of a power grid to regain the stability of the voltage lost due to the large variation in the active power demand of a PQ consumption node. The voltage profile of the entire electricity transmission network is used by the continuation power flow (CPF) method to observe the voltages of the network nodes in order to determine the critical point and predict the voltage stability of the said power grid. Using a stepped shunt compensation methodology developed in this study, the value of the shunt to be connected to the node where the voltage is critical due to the increased load was determined. This methodology also makes it possible to improve the performance of the power grid through parameters such as the critical voltage, the maximum voltage while respecting the constraints related to the voltages, the load factor and the voltage sensitivity factor. The results obtained for the case of the power grid of the Electricity Community of Benin (CEB) showed that thanks to the compensation by shunt at node 6 of this power grid, we note with an increasing evolution of the load factor, the rise in voltages initially low, with values which respect the constraints linked to the tensions of the various nodes. This study will help a power grid operator to avoid voltage instability in the grid.**

Keywords - continuation power flow, Newton-Raphson, voltage profile, Shunt compensation, voltage stability sensitivity factor

I. INTRODUCTION

Electrical systems are characterized by nodes with associated generation groups, loads (consumption), lines and electrical energy transformers. It includes the production, transport and consumption (charges) of electrical energy. The essential objectives of electrical systems are the search for quality and the reduction of operating costs while respecting the security constraints of said system. The major safety constraints in an HV power grid are the stability limit and the voltage profile [1-3]. The profile of the voltages in the power grid nodes makes it possible to evaluate the variation in the voltage of each node of the power grid in order to control the stability of the grid within its limits to guarantee a production - consumption adequacy [4].

Thanks to the CPF, several studies in [5,6], [7,8] have been made on voltage drops at nodes of power grid.

Thus the objective of this paper is to rely on the CPF to define a methodology which consists in determining the critical voltage point and the limit of increase in the demand for electrical energy in order to prevent the voltage instability of the power grid by shunt compensation. The case of the electricity network of the Electric Community of Benin is studied in this paper. First it is exposed after the introduction, the CPF method used, followed by the presentation of the CEB's HV power grid. Then the data processing in a Matlab environment with the results is carried out and finally analyzes and discussions followed by the conclusion are presented.

II. THE CONTINUATION POWER FLOW METHOD: CPF

The CPF method begins with the basic conditions using conventional solutions of load distribution (Load Flow: LF) from the Newton-Raphson algorithm to calculate the basic parameter denoted λ .To do this, we reformulate the Load Flow equation to introduce a load parameter λ .We rewrite the Load Flow equation in a matrix form known as the Jacobian matrix J.

Consider the conventional Load Flow equation defined in relation (1), [9]:

$$\begin{bmatrix} P_i - P_{gi} + P_{Li} \\ Q_i - Q_{gi} + Q_{Li} \end{bmatrix} = 0 \quad , \qquad (1)$$

avec:

$$P_i = \sum_{k=1}^{n} V_i V_k V_{ik} \cos(\delta_i - \delta_k - \theta_{ik}) \quad , \qquad (2)$$

$$Q_i = \sum_{k=1}^{n} V_i V_k V_{ik} \sin(\delta_i - \delta_k - \theta_{ik}) \, , \qquad (3)$$

where: P_i and Q_i are respectively the active and reactive powers at node *i*; P_{gi} and Q_{gi} the active and reactive powers generated at node *i*; PL_i and QL_i the active and reactive power consumed at the bus *i*; $V_i\angle\delta_i$ *et* $V_k\angle\delta_k$ the voltages at buses *i* and *k*; $Vik\angle\theta ik$ the admittance (*i*, *k*) element of the Y_{bus} admittance matrix; *n* is the total number of buses in the power grid.

By asking $P_i^{inj} = P_{gi} - P_{Li}$ and $Q_i^{inj} = Q_{gi} - Q_{Li}$ we rewrite relation (1) in relation (4):

$$g(\partial, V) = \begin{bmatrix} P(\delta,V) - P^{inj} \\ Q(\delta,V) - Q^{inj} \end{bmatrix} = 0 \, , \qquad (4)$$

where: $P(\delta,V)$ *and* $Q(\delta,V)$ are the vectors of the active and reactive power of the power grid; (δ,V) variable vector composed of the angle and the magnitude of the voltage of each bus of the power grid; P^{inj} *et* Q^{inj} are the vectors of the active and reactive power injected from each bus of the network.

In order to know the state of the electrical system for different load factors, we must add a state variable λ to Eq. (4); we can obtain the plot of δ "and *V*" by varying λ [7]. The system of Eq. (4) then becomes that of relation (5):

$$f(\delta, V, \lambda) = \begin{bmatrix} P(\delta,V) - \lambda P^{inj} \\ Q(\delta,V) - \lambda Q^{inj} \end{bmatrix} = 0 \, , \qquad (5)$$

where: λ is the continuous parameter such that $\lambda \le 0 \le \lambda_{\max}$.

In the Newton-Raphson method (method not developed in this paper) for Load Flow, the reformulated Jacobian matrix of the system of Eqs. (5) is written at relation (6), [7]:

$$J(\partial, V, \lambda) = \begin{pmatrix} \frac{\partial P_2}{\partial \delta_2} & \cdots & \frac{\partial P_2}{\partial \delta_n} & \frac{\partial P_2}{\partial V_{m+2}} & \cdots & \frac{\partial P_2}{\partial V_n} & \frac{\partial P_2}{\partial \lambda} \\ \vdots & & \vdots & \vdots & & \vdots & \vdots \\ \frac{\partial P_n}{\partial \delta_2} & \cdots & \frac{\partial P_n}{\partial \delta_n} & \frac{\partial P_n}{\partial V_{m+2}} & \cdots & \frac{\partial P_n}{\partial V_n} & \frac{\partial P_n}{\partial \lambda} \\ \frac{\partial Q_{m+2}}{\partial \delta_2} & \cdots & \frac{\partial Q_{m+2}}{\partial \delta_n} & \frac{\partial Q_{m+2}}{\partial V_{m+2}} & \cdots & \frac{\partial Q_{m+2}}{\partial V_n} & \frac{\partial Q_{m+2}}{\partial \lambda} \\ \vdots & & \vdots & \vdots & & \vdots & \vdots \\ \frac{\partial Q_n}{\partial \delta_2} & \cdots & \frac{\partial Q_n}{\partial \delta_n} & \frac{\partial Q_n}{\partial V_{m+2}} & \cdots & \frac{\partial Q_n}{\partial V_n} & \frac{\partial Q_n}{\partial \lambda} \end{pmatrix}, \qquad (6)$$

This Jacobian matrix makes it possible to find the point of bifurcation of the system by systematic gradual increase of the load factor λ of the system thanks to the CPF. CPF techniques are a very robust tool for the calculation of trajectories of one or more parameters [7]. The considered system is summarized by relation (5).

Continuation Power Flow (CPF) is an iterative process which from an initial solution defined by $(\delta^j, V^j, \lambda^j)$, consist to calculate a new situation $(\delta^{j+1}, V^{j+1}, \lambda^{j+1})$ avec $\lambda^j > \lambda^{j+1}$. This process thus converges towards $\lambda_{\max}$.

The CPF is then carried out in three steps, namely parametrization, prediction and correction.

A. Parametrization

Parametrization is mathematically a means of identifying each solution so that the next or previous solution can be evaluated. In this paper, the natural parametrization which takes directly λ as a parameter has been used according to relation (7):

$$p^j(\delta, V, \lambda) = \lambda - \lambda^j - \sigma = 0\,, \qquad (7)$$

where: λ^j is the initial parameter; λ the new parameter and σ continuous measurement of the step.

B. Prediction

Prediction is the process of producing an estimate $(\hat{\delta}^{j+1}, \hat{V}^{j+1}, \hat{\lambda}^{j+1})$ of the new solution according to relation (8):

$$\begin{bmatrix} \hat{\delta}^{j+1} \\ \hat{V}^{j+1} \\ \hat{\lambda}^{j+1} \end{bmatrix} = \begin{bmatrix} \delta^j \\ V^j \\ \lambda^j \end{bmatrix} + \sigma \overline{z_j}\,, \qquad (8)$$

with:

$$\overline{z_j} = \frac{z_j}{\|z_j\|_2}\,, \qquad (9)$$

$$\begin{bmatrix} f_\delta & f_V & f_\lambda \\ & e_k & \end{bmatrix} z_j = \begin{bmatrix} 0 \\ 1 \end{bmatrix}, \qquad (10)$$

where: $z_j = [d\delta \quad dV \quad d\lambda]$ is the tangent vector, $\overline{z_j}$ is the normalized tangent vector; $e_k = \left[p_\delta^{j-1} p_V^{j-1} p_\lambda^{j-1}\right]$ is the appropriate and dimensioned row vector such that all its elements are zero except the $k^{ième}$ element that is worth ± 1 he sign of the variation; *k* is the index of the maximum component of the tangent vector respecting the Eq. (11), [10]:

$$(\delta_{k,} V_k) : |z_k| = \max\{|z_1|, |z_2|, \ldots |z_N|\}\,, \qquad (11)$$

where: $N = 2_{n_1} + n_2 + 1$ with n_1 the number of buses *PQ* et n_2 the one of generation buses *PV*.

C. Correction

The correction step provides the new solution $(\delta^{j+1}, V^{j+1}, \lambda^{j+1})$ by correcting the predicted solution $(\hat{\delta}^{j+1}, \hat{V}^{j+1}, \hat{\lambda}^{j+1})$ The Newton-Raphson method is used to find this new solution by solving the equation system of relation (12):

$$\begin{bmatrix} f(\delta, V, \lambda) \\ p^j(\delta, V, \lambda) \end{bmatrix} = 0\,. \qquad (12)$$

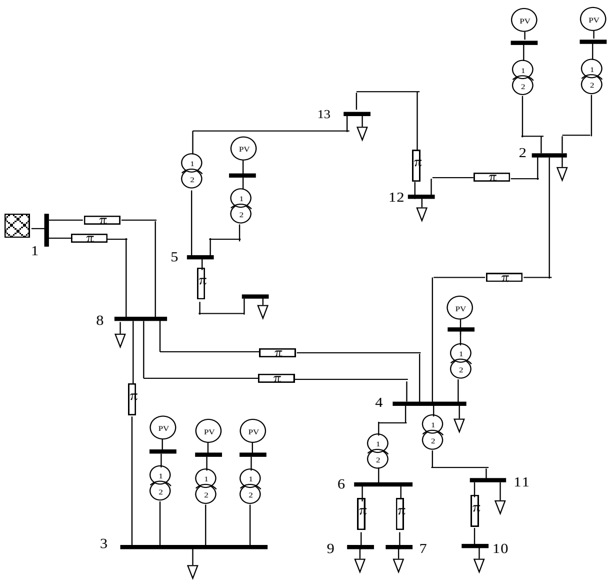

Figure 1. CEB's HV power grid

TABLE I. THE DATA OF THE CEB'S HV POWER GRID BUSES.

a	b	c	d	e	f	g	h	i	j	k	l	m	n
VRA	1	3	0	0	0	0	1	1	0	161	1	1.3	0.9
ATA	2	1	3.9	2.8	0	0	1	1	0	161	1	1.3	0.9
AVA	3	1	2.6	1.59	0	0	1	1	0	161	1	1.3	0.9
BOH	4	1	6.5	4.5	0	0	1	1	0	161	1	1.3	0.9
CVE	5	1	36.6	17.89	0	0	1	1	0	161	1	1.3	0.9
KAR	6	1	7.745	3.786	0	0	1	1	0	161	1	1.3	0.9
LAF	7	1	37.17	18.172	0	0	1	1	0	161	1	1.3	0.9
LPO	8	2	21.23	12.99	0	0	1	1	0	161	1	1.3	0.9
MAG	9	2	0	0	0	0	1	1	0	161	1	1.3	0.9
MOM	10	1	9.186	5.92	0	0	1	1	0	161	1	1.3	0.9
NAN	11	2	0	0	0	0	1	1	0	161	1	1.3	0.9
ONI	12	1	2.9	5.7	0	0	1	1	0	161	1	1.3	0.9
SAK	13	1	0.6	0.3	0	0	1	1	0	161	1	1.3	0.9

Legend: ATA : Atakpamé ; AVA : Avakpa ; BOH : Bohicon ; CVE : Cotonou-Vedogou ; KAR : Kara ; LAF : Lomé-Aflao ; LPO : Lomé-Port ; MAG : Maria-Gleta ; MOM : Mome-hagou ; ONI : Onigbo, SAK : Sakete ; a : Design ; b : Bus type (1 = PQ, 2 = PV, 3 = Slack, 4 = isolated); c : bus number (positive integer); d : real power demand Pd [MW] ; e : reactive power demand Qd [MVAr] ; f : shunt conductance Gs (MW demanded at V = 1.0 p.u.) ; g : shunt susceptance Bs (MVAr injected at V = 1.0 p.u.) ; h : area number (positive integer); i : voltage magnitude Vm (p.u.) ; j : voltage angle Va (degrees) ; k : base voltage (kV) ; l : loss zone (positive integer); m : maximum voltage magnitude Vmax (p.u.) ; n : minimum voltage magnitude Vmin (p.u.).

TABLE II. DATA OF THE TRANSMISSION LINES OF THE CEB'S HV POWER GRID.

1	2	3	4	5	6	7	8	9	10	11	12	13
9	13	0.029	0.086	0.040	404	444	485	0	0	1	-360	360
12	13	0.024	0.742	0.034	404	445	485	0	0	1	-360	360
5	9	0.007	0.017	0.007	405	446	486	0	0	1	-360	360
3	9	0.029	0.061	0.026	406	446	487	0	0	1	-360	360
9	10	0.651	0.149	0.065	406	446	487	0	0	1	-360	360
3	10	0.038	0.087	0.038	406	447	487	0	0	1	-360	360
7	10	0.039	0.090	0.039	407	447	488	0	0	1	-360	360
10	11	0.613	0.183	0.084	407	448	488	0	0	1	-360	360
7	8	0.009	0.027	0.012	407	448	489	0	0	1	-360	360
2	6	0.126	0.377	0.171	408	449	490	0	0	1	-360	360
2	11	0.019	0.057	0.026	409	449	490	0	0	1	-360	360
4	11	0.042	0.126	0.058	409	450	491	0	0	1	-360	360
4	12	0.039	0.118	0.054	409	450	491	0	0	1	-360	360
7	1	0.091	0.208	0.091	408	449	490	0	0	1	-360	360

Legend: 1 : F_BUS " from" bus number ; 2 : T_BUS " to" bus number ; 3 : BR_R resistance (p.u.) ; 4 : BR_X reactance (p.u.) ; 5 : BR_B total line charging susceptance (p.u.) ; 6 : RATE_A MVA rating A (long term rating), set to 0 for unlimited; 7 : RATE_B MVA rating B (short term rating), set to 0 for unlimited; 8 : RATE_C MVA rating C (emergency rating), set to 0 for unlimited; 9 : TAP transformer off nominal turns ratio, (taps at " from" bus, impedance at " to" bus, i.e. if r = x = b = 0, tap = |Vf /Vt|) ; 10 : SHIFT transformer phase shift angle (degrees), positive) delay ; 11 : BR_STATUS initial branch status, 1 = in-service, 0 = out-of-service; 12 : ANGMIN minimum angle difference, θf - θt (degrees) ; 13 : ANGMAX maximum angle difference, θf - θt (degrees).

III. MATERIALS

The CEB's HV power grid shown in Fig.1 and made up of 13 buses and 14 power transmission lines is used in this paper. Matpower 6.0 [11] software in a Matlab R2016a environment was used.

The data from the HV power grid were processed and modeled according to the format of Matpower, [12,13]. The data of the CEB's HV power grid buses are presented in Table I. The buses are distributed as follows: 03 PV bus, 01 slack bus and 09 PQ bus. Table II contains the formatted data of the electrical energy transmission lines of the CEB's HV network.

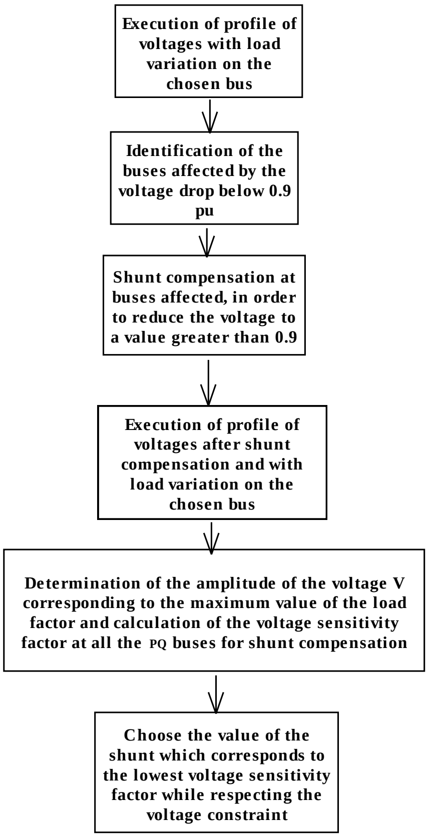

Figure 2. Shunt compensation methodology.

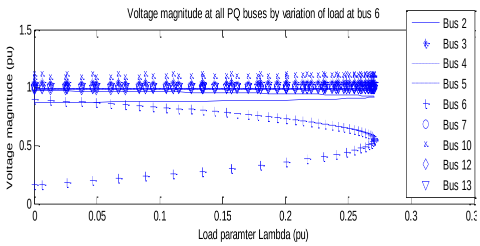

Figure 3. Voltage magnitude at all PQ buses by variation of load at bus 6.

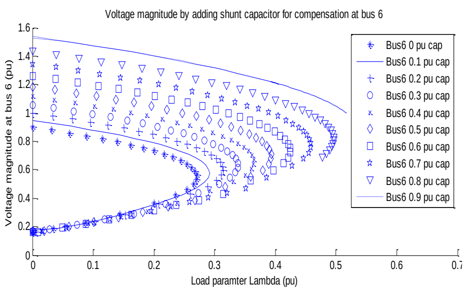

Figure 4. Voltage magnitude by adding shunt capacitors for compensation at bus 6.

IV. Methodology

The adopted compensation comparison methodology is presented in Fig. 2. In this methodology, we define at each load bus i *PQ* the sensitivity factor S_{vi} of the voltage stability by Eq. (13):

$$S_{Vi} = \left| \frac{dV_i}{dP_{Total}} \right|, \tag{13}$$

where dV_i is the variation of the voltage in per unit (pu) at the bus *i* and dP_{Total} The lower this sensitivity factor to a bus *i* compared to another bus j, the more stable the bus *i*. The voltages of the buses of the power grid are subjected to a constraint of magnitude margin *V* according to Eq. (14) to guarantee the stability of the network:

$$V_{\min} \le V \le V_{\max} \,. \tag{14}$$

V. Results and Discussion

By varying the active power demand on bus 6 of the CEB's power grid via the load factor lambda λ, the voltage magnitude of the nine (09) PQ buses is obtained through the network voltage profile. Fig. 3 shows the voltage profile.

The critical voltage at bus 6 is 0.5616 pu for a maximum load factor $\lambda_{\max}$ equal to 0.2705. This led to making the shunt compensation to bus 6 of the CEB's power grid. Fig. 4 shows the voltage profile curves of the two types of compensation at bus 6.

According to the constraints related to the minimum and maximum magnitudes on bus 6, the results retained for the choice of the shunt compensation are summarized in Table III.

After having found the optimum value of the shunt compensator at node 6, one proceeds to an execution of the voltage profile at all the nodes with an increasing variation of the load at node 6. The results obtained for the PQ nodes are shown at Fig. 5 and recorded in Table IV.

TABLE III. RESULTS OF OPTIMAL SHUNT COMPENSATION AT BUS 6 IN CEB'S POWER GRID.

Value of shunt compensation [pu]	**V_{6max} [pu]**	**$V_{6critical}$ [pu]**	**Load para meter λ_{max} [pu]**	**Voltage stability sensitivity factor : Sv_6**
0.6	1.25	0.97	0.45	0.010

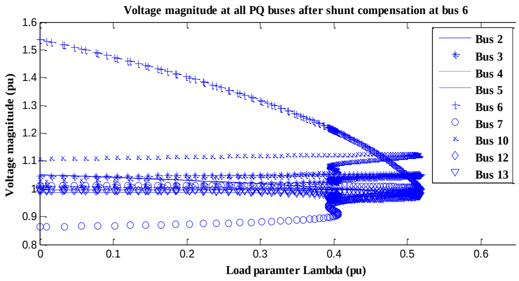

Figure 5. Voltage magnitude at all PQ buses after shunt compensation at bus 6.

TABLE IV. NEW VALUES OF CRITICAL VOLTAGE MAGNITUDE AND SENSITIVITY FACTOR FOR ALL PQ BUSES AFTER SHUNT COMPENSATION AT BUS 6 IN CEB'S POWER GRID.

λmax = 0.4517 pu after shunt compensation at bus 6		
PQ Bus N°	**$V_{critical}$ [pu]**	**Voltage stability sensitivity factor Sv**
2	0.972	0.0014
3	1.05	0.00011
4	0.978	0.00013
5	0.996	1.47E-17
6	0.969	0,01018
7	0.998	0.00028
10	1.122	0.00025
12	0.983	0.00017
13	0.976	0.00041

We observe from the results of Table IV and Fig. 5 that although the maximum value of the load factor has increased from 0.2705 to 0.45, the voltage of all the consumption nodes PQ is greater than 0.9, the lower value of the constraint. This acceptable result is obtained from the shunt compensation carried out at node 6 of the power grid.

VI. CONCLUSION

The results of this study sufficiently show that the voltage instability of a power grid can be avoided from shunt compensation at the node where the energy demand increases. The methodology developed in this paper is based on the continuation power flow (CPF) to determine the voltage profiles, the value of the critical point of the voltage according to the limit of the load factor in the power grid. The results are satisfactory, however shunt compensation can be combined with another type of compensation to improve these results.

REFERENCES

[1] Ammari, S. (2000). Interaction des dispositifs FACTS avec des charges dynamiques dans les réseaux de transport et d'interconnexion. Thèse de doctorat de l'Institut National Polytechnique de Grenoble. Spécialité Génie Electrique.

[2] Miller T. J. E. (1982). *Reactive power control in Electric System*. John Wiley & sons.

[3] Yao, B., Adekunlé, S., Mawugno Kodjo, K., Dotche K., & Koffi-Sa. B. (2019). Comparative Study of the Voltage Drops Estimation on Electrical Distribution grid: Case study of the Togolese Company of Electricity and Energy grid. In *Conference IEEE PES/IAS PowerAfrica, Abuja, Nigeria*, (pp. 255-260), doi: 10.1109/PowerAfrica.2019.8928838.

[4] Ladjici A. A. (2005). Calcul évolutionnaire : Application sur l'optimisation de la planification de la puissance reactive. Mémoire de Magister en Electrotechnique. Ecole Nationale Polytechnique d'Alger. Algérie.

[5] Anand U. P., & Dhurmeshkumar P. (2013). Voltage Stability assessment using Continuation Power Flow. *International Journal of Advanced Research in Electrical Electronics and instrumentation Engineering*. *2*(8), 4013-4022.

[6] Jinquan, Z., Xiaolong, F., Changnian, L., & Wei Wenhui. W. (2015). Distributed continuation power flow method for integrated transmission and active distribution network. *J. Mod. Power Syst. Clean Energy*: 573-582. DOI 10. 1007/140565-015-0167-2.

[7] Satish, K. et al. (2015). Analysis of Power Flow, Continuous Power Flow and Transient Stability of IEEE-14 Bus integrated Wind Farm Using PSAT. In *International Conference on Energy Economics and Environment (ICEEE), Noid* 978-1-4673-7492-7/15.

[8] Ajjarapu, V., & Colin, C. (1992). The Continuation Power Flow: a tool for steady state voltage stability analysis. *Transactions on Power Systems*, *7*(1), 416-423.

[9] Castro, A. J., & Phulpin, Y. (2007, Septemer). Estimation locale de la stabilité en tension. In Conférence EF, ENSEEIHT, Toulouse, (pp. 6-7).

[10] Bokovi, Y., Adjamagbo, C., Salami, A. A., & Ajavon, A. S. A. (2020). Comparative Study of the Voltage Stability of an Hight Voltage Power Grid: Case of the Power Grid of the Electric Community of Benin. *Science Journal of Energy Engineering*. *8*(2), 15-24. doi: 10.11648/j.sjee.20200802.11

[11] Keskin, M. B. (2007). Continuation Power Flow and Voltage Stability in Power Systems. Thesis M. Sc.

Departement of Electrical and Electronics Engineering. Middle east Technical University, USA.

[12] Zimmerman, R. D., & Murillo-Sanchez, C. E. (2016). Matpower 6.0 User's manuel.

[13] Bircheld, A. B., Xu, T., Gegner, K. M., Shetye, K. S., &. Overbye, T. J. (2017). Grid Structural Characteristics as Validation Criteria for Synthetic Networks. *IEEE Transactions on Power Systems* D-17.

Seismic Waves Incurred as a Result of Blasting Operations

Suzana Lutovac[1], Luka Crnogorac[2], Jelena Majstorović[3], Rade Tokalić[4]

[1,2,3,4]University of Belgrade – Faculty of Mining and Geology, Belgrade, Serbia, suzana.lutovac@rgf.bg.ac.rs[1]; luka.crnogorac@rgf.bg.ac.rs[2]; jelena.majstorovic@rgf.bg.ac.rs[3]; rade.tokalic@rgf.bg.ac.rs[4]

Abstract—**The application of explosive energy is an important discipline of modern mining technology. In mining, explosives are primarily used in the extraction of mineral raw materials from solid rocks. The development of production capacities has conditioned the use of large quantities of explosives during blasting operations. On the one hand, this leads to the improvement of technical and economic indicators while, on the other hand, it results in the increase of negative effects that accompany blasting operations. By negative effects of blasting, we are implying the seismic action of blasting, action of air wave, sound effect, scattering of demined rock mass, etc. During blasting, the potential energy of the explosive is converted into mechanical work. This energy (near the place of blasting) destroys, crushes the rock mass, creates cracks and permanent deformations at a slightly greater distance, and – at an even greater distance – it turns into elastic deformations. In this zone, there is no destruction but, rather, oscillation of rock mass particles which feels like a quake; it is the seismic effect of an explosion. Seismic waves that spread through the rock mass cause oscillations of the ground and buildings. This paper describes the types and characteristics of seismic waves which spread through, and on the surface of, the rock massif. In addition, the basic factors that influence the formation of the seismic waves and determine the intensity of the seismic vibrations have been presented.**

Keywords – blasting, seismic vibrations, seismic wave, parameters of rock mass oscillation

I. Introduction

The energy of explosives is contained in an explosive substance. Explosives are simple or complex chemical substances that hold the property of decomposing abruptly under the influence of external stimuli and then, consequently, turning into a gaseous state. The most effective form of decomposition of explosive substances in the destruction of rock mass is detonation. Detonation is a form of explosion in which the chemical reaction takes place at high speed, creating high pressure and a very high temperature in the zone of the explosive substance. Thereby the detonation wave moves through the explosive substance at a constant speed. High pressures caused by detonation are transferred from the explosive charge to the surrounding rock mass. This pressure is transmitted in the form of a pulse, so that the application of pressure to the working environment surrounding the explosive charge is of a wave nature, via a shock wave. With greater distance from the center of the explosion, the shock wave becomes less and less intense. Depending on the distance from the center of the explosion, there are different changes noticed in the rock mass. In homogeneous and isotropic environments, three zones can be distinguished: crumbling zone, destruction zone and quake (vibration) zone [1].

Crumbling zone – in this zone, the shock wave exerts pressure on the surrounding rocks at a speed higher than the speed of sound while in the zone around the explosion, – and at a distance of $(3 \div 7)r$ (where r is the radius of explosive charge) – rock material crumbles and is compacted into a rock massif. The resulting pressure is exponentially higher than the compressive strength of the rock (40÷400 times). In this zone, the breaking of the rock is the most intense and the largest amount of available energy is consumed.

Destruction zone – occurs at a distance greater than $(3 \div 7)r$. In this zone, the shock wave is significantly weakened and moves at the speed of sound. It causes stresses in the surrounding rock material which result in the creation of cracks of

ISBN: 978-86-80616-07-0

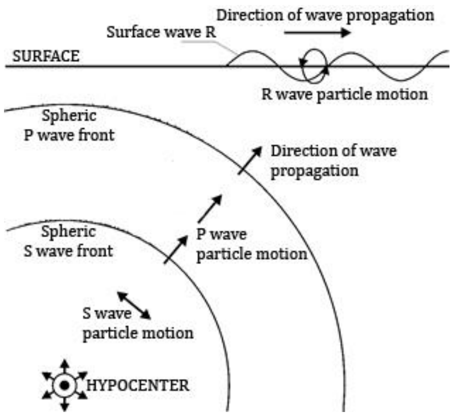

Figure 1. Schematic representation of the propagation of seismic waves

different directions and orientations. Radial or concentric cracks, or a combination of the two, can occur.

Seismic vibration (quake) zone – occurs when the shock wave is so weakened that it can move particles in the domain of elastic deformations. In this zone, there is no destruction but the movement of particles of rock masses can make it feel like a quake.

From the seismic point of view, the vibration (quake) zone is of special importance because the elastic waves that propagate in this zone have the nature of seismic waves. Their actions and consequences have the same character as seismic waves caused by an earthquake. What distinguish seismic waves – i.e., those caused by earthquakes and explosives – are the amounts of released energy, ranges of influence and durations of the seismic wave.

What distinguishes an uncontrolled explosion in the earth's crust (e.g. an earthquake) from a controlled explosion (e.g. the detonation of explosive substances), is the knowledge of the amount of energy released. We discover the amount of energy released during an earthquake only after the earthquake has happened and after ascertaining the consequences of its action. In the detonation of explosive substances (controlled explosions), however, we can determine – in advance – the amount of energy released and define the part that will be the carrier of the quake (seismic vibrations). This knowledge has therefore made it possible to estimate the range and intensity of the seismic wave for controlled explosions.

II. TYPES OF SEISMIC WAVES

Seismic waves propagate through a rock mass in the form of concentric spheres until they reach the earth's surface. When the waves reach the surface, they cause the ground to move, which is called seismic vibrations. According to their behavior and propagation, seismic waves can be divided into two groups:

- spatial or volumetric waves - which extend through the rock mass and
- surface waves - which spread over the surface of the terrain.

Fig.1. shows a schematic representation of the propagation of seismic waves:

If the wave leaving the blasting site encounters an acoustically different environment, it may bounce or refract. This means that spatial or volumetric waves can be different, as follows:

- direct,
- rejected (reflected), and
- refracted (refracted) waves.

Spatial, longitudinal, seismic P wave – which propagates through the rock mass and leads directly to the observed point; at the same time, this wave causes compressive stresses in the rock mass, i.e. compression (compaction) of the rock mass. The material particles of the rock mass oscillate in the direction of propagation of the elastic wave. These waves, due to the movement of material particles in the direction of wave motion, are called longitudinal (primary) and in seismology, P-waves [2]. A schematic representation of the deformations that occur during the propagation of a longitudinal seismic wave is given in Fig. 2.

The propagation velocity of the longitudinal seismic c_p wave is defined by Eq. (1):

$$c_p = \sqrt{\frac{E\gamma}{g}} \left[\frac{m}{s}\right], \tag{1}$$

where:

E – modulus of elasticity,
γ – volume density of rock,
g – gravity of Earth.

Longitudinal seismic waves can propagate in solid, liquid and gaseous state of matter.

The values of the propagation velocities of longitudinal seismic waves, for some rock materials, are shown in Table I.

The spatial, transverse, seismic S wave – propagates through the rock mass causing shear stresses. In this case, the material particles of the rock mass oscillate perpendicular to the direction of propagation of the elastic wave. That is why these waves are called transverse (secondary, shear, transverse) waves and in seismology, S-waves. A schematic representation of the propagation of transverse seismic waves is given in Fig. 1.

The speed of propagation of the transverse seismic wave c_s is defined by Eq. (2):

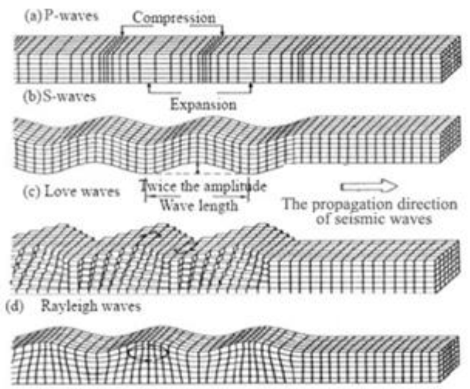

Figure 2. Schematic representation of deformations of rock material under the influence of seismic waves: a – influence of longitudinal (pressure-tension) wave, b – influence of transverse (shear) wave, c – influence of surface Love wave, and d – influence of surface Rayleigh wave [3].

TABLE I. LONGITUDINAL SEISMIC WAVE PROPAGATION VELOCITY VALUES FOR SOME ROCK MATERIALS.

Rock material	c_p $[km/s]$
Granite	5.0 – 5.7
Limestone, sandstone	2.5 – 4.5
Gypsum	1.7 – 3.0
Crumbs, gravel	0.9 – 2.1
Sandy soil	0.6 – 1.6
Clay soil	0.5 – 1.5
Loose soil	0.2 – 0.5
Water	1.73
Air	0.34

$$c_s = \sqrt{\frac{E \cdot g}{2\gamma(1+\mu)}} \left[\frac{m}{s}\right], \qquad (2)$$

where:

μ – Poisson’s ratio for rocks ranges from 0.2-0.35.

The speed of propagation of transverse waves is less than the speed of propagation of longitudinal waves which can be seen from the formulas for their calculation. Based on the performed experiments, the relationship between these two velocities was, in many cases, very close to the following Eq. (3):

$$c_P = 1.73 \cdot c_s \left[\frac{m}{s}\right]. \qquad (3)$$

Transverse seismic waves can propagate only through a solid state of matter, since shear stresses are possible only in this state. A schematic representation of the deformations that occur during the propagation of a transverse seismic wave is given in Fig. 2.

Surface waves – when the wave reaches the surface of the terrain, it encounters a much acoustically rarer state of matter –i.e. air, due to refraction. The waves that were formed propagate through the surface layer of the terrain and are called surface waves. The direction of movement of particles caused by surface waves can be in all three directions (longitudinal, transverse, vertical).

The most significant of the surface waves are Rayleigh waves, known in seismology as R-waves. The trajectories of particle oscillations, during the propagation of these waves, are in the vertical plane and in the direction of the propagation of seismic waves.

There are also purely surface waves which occur at the contact of two, differently elastic state of matter (soil - air) – and only if there is a thin surface layer. These waves occur only in the case where, at a shallower depth, there is an elastic layer matter with significantly different elastic properties than that at a surface layer. These purely surface waves are called Love waves and are horizontally polarized (i.e. the direction of propagation and the direction of oscillation form one ‘horizontal’ plane). A schematic representation of the propagation of Rayleigh and Love surface waves is given in Fig. 1 while a schematic representation of the deformation of the rock material, during the propagation of surface Rayleigh and Love waves, is given in Fig. 2.

The speed of propagation of the Love wave is slightly higher than the speed of propagation of the Rayleigh wave.

The ratio of propagation velocities between Rayleigh waves c_R and transverse waves c_s is given by Eq. (4):

$$c_R = 0.92 \cdot c_s \left[\frac{m}{s} \right] . \tag{4}$$

Based on the above, it can be determined that – according to the speed of propagation through the rock mass – longitudinal waves are the fastest, transverse are somewhat slower, and surface waves, the slowest.

III. Parameters of Rock Mass Oscillation

When a seismic wave encounters a point on the ground, the soil particles are expelled from the equilibrium position at that point and oscillate around their equilibrium position for some time until they calm down completely. The oscillation of particles of rock material is what manifests and feels like, a quake, i.e. ground vibration. Therefore, the important difference between a seismic wave and a quake is: ground vibration.

The waves move at high speeds and at great distances through the rock mass (300 ÷ 7000 *m/s*) thus exciting the oscillations of the particles at the points they encounter. The material particles of the massif do not move anywhere but, instead, oscillate around their equilibrium position at much lower speeds (of the order of [mm/s]) until the oscillations are attenuated –i.e. until the rock mass settles [4].

Ground vibration, or vibration of a rock mass, is an effect of blasting that can be felt on the ground, causes damage to buildings, and instills an unpleasant feeling and fear in people.

The intensity of the quake (seismic vibration) caused by blasting can be determined by measuring one of the three basic parameters that characterize the oscillation of the aroused (excited) soil, and they are:

- displacement of rock mass particles x - the distance at which the particle moves away from its equilibrium position during oscillation,
- ground particle oscillation velocity v - particle velocity during oscillation, and
- acceleration of particles of the aroused environment a - shows the change in oscillation speed, i.e. particle motions.

The magnitudes (size) of these three parameters indicate the intensity of the force with which they are caused, hence the degree of hazard that the vibration of a rock mass induces. These parameters represent the basic dynamic parameters of a vibration of rock mass.

IV. Recording Rock Mass Oscillation Velocity

When blasting, several types of waves arrive almost simultaneously on one point of the terrain, causing oscillations of the particles of the rock mass in different directions. Therefore, the resulting spatial trajectory of particle motion around its equilibrium position is a complex shape. For that reason, the oscillation parameters of the rock mass are measured in three directions, i.e. through three components:

v_t – horizontal component, normal to the direction of wave spreading - transversal component,

v_l – horizontal component, in the direction of wave spreading - longitudinal component and

v_v – vertical component.

The recording of rock mass oscillation parameters is performed with instruments - seismographs. The main parts of the seismograph are the sensors with which the oscillation speed is registered. The oscillation detector contains three seismometers, which are housed within a common instrument casing, and oriented in the X, Y and Z - directions of the rectangular coordinate system. The seismograph is designed so that it can register the oscillation velocity *v*, whereby acceleration *a* and the displacement of the rock mass *x* are calculated along with the value of the frequency f . The oscillation curves are labeled as seismograms, velocigrams or accelerograms depending on whether the registered oscillations are proportional to displacement, velocity or acceleration.

The intensity of air blasts can be registered on the fourth channel using a microphone that is hooked to an external connector.

The oscillation speed of the aroused (excited) rock mass is most often taken as a parameter for estimating the seismic effect of blasting. It serves to connect and describe the danger of – as well as the damage caused by –a ground vibration. For this reason, appropriate ground vibration protection standards are based on data relating to the speed of oscillation.

Maximum oscillation speed of the rock mass $v_{\max}$ is determined by the Eq. (5):

$$v_{\max} = \sqrt{v_t + v_l + v_v} \quad , \qquad (5)$$

where:

v_t – transverse component of rock mass oscillation velocity,

v_l – longitudinal component of the rock mass oscillation velocity,

v_v – vertical component of rock mass oscillation velocity.

V. Influencing Factors on Seismic Vibrations

The main factors that affect the formation of seismic waves and determine the intensity of seismic vibrations caused by blasting are: energy of seismic vibration (quake), properties of the rock material through which the seismic wave passes, distance from the place of blasting to the point where the observation is performed and the delay interval [1].

A. *Energy of Seismic Vibrations*

Seismic energy means the total energy of elastic waves generated after the explosion of a certain amount of explosives or earthquakes. The energy supply is contained in the explosive substance. This energy is transmitted by elastic seismic waves. As it travels through the rock massif, from the place of excitation to the place of observation, it decreases so only a part of the total energy is registered at the place of observation. Energy dissipation occurs due to the reflection, diffraction and refraction of waves, as the starting energy is divided into several types of waves –i.e. on multiple types of seismic beams. In the case of spherical waves, there is a weakening due to the division of energy into an ever-increasing sphere.

The residual energy of the seismic wave E_{uk} which reaches the observed point, can be expressed as the sum of the kinetic E_k, and the potential energy E_p available to the seismic wave; this is expressed in the form of Eq. (6):

$$E_{uk} = E_k + E_p = \rho \cdot \delta \cdot v^2 \cdot \sin^2 \frac{2\pi}{T}(t - \frac{x}{c}) \quad , \qquad (6)$$

where:

ρ – rock mass density,

δ – an elementary particle of the state of matter through which a seismic wave passes,

v – the oscillation speed of the observed elementary point,

T – period of oscillation,

t – time,

x – displacement magnitude,

c – wave propagation velocity.

Under the influence of this energy, which is carried by the seismic wave, the material particles at the observed point are forced to oscillate at velocity v and reach the magnitude of displacement x . Therefore, the speed of oscillation – and the magnitude of the displacement of material particles – will depend on the amount of energy that the elastic wave carries with it.

It is understandable that, with the distance from the place of explosion, energy is wasted considering the nature of the propagation of the seismic wave as well as the consumption of energy needed to overcome the resistance in the path of its propagation. Therefore, with the distance from the center of the explosion, the energy of the seismic wave weakens. These changes can be defined by the Eq. (7):

$$E_r = \frac{1}{2}\gamma \cdot c \sum_{i=1}^{i=n} v_i^2 \cdot T_i \quad , \qquad (7)$$

where:

E_r – energy of vibration,

γ – volume density of rock,

c – wave propagation velocity,

v_i – oscillation velocity at the site of observation,

T_i – period of oscillation.

B. Properties of Rock Mass Through Which a Seismic Wave Passes

The characteristic of the geological composition of the terrain, for one locality where blasting is performed, is a naturally conditioned factor so it is necessary to adjust the parameters of blasting for the given conditions.

When blasting is performed in one geological environment and effects are observed in another, the seismic wave propagates from the blasting site to the observation site through different geological environments [4]. The energy along seismic wave *E* is given in the Eq. (8):

$$E = v^2 \cdot c \cdot \rho \quad . \tag{8}$$

Energy on both sides of the boundary plane, i.e. the surface separating the different elastic media, is equal and is given by Eq. (9):

$$E_1 = E_2 = v_1^2 \cdot c_1 \cdot \rho_1 = v_2^2 \cdot c_2 \cdot \rho_2 \ , \tag{9}$$

where:

v_1 i v_2 – oscillation velocity of rock mass in environment 1 and environment 2,

c_1 i c_2 – wave propagation velocity in environment 1 and environment 2,

ρ_1 i ρ_2 – volume density of rock 1 and volume density of rock 2.

It follows from this equation that the oscillation speed of rock mass v increases if acoustic impedance ρc decreases.

Based on the previous analysis, it is possible to conclude that the seismic intensity increases with decreasing rock mass strength and rock material coherence. Thus, in very hard rocks – such as with igneous and many sedimentary rocks (like granite, basalt, marble, limestone) – the consequences of seismic vibrations are significantly less than in soft and crumbly rocks like sand, gravel, clay, loess, humus, loose soil, etc. If the rock also contains a significant amount of water, the negative consequences are even greater.

This also means that the massive solid rock mass enables the transfer of energy over longer distances, i.e. faster propagation of seismic waves with less damping than the cracked rock mass. The cracked rock mass dampens it faster –

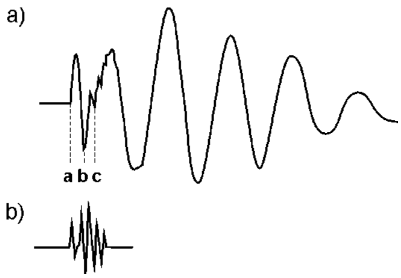

Figure 3. Examples of seismic wave oscillograms, a) in a water-saturated soft rock; sectors a,b,c – primary phase; b) in solid rock.

that is, the seismic wave in such an environment weakens faster and spreads over shorter distances. The cracked irrigated environment further transmits waves from the cracked dry environment, while in a porous unbound environment, the waves are attenuated the fastest.

These changes are most noticeable through, and can be monitored on, oscillograms. According to numerous results obtained during the research of this phenomenon – and in relation to the degree of coherence – it was noticed that in soft and water-saturated rocks, the oscillation of particles is much higher than in hard rocks [1]. Typical oscillograms for these two cases are shown in Fig. 3.

Based on the research on the intensity of seismic vibrations on different rock materials, it can be concluded that there is an increment of seismicity n according to the type of rock material. In this regard, all rocks are divided into seven categories. Table II shows the increment of seismicity by categories of rocks, in relation to granite as a standard (according to S.V. Medvedev).

TABLE II. INCREMENT OF SEISMICITY BY ROCK CATEGORIES IN RELATION TO GRANITE.

Rock category	**Rock**	**Increment of seismicity n**
I	Granite (etalon)	0
II	Limestones, sandstones	0.0 – 1.0
III	Marl soil	1.0
IV	Soil of gravel, fine and coarse gravel	1.0 – 2.0
V	Sandy soil	1.0 – 2.0
VI	Clay soil	1.0 – 2.0
VII	Fill loose ground	2.0 – 3.0

When there is a dilapidated, loose and degraded environment above the solid rock mass, which differs significantly from the solid substrate in its physical and mechanical properties, the oscillation speed on the terrain surface can be several times higher than on a solid substrate. The reason for that is the multiple refraction and repulsion of the seismic wave from the surface of the terrain – i.e. from the solid surface, on the way from the place of blasting to the place of vibration measurement.

C. Impact of Distance on Seismic Vibrations

The distance from the center of the explosion has a great influence on the seismic wave and the consequences of its action. It is understandable that, with greater distance from the center of the explosion, the seismic wave becomes weaker and weaker and the vibrations, smaller and smaller.

With a change in the distance from the place of blasting, in addition to the intensity of the vibrations, the character of the vibrations also changes. Namely, oscillations with high frequencies dominate at shorter distances. As the distance increases, the high-frequency oscillations disappear because they dampen faster; as a result, low-frequency oscillations become dominant which, in turn, have a more destructive effect on high-rise buildings.

To establish a correlation between the oscillation speed of the rock mass and the basic parameters that affect its size, several models have been developed. One of the most commonly used models is the M.A. Sadovskii which defines the change in the speed of oscillation depending on the distance, the amount of explosives and the way of performing blasting. The equation provides an opportunity to determine the seismic effect of blasting in the direction of an object. Here is an example of the equation of M. A. Sadovskii [5]: given in the form (10):

$$v = K \cdot R^{-n} = K \cdot \left(\frac{r}{\sqrt[3]{Q}}\right)^{-n} , \qquad (10)$$

where:

v – the oscillation speed of the rock mass [cm/s],

K – coefficient which is conditioned by the characteristics of the rock mass and the conditions of blasting; K is determined by field measurements

n – exponent which is conditioned by the characteristics of the rock mass and blasting conditions, and is also determined by field measurements,

r – distance from the place of blasting to the place of observation [m],

Q – total amount of explosives [kg],

R – reduced distance expressed as $R = \frac{r}{\sqrt[3]{Q}}$

Sadovskii's equation is determined on the basis of trial blasting for a specific working environment.

In the study of the nature of seismic vibrations behavior, its importance and its intensity changes with depth. This factor is important because massive blasting in mining is performed with large quantities of explosives, whether they are underground or on the surface, so it is necessary to determine how the intensity of the vibrations changes in depth. It has been experimentally determined that the intensity of oscillation of the rock mass decreases with depth, so that the horizontal component of the oscillation speed decreases faster than with the vertical one.

D. Influence of Delay Interval on Seismic Vibrations

Blasting with a delayed effect works in such a way that, instead of one high-intensity wave in a one-time initiation of one blast series, we have more low-intensity waves. A wave caused by one initiated blast-hole (or a group of simultaneously initiated blast-holes), given its velocity, reaches a considerable distance before the next group of blast-holes is activated.

For this process to take place successfully, it is necessary to determine the appropriate delay time. The seismic wave caused by the activation of one blast-hole (or group of blast-holes) should come out of the minefield before any subsequent blast-hole (or group of blast-holes) detonates. Since both the first and the second wave pass through the rock mass or soil at the same speed, the second wave can never reach the first and cannot, therefore, affect it [6].

In the case that the delay time is not enough, seismic waves meet which results in an increase in seismic vibration (quake). Fig.4 shows the encounter of waves at a small-time delay:

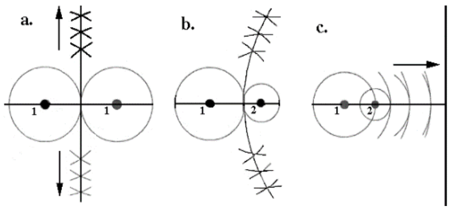

Figure 4. View of the encounter of waves when activating blast-holes: a) – instantaneous activation, b), c) – delay activation, 1 – currently-activated mine, 2 – mine activated with delay [6].

Case a) – shows the instantaneous activation, without delay, between blast-holes. Seismic vibration intensifies at the place where seismic waves meet. The biggest seismic vibration is at the point of intersection of the line connecting the blast-holes and the bisector, i.e. the line where the waves meet. As you move along the line of contact, the intensity of the vibration decreases because the waves propagate over a longer length. It is therefore a well-known empirical observation that vibrations during the instantaneous initiation of several blast-holes are the largest in front of, and behind, the mine series.

Case c) – shows the activation, with delay, between the blast-holes so that the next blast-hole is activated at the moment when the seismic wave, caused by the previous blast-hole, passes over it. In that case, the direction of meeting the waves will be in the direction of connecting the line of blast-holes. For this reason, if an object is to be protected from vibrations, the mine series should be initiated so that the process of destruction of the rock mass moves away from the object that is being protected.

Case b) – shows the encounter of seismic waves between the previous two cases, a) and c) respectively. The line of encounter of the waves, in this case, is curved and has the shape of a hyperbola. The direction and curvature of this line will depend on the order of initiation and delays between the blast-holes.

When seismic waves meet, the oscillation parameters change in the following ways:

- amplitudes increase, i.e. the maximum oscillation speed increases,
- upon which, the period of oscillation in two phases, increases which means a decrease in frequency; reducing the frequency of vibrations increases the risk of damage to buildings because oscillations with lower frequencies are more dangerous for high-rise buildings – i.e. for residential buildings. Increasing the period of oscillation also means that the wider area is more intensely affected by the vibrations.

Based on the above, we can say that delayed blasting reduces vibrations – compared to the instantaneous blasting; but in the case of insufficient delay at certain points in space, it causes increased vibrations – compared to vibrations with proper delay.

VI. Conclusion

In mining, explosives are primarily used to extract minerals from solid rocks. Today, explosive charges with hundreds of kilograms per blast-hole – and blasting with tens of tons of explosives – are used in the world. Such large quantities of explosives can cause seismic vibrations of such intensity which adversely affect the environment, i.e. with the disruptive movements of objects. The basic factors that affect the formation of seismic waves and determine the intensity of vibrations caused by blasting are: energy of seismic vibrations (quakes), the properties of rock material through which the seismic wave passes, and the distance from the blasting site to the point where the observation and delay are interval. The intensity of the vibration can be established by measuring one of the three basic dynamic parameters, which are: displacement, velocity and acceleration of the motion of the rock mass particles.

This paper describes the mechanism of generating seismic waves caused by blasting as well as the factors that determine the intensity of seismic vibrations. Based on precisely defined parameters of rock mass oscillation, as well as on knowledge of factors that affect the strength of seismic vibrations, it is possible to optimally use the energy of explosives and minimize the negative effects of blasting.

References

[1] Trajković, S. (1993). Area of Application of Laws of Rock Mass Oscillation Caused by Blasting, with Reference to Mining Works. Ph.D. Thesis, Faculty of Mining and Geology, Belgrade, Serbia.

[2] Zhang, Q., Li, Z., & Yu., T. (2018). Seismic Response for Wave Propagation across Joints with Equally and Unequally Close-Open Behaviours. *Advances in Civil Engineering.*

[3] *Types of seismic waves.* Available at: https://www.geographyforyou.com/2017/09/how-

many-types-of-seismic-waves-geography-for-you.html

[4] Slimak, Š. (1996). *Engineering geophysics*.University of Belgrade – Faculty of Mining and Geology, Belgrade, Serbia, (pp. 176-178).

[5] Medvedev, S. V. (1964). *Seismics of Mountainous Explosions*. Nedra: Moscow, Russia (pp.42–43).

[6] Savić, M. (2000). *Blasting at of the Open Pits*. Monograph, RTB Bor; Cooper Institute Bor, Indok Center: Bor, Serbia (pp. 314–316).

Effect of Surface Treatment of Substrates on Optical and Morphological Properties of Multilayer Selective Solar Surfaces (Cr/Si)

Camila Rêgo de Andrade[1], Beatriz Ferreira de Oliveira[2], Maycon Fagner de Oliveira Meneses[3], Kelly Cristiane Gomes da Silva[4]

[1,2,3,4]Federal University of Paraíba, João Pessoa, Brazil, camila.andrade@cear.ufpb.br[1]; beatriz.oliveira@cear.ufpb.br[2]; maycon.menezes@cear.ufpb.br[3]; gomes@cear.ufpb.br[4]

Abstract—**In the midst of the search for sustainable development, renewable energy sources are an important energy alternative, especially solar energy. One of the ways to use this energy is through its thermal conversion through solar collectors. To improve the performance of these collectors, coatings called selective surfaces are applied which aim to increase the absorption of solar radiation and reduce thermal losses by emission in the infrared. In this context, this work proposes to produce selective surfaces of Cr and of Cr/Si using the Magnetron Sputtering technique, varying the deposition time and using substrates subjected to different surface treatments (cleaning with hexane and electropolishing), in order to evaluate the influence of these parameters on the optical and morphological properties of the films. These coatings were characterized from the techniques: UV-Vis-NIR Spectrophotometry, Optical Perfilometry and Scanning Electron Microscopy (SEM). The results showed that the surface treatment influences the optical and microstructural characteristics of the films. Among the treatments used, electropolishing was more favorable, because the films deposited on electropolished substrates showed greater absorbances (≥ 95%). Moreover, longer deposition times and the addition of the Si layer, favored the achievement of better optical properties. Regarding the microstructural characteristics, the films presented nanometric thicknesses and those that were deposited on electropolished substrates had lower roughness values. Thus, it was found that Cr/Si films showed better optical performance, especially in longer deposition times, and that electropolishing is an effective surface treatment for preparing SSS with thin films deposited by Magnetron Sputtering.**

Keywords - multilayer selective surfaces, sputtering, chromium, silicon, electropolishing

I. INTRODUCTION

The industrialization process marks the beginning of a strong economic development that promoted changes in the lifestyle and consumption habits of society, being associated with an exponential increase in energy consumption. Much of this energy demand was supplied using fossil fuels, which resulted in an aggravation of environmental problems, especially global warming [1-3].

In this context, renewable energy sources prove to be an important energy alternative, because they are clean and could promote technological development and bring indirect economic benefits [4-6] Among renewable sources, solar energy stands out for being one of the cleanest and most abundant. One of the ways to use this energy is through its thermal conversion in solar collectors [7,8].

Although it has a good cost-benefit ratio, solar thermal conversion has limitations for applications at temperatures above 100°C (medium and high temperature applications), due to emission losses and low thermal stability of materials in these temperatures [9,10].

To increase the efficiency of these collectors, coatings called selective solar surfaces (SSS) are applied, which aim to increase the absorption of incident solar radiation and reduce thermal losses by emission in the infrared region [11].

The optical and morphological properties of the SSS are influenced both by the material and the deposition technique used in its construction [10].

Among the different types of materials used in the construction of these coatings, black chrome stands out, because it has high solar absorption (92-95%), low total hemispheric emissivity at 100°C (≈ 9%) and is thermally stable up to 400°C in the vacuum [12,13]. Another important material is silicon, which is an absorber of solar radiation in the ultraviolet and visible regions and has been widely used as a basis for the construction of anti-reflective coatings, which contribute to increase the performance of films [14,15].

Among the techniques, sputtering excels for ensuring greater control over the morphology of the films and for being considered a clean technique when compared to electrochemical processes, because it does not generate effluents to be eliminated at the end of the deposition [16].

Therefore, the objective of this work is to obtain selective surfaces with a single layer of chromium (Cr) and multilayer of chromium (Cr) and silicon (Si) through the Magnetron Sputtering technique with different deposition times and using substrates subjected to different treatments superficial (cleaning with hexane and electropolishing).

II. MATERIALS AND METHODS

A. *Surface Treatment of Substrates*

AISI 304 stainless steel substrates with dimensions of 30 mm x 30 mm were used. Before deposition, the substrates were subjected to two types of surface treatment:

- Cleaning with hexane: half of the substrates was subjected to cleaning with hexane. They were immersed in a beaker containing hexane for 10 minutes, being, posteriorly, washed in distilled water.
- Electropolishing: the other half of the substrates was electropolished. It was used a solution of phosphoric acid, sulfuric acid and glycerol in the proportion of 2:1:1. For closing the circuit, a mesh of AISI 304 stainless steel was used. A DC voltage source was applied to the circuit with the negative pole connected to the steel mesh and the positive pole connected to the substrate. The voltage at the source was set to 6 V and the current was maintained at values close to 1.35 A. Each substrate was electropolished for 10 minutes, being, subsequently, washed in distilled water.

After the surface treatment, the substrates were immersed in isopropyl alcohol and submitted to an ultrasonic bath for 15 minutes.

B. *Deposition process*

This study proposes to obtain two types of thin films: (a) films with a single layer of Cr and (b) multilayer films of Cr and Si.

The deposition of the films was performed by a Magnetron Sputtering RF Orion 5 system, supplied by AJA Instruments Inc.

Two targets were used: chromium (Cr) and silicon (Si), both manufactured commercially and high purity. The Cr target was 99.950% pure, 2” (50.8 mm) diameter and 0.125” (3.175 mm) thick. The Si target was 99.99% pure, 2” (50.8 mm) in diameter and 0.118” (3 mm) thick.

To initiate the depositions, the targets were positioned in the vacuum chamber at a distance of 105 mm from the substrates. The chamber was evacuated to a pressure of 1.3 x 10^{-3} Pa and then the gas was injected to form the plasma. Argon 5.0 gas was used, with a flow of 10 sccm into the chamber, causing a new pressure balance to be reached at 0.7 Pa. The equipment was supplied with the desired working power value for each target (Table I) and the deposition process started. During the process, the substrate rotated at a speed of 20 rpm.

TABLE I. DEPOSITION PARAMETERS.

Target	**Power (W)**	**Deposition Time (min)**
Cr	60	10
		20
		30
Si	200	10
		20
		30

TABLE II. NOMENCLATURE OF SAMPLES.

Sample	Composition	Surface Treatment	Deposi-tion time
C1	Cr	Hexane	10 min
C2			20 min
C3			30 min
C4		Electro-polishing	10 min
C5			20 min
C6			30 min
CS1	Cr/Si	Hexane	10 min/ 10 min
CS2			20 min/ 20 min
CS3			30 min/ 30 min
CS4		Electrop-olishing	10 min/ 10 min
CS5			20 min/ 20 min
CS6			30 min/ 30 min

Based on the different surface treatments and the parameters adopted in the depositions, 12 conditions were obtained, according to Table II. Then, three samples were produced for each set of conditions, totalizing the production of 36 samples.

C. *Characterization of films*

A fundamental characteristic in the study of selective solar surfaces is the absorptivity of these films. Therefore, to evaluate this parameter, the coating was subjected to UV-Vis-NIR spectrophotometry. The equipment used was a UV-Vis-NIR Spectrophotometer, model UV-2600, by Shimatzu, operating in the region between 220 nm e 1400 nm with measurements of reflectance, using the integration accessory, which allows an analysis of reflectance in all directions.

The absorptivity is defined as the ratio of the radiation absorbed by the surface to the radiation incident on that surface. Therefore, it is possible to calculate the solar absorptivity of a surface using (1):

$$\alpha = \frac{\int_{300}^{2500} \alpha_\lambda I_{sun} d\lambda}{\int_{300}^{2500} I_{sun} d\lambda} , \qquad (1)$$

where α_λ is the spectral absorptance of the solid, I_{sun} is the spectral distribution of the solar irradiation and α is the total hemispherical absorptance.

Considering that the samples obtained are opaques (transmittance is zero), the total hemispherical absorptance α can be calculated from (2):

$$\alpha = \frac{\int_{300}^{2500} (1-\rho_\lambda) I_{sun} d\lambda}{\int_{300}^{2500} I_{sun} d\lambda} , \qquad (2)$$

where ρ_λ is the solid spectral reflectivity. So, according to (2), the solar absorptivity of the films can be obtained from the spectral reflectance measurements, which are determined in the UV-Vis spectrophotometry. The integral in (2) was calculated using the trapezoidal rule, considering the radiation range of 300 nm to 1400 nm.

In order to determine the roughness and thickness of the obtained films, an optical perfilometry analysis was performed. The measurements were made by the CCI MP non-contact optical profiling device, manufactured by Taylor Hobson, connected to a computerized unit containing the Talysurf CCI software (Taylor Hobson, England) to obtain and analyze the data.

The visualization of the microstructure of the coatings was obtained using a Scanning Electron Microscope (SEM), model Quanta 450, manufactured by FEI, with detection of secondary electrons, which allows the visualization of the topography of the surface.

III. RESULTS AND DISCUSSION

A. *UV-Vis-NIR Spectrophotometry*

The Cr and Cr/Si absorbing films obtained via Magnetron Sputtering with variations in the time of deposition and in the surface treatment of the substrates were subjected to radiation with a wavelength between 220 nm and 1400 nm in order to determine their spectral absorbances, which are represented in the curves of Fig. 1.

As shown in Fig.1, the samples that have been treated with electropolishing presented high values of spectral absorptivity and greater absorption stability throughout the spectrum. Meanwhile, samples cleaned with hexane had a more unstable behavior along the spectrum.

To facilitate the comparison between the different films, the solar absorptivity for each condition was calculated, as well as their respective standard deviation. These values are shown in Fig. 2.

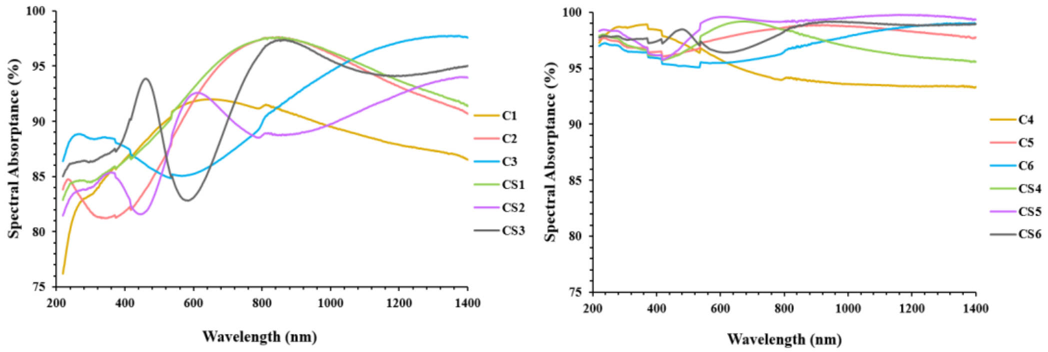

Figure 1. Spectral absorbance: (a) Cleaning with hexane and (b) Electro-polishing

The data in Fig. 2 show that the electropolished samples showed the highest values of solar absorbance, greater than 95%, associated with standard deviations between ±0.21% e ±3.77%. On the other hand, the samples cleaned with hexane obtained lower solar absorbance with values between 88.75% and 93.13%, and standard deviations varying between ±0.48% and ±2.21%.

Furthermore, it is observed that, in most samples, the addition of a Si layer contributed to an increase in the absorption of the films, the only exception is CS2. Among the samples cleaned with hexane, CS1 stands out, because after applying the silicon layer, it reached an average absorption of 93.13%, corresponding to an increase of 3.21% in the level of absorption in relation to C1. Among the electro-polished samples, CS5 obtained the best result, because it showed a solar absorptivity of 98.74%, resulting in an increase of 0.98% in the level of absorption after the application of silicon.

TABLE III. SOLAR ABSORPTIVITY AND STANDARD DEVIATION.

Sample	Solar Absorptivity (%)	Standard Deviation (%)
C1	89.92	1.92
C2	91.75	0.69
C3	89.11	0.48
C4	95.31	3.77
C5	97.76	0.83
C6	96.38	1.23
CS1	91.74	0.38
CS2	88.75	2.21
CS3	91.09	0.51
CS4	97.55	0.99
CS5	98.74	0.36
CS6	97.85	0.21

Table III shows the values of solar absorptivity and the standard deviation of all deposited films, where the best results for each film composition and surface treatment were highlighted.

Based on Table III, it is observed that the deposition time of 20 minutes per layer proved to be ideal in most conditions, except for Cr films treated with hexane (CS1 obtained the best result in that condition).

It is noticeable that CS5 was the one that presented the best performance, as it obtained the highest solar absorbance (98.74%) and a small standard deviation (± 0.36%), which indicates that this condition is reproducible.

Fig. 3 presents a comparison of the chrome films produced in this research with commercial films and those obtained in the literature.

When comparing the SSS obtained in the research with the commercially available films and in the literature [13,16-18], it is clear to observe that the best chromium films that were produced, C5 and CS5, present very satisfactory results, since their absorbance values are at a

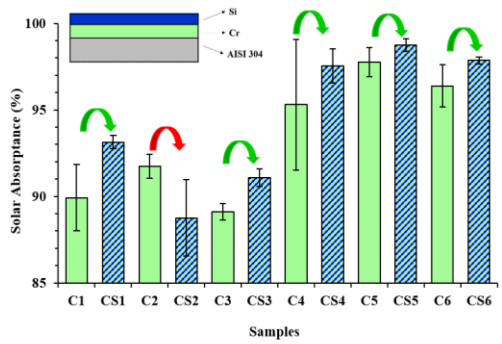

Figure 2. Solar absorbances and their respective standard deviations.

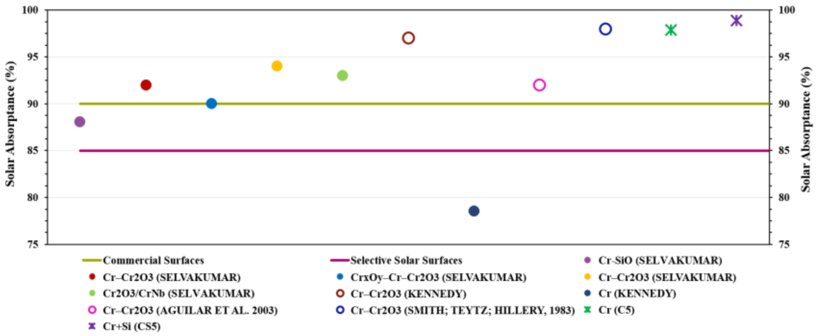

Figure 3. Results in literature and commercial SSS.

higher level comparing other surfaces. They obtained better results than so many SSS produced via *Sputtering* (●) and reached a level above the recommended (90%) to be considered commercial absorbent surfaces.

B. *Optical Perfilometry*

All films were subjected to optical profilometry analysis, from which the following parameters were obtained: Ra (arithmetic roughness, that is, the mean deviation with respect to the roughness profile) and the thickness values of the films. The data obtained are shown below in Table IV.

In Table IV, the films that obtained the highest (in **bold**) and the lowest (in *italic*) solar absorbances for each film composition and surface treatment of the substrate were highlighted, in order to compare their roughness and thickness parameters.

Table IV shows that, in coatings deposited on substrates cleaned with hexane, the highest levels of absorption are associated with higher values of Ra. For Cr coatings deposited on clean substrates with hexane, C2 showed the highest values of Ra at the same time it presented the highest solar absorbance. An analogous behavior was observed in the multilayered Cr/Si films deposited on clean substrates with hexane, so that CS2, with the lowest values of Ra, presented the lowest average absorption.

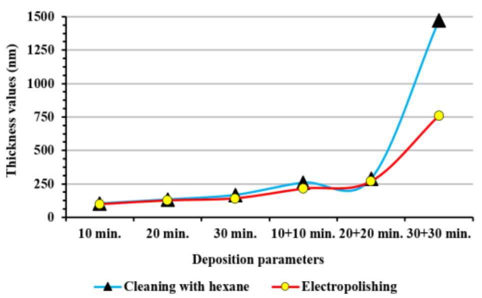

Figure 4. Films thickness.

On the other hand, the opposite behavior was observed in the films deposited on electropolished substrates: the reduction in Ra contributed to an increase in the solar absorptivity of the Cr surfaces and the Cr/Si multilayer surfaces. In addition, it was observed that the films deposited on electropolished substrates had the lowest values of roughness and the highest values of solar absorbance. This reduction in roughness is justified by the fact that, in electropolishing, metallic material is removed from the surface, resulting in a more homogeneous morphological profile.

Table IV also shows a correlation between the composition of the coatings and their Ra. The multilayer films showed a rougher surface (higher values of Ra) for both surface treatments.

TABLE IV. ROUGHNESS AND THICKNESS.

Sample	Ra (nm)	Thickness (nm)	Solar Absorptivity (%)
C1	*99.6*	*101.60*	*89.92*
C2	**111.0**	**132.03**	**91.75**
C3	103.6	166.48	89.11
C4	*19.0*	*97.33*	*95.31*
C5	**13.5**	**125.18**	**97.76**
C6	7.54	140.60	96.38
CS1	**115.7**	**258.00**	**91.74**
CS2	*111.6*	*286.75*	*88.75*
CS3	145.2	1472.00	91.09
CS4	*58.6*	*212.80*	*97.55*
CS5	**16.5**	**267.50**	**98.74**
CS6	12.3	758.67	97.85

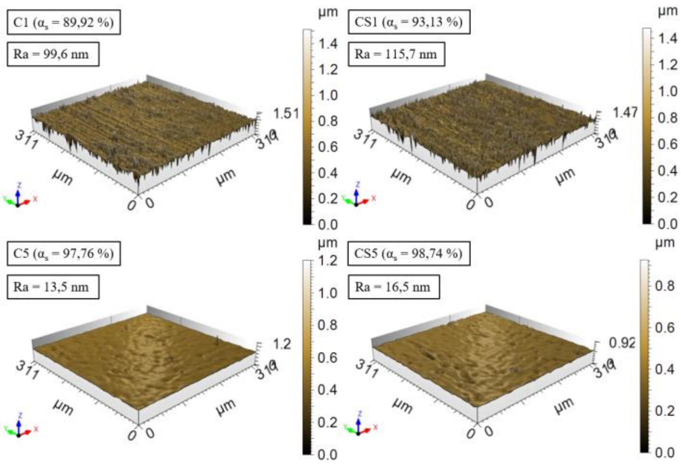

Figure 5. 3D morphological profile of the surfaces.

The films obtained nanometric thicknesses, except CS3. And the thickness values of the films increased after the application of the silicon layer and with the increase in the deposition time, as shown in Fig. 4.

Fig. 5 shows the 3D microstructures of the Cr and Cr/Si films, which presented the best solar absorptivity considering both surface treatments. It shows that the films that presented a more homogeneous surface and with lower values of roughness, notably those deposited on electropolished substrates, presented better performance in terms of absorption.

C. *Scanning Electron Microscope (SEM)*

Fig. 6 shows the micrographs obtained by scanning electron microscopy (SEM) with magnitudes of 5000 and 10000 times for the chrome films deposited on substrates subjected to cleaning with hexane.

In Fig. 6, it can be seen that the films which had longer time deposition (C2 and C3) presented a rougher surface with some groves and peaks scattered along their structure. These films also presented obtained higher levels of absorption and with close values, indicating that the increase in the roughness of the surfaces favored the increase in the average absorption.

This observation corroborates with the data verified in the perfilometry, from which it was shown that, for substrates cleaned with hexane, the highest absorbances were associated with the highest roughness values.

In general, the films presented a similar morphological structure, because they have the

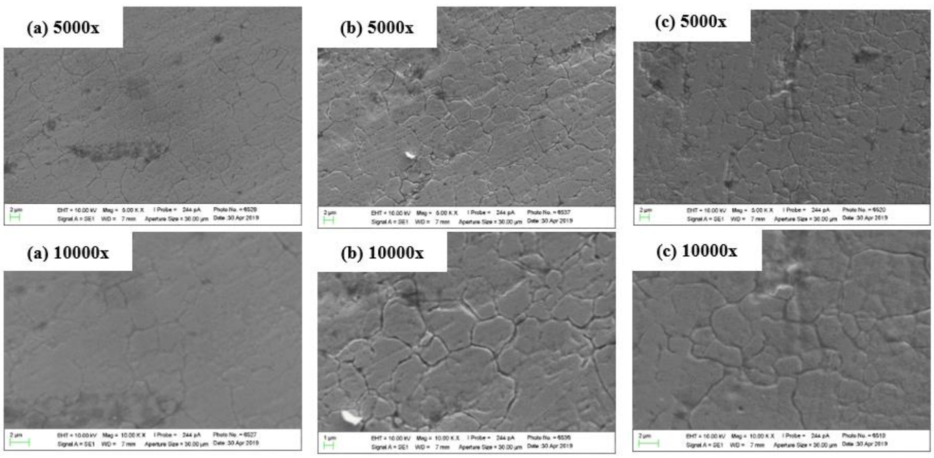

Figure 6. Micrographs of Cr films: (a) C1, (b) C2, (c) C3.

same composition, were deposited on substrates subjected to the same surface treatment (cleaning with hexane) and are very thin films, so they replicate to some degree the morphological profile of the substrate.

IV. CONCLUSIONS

The surface treatment influences the optical and microstructural characteristics of the films. Among the surface treatments used, electropolishing proved to be more efficient and contributed to the achievement of better performances, because the films deposited on electropolished substrates showed the highest solar absorptances ($\geqslant$ 95%). These films also had the lowest roughness parameters (Ra).

It was observed that the application of the silicon layer provided an increase in the level of absorption in most samples.

Regarding the deposition time, 20 minutes of deposition per layer is highlighted, because it proved to be the ideal time in most of the analyzed conditions.

The best performance was obtained by CS5, which achieved a solar absorptivity equal to 98,74% with a small standard deviation of ±0.36%.

Therefore, it is concluded that the Cr/Si films presented better optical performance, mainly in longer deposition times, and that the electropolishing is effective in the treatment of steel substrates for thin films deposited by Magnetron Sputtering.

ACKNOWLEDGMENT

The authors would like to thank the technical support provided by Integrated Biomaterials Laboratory – LABIO/UFPB, New Materials Technology Laboratory – TECNOMAT/UFPB and Laboratory of Synthesis and Characterization of Thin Films – LABFILM/UFPB, as well as the financial support of CAPES, CNPq and CEAR/UFPB.

REFERENCES

[1] Goldemberg, J., & Lucon, O. (2011). *Energy, Environment and Development*. Energia, Meio Ambiente e Desenvolvimento. São Paulo, Brazil.

[2] Hinrichs, R. A., & Kleinbach, M. (1999). *Energy and Environment*. Energia e Meio Ambiente. Thomson, São Paulo, Brazil: Editora da Universidade de São Paulo.

[3] Pompelli, M. F., Orozco, A. J., Oliveira, M. T, Rodrigues, B. R. M., Barbosa, M. O., Santos, M. G., Oliveira, A. F. M., & Almeida-Cortez, J. S. (2011). Global energy crisis and the Brazilian role in the bio-fuels issue. Crise energética mundial e o papel do Brasil na problemática de biocombustíveis. *Agronomía Colombiana*, *20*(2), 231–240.

[4] Editorial. (2015). The 3rd International Conference on Renewaible Energy: Generations and Applications (ICREGA 2014). *Renewable Energy*, 82, 1-3.

[5] Ueckerdt, F., Brecha, R., & Luderer, G. (2015). Analyzing major challenges of wind and solar variability in power systems. *Renewable Energy*, *81*, 1-10.

[6] Voinov, A., Arodudu, O., Duren, I. V., Morales, J. & Qin, L. (2015). Estimating the potential of roadside vegetation for bioenergy production. *Journal of Cleaner Production*, 102, 213-225.

[7] Solangi, K. H., Islam, M. R., Saidur, R., Rahim, N. A., & Fayaz, H. (2011). A review on global solar energy policy. *Renewable and Sustainable Energy Reviews*, *15* (4), 2149–2163.

[8] Weiss, W., & Rommel, M. (2008). Process Heat Collectors: State-of-the-Art Within Task 33/IV, IEA SHC-Task 33 and Solar PACES-Task IV: Solar Heat for Industrial Processes.

[9] Sani, E., Mercatelli, L., Janfrancesco, D., Sans, J. L., & Sciti, D. (2012). Ultra- High Temperature Ceramics for solar receivers: spectral and high-temperature emittance characterization. *Journal Of The European Optical Society-Rapid Publications*, 7, 12052.

[10] Neto, S., & J. F. (2017). Development of Selective Surfaces for Solar Collectors with Multilayer Deposition Development of Selective Surfaces for Solar Collectors with Multilayer Deposition of Cr and SiO_2. (Desenvolvimento de Superfícies Seletivas para Coletores Solares com Deposição Multicamadas Desenvolvimento de Superfícies Seletivas para Coletores Solares com Deposição Multicamadas de Cr e SiO_2. Tese Doutorado em Engenharia Mecânica), Universidade Federal da Paraíba, Paraíba, Brazil.

[11] Martins, M. (2010). Production of selective surfaces by Magnetron Sputtering for application in solar collectors. (Mestrado em Engenharia Metalúrgica e dos Materiais), Universidade Federal do Rio de Janeiro, Rio de Janeiro, Brazil. (In Portugese)

[12] Axelbaum, R. L., & Brandt, H. (1987). The Effect of Substrate Surface Preparation on the optical properties of a black chrome solar absorber coating. *Solar Energy*, *39*(3), 233–241.

[13] Kennedy, C. E. (2002). Review of Mid- to High-Temperature Solar Selective Absorber Materials, National Renewable Energy Laboratory, Colorado.

[14] Gomes, C. A. S. (2001). Comparative study of selective surfaces for solar collectors. (Mestrado em Engenharia e Ciência dos Materiais), Universidade Federal do Ceará, Fortaleza, Brazil. (In Portugese)

[15] Raut, H. K., Ganesh, V. A., Nair, A. S., & Ramakrishna, S. (2011). Anti-reflective coatings: A critical, in-depth review. *Energy & Environmental Science*, *4*(10), 3779-3804.

[16] Selvakumar, N., & Barshilia, H. C. (2012). Review of physical vapor deposited (PVD) spectrally selective coatings for mid- and high-temperature solar thermal applications. *Solar Energy Materials and Solar Cells*, 98, 1–23.

[17] Aguilar, M., Barrera, E., Palomar-Pardavé, M., Huerta, L., & Muhl, S. (2003). Characterization of black and white chromium electrodeposition films: surface and optical properties. *Journal of Non-Crystalline Solids*, *329*(1-3), 31-38.

[18] Smith, G. B., Teytz, K., & Hillery, P. (1983). The substrate impact on the structure and thermal stability of solar selective black chrome. *Solar Energy Materials*, *9*(1), 21–41.

The Analysis of Suitable Area for Solar Plant Construction in Nišava District: A GIS-MCDM Approach

Petar Vranić[1], Lazar Velimirović[2]

[1,2]Mathematical Intitute MISANU, Belgrade, Serbia, petarvvv@mi.sanu.ac.rs[1]; lazar.velimirovic@mi.sanu.ac.rs[2]

Abstract—**The Republic of Serbia is a signatory of the 2015 Paris Agreement on Climate Change. Like other signatories to the agreement, Serbia is legally compelled to fulfill the agreed goals which among others includes the increased use of renewable energy sources (RES). Building on previous studies, the objective of this paper is to analyze the suitable location for solar plants, in this way contributing to the objectives stated in Energy Strategy 2030 that are among others based on the activities that include more intense use of RES, by the promotion of RES to be included in energy plans of cities and local communities as part of local energy strategies. The study area of this research comprises the land territory of the Nišava District. The analysis in this research employs GIS multi-criteria decision-making approach (GIS-MCDM) to evaluate spatial, geomorphological, climate, and environmental criteria and generate a solar plant construction suitability index.**

Keywords – GIS, MCDM, energy, Serbia, solar plant, spatial analysis

I. Introduction

International Energy Agency (IEA) estimated an increase by 40% in primary energy consumption for the period from 2005 until 2025. Energy sector is driver of the economy of each country, therefore, it has to be particularly considered in strategic planning to secure welfare of the entire economy, otherwise, the country can expect reverse effects. Regardless of its importance, contemporary energy production patterns have the highest negative environmental offset among other economy sectors, due to its large dependence on conventional energy sources. The outlook of global development considers economy established on clean energy sources, with lowest possible environmental footprint of its supply and consumption [1]. As highlighted by Serbian national Energy strategy 2030 energy sector is seen as one of the frontiers in aiding future more dynamic and quality economy growth and its sustainable development, thus, sectoral policy by 2030 sees provision of energy security, energy market development and general transition towards sustainable energy sector as a core development axis of energy sector in republic of Serbia [1].

The Republic of Serbia is a signatory of the 2015 Paris Agreement on Climate Change. Like other signatories to the agreement, Serbia is legally obliged to fulfill the agreed goals which among others includes the increase use of renewable energy sources (RES) to reduce greenhouse gas emissions generated by the exploitation of fossil fuels [2]. Among other means of RES, because of its multiple benefits, solar energy (SE) is one of the most suitable, since it is fully environmentally friendly and can be exploited directly. It represents energy potential of the Republic of Serbia both for the generation of electricity and heating energy.

The exploitation of SE also contributes the reduction of fossil fuels imports, local industry development and job creation. The average solar radiation in Serbia is about 40% higher than the European average (between 1500 and 2200 hours per year), but on the other hand, the use of SE for electricity production lags far behind the EU countries [3]. Total solar energy potential is about 30% higher in comparison to East Europe, and the intensity of solar radiation is among the highest in Europe.

Average daily energy of global radiation for a flat surface in the winter reaches between 1.1 kWh/m2 in the north and 1.7 kWh/m2 in the

ISBN: 978-86-80616-07-0

south, while in the summer between 5.9 kWh/m2 in the north and 6.6 kWh/m2 in the south. For comparison, the average value of global radiation for the territory of Germany is about 1000 kWh/m^2, while for central Serbia the value is about 1400 kWh/m^2 [1,3]. In technical terms, usable energy potential for the conversion of solar energy into heating energy is estimated at 0.194 million toe per year assuming of installation of solar thermal collectors at 50% available facilities in the country [1]. Data presented clearly points out that Serbia has solar energy resources with an extremely favorable seasonal distribution.

In case of Serbia, solar energy is mainly used to generate heat energy (in a very small percentage), where it is proved to be very cost-effective. That is why solar collectors have become relatively popular in household water heating systems across the country. On the other hand, employing SE for obtaining electricity and installation of photovoltaic modules is symbolic, despite the favorable conditions [4]. The affirmation and` development of a sustainable market photovoltaic systems is necessary for the economy and environmental protection in Serbia.

Analyzing suitable location for solar plants, this research aims to contribute to objectives stated in Energy Strategy 2030 that are among others based on the activities that include more intense use of RES, by promotion of RES to be included in energy plans of cities and local communities as part of local energy strategies.

II. MATERIALS AND METHODS

The study area of this research is the land territory of The Nišava District (Fig. 1), situated in South-East Serbia. The land territory covers 2.729 km^2 and population of 372.404. Due to its geographical position and climate characteristics it is a good candidate for solar energy exploitation.

The analysis in this research employs GIS multi criteria decision making approach (GIS-MCDM). Geographic Information System (GIS) and geospatial modeling are common tool in renewable energy data processing [5]. The degree of utilization of RES depends on multiple features specific to a given context, therefore, the selection of the suitable sites for the installation of solar power plants is conditioned by number of factors that have to be taken into consideration during the analysis. In this modeling exercise we

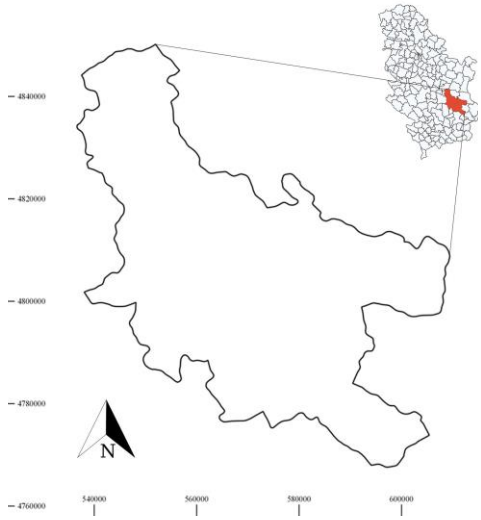

Figure 1. Study area.

focus on climatic, spatial and environmental parameters. This study primarily relies on open data for creation of a GIS data set: global horizontal irradiation (GHI) is derived form Global Solar Atlas (www.globalsolaratlas.info), for protected area we used data from the Institute for Nature Conservation of Serbia, settlements, railways, roads, and waterbodies are generated form Open Street Map (OSM) (the OSM data timeframe is 2018.), Corine Land Cover European seamless vector database (RELEASE v18_5) was used for the land cover data, the geomorphological variables slope, aspect, and elevation gradient maps are calculated based on the - shuttle radar topography mission (SRTM) digital elevation model with a resolution of 30 km. The analysis is conducted in open source GIS software QGIS 3.4 environment applying tools for spatial analysis. Applying the 25% rule each parameter is reclassified on the on the scale from 0 to 1, where the value p_j=0 is considered as the least favorable and value p_j=1 as the most favorable location for the given parameter (Table I). The relative weights (w_j) of the parameters are assigned by expert form the energy industry applying Analytical Hierarchy Process. AHP widely employed a non-compensatory, subjective MCDA method, frequently utilized in its crisp form [6]. It was frequently employed in various domains of environmental development and research [7,8]. Finally, to generate of solar plant suitability map the arithmetically weighted overlay approach is used to integrate all parameters using Eq. (1):

$$SUI_i = \sum_{j=1-n}^{i=1-n} w_j p_{ij} \quad , \qquad (1)$$

where SUI_i is the suitability index of the *i-th* cell, w_j is the relative weight of the *j-th* parameter, and p_{ij} is the value of the *j-th* parameter in the *i-th* cell.

A. *Global Horizontal Irradiation (GHI)*

GHI is the single most important parameter for energy yield calculation and performance assessment of flat-plate photovoltaic technologies. Da date is derived form Global Solar Atlas. The solar resource map provides a summary of estimated solar energy accessible for various energy applications. It represents the average daily/yearly sum of global horizontal irradiation (GHI) covering a period of 25 years (1994-2018). The underlying solar resource database is calculated by the Solargis model from atmospheric and satellite data with 15-minute and 30-minute time step. The effects of terrain are considered at nominal spatial resolution of 250m. There is some level of uncertainty in the yearly GHI estimate due to limited potential for regional model validation due to lack of high quality ground measurement data, which is estimated to vary regionally form approximately 5-6%.

TABLE I. CRITERIA CONSIDERED IN THE ANALYSIS.

Criteria (*w*)	**Sub-Criteria (*w*)**	**Values**	**Reclassified value (p_j)**
Spatial (0.1718)	Distance to settlements (0.5736)	0-1000m 1000-5000m 5000-10000m 10000-20000m >20000m	1 0.75 0.5 0.25 0
	Distance to roads (0.3614)	0-750m 750-1500m 1500-2250m 2250-3000m >3000m	1 0.75 0.5 0.25 0
	Distance to railway (0.0650)	0-5000m 5000-10000m 10000-15000m 15000-20000m >20000m	1 0.75 0.5 0.25 0
Environmental (0.2425)	Land Cover (0.2425)	Pastures and natural grasslands Sparsely vegetated areas Heterogeneous agricultural areas Arable land Other	1 0.75 0.5 0.25 0
Geomorphological (0.0838)	Slope (0.6267)	<25% >25%	1 0
	Orientation (0.2797)	South East, West North	1 0.5 0
	Elevation (0.0936)	<300masl 300-450masl 450-650masl >650masl	1 0.75 0.5 0
Climate (0.5019)	GHI (0.5019)	>1387kWh/m^2 1314-1387kWh/m^2 <1314 kWh/m^2	1 0.75 0.5

B. Protected Areas

The research eliminated some areas where energy plants can not be installed disregarding of their other characteristics due to environmental protection issues. Such areas are perceived as unsuitable locations. In order to not to undermine their protection regime, following recommendation form [9], the extra buffer of 200m was used.

C. Hydrology

Future climate scenarios indicate decline of water in rivers in Serbia, especially in the period 2071-2100. Also, scenario A2 envisages a drier climate in the last observed period, with a reduction in precipitation of over 30% in some parts of Serbia [10]. Estimates point out that for the case of an average increase of annual temperatures of 2°C we can expect average 40-50% less water in rivers [11]. In this study, the water bodies are considered as a constrain parameters as well as the area distanced 100 m from them, both in terms of protection and flooding prevention. Study take into network of the permanent waterways.

D. Distance to Settlements

As pointed by [12], assuming that solar plants should be built near electricity consumers, they has to be close to settlements. Lareger cities have a tendency to sprawl, in contrast to smaller towns, settlements and villages, thus, some studies [13], recommends buffer of this study apply buffer of 5 km in case of a big cities, the small ones buffer of 2 km. City of Niš is the only big city in the study are, however, due to its development patters it does not have prominent sprawling trends in past decades. Therefore buffer of 500m is applied for the urban area of Niš and 100m for the rest of the towns and settlements as a constrain area.

E. Distance to Infrastructure

Solar power plants has to be accessible both because the installation and maintenance purposes, therefore, proximity to roads and railways is an important criterion. Following [14], the maximum acceptable distance to roads is set to 3 km and to the railway to 20 km, where the location which is further form the origin of the infrastructure is considered as the less suitable.

F. Land Cover

Corine Land cover land recognize five main classes: artificial surfaces, agricultural areas, forest and semi natural areas, wetlands and water bodies, with fifteen land cover subclasses. When installing solar power plant it is important to avoid economically valuable lands. The most suitable classes for construction are barren land, grasslands, and bushlands, since they are economically least valuable lands and easy to exploit. Besides them emerging forests and pastures can be taken into consideration. Forests and agricultural lands are seen as the more valuable lands in economical terms, however, decision of (not)-including them is context dependent.

Serbia is suffering deforestation. Global climate change will cause changes in function and structure of forest ecosystems, and consequently, its capacity to sequestrate carbon and produce biomass, and thus, aid mitigation of climate change [15]. Considering the fact that new afforestation will be rather difficult, and potential multifold increased risks of forest fire in the region in coming decades [16], the preservation of existing forests is one of the imperatives of the climate change adaptation process [11], thus, forest lands are considered as constraint parameter in this research.

On the other hand, the agricultural land can be categorized according to land quality classes where the least productive lands can be allocated for energy production purposes, however, land productivity analysis is beyond the scope of this research. Finally, according to Corine Land Cover this analysis consider following available classes: natural grasslands, non-irrigated arable land, pastures, sparsely vegetated areas, land principally occupied by agriculture with significant areas of natural vegetation, and complex cultivation patterns as the potentially suitable areas for SE power plants.

G. Slope

The slope of the terrain is an important criterion, since the increase in the terrain incline highly affects the feasibility and the cost of any solar project [17,18]. Also the inclined terrain makes the installation of solar power plants more difficult. Following the [19] for this research 25% (14 degrees) is set as a maximum acceptable slope. The slopes higher than 25% are considered as unsuitable locations for construction of solar power plant with allocated value of 0.

H. Orientation

The aspect is another key orographic factor. The south-facing areas, followed by east-west oriented terrains are more favorable in comparing to north-facing slopes. The south-facing location are more exposed to solar radiation, therefore, more suitable for exploiting the solar potential. The value distribution for the area orientation are given in the Table I.

I. Elevation

The elevation as a third orographic parameter, is considered as parameter that influence feasibility and cost of the construction like slope. The locations positioned at the higher altitude requires higher transportation costs. 500m above the lowest point in study area is taken as the maximum acceptable elevation. Above this elevation location are considered as unsuitable, while the suitability level increases towards lower altitudes.

III. RESULTS

Fig. 2 indicates a spatial distribution of each selected criteria. When it comes to spatial criteria, we can observe that 92.2% of the area falls in the category of highly to moderately suitable locations considering the proximity to the settlements, 95.6% in case of proximity to the roads, and 70% in case of distance to the railway. On the other hand, environmental criteria have a somewhat different distribution ratio. A 38% of the analyzed territory, according to land cover classes, is marginally suitable (arable land), 55.1% is suitable (heterogeneous agricultural areas), 0.35% moderately (sparsely vegetated areas), and only 6.6% as highly suitable land (pastures and natural grasslands). In the case of geomorphological criteria, 60.7% of the territory is at elevation highly or moderately suitable for solar plant installation, 24.7% at suitable, and 14.7% at a marginally suitable elevation. Looking at the slope criteria, 94.8% of the area is at a slope lower than <25%, and only 5.2% lays at steeper slopes, thus, categorized as unsuitable. Moreover, 27.6% of the area has a southern orientation, and thus, perceived as highly suitable, 52.7% western or eastern, and 19.7% face north. Finally, in terms of climate criteria 26.6% has GHI >1387kWh/m^2, 58.0% has GHI value between 1314-1387kWh/m^2, and 15.4% falls in range lower than 1314 kWh/m^2.

Based on expert evaluation, applying AHP, we assigned local weights to the reclassified raster's, and by summing them up calculated solar plant construction suitability index for the territory of Nišava district. As indicated in Table I, climate (GHI) is perceived as the single most dominant criteria, followed by environmental and spatial criteria.

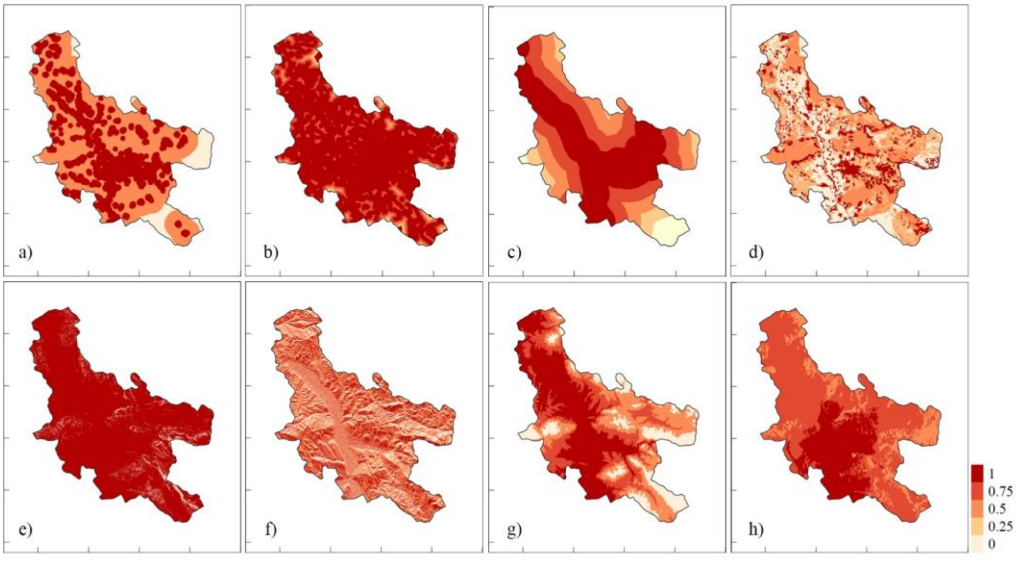

Figure 2. Reclassified values for the criteria: a) distance to settlements, b) distance to roads, c) distance to railway, d) land cover, e) slope, f) orientation, g) elevation, and h) GHI.

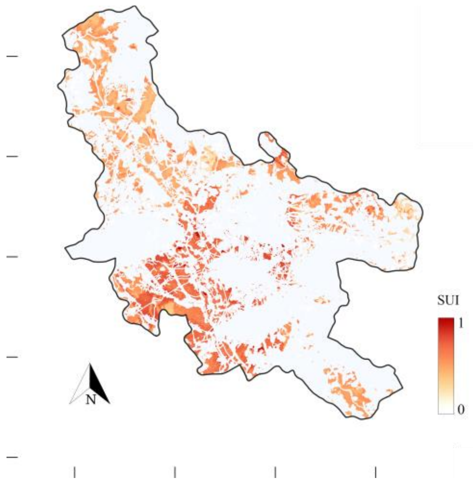

Figure 3. Suitability map for solar plant installation; 1 – highly suitable, 0.75 - moderately suitable, 0.5- suitable, 0.25 – marginally suitable, 0 – unsuitable.

The resulting suitability index reveals the distribution of the area for solar plant construction categorized on a scale from 0, meaning unsuitable, to 1 meaning highly suitable (Fig. 3). A substantial share of the entire area (80%) is under the constrained parameters, and so, considered unsuitable. The available land for solar plant construction is 20% of the district. As the resulting map indicates, all the remaining territories fall in the categories of the index values between 0.5 (moderately suitable) and 1 (highly suitable), in this way, pointing to the more significant spatial, environmental, and geomorphological potential for solar plant installation. As the SUI map indicates, we can observe a somewhat equal distribution of suitable area across the district, with the larger share of suitable area in the North-west part of the region and central-South.

IV. Concluding Remarks

The goal of this research was to explore suitable areas for the solar plant construction with the territory of Nišava district. In doing so, we employed the GIS-MCDM approach. The obtain results stand true for the selected criteria and expert evaluation. The applied approach can be further explored in several directions. In methodical terms, further research can consider comparative studies with different MCDM, and remote sensing approaches. In terms of selected criteria reconsideration of land use, criteria might affect results in further studies. In this study, the agricultural land is considered suitable, though with the lower weights. In further studies the agricultural land can be categorized according to land quality classes where the least productive lands can be allocated for energy production purposes, however, land productivity analysis was beyond the scope of this research. In this type of study distance to electricity, infrastructure is frequently considered as one of the criteria in terms of available connection nodes. However, distance to the electricity grid is insufficient criteria by itself, since the connection of solar power plant to network often requires reconstruction of the network itself, where related costs might out-weight the proximity to the network. Further research might take this criterion for the territories selected as the most suitable for the solar plant construction in the given context. Finally, the higher resolution of official data can result in the accuracy of the result.

Acknowledgment

This work was supported by the Serbian Ministry of Education, Science and Technological Development through Mathematical Institute of the Serbian Academy of Sciences and Arts.

References

[1] RSE - Republic of Serbia Ministry of Mining and Energy (2016). Energy Sector Development Strategy of the Republic of Serbia for the period by 2025 with projections by 2030.

[2] UNFCCC. (2015). Adoption of the Paris Agreement, FCCC/CP/2015/Add.1; United Nations Framework Convention on Climate Change: Paris, France..

[3] Lepotic-Kovacević, B., & Lazarević, B. (2016). *Construction of plants and electricity generation from photovoltaic plants in the republic of Serbia - Guide for investors*. UNEP: Belgrade

[4] Radičević, B., Mikičić, D., & Vukić, Đ. (2009). Energetski potencijal sunca u srbiji i primena energije sunca u poljoprivredi. *Poljoprivrdna tehnika 34*(4), 53-62.

[5] Vranić, P., & Milovanović, M. (2018, October). Review of GIS application in energy research. In *4th Virtual International Conference on Science, Technology and Management in Energy – eNergetics.* ISBN 978-86-80616-03-2

[6] Zyoud, S. H., & Fuchs-Hanusch, D. (2017). A bibliometric-based survey on AHP and TOPSIS techniques, *Expert Systems with Applications*, doi: 10.1016/j.eswa.2017.02.016

[7] Singh, R. P., & Nachtnebel, H. P. (2016). Analytical hierarchy process (AHP) application for reinforcement of hydropower strategy in Nepal. *Renewable and Sustainable Energy Reviews*, *55*, 43-58.

[8] Brandt., P, Kvakić., M, Butterbach-Bahl., K, & Rufino., M. C. (2017). How to target climate-smart agriculture? Concept and application of the consensus-

driven decision support framework target CSA. *Agric Syst 151*, 234-245.

[9] Georgiou, A. G., & Skarlatos, D. (2016). Optimal site selection for sitting a solar park using multi-criteria decision analysis and geographical information systems. Geosci. Instrum. *Methods 5*, 321–332.

[10] Ministarstvo poljoprivrede i zaštite životne sredine (2015). *The first national plan for adaptation to changed climatic conditions for the Republic of Serbia Draft* [Prvi nacionalni plan adaptacije na izmenjene klimatske uslove za Republiku Srbiju Nacrt] Beograd (In Serbian).

[11] Ministarstvo zaštite životne sredine (2017). *Second Report of the Republic of Serbia under the United Nations Framework Convention on Climate Change [Drugi izveštaj Republike Srbije prema Okvirnoj* konvenciji Ujedinjenih nacija o promeni klime]. Beograd. (In Serbian)

[12] Uyan, M. (2013). GIS-based solar farms site selection using analytic hierarchy process (AHP) in Karapinar region, Konya/Turkey. *Renew. Sustain. Energy Rev. 28*, 11–17.

[13] Merrouni, A. A, Elalaoui, F. E., Ghennioui, A., Mezrhab, A., & Mezrhab, A. (2018). A GIS-AHP combination for the sites assessment of large-scale CSP plants with dry and wet cooling systems. Case study Eastern Morocco. *Solar Energy 166*, 2–12.

[14] Gašparovic, I., & Gašparovic, M. (2019). Determining Optimal Solar Power Plant Locations Based on Remote Sensing and GIS Methods: A Case Study from Croatia. *Remote Sens. 11*(12), 1481; doi:10.3390/rs11121481

[15] Xie, Y., Wang, H., & Lei, X. (2020). Simulation of climate change and thinning effects on productivity of Larix olgensis plantations in northeast China using 3-PGmix model. *Journal of Environmental Management* 261, 110249. DOI: 10.1016/j.jenvman.2020.110249

[16] Khabarov et. al. (2016). Forest fires and adaptation options in Europe. *Regional Environmental Change* 16, 21-30. DOI:10.1007/s10113-014-0621-0

[17] Bravo, J. D., Casals, X. G., & Pascua, I. P. (2007). GIS approach to the definition of capacity and generation ceilings of renewable energy technologies. *Energy Policy* 35, 4879–4892.

[18] Gastli, A., Charabi, Y., & Zekri, S. (2010). GIS-based assessment of combined CSP electric power and seawater desalination plant for Duqum-Oman. Renew. *Sust. Energy Rev*. 14, 821–827.

[19] Tahri, M. Hakdaoui, M., & Maanan, M. (2015) The evaluation of solar farm locations applying Geographic Information System and Multi-Criteria Decision-Making methods: Case study in southern Morocco. Renew. *Sustain. Energy Rev.* 51, 1354–1362.

Thermal Analysis of Rotary Regenerator from Changes in Mass Flow Rate

Guilherme Henrique da Cunha[1], Paulo Cesar Mioralli[2], Elson Avallone[3], Paulo Henrique Palota[4], Murilo Secchieri de Carvalho[5]

[1,2,3,4,5]Federal Institute of São Paulo - IFSP, Catanduva, Brazil, cunha.h@aluno.ifsp.edu.br[1]; mioralli@ifsp.edu.br[2]; elson.avallone@ifsp.edu.br[3]; palota@ifsp.edu.br[4]; murilo.carvalho@ifsp.edu.br[5]

Abstract—**Thermal analysis of typical rotary regenerators under the laminar flow regime is computationally performed from changes in mass flow rate of gas streams. High mass flow rates may imply good thermal exchange in the regenerator, however, they can result in high pressure drop which negatively impacts the pumping power cost. On the other hand, if the mass flow rate is considerably low, significant contamination between the gases can occur from the fluid carryover leakage. The ratio of residence time t_{res} of flow on each side of the equipment to the time t_0 required for a complete matrix rotation is calculated for the regenerators, representing the fluid carryover leakage. The total heat transfer in the regenerator and the pressure drop in each gas stream are also obtained for each simulated case. Conditions for acceptable fluid carryover leakage, suitable pressure drop and good heat transfer in the regenerator were assumed based on literature and practical observations. A mass flow rate range that associates these conditions was chosen as good operating situations for each simulated equipment.**

Keywords – rotary regenerator, heat transfer, carryover leakage, pressure drop, computational analysis

I. Introduction

Rotary regenerator is a compact heat exchanger commonly used as waste heat recovery device. This equipment is adopted widely in large power plant boilers and air conditioning systems. The growing demand for energy recovery has driven researchers to search better performance in rotary regenerators. Many works aim the optimum use of equipment, focusing on lower pressure drop and higher efficiency. In general, optimization techniques require numerical analysis and including the simultaneous study of various parameters of rotary regenerator, such as matrix porosity, matrix rotation, pressure drop, carryover leakage, inlet temperatures and mass flow rate of streams. Some optimization studies with modeling and numerical analysis of rotary regenerator can be highlighted. Different algorithms were used to maximize the regenerator effectiveness [1-3]. Performance parameters and thermal behavior of a rotary regenerator were investigated using finite difference method [4], finite volume method [5-9], a porous media approach [10-11] and genetic algorithm [12-15].

Optimization techniques are often complex and laborious. Results that estimate the regenerator performance close to optimal operating conditions can be obtained through simpler procedures. Studies about the rotary regenerator that include the prescription of parameter ranges that imply satisfactory operating conditions and the use of a simple methodology are few explored in the literature [16-19]. The goal of present work is to establish a mass flow rate range that implies good operating conditions of three typical rotary regenerators. These conditions take into account acceptable fluid carryover leakage, typical pressure drop and good heat transfer, whose values considered as suitable are based on literature and practical observations.

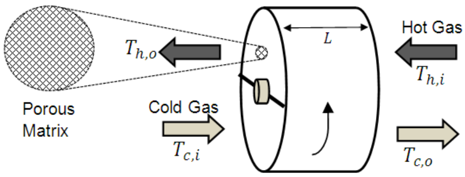

Figure 1. Schematic diagram of the rotary regenerator.

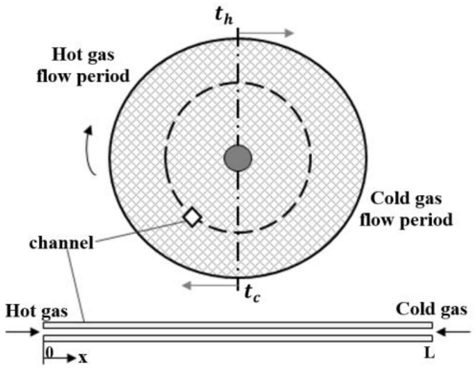

Figure 2. Cold and hot periods of the rotary regenerator.

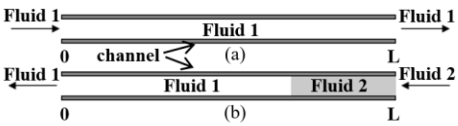

Figure 3. Contamination from the fluid carryover leakage: (a) The end of period 1; (b) The beginning of period 2.

II. Problem Description

A. The Rotary Regenerator

In the rotary regenerator, Fig. 1, two gas streams are introduced counterflow-wise through the parallel ducts of the air preheater. Cold gas is injected inside one duct and hot gas inside the other. The porous matrix, that stores energy, continuously rotates through these parallel ducts. The matrix receives heat from the hot gas on one side and transfers this energy to the cold gas on the other side. The matrix channels were assumed smooth. The fluid velocity was considered constant inside each channel.

The actual time that cold gas takes to flow through a hot regenerator matrix is called the cold period and the time that hot gas flows through the cold regenerator matrix is called the hot period. Fig. 2 illustrates a fixed point in the matrix of the regenerator, represented by a channel, which runs through the sides of the cold and hot gas streams during one revolution of the matrix. The parameters t_c and t_h represent the cold and hot periods, respectively.

Contamination between the fluids streams occurs when an amount of one of the fluids in the matrix passages is lugged from one fluid stream to the other by the rotation of the matrix [20]. For negligible contamination, the time it takes the gas particles to travel through the matrix passages must be sufficiently less than the rotation time of the matrix. Fig. 3 illustrates the contamination from the fluid carryover leakage.

The time of fluid particle passing through the matrix ducts is called the residence time t_{res} defined as the ratio of the length L of the matrix ducts to the bulk stream velocity u in ducts:

$$t_{res} = L/u \ . \tag{1}$$

To describe the propagation of carryover leakage, Banks [21] introduced a parameter defined as the ratio of residence time t_{res} of flow on each side to the time t_0 required for a complete matrix rotation. Analysis of typical rotary regenerators operating close to optimal conditions showed that this ratio must be up to 1.5% for negligible contamination between fluids [22], that is:

$$\left(t_{res}/t_0\right) \le 0.015 \ . \tag{2}$$

Geometric parameters of the rotary regenerator can be expressed based on Figs. 1 and 2. The total frontal cross-sectional area A_T is determined by the sum of the free flow cross-sectional area A and the matrix cross-sectional area A_m of the air preheater:

$$A_T = A + A_m \ . \tag{3}$$

The matrix porosity σ is defined by the ratio between A and A_T :

$$\sigma = A/A_T \ . \tag{4}$$

The hydraulic diameter D_h of the matrix ducts can be written as function of the porosity and the matrix duct wall thickness e that is:

$$D_h = \frac{4\sigma}{1-\sigma}\left(\frac{e}{2}\right) . \quad (5)$$

The use of hydraulic diameter is justified in the correlations for friction factor and Nusselt number.

B. Effectiveness-NTU Method for Rotary Regenerator

The Effectiveness-NTU method for rotary regenerators [23] consists of calculating the effectiveness ε_0 of a conventional counterflow heat exchanger and correcting this effectiveness by a correction factor φ_r that takes into account the rotational speed and the matrix heat capacity rate of the exchanger. Thus, the effectiveness of the regenerator ε_r is given by Eq. (6):

$$\varepsilon_r = \varepsilon_0 \, \varphi_r \ . \quad (6)$$

The effectiveness ε_0 of a conventional counterflow heat exchanger is defined by following Eq.:

$$\varepsilon_0 = \begin{cases} \dfrac{1-exp\left[-NTU\left(1-C^*\right)\right]}{1-C^* exp\left[-NTU\left(1-C^*\right)\right]} ; \ C^* < 1 \\ \dfrac{NTU}{1+NTU} ; \ C^* = 1 \end{cases} \quad (7)$$

where C^* is the ratio between the fluids heat capacity rates and NTU is the number of heat transfer units defined as follows:

$$C^* = C_{mim}/C_{max} \ , \quad (8)$$

$$NTU = \frac{1}{C_{min}}\left[\frac{1}{\left(1/hA_{tr}\right)_c + \left(1/hA_{tr}\right)_h}\right] , \quad (9)$$

where h is the convective heat transfer coefficient and A_{tr} is the matrix thermal exchange area on the side of the hot or cold stream. The parameters $C_{\min}$ and $C_{\max}$ correspond to the minimum and maximum values of the fluids heat capacity rates.

The correction factor φ_r in Eq. (6) is given by [24] that provides good results even for very low rotational speeds:

$$\varphi_r = \frac{1}{\left[1+3\left(\varepsilon_0/C_r^*\right)^2 + \left(\varepsilon_0/C_r^*\right)^4\right]^{1/4}} , \quad (10)$$

$$C_r^* = C_r / C_{min} \ , \quad (11)$$

$$C_r = \frac{n}{60} m_m \, c_m \ , \quad (12)$$

where C_r is the matrix heat capacity rate, n is the matrix rotational speed, m_m is the matrix mass and c_m is the specific heat of matrix.

The total heat transfer Q in the rotary regenerator is obtained in the same way as the Effectiveness-NTU method for conventional heat exchangers:

$$Q = \varepsilon_r \, Q_{max} \ , \quad (13)$$

$$Q_{max} = C_{min}\left(T_{h,i} - T_{c,i}\right) , \quad (14)$$

where $Q_{\max}$ is the maximum possible heat transfer and the term between parenthesis corresponds to the difference between the inlet temperature of the hot stream and the inlet temperature of the cold stream.

C. Hydrodynamic and Thermal Analysis

The hydrodynamic and thermal analysis are performed for each gas stream. The distributed pressure drop ΔP in the matrix ducts and the convective heat transfer coefficient h are obtained from correlations for Darcy friction factor f and Nusselt number Nu Correlations for smooth ducts with circular cross-sectional area were used based on the hydraulic diameter of matrix ducts for laminar flow regime. The correlations take into account hydrodynamically fully developed flow with thermal entrance length and constant wall temperature boundary condition.

$$f = \frac{64}{Re_{D_h}} \ , \quad (15)$$

$$Nu = 3.66 + \frac{0.0668\left(\frac{D_h}{L}\right)Re_{D_h}Pr}{1+0.04\left[\left(\frac{D_h}{L}\right)Re_{D_h}Pr\right]^{\frac{2}{3}}}, \quad (16)$$

where Re_{Dh} is the Reynolds number and P_r is the Prandtl number.

The distributed pressure drop ΔP is given by equation of Darcy-Weisbach and the convective heat transfer coefficient h is expressed in terms of Nusselt number:

$$\Delta P = f\ \rho \frac{L}{D_h}\frac{u^2}{2}, \quad (17)$$

$$h = \frac{Nu\, k}{D_h}, \quad (18)$$

where ρ and k are the fluid density and the fluid thermal conductivity, respectively.

D. *Fluid and Matrix Properties*

The fluid properties were obtained at the average temperature of each gas stream. The gases density ρ were calculated by the equation of state of an ideal gas, considering air with moderate values of pressure and temperature:

$$\rho = \frac{p}{RT}, \quad (19)$$

where p is the pressure of fluid, T is the average temperature of gas stream and R is the ideal gas constant. The values of air atmospheric pressure $p = 10^5 Pa$ and ideal gas constant for air $R = 287 Nm/kgK$ were assumed.

The dynamic viscosity μ and the thermal conductivity k of fluids can be approximated by the Sutherland equations [25] as follow:

$$\frac{\mu}{\mu_0} \approx \left(\frac{T}{T_0}\right)^{3/2}\frac{T_0+S}{T+S}, \quad (20)$$

$$\frac{k}{k_0} \approx \left(\frac{T}{T_0}\right)^{3/2}\frac{T_0+S}{T+S}, \quad (21)$$

where S is the Sutherland constant temperature, which is characteristic of each gas. Considering air, $S = 111K$ for dynamic viscosity and $S = 194K$ for thermal conductivity. The parameters T_0, μ_0 and k_0 are reference constants, whose values are $T_0 = 273K$, $\mu_0 = 1.76x10^{-5} Pa.s$ and $k_0 = 0.0241 W/mK$ for air.

The specific heat of gas under constant pressure c_p is obtained by a polynomial equation [26] with application for several gases in the temperature range between *300* and *1,000 K*

$$\frac{c_p}{R} = \alpha_0 + \beta_0 T + \gamma_0 T^2 + \delta_0 T^3 + \lambda_0 T^4, \quad (22)$$

where $\alpha_0 = 3.653$, $\beta_0 = -1.337x10^{-3}$, $\gamma_0 = 3.294x10^{-6}$, $\delta_0 = -1.913x10^{-9}$ and $\lambda_0 = 0.2763x10^{-12}$ are the constants for air.

The Prandtl number P_r is obtained from the ratio between some fluid properties, as follow:

$$Pr = \frac{\mu\, c_p}{k}. \quad (23)$$

The matrix properties of the rotary regenerator were assumed constant. The AISI 1010 low alloy carbon steel and the 2024-T6 aluminum alloy materials were considered for the matrix in this work. Table I shows the matrix properties used for the simulated regenerator cases, where c_m and p_m are the specific heat and the density of matrix, respectively.

E. *Computer Program*

A computer program written in *C* programming language was developed for the simulation of rotary regenerator. The *Dev-C++*

TABLE I. MATRIX PROPERTIES OF THE ROTARY REGENERATOR.

Matrix Material	***c_m* (J/kg K)**	***ρ_m* (kg/m³)**
2024-T6 Aluminum	875	2.770
AISI 1010 Steel	434	7.832

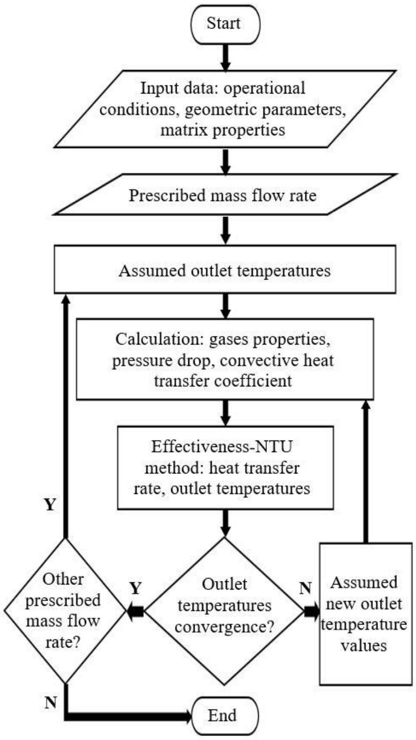

Figure 4. Schematic diagram of the calculation process.

software was used for compilation and recording results. Three typical sizes of equipment were simulated: small, medium-sized and large. The material AISI 1010 low alloy carbon steel was used for the medium-sized and the large regenerators in the simulations. The 2024-T6 aluminum alloy was used for the small regenerator. The total heat transfer in the rotary regenerator and the outlet temperatures of gas streams were calculated for different mass flow rate of gas stream. The mass flow rate of both streams were considered with the same value. The other operational conditions and the geometric parameters of the equipment were fixed.

An iterative process was used to obtain the fluid flow and the heat transfer. An outlet temperature values of each stream was assumed at the beginning of this process. Then, the fluid properties were evaluated at the average temperature of each gas stream. Based on these properties, the fluid flow and the heat transfer were obtained from correlations and the Effectiveness-NTU method for rotary regenerators. The iterative process continued until convergence of the outlet temperatures for both streams. The whole process was repeated for each assumed mass flow rate of streams. The subrelaxation factor 0.5 was used to the convergence of the outlet temperature values. The tolerance for convergence iterative procedure was adjusted as 10^{-3} for the outlet temperatures. The calculations were performed considering the steady-periodic condition of the regenerator. The schematic diagram of the calculation process is shown in Fig. 4.

In order to validate the computational code, the outlet temperatures of gas streams were calculated at a medium-sized rotary regenerator with corrugated ducts. Correlations for corrugated ducts [27] were used for the hydrodynamic and thermal analysis in this case. The results were compared with field data from a rotary regenerator operating in a petroleum refinery. Table II shows the comparison between the results of the present study and the field data. Reasonable agreement between results is observed. Since the pressure leakage and fluid bypass of rotary regenerator are not considered in this study, this difference could be minimized by including these parameters.

III. RESULTS AND DISCUSSION

Table III shows the input data for computer program of three typical rotary regenerators simulated: small, medium-sized and large. The simulations were carried out from different mass flow rate m values and considering the gas streams under the laminar flow regime. The

TABLE II. COMPARISON OF THE PRESENT DATA WITH FIELD DATA.

Outlet Temperature (°C)	Present work	Field data	Difference
$T_{c,o}$	439.89	405.65	8.44
$T_{h,o}$	158.44	194.27	18.44

TABLE III. INPUT DATA FOR COMPUTER PROGRAM OF TYPICAL ROTARY REGENERATORS.

Regenerator	Small	Medium-sized	Large
σ	0.83	0.90	0.90
L (m)	0.2	1.5	3.5
e (m)	0.00035	0.00050	0.00060
D (m)	0.7	6.0	15.0
n (rpm)	8	3	2
$T_{h,i}$ (°C)	50	450	600
$T_{c,i}$ (°C)	20	80	150
$\dot{m}$ (kg/s)	0.2 a 2.0	10 a 100	80 a 530

mass flow rate values were considered to be the same for both streams of each regenerator. The parameter D is the matrix diameter.

The total heat transfer, the pressure drop and the ratio (t_{res}/t_0) for both streams were obtained for each simulated case. From these results, a mass flow rate range was chosen, that provide: acceptable fluid carryover $(t_{res}/t_0 \leq 0.015)$, acceptable pressure drop, whose values approximate those observed in typical regenerators operating close to optimal conditions [22] and; good heat transfer rate, whose value is limited to up to about 20% less than the maximum possible value considering laminar flow regime.

Fig. 5 shows the total heat transfer in the small regenerator as a function of the mass flow rate. The total heat transfer increases as the mass flow rate values increase. In this case, for mass flow rate values greater than 1.8 kg/s, at least one of the streams reaches the turbulent flow regime. Fig. 6 shows two results simultaneously: the ratio (t_{res}/t_0) for both streams of the regenerator as a function of the mass flow rate (vertical bars) and also the pressure drop for both streams of the equipment as a function of the mass flow rate (continuous lines). The pressure drop increases linearly as the mass flow rate increases. Practical observations of typical small rotary regenerators, operating close to optimal conditions under laminar regime, show that the pressure drop values are lower than 200 Pa [22]. Fig. 6 shows that both streams are within this condition. Regarding to the ratio (t_{res}/t_0), Fig. 6 demonstrates that the increase in mass flow rate implies less contamination between fluids. Additionally, the mass flow rate values must be greater than 0.35 kg/s for negligible contamination between fluids in the small rotary regenerator, as reported by Eq. (2). According to Fig. 5, the total heat transfer is close to 6.5 kW for 0.35 kg/s. This result is 59% lower when compared to the maximum heat transfer (close to 16 kW) for the mass flow rate 1.8 kg/s. Assuming a decrease of around 20% in the maximum heat transfer, the mass flow rate 1.1 kg/s is obtained, corresponding to heat transfer rate close to 13 kW. So, based on the discussions above, the range $1.1 \leq \dot{m} \leq 1.8$ kg/s can be chosen as suitable for good heat transfer rate, pressure drop close to optimal operating conditions and acceptable fluid carryover leakage in the small rotary regenerator.

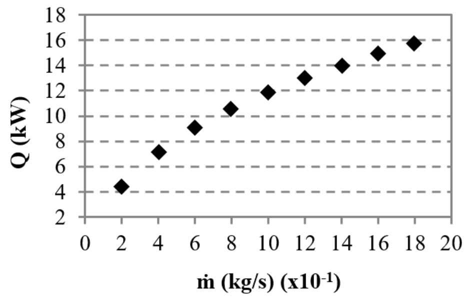

Figure 5. Total heat transfer in the small regenerator.

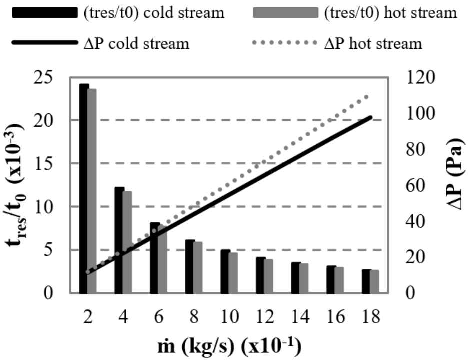

Figure 6. Ratio (t_{res}/t_0) and pressure drop versus mass flow rate for the small regenerator.

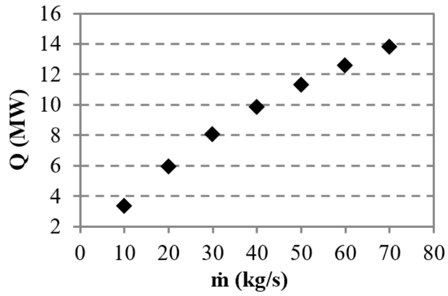

Figure 7. Total heat transfer in the medium-sized regenerator.

The medium-sized regenerator can be analyzed in a similar way to the analysis made for the small regenerator. Fig. 7 shows the total heat transfer in the mediu-sized regenerator as a function of the mass flow rate. Fig. 8 shows the ratio (t_{res}/t_0) for both streams of the regenerator as a function of the mass flow rate and also the pressure drop for both streams of the equipment as a function of the mass flow rate.

Figs. 7 and 8 show a similar behavior to that presented by the small regenerator (Figs. 5 and 6). In the medium-sized regenerator, the flow regime of at least one of the streams becomes turbulent for mass flow rate values greater than 70 kg/s. Practical observations of

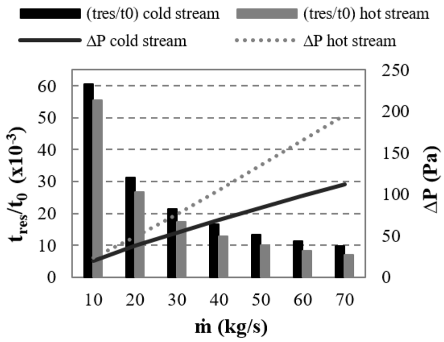

Figure 8. Ratio (t_{res}/t_0) and pressure drop versus mass flow rate for the medium-sized regenerator.

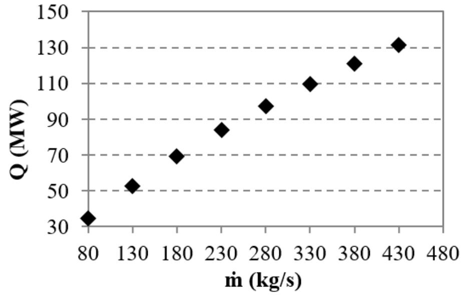

Figure 9. Total heat transfer in the large regenerator.

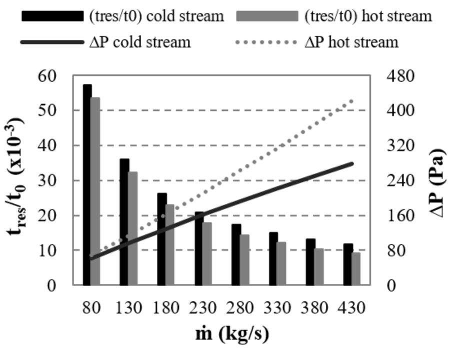

Figure 10. Ratio (t_{res}/t_0) and pressure drop versus mass flow rate for the large regenerator.

typical medium-sized rotary regenerators, operating close to optimal conditions under laminar regime, show that the pressure drop values are lower than 350 Pa [22]. Fig. 8 shows that both streams are within this condition. Fig. 8 also shows that the contamination between fluids, Eq. (2), is negligible for mass flow rate values greater than 45 kg/s that implies in a heat transfer rate, Fig. 7, close to 11 MW. This result is approximately 20% less than the maximum heat transfer (close to 14 MW) observed for 70 kg/s in Fig. 7. Thus, the range $45 \leq \dot{m} \leq 70$ kg/s can be chosen as suitable for good heat transfer rate, pressure drop close to optimal operating conditions and acceptable fluid carryover leakage in the medium-sized rotary regenerator.

Analyzing the large rotary regenerator, Fig. 9 shows the total heat transfer as a function of the mass flow rate. Fig. 10 shows the ratio (t_{res}/t_0) for both streams of the large regenerator as a function of the mass flow rate and also the pressure drop for both streams of the equipment as a function of the mass flow rate.

Figs. 9 and 10 exhibit an analogous behavior to that observed for the small and medium-sized regenerators. In these figures, at least one of the streams reaches the turbulent flow regime for mass flow rate values greater than 430 kg/s. Practical observations of typical large rotary regenerators, operating close to optimal conditions under laminar regime, show that the pressure drop values are lower than 600 Pa [22]. Fig. 10 shows that both streams are within this condition. Fig. 10 also shows that the contamination between fluids is acceptable for mass flow rate values greater than 330 kg/s that implies in a heat transfer rate, Fig. 9, close to 110 MW. This result is 15% less than the maximum heat transfer (close to 130 MW) observed for 430 kg/s in Fig. 9. Finally, the range $330 \leq \dot{m} \leq 430$ kg/s can be chosen as suitable for good heat transfer rate, pressure drop close to optimal operating conditions and acceptable fluid carryover leakage in the large rotary regenerator.

IV. Conclusions

Three typical rotary regenerators were computationally analyzed from changes in mass flow rate of gas streams. Conditions for acceptable fluid carryover leakage, suitable pressure drop and good heat transfer in the regenerator were assumed based on literature and practical observations. A mass flow rate range that associates these conditions was chosen for each simulated equipment. The mass flow rate ranges $1.1 \leq \dot{m} \leq 1.8$ kg/s, $45 \leq \dot{m} \leq 70$ kg/s and $330 \leq \dot{m} \leq 430$ kg/s were chosen for the small, medium-sized and large rotary regenerator, respectively.

The limit values of the mass flow rate ranges chosen for the medium-sized and large regenerators were defined by the condition of maximum acceptable contamination (minimum limit) and by the satisfactory pressure drop (maximum limit). For the small regenerator, the minimum limit was defined by the heat transfer rate up to 20% lower when compared to the maximum value observed in this case. Similarly to the medium-sized and large regenerators, the satisfactory pressure drop also defined the maximum limit in the small equipment. The results can help to establish good operating conditions for rotary regenerators.

REFERENCES

[1] Ghodsipour, N., & Sadrameli, M. (2003). Experimental and Sensitivy Analisys of a Rotary Air Preheater for the Flue Gas Heat Recovery. *Applied Thermal Engineering, 23*, 571-580.

[2] Rao, R. V., & Patel, V. (2011). Design optimization of rotary regenerator using artificial bee colony algorithm. *Proc. of the Institution of Mechanical Engineers, Part A: Journal of Power and Energy, 225(8)*, 1088-1098.

[3] Raja, B. D., Jhala R. L., & Patel, V. (2016). Multi-objective optimization of a rotary regenerator using tutorial training and self-learning inspired teaching-learning based optimization algorithm (TS-TLBO). *Appl. Therm. Eng., 93*, 456-467.

[4] Chen, X., et. al. (2016). Influence of rotational speed on thermal performance of tri-sector rotary regenerative air preheater. In *American Society of Mechanical Engineers ASME - Power Conference, POWER 2016, collocated with the10th International Conference on Energy Sustainability and the 14th International Conference on Fuel Cell Science, Engineering and Technology*, Charlotte, North Carolina, USA, (Paper No. POWER2016-59551).

[5] Mioralli, P. C., & Ganzarolli, M. M. (2005). Temperature Distribution in a Rotary Heat Exchanger. In *Proceedings of COBEM* (paper code 0356).

[6] Mioralli, P. C. & Ganzarolli, M. M. (2006). Influence of Porosity in a Rotary Regenerator Performance. In *Proceedings of ENCIT* (paper code CIT06-0549) (In Portuguese).

[7] Mioralli, P. C., & Ganzarolli, M. M. (2007). Optimal Porosity of a Rotary Regenerator with Fixed Pressure Drop. In *Proceedings of ECOS* (pp.1307-1314).

[8] Mioralli, P. C., & Ganzarolli, M. M. (2008). Thermal Optimization of a Rotary Regenerator with Fixed Pressure Drop. In *Proceedings of ENCIT* (paper code 7-5302).

[9] Mioralli, P. C., & Ganzarolli, M. M. (2013). Thermal analysis of a rotary regenerator with fixed pressure drop or fixed pumping power. *Applied Thermal Engineering, 52*, 187-197.

[10] Alhusseny, A., & Turan, A. (2016). An effective engineering computational procedure to analyse and design rotary regenerators using a porous media approach. *International Journal of Heat and Mass Transfer, 95*, 593–605.

[11] Dallaire, J., Gosselin, L., & da Silva, A. K. (2010). Conceptual optimization of a rotary heat exchanger with a porous core. *International Journal of Thermal Science, 49*, 454–462.

[12] Sanaye, S., Jafari, S., & Ghaebi, H. (2008). Optimum operational conditions of a rotary regenerator using genetic algorithm. *Energy and Buildings, 40(9)*, 1637-1642.

[13] Mohammadian Korouyeh, M., Saidi, M. H., Najafi, M., & Aghanajafi, C. (2019). Evaluation of desiccant wheel and prime mover as combined cooling, heating, and power system. *International Journal of Green Energy, 16(3)*, 256–268.

[14] Wang, L., Bu. Y., Li, D., Tang, C., & Che, D. (2019). Single and multi-objective optimizations of rotary regenerative air preheater for coal-fired power plant considering the ammonium bisulfate deposition. *International Journal of Thermal Sciences, 136*, 52–59.

[15] Abroshan, H., & Goodarzi, M. (2020). Optimization of a three-layer rotary generator using genetic algorithm to minimize fuel consumption. *Journal of Mech. Eng. and Sci., 14(1)*, 6304–6321.

[16] Mioralli, P. C., Silva, M. A. B., Avallone, E., Palota, P. H., & Natividade, P. S. G. (2018). Range of Porosity in Typical Regenerators for an Appropriate Balance Between Heat Exchange and Pressure Drop. In: Energetics. In *4th Virtual International Conference on Science,Technology and Management in Energy, Energetics.*

[17] Mioralli, P. C., Silva, M. A. B., Avallone, E., Palota, P. H., & Natividade, P. S. G. (2019). Computational Analysis for Good Thermal Exchange and Low Pressure Drop in Regenerative Air Preheaters. *Journal of Energy Research and Reviews, 2*, 1-15.

[18] Mioralli, P. C., Avallone, E., Palota, P. H., Natividade, P. S. G., & Luizete, C. E. (2019). Pressure Drop and Heat Transfer Analysis for Satisfactory Operating Conditions of Rotary Heat Exchangers. *Current Research in Science and Technology, 2*, p. 81-97.

[19] Mioralli, P. C., Ernandes, G. L., Avallone, E., Palota, P. H., Luizete, C. E., & Natividade, P. S. G. (2020). Matrix Rotation Range of Rotary Regenerators for Good Heat Transfer and Acceptable Fluid Carryover Leakage. *International Journal of Innovation Engineering and Science Research, 4*, 10-25.

[20] Shah, R. K. (1981). Thermal design theory for regenerators. In Kakaç, S., Bergles, A. E., & Mayinger, F. (Ed.). *Heat Exchangers: Thermal Hydraulic Fundamentals and Design,* DC: Hemisphere, 721-763.

[21] Banks, P. J. (1982). Effect of fluid carryover on regenerator performance. *Journal of Heat Transfer, 104(1)*, 215-217.

[22] Mioralli, P. C. (2009). *Heat transfer in a rotary regenerator with fixed pressure drop*. Doctoral thesis, Faculty of Mechanical Engineering, State University of Campinas, Brazil. (In Portuguese).

[23] Kays, W. M., & London, A. L. (1964). *Compact Heat Exchangers,* New York, USA: McGraw-Hill, 3rd.

[24] Buyukalaca, O., & Yilmaz, T. (2002). Influence of Rotational Speed on Effectiveness of Rotary-Type Heat Exchanger. *Journal of Heat and Mass Transfer, 38*, 441-447.

[25] White, F. M. (1974). *Viscous Fluid Flow,* New York, USA: McGraw-Hill.

[26] Wark, K. (1983). *Thermodynamics,* New York, USA: McGraw-Hill, 4th. Based in NASA SP-273. U. S. Government Printing Office: Washington, 1971.

[27] Mioralli, P. C. (2005). Thermal analysis of a rotary regenerator. Master diss., Faculty of Mechanical Engineering, State University of Campinas, Brazil, 2005. (In Portuguese)

A Literature Survey on Health Index Approach for Transformer's Condition Assessment

Sanja Stanković[1], Zoran Stajić[2]

[1]Faculty of Electronic Engineering, Niš, Serbia, sanja.stankovic@elfak.ni.ac.rs
[2]R&D Center "Alfatec", Niš, Serbia, zoran.stajic@alfatec.rs

Abstract—**Health Index (HI) is a practical and mostly used method for asset's overall condition assessment. As power transformer is one of the crucial assets in power distribution, utility companies are nowadays trying to implement HI approach in their regular asset management. This paper surveys different researches and scientific papers that have applied HI method, briefly explains their approach and summarize their results.**

Keywords – health index, condition assessment, power transformer

I. Introduction

Power transformer has the most important role in electricity distribution and represents also one of the greatest expenditures for electrical utilities. Due to the high demand for reliable, safe and continuous supply of electricity, there is a need for reliable and uninterrupted performance of power transformers. Therefore, power utilities are challenged nowadays to properly assess costs and risks and according to that, to choose appropriate maintenance plan. Most of the utilities perform maintenance actions periodically, which is called Time-based Maintenance (TBM). This is not the most optimal and cost-effective type of maintenance, because some transformers, despite their average lifespan of 30-40 years, are still operational after 50 or even 60 years in service, and often with only minor deteriorations [1,2]. This is why it is preferable to assess the condition of such assets and perform necessary actions when they are needed, which is called Condition-based Maintenance (CBM).

The Health Index (HI) is practical, simple and mostly used method to calculate the overall health of power transformers. It utilizes the results of on-line and off-line condition monitoring of transformers, as well as the results of different laboratory tests and routine inspections and then calculates one simple value that represent transformer's health condition [3].

This paper surveys a large number of practical examples found in scientific literature that have developed and applied HI algorithm on power transformers, presents their results and points out important findings and their contribution to HI methodology.

II. Diagnostic Tests and Procedures for Obtaining HI Input Parameters

Condition assessment is the key component in the process of asset management. Starting point for condition assessment, as well as for HI calculation is data collection, and it is a result of previously mentioned condition monitoring, tests and inspections. All data must be collected simultaneously, and tests are usually standardized for each asset and its parts. For power transformer, insulation oil is the most important part in terms of ageing and failure rate. However, when determining the overall transformer's condition, other parts must be observed too, because their ageing is not simultaneous as ageing of insulation [2,3].

Although there are numerous diagnostic procedures and tests that are done to obtain transformer's condition, they can be roughly classified into 4 main groups:

- dissolved gas analyses in oil and load tap changer,
- oil quality tests,
- operation, maintenance and failure records,

ISBN: 978-86-80616-07-0

- off-line and on-line condition inspections.

For general transformer's diagnostics recommendations, standard IEEE Std C57.152 represents a document that has great significance when condition assessment is performed. According to this standard, all tests, inspections and measurements are classified in 3 categories – recommended, as-needed and optional. Diagnostic tests are listed and classified depending on particular parts of transformer. The standard also briefly explains procedures for basic tests and measurements [4]. Examples of other important standards that focus on specific test procedures are presented in Table I.

Dissolved Gas Analyses (DGA) in oil is commonly used procedure for transformer's insulation health assessment, and at the same time, dissolved gases are indicators of the overall health of transformer itself. This is due to the fact that distribution of each gas dissolved in oil is related to different fault in transformer. The percentage of each gas, or their ratios can indicate the severity of deterioration or type of fault. However, the results of DGA can sometimes be ambiguous, because a lot of other factors have impact on transformer's health and failures. Regardless of that, DGA is one of the most affordable diagnostic procedures, so it is widely used to assess health condition of transformers.

The IEEE C57.104 [5] and IEC 60599 [6] are two standards that lead in the interpretation of DGA. These have been developed from empirical data and experience based on findings of case studies during long period of time. Example of ranges for common dissolved gases that these standards recommend as typical are presented in Table II. More detailed recommendations and sub-ranges can be found in [5,6]. Also, different methods for fault type detection based on dissolved gases ratios like Duval's triangle, C_2H_4/C_2H_2 ratio, Rogers ratio, Doernenburg ratio and Pentagon method are recommended and explained in these standards.

HI is a practical method that uses parameters obtained during previously mentioned condition monitoring and diagnostic tests, and then calculates one quantitative index that represents overall health of transformer. There are different approaches for HI calculations, but mostly used is scoring and ranking method. Each parameter is assigned with appropriate score and weight. Scores are obtained from previously mentioned standards and guides. They represent typical or limit values for each parameter. Weight represents the degree of importance and it is usually assigned based on expert's experience and judgment. Empirical equations developed by utilities and international working groups in the domain of power engineering like CIRED, CIGRE and others are used for HI calculation. Regardless of the methods, the result of HI is a number from various ranges, like 0-100, 1-10 and 0-1 with each value having its meaning for health condition of power transformer [3]. The algorithm for HI calculation has evolved as the condition monitoring has progressed. This is reviewed in the next chapter of this paper.

TABLE I. COMMON STANDARDS FOR TEST PROCEDURES.

Test	Standard
Dissolved gas analyses (insulating oil)	IEEE Std C57.104 IEC 60599 ASTM D3612
Dissolved gas analyses (load tap changer)	IEEE Std C57.139
Partial discharge measurement	IEEE Std C57.113
Frequency response analyses	IEEE Std C57.149
Dielectric breakdown voltage test	ASTM D877
Interfacial tension test	ASTM D971
Furan compounds test	ASTM D5837
Visual examination	ASTM D1524
Water content measurement	ASTM D1533
Power factor measurement	ASTM D924
Acidity measurement	ASTM D974

TABLE II. RANGES OF 90% TYPICAL GAS CONCENTRATION IN POWER TRANSFORMERS IN μL/L [6,7].

Gas	IEEE range	IEC range
H_2	40-100	50-150
CH_4	20-110	30-130
C_2H_6	15-150	20-90
C_2H_4	25-90	60-280
C_2H_2	1-2	2-20
CO	500-900	400-600
CO_2	3500-10000	3800-14000

III. Evolution of HI Through Literature Survey

A. Early Researches and Works on HI

The concept of HI in engineering has been used commonly in previous two decades. Some early works are presented in [9,10], where HI concept was used for power distribution and transmission asset management. Multi-criteria analyses approach was applied on a typical substation assets and composite HI was obtained. In [11], the research was extended on relationship between HI, end-of-life and probability of failure of assets. One of the early approaches that involves HI of power transformers is shown in [12]. Authors present a program for determining the equipment health rating, which is actually simple HI. It uses available condition data obtained through tests and inspections, as well as operation and maintenance history records. The output of this program is rating value from 0 (bad) to 100 (good) and recommendation for maintenance action to be performed.

B. Evolution of Classic HI method

Mathematical equation or algorithm, which involves scoring and weighting technique, represents core of most researches about HI done until today. Some representative scientific papers [13-22] are briefly reviewed in this chapter.

In [13], HI was formulated based on 20 input parameters, including dissolved gases, oil quality parameters, furfural content, electrical parameters, gases in tap changer and operation and maintenance records. Scores used in this paper were developed from IEEE and IEC guides' recommendations, as explained in previous chapter, and weights were assigned subjectively by expert's judgement. The method was applied to 1402 units, and results showed that 86% of transformers had HI more than 70 (good and very good). Similar research has been done in [14], with number of parameters increased to 24. Authors in both papers used the equation for overall HI that was sum of two components, one representing HI of transformer and second representing HI of load tap changer (LTC). Weighting factors assigned to them were 60% and 40%, respectively. These weighting factors are based on CIGRÉ's working group survey from 1983 that found approximately 40% of failures in transformer were because of failure in LTC [7,8,14]. However, later survey from 2012. has shown that this percentage had decreased, and by that time it was concluded to be 26% [15]. Also, in [14] it was proposed that utilities use their own failure rate for LTC, if they have appropriate failure records.

As on-line monitoring systems and equipment have advanced, so have the formulations of HI. In [16], three electrical factors have been added to the list of input parameters - dielectric losses at low frequencies, conductivity factor and polarization index. The reason for including these three parameters authors explained as the fact that experiments had shown these factors had varied with ageing of transformer. With such approach, the calculation of HI has given more accurate output values.

Another group of researchers had disaggregated approach for obtaining HI [17,18]. The paper [17] presented experience in asset management and condition assessment in Malaysian utility company, which resulted in formulation of transformer's HI. The approach consisted of three diagnostic groups or "tiers", and it was applied on 707 transformer units. Each group had specific diagnostic procedures and separate HI calculations. First group of tests was applied to all units, while second and third group to only those that couldn't get precise HI with first group of diagnostics. According to the results obtained, utility managed to plan and perform appropriate maintenance actions. Such "grouping" of diagnostics was also proposed in [19], and two groups were condition parameters and history parameters. Method was applied on three transformers and HI values were placed in risk matrix which reflected failure risk for each examined transformer.

A practical example of developing composite HI for a large electrical utility is presented in [20]. HI was calculated for four groups of parameters – electrical, thermal, mechanical and oil, and finally overall HI was determined for more than 700 units. Based on the results of this study, it could be concluded that HI was independent of transformer's service age, because some young transformers were denoted to be in a bad condition, while on the contrary some very old transformers were in excellent condition. This conclusion proves and justifies calculation of HI, as well as CBM. Reference [21] also emphasizes the fact that age is not the indicator of transformer's condition, as well as load factor. Calculation of HI with these two factors led to ambiguous results, so they were excluded from the analyses. Degree of polymerization was used instead, because it reflects the age, and incorporates the load factor as well.

One more recent study from Polish 110kV grid is presented in [22]. The aim of this study was to improve the overall effectiveness of condition assessment by using two HI algorithms and comparing the results with results of the official expert system used by utility. Methodology for both algorithms from this study was similar to the one in [20]. The main difference between two developed algorithms was that weights and scores were adopted from IEC standard for the first one, while empirical results from experience of the system operators were considered for the second one. The latter gave more precise and logical results, and they were consistent with values obtained from expert system. It was concluded once again that age was not always essential factor, but rather technical and exploitation conditions were much more of importance for calculating proper HI.

C. Advanced HI Techniques

Conventional HI scoring method is mostly used because of its simplicity, but there are some uncertainties that restrain accurate implementation of this method. Even if excessive amount of data is obtained through diagnostic tests and condition monitoring, expert subjectivity in defining weights and scores is factor that reduces reliability and validity of method. In order to overcome this issue, some more sophisticated methods are used for calculation of HI and they are mostly based on machine learning (ML) and artificial intelligence (AI).

Application of artificial neural networks (ANN) for obtaining the overall HI of transformers is presented in [23]. Diagnostics data, such as acidity, dissolved gases, furan, water content and a few more, obtained for 88 oil-filled transformers were used as input values for a feed forward ANN. Actual values of HI for these transformers were also calculated by company specialized in asset management, and 59 of them were used as training dataset. ANN used in this study had four layers – one input layer, one output layer and two hidden layers. Output values were very similar to actual values, so ANN was applied to testing dataset (29 units). The method successfully calculated HI for 28 transformers with accuracy of 96.55%.

Another type of ANN, multi-layer back propagation ANN, is presented in [24] and used for determining HI of transformers. It consisted of two tiers and each tier had different input parameters. First tier parameters consisted of dissolved gases, furan, power factor and operation and maintenance history. Second tier parameters were turn ratio, short circuit impedance, direct current resistance, frequency response analyses result and degree of polymerization. Training set for this network was composed of calculated HI values. The accuracy of the network was determined to be 92.4% for first tier and 99.5% for second tier. Validation of the results was performed by using k-fold cross validation method.

In [25], a type of probabilistic neural network was presented, which used Gaussian kernel for obtaining the best fitting scores of six parameter measurements, and thus determining more accurate HI values of power transformer. The method was tested using measurements from 100 transformers, and then compared with already available HI values that were calculated by utility's experts. The results matched in 83% of transformers.

Beside ANN, another common technique that is often used for condition assessment and HI calculation is fuzzy logic. Unlike ANN, where network "learns" from training sets without any rule specified or previous knowledge about system, fuzzy logic must use strictly defined rules based on empirical data of the system. Certainty of the output values depends solely on rules defined in linguistic rule database [3].

Reference [26] is one example of fuzzy logic application for health assessment of high voltage transformers that use thermal upgraded paper as winding insulation. Fuzzy logic functions, or so-called "membership" functions were formed for 6 diagnostic parameters, respecting limits given in ASTM standards. Membership function was also formed for overall HI, with total of 80 derived rules, and HI values were obtained. In [27,28], similar approach was used, but number of indicators was increased to 20 and HI was obtained for "criticalities" of transformer, in range 0-1, where 1 was considered as severe criticality. A complex fuzzy logic model for transformer's management and decision making was developed. The model effectively addressed critical parts of transformer, and as final result, the overall transformer's health condition was obtained. It was pointed out that accuracy of the model was affected by accuracy of diagnostic parameters that were used as input variables and by their dependence on each other.

Reference [29] presents the experience of using fuzzy expert system developed in Hungarian distribution system. The system was named "Transformer Status Indicator" and it was tested on several medium and high voltage transformers. However, it couldn't be denoted as accurate, because the experts were not able to obtain all necessary data of condition monitoring and measurements for all transformers in the same time. This is a practical example which shows actual issues with implementation of advanced methods for condition and health assessment of power transformers.

Technical issues that can occur with application of ANN and fuzzy logic for HI calculation can be overcome by using hybrid algorithms, such as artificial neural-fuzzy inference systems (ANFIS). This approach is presented in [30-32]. The case study in [31] pointed out the advantages of ANFIS over ANN, because of its robustness and applicability on large number of input datasets. The system was applied on data of 226 transformers, and the results were compared with calculated HI. 80% of the results matched. In [32], two different datasets were used, one consisting of real in-service measurement data, and another one was obtained by Monte Carlo simulation. Neuro-fuzzy algorithm was applied for both of them and tested on 15 transformers. Results were compared with scoring HI method, and it appeared that Monte Carlo simulation method was very reliable and more accurate than using raw in-service condition data.

Beside two aforementioned AI-based methods for HI calculation, which are mostly used among researchers, there are some other advanced methods and techniques that can be found in literature [33-36]. Probabilistic technique Markov Model was applied on 3195 oil samples from 373 transformers in [33], in order to predict future HI of transformers. The prediction accuracy reached up to 95.49%. In [34], logistic regression was used to calculate HI for 30 oil-immersed transformers, whereas parameters for regression model were estimated by function developed with Poisson distribution. The results of technique were compared to existing expert's HI values, and they proved to be quite accurate.

References [35,36] introduced complex and intelligent ML technique called Support Vector Machine (SVM) for purpose of HI algorithm formulation. SVM is common ML technique for data classification that uses training datasets for extracting valuable knowledge and classifies data based on it. In [36], SVM was used to develop intelligent mathematical model, and fuzzy c-mean algorithm was adopted to remove unnecessary noise that occurred in samples. Training datasets consisted of actual oil quality samples from 181 transformers. Pre-processing was also implemented in algorithm to correct class imbalance between training datasets, and method that attained the highest accuracy was synthetic minority over-sampling method.

One excellent comparative analysis for selecting most suitable parameters for HI method was described in [36]. A certain number of researchers emphasizes the fact that the number of parameters has to be large in order to obtain accurate HI. Reference [36] explores which parameters have negligible impact on HI, and which are crucial, by applying six different classifying algorithms: Random forest, J48, SVM, ANN and k-nearest neighbor. The best accuracy was reached with Random forest method. Among 9 different examined parameters, water content, acidity, breakdown voltage and furan content were found the most important for transformer's HI calculation. This approach enables utilities to reduce their unnecessary costs by optimizing condition monitoring.

IV. DISCUSSION

Scientific papers that are reviewed have important role for understanding and implementation of HI methodology nowadays. Some of them introduced formulations that are still in use among researchers, while some focused at procedures for determining parameters necessary for HI calculation. The majority indicates that not all parameters have the same importance for condition assessment, and that proper weighting is the key factor in HI formulation.

TABLE III. OVERVIEW OF DIFFERENT HI APPROACHES.

Ref.	No. of inputs	HI output (range of values)	Contribution to HI methodology	Summary
[13]	20	0-100 (0-very poor , 100-very good)	The paper introduced and listed an excessive number of parameters. It explained in detail the process of obtaining scores and assigning weights in tabular form.	HI calculation should be composed of two components, transformer and LTC. Weight for LTC is used from CIGRE survey that indicates 40% percent of all failures in transformer are due to LTC.
[14]	24	0-100 (0-very poor, 100-very good)	Four new parameters are added to the list, alongside with scores and weights. Probability of failure, effective age and remaining useful life are determined based on HI. Replacement capital plan is proposed.	It is proposed that weight for LTC's HI should be actual failure rate that utilities have in possession. If not, value of 40% can be used for this purpose.
[16]	27	0-1 (0-very poor, 1-very good)	Three new electrical parameters are added to the list: loss factor, polarization index and conductivity.	Experiments have shown that HI values were strongly influenced by variation of three new parameters. They were assigned maximum weight.
[21]	23	0-100 (0-very poor, 100-very good)	Degree of polymerization is presented as valuable parameter and used instead of load factor and age.	Age is not always a proper indicator of transformer's heath condition. It should be considered in relation to other available parameters.
[22]	15	0-100 (0-good, 100-risky)	Two formulations of HI are applied on power transformers. Different weights were assigned to ageing factors.	The main problem for HI calculation is the choice of parameters and determining their weights, because this is based on experts' knowledge and experience in the domain of power transformers. It must be done with caution.
[25]	6	0-1 (0-very good, 1-very bad)	Advanced probabilistic neural network is introduced for HI calculation. It is totally free of any assumptions or subjective impact.	The proposed method can be improved by adjustment of already available limitations of parameters from international standards and guidelines.
[28]	20	0-1 (0-normal/good, 1-poor/severe)	Complex and intelligent fuzzy inference model for condition assessment and transformer's criticalities is developed. It can indicate transformer's increased probability of failure.	There is an inevitable dependence of parameters on each other. In order to accurately assess condition of transformer, this dependence must be understood and considered.
[32]	15	0-100 (0-very bad, 100-very good)	Neural-fuzzy network where ambiguity of fuzzy logic has been overcome by neural learning from training datasets is developed. Monte Carlo simulation is introduced for obtaining training datasets.	Completely different approaches for calculation of HI can cause deviations of results. Better accuracy can be accomplished by using techniques like Monte Carlo simulation, because it doesn't depend on real in-service condition data.

Table III presents an overview of certain references surveyed in this paper. First column of the table is reference number, while the second column shows variations in number of input parameters. Third column represents various ranges of HI output that are used in these references. Fourth column presents progress of method and contribution to HI methodology. Finally, fifth column is a summary with some highlights from the papers, which are either conclusions, actual problems or proposals for further researches.

V. CONCLUSION

Through presented literature survey, it can be concluded that HI approach for the purpose of condition assessment is very valuable and practical tool. It has significantly progressed in previous two decades, as it can be concluded from reviewed references. However, advanced on-line condition monitoring equipment is not available to all distribution systems, either because of its costs, or complexity of distribution system. When this equipment becomes widely used, more experts could gain experience in the domain of CBM, and thus HI approach could be further and more rapidly improved.

ACKNOWLEDGMENT

This paper is a part of the research supported by the Ministry of Education, Science and Technological Development of the Republic of Serbia within the framework of technological development.

REFERENCES

[1] R&D Center "Alfatec". (2017). Racionalizacija rezervne opreme i poboljšanje pouzdanosti elektrodistributivnih objekata 110 kV i 35 kV. Niš, (In Serbian)

[2] Reichlet, D., Frey, A., & Schonneberg, M. (1996). Life Expectancy of Power Systems Apparatus and Components, CIGRE session, Paris.

[3] Stanković, S., Stajić, Z., & Rašić, M. (2019, October). Condition–based maintenance of power transformers, In *Proceedings of 5th Jubilee Virtual International Conference on Science, Technology and Management in Energy*, Niš, 28-29 (pp. 163-170).

[4] CIGRE Working Group 05. (1982). An international survey of failures in large power transformers in service. *Electra*, 88, 21–48.

[5] IEEE C57.152-2013, IEEE Guide for diagnostic field testing of fluid-filled power transformers, regulators, and reactors

[6] IEEE Std C57.104-2019, IEEE Guide for the interpretation of gases generated in mineral oil-immersed transformers

[7] IEC 60599-2015, Mineral oil-filled electrical equipment in service - Guidance on the interpretation of dissolved and free gases analysis

[8] Wang, M., Vandermaar, A. J., & Srivastava, K. D. (2002). Review of condition assessment of power transformers in service. *IEEE Electrical Insulation Magazine, 18*(6), 12-25.

[9] Hjartarson, T., & Otal, S. (2006, October). Predicting future asset condition based on current health index and maintenance level. In *IEEE 11th International Conference on Transmission & Distribution Construction, Operation and Live-Line Maintenance,* Albuquerque, USA, 15-19 (pp.1-8).

[10] Hughes, D. T. (2003, May). The use of "health indices" to determine end of life and estimate remnant life for distribution assets. In *17th International Conference on Electricity Distribution*, Barcelona, 12-15 (pp.1-4).

[11] Dominelli, N., Lau, M., Olan, D., & Newell, J. (2004, September). Equipment health rating of power transformers, *IEEE International Symposium on Electrical Insulation, Indianapolis*, USA, (pp.163-168).

[12] Naderian, A., Cress, S., Piercy, R., Wang, F., & Service, J. (2008, June). An approach to determine the health index of power transformers. In *IEEE International Symposium on Electrical Insulation*, Vancouver, (pp. 192-196).

[13] Jahromi, A., Piercy, R., Cress, S., Service, J., & Wang, F. (2009). An approach to power transformer asset management using health index. *IEEE Electrical Insulation Magazine, 25*(2). 20-34.

[14] CIGRE Working Group A2.37. (2012). Transformer Reliability Survey: Interim Report. *Electra*, 261, 46-49.

[15] B. Gorgan, Nothinger, P. V., Badicu, L. V., & Tanasescu. (2010). Calculation of power transformers health indexes. *Annals of the University of Craiova, Electrical Engineering Series*, (34), 13-18.

[16] Ghazali, Y. Talib, M. A., & Rosli, H. A. (2009, June). TNB experience in condition assessment and life management of distribution power transformers. In *20th International Conference on Electricity Distribution,* Prague, (CIRED Session 3, paper no. 0686).

[17] Malik, H., Azeem, A., & Jarial, R. K. (2012, March). Application research based on modern-technology for transformer health index estimation. In *International Multi-Conference on Systems, Signals & Devices,* Chemnitz, (pp. 1-7).

[18] Taengko, K., & Damrongkulkamjor, P. (2013, May). Risk assessment for power transformers in PEA substations using health index. In *10th International Conference on Electrical Engineering/Electronics, Computer, Telecommunications and Informaton Techology,* Krabi, (pp. 1-6).

[19] Scatiggio, F., & Pompili, M. (2013, June). Health index: the TERNA's practical approach for transformers fleet management. In *Electrical Insulation Conference*, Ottawa, (pp. 178-182).

[20] Jürgensen, J. H., Godin, A. S., & Hilber, P. (2017, June). Health index as condition estimator for power system equipment: a critical discussion and case study. In *24th International Conference & Exhibition on Electricity Distribution (CIRED),* (pp. 202-205).

[21] Bohatyrewicz, P., Plowucha, J, & Subocz, J. (2019). Condition assessment of power transformers based on health index value. *Applied Sciences, 9*(22), 4877.

[22] Abu-Elanien, A. Salama, M., & Ibrahim, M. (2011, June). Determination of transformer health condition using artificial neural networks. In *International Symposium on Innovations in Intelligent Systems and Applications*, Istanbul, (pp. 1-5).

[23] Mukti, P. H. Pamuji, F. A., & Munir, B. S. (2014, May). Implementation of artificial neural networks for determining power transfomer condition. In *5th International Symposium on Advanced Control of Industrial Processes*, Hiroshima, (pp. 473-477).

[24] Islam, M. M. Lee Dr., G., & Hettiwatte Dr., S. N. (2017). Application of a general regression neural network for health index calculation of power transformers. *International Journal of Electrical Power & Energy Systems,* 93, 308-315.

[25] Medina, R. D. Lata, J. P., & Chacón, D. P. (2016, September). Health index assessment for power transformers with thermal upgraded paper up to 230kV using fuzzy inference systems. In *51st International*

Universities Power Engineering Conference (UPEC), Coimbra, (pp. 1-6).

[26] Arshad, M. Islam, S. M., & Khaliq, A. (2014). Fuzzy logic approach in power transformers management and decision making. *IEEE Transactions on Dielectrics and Electrical Insulation, 21*(5), 2343-2354.

[27] Chantola, A. Sharma, M., & Saini, A. (2018, April). Integrated fuzzy logic approach for calculation of health index of power transformer. In *2nd International Conference on Inventive Communication and Computational Technologies,* Coimbatore, (pp. 1045-1050).

[28] CIGRE Working Group A2-103. (2014). Health index as one of the best practice for condition assessment of transformers and substation equipments – Hungarian experience, CIGRE Session 2014, Paris (pp. 1-8).

[29] Forouhari, S., & Abu-Siada, A. (2018). Application of adaptive neuro fuzzy inference system to support power transformerl estimation and asset management decision. *IEEE Transactions on Dielectrics and Electrical Insulation, 25*(3), 845-852.

[30] Zeinoddini-Meymand, H., &Vahidi, B. (2016). Health index calculation for power transformers using technical and economical parameters. *IET Science, Measurement & Technology, 10*(7), 823–830.

[31] Kadim, E. J., Azis, N., Jasni, J. Ahmad, S. A., & Talib, M. A. (2018). Transformers health index assessment based on neural-fuzzy network. *Energies,* 11, 710.

[32] Yahaya, M. Azis, N., Ab Kadir, M., Jasni, J. Hairi, M., & Talib, M. (2017). Estimation of transformers health index based on the Markov chain. *Energies, 10*(11), 1824.

[33] Areffin, S., Hasan, M. I., & Chowdhury, B. A. (2017, December). Assessment of the health condition of oil-immersed transformers using logistic regression and Poisson distribution. In *3rd International Conference on Electrical Information and Communication Technology (EICT*), Khulna, (pp.1-5).

[34] Cui, Y., Ma, H., & Saha, T. K. (2013, October). Power transformer condition assessment using support vector machine with heuristic optimization. In *Australasian Universities Power Engineering Conference (AUPEC)*, Hobart, (pp. 1-6).

[35] Ashkezari, A. D., Ma, H., Saha, T. K., & Ekanayake, C. (2013). Application of fuzzy support vector machine for determining the health index of the insulation system of in-service power transformers. *IEEE Transactions on Dielectrics and Electrical Insulation, 20*(3),965-973.

[36] Benhmed, K., Mooman, A., Younes, A., Shaban, K., & El-Hag, A. (2018). Feature selection for effective health index diagnoses of power transformers. *IEEE Transactions on Power Delivery, 33*(6), 3223-3226.

Global Energy Transition: Nearly Free and Sustainble Electric Power for All

Rajendra Singh[1,2], Prahaladh Paniyil[3], Vishwas Powar[4], Naireeta Deb[5]

[1,3,4,5]Holcombe Dept of Electrical and Computer Engineering, Clemson, USA 29631,
srajend@clemson.edu[1]; ndeb@clemson.edu[5]
[2]Holcombe Dept. of Automotive Engineering, Clemson, 29607 USA

Abstract—**Free fuel-based energy sources (solar and wind) are demonstrating long term trends toward a future in which sustainable energy in the form of electricity is affordable, abundant, and deployed with high energy efficiency. On the capacity basis, at the end of 2019, photovoltaics has emerged as the fourth largest global source of electrical power. Advancement in technology and volume manufacturing, similar to photovoltaic modules is mainly responsible for the cost reduction of lithium ion batteries. Ultra large scale manufacturing of PV and battery based power networks, no trade barriers, vertically integrated business model and energy and financial policies in the interest of public at large can provide the cost of electric power around the clock in the range of \$0.02-\$0.03 per kWh in the next 2-3 years. In this paper we have provided key technical directions, new business models, equitable financial and energy policies that will provide sustainable electric power to all.**

Keywords - photovoltaics, batteries, local DC power, transportation, access to all

I. INTRODUCTION

Providing sustainable electrical power to the current global population of about 7.6 billion and potential population of 11.5 billion by the end of 21st century is a huge challenge. Free fuel-based energy sources (solar and wind) are demonstrating three long term trends in the electrification of energy. The three trends point toward a future in which sustainable energy is affordable, abundant, and deployed with high energy efficiency. These three trends are going to have major economic, geo-political and environmental benefits to humanity [1]. One of the important characteristics of electricity as an energy currency is that it can be conveniently transportable all the way from point-of-creation to end point-of-use. Local generation of electrical power by sun and wind further reduces the cost of electrical power due to the absence of long-haul transmission of electrical power. The other important characteristic of electricity as energy currency is that due to its inherent compatibility with electromagnetic and semiconductor technologies, electrical energy can be transformed easily and with high efficiency into other forms of energy [1]. Without providing electrical power, one cannot even fight poverty [2]. The signs of global warming are everywhere and are more complex than just climbing temperature [3]. To a larger degree, the use of fossil fuel-as energy source is responsible for climate related challenges [4]. Thus, there is an urgency to combat climate change related challenges and replace fossil fuel-based energy sources by solar and wind energy. The objective of this paper is to establish that photovoltaics system can provide nearly free sustainable electric power to virtually all. There are few places on the earth (e.g. Scandinavian countries) where solar intensity is low and there is abundance of wind energy. As shown in Fig. 1 [5], in such places, photovoltaics can provide additional electrical power to wind turbines. The objective of this paper is to establish that

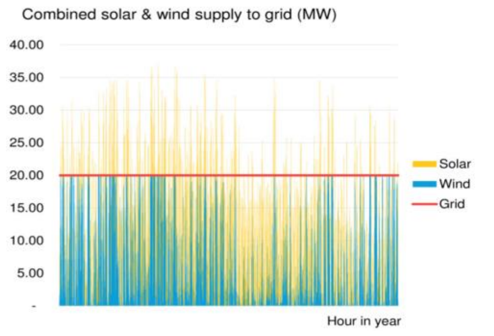

Figure 1. Supplemental role of photovoltaics in places where wind is not blowing [5].

implementing free fuel solar and wind generated electrical power and use of batteries for storing electrical power can provide sustainable electric power to all. In the next section, the challenges associated with power systems in the current and future scenarios are discussed. The challenges revolve around fuel depletion, climate change, energy poverty and supplementing the new and emerging electrified transport sector. In section 3, the status of photovoltaic systems and batteries are also discussed. The cost and demand trends for both systems are focused on in this section. In section 4, the transformative role of photovoltaic systems is established by discussing the importance of decentralizing the power grid and proposed local direct current power network in place of the currently utilized centralized AC power grid. The important research areas to be focused for further enhancement of photovoltaic systems in the future are discussed in section 5. Finally, the paper is concluded in section 6.

II. Current and Future Challenges of Power Systems

The sustainability of any power system is governed by the abundance of fuel used to obtain electrical power that can provide ultra-low-cost power system. Along with the costs, reliability and resiliency of the systems need to be considered. Resiliency is required against both natural threats (solar storms, hurricanes etc.) and man-made threats (cyber-attacks, electromagnetic pulse (EMP) attacks). Conservation of the ecosystem, re-use and recycle of majority products has become extremely necessary. The modern power system must consider its impact on the ecosystem and strive to have minimal adverse impacts. Accessibility is another major concern when designing power systems for the future. A novel power network should encompass access to everyone. Lastly, the power network must have highest energy efficiency. It must include smart sensors and their associated network capabilities to achieve efficiency higher than existing power networks. The Internet-of-Things (IoT) is an enabler for achieving efficient systems and the power networks must comply with IoT to achieve the highest efficiency at all levels [6,7].

In this section we will discuss how the combination of Photovoltaics (PV), wind turbines and batteries can provide a sustainable power network

A. Adoption of Free Fuel based Energy Sources for Sustainable Electric Power

The use of fossil fuel has been responsible for all economic and political events since the energy crisis of 1973. Fig. 2 [8] shows the prices of crude oil and all major political and economic events since 1973. For sustainable global economic growth, fossil fuel-based economy must be replaced by free fuel-based economy. As shown in Fig. 3 [9], the availability of solar power is greater than any other energy source known to mankind. According to [10], the global energy consumption in 2017 was approximately 22000 TWh and the availability of solar energy is 23000 TWy/year (1 TWy = 8760 TWh) as seen in Fig. 3 [11].

Thomas Edison in 1931 stressed the importance of solar energy for generating electrical power [12]. To demonstrate the global role of PV systems, we combined theŁ population density data with the availability of PV output across the world. The population density data was obtained from [12]. Incident solar intensity data was obtained from [13]. The color-coded population density map was combined with the incident solar intensity data and assigned different colors accordingly to generate the new combined data map. This is demonstrated in Fig. 4. The data clearly indicates that vast majority of the world population can produce substantial amount of PV power per day. The northern regions of Europe and Russia are the only countries with a low amount of PV

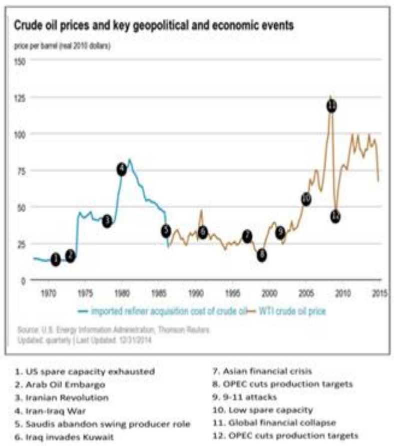

Figure 2. Crude oil prices and key geopolitical and economic events [8].

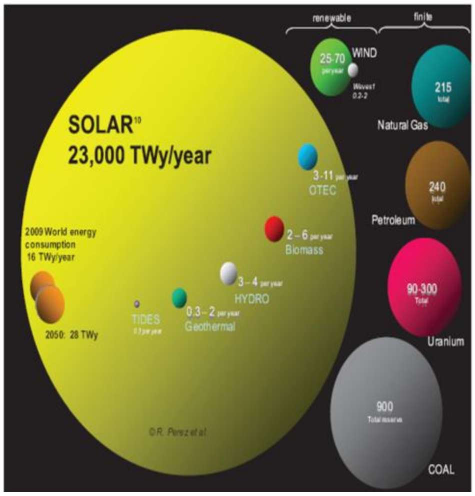

Figure 3. Availability of different energy sources on the earth [9].

output for the population density. In addition to low population density in these regions, however, it is possible to harness sufficient wind energy. Solar farms and wind farms can be paired on the same site. A 2-MW turbine and 500-kW solar installation share an inverter and grid connection, reducing equipment costs compared to two separate projects [14]. Clearly, pairing of PVs and wind energy in some locations in combination with storage of electrical power can meet the energy need of all the people on planet earth.

Although, nuclear power has its positive aspect with respect to greenhouse emissions, nuclear power is not cost-effective. Providing cost-effective safety is one major challenge. Nuclear disaster related final cost of Japan's Fukushima reactor will approach one trillion dollars [15]. Waste management is another major issue. The costs associated with the waste management and construction of plants are enormous. Lastly, nuclear resources are not renewable [16]. Ultimately, the world will run out of it. For economic and safety reasons, there is no need to build new nuclear reactors.

B. Addressing Climate Related Challenges

Climate change is a major concern faced by the world today. According to [17], the oceans are retaining heat faster than the previously estimated rate. This is leading to a faster rate of global warming. The three major sources of carbon emissions are electric power generation, transportation, and animal agriculture. The electric power generation sector can reduce its share of carbon emission greatly by the utilization of solar and wind energies. Fig. 5 [18] clearly indicates the reduction in CO_2 emissions in the US alone by the utilization of solar and wind energy for electric power generation.

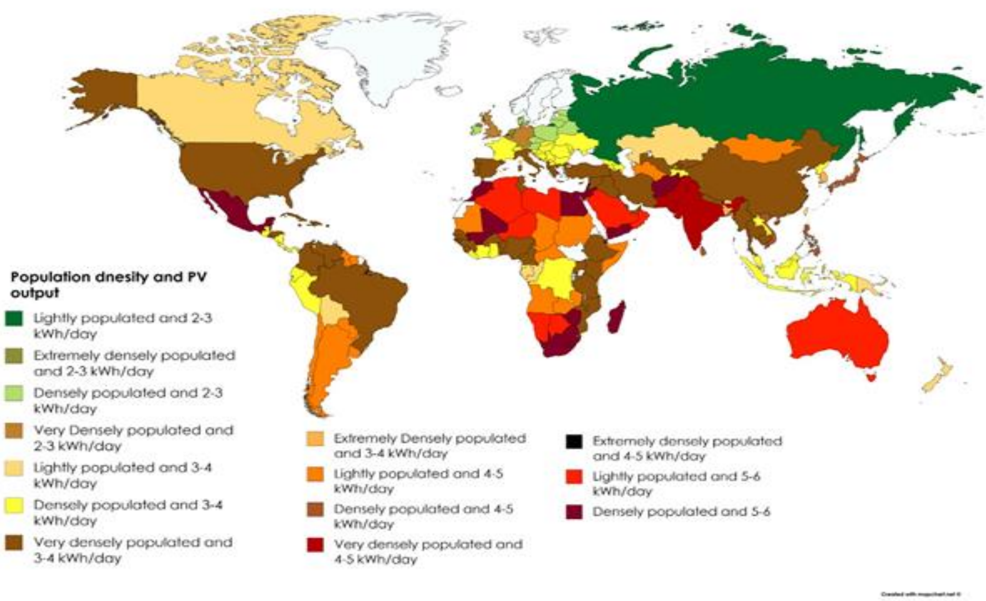

Figure 4. PV output combined with populaton density. The colors represent the data as indicated in the legend.

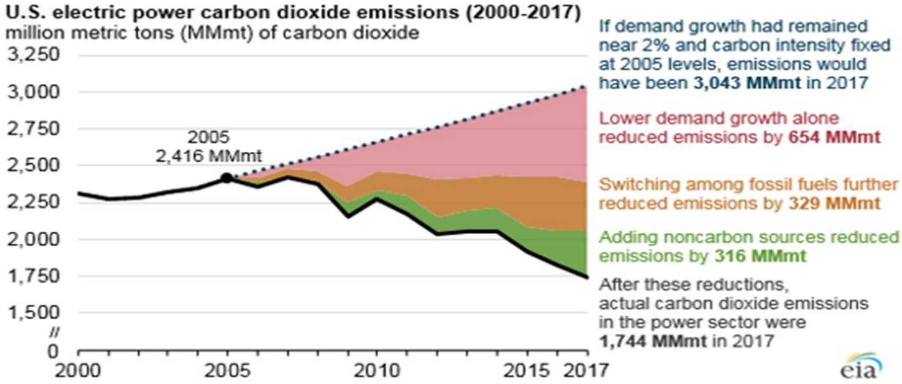

Figure 5. Solar and Wind help curb CO_2 power emissions by 28% since 2005 [18].

Apart from the power generation sector, the transportation sector also can considerably reduce their CO_2 emission contribution through electrification. The effects of electrification of the transport sector will be discussed in detail in the following section. The contribution of CO_2 emissions from animal agriculture is another concern which is discussed in [19] and plant-based diet is recommended to combat climate change [20].

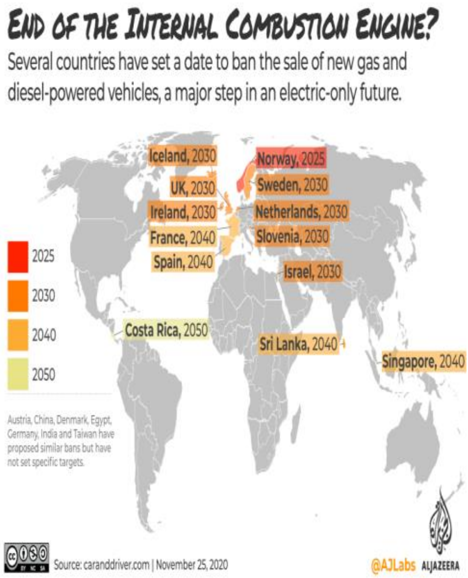

Figure 6. Proposed plan if various countries to end fossil fuel based surface transportation [21].

C. *Transformation of the Transportation Sector*

Transport sector which covers surface, water and air transportation is going to undergo a major change owing to electrification and its advantages over conventional modes. Fig. 6 [21] shows the plan of various countries to end fossil fuel based surface transportation. There are four drivers for change in the auto sector: electrification, autonomous driving, diverse mobility and connectivity [22]. In addition to electrification, major advancements in information technology (IT) and new business models will transform the field of mobility in following areas: (i) connected autonomous electric vehicles, and (ii) ride sharing. These three innovative technologies of, autonomous driving, diverse mobility and connectivity will progress independently, but their impact on surface transportation will overlap. Due to inherent advantages of electric vehicles over internal combustion vehicles, the electric power required for sensors and on-board computers of autonomous vehicles (AVs), the 12-volt auxiliary battery cannot supply the electric power required by AVs. Electric autonomous vehicles are expected to drastically reduce greenhouse gas emissions, traffic congestion, parking demand, insurance costs and traffic fatalities. The convergence of electric drive, autonomy and connectivity will have following positive impacts: (a) cars will last longer, (b) mobility will become cheaper, (c) cars will interact like phones and (d) reduced parking space will be covered with Asphalt. The increase in battery capacity and battery-life, and reduction in its cost has enabled more efficient electric vehicles with cost of ownership less than internal combustion engines and higher reliability [23]. If the electrification aspect for EVs is combined with low cost PV power generation, EVs are much cheaper to fuel as compared to Internal Combustion Engine (ICE) based vehicles [24]. The concern of long charging times for EVs is now being addressed by DC fast charging through the implementation of more and more PV for charging. Once the charging infrastructure picks up speed due to the EV demand, a more efficient surface transportation network can be easily realized.

Electric Vehicles have considerably lesser contribution to CO_2 emission as compared to ICE based vehicles. According to a study in [24], an average EV contributes 0.96 tons of CO_2 emissions per 10.000 miles of driving as compared to 2.99 tons for a petrol vehicle and 2.88 tons for a diesel vehicle. Thus, electrification of the surface transport sector alone can reduce CO_2 emissions by a considerable amount and help in resolving the climate change related challenges. Recently, there have been major explorations in electrification of the air and water transportation sectors as seen in [25] and [26]. Using PV as the source for efficient power generation and batteries for storage, the dream of a lesser carbon footprint from the transportation sector can be realized.

D. Energy Efficiency, Energy Poverty, and Clean Water

The traditional centralized generation of large base-load AC power and its long-haul distribution via high-voltage transmission followed by conversion to lower voltages approximately 70% of electricity produced globally is lost in generation, transmission, and distribution [27]. At the rate of \$0.1/kWh, the annual loss of 41 trillion kWh energy amounts to about \$4.1 trillion [28]. Thus, with the use of a decentralized, direct current (DC) based power network the efficiency for energy generation can be enhanced at various levels.

As described in [29], approximately 13.3% of the global population still do not have access to electricity as of 2016. Accessibility issues are mostly due to the inability of the centralized infrastructure to reach remote rural areas. The decentralized, DC power network encompassing PV and batteries can address the accessibility even in remote rural regions.

The water crisis has been rated 5th in terms of impact as a global risk [29]. Humanity will have to turn to methods like ground water elevation and desalination to cope with this risk. These processes will require a significant amount of electric power. Their power needs can be effectively met by PV based DC power networks.

III. Current Status of Photovoltaic Systems with Energy Storage

PV systems along with batteries have come a long way in the last 40 years. The cost of PV systems has significantly reduced owing to advancements in technology and an increase in their demand. Due to the increased demand for EVs recently, the cost of lithium-ion batteries has also followed a similar cost reduction trend of photovoltaic modules. The reduction in battery cost is a boon to the PV power networks as it provides an effective storage option for the time of the day when sunlight is not available. The increase in PV availability is an added benefit for the DC fast charging mechanisms associated with EVs. Thus, it can be concluded that PV, batteries and EVs have a triangular, bi-directional relationship.

A. Cost Reduction Trends of Photovoltaic Modules and Batteries

In the last ten years, the cost of PV modules has dropped exponentially and, the manufacturing capacity (related directly to number of installations) per year has also increased almost exponentially as seen in Fig. 7 [30]. Current trend is in the direction of

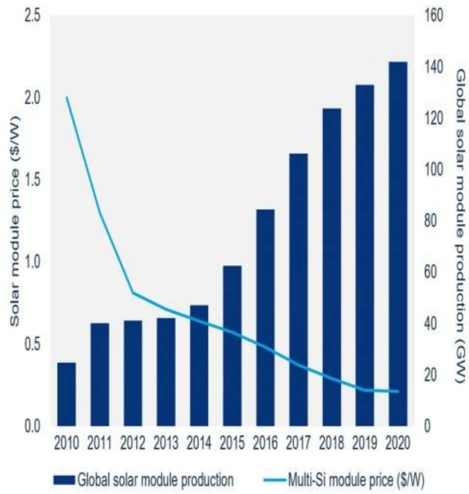

Figure 7. Global PV manufacturing capacity vs. module cost (2010-2020E) [30].

dominance of free fuel solar and wind for generating electric power. Globally in 2019, solar and wind reached 67% of new power capacity while fossil fuel reduced to 25% [31]. Photovoltaics has made enormous strides in a decade, rising from just 43.7 GW of total capacity installed in 2010 to 651GW as of year-end 2019 [31]. As shown in Table I, capacity wise globally photovoltaics is ranked fourth [31]. There is now more free fuel solar and wind capacity online worldwide than total capacity from all technologies (clean or dirty), in the United States of America. PV in 2019 also moved past wind (644GW). It is worth mentioning here that this trend of more PV and less wind is in concert with our earlier prediction where the first author pointed out in 2010 [32], that due to inherent advantages of solar cells as solid-state devices, PV will take over wind energy.

For storing electric power generated by solar and wind a number of techniques have been explored since the energy crisis of 1973. Other than hydro, only batteries capacitors and fuel cells have practical use. Globally there is huge investment and interest in the development of fuel cells. However due to fundamental technical and economic reasons, today hydrogen economy does not make sense [33]. With any material breakthrough and or policy change it is possible that for long haul air and water transportation, in future hydrogen may be used. For these reasons we will not discuss hydrogen anymore in this paper.

Although there are several battery options available in the market, lithium-ion batteries are the most attractive ones due to their high energy density per weight. In case of the consumer products, lithium-ion batteries have already occupied their niche for a long time. As shown in Fig. 8 [34], due to the advancements in technology of lithium-ion batteries the cost is reducing, and the energy density is increasing. Volume manufacturing, similar to photovoltaic modules is playing a very important role in the cost reduction of lithium-ion batteries. Doubling the volume of cumulative manufacturing leads to a cost reduction of about 22% in lithium ion batteries [35]. Similar to Tesla's Gigawatt factory in the United States, several manufacturers in China, Japan, and South Korea are setting up ultra-large-scale manufacturing of lithium-ion batteries. State of the art lithium-ion batteries are highly reliable. After driving 250,000 km the battery pack of Tesla EV has 90% of its power capacity [23]. It can be easily concluded from these cost reduction trends and reliability data that the PV and battery-based power networks will provide the cheapest energy generation and storage framework for the modern era.

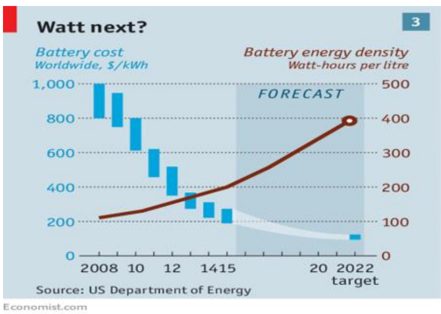

Figure 8. Lithium-ion battery cost vs. Energy density [34].

B. *Cost Reduction Trends of Electric Power generated by PV systems*

PV electric power cost without storage has been reported as low as $0.0132/kWh in Portugal [36]. At utility scale the cost of storing electric power in US in the range 0f of 0.8-1.4 cents per kWh [37]. By 2022, the expected cost of storing electric power by lithium ion batteries is 0.4-0.9 cents per kWh [37]. The cost associated with generation of power also depends on the implementation scale of the system. The larger the scale of the implementation, the lesser is the cost for generation. In an earlier paper [27], we predicted the cost for generation by PV with storage can reach $0.02 per kWh by 2022-2024. If the cost reduction trends mentioned in this paper continue, this cost of PV generated electric power can be achieved even sooner.

In essence PV and battery storage are emerging as default energy for new infrastructure. As an example, Florida Power and Light has announced on March 29, 2019 the plan for the construction of a 409 megawatt

TABLE I. GLOBAL RANKING OF SOURCE OF POWER RANKED CAPACITY-WISE [31].

Source of Power	Capacity	Rank
Coal	2.089 GW	1
Gas	1.812 GW	2
Hydro	1.169 GW	3
Photovoltaics	651 GW	4

(MW) / 900 megawatt-hour battery installation at what will be called the FPL Manatee Energy Storage Center [37]. Tesla deployed 759 MWh of stationary battery storage in Q3 of 2020 [38].

C. Transformative Role of Photovoltaic Systems

PV systems have an important role in the future. As we have already discussed, in addition to electric power generation for conventional applications of electrical power, PV systems are going to greatly impact the next major change in the electrification of transportation. The electrification of the transportation sector is fortified with DC power as its base, majorly owing to the utilization of lithium-ion batteries. The major obstacle with EVs is the charging time for the lithium-ion battery. As shown in Table II [39], the solution to this problem is DC fast charging. PV systems is the only source that generates DC power. Thus, PV systems can enable DC fast charging for lithium-ion batteries in EVs. As PV systems are based on free fuel based solar energy, the cost for charging will also be minimal.

The local DC power networks consisting of PV and battery can access regions that even today have no access to electrical power. The low costs associated with PV systems for power generation empowers electrification of rural regions across the world. An ideal example for bolstering the argument would be the recent electrification of rural India through solar power. Solar projects have started to provide electricity for various applications in rural India as seen in [40].

For long-haul transmission high voltage DC (HVDC) has proven better than high voltage AC. However, local low voltage (< 1,500 V) DC power networks are more lucrative when it comes to PV systems. Local DC power [41] network has its own power generation, power storage, and intelligent loads. The bi-directional flow of electric power from one generation and storage node to other nodes provide transformative features of photovoltaic system. The concept is applicable to a new sub-division, new mall, new manufacturing facility, new commercial entity etc. Many new business models are feasible in our concept of local DC power network. As an example, in a new smart sub-division, individual house owners can have PV on the roof of their house and some storage in their garage. However, a solar farm in the neighborhood and large-scale storage can be owned by another investor. In this scenario, the generation, distribution, and storage deals with DC power except for a few necessary inductive loads, which can be served by local inverter. By eliminating the need for conversion and losses in transmission, we can create a highly efficient power network. Due to less attack surface area, DC power network provide better cyber security as compared to identical AC power network based on PV for power generation and batteries for storage.

IV. Important Research Areas to Future Increase the Performance, Reliability, and Cost of PV Systems

PV systems with batteries are the key to a sustainable source of electric power for humanity. In this section, we have investigated areas where improvements can be made for future generation of PV systems.

A. Higher Efficiency and Higher Reliability of PV Modules through IoT

IOT can be major enabler for increase in efficiency and reliability of PV modules. IoT has already entered the consumer product market by offering highly efficient and connected devices. The loads can significantly reduce their power usage through efficient monitoring and control through IoT modules. The IoT modules utilize sensors that relay information to servers via the internet for increasing the efficiency of any device. These devices have coined the term ‘smart devices’ due to their effective power

TABLE II. Comparison of extremely fast charging (XFC) of EVs with currently available charging infrastructure [39].

Unit of measure	Charging techniques				
	Level 1 (110V, 1.4kW)	**Level 2 (220V, 7.2kW)**	**DC Fast Charger (480V, 50kW)**	**Tesla SuperCharger (480V, 140 kW)**	**XFC (800+V, 400 kW)**
Range per minute of charge (miles)	0.0082	0.42	2.92	8.17	23.3
Time to charge for 200 miles (minutes)	2.143	417	60	21	7.5

management. PV modules can also benefit from the wave of IoT sensors by incorporating the IoT modules in their network. These sensors can track, monitor, and relay data effectively with minimum power usage. The data can be utilized for increasing the efficiency through research and analysis of big data. The reliability of PV systems can also be enhanced by more effective maintenance with the help of the IoT modules. On the other hand, when the ‘smart’ PV system is combined with intelligent loads it can minimize the power wastage and generate efficient storage mechanisms by analyzing the peak usage data.

B. *Further Cost Reduction for PV Systems and Batteries*

Further cost reduction is necessary in all sub-systems of PV system. Although the cost of PV modules by the end of 2020 has reached as low as \$0.20/W_p [30], both increase in efficiency and further advancements in the technology are required to bring the cost of PV modules in sub-\$0.10 per W_p. The best efficiency of single junction silicon solar cells measured under global AM 1.5 spectrum is $26.7 \pm 0.5\%$ [42]. The efficiency of silicon PV modules can be increased by using the concept of multi-terminal multi-junction solar cells [43]. The co-location of glass manufacturing and PV module manufacturing facilities will further reduce the cost of PV system. PV systems also have soft costs associated with them. Soft costs are the indirect costs in any system that must be considered pre- and post-setup of that system. These soft costs for PV include installation charges, taxes and legal fees, service fees, maintenance charges, etc. A reduction in these soft costs are necessary for PV systems to become a reality in every household or commercial institution. Public policies that can empower PV installation is another important aspect that will affect the costs associated with PV systems. It is worth mentioning here that contrary to opinion of many reports [44], perovskite solar cells will have no significant impact on PV industry. We have analyzed technical and economic consideration in reference [45].

Based on very recent (3 December 2019) cost data published by Bloomberg New Energy Finance [46], the average battery pack capital cost in the years 2020 and 2030 is expected to be USD 144 and USD 61 per kWh, respectively. A similar trend must continue in the future to make battery systems more viable in the electric power network as well as the transportation sector. Without inventing any new battery chemistry, the cost of lithium-ion battery can be further reduced by introducing some of the concepts used in semiconductor industry and implement industrial IoT in battery manufacturing [47]. Recently, solid-state batteries have started capturing some attention as some automotive companies are looking for more attractive options than the liquid electrolyte-based lithium-ion batteries. Solid-state batteries can provide higher energy density, longer life cycles, faster charging and are non-flammable [48]. However, a lot of research is still pending on their commercial viability. If at all solid-state batteries can become commercially viable, they can be the next breakthrough in energy storage for the power network.

C. *Lower Cost and High-Performance Power Electronics based on Wide Bandgap (WBG) Semiconductors*

Power Electronics go hand in hand with the PV power generation industry. Power electronics offer switching capabilities at a high frequency for DC to AC and DC to DC conversion. The inverters currently in use incorporate Silicon (Si) transistors for switching. However, Wide Bandgap (WBG) transistors like Silicon Carbide (SiC) or Gallium Nitride (GaN) have higher power handling density as compared to their Si counterparts. This results in much smaller inverter size. The WBG transistors can also operate at a much higher temperatures and hence require smaller heat sinks. Higher switching frequencies can also be achieved using WBG transistors. Thus, the utilization of WBG transistors provides an effective reduction in the inverter size and an increase in the switching frequency with the ability to operate at much higher voltages. However, the most important factor in which Si transistors triumph the WBG transistors is the cost. The WBG transistors are expensive and can increase the system cost by a significant amount. To illustrate this point, we purchased Si MOSFETs and GaN MOSFETs for a project in progress. The Si MOSFET costs \$1.78 a piece versus the GaN MOSFET that costs \$17 a piece. This is just a miniaturized scale for the cost difference between the two technologies. Larger the scale, greater is the cost difference. Hence, a low-cost solution is required for power electronics with WBG materials at their core.

D. Recycling, Builidiung-Integrated PV, and Grid bypass

Every PV module manufacturer provides warranty of at least 25 years. Many solar panels are rated with a lifespan of 30 years. Sunpower has announced that after 40 years, 99% of their modules will have at least 70% [49]. The panels get replaced with new infrastructure after they stop generating significant amount of power. Eying a future with PV power generation for majority of the world, this will generate a huge amount of waste as old panels if not recycled. Hence, recycling of panels is a necessary measure if the goal of clean energy through PV is to be realized. Fortunately, research studies conducted on the topic of recycling solar panels have resulted in an astonishing 96% recycling efficiency, but the aim is to raise the bar further [50]. Silicon is a material with a myriad of applications. The recycled panels can be utilized towards PV or towards any other application.

Building-Integrated PV (BIPV) is another attractive design consideration for commercial and non-commercial buildings to maximize their power efficiency. The PV systems can be integrated in the building structure like shingles, walls, rooftops, etc. BIPVs are an efficient solution to solving the power needs of a building without majorly affecting its aesthetic appeal. The design considerations and specifications of some BIPV structures can be found in [51]. Fig. 9 [52] illustrates the difference in PV integration to a residential building.

E. DC Appliances and Equipment with Higher Energy Efficiency and Lower Cost

Currently, majority of the power network is based on AC transmission and distribution. In the United States, the wall outlets output is either 110V or 220V AC voltage. However, majority of loads that we utilize today ranging from consumer electronics to HVAC systems are DC powered. The conversion takes place within the load through transformers, rectifiers, filters, etc. PV and batteries generate DC power that can be utilized with the loads without conversion. Without the conversion losses and equipment, the efficiency, the cost, and size can be reduced for appliances. Hence, it has become necessary to manufacture and commercialize DC appliances. Table III [53] illustrates the power savings with DC appliances as compared to their AC counterparts.

Figure 9. Different levels of PV integration in a residential builiding [52]

F. Solar Farms in Space

As early as 1968 Peter Glaser envisioned a way to harness limitless solar power in space and transmit it for use on Earth via invisible microwaves [54]. The research involves launching and setting up a solar farm of panels in space that would orbit the earth and relay power to a receiving station on earth. After some initial investigation, the concept was not pursued further. Recently, China has announced plans to build solar farms in space [55]. The power can be relayed to the earth either by laser or microwaves. For all practical purpose, this is not a cost-effective approach.

TABLE III. POWER SAVINGS WITH DC APPLIANCES [53].

Description	Consumption (in Watts)	
	48V DC Appliances	**230V AC Appliances**
Ceiling Fan	30	70
Tube light	18	40
Bulb/ CFL	5	18
Mobile Charger	5	5
21” Television	36	100
24” Television	40	120
Laptop Adapter	65	100
Television adapter	100	100
Cooler	-	150
Refrigerator	-	150
2*2 Downlight	33	36
Linear Light	18	22
Down Light Circular	9	11
Down Light Rectangular	9	11
Exhaust Fan	48	80

V. CONCLUSION

The challenge of a clean and sustainable power system for the world is most efficiently realized by free fuel PV systems and or wind turbines combined with batteries. Considering the declining cost trends for both PV and battery, it can be concluded that it is also the most low-cost energy generation and storage technique. The use of local direct current power in place of alternating current power can further reduce the power generated by local DC PV systems. Public policies are already being adopted across several nations in the world to realize a clean and eco-friendly future in transport and power networks. The important issue of climate change can only be tackled if these policies accelerate and empower more PV and battery growth, with more research, PV systems can achieve milestones in providing clean and sustainable energy for all.

REFERENCES

[1] Tsao, J. Y., Schubert, E. F., Fouquet, R., & Lave, M. (2018). The electrification of energy: Long-term trends and opportunities. *MRS Energy & Sustainability, 5.*

[2] The Beam. (2019). *Electricity: You can't fight poverty without it*. Available at: https://cleantechnica.com/2019/04/13/electricity-%e2%80%8ayou-cant-fight-poverty-without-it/

[3] National Geographic. *Causes and Effects of Climate Change.* Available at: https://www.nationalgeographic.com/environment/global-warming/global-warming-effects/

[4] Takepart Flashcards. *What is climate change*. Available at: http://www.takepart.com/flashcards/what-is-climate-change/

[5] BloombergNEF. *Adding Solar to Wind Farms Lights Up Project Returns.* Available at: https://about.bnef.com/blog/adding-solar-wind-farms-lights-project-returns/

[6] Bedi, G., Venayagamoorthy, G. K., Singh, R., Brooks, R. R., & Wang, K. C. (2018). Review of Internet of Things (IoT) in electric power and energy systems. *IEEE Internet of Things Journal, 5*(2), 847-870.

[7] Bedi, G., Venayagamoorthy, G. K., & Singh, R. (2020). Development of an IoT-Driven Building Environment for Prediction of Electric Energy Consumption. *IEEE Internet of Things Journal, 7*(6), 4912-4921.

[8] Wood, E. (2015). *Energy Waste Worries American Business Now.* Available at: http://energyefficiencymarkets.com/energy-waste-worries-american-businesses/

[9] Perez, R., Zweibel, K., & Hoff, T. *Solar Power Generation in the US: Too expensive, or a bargain?* Available at: http://www.asrc.cestm.albany.edu/perez/2011/solval.pdf

[10] Enerdata. *Global Energy statistical Yearbook 2018*. Available at: https://yearbook.enerdata.net/electricity/electricity-domestic-consumption-data

[11] Quote investigator. Available at: https://quoteinvestigator.com/2015/08/09/solar/

[12] MapsofIndia.com. *World Population Density Map*. Available at: https://www.mapsofindia.com/worldmap/population-density

[13] Energydata.info. *Global Solar Atlas.* Available at: https://globalsolaratlas.info

[14] Powergrid International. Electric Light & Power. (2019). *Juhl Energy pairs wind and solar power in hybrid project*. Available at: https://www.elp.com/articles/2019/03/juhl-energy-pairs-wind-and-solar-power-in-hybrid-project.html

[15] Barabard, M. (2019). *Fukushima's Final Costs Will Approach A Trillion Dollars Just For Nuclear Disaster.* Available at: https://cleantechnica.com/2019/04/16/fukushimas-final-costs-will-approach-one-trillion-dollars-just-for-nuclear-disaster/

[16] Renewable Resources Coalition. (2016) *Nuclear Energy: Pros & Cons.* Available at: https://www.renewableresourcescoalition.org/nuclear-energy-pros-cons/

[17] Mooney, C., & Dennis, B. (2018). *Scientists acknowledge key errors in study of how fast the oceans are warming.* Available at: https://www.washingtonpost.com/energy-environment/2018/11/14/scientists-acknowledge-key-errors-study-how-fast-oceans-are-warming/

[18] Lillian, B., & SolarIndustryMag.com. (2018). *Solar and Wind Help Curb CO2 Power Emissions 28% Since 2005*. Available at: https://solarindustrymag.com/solar-and-wind-help-curb-co2-power-emissions-28-since-2005/

[19] Elliott, D. (2018). *Is Renewable Energy Enough To Stop Global Warming/ What About Animal Agriculture?* Available at: https://cleantechnica.com/2018/12/09/is-renewable-energy-enough-to-stop-global-warming-what-about-animal-agriculture/

[20] Drayer, L. (2019). *Change your diet to combat climate change in 2019.* Available at: https://www.cnn.com/2018/10/18/health/plant-based-diet-climate-change-food-drayer/

[21] *The End of the Internal combustion engine*. Available at: https://www.aljazeera.com/amp/features/2020/11/27/the-end-of-the-internal-combustion-engine

[22] Beiker, S., Hansson, F., Suneson, A., & Uhl, M. (2016). *How the convergence of automotive and tech will create a new ecosystem.* Available at: http://www.mckinsey.com/industries/automotive-and-assembly/our-insights/how-the-convergence-of-automotive-and-tech-will-create-a-new-ecosystem

[23] Pressman, M. (2018). *Forbes: Electric Cars = The Future, Gas mobile killers.* Available at: https://cleantechnica.com/2018/09/28/forbes-electric-cars-the-future-gasmobile-killers

[24] Carbon Footprint. (2016). *What makes electric cars better for the environment than conventional cars?*

Available at: https://www.carbonfootprint.com/electric_vehicles

[25] Zart, N. (2019). *Electric Aircraft Will Help Save The World.* Available at: https://cleantechnica.com/2019/05/06/electric-aircraft-will-help-save-the-world/

[26] Elect!. *Exploring new horizons – with electric ships.* Available at: https://www.elect-expo.com/en/electrifying-stories/exploring-new-horizons-with-electric-ships/

[27] Singh, R., Alapatt, G. F., & Bedi, G. (2014). Why and how photovoltaics will provide cheapest electricity in the 21st century. *Facta Universitatis, Series: Electronics and Energetics, 27*(2), 275-298.

[28] The World Bank – Data. *Access to electricity (%of population}.* Available at: https://data.worldbank.org/indicator/

[29] World Economic Forum. (2018). *The Global Risks Report 2018 – 13th Edition.* Available: http://www3.weforum.org/docs/WEF_GRR18_Report.pdf

[30] GTM. *Solar Technology Got Cheaper and Better in the 2010s*. Available at: https://www.greentechmedia.com/amp/article/solar-pv-has-become-cheaper-and-better-in-the-2010s-now-what

[31] BloombergNEF. *Solar and Wind Reach 67% of New Power Capacity Added Globally in 2019, while Fossil Fuels Slide to 25%.* Available at: https://about.bnef.com/blog/solar-and-wind-reach-67-of-new-power-capacity-added-globally-in-2019-while-fossil-fuels-slide-to-25/

[32] Renewable Energy World. (2010). *Champions of photovoltaics technology*. Available at: http://www.renewableenergyworld.com/articles/2010/10/champions-of-photovoltaics

[33] Bossel, U. (2006). Does a hydrogen economy make sense?. *Proceedings of the IEEE, 94*(10), 1826-1837.

[34] The Economist. (2017). *Electrifying everything – After electric cars, what more will it take for batteries to change the face of energy?* Available at: https://www.economist.com/news/briefing/21726069-no-need-subsidies-higher-volumes-and-better-chemistry-are-causing-costs-plummet-after/

[35] Sivaram, V. (2015). *Why Moore's Law Doesn't Apply to Clean Energy Technologies*. Available at: http://www.greentechmedia.com/articles/read/why-moores-law-doesnt-apply-to-clean-technologies

[36] PVmagazine. *Portugal's second PV auction draws world record low bid of $0.0132/kWh.* Available at: https://www.pv-magazine.com/2020/08/24/portugals-second-pv-auction-draws-world-record-low-bid-of-0-0132-kwh/

[37] The Mottley Fool. (2020). *This Renewable Energy Juggernaut Wants to Supercharge America's Battery Storage Capacity*. Available at: https://www.fool.com/amp/investing/2020/09/05/this-renewable-energy-juggernaut-wants-to-supercha/

[38] Electrek (2020). *Watch Tesla Megapack 15 MWh battery system being deployed on impressive timeline.* Available at: https://electrek.co/2020/11/16/tesla-megapack-batteries-being-deployed-video/

[39] U.S. Department of Energy. Office of Energy Efficiency & Renewable Energy. (2017). *Enabling Fast Charging: A Technology Gap Assessment.* Available at: https://www.energy.gov/sites/prod/files/2017/10/f38/XFC%20Technology%20Gap%20Assessment%20Report_FINAL_10202017.pdf

[40] Dawra, V. (2016). *How solar power is turning rural India bright and shining.* Available at: https://www.thehindubusinessline.com/specials/how-solar-power-is-turning-rural-india-bright-and-shining/article9277415.ece

[41] Singh, R., & Shenai, K. (2014). *DC Microgrids and the Virtues of Local Electricity.* Available at: http://spectrum.ieee.org/green-tech/buildings/dc-microgrids-and-the-virtues-of-local-electricity

[42] Green, M., Hishikawa, Y., Dunlop, E., Levi, D., Hohl-Ebinger, J., Yoshita, M., & Ho-Baillie, A. (2018). *Solar cell efficiency tables (Version 53)*. Available at: https://onlinelibrary.wiley.com/doi/full/10.1002/pip.3102

[43] Singh, R., Alapatt, G. F., & Lakhtakia, A. (2013). Making solar cells a reality in every home: Opportunities and challenges for photovoltaic device design. *IEEE Journal of the Electron Devices Society, 1*(6), 129-144.

[44] PVmagazine. *Large-scale printing for perovskites*. Available at: https://www.pv-magazine.com/2020/11/27/large-scale-printing-for-perovskites/

[45] Asif, A. A., Singh, R., & Alapatt, G. F. (2015). Technical and economic assessment of perovskite solar cells for large scale manufacturing. *Journal of Renewable and Sustainable Energy, 7*(4), 043120.

[46] Bloomberg NEF. *Battery Pack Prices Fall as Market Ramps up with Market Average at $156/kWh in 2019*. Available at: https://about.bnef.com/blog/battery-pack-prices-fall-as-market-ramps-up-with-market-average-at-156-kwh-in-2019/(accessed on 5 June 2020).

[47] Asif, A. A., & Singh, R. (2017). Further cost reduction of battery manufacturing. *Batteries, 3*(2), 17.

[48] Stereax. Ilika. (2016). *Accelerated materials innovation.* Available at: https://www.ilika.com/images/uploads/general/Ilika_Stereax_FAQ-V1.01.pdf

[49] SunPower. *SunPower A-Series 400-425 W Residential Module Datasheet.* Available at: https://us.sunpower.com/solar-resources/sunpower-series-400-425-w-residential-module-datasheet

[50] NERC. (2019). *The Opportunities of Solar Panel Recycling*. Available at: https://nerc.org/news-and-updates/blog/nerc-blog/2019/01/29/the-opportunities-of-solar-panel-recycling

[51] Eiffert, P., & Kiss, G. Building-Integrated Photovoltaic *Designs for Commercial and Institutional Structures.* Available at: https://www.nrel.gov/docs/fy00osti/25272.pdf

[52] James, T., Goodrich, A., Woodhouse, M., Margolis, R., & Ong, S. (2011). Building-Integrated Photovoltaics (BIPV) in the residential sector: an analysis of installed rooftop system prices (No. NREL/TP-6A20-53103). National Renewable Energy Lab.(NREL), Golden, CO (United States).

[53] Cygni. *DC Appliances*. Available at: http://www.cygni.com/wp-content/uploads/2016/08/DC-Appliances-leaflet.pdf

[54] American Security Project. *Space based Solar Power*. Available at: https://www.americansecurityproject.org/climate-energy-and-security/energy/future-investment/space-based-solar-power/

[55] Unwin, J. (2019). *More details revealed on China's plans for solar farm in space.* Available at: https://www.power-technology.com/news/chinese-solar-farm-space/

A Secure Hybrid Cloud-based Architecture to Support Dynamic Line Rating Systems

Slavica V. Boštjančič Rakas[1], Mirjana D. Stojanović[2]

[1]University of Belgrade, Mihailo Pupin Institute, Belgrade, Serbia, slavica.bostjancic@pupin.rs

[2]University of Belgrade, Faculty of Transport and Traffic Engineering, Belgrade, Serbia, m.stojanovic@sf.bg.ac.rs

Abstract—**Dynamic Line Rating (DLR) systems and methods for prediction of the maximum transmission line's load, as a functional part of smart grids, contribute to efficient load management in power utility network and optimization of electric energy distribution. This paper considers DLR systems in the cloud computing environment. Special attention is dedicated to cyber security issues, including public and private cloud infrastructures. A secure hybrid cloud infrastructure is proposed to support DLR systems as a solution that can benefit from cost efficiency of public cloud services, while retaining high level of security for critical applications that are executed in the private cloud.**

Keywords - cloud computing, cyber security, dynamic line rating, overhead transmission line

I. Introduction

Dynamic line rating (DLR) systems provide energy optimization, prevention from the conductor overheating, and enhance the overall security and reliability of the power system based on continuous data acquisition and analysis. DLR systems perform a real-time control of the transmission line, based on: (1) continuous evaluation of the actual thermal and other operating conditions, (2) estimation of the acceptable transmission line's load and (3) other relevant parameters regarding operational limitations. These systems detect additional available capacities and provide advantageous conditions for power system management procedures, and are commonly integrated with the power utility's supervisory control and data acquisition (SCADA) system [1,2]. DLR also plays an important role in implementing the smart grids in the transmission network, since it provides prompt response in the case of detected incidents [3].

This paper considers application of cloud computing services to support DLR systems. Cloud computing is a prospective technology for smart grid applications because of its advanced computing and data storage capabilities, flexibility, provision for big data analytics, as well as cost savings [4]. However, cloud computing also brings in some risks, primary in terms of security and reliability [5]. Additionally, operation of DLR systems depends strongly on receiving accurate data in real time, therefore the information security is of the most importance. In fact, implementation of the DLR system requires a proper level of information and network infrastructure security.

The rest of the paper is organized as follows. Section II surveys the basic concepts of integrated DLR systems. Section III discusses application of cloud computing in DLR systems. Cyber security issues of cloud-based DLR systems are considered in Section IV. Section V presents proposal of a secure hybrid cloud-based architecture that supports DLR systems. Section VI concludes the article.

II. Integrated DLR Systems Basics

Traditionally, the operation of overhead transmission lines (OHLs) is evaluated with static thermal rating, which is normally based upon the worst-case weather assumptions and specific conductor parameters. Due to increase of renewable energy generation sources worldwide, power generation becomes highly dependent on the weather and climate conditions. Power generation from most renewable energy sources (wind farms, solar panels, etc.) is directly dependent on the onsite meteorological conditions [6]. Hydro-power is also dependent on weather conditions, but with less variable dynamics [7].

A significant improvement was gained with the introduction of DLR concept, since it dynamically increases transmission capacity of power lines and improves operating security of power grids [8]. It performs real-time management of the OHLs, i.e., continuously estimates transmission line’s acceptable carrying capacity (ampacity), based on the actual operating and thermal conditions. DLR system’s main task is to properly react to transmission line capacity limit, while preserving system's reliability, availability, and security.

The integrated DLR systems represent an important smart grid application and are capable of measuring a set of weather and/or mechanical variables, in order to compute OHL rating. This new limit is then forwarded to SCADA system.

Integrated DLR systems are composed of different layers: sensing and measuring, communications, management information system, and analysis and optimization, as illustrated in Fig. 1 [1].

Calculation of DLR ratings can be performed by two main categories of methods,

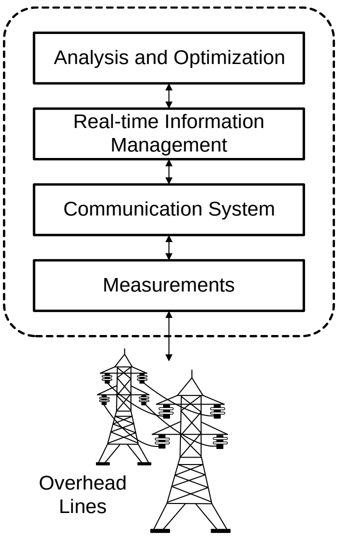

Figure 1. Integrated DLR system layers.

which either use direct or indirect monitoring sensors. Direct monitoring sensors are used for observation of different conductor's variables (line tension, line sag, conductor temperature, etc.), while indirect monitoring sensors are used for measuring the weather parameters (wind speed, wind direction, solar radiation, ambient temperature, air pressure) [3,9,10].

In order to get the most out of the DLR system, it is also important to provide for short term (few hours) and long term (up to two days) forecasting. In case of unpredictable situations or variations in energy generation from wind farms, dispatchers can make the right decision based on short term forecasting, while long term forecasting improves energy trading, particularly in the case of renewable energy resources [11].

The main benefits of the DLR system are: (1) increase of the transmission system efficiency; (2) operational flexibility of the transmission system; (3) improved utilization of the existing assets (decrease of overall costs); (4) reduction of greenhouse gas emissions, through integration of renewable energy resources; (5) security improvement of the power grid's operation in normal operating conditions.

III. Application of Cloud Computing in DLR Systems

In the past few years, cloud computing has gradually moved its focus from consumer applications toward corporate control systems. The cloud-based services, provided through the public, private, or hybrid infrastructures, add to cost-efficiency and simplification of the industrial processes. The world’s leading cloud service providers are offering cloud solutions that can meet the needs of industry organizations; this paradigm is known as “Industry cloud” or “Manufacturing cloud” [12,13]. Industry cloud is not restricted to public clouds; hybrid and private industry cloud infrastructures can be built with the assistance of professional system integration companies.

In the electric power industry, cloud computing is usually used for distributed energy management and information management [5]. Another important application area of industry cloud computing is electrical distribution systems. The web-based cloud platforms help consumers to organize their energy consumption and reduce bills, based on the real-time information about energy usage and cost of energy.

Regarding the DLR system, migration of SCADA toward cloud environment may impact the cloud-based DLR system architecture, due to integration of both systems. The DLR system follows client-server paradigm, where results of measurements, software and specialized algorithms are located in the DLR server. The DLR server is typically configured to send standard telecontrol frames to the power utility's SCADA acquisition units. A detailed discussion on migration scenarios of SCADA systems to the cloud computing environments can be found in [14].

Taking into account principles from [14], the first migration scenario refers to the public cloud, where the DLR server is running on company's premises, and is directly connected to sensor elements. The data is transferred to the cloud where they can be stored and distributed to remote work stations. The second migration scenario assumes private/hybrid cloud, in which distributed DLR application is remotely connected to sensor elements, via appropriate communication links, and is entirely executed in the cloud environment.

TABLE I. APPLICATION OF CLOUD COMPUTING SERVICES IN DLR SYSTEMS.

Cloud Service	**Features**	
	Applications	**Type of cloud**
SaaS	Geospatial data Weather reports & forecasts	Public
PaaS	Platforms for big data analysis Platforms for visualization	Public or private
IaaS	Storage Web hosting Network performance monitoring High performance computing	Public or private
CompaaS	Processing resources for utility applications	Public or private
DaaS	Data management/ aggregation Data optimization	Public

Apart from the three basic cloud service models defined by U.S. NIST [15], namely Software as a Service (SaaS), Platform as a Service (PaaS) and Infrastructure as a Service (IaaS), the ITU-T specifies four additional categories [16]: Communications as a Service (CaaS), Compute as a Service (CompaaS), Data storage as a Service (DaaS) and Network as a Service (NaaS).

Possible applications of cloud computing in DLR systems, in terms of different cloud services and different types of cloud infrastructure, are summarized in Table I. They include:

1. *Storage for big data* that are collected from the large number of sensor elements over a long period of time, as well as for the relevant meteorological data. These databases can be implemented using either DaaS or CompaaS services. DaaS enables data management and optimization in the cloud, and is usually offered as a public cloud service. CompaaS represents cloud processing resources (e.g., virtual machines), that are used to install and run utility's own database management software. It can be used as a public cloud service or implemented in the private cloud.
2. *Processing of the collected data* using different algorithms for short and long term prediction of the maximum transmission line's load. These algorithms can be implemented using cloud services like PaaS and IaaS. PaaS provides platforms for big data analysis and visualization of results, while IaaS provides infrastructure resources required for data storage, web hosting, network performance monitoring, and high performance computing. Both services can be implemented in the public and private/hybrid cloud environments; however security makes a great difference, which is discussed in the next Section.
3. *SaaS-based DLR solution*, offered as a public cloud service, which provides geospatial data as well as weather forecasting at any location of the weather station and managing the data collected from weather stations [17]. These services help users to track changes of current load in a real time, and to appropriately react based on that information.

IV. CYBER SECURITY ISSUES

Cyber security and privacy are essential issues in cloud-based DLR systems. Cyber security refers to defending information and infrastructure from malicious attacks, while the privacy is associated to company's rights to control confidential information and the way it is used.

Industrial systems' information and infrastructure security typically require solutions customized for the control environment. Security management assumes definition and implementation of the appropriate security policies, risk assessment, design of the overall security architecture, as well as selection and implementation of the appropriate security mechanisms.

DLR systems require reliable real-time data acquisition; therefore, information and equipment protection assumes a set of different measures like authentication and access control, antivirus software installing, data encryption, firewalls, as well as intrusion detection and prevention systems (IDPSs) [18].

In general, when discussing cyber security of cloud-based industrial systems, a distinction should be made between public and private cloud infrastructures [19].

A. Public Cloud Infrastructure and Services

The use of public cloud services increases cyber security risks. Besides cyber security threats that are present in the traditional computing platforms and networks, public cloud services cope with a number of additional vulnerabilities such as: attacks by other customers; shared technology issues; malfunctions and/or flawed integration of provider's or customer's security systems; insecure application programming interfaces; data loss or leakage; insider attacks; account or service hijacking; legal and regulatory issues [20]. In addition, the user cannot control the network performance; even servers' locations are unknown to their users.

Vulnerability also depends on the type of cloud service. For example, IaaS is susceptible to most of the threats that are recognized in the traditional information and communication systems. Customers are responsible for securing their applications, because all of them are running on the virtual machines. PaaS is particularly susceptible to shared technology issues, because of different security settings for various kinds of resources and potential data leakage. SaaS typically requires only a web browser and the Internet connection; hence, it is mainly susceptible to data security and confidentiality. The other issues with SaaS encompass data backup, data access, storage locations, availability, authentication, etc.

Cloud-based DLR systems suffer from the same cyber security risks as general-purpose cloud services. However, some threats in cloud environments can make DLR systems more vulnerable: (1) denial of service (DoS), distributed DoS (DDoS), and man-in-the-middle (MITM) attacks like active eavesdropping, protocol spoofing, etc.; (2) insecure network connections between DLR systems and the cloud; (3) lack of protection for some proprietary protocols used in the power utility; (4) use of commercial off-the-shelf solutions.

Securing DLR system that uses public cloud services assumes several steps, as illustrated in Fig. 2.

The first and the most important step is *the right choice of a cloud service provider*, according to the offered service maturity. Service maturity is assessed through a set of criteria including quality of service, mutual isolation of traffic originating from different sources, customer's control level concerning changes in the provider's infrastructure, data encryption, response to detected attacks, continuous assessment of security mechanisms

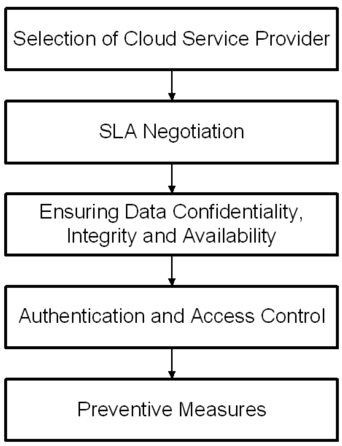

Figure 2. Securing DLR system that uses public cloud services.

efficiency, capability of detecting intrusions in real time, etc. This should be followed by *establishing well-defined service level agreement (SLA)* between the provider and the customer [5,19].

The third step refers to *ensuring data confidentiality, integrity and availability.* In DLR systems, input and output data are not the same regarding the requirements for confidentiality. A part of input data is publicly available (weather reports, weather forecast, etc.), while the output information (estimated ampacity) is strictly confidential. Hence, strong encryption algorithms should be applied [21,22]. Data availability and data integrity are vital for both input and output data. The input data is used for estimation of the maximum transmission line's load; therefore, it has to be available in a real time and unmodified. This goes for the output data as well, since it provides inputs to SCADA system. A detailed discussion on security solutions related to data confidentiality, integrity and availability in cloud computing can be found in [23].

The fourth step encompasses *authentication and access control.* In the cloud environment, authentication is requested for the persons and the equipment. Automated actions such as online backup, patching and updating operating systems and remote monitoring require authorization. Strong authentication techniques are needed, because the cloud services are accessed through various devices and interfaces. These techniques may include username and password, mobile trusted module (MTM), multifactor, public key infrastructure (PKI), single sign-on and biometric authentication [24,25]. Other mechanisms that can be implemented at different network and cloud layers, encompass firewalls, IDPS solutions customized for smart grids [26], and clear delineation of responsibilities between the user and the cloud service provider.

Finally, a set of *preventive measures* should be applied. For example, prevention of breaking authentication, session and access control refers to establishing and implementation of well-defined strong authentication and session management controls, checking access from unknown or untrusted sources, automated verification of authentication deployment, etc. Other useful preventive measures may encompass data segregation techniques to mutually isolate data from different users, strong encryption techniques for the backup data, etc.

B. Private Cloud Infrastructure and Services

In this case the network owner is responsible for the overall security solutions and functions, including the design of security architecture, selection of appropriate security mechanisms and definition of security policies. In comparison with the public cloud, private cloud provides several benefits that improve the overall security:

- Flexible virtualization, e.g., the possibility of managing multiple groups of virtual machines with separate administrators.
- Limitless selection of the operating systems templates and versions, as well as configuration options.
- Implementation of specific security controls.
- Visibility of security logs, real-time security threats, and other activities;
- Detailed real-time view into cloud operating, statistics, metering, and performance;

Specification of location for data storage. These benefits are particularly visible in private PaaS and IaaS solutions. The private PaaS software can be established on any type of infrastructure, allowing Power Company to deploy and manage its business and operational applications, and at the same time meeting strict security and privacy requirements. Private IaaS, as a unique instance of the cloud service can be customized by Power Company to a much greater degree than the public cloud service. The situation is slightly different with the private SaaS, because cost savings that are the main benefit of public SaaS model are almost neutralized with the private cloud.

V. Proposal of a Hybrid Cloud-based DLR System

Hybrid cloud allows companies to combine their own data center and/or private cloud setup with public cloud resources such as SaaS. One of the most common applications of hybrid cloud is to keep sensitive, mission-critical data and applications in the private cloud, and to use public cloud when capacity is needed for less sensitive development or testing activities.

The basic idea is to take advantage of cost benefits of public cloud services, while preserving high level of security for critical applications that are executed in the private cloud [27,28].

In the context of dynamic line rating, this means that DLR server is remotely connected to sensor elements, via secure communication links, and DLR application is entirely executed in the private cloud. Public cloud services are used to provide weather reports and forecasts, as well as storage/management of less sensitive data. Architecture of the DLR system using hybrid cloud is illustrated in Fig. 3. Such architecture can easily be extended to support other smart grid applications.

DLR application makes use of the private PaaS to perform the following functions:

- Real-time acquisition of measured data from DLR sensors, regarding transmission line's parameters;
- Data aggregation, storage and management, including database management and file hosting service;
- Data processing, i.e., running algorithms to compute OHL rating;
- Sending the results to SCADA system using standard or proprietary telecontrol protocol. Protocol converter is used, if needed, to allow interoperability between the DLR and SCADA systems.

Private PaaS allows support of different software platforms that are tailored to other critical applications in the power utility.

Public SaaS is used for provisioning of publicly available information on weather reporting and forecasting at the particular locations. Public DaaS can optionally be used for storage of less sensitive data.

Achieving high level of security and privacy assumes implementation of security measures described in Section IV. This means a careful selection of the cloud service provider with a well defined SLA for each service.

Securing the private cloud is complete responsibility of the power company, and it starts from definition of security objectives and corresponding security policies, followed by implementation of mechanisms that ensure data confidentiality, integrity and availability; authentication and access control; intrusion detection and prevention, as well as a set of other preventive measures.

In Fig. 3, four inline network-based IDPSs are installed together with firewalls at network's vulnerability points to cyber attacks. IDPSs monitor the traffic in specific network segments and observe the activities of network and application layer protocols to identify and stop

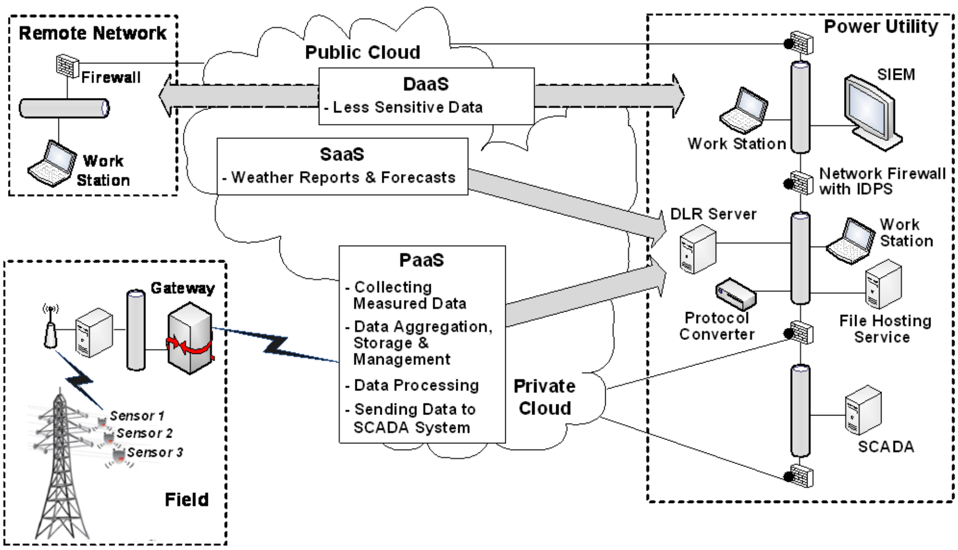

Figure 3. Architecture of the DLR system using hybrid cloud.

suspicious activities and events. They also typically record information about these activities, notify the administrator about important events with warnings and alarms, and generate reports.

Security information and event management (SIEM) software collects and aggregates security-related logs, generated throughout the private cloud infrastructure, and performs correlation of the corresponding events.

VI. CONCLUSION

Although smart grids have been widely addressed in the literature, insufficient attention has been paid to cloud-based DLR systems. Hybrid cloud infrastructures are a prospective solution because they can benefit from cost efficiency of public cloud services, while retaining high level of security for critical applications that are executed in the private cloud. Using PaaS in the private cloud allows power utilities to build, test, debug, deploy, host, and update other smart grid applications, all in the same environment. On the other hand, public SaaS is a low-cost solution for acquisition of dynamic data that are not confidential, such as weather reports and forecasts for different locations. Additionaly, public cloud can provide resources for storage of massive amount of less sensitive data (historical data, backup data), e.g., through the DaaS service.

Securing the private cloud infrastructure assumes that the power utility takes responsibility for the overall security of its system, while maintaining technical benefits of cloud computing. Besides, world's leading cloud providers are becoming capable to offer highly reliable and secure services through so-called industry cloud.

ACKNOWLEDGMENT

This work was partially funded by the Ministry of Education, Science and Technological Development of Serbia.

REFERENCES

[1] Alvarez, D. L., Rosero, J. A., Faria da Silva, F., Bak, C. L., & Mombello, E. E. (2016). Dynamic line rating – Technologies and challenges of PMU on overhead lines: A survey. In *51st International Universities Power Engineering Conference – UPEC* (pp. 1-6).

[2] Bostjancic Rakas, S., Timcenko, V., Kabovic, A., & Kabovic, M. (2016). Cyber security issues in conductor temperature and meteorological measurement based DLR system. In *Mediterranean Conf. Power Generation, Transmission, Distribution and Energy Conversion* (pp. 1-7).

[3] Akpolat, A. N., Nese, S. V., & Dursun, E. (2018). Towards to smart grid: Dynamic line rating. In *6th International Istanbul Smart Grids and Cities Congress and Fair – ICSG* (pp. 96-100).

[4] Dileep, G. (2020). A survey on smart grid technologies and applications. *Renewable Energy*, *146*, 2589-2625.

[5] Raković, R. M. (2020). Application of cloud computing in electric power utility systems: Advantages and risks. In: M. Stojanović & S. Boštjančič Rakas (Eds.), *Cyber Security of Industrial Control Systems in the Future Internet Environment* (pp. 229-247). Hershey, PA: IGI Global.

[6] Michiorri, A., Nguyen, H-M., Alessandrini, S., Bjørnar Bremnes, J., Dierer, S., Ferrero, E., et al. (2015). Forecasting for dynamic line rating. *Renewable and Sustainable Energy Reviews*, *52*, 1713-1730.

[7] Ramos, M. H., Castelletti, A., Pulido-Velazquez, M., & Gustafsson, D. (2016). Weather and climate services for hydropower management. In *Hydropower and Environmental Sustainability*.

[8] McCall, J. C., & Goodwin, T. (2015). Dynamic Line Rating as a means to enhance transmission grid resilience. In *CIGRÉ Colloquium – Grid of the Future* (paper 49).

[9] Kabovic, A., Kabovic, M., Bostjancic Rakas, S., & Timcenko, V. (2018). Models for short-term forecasting of parameters used for calculation of the overhead line ampacity. In *Telecommunications forum TELFOR 2018* (pp. 687-690).

[10] Estanqueiro, A., Ahlrot, C., Duque, J., Santos, D., Gentle, J. P., Abboud, A. W., et al. (2018). DLR use for optimization of network design with very large wind (and VRE) penetration. In *Wind Integration Workshop* (article 263).

[11] Aznarte, J. L., & Siebert, N. (2017). Dynamic line rating using numerical weather predictions and machine learning: A case study. *IEEE Transactions on Power Delivery*, *32*(1), 335-343.

[12] Sanders, J. (2019). *Guide to industry cloud: What businesses need to know*. Available at: https://www.zdnet.com/article/guide-to-industry-cloud-what-businesses-need-to-know/

[13] Devare, M. H. (2019). Convergence of manufacturing cloud and Industrial IoT. In G. Kecskemeti (Ed.), *Applying Integration Techniques and Methods in Distributed Systems and Technologies* (pp. 49-78). Hershey, PA: IGI Global.

[14] Stojanović, M. D., Boštjančič Rakas, S. V., & Marković-Petrović, J. D. (2019). SCADA systems in the cloud and fog environments: Migration scenarios and security issues. *Facta Universitatis Series: Electronics and Energetics*, *32*(3), 345-358.

[15] Mell P., & Grance, T. (2011). The NIST definition of cloud computing. NIST Special Publication 800-145. Gaithersburg, MD: U.S. National Institute of Standards and Technology.

[16] International Telecommunication Union – Telecommunication Standardization Sector (ITU-T). (2014). Information technology – Cloud computing –

Overview and vocabulary. ITU-T recommendation Y.3500. Geneva, Switzerland: ITU-T.

[17] Gentle, J. P. (2016). *Operational and strategic implementation of dynamic line rating for optimized wind energy generation integration. (TR No. INL/EXT-16-40751; TRN: US1702282).* Available at: https://www.osti.gov/servlets/purl/1364098

[18] Fang, B., Yin, X., Tan, Y., Li, C., Gao, Y., Cao, Y., & Li, J. (2016). The contributions of cloud technologies to smart grid. *Renewable and Sustainable Energy Reviews*, *59*, 1326-1331.

[19] Stojanović, M., & Boštjančič Rakas, S. (2020). Challenges in securing industrial control systems using Future Internet technologies. In: M. Stojanović & S. Boštjančič Rakas (Eds.), *Cyber Security of Industrial Control Systems in the Future Internet Environment* (pp. 1-26). Hershey, PA: IGI Global.

[20] Hari Krishna, B., Kiran, S., Murali, G., & Pradeep Kumar Reddy, R. (2016). Security issues in service model of cloud computing environment. *Procedia Computer Science*, *87*, 246-251.

[21] Khanezaei, N., & Hanapi, Z. M. (2014). A framework based on RSA and AES encryption algorithms for cloud computing services. In *IEEE Conf. Systems, Process and Control* (pp. 58-62).

[22] Awan, I. A., Shiraz, M., Hashmi, M. U., Shaheen, Q., Akhtar, R., & Ditta, A. (2020). Secure framework enhancing AES algorithm in cloud computing. *Security and Communication Networks*, *2020*, Article ID 8863345, 16 pages.

[23] Ravi Kumar, P., Herbert Rajb, P., & Jelcianac, P. (2018). Exploring data security issues and solutions in cloud computing. *Procedia Computer Science, 125,* 691-697.

[24] Babaeizadeh, M., Bakhtiari, M., & Mohammed, A. M. (2015). Authentication methods in cloud computing: A survey. *Research Journal of Applied Sciences, Engineering and Technology*, *9*(8), 655-664.

[25] Farooq, H. (2017). A Review on cloud computing security using authentication techniques. *International Journal of Advanced Research in Computer Science*, *8*(2), 19-22.

[26] Radoglou-Grammatikis, P. I., & Sarigiannidis, P. G. (2019). Securing the smart grid: A comprehensive compilation of intrusion detection and prevention systems, *IEEE Access*, *7*, 46595-46620.

[27] Aryotejo, G., Kristiyanto, D. Y., & Mufadhol, M. (2018). Hybrid cloud: Bridging of private and public cloud computing. *Journal of Physics Conference Series*, *1025*(1):012091.

[28] Lee, I. (2019). An optimization approach to capacity evaluation and investment decision of hybrid cloud: a corporate customer's perspective. *Journal of Cloud Computing:Advances, Systems and Applications, 8*(15), 1-13.

Wind based Phase-Fault Tolerant Induction Generator for Grid-secluded Application

Arunava Chatterjee

Dept. of Electrical Engineering, Raghunathpur Govt. Polytechnic, Purulia, India.
EE Dept., Meghnad Saha Inst. of Technology (on-line), Kolkata, India,
arunava7.ju@gmail.com

Abstract—**Three-phase induction generators are widely used to harness power from wind. This paper proposes a fault tolerant induction generator for standalone operation suitable for microgeneration schemes in remote and grid inaccessible areas as a means of extracting electric power from wind. During phase faults, the same induction generator will be used to generate power using asymmetric phase excitation using a single-phase inverter. The inverter acts as a source of variable excitation and regulates the load voltage during fluctuating loads or low wind speeds. The obtained power is converted to DC and the same can be fed to single-phase loads via a constant frequency inverter. The DC bus can be energized from a photovoltaic (PV) panel combined with a storage battery for improved reliability as regards availability of power. Appropriate simulation and experimental results validate the proposed strategy.**

Keywords – induction generator (IG), wind power, balanced current control, fault tolerant operation

I. INTRODUCTION

The usage of renewable sources of energy such as wind and solar photovoltaic (PV) has become critical with an increased global energy demand and with soaring fossil fuel costs. Due to economic considerations of high cost of transmission lines and associated losses, establishing remote electrification is difficult especially in a developing country. A suitable standalone renewable source of generation is thus the need of the hour for such places. Wind among other renewable sources is a confined, mostly copious and a clean source although it is intermittent in nature [1]. Mostly three-phase induction generators (IG) are used for power generation from wind owing to a large number of advantages viz., economic, robust, almost maintenance-less and no obligation of dc excitation. One big problem is the voltage regulation for such systems and thus proper control is essential [2]. Single-phase induction generators in self excited mode (SEIG) are used to supply residential loads, since most of the residential loads are of single-phase type but are costly and are also prone to faults than their three-phase counterparts off similar rating [3]. Previously, different generation systems were realized using SEIGs [4-6]. Three-phase IGs can be used to supply grid isolated single-phase AC loads either by converting it to DC and inverting the same at fixed frequency to supply single-phase AC loads. Also, same three-phase IGs can be used quite effectively as standalone generators for supplying grid-isolated loads using asymmetrical excitation or asymmetric loading [7,8]. The latter can be quite advantageous but it can cause uneven loading, heating due to uneven stator current flow and this may lead to torque pulsations and winding faults [9]. Thus, again a suitable control is essential. A suitable closed loop variable excitation with balanced current based IG control scheme can be used in such cases [10]. Electronic load controllers are used before to keep the output power constant with variable terminal loads with uneven excitation for a three-phase IG [11]. These controllers increases the overall system cost and is thus not suitable.

In this paper, three-phase induction machine is used as generator for supplying single-phase grid-isolated loads. For this purpose, a balanced excitation is provided in the stator which makes the IG work like a two-phase generator. The

ISBN: 978-86-80616-07-0

three-phase IG can be used as a single-phase IG when there is a phase-fault and any one of the phases are shorted. A capacitor bank is connected across the stator winding terminals for initial bulk excitation. An inverter is connected across the stator terminals for providing variable excitation. The experimental and simulation results justify the suitability of the concept for remote and grid isolated purposes.

II. Asymmetric Excitation

A three-phase induction machine can be operated as a generator by driving the machine above its synchronous speed with a suitable source of reactive power connected across its stator winding. The reactive power source helps to maintain the magnetic field and it is almost often a three-phase capacitor bank. It is also observed that even if instead of a three-phase capacitor bank, a single-capacitor is connected across a phase and neutral, similar excitation will take place and generation of voltage will take place across other phases. The same is also true with a suitable valued capacitor when connected across two-phases and one phase and neutral kept open. This self-excitation phenomena was also used previously for short duration dynamic braking of induction motor [12].

The problem is when this phenomenon is utilized for generation purpose, there are long term effects of this unbalance, leading to unbalanced current flow in stator and finally culminating to phase-faults due to excessive heating. The unbalanced currents also lead to torque pulsations which damages the motor mechanically. Such scheme is shown in Fig. 1.

The stator current i_s and rotor current i_r are expressed as positive and negative sequence current vectors I_p, I_n as:

$$i_s = \frac{3}{\sqrt{2}}\left[I_{sp}e^{j\omega_s t} + I_{sn}^{*}e^{-j\omega_s t}\right], \quad (1)$$

$$i_r e^{j\theta} = \frac{3}{\sqrt{2}}\left[I_{rp}e^{j\omega_s t} + I_{rn}^{*}e^{-j\omega_s t}\right], \quad (2)$$

where, ω_s, θ are stator frequency, rotor angle respectively. Induction machine electromagnetic torque [9] can be modified using the above sequence currents as given by:

$$T = \frac{3P}{2} L_m \operatorname{Im}\Big[(I_{sp}e^{j\omega_s t} + I_{sn}^{*}e^{-j\omega_s t})(I_{rp}^{*}e^{j\omega_s t} + I_{rn}e^{-j\omega_s t})\Big]. \quad (3)$$

One may express (3) as:

$$T = \frac{3P}{2} L_m \operatorname{Im}\Big[(I_{sp}I_{rp}^{*}) + (I_{sn}^{*}I_{rn}) + (I_{sp}I_{rn}e^{j2\omega_s t}) + (I_{sn}^{*}I_{rp}^{*}e^{-j2\omega_s t})\Big]. \quad (4)$$

Interactions from the positive and negative sequence current vectors produces electromagnetic torque which is useful and the dissimilar quantities of positive and negative sequence current vectors produce a pulsating torque with twice stator frequency which can cause torque pulsations which are harmful to the IG. A suitable control to minimize this effect is discussed in the next Section IV.

III. Proposed Generation Scheme

For grid-isolated operation, a three-phase induction generator coupled to a wind turbine is chosen. The output is converted to DC and fed to a bus. Alternatively, a PV panel of suitable rating may be used connected to the DC bus for operation and supplying to isolated loads. The DC power is converted to fixed frequency AC for supplying the single-phase loads connected. During single-phase faults in the IG, an alternative connection as mentioned a s asymmetric connection is chosen which can supply the DC bus with some reduction in output. The generation scheme is shown in Fig. 2.

IV. Proposed Control for the IG During Phase Failure

The main aim of the control during a phase failure is to provide balanced current control as well as voltage regulation. The same is done using a balanced current control loop. The IG is modeled in stationary $\alpha-\beta-axes$ as:

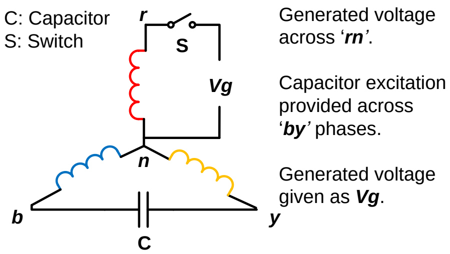

Figure 1. Asymmetric excitation for three-phase induction generator.

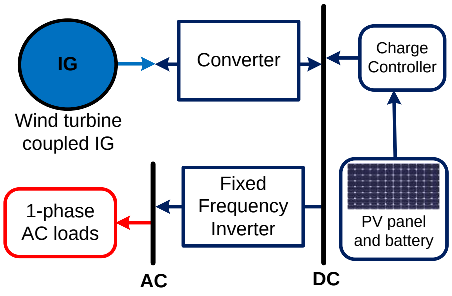

Figure 2. Proposed isolated generation scheme.

$$V_{\alpha s} = R_{\alpha s} i_{\alpha s} + \frac{d}{dt}\psi_{\alpha s} \ , \tag{5}$$

$$V_{\beta s} = R_{\beta s} i_{\beta s} + \frac{d}{dt}\psi_{\beta s} \ , \tag{6}$$

$$0 = R_{\alpha r} i_{\alpha r} + \frac{d}{dt}\psi_{\alpha r} + \omega_r \psi_{\beta r} \ , \tag{7}$$

$$0 = R_{\beta r} i_{\beta r} + \frac{d}{dt}\psi_{\beta r} + \omega_r \psi_{\alpha r} \ , \tag{8}$$

where, $R_{\alpha s}$ $R_{\beta s}$, are the respectively the α and β axis stator resistances, $v_{\alpha s}$, $v_{\beta s}$ are the α-$\beta - axes$ stator voltages, $i_{\alpha s}$, $i_{\beta s}$, $i_{\alpha r}$ and $i_{\beta r}$ are the stator and rotor α-axis and β-axis currents respectively. ω_r is the speed of the rotor. The corresponding flux linkages are represented as ψ and are not provided here for simplicity. The control schematic details is shown in Fig. 3 when operating in asymmetrical excitation mode.

A. *Normal Operation*

When there is no phase fault, the three-phase IG operates normally just like any other three-phase wind turbine generator. For this purpose, a capacitor bank is used across the stator windings for bulk excitation during start. For operation during wind or load transients, a three-phase inverter as a variable source of excitation is used with voltage control.

B. *During Phase-Faults*

During a phase fault when one of the IG windings is having a fault, the IG is operated in asymmetric mode as shown in Fig. 3. In this condition of operation, the control scheme is shown which provides balanced current flow in the stator winding thereby reducing torque pulsations and improving machine life. Also, it should be noted here that during such an operation. Only about 90% of power can be obtained than normal three-phase IG operation theoretically without exceeding the machine current ratings of the windings [13]. A hysteresis band controller (HBC) is used for the inverter control to provide balanced current control for switching the inverter. The inverter used in this case is in single-phase configuration. Thus, an extra leg of inverter is needed for the said operation. Output voltage is maintained at a constant level by using a voltage loop with a current loop to control the current to remain balanced like a balanced two-phase system. A DC motor is used as prime mover for emulating wind turbine characteristics in laboratory

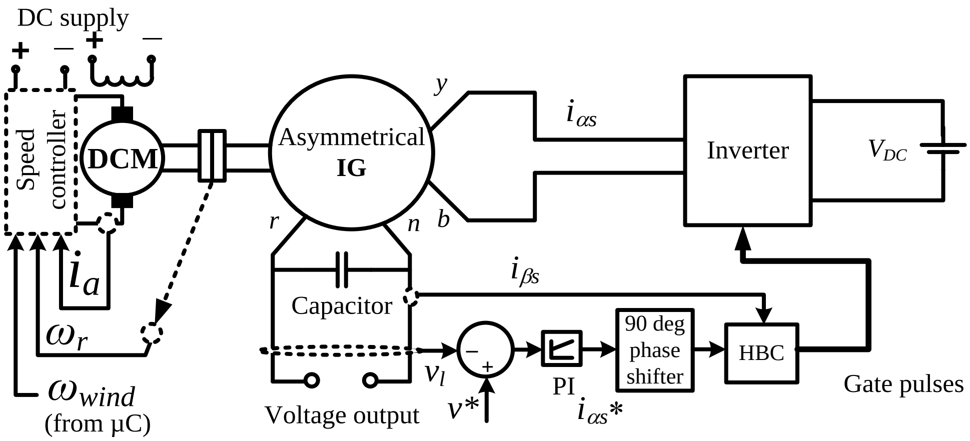

Figure 3. Proposed IG with control scheme during phase fault (asymmetrical IG operation).

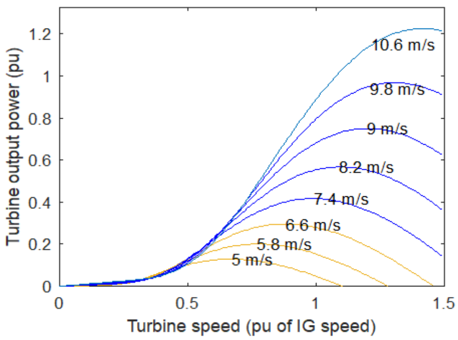

Figure 4. Wind turbine power characteristics used.

environment. Wind turbine data is fed to the speed controller for the prime-mover along with speed data used for the machine. The torque-based control scheme is used to provide speed control for the prime mover [14]. The wind turbine power curves for different wind speeds are shown in Fig. 4.

V. Results and Discussion

The IG along with the control is simulated in *MATLAB* environment with suitable experiments done on a laboratory prototype. A three-phase induction machine of 1.5kW, 400V, 50Hz is used for the proposed scheme. The generated voltage profile for the three-phase IG is shown in Fig. 5.

When there is a phase fault, the generated voltage becomes single-phase and also the load voltage output is reduced to arounf 90% of rated three-phase IG output. With the proposed control as discussed in previous section, the generated voltage can be maintained to a constant value. Also phase balance can be maintained in the stator windings. With the proposed control, the generated voltage comparison is shown in Figs. 6. and 7 shows the variation of the DC bus voltage with and the IG generated power when there is a phase fault in the IG. As observed from the Fig. 7, with a phase fault, the IG is able to deliver around 90% of the generated power than when IG is operated in three-phase mode.

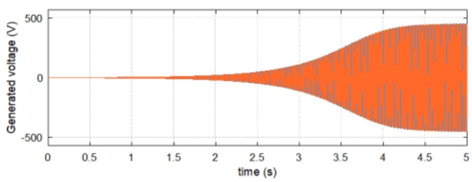

Figure 5. Generated voltage for the normal three-phase IG operation.

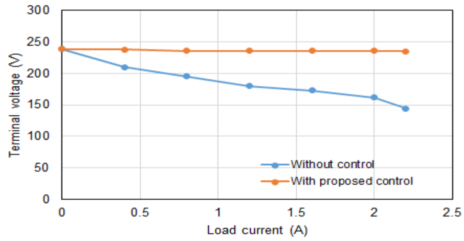

Figure 6. Terminal voltage variation with load current during phase fault with and without proposed control.

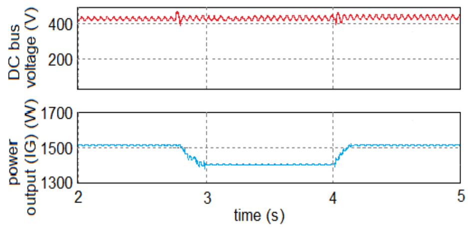

Figure 7. Variation of DC bus voltage and power output from the IG with phase fault.

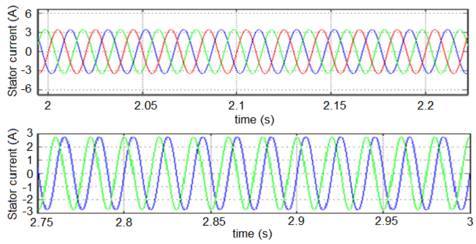

Figure 8. Stator currents during nornal three-phase IG operation at rated load and stator currents during balanced asymmetric IG operation with rated load.

Thus there is a reduction in generated power but it can still safely sustain around 90% of the load. During the fault, the bus voltage is compensated from the PV generated voltage and the storage battery and thus the bus voltage is maintained at a constant value.

Fig. 8 shows stator currents during nornal three-phase IG operation at rated load and stator currents during balanced asymmetric IG operation with rated load. It is observed that with the proposed control, the IG currents are in two-phase balance during single-phase fault or asymmetric mode of operation. Fig. 9 shows the electromagnetic torque pulsations when the IG is running in asymmetric mode. After 1s time, the proposed balanced current control is effected and the torque pulsations are much reduced as shown. The reduced torque pulsations will also help in achieving better machine life with lesser

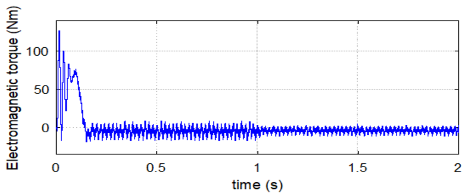

Figure 9. Electromagnetic torque pulsations for the IG when operated in single-phase asymmetrical mode.

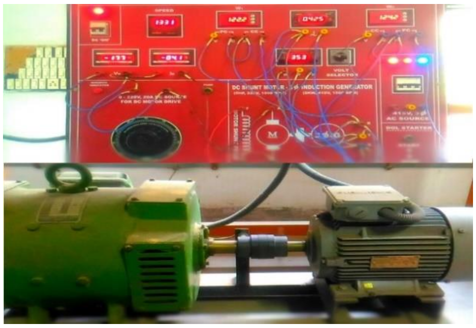

Figure 10. Laboratory experimental test rig.

mechanical faults and lower downtime than unbalanced operation during normal phase fault occurrence. The laboratory experimental setup is shown in Fig. 10.

VI. CONCLUSION

A scheme for three-phase induction generator is proposed which can operate in asymmetrical excitation mode during phase faults. The control scheme during such operation is maintained at two-phase balanced mode. The generator scheme can be easily fabricated in remote and grid isolated areas with a wind turbine for domestic microgeneration applications. The proposed control strategy also overcomes the problem of voltage regulation during variable load or wind speeds. A PV panel also aids in the operation of the IG during low or no winds. The induction generator and associated microgrid can be a suitable option for feeding electricity for remote locations even during faults with minimal disturbances and thus is a viable option for standalone, grid secluded applications.

ACKNOWLEDGMENT

The Author thanks Electrical Engineering department of Meghnad Saha Institute of Technology for providing the experimental infrastructure in carrying out this work.

REFERENCES

[1] Patel, M. R. (2006). *Wind and Solar Power Systems 2nd edn.*, CRC Press, Boca Raton, USA.

[2] Trzynadlowski, A.M. (2001). *Control of Induction Motors, 1st edn.*, Academic Press, USA.

[3] Chatterjee, A., Roy, K., & Chatterjee, D. (2014). A gravitational search algorithm (GSA) based photo-voltaic (PV) excitation control strategy for single phase operation of three phase wind-turbine coupled induction generator. *Energy*, *74*, 707-718.

[4] Bansal, R. C. (2005). Three-phase self-excited induction generators: an overview. *IEEE transactions on energy conversion*, *20*(2), 292-299.

[5] Bansal, R. C., Bhatti, T. S., & Kothari, D. P. (2003). A bibliographical survey on induction generators for application of nonconventional energy systems. *IEEE transactions on energy conversion*, *18*(3), 433-439.

[6] Chauhan, P. J., & Chatterjee, J. K. (2019) A novel speed adaptive stator current compensator for voltage and frequency control of standalone SEIG feeding three-phase four-wire system. *IEEE transactions on sustainable energy*, *10*(1), 248-256.

[7] Chan, T. F., & Lai, L. L. (2004). A novel excitation scheme for a stand-alone three-phase induction generator supplying single-phase loads. *IEEE transactions on energy conversion*, *19*(1), 136-143.

[8] Arthishri, K., Kumaresan, N., & Ammasai Gounden, N. (2019). Analysis and application of three-phase SEIG with power converters for supplying single-phase grid from wind energy. *IEEE systems journal*, *13*(2), 1813-1822.

[9] Chatterjee, A., & Chatterjee, D. (2015). An improved excitation control technique of three-phase induction machine operating as dual winding generator for micro-wind domestic application. *Energy conversion and management*, *98*, 98-106.

[10] Chatterjee, A., Ghosh, S., & Chatterjee, D. (2017). Analysis and control of a two winding IG based wind-photovoltaic generation scheme for domestic application. In *Proc. IEEE Calcutta conference (CALCON)* (pp. 292-297).

[11] Singh, B., Murthy, S.S., & Gupta, S. (2006). Analysis and design of electronic load controller for self-excited induction generators. *IEEE transactions on energy conversion*, *21*(1), 285-293.

[12] Murthy, S. S, Berg, G. J., Jha, C. S., & Tandon, A. K. (1984). A novel method of multistage dynamic braking of three-phase induction motors. *IEEE transactions on industry applications*, *20*(2), 328-334.

[13] Chatterjee, A., & Chatterjee, D. (2016). Analysis and control of photovoltaic-assisted three-phase induction machine operating as single-phase micro-wind generator. *IET generation, transmission & distribution*, *10*(9), 2165-2176.

[14] Cardenas, R., Pena, R., Proboste, J., et al. (2005). MRAS observer for sensorless control of standalone doubly fed induction generators. *IEEE transactions on energy conversion*, *20*(4), 710-718.

Battery Energy Storage Schedule Optimization Considering Different Forecast Scenarios

Vladislav Lazić[1], Aleksandar Janjić[2], Bratislav Trojić[3], Uroš Ilić[4]

[1,2,3,4]Faculty of Electronic Engineering, Niš, Serbia, vladislav.lazic@gmail.com[1]; aleksandar.janjic@elfak.ni.ac.rs[2]; bratislav.trojic@gmail.com[3]; urosilic@elfak.rs[4]

Abstract—**This paper deals with the optimization of battery energy storage in a microgrid with renewable energy sources and a connection to the utility grid with an option to buy or sell electrical energy. Due to the intermittency of renewable sources, battery energy storage is an integral part of microgrids, not just to provide energy continuously in times when renewables don't deliver energy, but also to lower the costs of purchasing energy from the utility. In the paper, a model for optimization of battery storage scheduling is derived using the software package MATLAB. Since model parameters such as wind speed, solar irradiance, load, and electricity prices are subject to significant forecast errors, five different scenarios are created to assess possible changes in optimal results.**

Keywords - battery energy storage schedule optimization, microgrid, renewable energy, forecast uncertainty

I. INTRODUCTION

In the 21st century, humankind is set to face the most challenging problems. Many of these problems are related to energy generation and its use. While on the one hand human need and dependence on energy increases, on the other hand, climate and environmental issues force us to find a sustainable and carbon-free way of generating energy. Renewable energy sources provide a solution. In the past decade, due to increased attention towards renewable sources and technological improvements, the renewable power generation price has seen a significant fall, especially for wind and solar energy [1].

One of the major issues concerning renewable energy is the intermittency and the unpredictability of its sources. To address these issues, battery energy storage systems are used in parallel with renewables as they provide the flexibility necessary for the integration of these variable renewable energy sources into the energy system in an efficient way [2,3].

Renewable energy sources are often used inside the microgrids, in standalone or grid-connected mode. The concept of microgrids is introduced in order to get higher reliability and better power quality for users [4,5]. Energy sources are closer to the end-users, providing lower operating costs, as well as higher controllability and flexibility in power system operation. Besides energy sources, energy storage facilities are an important part of microgrids for the reasons mentioned above. Microgrids are often used connected to the grid, but they can be operated in an islanded mode in case of faults in the utility grid, which minimizes the outage time of users in the microgrid area. To use the most out of the microgrids, optimization tools have to be employed.

In order to do so, the mathematical models of the renewable energy sources [6,7], the battery energy storage [8,9], and all other elements in the microgrid need to be derived. Once the mathematical model of the microgrid is built, different algorithms can be used for optimization. In [10] authors propose an algorithm for optimal sizing of the battery energy storage through peak shaving and energy-saving techniques. In [11] authors use and compare different solvers within MATLAB's Optimization Toolbox. For minimizing the power generation costs in the microgrid and maximizing the useful life of lead-acid batteries, in [12] authors use NSGA-II (nondominated sorting genetic algorithm). The particle swarm optimization (PSO) algorithm is often used for hybrid energy scheduling and economic analysis in microgrids [13-15].

Another big issue with renewable energy sources is their unpredictability. Both solar irradiance and wind speed are prone to uncertainties, as well as load and electricity prices [16-21]. All these uncertainties can produce significant errors in a day-ahead forecasted amount of power that needs to be purchased and in battery scheduling. This can lead to higher costs as energy prices on the intraday market are usually higher [22].

In this paper, five different scenarios were generated to assess the effects of input parameters' uncertainties. For this purpose, an optimal battery schedule was found for each of the scenarios, and these schedules were then used crosswise in other scenarios. After that, it was analyzed how results change when all scenarios are taken into account for optimization. Also, it was assessed what the effects of using the probability of scenario occurrence are.

II. MODEL OF THE MICROGRID

A. Solar Energy Generation Modeling

PV generation depends on weather conditions. Specifically, solar irradiance and ambient temperature are the factors that condition PV generation output power. The mathematical model by which this is conditioned is presented in [6]. The main part of the PV system is a photovoltaic array that accepts solar energy and converts it to electrical energy by forming a DC current. Generated DC current is subsequently converted to AC current to deliver the desired output power. The output power P_{pv} of a PV panel can be calculated as follows:

$$P_{pv} = P_{stc}\left[1 + k(\mathrm{T}_c - T_{ref})\right]\frac{G_t}{G_{stc}}, \qquad (1)$$

where P_{stc} is the output power of PV cells in standard test conditions $(G_t = G_{stc} = 1000\frac{W}{m^2}, \quad T_c = T_{ref} = 25^0 C), \quad G_t$ is the light intensity incident on a PV panel. The coefficient k is a power-temperature coefficient and is equal to $-0.47\frac{\%}{k}$ while T_C is the working temperature of solar panels and it depends on ambient temperature T_a and solar radiation inflicted on a horizontal panel G and is calculated using (2):

$$T_c = T_a + \frac{NOCT - 20}{0.8}G, \qquad (2)$$

where $NOCT = 48^0 C$.

B. Wind Energy Generation Modeling

The wind power output is dependent on wind speed that is measured at the height of the wind turbine. Usually, wind speed is measured closer to ground level, so it is important to know the characteristics of the terrain where the turbine is placed, so it would be possible to recalculate the wind speed at another height. Other parameters that are important are the size of the turbine and the wind density of the surrounding air but for the wind turbine for a given place and height, we can write the conditioned relation between wind speed and output wind turbine power as [6]:

$$Pw = \begin{cases} 0, 0 \le v \le v_r \\ \mathrm{P}_{rated}\frac{(\mathrm{v}^3 - \mathrm{v}_{ci}{}^3)}{(v_r{}^3 - v_{co}{}^3)}, v_{ci} \le v \le v_r \\ P_{rated}, v_r \le v \le v_{co} \end{cases}, \qquad (3)$$

where P_{rated} is the rated power of the wind turbine, v is the measured wind speed, v_r, v_{ci}, and v_{co} are rated speed, cut-in-speed and cut-off-speed of the wind turbine, respectively. v_{ci} is the speed bellow which power generation cannot work and v_{co} is the speed above which the turbine gets into the danger of a mechanical failure.

C. Batter Energy Storage Modeling

As mentioned in the paper, battery energy storage is a very important part of microgrids. It can store energy and supply it when it is needed, to complement the lack of renewable energy in certain periods of a day, especially when electricity prices are higher. Some of its other characteristics are a bidirectional flow of energy (charging and discharging) and a fast response. The latter is very useful in terms of frequency regulation inside of a microgrid, thus making battery energy storage crucial in ensuring the microgrid's stable operation.

Apart from the benefits gained using a battery as often as possible, its use also brings additional costs. It should be taken into consideration that every time the battery is used, it loses a fraction of its remaining useful life, so the costs of a battery depreciation should also form part of the optimization target function. For simulations in this paper, a lead-acid battery is used and the battery energy storage mathematical model is constructed as in [13].

One of the crucial parameters for battery modeling is a state of charge (*SOC*). It shows the battery's remaining capacity. In (4) it is presented how SOC is updated after each charging/discharging cycle. $P_{bat}(i)$ is the battery power during i-th hour of the day and lasts for a period $\Delta t = 1h$. The value is positive if the battery is discharging and negative if the battery is charging. C_{bat} is the battery capacity, while $SOC(i)$ and $SOC(i+1)$ are SOC values in i-th and $(i+1)-th$ time step:

$$SOC(i+1) = SOC(i) - \frac{P_{bat}(i)}{C_{bat}} \Delta t \ , \qquad (4)$$

where $SOC(0)$ is the initial state of charge.

The fact that the battery loses its remaining useful life with every cycle is taken into account using following Eq.:

$$c_{storage} = \frac{c_{init}}{a_1 e^{a_2 D_n} + a_3 e^{a_4 D_n}} \ , \qquad (5)$$

where the denominator represents equivalent cycle number when the depth of the discharge is D_n .The correlation coefficient factors a_1, a_2, a_3, and a_4 are equal to −16.27, 2.679, 4110 and −1.85, respectively [13].

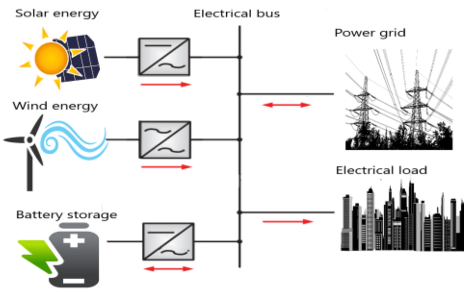

Figure 1. Microgrid diagram.

III. Problem Formulation

A. Problem Setting

The microgrid that was used in this paper for analysis consists of a PV power plant, wind power plant, and battery energy storage (Fig. 1).

The microgrid is connected to the power grid and has the possibility of exchanging electrical energy with the grid. The goal is to forecast weather, load, and prices condition, which would subsequently be used for battery schedule optimization in order to get the lowest operating costs of a microgrid. The energy is bought on the day-ahead market based on forecasted parameters, but if, due to errors in forecasting, the power balance condition isn’t satisfied, the energy difference would be bought or sold on the intraday market, where prices are bigger and more volatile.

B. Input Parameters

As an input to the model, forecasted 24-hour vectors of solar irradiance, wind speed, load, and electricity prices were inserted. These, along with other parameters, defined the framework inside of which the algorithm would propose battery output power for each hour of the next day. However, as was mentioned before, all four parameters are highly susceptible to errors in forecasting, which are almost impossible to avoid. Solar irradiance forecast uncertainty, that follows the Beta distribution function, and wind speed forecast uncertainty, that is matched by Weibull distribution, are a consequence of the weather stochasticity, while load forecast uncertainty and electricity price uncertainty can be modeled by Gaussian distribution [17]. While solar and wind production comes with uncertainties, their profiles cannot be significantly different. For example, solar generation almost always peaks around noon and has a zero output during the night. Weather forecast for the next day is often sufficiently accurate, even though significant errors are still possible. Load profiles are also quite stable, but electricity price profiles can change significantly and our analysis shows they have the biggest impact on optimization results. This is especially true for electricity prices on intraday markets that are not strong enough to keep very stable prices [22].

To assess the effects of uncertainty in input parameters on battery schedule optimization, five different scenarios were generated (Fig. 2). Weather forecast changes in several consecutive

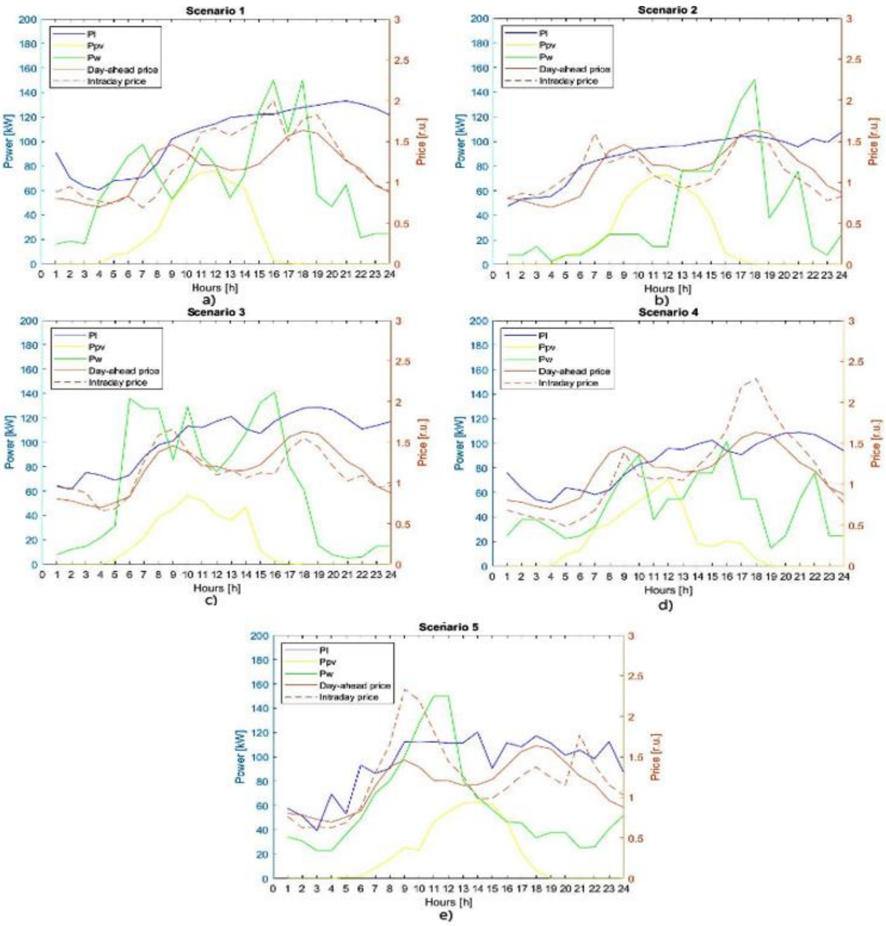

Figure 2. Forecast scenarios:
a) Scenario 1, b) Scenario 2, c) Scenario 3, d) Scenario 4, e) Scenario 5.

days for a fixed location near Niš, Serbia were used as a basis for different scenarios. After that, scenarios have been moderately altered to insert occasional spikes and drops that would be a consequence of unexpected cloudiness, for example. The goal was to change profiles a bit, where the bigger changes were made to a wind profile. The same was done for the load profile, but the evening peak and lower loads during the night had to be left intact to preserve credibility.

The biggest changes were made to the intraday market prices profile compared to the day-ahead prices profile, which was fixed in this problem. The prices for each hour were considered to be subjected to change within ± 20% range, with occasional spikes in prices arbitrarily placed. Scenario 1 was considered to actually have happened on the day for which the scheduling was made, so this scenario was used as the baseline scenario for analysis. Price values are used in relative units, where they are relative to $50\frac{€}{MWh}$.

C. Objective Function

The goal of the optimization algorithm in this paper was to minimize the operating costs of the microgrid for the day ahead. That means that the battery charging/discharging schedule should have been proposed in such a way to reduce the cost of purchasing the electricity from the grid while considering the costs of the energy storage usage. Maintenance costs are relatively small and they are excluded from the objective function. Furthermore, the prices of buying and selling electricity are considered to be the same.

The optimization was performed for each scenario k and the optimization function consisted of three terms: the costs of purchasing energy from the grid on the day-ahead market, the costs of purchasing energy from the grid on the intraday market if there is a need, and the costs of battery storage usage. First optimal results were calculated for the baseline scenario, where it is presumed that all forecasts were correct. After that, the objective function is calculated for all other scenarios relative to the baseline scenario:

$$f^k = P_{grid}^k \pi_{d,a} + (\mathrm{P}_{grid}^k - \mathrm{P}_{grid}^{bs})\pi_{i,d}^k + c_{storage}^k , \quad (6)$$

where f^k is the objective function value of scenario $k, \pi_{d,a}$ k is the 24 h vector of day-ahead energy prices which is the same for all scenarios, $\pi_{i,d}^k$ is the 24 h vector of intraday prices for scenario k , the difference $P_{grid}^k - P_{grid}^{bs}$ is the amount of energy needed to buy on the intraday market for each scenario, while $c_{storage}^k$ is the price of the storage for the optimal solution in the scenario k . It is possible to find the solution of the battery schedule to be optimal across all scenarios. By this mean, the risk of the occurrence of each of the scenarios other than baseline scenario would be mitigated:

$$f = \sum_{k=1}^{n} f^k , \quad (7)$$

where n is the number of scenarios.

Finally, the coefficient ρ which represents the probability of the baseline scenario occurrence was introduced to assess the importance of the forecast quality. All other scenarios have the same probability of happening. This is expressed by the following Eq.:

$$f = pf^{bs} + \frac{1-\rho}{n}\sum_{k=2}^{n} f^k \ . \quad (8)$$

D. Constraints

Equation (9) represents the power balance constraint which needs to be fulfilled in every iteration and in every scenario:

$$P_{load}^k(i) = \mathrm{P}_{pv}^k(i) + \mathrm{P}_w^k(i) + P_{bat}^k(i) + P_{griod}^k(i) , \quad (9)$$

where $P_{load}^k(i)$, $P_{pv}^k(i)$, $P_w^k(i)$, $P_{bat}^k(i)$, and $P_{griod}^k(i)$ are load demand, PV generation output, wind generation output, battery power and energy provided from the grid in $i-th$ hour for $k-th$ scenario, respectively.

The battery has to be charged between 20% and 100% of its full capacity at all times, it cannot go below 20%. The initial state of charge is 80% and at the end of the day it also needs to be 80%, so another condition is that the sum of battery power for each hour during the day is 0, which is represented by (10). Battery power is considered negative when the battery is charging and positive when the battery is discharging:

$$\sum_{i=1}^{24} P_{bat}^k(i) = 0 \ . \quad (10)$$

Equation (11) represents the condition that battery charging and discharging power at each hour has to be less than the maximum charging or discharging power, which are in this case 10 kW for charging and 20 kW for discharging:

$$\begin{cases} P_{bat,ch} \le P_{bat,ch,max} \\ P_{bat,dis} \le P_{bat,dis\,max} \end{cases} . \quad (11)$$

IV. Simulation Results

A. Baseline Scenario Optimal Schedule

In Table I the optimal battery energy storage schedule for the baseline scenario is given. PV power plant and wind power plant that were modeled in this paper have rated powers of 100 kW and 150 kW, respectively. The capacity of the battery energy storage is 100 kWh and need to have the same state of charge at the end of day as it was at the beginning of day. The results are obtained using *Matlab's* optimization solver *fmincon.*

As can be seen in the table, at certain times there is a possibility of selling energy to the grid. Due to the cost of battery usage, the algorithm leaves several hours with a zero or low power output. The battery is discharged with maximum discharging power in the hours 15-16, 17-18, and 18-19 because the prices are highest at that time. It leaves a few cycles for charging at later evening because prices are lower and it is necessary to satisfy the constraint of leaving the same SOC as was at the beginning of the day.

TABLE I. THE OPTIMAL BATTERY SCHEDULE FOR THE BASELINE SCENARIO.

Hour [h]	**Power[kW]**				
	P_{pv}	P_w	P_{bat}	P_{grid}	P_{load}
00-01	0.00	16.01	3.03	72.17	91.21
01-02	0.00	18.41	6.97	44.62	70.00
02-03	0.00	16.46	-10.00	56.68	63.14
03-04	0.00	51.88	-10.00	18.60	60.48
04-05	6.87	70.08	-10.00	0.88	67.83
05-06	9.13	88.05	0.00	-28.30	68.88
06-07	17.56	97.37	0.00	-44.37	70.56
07-08	27.24	72.32	0.00	-17.94	81.62
08-09	51.97	52.80	0.00	-2.92	101.85
09-10	66.35	68.97	0.00	-28.44	106.89
10-11	74.81	94.64	2.16	-60.46	111.16
11-12	75.62	80.54	6.59	-48.44	114.31
12-13	67.04	53.73	-8.75	7.33	119.35
13-14	61.56	72.32	0.00	-13.14	120.75
14-15	31.52	124.23	0.00	-33.67	122.08
15-16	2.48	150.00	20.00	-50.26	122.22
16-17	0.00	107.31	4.95	13.05	125.30
17-18	0.00	150.00	20.00	-42.25	127.75
18-19	0.00	56.58	20.00	52.92	129.50
19-20	0.00	46.57	-4.22	89.24	131.60
20-21	0.00	64.67	-10.00	78.33	133.00
21-22	0.00	21.32	-10.00	119.30	130.62
22-23	0.00	24.61	-10.00	112.44	127.05
23-00	0.00	24.61	-10.00	106.91	121.52

TABLE II. OPTIMAL OUTPUT ACROSS DIFFERENT SCENARIOS.

x_{opt}^k	**Costs [$r.u.$]**				
	S^1	S^2	S^3	S^4	S^5
x_{opt}^1	**1100.28**	1701.94	1596.16	2051.31	1744.38
x_{opt}^2	1143.98	**1670.62**	1574.48	2049.37	1707.66
x_{opt}^3	1145.76	1680.02	**1559.62**	2044.15	1689.69
x_{opt}^4	1118.51	1683.99	1572.25	**2030.90**	1712.52
x_{opt}^5	1177.70	1714.56	1590.32	2103.00	**1667.10**
x_{opt}^{1-5}	1125.77	1677.00	1565.77	2035.94	1690.03

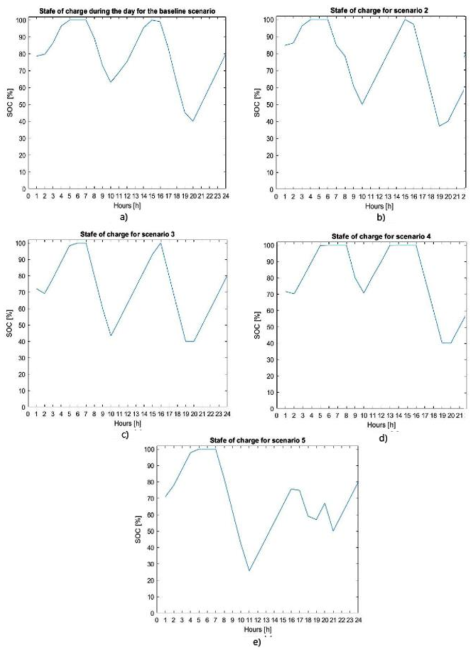

Figure 3. SOC for all scenarios; a) Scenario 1, b) Scenario 2, c) Scenario 3, d) Scenario 4, e) Scenario 5.

B. *The Optimization across Different Scenarios*

The optimal battery schedule for one scenario doesn't provide the best solution for other scenarios. This is where it can be seen how important the accuracy of the forecast is. Luckily, even though big errors are possible, solar energy, wind energy, and load have profiles that are usually stable. The electricity price profile has the biggest impact on the difference in optimal results across scenarios.

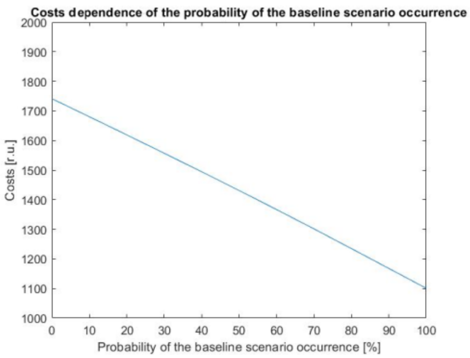

Figure 4. Costs dependence of the probability of the baseline scenario occurrence.

To analyze the difference between the results in different scenarios, the optimization was performed for all scenarios using the optimization function described in (6). Then the optimal battery schedule x_{opt}^{k} of one scenario S^{k} is then applied to the costs function of other scenarios. The results showed differences in costs function output depending on which scenario's optimal battery schedule was used. After that, the optimization function considering all scenarios that is described in (7) was evaluated and the resulting schedule x_{opt}^{1-5} was obtained. The results are presented in Table II.

The schedule x_{opt}^{1-5} didn't provide the best solution for any of the scenarios individually, but the sum of the costs of all scenarios is the smallest when x_{opt}^{1-5} is used as a solution. Other than that, in almost all cases it provides the second-best result for an individual scenario. When there are a lot of forecasting uncertainties, this procedure may represent an easy solution to lower the risk of the worst-case scenario occurrence.

It should be noted that differences in Table II are not too big because for all scenarios the proposed charge/discharge strategy was similar. This can be best seen by comparing the battery's SOC cycles for all scenarios (Fig. 3). More significant differences can be seen in scenario 5 SOC schedule, which means that the forecasted quantities' profiles for scenario 5 were more distorted compared to the others.

C. *The Optimization Consideringt the Probability of the Scenario Occurrence*

If some of the parameters or circumstances are known, then a certain probability can be assigned to the occurrence of the forecast scenario. To assess how the probability affects the optimization results, the optimization function presented in (8) was used. Fig. 4 depicts how the optimal battery energy storage scheduling output gives the smaller operating costs when the probability of baseline scenario occurrence is higher, which is expected as in this case all scenarios were worse than the baseline scenario in terms of needed operating costs. Fig. 4 actually represents how much we have to give up on baseline optimal solution in order to lower the risk of bigger costs.

V. Conclusion

This paper assesses the battery energy storage schedule optimal results in a microgrid across different forecast scenarios. It shows how differences in input parameters, such as solar, wind, load, and electricity prices, which are susceptible to forecasting errors, may invoke changes in the optimal schedule and higher costs than expected. To minimize the risk of the worst-case scenario occurrence, more scenarios have to be taken into account when finding the optimal scheduling output. This can either be done by just adding all scenarios and finding the optimal solution across all of them, or use the probability of the scenario occurrence if it is available.

For future work, a more comprehensive model that encompasses more of the significant factors and gives a closer representation of the grid can be built. Also, more elements of modern microgrids can be included, especially electric vehicles that are becoming more and more important.

Acknowledgment

This work was supported by the Ministry of Science and Technological Development, Republic of Serbia (Project number: III 44006).

References

[1] IRENA (2020). Renewable Power Generation Costs in 2019. International Renewable Energy Agency, Abu Dhabi.

[2] IRENA (2019). Innovation landscape brief: Utility-scale batteries. International Renewable Energy Agency, Abu Dhabi.

[3] De Sisternes, F. J., Jenkins, J. D., & Botterud, A. (2016). The value of energy storage in decarbonizing the electricity sector. *Applied Energy, 175*, 368-379.

[4] Datta, U., Kalam, A., & Shi, J. (2018). Hybrid PV–wind renewable energy sources for microgrid application: an overview. *Hybrid-Renewable Energy Systems in Microgrids*, 1-22.

[5] Laaksonen, H., & Kauhaniemi, K. (2008). Microgrid-Network Concept of the Future. In *Proc. of Renewable Efficient Energy, Nordic Conference on Production and Use of Renewable Energy.*

[6] Milosavljevic V. (2011). *Distributed Energy Sources*. Akademska misao, Belgrade.

[7] Bhandari, B., Poudel, S. R., Lee, K., T., & Sung-Hoon, A. (2014). Mathematical modeling of hybrid renewable energy system: A review on small hydro-solar-wind power generation. *Int. J. of Precis. Eng. and Manuf.-Green Tech. 1*, 157–173.

[8] Anvari-Moghaddam, A., Dulout, J., Alonso, C., Jammes, B., & Guerrero, J. (2017). Optimal Design and Operation Management of Battery-Based Energy Storage Systems (BESS) in *Microgrids*. 10.5772/intechopen.71640.

[9] Moncecchi, M., Brivio, C., Mandelli, S., & Merlo, M. (2020). Battery energy storage systems in microgrids: Modeling and design criteria. *Energies, 13*(8), 2006.

[10] Garmabdari, R., Moghimi, M., Yang, F., Lu, J., Li, H., & Yang, Z. (2017, December). Optimisation of battery energy storage capacity for a grid-tied renewable microgrid. In *2017 IEEE Innovative Smart Grid Technologies-Asia (ISGT-Asia)* (pp. 1-6). IEEE.

[11] Marinova, G. I., & Guliashki, V. G. (2016). Optimization of the Battery Schedule for Residential Microgrid Applications. *IFAC-PapersOnLine, 49*(29), 226-231.

[12] Zhao, B., Zhang, X., Chen, J., Wang, C., & Guo, L. (2013). Operation optimization of standalone microgrids considering lifetime characteristics of battery energy storage system. *IEEE transactions on sustainable energy, 4*(4), 934-943.

[13] Liu, Z., Chen, C., & Yuan, J. (2015). Hybrid energy scheduling in a renewable micro grid. *Applied Sciences, 5*(3), 516-531.

[14] Meiqin, M., Shujuan, S., & Chang, L. (2011, May). Economic analysis of the microgrid with multi-energy and electric vehicles. In *8th International Conference on Power Electronics-ECCE Asia* (pp. 2067-2072). IEEE.

[15] Mohammed, O. H., Amirat, Y., & Benbouzid, M. (2019). Particle swarm optimization of a hybrid wind/tidal/PV/battery energy system. Application to a remote area in Bretagne, France. *Energy Procedia, 162*, 87-96.

[16] Wang, Z., Negash, A., & Kirschen, D. S. (2017). Optimal scheduling of energy storage under forecast uncertainties. *IET Generation, Transmission & Distribution, 11*(17), 4220-4226.

[17] Zheng, Y., Zhao, J., Song, Y., Luo, F., Meng, K., Qiu, J., & Hill, D. J. (2017). Optimal operation of battery energy storage system considering distribution system uncertainty. *IEEE Transactions on Sustainable Energy, 9*(3), 1051-1060.

[18] Michiorri, A., Bossavy, A., Kariniotakis, G., & Girard, R. (2013, June). Impact of PV forecasts uncertainty in batteries management in microgrids. In *2013 IEEE Grenoble Conference* (pp. 1-6). IEEE.

[19] Hanna, R., Kleissl, J., Nottrott, A., & Ferry, M. (2014). Energy dispatch schedule optimization for demand charge reduction using a photovoltaic-battery storage system with solar forecasting. *Solar Energy, 103*, 269-287.

[20] Hobbs, B. F., & Rijkers, F. A. (2004). Strategic generation with conjectured transmission price responses in a mixed transmission pricing system-Part I: formulation. *IEEE Transactions on power systems, 19*(2), 707-717.

[21] Hossain, M. A., Pota, H. R., Squartini, S., Zaman, F., & Guerrero, J. M. (2019). Energy scheduling of community microgrid with battery cost using particle swarm optimisation. *Applied Energy, 254*, 113723.

A Management Proposal of Quality Requirements to Cogeneration of Electric Energy from Sugarcane Biomass

Paulo Henrique Palota[1], Murilo Secchieri de Carvalho[2], Elson Avallone[3], Paulo César Mioralli[4]

[1,2,3,4]Federal Institute of Education, Science and Technology of São Paulo, Catanduva-SP, Brazil, palota@ifsp.edu.br[1]

Abstract—**The main objective of this work is to investigate the quality requirements used in the cogeneration of electric energy from sugarcane biomass in order to propose a management model that facilitates the attainment of these requirements on this production chain. To meet this objective, an empirical research of multiple cases was performed in this production chain in order to find these requirements and investigate the use of practices of the element "process management" from the "internal process" theory. The finding showed that there is a lack of a system of continuous improvement on the agents of the cogeneration production chain. The proposal model presents solutions to perform all the practices of the element "process management". Besides, it can corroborate towards the attendance of the quality requirements on the chain's agents, which could result better product's quality of sugarcane biomass agents.**

Keywords – biomass, cogeneration quality requirements, process management, internal process

I. INTRODUCTION

Sugarcane generates foreign exchange for Brazil through the production of sugar, ethanol and more recently the cogeneration of electric energy that has been gaining prominence as an alternative source in the Brazilian energy matrix. The sugarcane generates leaves (fresh, dry, and tops) before harvesting and bagasse throughout the process of juice extraction on the milling planting. Both are byproducts from sugarcane that can be used for electric energy and for second-generation ethanol.

With the advent of open markets, globalization and the prices of sugarcane main products are tied to commodity exchange and futures; the Brazilian sugarcane agribusiness needs to be competitive. The competitiveness and survival of the sugar-energy chain is subject to a management that add value to this chain through the improvement of the quality of its products and its processes for obtaining more competitive costs for the production chain. The agents of the cogeneration production chain should attend the products requirements. This could be supported by internal process (IP) elements. According to [1], a successful implementation of supply chain quality management needs add the (IP), compound by the following elements: product/service design, process management (PM) and logistics. However, this work considers the element "process management", once it is related with the management of the quality requirements of the chain.

The main objective of this work is to investigate the main products and processes requirements on the cogeneration production chain and the (PM) practices in order to identify agreement and disagreement for proposing a framework that facilitates the attainment of these requirements on this chain. Within this context, the research aims to answer the following question:

- How to manage the product and process requirements of the cogeneration production chain?

To achieve this proposal, some specific objectives are considered:

- Identify IP management in the literature;
- Find the main elements of this topic.
- Find the main practices of this element in the literature;
- Investigate these practices on the cogeneration production chain in field research.
- Investigate in field research the process requirements demanded by the cogeneration production chain;
- Present a proposal based on what was identified in the previous steps.

II. Internal Process/Ethanol Production Chain

The internal process (IP) refers to all the activities of a company. This concept includes three elements: product and service design, process management and logistics. The successful implementation of the practices of these elements can generate a significant impact on the operational performance [1]. The IP, when properly managed, facilitates the integration and rationalization of the internal operational activities of a company [2]. The authors state that (IP) management has positive effects on both external and internal operating performance.

As the objective of this work is to propose a model for managing the necessary requirements for cogeneration chain production, the focus in this work is on the element "Process Management", which will be addressed in the next topic.

A. *Process Management*

According to [3], PM can generate quality for the final product in addition to improving the efficiency, effectiveness, and flexibility of production. IP management has positive effects on internal and external operating performance. However, external process management has a positive effect on external operational performance [2] .

When IP has standardization, clear instructions and statistically controlled, they assist in the delivery of products and services that improve a company's operational performance [2]. The process control is critical to the success of supply chain and can be achieved through performance measurement of supply chain [4]. Companies can identify weaknesses in its internal supply chain to maximize process performance [5]. Organizations need to review and improve processes continuously in order to reduce errors [6]. A synchronous connection between different processes and / or operations is considered critical for an efficient supply chain [7]. PM refers to the use of statistical techniques, which increases the level of process and error-proofing process design and minimizes the chance of employees' mistakes [8]. PM refers increases automatic level of processes and fool-proof in designing process [8] . The reliability of equipment and restricting disruption in production can be improved using the preventive maintenance [9].

Summarizing, it can be identified the following main practices related to the PM element:

- Control and improve continuously the processes.
- Use of statistical techniques.
- Use of fool-proof for process design.
- Use of automatic processes.
- Use of the preventive equipment maintenance.
- Clarity of work or process instruction.

B. *Sugarcane Production Chain*

The configuration of the sugarcane production chain can be seen in Fig. 1, where the main agents that make up of it are showed, as follow:

- Seedling’s growers: the companies and/or institutions responsible for the development of new cultivars for sugarcane farms.
- Agricultural inputs: the industries of correctives, fertilizers, agricultural defenses and irrigation systems for the farms of the sugarcane’s growers.
- Manufacturers of machinery and equipment: the harvesters, tractors, trucks, trailers, sprayers and various implements used for the cultivation of land (subsoilers, plows, furrows, among others).
- Farms: the growers that supply sugarcane and straw to the millings, which can be both independent suppliers and integrated into the milling itself.

- Milling: the industry manufacturer of products, such as: ethanol, various types of sugar, electric energy from
- cogeneration, yeast and additives.

The study object selected for field research, indicated on Fig. 1, covers only the raw material-related agents for the cogeneration from byproducts of sugarcane: seedling growers, sugarcane producers with focus on the byproduct of sugar cane straw (leaves), and the milling focused on cogeneration from bagasse, byproduct of extracting process.

III. Methodology

The research method used in this work is the study of multiple cases, as it investigates deeply the phenomenon of the object of analysis.

The research is aimed at the elaboration of a proposal through the verification of the PM element from the IP theory for different approaches and with replication of it in the agents that holds part of the energy cogeneration as: seedling grower, sugarcane grower and milling. The field research seeks investigating the practices of the PM element, the product and QM requirements that are used on these agents.

The method of research planning for the conduction of the field research has three topics and five steps is showed on the Table I. Each step is identified by the letter "S".

The elaborated research protocol aimed at, in overall way, to investigate the following questions:

- What are the main quality product and QM requirements for energy cogeneration from byproducts of sugarcane (leaves and bagasse)?
- What practices of the PM element on these agents (seedling grower, sugarcane grower and milling) are executed?

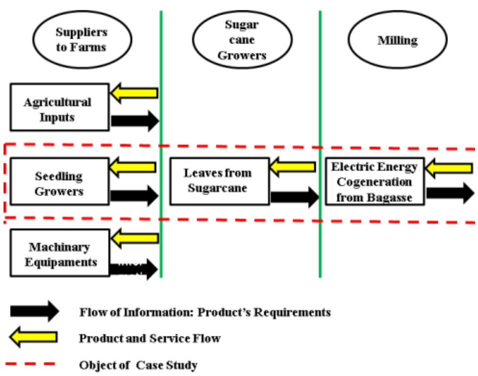

Figure 1. Production chain of cogeneration from bagasse and leaves of sugarcane.

The interviews were conducted on the seedling and sugarcane growers and quality coordinator of the milling plant.

IV. Case Studies and Proposal For Requirement's Management in the Chain

In this topic, the analysis of the results from the cases is presented. The presentation of the case study follows the topics: a brief characterization of the agents, what was found about the (PM) element and ending with the identification and description of the product and QM requirements.

TABLE I. The Research Planning Method

Topics	Steps	Description	Results for the research
Literature Review	S1	Internal process	Definition of the theory of IP, explanation of the elements PM with its practices.
Field Research	S2	Establishment of criteria for case selection.	Identification and selection of companies for cases.
	S3	Elaboration and evaluation of the research protocol.	Better understanding of themes, validation and improvement of the questionnaire.
	S4	Conducting the interviews.	Field verification of the practices of the PM elements of the IP theory for the cases.
Analysis of Results	S5	Case report, cases analysis and solution proposal.	Comparative analysis of the existing practices and the missing ones investigated in the cases. Proposal solution.

Besides, a model is elaborated to manage the quality requirements in this chain.

A. Seedling Grower

The grower develops seedlings of commercial varieties with genetic and phytosanitary purity of early, medium and late maturation to be able to meet the total harvesting period from the beginning of April to November of each year.

1) Process Management

The development stages of the varieties of seedlings follow a standard with agronomic and phytosanitary characterization, whose analysis in comparison with the standard varieties defines discarded or released as new cultivars. In the validation process of the cultivars, statistical tests are performed in at least eight different regions in order to better adapt the cultivar to a given agricultural area.

The processes of obtaining the seedlings follow standardization with control and when any deviation occurs, it is evaluated, which can be discarded or maintained. However, actions plan is more corrective than preventive.

2) Seedling's Requirements

The development of a certain cultivar's attribute is based on a market need. If it needs for energy cogeneration, the seedling's grower develops varieties that contain 24% of fiber. The goal of the seedling's developer is to balance the attributes of sucrose and fiber contents in cultivars, as there is a negative correlation between these parameters, that is, by increasing the sugar content of the cultivar, the fiber content of the cultivar is decreased and vice versa.

The Brazil governmental requirements for the release of a new variety is based only on a morphological characterization of the sugarcane (color, stem diameter etc.). On Table II, follow the found QM requirements necessary to meet the requirements of the seedlings on its production phases.

B. Sugarcane Grower

The grower produces approximately 600,000 tons of sugar cane per year. This being its main product, however, it is also a supplier of straw, a byproduct of the sugarcane harvesting used for cogeneration of electricity in a milling plant near his farm.

TABLE II. QM REQUIREMENTS TO SEEDLINGS

Seedling Production		
Grower's production process steps	**QM Requirements**	**Product's Requirements**
Crossing	Construct a database containing the characterization of the whole germplasm.	Use on different soil condition.
	Test the germline capacity of caryopses.	Seeding production with capacity of germination.
Seeding	Meet good seedling production practices.	Ensuring sprouting and agronomic characteristics of seedlings.
Transplanting	Respect from 3 to 5 centimeters tall seedlings.	Tall of seedlings.
	Weekly pruning.	Decrease leaf perspiration.
	Get good stapling.	Need for plants with compaction and profiling.
Selection	Achieve natural field conditions such as: soil tillage, furrow spacing.	Meet the agronomic characteristics.
Multiplication	Phytopathological tests of coal and mosaic and technological analyses.	To be approved on phytopatological tests.
	Obtain the correct rate of: Brix of broth, POL% of broth, POL% of cane and fiber %.	Necessity of agronomic characteristics of seedlings.
	Perform tests in different climates.	Seedlings need to adapt on different climates.
	Perform heat treatment on seedlings.	Control of ratoon stunting disease on seedlings.
Commercial testing	Perform test of health risks.	Seedlings need to be free of health risks.

1) Process Management

Sugarcane harvesting is mechanized. The harvester cuts the sugar cane slices into pieces and deposits them in a container automatically. It removes green and dry straw and releases them into the soil automatically.

The straw baling process can be "without chipping" in which the straw left by the harvester is used. This process is characterized by less dense bales. Another baling process is "with chipping" in which a baling machine is used in order to bite the straw before baling it, which generates denser bales. Consequently, the grower receives a higher profit when compared to baling with straw "without chipping", due to a lower logistic cost of transporting the straw from the farm to the milling. However, the "chipping" bailing process demands a higher initial investment.

The straw bailing production processes are managed through daily monitoring and control, and any deviation in the process is reported to the responsible manager for the appropriate actions. The work process has clear instruction.

The producer makes use of a system to assist in the maintenance management of machines and equipment, called "Meta", which generates information about maintenance. The statistics are used to control the service life of parts in the maintenance department.

2) Product and QM Requirements

The moisture content and mineral impurity are the requirements demanded by the customer for the byproduct of sugarcane (straw).

On Table III, follow the found QM requirements necessary to meet the requirements of sugar cane on its production phases.

C. Milling

The main function of the sugarcane milling process is to extract the sugars (broth) through crushing. From this process, broth is obtained for the production of sugar and ethanol, while bagasse, the byproduct of this process, is sent to the boilers to generate electricity, which is used for the internal consumption of the milling plant and for electricity sale to concessionaires as well. Cogeneration can also be carried out by burning straw from the sugarcane harvest.

TABLE III. QM REQUIREMENTS TO SUGARCANE STRAW.

Sugarcane Grower		
Grower activities	**QM Requirements**	**Product's Requirements**
Soil preparation and cultural treatments	Application of the correct dosage of limestone and plaster for soil correction.	Greater vegetation and tillering
	Application of the correct amount of fertilizers and insecticides.	
Planting	Choice of variety with hither fiber content and tillering.	Greater vegetable impurity.
Baling (with and without chipping)	Soil humidity less than 15%.	Straw humidity below 15%.
	Proper adjustment of the harvester's cutting base.	Less mineral impurity of straw.

1) Process Management

There are criteria to manage and control the plant's automated cogeneration processes, which have clear work instructions through Standard Operating Procedures (SOP). Deviations are monitored and measured by laboratory analysis and the information obtained is sent via intranet "online" to those responsible for the industrial manufacturing process in order to take appropriated corrective actions.

The plant makes use of preventive and predictive maintenance procedures.

2) Cogeneration's Requirements

As for the bagasse, its moisture is analyzed, which is essential for the process of burning the bagasse by the boiler. The sugar content is also analyzed, the less sugar the bagasse contains, the better the extraction of the mill is. Bagasse analyzes are used to calculate the extraction efficiency.

On Table IV, follow the QM requirements necessary to meet the found requirements of the cogeneration on its production phases.

TABLE IV. QM REQUIREMENTS TO COGENERATION PROCESS.

Ethanol		
Milling's ethanol production steps	**QM Requirements**	**Ethanol's Requirements**
Sugarcane juice treatment	Obtaining the correct Ph range correction in sugarcane juice	Ph range
	Polymer dosage control in sugarcane juice	Residual lead and iron rates
Fermentation of sugarcane juice	Brix control of must	Alcohol rate
	Dosing control of sulfuric acid	Ph; Residual lead and iron rates; electric conductivity rate
Distillation	Ph range control	Ph range
	Alcohol level control	Alcohol rate
	Total acid control	Total acidity rate
	Electric conductivity control	Electric conductivity rate

D. Management Proposal for Cogeneration Production Chain Requirements

1) Meeting the requirements

All the products requirements of the cogeneration production chain must be accomplished by each one of its agents (seedling grower, sugarcane grower and milling). Then, the quality of these process needs of a management that enables the attainment of these requirements identified based on the practices of the PM element of the (IP) theory in the cogeneration production chain.

The investigation showed that in all of the agents of the field research, when applied, the following PM practices are used: use of statistical techniques, use of fool-proof for process design, use of automatic processes, use of the preventive equipment maintenance and clarity of work or process instruction. However, the PM practice of "control and improve continuously the processes" is not implemented on the agents investigated on this field research. It was evident a lack of a culture of continuous improvement on all the agents of the cogeneration chain investigated.

To perform this gap, a Quality Management (QM) proposal is presented, which seeks to solve the lack of a continuous improvement culture in the agents that forms the cogeneration production chain. This model, once implemented, could help the main agents of this chain attain the product quality requirements, having the PM practices, as a basis for the implementation of the proposal.

An illustration of the proposal to manage the product requirements in the cogeneration production chain is shown on Fig. 2.

The proposal is based on meeting the product requirements demanded by customers in the cogeneration production chain (yellow arrows). To meet these requirements, suppliers must meet the QM requirements (orange arrows). If at each stage of cogeneration production, the requirements of QM are met (blue arrows), consequently the product requirements of the agents will be met (green arrows).

Product requirements must be defined for all agents in the production chain in order to develop and produce products that meet customer needs. These requirements are obtained both from regulatory agencies and by specifications of chain customers.

QM requirements must be defined and specified for each agent to meet the cogeneration product requirements. These requirements are those used and necessary for the definition of the management procedures with the objective of achieving the expected quality of the product, also contemplating the reduction of costs and losses in cogeneration production from biomass.

2) Process Management (PM)

The execution of the practices of the PM element is a basis to support the quality management model.

In order to meet the PM element practices at the cogeneration production chain, discussed in the previous topic, it is necessary to identify, investigate and update these practices in order to improve transparency and trust among the agents of the chain through actions that

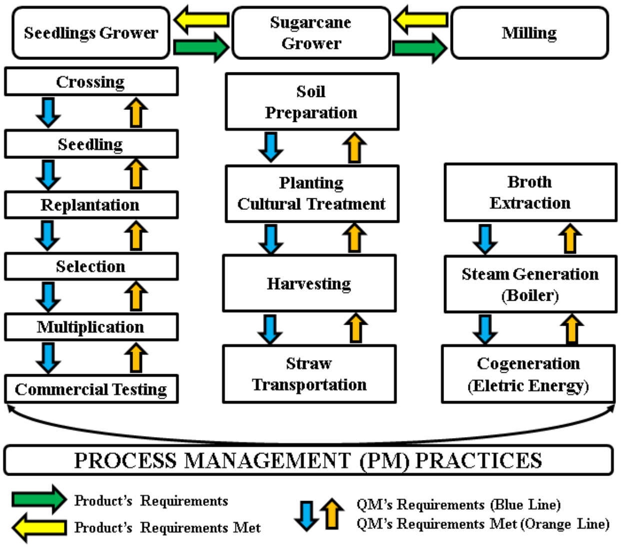

Figure 2. Illustration for managing the product requirements of the cogeneration production chain.

compliance with QM requirements. This is to improve product quality and efficiency in the activities of the cogeneration production chain. An evaluation of the PM practices regarding their effectiveness in the timeline should be undertaken. If they are effective, they should be maintained. If they are ineffective, the cause of ineffectiveness must be identified and eliminated. On Fig. 3 is shown a flowchart that assists in the evaluation of PM element practices.

V. Conclusion

The PM element from IP theory and its main practices were identified in the literature. The empirical research of multiple cases investigated the use of the practices of this element in the cogeneration production chain. The product requirements were identified on the agents of this chain as well QM requirements demanded by each (IP) of the agents. The main deficiency identified in relation to the agents was the lack of quality preservation actions to lead to continuous improvement actions. To fill this gap and to meet the requirements of the chain, a model was proposed in order to establish a flow

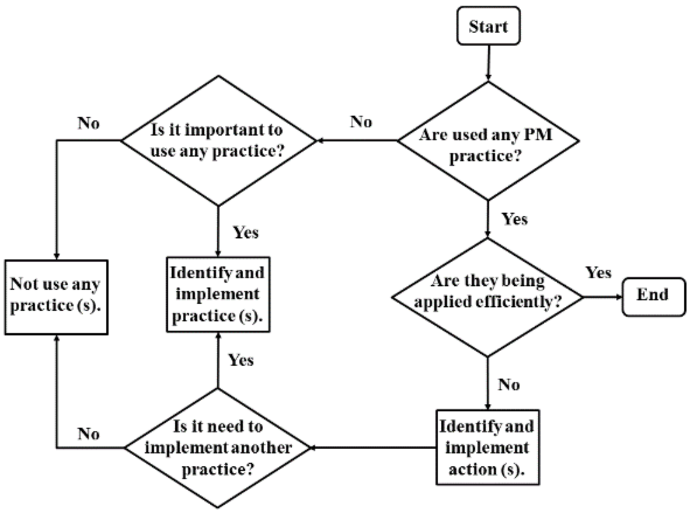

Figure 3. Flowchart of the information flow of the practices of the PM element.

of information to meet the QM requirements, based on the PM practices that support it. This proposal could corroborate the improvement on the quality of product requirements among agents in the cogeneration chain, which could result on the attainment of the products requirements of the agents.

The main objective of this work, which is to present a proposal to manage the requirements of the cogeneration chain, was performed. However, the proposal does not address aspects related to the external activities of this chain. This is a suggestion for a future work.

ACKNOWLEDGMENT

To the Federal Institute of Education, Science and Technology of São Paulo, Catanduva-SP.

REFERENCES

[1] Sampaio, P., Carvalho, M. S., Fernandes, A. C., Quang, H. T., An, D. T. B., & Vilhenac, E. (2016). An extensive structural model of supply chain quality management and firm performance. *International Journal of Quality & Reliability Management 33*(4).

[2] Prajogo, D., Toy, J., Bhattacharya, A., Oke, A., & Cheng, T. C. E. (2018). The relationships between information management, process management and operational performance: Internal and external contexts. *International Journal of Production Economics, 199*, 95-103.

[3] Chiarini, A., & Vagnoni, E. (2015). World-class manufacturing by Fiat. Comparison with Toyota production system from a strategic management, management accounting, operations management and performance measurement dimension. *International Journal of Production Research, 53*(2), 590-606.

[4] Gunasekran, A., Patel, C., & McGaughey, R. E. (2004). A framework for supply performance measurement. *International journal of production economics, 87,* 333-347.

[5] Brusset, X. (2016). Does supply chain visibility enhance agility?. *International Journal of Production Economics, 171,* 46-59.

[6] Chow, W. S., & Lui, K. H. (2003). A structural analysis of the significance of a set of the original TQM measurement items in information systems function. *Journal of computer information systems, 43*(3), 81-91.

[7] Robinson, C. J., & Malhotra, M. K. (2005). Defining the concept of supply chain quality management and its relevance to academic and industrial practice. *International journal of production economics, 96*(3), 315-337.

[8] Kaynak, H. (2003). The relationship between total quality management practices and their effects on firm performance. *Journal of operations management, 21*(4), 405-435.

[9] Ho, D. C., Duffy, V. G., & Shih, H. M. (1999). An empirical analysis of effective TQM implementation in the Hong Kong electronics manufacturing industry. *Human Factors and Ergonomics in Manufacturing & Service Industries, 9*(1), 1-25.

Assessment of Renewable Electricity Generation in Low and High Income Countries

Ivana Veličkovska

Mathematical Institute SANU, Knez Mihailova 36, Belgrade, Serbia,
ivana993@turing.mi.sanu.ac.rs

Abstract—**Directing electricity production towards renewable energy sources has been attractive topic in energy literature for years. The role of renewable energy sources in a modern society that is technologically advanced is very important due to the constant growth of the electricity demand. In the process of developing the use of renewable energy sources, European countries are more or less successful. Therefore, the subject of this research is reflected in the assessment of electricity production from renewable energy sources in relation to the total electricity production and the economic development. The survey refers to 35 European countries that are distributed according to the level of GDP and data have been gathered for the period from 2004 to 2018. For the purposes of the analysis, the Autoregressive Distributed Lag (ARDL) model was applied, which determines the short-run and long-run impact of the regressors on the dependent variable. The obtained ARDL model in the short run indicates on a high reliability that exceeds 99.9%. In the long-run, the model highlights total energy consumption from renewable energy sources as a variable that has a significant long-run effect on the production of electricity from renewable energy sources.**

Keywords – renewable electrical energy, electrical energy supply, autoregressive distributed lag

I. INTRODUCTION

Accelerated progress of the modern society brings numerous challenges, among which is the problem of using conventional sources of electricity generation. Electricity is one of the fundamental resource for economic development [1]. In order to reduce the production of electricity from conventional energy sources and reduce consumption, governments of most of the countries have directed their energy policies towards the introduction of renewable energy sources that are sufficient to ensure the electrical energy supply. EU’s considers transformation of the electricity generation sector as the main task in developing energy policy [2]. Developed countries are already moving towards renewables by targeting high future shares of the renewable energy sources. EU’s regulation regarding energy and climate plan to 2030 is committed to reduce 40% of the greenhouse gas emissions, reach the share of 32% of renewables and increase energy efficiency for 32.5% [3]. However, the long-term strategy until 2050 predicts net-zero greenhouse gas emissions in the EU [4]. Therefore, Germany’s energy target as a part of the EU long-term energy strategy is to reach 100% renewable electricity supply by 2050 [5]. Hence, the realization of this target is coordinated by adapting national energy plan and corresponding regulations. On the other side, Finland’s energy and climate plan predicts 2035 as the target year for becoming carbon neutral society [6]. While Denmark’s government has set ambiguous target of increasing the share of renewables in the total energy consumption for 55% until 2030 [7]. Proceeding with energy plans in terms of renewable electrical energy (REE) needs to be supported by numerous researches that investigate the effects of different factors on the REE trends [8]. Therefore, the main goal of this survey was to explain the nature of the short-run and long-run cointegration among REE and observed variables by means of electrical energy indicators and renewable energy data. The most fitting methodology for fulfilling this research objective was Autoregressive Distributed Lag

TABLE I. ASSESSED DATA AND SOURCES.

Label	Indicator name	Unit	Source
Total_REG	Total renewable electrical energy generation	Ktoe	[10]
Total_EG	Total electrical energy generation all sources	Ktoe	[10]
Gross_REC	Gross final consumption of energy from renewable sources	Ktoe	[10]
EC	Electrical energy consumption	MWh	[11,12]
GDP	GDP per capita	US$	[13]

(ARDL) model. ARDL methodology is successfully applied in discovering short-term and long-term influence of various factors on the development trend of a certain phenomenon [9]. The data have been analysed from the European perspective of REE generation in the framework of countries' economic development. The expected scientific contribution of the study is to reveal the nature of the REE trend and acknowledge the most prominent variables that shape this trend. The research outcome could be valuable for considering the implementation effectiveness of European national energy plans.

II. RESEARCH DATA AND METHODOLOGY

Developing bound's testing for REE generation required employing several data sources. For constructing a coherent database, five different variables dating from 2004 to 2018 were gathered. The survey considered 35 European countries that were divided according to their incomes into high-income and low-income countries. Considered low-income countries were Bulgaria, Romania, Montenegro, Serbia, Albania, North Macedonia and Bosnia and Herzegovina, while the rest of the countries were added to the high-income group. Summarized definitions of indicators that were used in the study are presented in the Table I.

A comprehensive overview of the data provided the information about the top five consumers of electrical energy according to the data from 2018 that are Iceland (54.6 MWh), Norway (24.1 MWh), Finland (15.8 MWh), Sweden (13.5 MWh) and Luxembourg (13.3 MWh). The largest consumers are technologically advanced economies.

Fig. 1 and Fig. 2 are graphical representation of the average REE generation and gross final consumption of energy from renewable sources in the considered timespan. The trend of REE generation is fluctuating and the data depend on the observed country. Fig. 1 points out developed countries like Denmark, Greece, Spain, France, Sweden that achieved high REE, with Germany and Norway as leaders. Fig. 2 illustrates energy consumption from renewables. The similarity between those two trends demonstrate that electrical energy is the major form of energy from renewable sources.

Methodological approach that has been used in the study is ARDL. ARDL models are frequently used in recent studies that investigate short run and long run relationship among dependent and regressor variables. The methodology has been introduced by [14]. References [15] and [16] give detailed computational procedure for ARDL models.

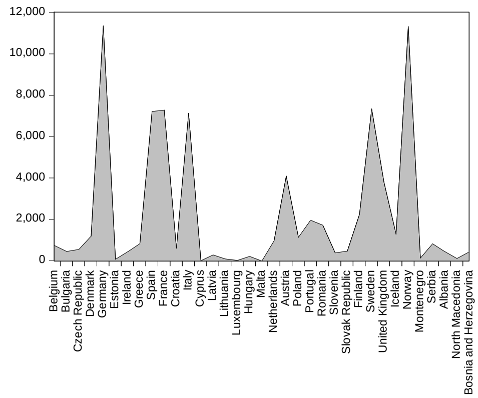

Figure 1. Total renewable electricity generation [10].

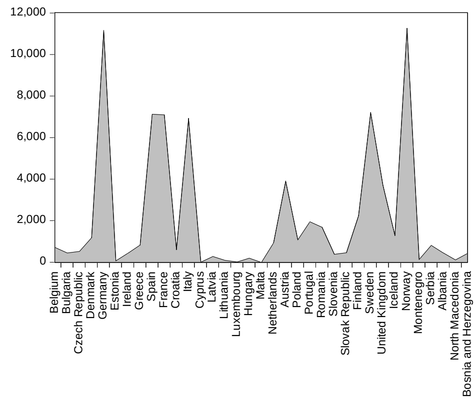

Figure 2. Gross final consumption of renewable energy [10].

ARDL methodology is often used in research problems in energy sector. It was proven to be a suitable method for assessing the long-run cointegration among electricity consumption and economic growth in 11 MENA countries [17]. Moreover, ARDL bound testing approach has been applied to investigate the long-run cointegration among renewable electricity consumption, direct foreign investments and economic growth in Egypt [18]. The outcome of the estimations presented the existence of positive long-run cointegration of electricity consumption and direct foreign investments with economic growth. Another study explored the cointegration between carbon emissions, energy consumption and industrial growth by employing ARDL [9]. Furthermore, a recent survey confirmed the positive cointegration between increasing the use of renewable energy sources to secure energy stability and protect the environment [19].

III. RESULTS AND DISCUSSION

Before estimating an ARDL model several statistical measures should be calculated and their values should be checked. The outcome of descriptive statistics is presented in the Table II and is considering mean, median, maximum and minimum, standard deviation, skewness and kurtosis. The difference between minimum and maximum values for considered countries is high and can be explained in terms of large deviations in recorded renewable and non-renewable electricity generation, electricity consumption and GDP in developing and developed countries.

The nature of the relationship among variables is described using correlation. The computational outcome of the correlation is presented in the Table III. By looking at the results of comparison between dependent variable total renewable electricity generation and other regressor variables the highest correlation is achieved with gross final consumption of renewable energy (r=0.999). More specifically, increase in final consumption of renewable energy leads to increase in REE generation. Another significant relationship is achieved between REE generation and electricity generation from all sources (r=0.786). The analysis also indicates high positive correlation between GDP per capita and electricity consumption (r=0.572) meaning that economic growth follows increase in electrical energy demand and opposite.

The problem of heteroscedasticity is often present in researches that include time series data. Several methods are used to examine heteroscedasticity. In this case, to prevent any computational errors, a Breusch-Pagan-Godfrey test for discovering heteroscedasticity was performed.

The results of the test are described in the Table IV and are reporting acceptable value of the Chi-square probability of ($p<0.05$) for the observed coefficient of determination meaning that the problem with the heteroscedasticity was overcame.

TABLE II. DESCRIPTIVE STATISTICS.

	TOTAL_REG	TOTAL_EG	EC	GROSS_REC	GDP
Mean	2215.509	8591.270	7.758705	2174.830	30329.27
Median	746.4679	3258.814	5.426667	718.1242	22799.28
Maximum	11359.04	51766.02	47.28667	11272.23	103941.2
Minimum	4.326465	197.2754	1.926667	4.326465	3984.193
Std. Dev.	3204.473	12650.79	8.170356	3154.527	23495.00
Skewness	1.728322	2.128092	3.623872	1.746325	1.147097
Kurtosis	4.814117	6.731775	17.16438	4.899211	4.223669
Observations	35	35	35	35	35

TABLE III. CORRELATIONS.

	TOTAL_REG	TOTAL_EG	EC	GROSS_REC	GDP
TOTAL_REG	1				
TOTAL_EG	0.786	1			
EC	0.239	-0.016	1		
GROSS_REC	0.999	0.782	0.243	1	
GDP	0.421	0.225	0.572	0.422	1

TABLE IV. HETEROSKEDASTICITY TEST.

F-statistic	1.994818	Prob. F(11,19)	0.0898
Obs*R-squared	16.61415	Prob. Chi-Square(11)	0.1198
Scaled Explained SS	12.59792	Prob. Chi-Square(11)	0.3204

In order to define the short run effect of the regressor variables on the renewable electricity generation, ARDL model was employed. The selection of the optimal number of lags for each dependent and regressor variable was automatically determined and the number of lags equal to four. Method for model selection was Hannan-Quinn criterion and the total number of models that have been evaluated is 2500. The estimation outcome of the ARDL model is presented in the following Table V. The final selected model is described as ARDL (1, 4, 1, 0, 1). Probability for selected variables is below 5%, meaning that all variables are statistically significant. Calculated values for T-statistics for selected regressor variables are in their absolute form above 2 and within the limit value. Performance indicators of the constructedmodel point out on a high value of coefficient of determination (R^2=0.9999). Reported coefficient of determination highlights the potential of investigated regressor variables to explain the variation of the electricity generation from renewable sources.

Fig. 3 is illustrating how strongly the selected model is preferred over the other models. The lowest value of Hannan-Quinn criteria is the preferred value.

The outcome of the investigation of short-run effects is acceptable so the ARDL estimation was analyzed to discover the long-run effects of the regressor variables. For that purpose the cointegration test and bounds test were performed. As expected, the outcome of the performed bounds testing presented in the Table VI is indicating that the F-statistics value (F=43,796.53) is higher than the lower I(0) and upper I(1) bounds critical values at significance at 5% and is confirming the long-run cointegrating relationship among investigated variables.

TABLE V. ARDL MODEL SUMMARY.

Variable	**Coefficient**	**Std. Error**	**t-Statistic**	**Prob.***
TOTAL_REG(-1)	0.010977	0.004825	2.275022	0.0347
TOTAL_EG	-0.002200	0.001334	-1.648873	0.1156
TOTAL_EG(-1)	-0.002196	0.001067	-2.057623	0.0536
TOTAL_EG(-2)	0.000649	0.000466	1.391485	0.1802
TOTAL_EG(-3)	-0.000505	0.000461	-1.095974	0.2868
TOTAL_EG(-4)	-0.001002	0.000454	-2.205404	0.0399
EC	-1.183314	0.910782	-1.299228	0.2094
EC(-1)	-7.056834	1.779222	-3.966246	0.0008
GROSS_REC	1.028221	0.005776	178.0101	0.0000
GDP	0.000400	0.000327	1.223262	0.2362
GDP(-1)	0.000986	0.000350	2.815608	0.0110
C	20.96063	14.44593	1.450972	0.1631
R-squared	0.999949	Mean dependent var		2405.442
Adjusted R-squared	0.999919	S.D. dependent var		3361.683
S.E. of regression	30.25787	Akaike info criterion		9.942035
Sum squared resid	17395.23	Schwarz criterion		10.49713
Log likelihood	-142.1015	Hannan-Quinn criter.		10.12298
F-statistic	33662.25	Durbin-Watson stat		1.477565
Prob(F-statistic)	0.000000			

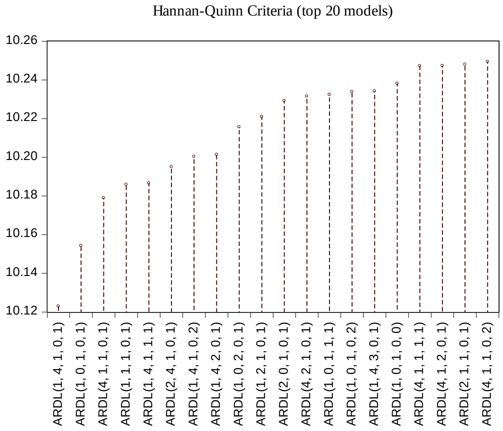

Figure 3. Top 20 models by Hannah-Quinn criteria.

TABLE VI. SUMMARIZED RESULTS OF THE BOUNDS TEST.

Test Statistic	Value	Significance	I(0)	I(1)
F-statistic	43796.53	10%	2.2	3.09
k	4	5%	2.56	3.49
		2.5%	2.88	3.87
		1%	3.29	4.37

The most important results of the cointegration test are presented in the following Table VII. Probability values for the regressor variables that are lower than the limit value of 5% indicate the long-run relationship with the dependent variable. By looking at the results of the cointegration, all examined regressor variables in the constructed ARDL model are statistically significant ($p<0.05$) meaning that each particular regressor variable achieved the long-run relationship with the dependent variable. Furthermore, the integral part of the cointegration test is coefficients calculation that was used to construct model equation for estimating European total renewable electrical energy generation.

TABLE VII. SUMMARIZED RESULTS OF THE COINTEGRATION TEST.

Variable	Coef.	t-Stat.	Prob.
TOTAL_EG	-0.0053	-2.1288	0.0466
EC	-8.3316	-4.1391	0.0006
GROSS_REC	1.0396	104.0937	0.0000
GDP	0.0014	2.7030	0.0141
C	21.193	1.4486	0.1637

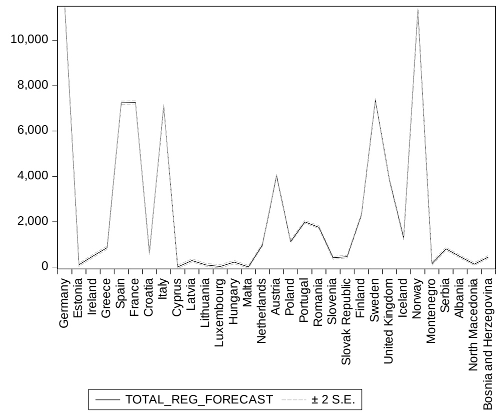

Figure 4. Forecast of the total renewable electricity generation.

Next Fig. 4 is illustrating the effectiveness of the estimation model described in the previous Table VII. The forecasted trend closely follows the realized renewable electricity generation data with ±2 standard error. The calculated root mean squared error (RMSE) for the estimated model equals to 23.73, mean absolute error (MAE) equals to 16.46, while mean absolute percent error (MAPE) equals to 5.89.

The outcome of the realized cointegration testing performed on four regressors demonstrated the statistically significant variables. With the probability of 99.99%, the short-run trend of total electricity generation from renewables can be explained using regressor variables TOTAL_EG, EC, GROSS_REC and GDP. Empirical evidence from the ARDL analysis showed that 1% increase in electricity consumption would lead to decrease in renewable electricity generation by -7.056834% in a short-run. Another important short-run outcome describes the relationship between renewable energy consumption and renewable electricity generation as positive and underlines that 1% increase in renewable energy consumption leads to 1.028221% increase in renewable electrical energy generation.

The long run results suggest that 1% increase in total electrical energy generation follows decrease in electrical energy generation from renewables for -0.0053%. Derived results showed that majority of the investigated countries are not using enough renewable sources in producing clean electrical energy so increase in total electrical energy generation is related to decrease in renewable electrical energy generation. Additionally, empirical evidence imply on a negative long-run cointegration between electricity consumption per capita and renewable electricity generation, where 1% increase of electricity consumption leads to decrease in renewable electrical energy generation by -8.3316%. The two analyzed regressors indicate that governments of investigated countries should target their energy policies and tax policies towards more challenging goals such as further increase in the share of renewable energy sources. This is highly important in developing countries in Balkans such as Serbia and North Macedonia that record low renewable electricity generation. Two Balkan countries that record high renewable electrical energy generation are Albania and Montenegro. In 2018, Albania covered approximately 92% of electrical energy production from renewable energy sources with annual electricity consumption of 2.3 MWh that is considered as the lowest electricity consumption per capita in Europe. On the other side, Montenegro recorded a bit lower percentage of renewable electrical energy generation that equals to 52% of the total electricity production followed by 4 MWh electricity consumption per capita. However, low renewable electrical energy production is also a challenge in some developed countries like Cyprus, Luxembourg, Hungary and other similar economies to generate and consume low amount of renewable electrical energy. For example, Luxembourg is one of the country with high electricity consumption per capita (average consumption is ≈13 MWh) and less than 10% of the total electricity generation is from renewable sources. However, Luxembourg is ranked as the European country with the highest GDP per capita in 2018. In favor of increasing renewable energy is the positive relationship between the final consumption of renewable energy and electricity generation from renewable sources where 1% increase in final consumption of renewables leads to 1.0396% increase in generating renewable electrical energy.

Another important precondition for generating and consuming large amount of renewable electrical energy is how a particular economy is developed. Dataset for low and high-income countries suggests that the use of renewables is more likely in developed countries with high GDP per capita than in developing countries with low GDP. Leaders in consuming renewable energy in Europe are economies with GDP per capita higher than 40,000 US$. Increase of 1% in GDP per capita, the electricity generation from renewable sources increases in 0.0014%. Significance of producing renewable electrical energy is also recognized in developed economies such as Iceland and Norway that are trendsetters in this field. The two mentioned economies are the only developed countries in Europe that satisfy their total electrical energy demand from renewable sources making them pioneers in introducing renewable electricity generation. Data for 2018 showed that the supply of electrical energy in Iceland is 98.5% secured from the renewable sources, while Norway exceeds electrical energy supply from renewable sources by 106.82%. The largest European producer of electrical energy is Germany with production volume higher than 50 thousand Ktoe every year. The second largest producer is France, another developed economy whose electricity generation exceeds 44 thousand Ktoe every year. Germany as the largest electrical energy producer is covers around 38% of total electricity generation from renewable sources. Even though France is second ranked electricity producer in Europe, only 21% is generated from renewable energy sources. Therefore, it is necessary to adopt adequate government's measures in the form of incentives for using renewables in generating electrical energy. The governments of countries with low renewable electricity generation should provide appropriate financial boost to motivate producers to make clean electrical energy and on the other side should intervene in high-energy consuming industries to start using renewables.

IV. Conclusion

Production of electrical energy obtained from renewable sources in Europe grows day by day. The greatest growth trend was registered in countries with strong economy like Germany that improved its REE generation result for more than 14 thousand Ktoe in 2018 in respect to the initial observed year 2004. This successful outcome is supported by proper energy policy and strong government's role in arranging the legislation in energy sector. Furthermore, efforts that were devoted to enhance REE generation in Germany can be used as an example for benchmarking other countries with one of the best representative in the energy field. When comparing data from 2004 and 2018 Poland has the largest increase in electricity generation among high-income countries while UK has drastically decreased its electricity production.

Luxembourg has the significant decline of electrical energy consumption in the end of the considered timespan for -2.8 MWh per capita while Iceland has increased its electricity consumption for 26.4 MWh per capita for the last15 years. The decline of electrical energy consumption in Luxembourg is followed by the highest increase in GDP among high-income countries when comparing 2004 and 2018.

The data for low-income countries discovered great differences among high-income and low-income economies. The low-income economies are small-scale producers and consumers of REE. The leader in REE generation in this group of countries is Romania that has expanded its REE generation for more than 800 Ktoe in 2018 in respect to the 2004. Romania is also superior in the growth of electricity generation and incomes. Even Romanian's economy has increased, the growth was followed by 0.5 MWh per capita in electricity consumption that is far less than other countries. The lowest score in REE generation is associated with North Macedonia that has increased its REE generation outcome for less than 100 Ktoe in in 2018 as for 2004, with the same electricity consumption per capita that equals to 3.1 MWh per capita. Montenegro expressed the highest growth of electricity consumption per capita of five MWh when comparing 2004 and 2018.

In order to increase the use of renewable energy sources it is necessary to work on improving energy policy and provide monetary incentives in industry and households. Initiating energy projects with the aim of increasing the production and consumption of electricity from renewable sources provides possibility to influence the structure of electricity consumption. This would increase awareness of the importance to use clean electricity in both private and public sectors. Future research may include additional parameters that be useful in carrying out a more detailed comparison of electricity generation from renewable sources.

Acknowledgment

This work was supported by the Serbian Ministry of Education, Science and Technological Development through Mathematical Institute of the Serbian Academy of Sciences and Arts.

References

[1] Gurgul, H., & Lach, Ł. (2012). The electricity consumption versus economic growth of the Polish economy. *Energy Economics, 34*(2), 500-510.

[2] Bianco, V., Driha, O. M., & Sevilla-Jiménez, M. (2019). Effects of renewables deployment in the Spanish electricity generation sector. *Utilities Policy, 56*, 72-81.

[3] European Comission. *2030 climate and energy framework*. Available at: https://ec.europa.eu/clima/policies/strategies/2030_en#tab-0-0. Accessed on: 15.09.2020.

[4] European comission. *2050 long-term strategy*. Available at: https://ec.europa.eu/clima/policies/strategies/2050_en. Accessed on: 15.09.2020.

[5] European Comission. *Germany's Integrated National Energy and Climate plan.* Available at: https://ec.europa.eu/energy/sites/ener/files/documents/de_final_necp_main_en.pdf. Accessed on: 16.09.2020.

[6] European Comission. *Finland's Integrated Energy and Climate Plan*. Available at: https://ec.europa.eu/energy/sites/ener/files/documents/fi_final_necp_main_en.pdf. Accessed on: 16.09.2020.

[7] European Comission. *Denmark's Integrated Energy and Climate Plan*. Available at: https://ec.europa.eu/clima/sites/lts/lts_dk_en.pdf. Accessed on: 16.09.2020.

[8] Pablo-Romero, M. P., Sánchez-Braza, A., & Galyan, A. (2020). Renewable energy use for electricity generation in transition economies: Evolution, targets and promotion policies. *Renewable and Sustainable Energy Reviews*, 110481.

[9] Rahman, M. M., & Kashem, M. A. (2017). Carbon emissions, energy consumption and industrial growth in Bangladesh: Empirical evidence from ARDL cointegration and Granger causality analysis. *Energy Policy, 110*, 600-608.

[10] Eurostat. Available at: https://ec.europa.eu/eurostat/web/energy/data/shares. Accessed on: 01.09.2020.

[11] World data bank. Available at: https://data.worldbank.org/indicator/EG.USE.ELEC.KH.PC?view=chart. Accessed on: 01.09.2020.

[12] International Energy Agency. Available at: https://www.iea.org/data-and-statistics?country=BELGIUM&fuel=Electricity%20and%20heat&indicator=ElecConsPerCapita. Accessed on: 01.09.2020.

[13] World data bank. Available at: https://data.worldbank.org/indicator/NY.GDP.MKTP.CD. Accessed on: 01.09.2020.

[14] Pesaran, M. H., & Smith, R. P. (1998). Structural analysis of cointegrating VARs. *Journal of economic surveys, 12*(5), 471-505.

[15] Rauf, A., Zhang, J., Li, J., & Amin, W. (2018). Structural changes, energy consumption and carbon emissions in China: empirical evidence from ARDL bound testing model. *Structural Change and Economic Dynamics, 47,* 194-206.

[16] Marques, A. C., Fuinhas, J. A., & Tomás, C. (2019). Energy efficiency and sustainable growth in industrial

sectors in European Union countries: A nonlinear ARDL approach. *Journal of Cleaner Production, 239*, 118045.

[17] Ozturk, I., & Acaravci, A. (2011). Electricity consumption and real GDP causality nexus: Evidence from ARDL bounds testing approach for 11 MENA countries. *Applied energy, 88*(8), 2885-2892.

[18] Ibrahiem, D. M. (2015). Renewable electricity consumption, foreign direct investment and economic growth in Egypt: An ARDL approach. *Procedia Economics and Finance, 30*, 313-323.

[19] Belaïd, F., & Zrelli, M. H. (2019). Renewable and non-renewable electricity consumption, environmental degradation and economic development: evidence from Mediterranean countries. *Energy Policy, 133*, 110929.

Optimal Allocation of Sectionalizing Switches in Smart Grid: A Problem-Solving Framework

Miodrag Forcan[1], Jovana Forcan[2], Mirjana Maksimović[3]

[1,3]University of East Sarajevo, Faculty of Electrical Engineering, East Sarajevo, BiH, miodrag.forcan@etf.ues.rs.ba[1]; mirjana.maksimovic@etf.ues.rs.ba[3]

[2]University of East Sarajevo, Faculty of Philosophy, Department of Mathematics and Informatics, East Sarajevo, BiH, jovana.forcan@ffuis.edu.ba

Abstract—**Reliability improvement of electricity supply represents one of the mandatory objectives of the future Smart Grid (SG) concept. In this paper, problem-solving frameworks for optimal allocation of Sectionalizing Switches (SS) in Distribution System (DS) are analyzed. The diversity of protection components available for SG with Distributed Generation (DG) is highlighted. The unique classification of input data sets for SS optimal allocation is proposed. Specific guidelines are recommended for the creation of a generalized problem-solving framework.**

Keywords – smart grid, sectionalizing switches, remote controlled switches, optimal allocation

I. INTRODUCTION

Distribution system (DS) reliability improvement is a mandatory task in the process of transformation towards Smart Grid (SG). The ultimate goal is to achieve the fully-automated self-healing DS. The distribution system operator (DSO) should be able to restore electricity supply automatically and fast for the majority of customers in the case of any fault event. A distribution management system (DMS) is expected to use advanced fault locating and isolation algorithms. These algorithms rely on locations of protection components that are widely geographically distributed. Fault isolation capability depends on the number of available sectionalizing switches (SS) in DS.

The selection of an adequate number of SS and their locations is a difficult task in DS planning [1]. This task requires solving a combinatorial constrained problem described by a nonlinear objective function [2,3]. Heuristic algorithms are used widely in the literature to solve the optimal switch placement problem. Since heuristic algorithms explore only a narrow region of the search space and tend to get stuck into locally optimal solutions [4], the mathematical optimization method mixed-integer linear programming (MILP) is proposed [5].

The optimal solution of SS allocation problem depends on both, economic and technical considerations. The objective is to minimize the overall costs, improve reliability indices, and satisfy all technical constraints at the same time. Various methodologies and problem-solving frameworks are proposed in the existing research papers. Consideration of SS additional possible locations on laterals is proposed recently [6]. Simultaneous placement of fault indicators (FI) and SS in DS is proposed in [7]. The impact of distributed generation (DG) is landing capabilities on the SS allocation problem is analyzed in [8-10]. Malfunction probability of SS is considered in [11]. A large diversity of the existing problem-solving frameworks in literature could be confusing, thus aggravating future research. The main objective of this paper is an attempt to create the guidelines towards a simple, clarified, and ultimate problem-solving framework, which would be based on the summary of all existing problem-solving frameworks.

The rest of this paper is organized as follows. Section II introduces the complexity analysis of the fault isolation problem in the new generation of DS. Remote-controlled SS

ISBN: 978-86-80616-07-0

are analyzed in Section III. The range of input data required for SS allocation problem solving is provided in Section IV. In Section V, the guidelines for generalized SS allocation problem-solving framework are proposed. The reliability indices and the objective function are considered in Section VI. Finally, the paper is concluded in Section VII.

II. Allocation of Protection Components in DS

In this paper, a protection component is defined as a device capable to cause a reconfiguration of DS. The most commonly used protection components are circuit breaker (CB), SS, recloser, and fuse. In the literature, previous components are often called switching devices [12]. The most common strategy to increase the reliability of DS is to install switching devices [13].

The example of modern DS with the existing protection components and possible locations of SS is presented in Fig. 1. Typical modern DS main feeders are constructed with ring topologies to enable alternative power supply using tie switches (TS). SG concept is expected to include various combinations of load and DG types. Main feeders are protected by CB in the main substation. Lateral connecting of a small hydropower plant is commonly protected using CB. A small solar power plant is often protected by its own incorporated CB, which operates whenever the voltage level drops below the acceptable limit. In general, laterals feeding loads are protected using either fuses or manual switches (MS). More often, laterals feeding industrial loads are protected with MS. Laterals protected by fuses can participate in fuse-saving and fuse-blowing schemes depending on DSO strategy. Some laterals or sub-laterals remain unprotected.

Relay protection algorithms are in charge of DS fault detection and clearing. These operate from main substations, but some DG could also be equipped with their relay protection algorithms. Reclosers are commonly used for fast restoration of power supply in the case of transient faults. In the case of a permanent fault, the main protection objective is to isolate the faulted component from the rest of the DS. Deployment of SS in main feeders enables the isolation of smaller DS area in the case of permanent faults, thus restoring the power supply to the majority of customers without a need to wait for faulted component repair. Installation of SS at every possible location is not economically justified and it is often unnecessary. Optimal SS allocation should be determined to meet DS's economical and technical requirements. However, in highly diversified SG, mainly due to DG, loads, and available protection components, this optimization problem is not an easy task and a proper problem-solving framework is required.

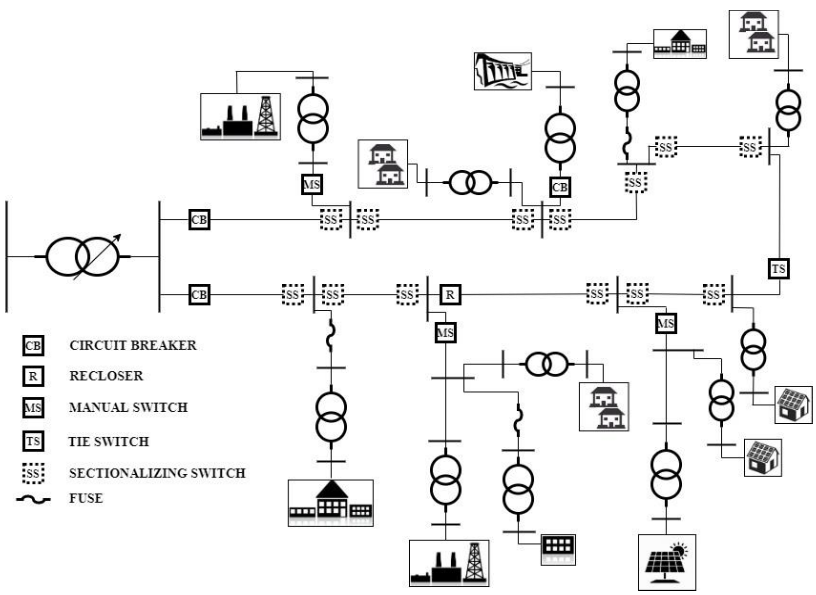

Figure 1. Protection components and possible locations of SS in distribution network with DG.

III. REMOTE CONTROLLED SWITCHES

When a fault occurs within the power distribution line, remote control of the switches to isolate the fault and restore the service is activated by the distribution automation system (DAS). Upon the occurrence of a fault in the distribution line, remote controllable switches (RCS) with communication capabilities send an alert to the operator for the localization of the fault. In this way, the physical-based distribution system model can be monitored in real-time, and switches on/off state can be modified by operators in remote control mode [14].

RCS are commonly installed on the sections of the main feeder. When SS is equipped with a transceiver it can operate shortly after the fault location is determined in such a way significantly lowering customer interruption time and consequently increasing reliability.

A. *Communication Technologies for RCS*

Among so many communication options available, electricity utilities are required to choose the most appropriate way of communication for the characteristics of distribution facilities. According to [15], the distribution automation system size and means of communication may be tailored to regional characteristics. High reliability and high-speed performance for switching operations are essential in a large-scale system in urban areas. Therefore, the optical fiber cable would be selected for the urban area. In the case of a small-scale system in a rural area that is concentrated on the low cost and downsizing structure for simple remote operation of switches, wireless and cellular communications would be a better option.

5G communications have the potential to enable high reliability and high-speed performance even in urban areas. Ultra-reliable command messaging for RCS in SG could be achieved with polar coding technology [16]. DSO can be adapted to use the future public 5G network infrastructure and in such a way reduce infrastructure and maintenance-related costs.

IV. INPUT DATA FOR SS OPTIMAL ALLOCATION PROBLEM SOLVING

The first step towards generalized problem-solving framework definition is input data availability and range analysis. Input data sets required for optimal allocation of SS problem solving are presented in Fig. 2. Input data can be divided into 4 groups according to corresponding data sources: distribution network data, load data, DG data, and SS data. The significance of every data group is explained as follows.

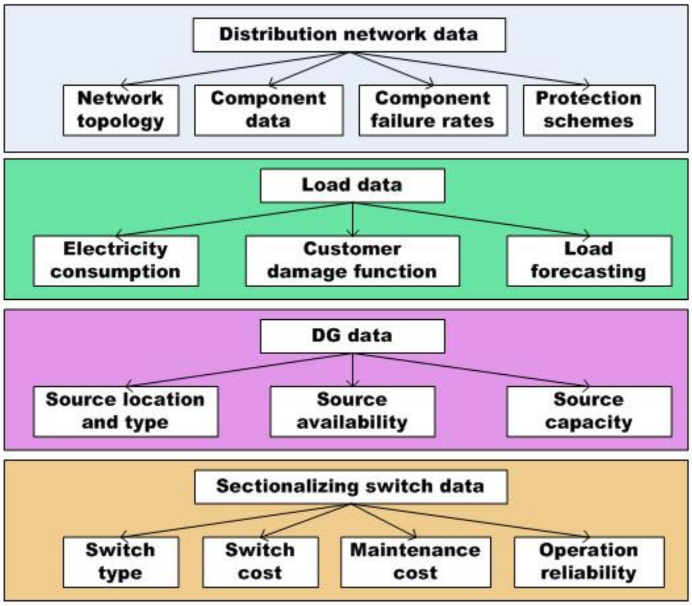

Figure 2. Input data sets required for SS optimal allocation problem solving.

A. Distribution Network Data

Network topology determines possible locations of SS. DS are mainly radially consisting of main feeders starting from the main substation. Downstream, along the feeder, there are buses (network nodes) at which laterals are connected. Load transformers are mainly connected to laterals, but sometimes they can be connected directly to the main feeder (e.g. industrial customers). Even laterals can have more than one network branch, depending on customer density and geographical constraints.

Components, such as overhead lines, cables, and transformers, enable power distribution to customers. Component data is required for state estimation and power flow calculation in the distribution network. SS operation affects loading and voltage levels of components, thus state estimation and power flow calculation should be performed after every network reconfiguration. Component data mainly consists of power, voltage, and current ratings and impedance data. Data about the types and locations of the components is required for protection schemes that affect the allocation of SS.

The component failure rate is defined as the number of component failures in the observed time interval. Failure rate values have a significant impact on the allocation of SS. If component failure rates are very high, it is more likely that the allocation of more SS will be justified. DSO should keep records of the component failures in their life-time long operation.

Data on used protection schemes is very important for optimal allocation of SS. The distribution feeder is protected by digital relays connected to circuit breakers located in the main substation. Reclosers are often used downstream to deal with transient faults that occur most frequently, thus shortening interruption times. The fuses are mainly used for the protection of laterals. The fuse blowing and the fuse saving protection schemes could be selected. Available protection devices operate in combination with SS to isolate the faulted section according to the selected protection scheme. SS optimal allocation problem solver should consider all other available protection devices and principles used in the distribution network.

B. Load Data

In addition to data on types and locations of loads in the distribution network, electricity consumption should be considered. Peak demands are of interest when considering component loading and voltage levels. Average demands are relevant for interruption cost estimations.

Customer damage function (CDF) explains the relationship between interruption duration and its customer economic losses and has a key role in interruption cost determination [17]. Interruption cost estimation is the most important factor in the analysis of profitability related to the installation of SS in DS.

Accuracy of load forecasting could have an important impact on SS optimal allocation problem since it depends on the long-term analysis (15 years ahead). It would be useful to also forecast CDF.

C. DG Data

The presence of DG in DS causes bidirectional power flows, thus affection protection schemes. Locations and types of DG should be considered first in the SS optimal allocation problem-solving. Commonly, in the case of a fault, DG is disconnected from DS by operation of its own CB. DG remains disconnected until the faulted component is being repaired. However, certain types of DG support islanding mode of operation, which could be beneficial for shortening the interruption time of selected customers in the case of permanent faults. Some types of DG could support ride-through mode of operation in the case of transient faults.

DG electricity production availability during fault event time should be also considered. Electricity production of solar and wind small power plants could be very limited during interruption time, thus they cannot be always available to supply customers.

If DG electricity production is available after fault isolation, DS islands can be formed to restore electricity supply to corresponding loads. However, islanding operation depends on DG production capacity. With higher production capacity DG could be used to restore electricity supply to more customers, thus improving reliability.

D. SS Data

There is a difference between SS types according to times required for operation. RCS enables faster fault isolation and electricity supply restoration than MS, due to communication capabilities. At the same time, RCS are more expensive when considering investment, installation, and maintenance costs. There is a trade-off between DS reliability gain and profitability, which should be analysed. A recent research paper [11] revealed the correlation between SS optimal allocation and SS malfunction probability. Operation reliability should be considered in practical DS to avoid overestimation of profitability.

V. Guidelines for Generalized SS Allocation Problem-Solving Framework

Since there are many SS allocation problem-solving frameworks, there is a need to identify and clarify relevant guidelines and methodology steps towards a generalized framework. The most relevant guidelines are analyzed in this paper and summarized in the form of a generalized framework prototype, which is presented in Fig. 3.

The very first step of every SS allocation problem-solving framework should be detailed input data range analysis. The framework would be significantly limited if input data is limited. In the next step input data, uncertainty should be considered. The statistical analysis of bad data and uncertainty indices is required. In some DS there are already SS placed on certain locations. Before further analysis it is necessary to determine initial conditions in terms of the existing SS allocation. The next important step includes the determination of the new SS number limit due to DS budget limitations. The decision on SS allocation on laterals is necessary to be made. In the case of including laterals for SS allocation, it would be required to consider the removal or adaptation of the existing protection components. To account for DG it is required to determine possible islanding areas depending on fault locations. Additional reconfiguration action sets should be identified with a goal to meet DG capacity. The next possible step is transient fault interruption consideration, which should include additional protection components, such as reclosers if they are available in DS. If both, permanent and transient fault interruptions are considered, the more precise estimation of optimal SS allocation will be achieved.

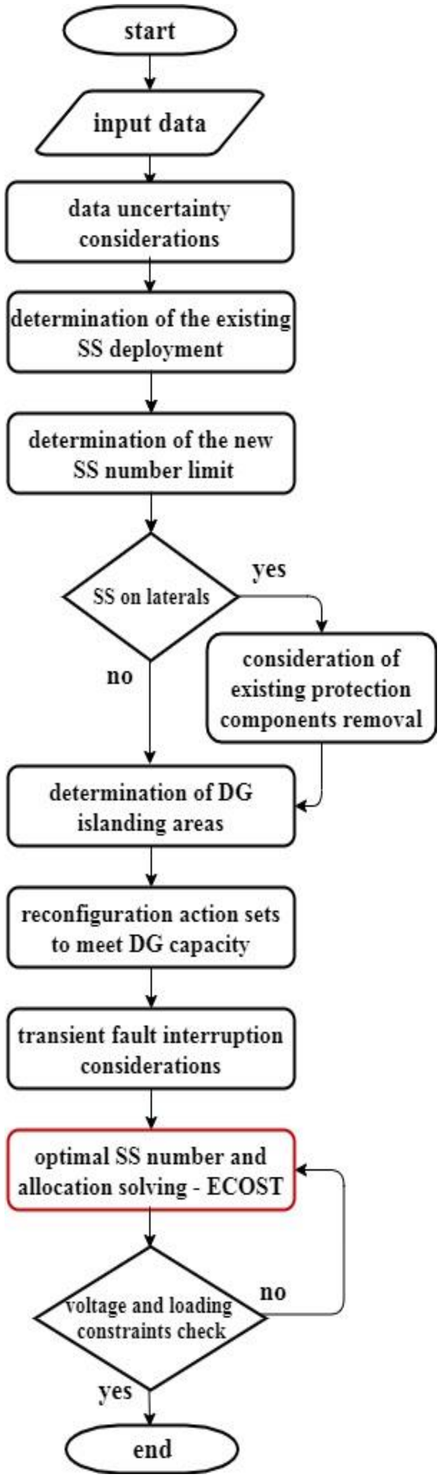

Figure 3. Generalized SS optimal allocation problem-solving framework prototype based on selected guidelines.

Following the previous steps and supporting guidelines the optimal SS number and allocation solving should be performed. The best reliability indicator should be selected and according to the majority of research papers, the most relevant indicator is System Expected Outage Cost to Customers (ECOST). The objective is to find the optimal solution which minimizes ECOST. Instead of getting the unique optimal solution, the research paper [18] proposes a multiobjective switch placement (MOSP) algorithm for solving the problem and providing multiple solutions to help DSO in dealing with the cost-reliability dilemma.

Every SS allocation solution should be analyzed for all possible fault and reconfiguration scenarios in DS to check voltage and loading constraints. Multiple power flow calculations are required to check if technical constraints are violated. In the case of unacceptable violations, it is necessary to find the second-best solution.

VI. RELIABILITY INDICATORS AND OBJECTIVE FUNCTION

In early research stages on SS optimal allocations, the following reliability indicators were used:

1) System Average Interruption Frequency Index (SAIFI):

$$SAIFI = \frac{\sum_i \lambda_i N_i}{\sum_i N_i}\ , \qquad (1)$$

where i is customer's location, N_i is the number of customers at location i and λ_i is the failure rate related to location i.

SAIFI is measured in units of interruptions per customer.

2) System Average Interruption Duration Index (SAIDI):

$$SAIDI = \frac{\sum_i U_i N_i}{\sum_i N_T}\ , \qquad (2)$$

where U_i is the annual outage time for location i and N_T - the total number of customers served.

SAIDI is often measured in minutes or hours.

Previous reliability indicators do not account for the effects of the system topology, interruption durations, load variations, equipment failure probability, and recognize the various customer types and their damage functions. The best way to quantify customer outage costs is the usage of ECOST [1]:

$$ECOST = \sum_{i=1}^{Ni}\sum_{j=1}^{Nj}\sum_{k=1}^{Nk} \lambda_i \times CDF_{i,j,k} \times L_{j,k}\ , \qquad (3)$$

where N_i is the total number of possible fault locations, N_j is the total number of load points, N_k is the total number of customer types, λ_i is an average failure rate of network component i, $L_{j,k}$ is the average load of the *k*th-type customers located at the *j*th load point and $CDF_{i,j,k}$ is customer damage function.

The cost of SS can be quantified by the following Eq. [5]:

$$SSCOST = \sum_{s=1}^{Ns} (CI_s + IC_s + MC_s) \times X_s\ , \qquad (4)$$

where N_s is the number of *SS*, CI_s is the *SS* capital investment cost, IC_s is the *SS* installation cost, MC_s is *SS* maintenance cost and X_s is a binary variable representing *SS* existence.

A. MILP Formulation for SS Optimal Allocation

The proposed MILP formulation for the SS optimal allocation in DS is defined as follows [5]:

$$\min \left[\sum_{t=1}^{Nt}\sum_{f=1}^{Nf} \left(\begin{array}{l} \frac{(1+q)^{t-1}}{(1+DR)^t} \times ECOST + \\ + \frac{1}{(1+DR)^t} \times SSCOST \end{array} \right) \right]\ , \qquad (5)$$

where N_t is the number of years, N_f is the number of feeders, *q* is the annual load increase rate and *DR* is the annual discount rate.

Objective function consists of ECOST and SSCOST. To account for transient (temporary) faults it is necessary to additionally include the corresponding interruption costs [9]:

$$ICT = \sum_{i=1}^{Ni}\sum_{j=1}^{Nj}\sum_{k=1}^{Nk}\lambda_i^T \times CDF_{i,j,k} \times L_{j,k} \quad , \quad (6)$$

where λ_i^T is temporary failure rate of network component i and $CDF_{i,j,k}^T$ is customer damage function of temporary faults.

The probability of availability and unavailability of the two-state model for DG is proposed in [9]. The probability of an island is given by [8]:

$$P_{IP} = \left(\sum_{j=1}^{Nj}(P_{GDG} \times P_{GLP_j})\right) \times (1 - P_f) \quad , \quad (7)$$

where P_{GDG} is DG probability to generate power greater than or equal to a certain level, P_{GLP} presents a load point probability to have a certain value and P_f is forced outage rate of a DG.

According to paper [9] the number of SS in the optimal solution increases as the number of DG increases.

VII. CONCLUSION

SS optimal allocation is one of the most important problems that should be analyzed in future DS since it has the potential to significantly improve reliability, which is the mandatory task in the SG concept. The complexity of DS protection with various types of protection components is emphasized in this paper. RCS's ability to improve the reliability of DS by shortening the interruption time of customers is revealed. Classification of all input data sets relevant for SS optimal allocation is proposed. Specific guidelines are recommended with the objective to create a generalized problem-solving framework. A clarification and summarization of various different proposed problem-solving frameworks are given, including consideration of transient faults and DG units. The obtained research results can be useful to DS planning departments considering the future SS investments and also to the research community attempting to create an ultimate problem-solving framework for SS optimal allocation.

REFERENCES

[1] Billinton, R., & Jonnavithula, S. (1996). Optimal switching device placement in radial distribution systems. *IEEE transactions on power delivery*, *11*(3), 1646-1651.

[2] Teng, J. H., & Lu, C. N. (2002). Feeder-switch relocation for customer interruption cost minimization. *IEEE transactions on power delivery*, *17*(1), 254-259.

[3] Tippachon, W., & Rerkpreedapong, D. (2009). Multiobjective optimal placement of switches and protective devices in electric power distribution systems using ant colony optimization. *Electric Power Systems Research*, *79*(7), 1171-1178.

[4] Abraham A., & Das S. (2010). *Computational Intelligence in Power Engineering*. Springer-Verlag.

[5] Abiri-Jahromi, A., Fotuhi-Firuzabad, M., Parvania, M., & Mosleh, M. (2011). Optimized sectionalizing switch placement strategy in distribution systems. *IEEE Transactions on Power Delivery*, *27*(1), 362-370.

[6] Izadi, M., Farajollahi, M., & Safdarian, A. (2019). Optimal deployment of remote-controlled switches in distribution networks considering laterals. *IET Generation, Transmission & Distribution*, *13*(15), 3264-3271.

[7] Farajollahi, M., Fotuhi-Firuzabad, M., & Safdarian, A. (2018). Simultaneous placement of fault indicator and sectionalizing switch in distribution networks. *IEEE Transactions on Smart Grid*, *10*(2), 2278-2287.

[8] Heidari, A., Agelidis, V. G., & Kia, M. (2014). Considerations of sectionalizing switches in distribution networks with distributed generation. *IEEE Transactions on Power Delivery*, *30*(3), 1401-1409.

[9] Heidari, A. et al. (2016). Reliability optimization of automated distribution networks with probability customer interruption cost model in the presence of DG units. *IEEE Transactions on Smart Grid*, *8*(1), 305-315.

[10] Isapour Chehardeh, M., & Hatziadoniu, C. J. (2019). Optimal placement of remote-controlled switches in distribution networks in the presence of distributed generators. *Energies*, *12*(6), 1025.

[11] Farajollahi, M., Fotuhi-Firuzabad, M., & Safdarian, A. (2017). Optimal placement of sectionalizing switch considering switch malfunction probability. *IEEE Transactions on Smart Grid*, *10*(1), 403-413.

[12] Izadi, M., Farajollahi, M., & Safdarian, A. (2018). Switch deployment in distribution networks. In *Electric distribution network management and control* (pp. 179-233). Springer, Singapore.

[13] Forcan, M., Maksimović, M., & Forcan, J. (2019, October). Cloud-based approach for real-time monitoring of smart grid topology. In *5th Jubilee Virtual International Conference on Science,*

Technology and Management in Energy – eNergetics (pp. 47-54). Nis, Serbia.

[14] Choi, T. I., Lee, K. Y., Lee, D. R., & Ahn, J. K. (2008). Communication system for distribution automation using CDMA. *IEEE transactions on power delivery*, *23*(2), 650-656.

[15] Choi, T. I., Koh, I. S., Kim, B. H., Song, W. S., & Jang, W. S. (1999, January). PC-based remote control and fault location system for distribution line. In *IEEE Power Engineering Society. 1999 Winter Meeting (Cat. No. 99CH36233)* (Vol. 2, pp.1085-1090). IEEE.

[16] Maksimović, M., & Forcan, M. (2020). Application of 5G Channel Coding Techniques in Smart Grid: LDPC vs. Polar coding for Command Messaging. In *7th International Conference on Electrical, Electronic and Computing Engineering, IcETRAN 2020* (pp. 746-751).

[17] Beni, S. A., Haghifam, M. R., & Hammamian, R. (2013). Estimation of customers damage function by questionnaire method.

[18] Bezerra, J. R., Barroso, G. C., Leão, R. P. S., & Sampaio, R. F. (2014). Multiobjective optimization algorithm for switch placement in radial power distribution networks. *IEEE Transactions on Power Delivery*, *30*(2),545-552.

New Software for Processing Weather Station Data

Jed Mohamed[1], Jed Mohamed El Hacen[2], Nabila Ihaddadene[3], Razika Ihaddadene[4]

[1,2]Nouakchott Al Aasriya university,Nouakchott, Mauritania, memjid2001@gmail.com[1]; hassenjid@gmail.com[2]

[3,4]M'Sila University, M'Sila, Algeria, MAZ1dz@gmail.com[3]; tassekurt1@gmail.com[4]

Abstract—**This work presents software designed using MATLAB software using the MATLAB GUI tool, which aims to process meteorological data such as temperature, solar irradiation, wind speed, humidity and other meteorological parameters, collected from meteorological station measuring instruments which are recorded instantly. The software is used to process this data and analyze it in order to present it in a way that is easier to manipulate and analyze. The first version of the software can present the daily, monthly and annual evolution in a simpler format for use in studies and helps to determine the extreme and average values of temperature, irradiance, insolation and speed wind for a specific period.**

Keywords - MATLAB GUI, renewable energy, data analysis

I. Introduction

According to new data released by the International Renewable Energy Agency (IRENA) in April 2019, the decade-long trend of strong growth in renewable energy production capacity continued in 2018, with an overall increase of 171 gigawatts (GW) [1].

All of this is due to climate change in recent decades which is also promoting a return to the uses of renewable energies which reduce greenhouse gas emissions and protect the environment. [2-6]. In addition, the depletion of fossil fuels which is certain due to the increased demand for energy is another important factor which has encouraged the exploitation of renewable sources [5].

Renewable energies are endless natural energies on the scale of human life from renewable sources such as the sun, wind, waterfalls, tides, etc. Unlike fossil fuels, every country in the world uses at least one renewable energy source. Hence, renewable energy is widely and easily available around the world. With conventional energy sources being depleted due to their continued use, all countries around the world have adopted policies to exploit their natural energy potential and to protect the environment. Solar energy is considered the most important renewable energy source [6-8]. It is the energy created by nuclear fusion between hydrogen atoms that takes place in the sun. This source of energy is clean and free and is at the origin of fossil fuels, wind and tidal power [2]. In addition, this source is accessible to everyone, but in different quantities depending on the location. North Africa receives a greater amount of solar radiation than northern Europe. Australia is the continent that receives most of the world's solar radiation [8].

Algeria is strongly dominated by solar energy (i.e. 169,000 TWh/year for thermal solar, 13.9 TWh/year for solar photovoltaic and 35 TWh/year for wind energy [9]). Thanks to its geographical location, Algeria has one of the largest solar fields in the world and in particular in the Maghreb region. The average number of hours of sunshine on the whole of the Algerian territory exceeds 2000 hours per year and reaches 3000 hours in the highlands and 3500 in the Sahara [10]. The average energy received daily on a horizontal surface is of the order of 5 kWh/m² over most of the national territory, and about 1700 kWh/m² / year in the North and 2263 kWh/m² /year to the south. [11].

ISBN: 978-86-80616-07-0

But still for the realization of installations producing renewable energy, a study of the meteorological situation of the place is a necessity [7,12,13] and this is only possible with the analysis of the data of the past decades by basing data collected from weather stations, such as solar radiation, ambient temperature, wind speed, precipitation, humidity, etc. Generally, this data is recorded instantaneously or according to a well-defined time interval (generally in second minute or hour), so to see the daily, monthly, seasonal and annual evolution which will better help to estimate the production of the future installation a long treatment should be carried out. The aim of this article is to simplify the processing and management of this data with software that was designed with Matlab software using the MALAB GUI tool [10].

The objective of this software is to help people who work on site weather data to process this data and visualize it in a clear and understandable way in order to save time while manually working on excel files.

II. Materials and Methods

A. *Matériels*

For the realization of the software, we used the MATLAB GUI tool of the MATLAB software (also known as Graphical User Interfaces or GUI) which allows Develop applications interactively using App Designer or by programming using MATLAB® functions which provides a simple point-and-click interface to code. Applications contain interactive commands such as menus, trees, buttons, and sliders that execute specific instructions when users interact with them (see Fig. 1). Applications may also contain graphics for visualization or data exploration [10].

In this article, the data processed by the software is that of the M'Sila weather station. The data collected are solar radiation, ambient

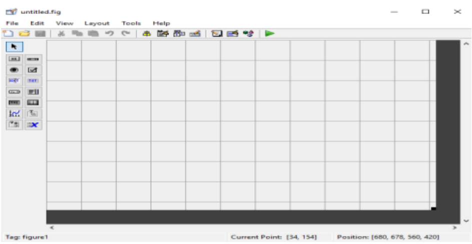

Figure 1. View of the MATLAB GUI tool.results for supercapasitor bank in case 4.

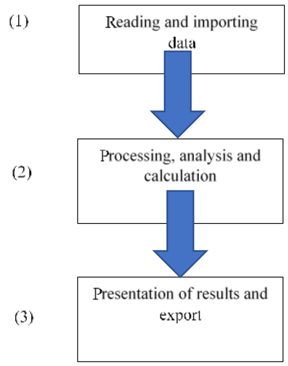

Figure 2. Software sequence diagram.

temperature, wind speed, precipitation and humidity for the period of one year between November 2016 and October 2017. The recording interval is 5 minutes and the files are in format csv, each day's data is saved in a separate file with the name of the file date.

B. *Methods*

During its execution, the operation of the software goes through three main parts as illustrated in Fig. 2.

1. *Importing and Reading Data*

Importing and reading files are important steps before moving on to the next step, for now this part must be customized by the user of the software according to the file format and the classification or position of the variables (studied parameters).

The user must define:

- File format: for the moment either .xls, .csv or .txt and then the software will use the appropriate function for each type of file to import and read the file. In the case of the application, the files are in .xls format.
- Location of variables: the files generated by the meteorological data recording system are not the same depending on the system, but generally for each parameter it has its own column and rows for the measurement points (measurement time interval). So for the software to understand what parameter it is, the user must declare the column number of each parameter as well as the time interval.

For example in our case file in .xls format:

Column 1: Time;

Column 2: Temperature;

Column 3: Wind speed;

Column 4: solar radiation;

Column 5: Solar energy

Column 6:……….;

Measurement interval every five minutes.

2. Processing, Analysis and Calculation

This second part is the heart of the software. From the data retrieved from the previous step (step 1), each parameter will be saved in a well-defined variable and the software will start to analyze these parameters.

Then calculations will be launched to calculate for example:

Extreme or average values;

Determine the irradiation if not given;

Daily, monthly and annual evolution;

Graphic interpretation;

You will find below some equations used in the calculation process:

To convert the irradiances into daily and monthly insolation we used successively Eq. (1) and Eq. (2):

$$H_{t,d} = \sum_{t=1}^{t=T_{rp}} G \times T_r \ , \qquad (1)$$

$$H_{t,m} = \sum_{d=1}^{N} H_{t,d} \ , \qquad (2)$$

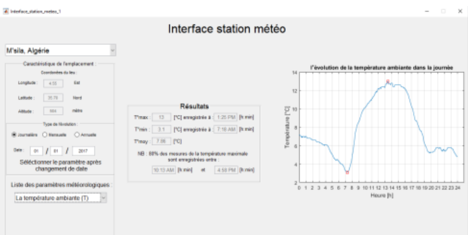

Figure 3. View of the the software.

where:

T_r : is the recording time interval;

T_{rp} : the reporting period;

N : the number of days in a month;

H_t : (d:daily; m :monthly) : total insolation Wh/m²;

G : irradiance W/m²

3. Presentation of Results and Export

This part represents the output results of the software. After the first two steps, the user can view the data after analysis and calculation available in several formats:

- Digital: thanks to panels which display the numbers with their meanings and units of measurement;
- Graphically: using the figures.
- Possibility to export the results in .xls format which will be displayed in table format.

III. Results and Discussion

In this part we will present screenshots of the software during these different functional stages for our study case the weather station of M'Sila. A full view of the software after execution is shown in Fig. 3. Note that the objective of the software is to help people who work on site weather data to process this data and visualize it in a clear and understandable

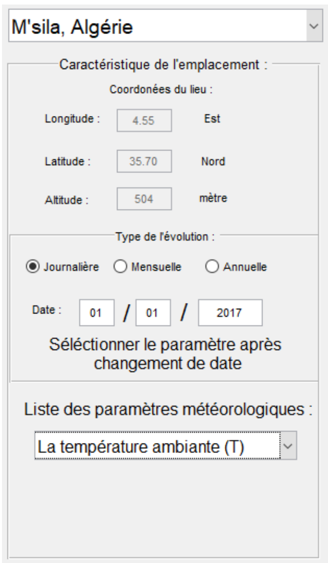

Figure 4. Evolution and paramters panel.

way in order to save time.

In “Fig. 4”, as soon as the software is executed, a panel with the possibility of choosing the type of evolution, either daily, monthly or annual, will appear with a menu containing the parameters (studied parameters, irradiance, insolation, temperature or wind speed) declared in the first part according to the availability of data from the weather station. This panel also shows the coordinates of the studied area.

In Fig. 5 and Fig. 6 we can see the digital panel of the results in the case of temperature and the case of solar radiation. Thanks to these panels we can determine:

- Extreme temperature (max and min) with recording time;
- Average temperature over a defined period;
- Interval of time or temperature is higher;
- Maximum solar radiation with recording time;
- Average solar radiation;
- Time interval where we capture 80% of energy per day;

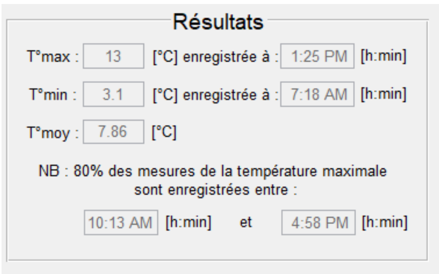

Figure 5. Digital results panel case temperature.

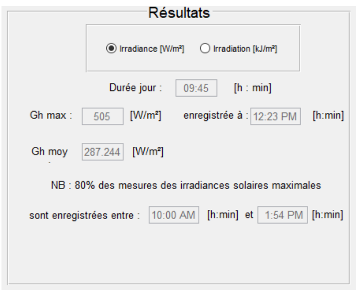

Figure 6. Digital results panel case solar irradiation.

In Fig. 7, graphical presentation of the hourly evolution of ambient temperature and solar radiation.

These kinds of figures give us a fair visualization and enlightenment on the extreme values and the type of evolution during the day.

In Fig. 8, the monthly evolution of temperature is presented with a trend which can be used as a judgment parameter on the capability of the parameter studied to increase or decrease or even remain stable.

IV. Conclusion

A software designed using MATLAB GUI, which aims to process meteorological data collected from weather stations which are

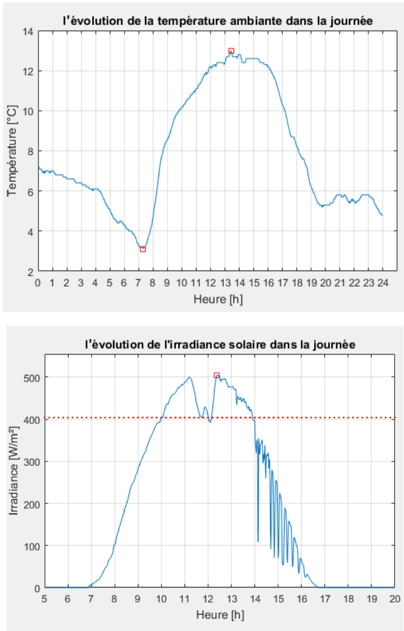

Figure 7. Hourly temperature and solar radaition evolution.

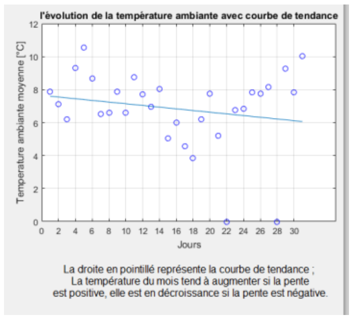

Figure 8. Monthly solar radiation evolution.

recorded instantly. The objective of the software is to help people who work on site weather data to process this data and visualize it in a clear and understandable way in order to save time while manually working on excel files.

It can be used to see:

- daily, monthly and annual evolution values of meteorological parameters;
- Extreme temperature (max and min) with recording time;
- Average temperature over a defined period;
- Interval of time or temperature is higher;
- Maximum solar radiation with recording time;
- Average solar radiation;
- Time interval where we capture 80% of energy per day;

REFERENCES

[1] Brunet, *Les énergies renouvelables devraient renouer avec une croissance vigoureuse en 2019, Le Monde de l'Energie* (2019). Available at : https://www.lemondedelenergie.com/energies-renouvelables-croissance-2019/2019/09/26/.

[2] Kalogirou, S. A. (2004). Solar thermal collectors and applications. Progress in Energy and Combustion Science, *30*(3), 231-295.

[3] Kim, J., Park, S. Y., & Lee, J. (2018). Do people really want renewable energy? Who wants renewable energy?: Discrete choice model of reference-dependent preference in South Korea. *Energy Policy*, 120, 761-770.

[4] Tian, Y., & Zhao, C. Y. (2013). A review of solar collectors and thermal energy storage in solar thermal applications. *Applied Energy*, 104, 538-553.

[5] Shahsavari, A., & Akbari, M. (2018). Potential of solar energy in developing countries for reducing energy-related emissions. *Renewable and Sustainable Energy Reviews*, 90, 275-291.

[6] Lau, K. K. L., Lindberg, F., Johansson, E., Rasmussen, M. I., & Thorsson, S. (2017). Investigating solar energy potential in tropical urban environment: A case study of Dar es Salaam, Tanzania. *Sustainable cities and Society*, 30, 118-127.

[7] Chegaar, M., & Chibani, A. (2001). Global solar radiation estimation in Algeria. *Energy conversion and management*, *42*(8), 967-973.

[8] Kabir, E., Kumar, P., Kumar, S., Adelodun, A. A., & Kim, K. H. (2018). Solar energy: Potential and future prospects. *Renewable and Sustainable Energy Reviews*, 82, 894-900.

[9] CDER. (2013). Les énergies renouvelables en Algérie: chiffres clefs, publication des services économiques. pp. 13.

[10] *MATLAB GUI*. Available at: https://www.mathworks.com/discovery/matlab-gui.html

[11] Saïd, B. (2010). L'énergie renouvelable en Algérie et l'impact sur l'environnement. *Journal of Scientific Research* 0, 1, 49.

[12] Ouagued, M., Khellaf, A., & Loukarfi, L. (2013). Estimation of the temperature, heat gain and heat loss by solar parabolic trough collector under Algerian climate using different thermal oils. *Energy Conversion and Management*, 75, 191-201.

[13] Hussain, M., Rahman, L., & Rahman, M. M. (1999). Techniques to obtain improved predictions of global radiation from sunshine duration. *Renewable Energy*, *18*(2), 263-275.

Numerical Modeling of SO_2 Turbulent Dispersion from Thermal Power Plants to Urban Environment: Influence of Realistic Terrain Topography

Rastko Jovanović

Department of Thermal Engineering and Energy, „VINČA" Institute of Nuclear Sciences - National Institute of the Republic of Serbia, University of Belgrade, Belgrade, Serbia, virrast@vin.bg.ac.rs

Abstract—**This work presents a workflow for calculation of SO_2 dispersion from thermal power plants "Nikola Tesla" to Republic of Serbia capital city Belgrade. Model is based on CFD simulations over terrains with a complex topography and treats urban environments as porous media. CFD part of the model, used for numerical calculations, is based on user modified comprehensive solver ANSYS FLUENT. The obtained results showed very good agreement with measured SO_2 concentrations. Thus, the suggested model can be used for the quantitative estimation of existing measures for air pollution reduction, as well as for the planning of the new measures.**

Keywords – CFD simulation, porous medium, topology, air pollution, SO_2 dispersion

I. INTRODUCTION

SO_2 is harmful gas emitted to the atmosphere from power plants firing fossil fuels, industrial processes (metals processing and smelting facilities), and vehicles powered by diesel fuel [1]. Thermal Power Plants (TPPs) burning low-quality lignite coals with high Sulphur content are by far the largest source of SO_2 in the Republic of Serbia (RS) [2]. TPP "Nikola Tesla" located about 30 km southwest of Serbian capital city Belgrade is the 9th largest SO_2 pollutant in the world [3].

Short-term SO_2 exposures negatively influence the human respiratory system and breathing. The most affected population groups are individuals with asthma and children. Increased SO_2 concentrations may influence the formation of other sulfur oxides. The newly formed Sulphur oxides may react with other air pollutants generating aerosol particles and thus increasing particulate matter (PM) pollution. PM can penetrate the lung's alveoli and further damage the human respiratory system [4]. Sulfur oxides are also the origin of acid rain, which has a harmful effect on plants and trees [5].

The main hypothesis of this work is that SO_2 emitted from TPP "Nikola Tesla" has the prevailing influence on the increased SO_2 concentration in Belgrade. The main subject of this work is three-dimensional computational fluid dynamics (CFD) modeling of SO_2 dispersion emitted from chimneys of TPPs "Nikola Tesla" TENT A and TENT B.

Although CFD modeling has a wide range of applications its usage in air pollutant dispersion simulation over large distances (bigger than ~10 km) is limited, mainly due to high computational requirements. Gaussian models are commonly used for local pollutant dispersion (domain length ~50–100 km). The main advantage of these models is their relatively low computational costs and fast calculation. However, these models have several limitations: they do not perform well for low wind velocities and utilize quite simplified turbulence representation. Moreover, the influence of topography is taken into account only by

ISBN: 978-86-80616-07-0

roughness height, which allows for arbitrary adoption of this, very important parameter [6]. Lagrangian models are based on the calculation of pollutant trajectory on its path from the source. Lagrangian models are often used for pollution dispersion modeling up to regional distances (domain length ~1000 km). Their main limitation is that pollutant's trajectory is calculated on an already generated Eulerian grid, which does not allow a user to refine the grid in regions with sharp topology changes. Eulerian grids are often coarse, with the lowest resolution of 1–5 km. This further decreases models' ability to accurately describe topology and consequently lowers their performance [7].

The main aim of the performed work is to suggest the CFD based model for SO_2 dispersion calculation, able to quantitatively predict SO_2 concentration distribution. The model utilizes high-resolution GIS files with realistic topography as geometry input. GIS files are used to generate highly resolved computational mesh for CFD calculations. The urban environment is represented using a porous medium with properties corresponding to real cities. The suggested model is used to calculate SO_2 concentration levels emitted from the chimneys of TPP "Nikola Tesla". Model is validated comparing calculated and measured SO_2 concentrations in Belgrade, RS. Measured SO_2 values are obtained from the Serbian Environmental Protection Agency (SEPA) open data portal [8].

II. Materials and Methods

A. Pollutant Sources

TPP "Nikola Tesla" consists of two sections: TPP TENT A and TPP TENT B, located at 30 km in the west-south-west (WSW) direction from the center of Belgrade, on the bank of river Sava. Distance between TENT A and TENT B is approximately 15 km, Fig. 1.

TENT A has two flue gas chimneys with heights of 150 m and 220 m, and diameters of 10.5 m and 16.9 m, respectively. TENT B has a single chimney with a height of 280 m and a diameter of 30 m. Continual in-situ measurements of SO_2 concentrations at the chimneys' outlets were used to calculate pollution source input values in the suggested model.

Figure 1. Site positions: red – TPPs TENT A and TENT B, green – weather station, and yellow – SEPA air pollution station.

B. Weather Parameters Measurements

Wind velocity, wind direction, and air temperatures were obtained from a weather station located between TPPs TENT A and TENT B, Fig. 1. Meteorological parameters were measured in real-time at mast height of 10 m, at time intervals of 1 s.

C. SO_2 Measurement Data

SO_2 is monitored at totally four different SEPA air pollution monitoring stations in the city of Belgrade. SEPA station located in the New Belgrade municipality (NB) was chosen for model validation based on the fact that this station is predominately influenced by SO_2 emitted from TPPs TENT A and TENT B. The other three stations are positioned at locations that may be influenced by air pollution emissions originating from other industrial facilities and/or intensive traffic jams [9]. All monitored data are

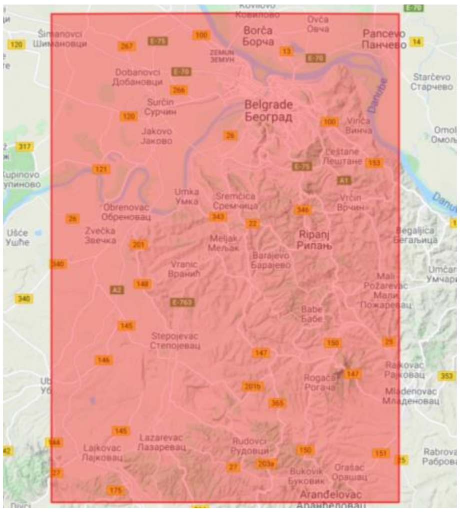

Figure 2. Geometry selected for 3d model creation.

available through the SEPA open data portal [8] as minute values for all stations.

III. Mathematical Model

A. Geometry Model

Modeled geometry is first selected and saved in OpenStreetMap (OSM) format [10]. OSM format stores XML-formatted data as nodes, connections, and tags (object properties). Selected geometry is shown in Fig. 2 in the red rectangle. OSM file is then imported into the open-source 3D computer graphics software Blender and prepared for further processing [11]. Geometry model is exported to CFD pre-processor GAMBIT 2.3.1 in .stl format, Fig. 3.

B. Computational Mesh and Mesh Independence Study

The computational mesh is created using the GAMBIT 2.3.1 pre-processor. Generated finite volume mesh consists of all hexagonal elements with a maximum size change of 1.05. Mesh is locally refined in regions of steep geometric height (altitude above mean sea level) changes (hills, mountains…), regions at chimney locations, and in the urban region of Belgrade. Great care was given to mesh generation to ensure high mesh quality and low numerical diffusivity.

Four meshes with a different number of control volumes were generated to perform grid independence study: coarse, medium, fine, and very fine consisting of about 1.5e+06, 7e+06, 12e+06, and 15e+06 computational cells respectively. A grid independence study was performed for turbulent flow with a velocity magnitude of 5 ms^{-1} from the southern direction. Calculated averaged velocity in middle x and y planes changed less than 2% when solving on fine and very fine meshes. Based on this fine mesh consisting of 12e+06 finite volumes was adopted for further calculations in this work, Fig. 4. Computational mesh at cross-section z = 0 m (ground level), obtained by remeshing the imported .stl file is shown in Fig. 5.

C. CFD Modeling – Governing Equations

CFD simulations were performed using comprehensive CFD code ANSYS FLUENT 2020 R2 [12]. Default FLUENT solver was adjusted for this work using a series of user-defined functions (UDFs) to define custom boundary conditions profiles, source terms, and porous medium characteristics [13].

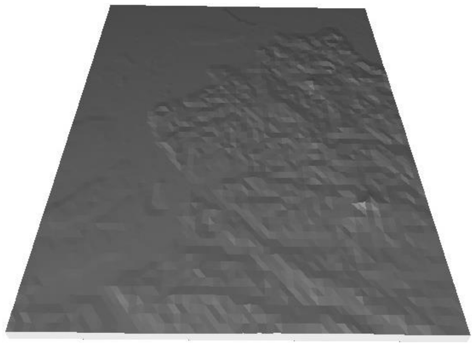

Figure 3. Three dimensional geometry model for CFD pre-processing.

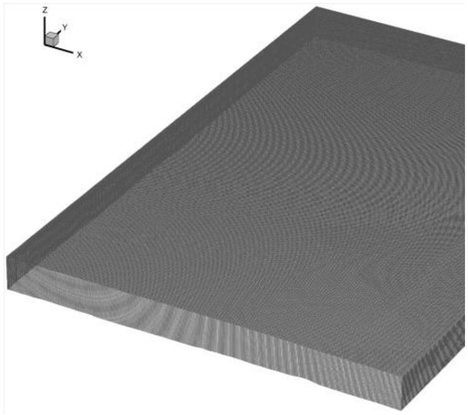

Figure 4. Finite volume mesh used for CFD calculations.

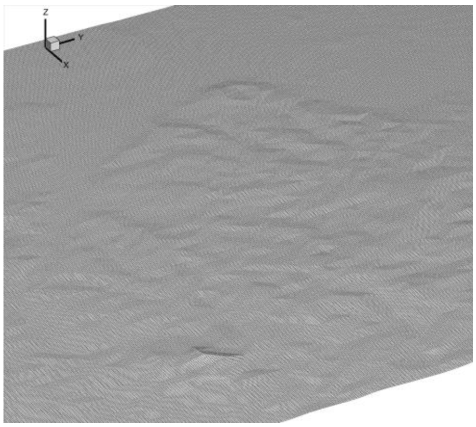

Figure 5. Detailed view of finite volume mesh cross-section z = 0 m.

The main assumptions are that the modeled flow is:

- three-dimensional,
- steady-state,

- incompressible,
- multi-component,
- turbulent.

The governing equation for the mass conversion is defined as:

$$\frac{\partial u_i}{\partial x_i} = 0 \ , \tag{1}$$

where u_i is the time-averaged component of velocity vector u in direction x_i.

The governing Eq. for momentum conversion is defined by the following expression:

$$\frac{\partial}{\partial x_i}(u_i u_j) = -\frac{1}{\rho}\frac{\partial p}{\partial x_i} + \frac{\partial}{\partial x_i}\left(\nu \frac{\partial u_i}{\partial x_j} - \overline{u_i^{'} u_j^{'}}\right) + S_{momentum,i} \ , \tag{2}$$

where ρ is the fluid density, p is mean pressure, ν is kinematic viscosity, $S_{momentum,i}$ is momentum source term due to SO_2 emissions, and $\overline{u_i^{'} u_j^{'}}$ are Reynolds stresses defined by the following Eq.:

$$-\overline{u_i^{'} u_j^{'}} = 2\nu_t S_{ij} - \frac{2}{3}\kappa\delta_{ij} \ , \tag{3}$$

where S_{ij} is strain rate tensor, turbulent viscosity, k is turbulent kinetic energy, and ν_t is kinematic turbulent viscosity defined as:

$$\nu_t = C_\mu \frac{k^2}{\varepsilon} \ . \tag{4}$$

Unknown turbulent quantities, k – turbulent kinetic energy, and ε – dissipation of turbulent kinetic energy are determined using realizable k-ε turbulent model, which solves two additional transport equations for the above defined turbulent quantities:

$$\frac{\partial}{\partial x_j}(k u_j) = \frac{\partial}{\partial x_j}\left[\left(\nu + \frac{\nu_t}{\sigma_k}\right)\frac{\partial k}{\partial x_j}\right] + P_k - \varepsilon \ , \tag{5}$$

$$\frac{\partial}{\partial x_j}(\varepsilon u_j) = \frac{\partial}{\partial x_j}\left[\left(\nu + \frac{\nu_t}{\sigma_\varepsilon}\right)\frac{\partial \varepsilon}{\partial x_j}\right] + C_{\varepsilon 1}\frac{\varepsilon}{k}P_k - C_{\varepsilon 2}\frac{\varepsilon^2}{k} \ , \tag{6}$$

where P_k is source term, which represents the production of k, σ_k and σ_ε are Prandtl numbers, and $C_{\varepsilon 1}$ and $C_{\varepsilon 2}$ are model constants.

Additional transport equation for the mass fraction of SO_2 has the following form:

$$\frac{\partial}{\partial x_j}(\mathrm{Y}_{SO_2} u_j) = \frac{\partial}{\partial x_j}\left[D_{eff}\frac{\partial SO_2}{\partial x_j}\right] + S_{species} \ , \tag{7}$$

where D_{eff} is the effective diffusive coefficient of SO_2 in air, and $S_{species}$ is mass source due to generation of SO_2 in the computational domain.

D. *Computational Domain and Boundary Conditions*

The main dimensions of the computational domain are 41788.56 m in the x-direction, 60000 m in the y-direction, and 2000 m in the z-direction, Fig. 6.

Velocity inlets were specified at southern and western lateral domain boundaries (Fig. 6) since the prevailing wind direction is south-west (SW). Wind velocity, turbulent kinetic energy, and dissipation of turbulent kinetic energy at inlets were specified using expressions, which correspond to the atmospheric boundary layer (ABL) flow [14]:

$$u(\mathrm{z})_{inlet} = \frac{u^*}{k}\cdot \ln\left(\frac{z+z_0}{z_0}\right), \tag{8}$$

$$\mathrm{k(z)}_{inlet} = \frac{u^{*2}}{\sqrt{C_\mu}}, \tag{9}$$

$$\varepsilon(\mathrm{z})_{inlet} = \frac{u^{*3}}{k(z+z_0)} \ , \tag{10}$$

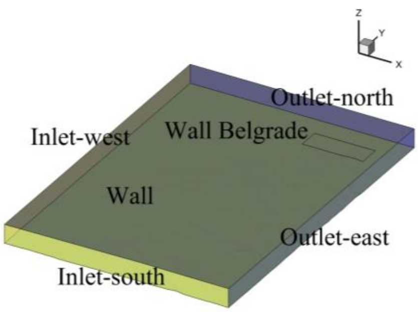

Figure 6. Computational domain and boundaries.

where u^* is friction velocity given by the following expression:

$$u^* = k \cdot \frac{u_{ref}}{\ln(\frac{z_{ref} + z_0}{z_0})} . \quad (11)$$

In the above Eqs. (7)-(10), z is domain height, z_0 is aerodynamic roughness length, $C_\mu = 0.09$ is turbulent viscosity constant, κ = 0.4 is von Karman constant, u_{ref} is reference velocity taken from measurements, and z_{ref} is reference height at which reference velocity was measured. Inlet value $z_0 = 0.25m$ was adopted from [15] for areas with high crops and scattered obstacles.

Outlet boundary conditions were applied to northern and eastern domain lateral boundaries. Pressure value was set to zero, as recommended for incompressible flows, and zero-gradient condition was applied for all other quantities at outlet boundaries, Fig. 6.

Symmetry boundary condition was applied to the top surface (open atmosphere).

No-slip wall boundary condition was applied for the bottom plain with the roughness height, k_s, calculated according to the following Eq.:

$$k_s = \frac{9.793 z_0}{C_s} , \quad (12)$$

where C_s = 7 is roughness constant.

Aerodynamic roughness length $z_0 = 0.25m$, same as for inlets, was used for all wall boundary sections except for the Belgrade area. Aerodynamic roughness length $z_0 = 1.15m$ was used for the Belgrade wall section, as recommended in [16] for urban areas with block buildings, industrial facilities, and city centers, Fig. 6.

Belgrade city urban region is represented as the porous medium with the porosity of $\varphi = 0.6$ adopted from [17]. Two additional inputs necessary for porous media modeling are the permeability, α, and inertial loss coefficient, C_2. These two quantities were derived based on the semi-empirical Ergun equation:

$$\alpha = \frac{D_p^2}{150} \frac{\varphi^3}{(1-\varphi)^2} , \quad (13)$$

$$C_2 = \frac{3.5}{D_p} \frac{(1-\varphi)}{\varphi^3} , \quad (14)$$

where D_p is characteristic packing diameter, calculated based on the average building hydraulic diameter [16].

IV. Model Validation Scenario

The model was validated using real weather conditions and TPPs operation conditions. Calculations were performed for the worst-case scenario determined based on the following criteria (in order of significance): 1) wind-direction, 2) wind intensity, 3) registered SO_2 concentrations in NB SEPA pollution station, 4) power production at TPPS TENT A and TENT B. The first criterion is fulfilled when the wind blows in the SW direction for the majority of the day, at least 35% od 24h monitored values. The target value set for the second criterion is that wind velocity magnitude must be in the range between 3 m/s and 5 m/s. The target set for the third criterion is that the recommended 24h mean SO_2 concentration of 20 μgm^{-3}, as defined in [18], has to be exceeded on all SEPA air pollution stations in Belgrade. Finally, the worst-case scenario was chosen as a 24h period with maximum power production for which all three targets were met, 29th of January 2018. Wind-rose plot for this date is used to define inlet boundary conditions, Fig. 7. Time-averaged

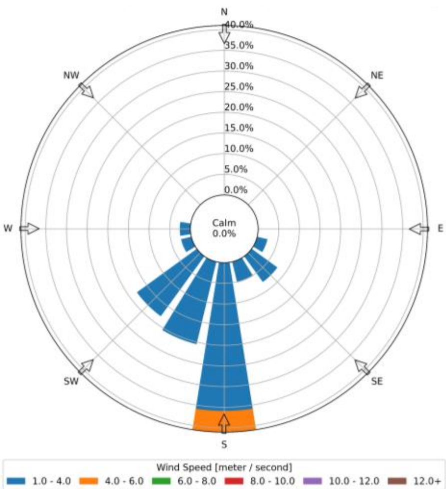

Figure 7. Windrose on the 29th of January 2018.

TABLE I. SO_2 SOURCES INPUT PARAMETERS.

Chimney	Position [decimal degrees]	Mass flow rate [kgs^{-1}]	Vertical velocity [ms-1]
TENT A1	Lat: 44.6719 Long: 20.1588	1.8734 [19]	10 [19]
TENT A2	Lat: 44.6706 Long: 20.1582	1.8734 [19]	10 [19]
TENT B	Lat: 44.6538 Long: 20.0049	2.5 [19]	10 [19]

velocity and turbulent quantities profiles were implemented using UDFs.

SO_2 flow from TENT A and TENT B chimneys was modeled employing mass and momentum sources incorporated in equations (2) and (7). Sources were applied to cell sets corresponding to the chimneys' outlet surfaces. Chimney locations and Belgrade urban central area positions inside the computational domain are shown in Fig. 8. Mass and momentum sources were defined using UDFs, specifying their positions in three-dimensional space, the mass flow rate in $kgs^{-1}m^{-3}$, and vertical flue gas velocity, Table I.

V. Results and Discussion

CFD calculated topological features are shown in Fig. 9. Terrain topology on the finite

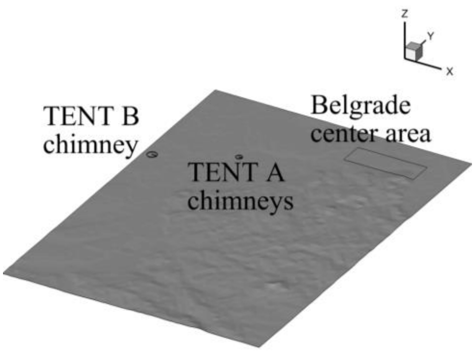

Figure 8. TPPs TENT A and TENT B chimneys and Belgrade urban center locations (real chimneys diameters are enlarged 100 times for visual purposes).

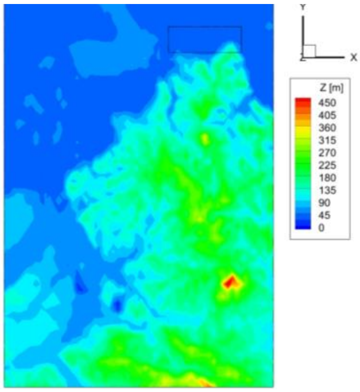

Figure 9. CFD calculated terrain height.

volume grid is presented in terms of height above sea levels. It can be seen that all important features imported from the OSM file are well preserved and represented accurately on fine finite volume mesh.

Velocity magnitude values in vertical cross-section y = 100 m. are shown in Fig. 10. It can be seen that the ABL velocity profile is accurately represented using UDFs incorporated into the default ANSYS FLUENT code. The influence of SW wind direction is visible in the left (x-axis origin) corner, where superimposing of the southern and western winds occurs. The strong influence of SW wind direction is visible in the horizontal plane z = 1.85 m, as shown in Fig. 11. Most importantly, a strong decrease of velocity magnitude, from 3 m/s to 1 m/s, is present in the urban region of Belgrade city.

Thus, it can be concluded that porous medium treatment of the urban areas strongly impacts velocity distribution inside these areas due to lower permeability and higher viscous resistance, Fig. 11.

The previous conclusions about porous medium treatment of the Belgrade urban area and prevailing influence of SW wind direction are presented in more detail by velocity vectors in

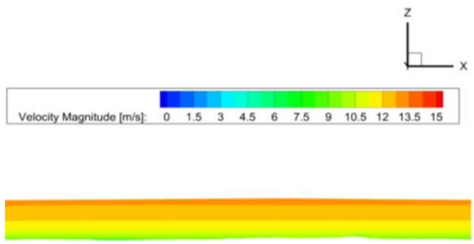

Figure 10. Velocity magnitude in middle vertical cross section y = 100 m.

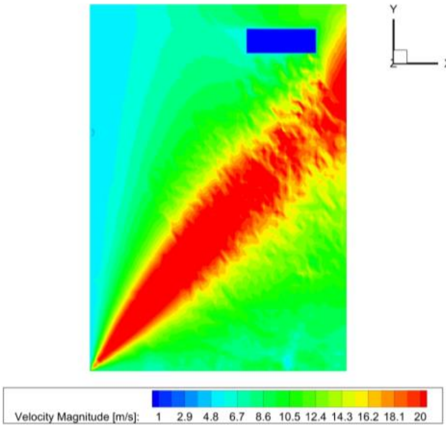

Figure 11. Velocity magnitude in horizontal cross section z = 1.5 m.

horizontal cross-section z = 1.5 m, shown in Fig. 12.

SO_2 distribution in horizontal plane z = 1.5 m is shown in Fig. 13. It can be seen that initial momentum from the chimneys' outlets impacts SO_2 concentration near the source position, and decreases at larger distances from the source. At bigger horizontal distances from the source and at lower heights, SO_2 concentration distribution is mainly influenced by the wind speed.

The influence of geo-topology can be seen comparing the velocity magnitude field shown in Fig. 12 with SO_2 concentrations presented in Fig. 13. Hill terrain in the NE direction of the Belgrade area lowers velocity magnitude and thus decreases SO_2 dispersion intensity.

Quantitative comparison between average daily SO_2 concentrations registered at USEPA air

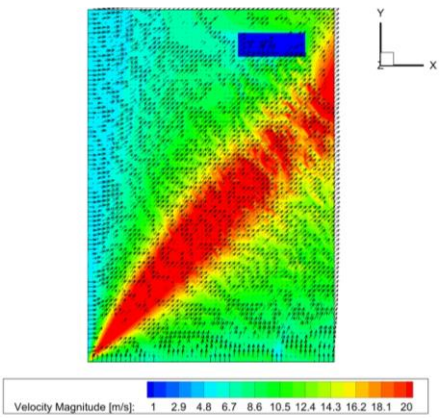

Figure 12. Velocity vectors and velocity magnitude in horizontal cross section z = 1.5 m.

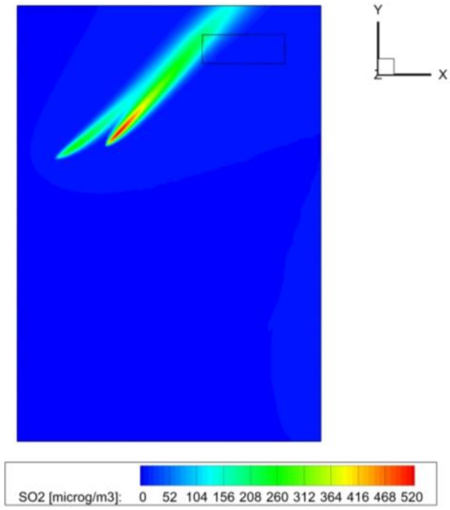

Figure 13. Contours of SO_2 concentration in horizontal cross section z = 1.5 m.

pollution station located in the NB area and numerically calculated SO_2 concentration value is shown in Fig. 14. The relative difference between the measured and model calculated value is about 3.4%. The small relative error of the model points out the model's high accuracy and its ability for quantitative predictions of SO_2 dispersion from point sources.

VI. Conclusions and Future Work

The following conclusions and possible directions for future work can be drawn based on the obtained results:

- Novel workflow for SO_2 dispersion calculation over large distances is suggested;

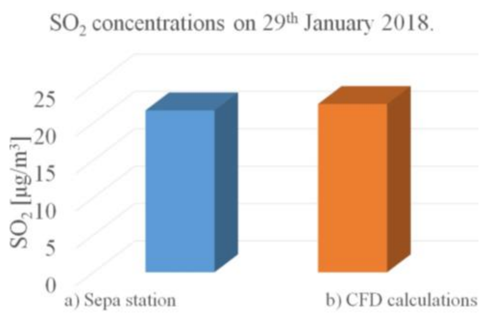

Figure 14. Comparison between meassured and numerically calculated SO_2 concentrations at NB location in horizontal cross section z = 1.5 m.

- The suggested model is based on CFD calculations over terrains with realistic complex topology;
- The model can quantitatively predict SO_2 concentrations at all spatial distances from the source;
- The suggested framework is not limited to the particular case presented in this paper, it can be applied to any terrain and for all types of air pollutants;
- This framework can be used to suggest the implementation of new measures for air pollution reduction and/or for control of the effects of existing measures;
- It is planned to continue suggested model sophistication to full automatization from geometry input to results calculation.
- It is also planned to include the possibility to calculate the spatial and temporal distribution of all main air pollutants into the existing model.

ACKNOWLEDGMENTS

This work was supported by the Ministry of Education, Science and Technological Development of Serbia.

The author would like to express his gratitude to dr. Milić Erić and dr. Zoran Marković for online in-situ measurement data from flue gas measurements at TPP "Nikola Tesla".

REFERENCES

[1] Stewart, M. J. (2010). Primary National Ambient Air Quality Standard for Sulfur Dioxide; Final Rule, Information Center, EPA/DC, EPA West, Room 3334, 1301 Constitution Ave., NW., Washington, DC.

[2] Electric Power Industry of Serbia. (2018). Environmental Report, Belgrade, Republic of Serbia.

[3] Sunil Dahiya, L. M., Anhäuser, A., Farrow, A., Thieriot, H. & Chanchal, A. (2020). *Ranking the World's Sulfur Dioxide (SO_2) Hotspots: 2019-2020 A closer look at the colourless gas that is poisoning our air and health*. Available at: https://environmentsee.eu/serbian-tpp-nikola-tesla-is-the-ninth-largest-sulfur-dioxide-pollutant-in-the-world/.

[4] Barbone, F. et al. (2019). A panel study on lung function and bronchial inflammation among children exposed to ambient SO_2 from an oil refinery. *International journal of environmental research and public health*, *16*(6), 1057.

[5] Likus-Cieślik, J., Socha, J., Gruba, P., & Pietrzykowski, M. (2020). The current state of environmental pollution with sulfur dioxide (SO_2) in Poland based on sulfur concentration in Scots pine needles. *Environmental Pollution*, *258*, 113559.

[6] Caputo, M., Giménez, M., & Schlamp, M. (2003). Intercomparison of atmospheric dispersion models. *Atmospheric Environment*, *37*(18), 2435-2449.

[7] Miller, A. J., Raduma, D. M., George, L. A., & Fry, J. L. (2019). Source apportionment of trace elements and black carbon in an urban industrial area (Portland, Oregon). *Atmospheric Pollution Research*, *10*(3), 784-794.

[8] Serbian Environmental Protection Agency (SEPA). (2020). *Open data*, (n.d.). Available at: http://data.sepa.gov.rs/en/.

[9] Jovašević-Stojanović, M., & Bartonova, A. (2010). Current state of particulate matter research and management in Serbia. *Chemical Industry and Chemical Engineering Quarterly/CICEQ*, *16*(3), 207-212.

[10] OpenStreetMap contributors. (2020). *Planet dump*. Available at: https://planet.osm.org.

[11] Blender Online Community. (2020). *Blender - a 3D modelling and rendering package*. Available at: http://www.blender.org.

[12] I. ANSYS. (2020). *Ansys® Fluent, Release 2020 r2*. Available at: https://www.ansys.com/products/fluids/ansys-fluent.

[13] I. ANSYS. (2016). *ANSY Fluent UDF Manual 17.1*.

[14] Hargreaves, D. M., & Wright, N. G. (2007). On the use of the k–ε model in commercial CFD software to model the neutral atmospheric boundary layer. *Journal of wind engineering and industrial aerodynamics*, *95*(5), 355-369.

[15] Wiernga, J. (1993). Representative roughness parameters for homogeneous terrain. *Boundary-Layer Meteorology*, *63*(4), 323-363.

[16] Grimmond, C. S. B., & Oke, T. R. (1999). Aerodynamic properties of urban areas derived from analysis of surface form. *Journal of applied meteorology*, *38*(9), 1262-1292.

[17] Hu, Z., Yu, B., Chen, Z., Li, T., & Liu, M. (2012). Numerical investigation on the urban heat island in an entire city with an urban porous media model. *Atmospheric environment*, *47*, 509-518.

[18] World Health Organization, WHO, Air quality guidelines for particulate matter, ozone, nitrogen dioxide and sulfur dioxide. Geneva 27, Switzerland, 2006.

[19] Eric, M., Markovic, Z., & Marinkovic, A. (2020). *Investigation about periodic investigation of emissions of air pollutants from thermal Power Plant "Nikola Tesla*". Obrenovac, Serbia.

Bioclimatic Classification of Locations in South-East Nigeria for Indoor Thermal Comfort

Stephen A. Ajah[1], Howard O. Njoku[2,3], Onyemaechi V. Ekechukwu[4]

[1]Department of Mechanical Engineering, Alex Ekwueme Federal University Ndufu-Alike, Abakaliki, Nigeria, stephen.aroh@funai.edu.ng
[2,4]Department of Mechanical Engineering, University of Nigeria, Nsukka, Nigeria, howard.njoku@unn.edu.ng[2]; nwokoma@gmail.com[4]
[3]Department of Mechanical Engineering Sciences, University of Johannesburg, Johannesburg, South Africa

Abstract—**The bioclimatic thermal comfort conditions at locations within Nigerian's south-east region were determined based on climate data for the period 1996 – 2019, obtained from the online NASA-SSE database. Data for seven cities in the region were used with the Givoni psychrometric chart to determine the predominant bioclimatic class of locations in the region. Locations in the region were found to have similar bioclimatic conditions with slight difference round the year. Generally, the region falls within the *natural ventilation and conventional* dry zone. Hence in these locations, indoor conditions that are within the bioclimatic comfort zone can be achieved by natural cooling of buildings besides conventional mechanical ventilation.**

Keywords – bioclimatic classification, thermal comfort, comfort zone

I. INTRODUCTION

A. Climatic Classifications in Nigeria

A crucial role of buildings is to adapt to the prevailing climate and provide internal environments which will be comfortable and conducive to the occupants [1]. Due to constant exposure to high solar radiation in tropical locations, the design of buildings in such locations should aim at achieving minimum heat gain indoors and maximum evaporative cooling to ensure the thermal comfort of occupants [2]. Occupants experience undesirable thermal conditions in buildings that are poorly designed in relation to the climate, which require a great deal of energy for cooling during climatic extremes [1]. For tropical climates, shading and ventilation effects are considered to be the most important environmental design factors for residential buildings [3]. These effects are mostly determined by the building orientations, height, and their exposure to the sky.

Climates in Nigeria are characterized by a strong latitudinal dependence, becoming drier as one moves towards the north from the coast. In terms of annual rainfall considerations, two precipitation regions are roughly identifiable -- a low precipitation region in the north leading to aridity and desertification and regions of high precipitation in the south which usually experience high flooding [4]. Nigeria is located in the tropical climate belt and wide climatic variations are witnessed all year round in different parts of the country. Around coastal area, temperatures are usually below 32℃ but humidity is relatively high with hot nights. Nigeria has basically two distinct seasons: wet season from April to October with lower temperatures, influenced by an air mass originating from the south Atlantic ocean, called the tropical maritime (TM) air mass and dry season from November to March, which blows from the Sahara Desert, known as the tropical continental (TC) air mass, with midday temperatures above 38℃ but relatively cool nights around 12℃ [5].

The climates in Nigeria have been studied to produce classifications that are f°C used on agricultural and weather prediction purposes with little or no application for building design [6]. Annually, two seasons are prevalent: a rainy (April-October) and a dry (November-March) season of approximately six months duration, with annual rainfall ranging from 500 m in the extreme north to 3000 m along the coast [7].

B. Architectural Based Classification

In a vernacular architectural study, locations in Nigeria have been classified into five climatic regions as hot-dry, temperate-dry, hot-humid, temperate-humid and temperate-dry with cool climate which are above sea level of 1520 m [6]. Alternatively, Ogunsote and Ogunsote [8] have classified Nigeria into six zones for architectural design purposes - the coastal zone, forest zone, transitional zone, savannah zone, highland and semi-desert zone. The translational, the savanna and the semi-desert zones were each further divided into two, a and b, resulting in nine distinct zones in all, with their respective responses but the information on monthly climate data of the selected locations is limited.

Some climatic classifications of Nigeria for architectural design purposes have been contradictory. E.g., the National Universities Commission divided the country into southern and northern regions, which is obviously over simplistic, without scientific justification and of not much use for architectural design [6]. Komolafe's classification also produced four climate divisions: hot-dry, temperate-dry, hot-humid and warm-humid [9]. The classification of Wladimir Peter Köppen resulted in four climate divisions: Warm Dessert Climate, Warm Semi-arid Climate, Monsoon Climate and Tropical Savanna Climate, while the Atkinson classification, using temperature, humidity, precipitation and sky conditions, resulted in four zones: composite, temperate, hot-dry and warm humid [10]. Roberto Costa [11] has classified Nigeria into Zone A (low vapour pressure, considerable number of hours of sunshine in a clear sky, great diurnal range in temperatures), Zone B whose characteristics are somewhere between those of zones A and C. Zone C (rain, short periods of clear sky, slight diurnal range in temperatures). Under these classifications, four separate regions are found in the country depending on the prevailing climatic zone: (RI) conditions of zone A prevalent; (RII) conditions of zone B prevalent; (RIII) characteristics of all

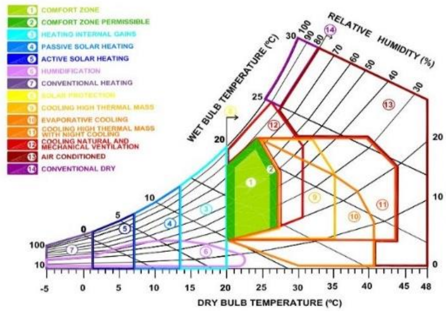

Figure 1. Psychrometric chart adopted from Givoni [15]

three zones present during the course of the year; and (RIV) conditions of zone C prevalent [11]. Eludoyin and Adelekan [12] concluded that the physiologic climate of Nigeria could not be explained based on the existing vegetation/rainfall climate classification systems but by a complex linkage of the influence of altitude, latitude and urbanization. Bioclimatic level of different regions/cities in Nigeria have been affected due to variation in the rainfall period and seasons of the year [13]. For decades now, there has been changes in Nigeria's climate which can be observed from the prevalent increases in temperature, periodic rainfall variation, slight altitudinal increment and flooding, drought and desertification, degradation of land resources, prevalent extreme weather conditions, fresh water resources destruction and different biodiversity losses [14].

Givoni psychrometric chart (GPC) [15], shown in Fig. 1, provides 14 zones for characterizing a locations bioclimatic condition. The zones include: 1) comfort zone, 2) permissible zone, 3) heating internal gains zone, 4) passive solar heating zone, 5) active solar heating zone, 6) humidification zone, 7) conventional heating zone, 8) solar protection zone, 9) high thermal mass cooling zone, 10) evaporative cooling zone, 11) nocturnal renovation with thermal mass cooling zone, 12) natural and mechanical ventilation cooling zone, 13) air conditioning zone and 14) conventional humidification zone.

II. THE STUDY AREA

The study sites are located within the South Eastern (SE) region of Nigeria. This region falls within the latitude 6°N and 8°N and longitude 4.5°E and 7.5°E (Fig. 2). The region which is densely populated covers an area of about 4×104 km^2 and represent 4.2% of the country's

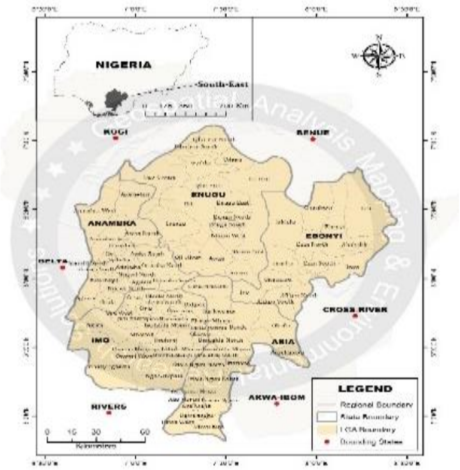

Figure 2. Map of South Eastern Nigeria with LGAs [16].

land mass. The SE zone is politically made up of five (5) States: Enugu, Anambra, Abia, Imo and Ebonyi state, which are generally referred to as the South-East geopolitical zone of Nigeria.

The climate of SE Nigeria is of the wet tropical type, with maximum mean annual temperatures in the range of between 27℃ and 34℃. The temperatures peak around March/April when the sun passes overhead of Nigerian latitudes [7]. This region is not known to for snow formation, though it has high precipitation limited to rainfall. Annual average rainfalls of roughly 1744 mm are recorded within the region, which drops inland from the Niger Delta area or the coast of Nigeria. This precipitation results in air moisture cooling sufficient enough to cause condensation.

In the absence of studies to determine the indoor thermal comfort classification of locations in Nigeria's SE region, this study undertook to determine this for seven locations in the region, which represent the major urban centres in the region. Thermal comfort classifications were determined on annual and quarterly bases, using climate data obtained from the NASA-SSE online database (1996 to 2019) [17].

III. METHODOLOGY

Daily annual average of relative humidities, dew point temperatures, dry bulb temperatures and the wet bulb temperatures of the locations were obtained. The five capital cities of states in the SE region (Abakaliki, Ebonyi State; Awka, Anambra State; Enugu, Enugu State; Owerri, Imo State and Umuahia, Abia State) and two other major population centres (Aba, Abia State and Onitsha, Anambra State) were considered in this study.

The climate data of each location was plotted on the GPC, the positions of the location's characteristic climatic conditions on the GPC were used to determine their annual thermal comfort classification and the classifications for different periods of the year.

IV. RESULTS AND DISCUSSION

From the data collected, the relative humidity of the South Eastern cities generally vary between 57% and 92%. The least value occur around January while the peak value occur around mid-June period. Similar trend is followed by the dew point temperature except that the third and last quarter of the year witnessed slight decrease. The maximum and minimum values of dew point temperature do recorded are 24.7℃ and 14.2℃ respectively. The cities were located in the GPC using the dry bulb temperature data.

A. Bioclimatic Classification of Aba City

Fig. 3 indicates the annual conditions of Aba on a GPC with dry bulb temperature data while the light green shaded area shows the desired comfort and permissible zone. This city is bound by prevalent temperature values of 23.6℃ and 28℃, relative humidity between 67% and 92%.

From the chart, the city falls mostly within the natural ventilation zone and slightly into the comfort permissible zone. Thus in addition to conventional mechanical ventilation, buildings in this city can be cooled by natural methods and to be in comfort zone. This can be done through the use of internal building plants and flowers,

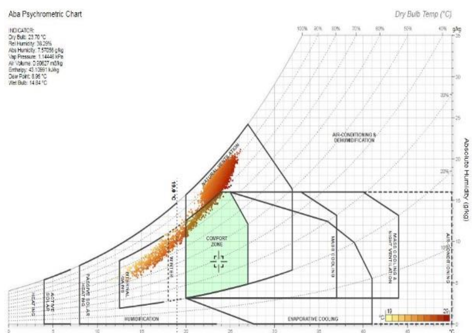

Figure 3. Annual climatic properties of Aba.

absorbent salts and saline cells, inducement of cross ventilation as natural ventilation strategy with vertical spaces within building.

B. Bioclimatic Classification of Abakaliki City

Fig. 4 indicates conditions in Abakaliki on a GPC. This city is bound by prevalent maximum temperature values of 23℃ and 27℃, relative humidities between 58% and 89%.

This indicates that conditions in Abakaliki mostly fall within the natural ventilation, internal heating zone but slightly within the permissible zone. Thus cool conditions within buildings located in the city can be acheived by the use of light and durable materials, wide windows and high walled spaces in addition to conventional mechanical ventilation like fans and blowers which consume small amounts of energy.

C. Bioclimatic Classification of Awka City

This city is bound by prevalent temperature values of 23℃ and 27℃, relative humidity between 59% and 90%. The classification (as shown in Fig. 5) indicated that Awka falls within the natural and mechanical ventilation and internal heating zone, though it is within the comfort zone for short periods.

For buildings within the city to be in comfort zone, natural ventilation through vertical spaces and wide windows in addition to conventional mechanical are needed with some tree shadings around the buildings.

D. Bioclimatic Classification of Enugu City

Enugu is bounded by temperature values of 24℃ and 27℃, relative humidity between 58% and 89% which are prevalent within the city. The annual classification of this city fall on the same zone as that of the Abakaliki city. The same

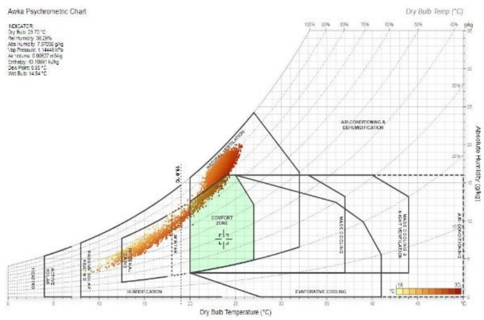

Figure 5. Annual climatic properties of Awka.

bioclimatic approaches can be applied to move the buildings in this location into comfort zone.

E. Bioclimatic Classification of Onitsha City

This city is bound by temperature values of 23.5℃ and 28℃, relative humidity between 61% and 90% that is prevalent within the city. The annual classification of this city falls in the same zone as that of Awka city.

The same bioclimatic approach as that of Awka can be applied to move the buildings in this location to comfort zone as seen in Fig. 6.

F. Bioclimatic Classification of Owerri City

Owerri city is bound by temperature values of 24.9℃ and 27℃, relative humidity between 70% and 90%. The annual classification of this city falls on the same zone as that of the Aba city. The same bioclimatic approach for buildings at Aba city can be applied to those in this location to achieve indoor comfort conditions.

G. Bioclimatic Classification of Umuahia City

Umuahia is bound by temperature values of 23.9℃ and 26.8℃, relative humidity between 64% and 90%. The annual classification of this city fall on the same zone as that of the Abakaliki

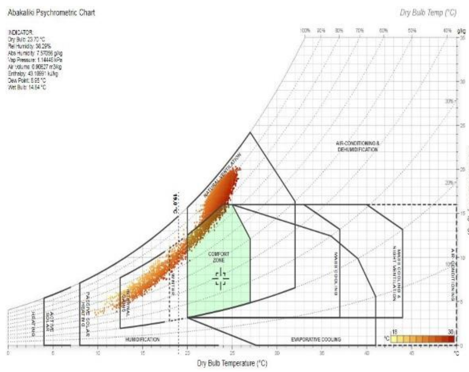

Figure 4. Annual climatic properties of Abakaliki.

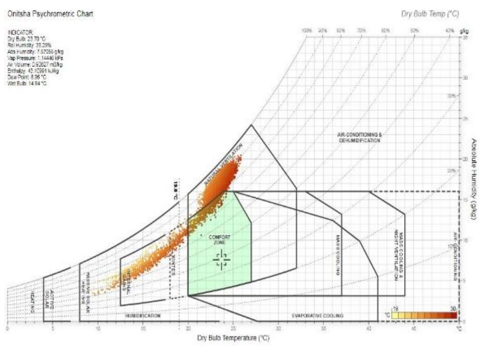

Figure 6. Annual climatic properties of Onitsha.

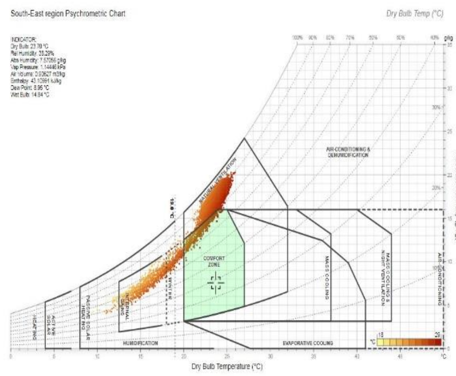

Figure 7. Annual climatic properties of SE region.

city and Enugu city. The same bioclimatic approach for buildings at Abakaliki city can be applied to those in this location to be in comfort zone.

H. *Bioclimatic Classification of South Eastern region*

Fig. 7 shows the annual conditions of SE region on a GPC. The average value of the data annual collected in the cities that make up the South Eastern region were used for the regions' classification. The region is annually bound by prevalent temperature values of 24℃ and 26.9℃, relative humidity between 62% and 90%.

The region falls natural ventilation and internal heating zone even though slight permissible comfort is witnessed within the region generally. Quarterly, the region is bound by temperature values of 25.1℃ and 26.1℃, relative humidity between 75% and 90% which is also within natural ventilation zone. Bioclimatic thermal control of the buildings with this region of the country do not require intense energy use.

V. Conclusion

Bioclimatic classification of the seven selected cities of the South Eastern region of Nigeria were individually done using their respective collected climate data. The classifications were done for annual basis to determine their different climatic properties. The average data of these selected cities in the region were used for the classification of the entire region. It has been found that the cities that made up the region as well as the region itself do not have wide climatic data difference throughout the year. The cities in the region have similar climatic conditions with slight difference. Generally, the region fall within non-comfort (natural ventilation and internal heating) zones. Thus buildings within the SE region need natural cooling in addition to conventional mechanical ventilation to be in comfort zone. This can be done through the use of internal building plants and flowers, inducement of cross ventilation as natural ventilation strategy with vertical spaces within building.

References

[1] Akande, O. K. (2010). Passive design strategies for residential buildings in a hot dry climate in Nigeria. *WIT Transactions on Ecology and the Environment*, *128*, 61-71.

[2] Zakaria, M. A., & Kubota, T. (2014). Environmental Design Consideration for Courtyards in Residential Buildings in Hot-humid Climates: A Review. *International Journal of Built Environment and Sustainability*, *1*(1).

[3] Ajibola, K. (2001). Design for comfort in Nigeria—a bioclimatic approach. *Renewable Energy*, *23*(1), 57-76.

[4] Akande, A., Costa, A. C., Mateu, J., & Henriques, R. (2017). Geospatial analysis of extreme weather events in Nigeria (1985–2015) using self-organizing maps. *Advances in Meteorology*, *2017*.

[5] Adedeji, O. O. (1997). Climatic zones for architectural design with climate in Nigeria.

[6] Dorcas Mobolade, T., & Pourvahidi, P. (2020). Bioclimatic Approach for Climate Classification of Nigeria. *Sustainability*, *12*(10), 4192.

[7] Uchechukwu, N. B., Agunwamba, J. C., Tenebe, I. T., & Bamigboye, G. O. (2018). Geography of Udi Cuesta Contribution to Hydro-Meteorological Pattern of the South Eastern Nigeria. In *Engineering and Mathematical Topics in Rainfall*. IntechOpen.

[8] Ogunsote, O. O., & Prucnal-Ogunsote, B. (2002). Defining climatic zones for architectural design in Nigeria: a systematic delineation. *Journal of Environmental Technology*, *1*(2), 1-14.

[9] Ajibola, K. (1997). Ventilation of spaces in a warm, humid climate—Case study of some housing types. *Renewable energy*, *10*(1), 61-70.

[10] Osinowo, A. A., & Okogbue, E. C. (2014). Correlation of Global Solar Irradiance with some Meteorological Parameters and Validation of some Existing Solar Radiation Models with Measured Data Over Selected Climatic Zones In Nigeria. *Int. J. Innov. Educ. Res*, *2*(1924), 41-56.

[11] Costa, R. (1989). Architecture in black Africa between development and tradition. *Solar & wind technology*, *6*(4), 383-387.

[12] Eludoyin, O. M., & Adelekan, I. O. (2013). The physiologic climate of Nigeria. *International journal of biometeorology*, *57*(2), 241-264.

[13] B. C. (1972). The variability of rainfall in Nigeria. *Niger. J. Sci.*, *6*, 87–91.

[14] Ebele, N. E., & Emodi, N. V. (2016). Climate change and its impact in Nigerian economy. *Journal of Scientific Research and Reports*, 1-13.

[15] Givoni, B. (1992). Comfort, climate analysis and building design guidelines. *Energy and Buildings*, *18*(1), 11-23.

[16] G. Archives. *South-East Nigeria on Map*. Available at: https://www.gamers.com.ng/south-east-nigeria-on-map/.

[17] NASA. *POWER Data Access Viewer: Prediction Of Worldwide Energy Resources*. Available at: https://power.larc.nasa.gov/data-access-viewer/.

Fog-based Architecture for Home Energy Management within the Smart Grid

Ivan Petruševski[1], Ivan T. Popović[2], Aleksandar Ž. Rakić[3]

[1,2,3]University of Belgrade, School of Electrical Engineering, Belgrade, Serbia
ivan.d.petrusevki@gmail.com[1]; popovici@etf.rs[2]; rakic@etf.rs[3]

Abstract—**The design and development of a home energy management system, as given in the Smart Grid vision, is burdened by complex integration requirements. Beside the integration of home-side equipment, like various home devices, smart appliances, distributed energy resources, it also assumes integration of electricity grid services, grid infrastructure and the consumer himself. In order to address such requirements, we have adopted an architectural approach to the design of home energy management systems, which is based on a fog computing model. The proposed approach enables rapid development and delivery of functionalities for energy management at residential level as a constituting part of foreseen distributed Smart Grid applications. The previous claim is supported by the case study of cross-fog application for peak shaving of home energy consumption.**

Keywords – home energy management, smart grid, fog computing, system architecture

I. Introduction

Smart Grid is an electricity network with the advanced capabilities of monitoring and control of all its entities in the segments of energy generation, transmission, distribution, and end-user consumption. The main goal of Smart Grid is to provide optimization and balance between the energy generation and demand by coordinating needs and capabilities of all stakeholders [1].

According to many analysts, the full potential of a Smart Grid cannot be achieved without the active involvement of energy management at the residential level [2,3]. Home Energy Management System (HEMS) is a constituent part of Smart Grid since it fulfills one of its primary goals - end-user integration into Smart Grid.

Smart Grid as a top-level concept integrates many different technologies in several different technology areas [4]. The wide-area monitoring and control area help system operators to understand and optimize power system components distributed over large geographic areas. Information and communications technology (ICT) integration area represents a communication infrastructure that supports two-way information exchange between stakeholders. The area of renewable and distributed generation (RDG) addresses technologies involved in integration of renewable resources on all levels, including the ones in residential buildings. The area of transmission enhancement applications covers technologies and applications for the optimization and maintaining stability of the transmission system. Distribution grid management area is aimed for technologies and applications that provides uninterrupted and stable electrical energy supply to end-customers. Advanced metering infrastructure (AMI) area involves several technologies that enable a two-way communication between utilities and end-customers. The area of electric vehicle charging infrastructure (EVCI) includes billing, scheduling during the low energy demand and other related features. Finally, area of Customer-side systems (CSS) covers both industrial and residential end-users with a variety of systems and applications for optimizing their energy consumption.

RDG, AMI, EVCI and CSS are technology areas that are in direct relation with end-users. HEMS inherently provides end-users with different CSS applications and services, but it should also provide interfaces to other end-user related technology areas. As a dedicated system for managing energy in home, HEMS is strongly coupled with locally available renewable energy sources, electrical vehicle charging and storage systems, as well as with the AMI.

The scope of Smart Grid is so broad that it has to include numerous standards from different technology areas in order to be interoperable and secure. The biggest challenge is to make systems in all areas interoperable for equipment delivered by a variety of producers and vendors. Even though there are standards that are addressing issues within certain technology areas, there is no broad integration framework. Considering HEMS as a coupling point of several technology areas, we are introducing a systematic approach to HEMS design that addresses all identified integration issues.

The rest paper of the paper is organized as follows. An overview of several state-of-the-art energy management concepts and solutions is given in Section II. The proposed fog-based HEMS architecture and the details on its software view are given in Sections III and IV, respectively. The case study illustrating peak shaving of home energy consumption is given in Section V. Concluding remarks and directions for future work are given in the final section.

II. RELATED WORK

The HEMS provides customers at the residential level the ability to monitor their energy consumption and production, but it also allows them to shape and optimize the profile of both consumption and production. Various techniques and system-level solutions were developed to support more efficient energy usage with minimized energy cost, like load scheduling, peaks shaving, demand response [5] consumption balancing, implementation of different pricing strategies [6], etc. Anyway, there are still many challenges regarding HEMS system design, implementation, and integration into the emerging concept of smart grid. Significant efforts of several industries and research working groups have been made to identify and develop the adequate approaches to address these challenges.

There are numerous HEMS related works presenting specific architectures [7,8] or control algorithm implementation through use cases [9]. The comprehensive study review [10] classifies optimization techniques and identifies various objectives of HEMS. Solving a particular problem of fair power demand sharing between consumers in the market with no sufficient electrical energy generation sources is presented in [11]. The study given in [12] is based on building model that combines thermal energy, heat pumps, photovoltaic and battery systems within a HEMS showed that a close-to-optimal performance can be achieved.

The survey on recent HEMS solutions [13] defines unified HEMS properties in the context of physical, operational and security constrains. The sensing and measuring devices, smart appliances, user interface, support for EV charging and central platform are identified as major HEMS components. Paper also presents the review of two approaches for centralized and distributed system management, in-operation goals, strategies to meet these goals, approaches in management of household appliances, uncertainties in HEMSs' decision-making and performance metrics.

The study [14] is covering the various technical and conceptual aspects of efficient power management at residential level with the focus on technological background, architectural and infrastructural challenged in the design and development of HEMS. The paper also proposes a novel methodology for reducing electricity consumption as a part of smart HEMS. The philosophy of the proposed smart HEMS is about creating awareness among the consumers, motivating them to actively participate in more efficient energy usage. The revealed potential of applying the peak load reduction technique together with optimization based residential energy management technique is reduction in electricity bills up to 35%. This could be influenced by various consumers' habits and behaviors. A survey on consumers' intention to use HEMS [15] recognized eight distinct types of consumers' energy saving behaviors based on different criteria such as demographic factors or the time spent at home.

The design of HEMS as a part of smart grid concept and its association with the functionalities of demand-side management and the plug-in electric vehicles' charging are given by vehicle-to-grid and grid-to-vehicle concepts in [16]. The study has identified that the contribution of HEMS application to the smart grid concept is not only in the improvement of the power system reliability, but also in the reduction of power losses and voltage fluctuations through coordinated EV charging and power peaks flattening.

The focus in [17] is prioritizing the operation of controllable appliances in price-based HEMS by introducing the lost load parameter of each appliance as an indication of its operational priority from the customer's perspective. The proposed HEMS is suggested to lead to the optimal scheduling of household electrical demand, minimizing the customer energy consumption and the reliability costs at the same time. The study also showed that incorporating the adequate tariff in the HEM program leads to the lower cost and flatten household load, which brings benefits to both the customers and distribution system operators.

The challenges identified in [18] are related to high implementation overhead on device vendors to manufacture HEMS compatible devices and lack of the ability to scale the HEMS solution to new device types and external variables. A novel architectural model and a functional framework for HEMS are introduced, where the focus is on simplicity and scalability of the solution that enables rapid system deployment.

The spectrum of the identified challenges in previously presented research emphasizes the need for a comprehensive HEMS architectural solution, and the research findings provide strong background for architecting a collection of primary viewpoints of the architecture. These views will be presented in following section.

III. HEMS Architecture

As already stated in this paper, a full HEMS potential and benefits can be gained only within the Smart Grid. HEMS, as a main energy manager on the residential level, directly correlates with the technology areas of RDG, AMI, EVCI, ICT and CSS. HEMS can be considered as an integration element of technology areas mentioned above. Therefore, the residential part of Smart Grid architecture will be in focus in this paper, as shown in Fig. 1.

RDG, AMI and EVCI are technology areas dealing with similar entities and services, such as energy consumption, energy production, energy demand and others. HEMS is responsible of connecting all mentioned technology areas together on the residential level. It can be referred to as a household interface for a Smart Grid, which integrates different systems from different vendors that belongs to any of the five mentioned technology areas.

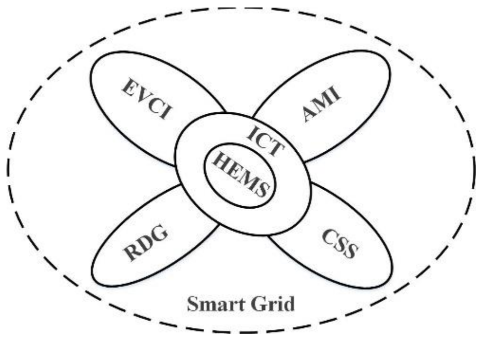

Figure 1. HEMS as a part of Smart Grid.

Interface toward EVCI enables implementation of smart grid-to-vehicle charging (G2V) and vehicle-to-grid (V2G) concepts which are introducing additional services for intelligent EV charging during low demand and/or low electricity price periods, management of capacity reserve for peak load shaving, etc.

Interface toward CSS enable monitoring and management of energy consumption via in-home displays or other energy dashboards, smart phone, or web applications. Energy management includes manual consumer control of smart appliances and smart sockets or intelligent automated control as a part of various services, supporting applications such as peak shaving or demand-side management.

Interface toward AMI enable gathering information about time and amount of consumed electricity supporting implementation of various services including monitoring services for collecting, storing and reporting of electricity usage, billing prediction, load desegregation, etc., all leading to more efficient energy usage. The interface could be realized in the form of two-way information flow supporting dynamic tariff, pre-paid pricing scheme and more effective debt management.

Management of renewable energy resources as a part of RDG at the residential level engage monitoring and control of generated and stored energy resources. This includes services for more efficient utilization of grid resources through demand-side energy management, maintenance of installed equipment, predictions of energy production, etc.

In order to manage such wide range of smart functionalities a home network has to be introduced, where different HEMS entities can exchange information in interoperable manner.

This involve usage of different wired and wireless communication technologies (ICT) and adequate communication equipment.

Thus, HEMS can be seen as complex system integrating different technology areas and smart functionalities distributed among them. The introduction of HEMS local interfaces does not eliminate the need for the interfaces toward upper levels of the Smart Grid. All of those interfaces should be operative and working in synergy in order to gain the full potential of Smart Grid concept.

A fog-based HEMS architecture is shown on Fig. 2. Different tiers provide scalability and interoperability within Smart Grid. Four tiers are shown on Fig. 2, but this number can vary in respect to the deployment size and area.

Device Integration Tier (Edge Tier) is responsible for the integration of different end-devices which belong to different Technology areas. Members of this tier are usually gateways toward the end-devices, provided by the end-device vendors. Node-to-device communication pathway, between this tier and end-devices, is implementing various communication protocols and technologies diversified among different products and vendors. Device Integration Tier fog nodes' main role is to provide services for uniform access to different devices produced by various vendors, from the higher levels of the Smart Grid. This tier can be considered as a device agnostic solution for integration of smart and legacy devices, mainly implementing data aggregation services. Those fog nodes are located close to the devices and are responsible for edge tier operations such as real-time device management and data gathering.

Residential Area Tier implements different application services available at the residential level, including user-interface service. Those services enable the development of various applications, including the applications for monitoring of energy usage, production and usage of renewable energy resources, demand management, node management, device maintenance, predictions of power peak and energy consumption and many others.

Neighborhood Area Tier provides implementation of services characteristic to the wider geographic area related to the specific household. Nodes closer to the network core services, located in the cloud, have higher processing capabilities. They perform more complex analytics to provide sophisticated services related to the smart grid, smart city, and other global applications.

Cross fog concept is based on distributed service execution that are deployed on different tires of the fog-based architecture, as depicted on the Fig. 2. One fog node can be a part of multiple cross fog applications, providing efficient deployment of various applications.

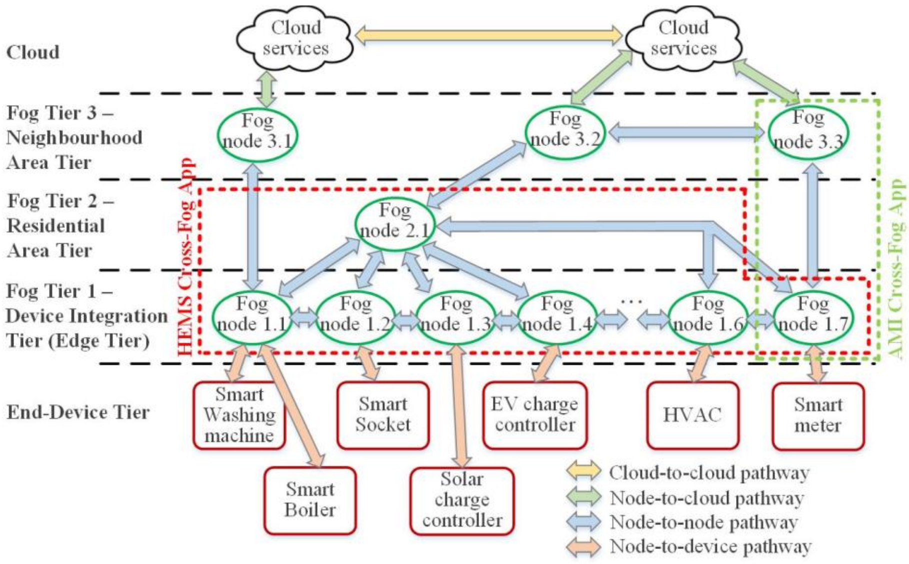

Figure 2. Fog-based HEMS architecture – logical view.

Taking into consideration previously described fog-based HEMS architecture, an example of physical deployment view is depicted in Fig. 3, which integrates devices and systems from all five previously mentioned technology areas. Electric vehicle charging, renewable energy generation, smart home devices, smart plugs, smart meter are all integrated on the level of Device Integration Tier. Fog node 1.7, as an edge tier node responsible for Smart Meter integration in the Smart Grid [19], is the joint node between two cross-fog applications. Main role regarding HEMS cross-fog application is to provide the total household electric energy consumption. Different wired and wireless communication technologies can be used for node-to-device communication, including UART, RS-232, RS-485, 3G, LTE, NB-IoT, LoRa, SigFox, WiFi, and BLE. Beside node-to-node communication pathway between two fog nodes, they can also communicate directly with cloud services over node-to-cloud communication pathway. For example, smart socket vendor can provide services for local integration, but also a cloud-based solution working in parallel. Vendors offer separate solutions in particular areas, such as smart sockets, electric vehicles chargers and others. HEMS deployed in the presented way offers integration of various vendors' devices and systems and development of additional energy management services.

IV. HEMS SOFTWARE ARCHITECTURE VIEW

Software architecture view of HEMS gives several structural software-related aspects of fog nodes that are the part of HEMS. In general, the elements of software architecture vary based on its position and role in tiered fog system deployment. Regardless of nodes processing and storage capabilities each fog node is required to have an ability to communicate with other entities within fog hierarchy, over node-to-device, node-to-node, or even node-to-cloud pathways. Also, each node must be able to discover and securely utilize services of other nodes in order to support building cross-fog application. By adopting micro-service architecture, fog computing is applicable in large-case and complex application scenarios.

As previously given, HEMS applications are also given as a collection of loosely coupled micro services physically distributed across the different nodes inside the fog computing infrastructure. According to the OpenFog reference architecture [20] software stack is organized into three software layers that are sitting on the top of the platform hardware layer (Fig. 4).

The software backplane layer contains common system software required to run other node software and to support inter-tier and intra-tier communications. This includes Operating system software, I/O device drivers and firmware, protocol stack, file system software, data confidentiality and integrity services, etc. On the other hand, node management services imply services for managing different stages of node life cycle, as node commission, provision, operational stage, node recovery and de-commission stage. Mentioned services provide support for automated discovery, registration, provisioning of connected devices, software updates, and sending alerts in the case of the system fault and abnormal operation.

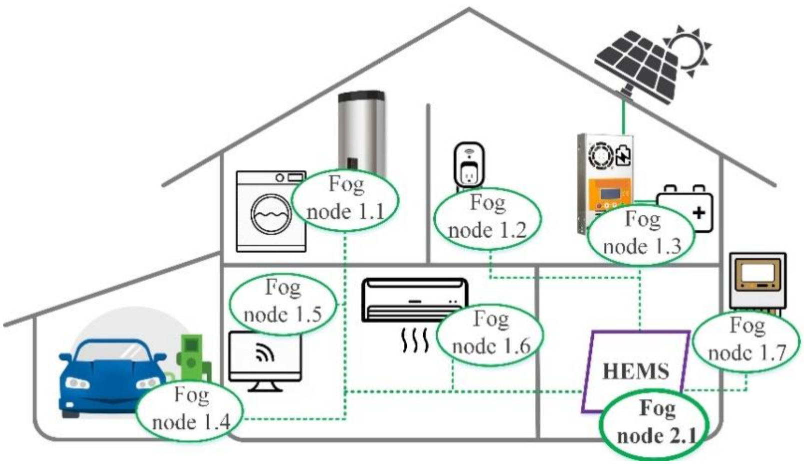

Figure 3. HEMS - physical deployment view.

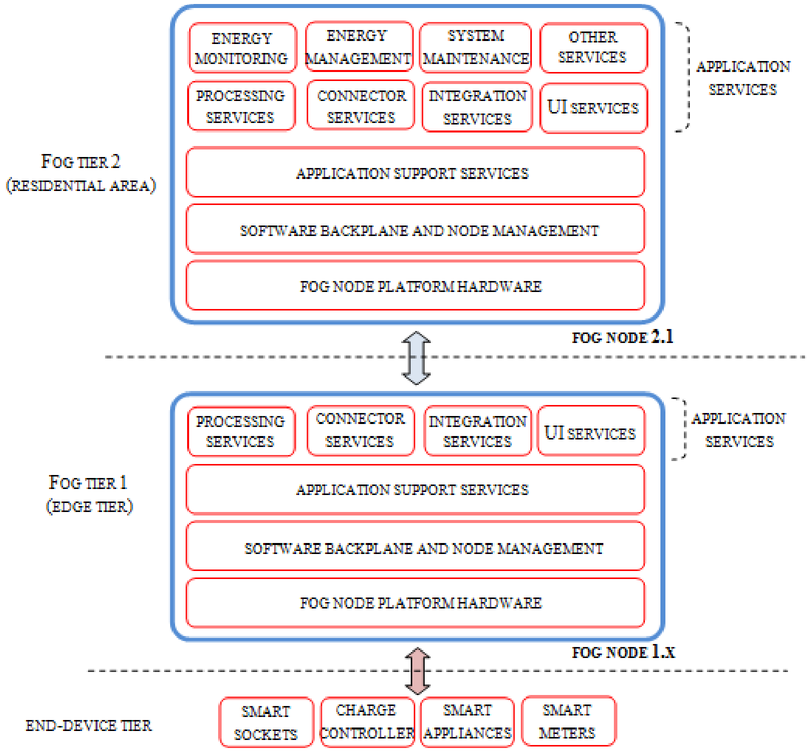

Figure 4. HEMS software architecture.

Application support layer services are not application specific but may be dependent on the underlying backplane and hardware layers. Application support layer contain variety of software tools and solutions, used and often shared by multiple application services, enabling application development, data and storage management, providing runtime execution environment for micro services and applications, application servers, security and middleware services, etc. Although not directly addressed at the service layers, other system perspectives, or cross cutting concerns related to the system performance, scalability, manageability, privacy, access control and security are employed through particular fog implementation.

Application services provide some application specific functionalities which vary based on node position and role in distributed architecture. Since the cross-fog application concept couples micro-services, which reside on different nodes, communication, integration, and orchestration of services is universally required. In order to support such requirements common application support services are deployed in both fog tiers. Connector services operate on the top of the protocol stack with the primary tasks of receiving and translating requests and responses into the common data structures and formats that are acceptable to destination services. Integration services enable inter-node communication by allowing outer nodes to request data of interest and providing the means to deliver such data using different communication mechanisms.

Processing services include different analytic capabilities encapsulated as reactive and predictive analytic services. At the edge tier data processing is mostly given in the form of simple data aggregation, segmentation, and filtering services, while the fog nodes at higher tiers perform more complex and sophisticated processing based on machine learning and other cognitive services.

In the case of HEMS, as previously given, different application domains are identified. These domains cover monitoring of energy usage and energy generation, node management and maintenance of residential devices and equipment, advanced energy management features related to peak shaving, load scheduling, support for dynamic tariffs, pre-paid billing,

billing prediction, etc. Each of the applications require underlying services at the application service layer as well as collection of remote-node services available through integration and fog connector services.

V. HEMS CASE STUDY

Smart Home Energy Balancing (SHEB) system is realized on presented principles and architecture as a case study of a cross-fog application for peak shaving. This system was installed in two households as a pilot project within EIT Climate-KIC Accelerator program. The main goal of this case study is to illustrate the implementation of peak shaving cross-fog application on the proposed HEMS architecture.

Peak shaving application utilizes processing services at Residential Area Tier for peak shaving algorithm, as well as data aggregation at Device Integration Tier providing aggregated one-minute based data. Peak shaving algorithm inputs are devices' priorities and total power limit value, which is configurable through user interface or through other cross fog applications, such as Peak-to-Average ratio application, demand management or others. Output of the algorithm is the control input for the micro services on the Device Integration Tier. Those micro services are used for allowing or denying the energy demand of a particular device over smart sockets. Algorithm uses simplified linear one step ahead prediction method for priority-based device control. Total household electrical energy consumption is provided by the dedicated node in Device Integration Tier, even though the same values could be gained from a fog node connected with a smart meter.

Illustration of described Peak shaving application operation is depicted in Fig. 5. Measurement and control over smart sockets are utilized only on the biggest electrical energy consumers in the household. Particular devices' data, presented in Fig. 5, is a one minute based average power, while data related to total engaged power in the household presents a 15-minute sliding window average, updated every minute. Once the algorithm detected that the total current 15-minute based average power will rise above the peak limit value, it sent command for denying the energy demand of the hot water boiler, since it has the lower priority. Therefore, a higher priority device, in this case the washing machine, could complete its cycle, after which the boiler was turned on again.

VI. CONCLUSION

Development of HEMS cross-fog applications bridges the gap between different smart grid technology areas at residential level. Since adopted fog computation model supports both horizontal and vertical inter-node communication pathways, the proposed architecture represents the highly scalable basis for the design of various distributed HEMS applications. Furthermore, the proposed HEMS architecture offers modularity and benefits of incremental design since such applications are built as collections of independently deployed and loosely coupled micro-services.

The proposed architecture has been implemented and successfully verified through the presented case study of peak shaving application.

Figure 5. Peak shaving application results.

Further refinement of the proposed architecture regarding the optimization framework and development of dedicated algorithms for energy management at the residential level are foreseen as a part of a future work.

ACKNOWLEDGMENT

This research was partially supported by the Serbian Ministry of Education, Science and Technological Development under contracts no. TR-32043 and TR 33024, as well as EIT Climate-KIC Accelerator programme.

REFERENCES

[1] IEC Smart Grid Standardization Roadmap. (2010). SMB Smart Grid Strategic Group, 1.

[2] Sintov, N. D., & Schultz, P. (2015). Unlocking the potential of smart grid technologies with behavioral science. *Frontiers in psychology*, *6*, 410.

[3] Kezunovic, M., McCalley, J. D., & Overbye, T. J. (2012). Smart grids and beyond: Achieving the full potential of electricity systems. *Proceedings of the IEEE*, *100*(Special Centennial Issue), 1329-1341.

[4] Smart Grids in Distribution Networks- Roadmap Development and Implementation. (2015). International Energy Agency.

[5] Shakeri, M., et al. (2017). An intelligent system architecture in home energy management systems (HEMS) for efficient demand response in smart grid. *Energy and Buildings*, *138*, 154-164.

[6] Abushnaf, J., Rassau, A., & Górnisiewicz, W. (2015). Impact of dynamic energy pricing schemes on a novel multi-user home energy management system. *Electric power systems research*, *125*, 124-132.

[7] Jebroni, Z., Afonso, J. A., & Tidhaf, B. (2020). Smart Home Energy Management System based on a Hybrid Wireless Network Architecture. *EAI Endorsed Transactions on Energy Web*, *7*(25).

[8] Kim, J. (2016). HEMS (home energy management system) base on the IoT smart home. *Contemporary Engineering Sciences*, *9*(1), 21-28.

[9] Shakeri, M., et al. (2018). Implementation of a novel home energy management system (HEMS) architecture with solar photovoltaic system as supplementary source. *Renewable energy*, *125*, 108-120.

[10] Qayyum, N., Amin, A., Jamil, U., & Mahmood, A. (2019). Optimization Techniques for Home Energy Management: A Review. In *2nd International Conference On Computing, Mathematics And Engineering Technologies (Icomet).*

[11] Abouelela, M. A., & Abouelela, M. M. (2016). Home Energy Management System (HEMS) For Fair Power Distribution. *Advanced Science Letters*, *22*(10), 2638-2641.

[12] Langer, L., & Volling, T. (2020). An optimal home energy management system for modulating heat pumps and photovoltaic systems. *Applied Energy*, *278*, 115661.

[13] Leitao, J., Gil, P., Ribeiro, B., & Cardoso, A. (2020). A survey on home energy management. *IEEE Access*, *8*, 5699-5722.

[14] Mahapatra, B., & Nayyar, A. (2019). Home energy management system (HEMS): concept, architecture, infrastructure, challenges and energy management schemes. *Energy Systems*, 1-27.

[15] Nakano, S., & Washizu, A. (2018). An analysis on Consumers' Introduction Intention to Home Energy Management Systems (HEMS). *Journal of the Japan Institute of Energy (Web)*, *97*(7), 205-215.

[16] Hartono, B. S., Mursid, S. P., & Prajogo, S. (2018). Home energy management system in a Smart Grid scheme to improve reliability of power systems. In *IOP Conference Series: Earth and Environmental Science* (p. 012081).

[17] Rastegar, M., Fotuhi-Firuzabad, M., & Zareipour, H. (2016). Home energy management incorporating operational priority of appliances. *International Journal of Electrical Power & Energy Systems*, *74*, 286-292.

[18] Dittawit, K., & Aagesen, F. A. (2013, August). Architecture and functional framework for home energy management systems. In *Meeting of the European Network of Universities and Companies in Information and Communication Engineering* (pp. 173-184). Springer, Berlin, Heidelberg.

[19] Petrusevski, I., Zivanovic, M., Rakic, A., & Popovic, I. (2014). Novel AMI architecture for real-time Smart Metering. In *22nd Telecommunications Forum Telfor (TELFOR)*.

[20] OpenFog Reference Architecture for Fog Computing, OpenFog consortium architecture working group, 2017.

Environmental Comparison of the Origin of Electric Power Consumed in Breweries

Daniel de Paula Diniz[1], Monica Carvalho[2]

[1]Graduate Program in Mechanical Engineering, Federal University of Paraiba, João Pessoa, Brazil, danieldiniz@cear.ufpb.br

[2]Department of Renewable Energy Engineering, Federal University of Paraiba, João Pessoa, Brasil, monica@cear.ufpb.br

Abstract—**Beer production in Brazil has been growing in recent years, and one of the reasons for this growth is a large number of micro and small breweries opened in the country, especially in the Northeast. The beer production process is a major consumer of electricity, especially in stages where cooling is required. This study compared greenhouse gas (GHG) emissions associated with electricity consumption from the Brazilian grid (electric mix) with solar photovoltaic electricity, applying to a real case of a brewery located in João Pessoa, Paraíba. The methodology used was the Life Cycle Assessment (LCA), with SimaPro v.9.0.0.35 software and Ecoinvent database. The environmental impact assessment method was IPCC 2013 GWP100a, which represents the values in terms of GHG (kg CO_2-eq). The partial replacement of the electric mix by photovoltaic solar energy proved to be very beneficial from an environmental point of view, representing -180 kg CO_2-eq for every 20% replacement in the case of the Brazilian mix. These values are associated with the consumption of 1 kWh of electricity, and a brewery consumes about 113.88 kWh per hectoliter of beer produced. It is concluded that there is potential for climate change mitigation associated with energy transition in breweries.**

Keywords – beer, life cycle assessment, electricity, photovoltaic solar energy, greenhouse gas emissions

I. INTRODUCTION

Beer is the most consumed alcoholic beverage in the world and its global consumption reached 2.5 billion hectoliters (hL) in 2016 [1]. Brazil has a large share of this market, according to the Brazilian Beer Industry Association - CervBrasil, recently the country reached the level of 140x106hL of beer produced, placing the country in the third position in the world rank, behind only China (460x106hL) and the United States (221x106hL), but in front of traditional brewing countries such as Germany (95x106hL) and Russia (78 x 106 hL) [2].

However, the large scale of beer production has resulted in substantial environmental impacts due to resource-intensive use. Alcoholic beverages, including beer, are estimated to account for 0.7% of global GHG emissions when the life cycle is considered [3]. Most of these emissions are associated with the energy consumption required for the production, transportation and distribution of beverages [4-7].

Energy decarbonization employs low-carbon fuels or energy vectors, thereby seeking to diversify the energy matrix, reduce dependence on fossil fuels and mitigate climate change [8-10]. An efficient way to decarbonize energy is to include renewable energy in full or partial replacement over fossil fuels.

In Brazil, the environmental benefit of the introduction of renewable energy generation has been proven, such as photovoltaic solar energy in the Brazilian electric mix [11]. According to the authors, despite being in full growth, photovoltaic solar energy is still inexpressive in the Brazilian energy matrix.

According to the National Energy Balance [12], base year 2018, electric power generation in Brazil reached the level of 636.4 TWh, with hydropower representing 66.6% of this amount

ISBN: 978-86-80616-07-0

while solar energy only 0.5%. Adding to other renewable sources, such as wind and biomass, 83.3% of total electricity generation in Brazil comes from renewable sources. In the Northeast region, the sources of electric power generation make up a matrix slightly different from the national scenario, especially the wind source. According to data from the National System Operator (ONS) Daily Preliminary Operating Information (IPDO), the wind source, in 2018, accounted for more than half of the northeast's electricity generation, reaching a percentage of 50.36% of the matrix of this region [13].

Electricity consumption by the industrial sector represents 37.7% of all electricity generated in the country, and 9.2% of this consumption refers to the food and beverage industry, making this industry the largest consumer of electricity in the country [14].

Brewing is an energy-intensive process, and its environmental impact has been the subject of several LCA studies [3,15-31]

Reference [32] conducted a study in a pilot beer plant, where the total electricity consumption for the production of 72 liters of beer was 82 kWh (31.7% for the activation of equipment and accessories, 20.7% for heating and 47.6% for cooling during brewing), totaling 113.88 kWh/hL. As beer production in the country has reached 140 million hL [2], the amount of energy required to sustain this production can reach 1.59 x 107 MWh. This amount demonstrates the importance of the inclusion of renewable energies in the beer sector.

The Brazilian Northeast region has been standing out as one of the largest beer producers in the country. In the last five years, the region's participation in the country's production grew by 1.2%. In total there has been a 26.2% increase in the region in the last five years, while the national average has been a 14.3% growth. The increase in consumption was mainly driven by the interior of the Northeast, with an increase of 40.6% [33].

As economic growth is related to energy consumption and consequently to GHG emissions, environmental and energy indicators can be employed for process evaluation. The carbon footprint is an important indicator for analyzing interactions between economic and human activity, energy consumption and GHG emissions.

A product's carbon footprint is a quantification of GHG emissions over its life cycle. All emissions within the value chain boundary of a specific product are accounted for and assigned to a functional unit, which may be very specific as to the nature of the product. Aggregated GHG emissions from all product-related activities from raw material extraction through manufacturing and distribution and including consumer use and end-of-life (recycling/disposal) are included in the carbon footprint of a product.

II. OBJECTIVE

The aim of this study is to apply the LCA methodology to quantify the carbon footprint associated with the consumption of electricity in the beer industry, using as a case study a brewery located in the city of João Pessoa, Paraíba, Brazil. Northeast Brazil.

III. METHODOLOGY

LCA is one of the most widespread methodologies used and consolidated for the calculation of environmental impacts, ranging from raw material extraction, manufacturing, transportation or distribution, use and final disposal of waste products or services.

The LCA is internationally standardized by the International Organization for Standardization [34,35], which in Brazil was translated by the Brazilian Association of Technical Standards (ABNT) into NBR ISO 14040 and NBR ISO 14044 [36,37].

LCA has four interrelated phases [34,35]: i) definition of the objective and scope, in this phase the boundaries of the analysis and the objective of the study and the functional unit that will be used are defined; ii) inventory formulation, which will be a quantified survey of data on all inputs (materials, energy and resources) and outputs (products, by-products and emissions) all associated with a previously established functional unit iii) identification and assessment in terms of Potential environmental impacts that can be associated with inventory data, this step applies an environmental impact assessment method to express the results; iv) interpretation of results.

To develop the LCA was used the software Simapro 9.0.0.35 [38] with Ecoinvent database [39]. The environmental impact assessment method applied was IPCC 2013 GWP 100a [40], which groups GHGs emitted over a 100-year horizon, expressing the results achieved in terms of kg CO_2-eq. The functional unit considered here was the consumption of 1 kWh of electricity.

For the consumption of electricity from the national grid, the methodology reported by Reference [11] was used to estimate the GHG emissions associated with the consumption of 1 kWh of electricity from the grid in Brazil in 2018, which used the National Electric System Operator [41] data for the period, dividing the sources of power generation into: hydroelectric 71.80%, thermal 16.70%, wind 8.30%, nuclear 2.70% and solar 0.50%.

For the electricity consumption from photovoltaic panels, the Electricity, low voltage {BR} | electricity production, photovoltaic, 3kWp slanted-roof installation, multi-Si, panel, mounted | APOS, S from the Ecoinvent database [39]. APOS refers to “At Point Of Substitution”, which is the attributional approach, where environmental burdens are allocated in proportion to the causative processes. S corresponds to "System".

The Brazilian process comprises the generation of electricity (low voltage) in a 3 kWp system installed on a sloping roof with 30-year service life. Includes the manufacture and installation of multi-crystalline silicon panel (mc-Si, with 13.5% efficiency and 270-300μm cell thickness), ancillary equipment, cabling, and maintenance (cleaning) water.

Table I shows the electricity consumption of the brewery, obtained from a quantitative survey.

IV. RESULTS AND DISCUSSION

Following [11], the carbon footprint associated with the electricity consumption of the national grid in 2018 was 0.259 kg CO_2-eq/kWh. For the electricity obtained from photovoltaic panels, the carbon footprint was 0.0766 kg CO_2-eq/kWh.

The factory production averages 50 hL/month, which corresponds to 116.85 kWh/hl of beer, very close to that found by [32], who obtained 113.88 kWh/hL in pilot scale.

Table II presents the results of GHG emissions associated with the progressive substitution of electricity from the Brazilian electric mix by photovoltaic solar energy, for the brewery installed in João Pessoa - PB.

With the total replacement of the energy source, using photovoltaic panels for power generation, the brewery emits about 448 kg CO_2-eq/month. This is much lower than the Business as Usual scenario, employing only the Brazilian electric mix, which emits 1513 kg CO_2-eq/month.

In a more realistic case, partial substitution is already very effective, representing about -213 kg CO_2-eq/month for each 20% substitution. Over the course of the year, considering the 12 months of operation, these values are quite significant: 2556 kg CO_2-eq/year when 20% of the electricity is substituted by photovoltaic.

Although the Brazilian electric mix is considered a low-carbon mix, in terms of significant hydroelectric contribution, it still presents an important share of fossil fuels. The partial introduction of solar photovoltaic electricity is quite beneficial in terms of GHG, as seen herein. The introduction of renewable

TABLE I. ELECTRICITY CONSUMPTION AT THE BREWERY [AUTHOR’S RESEARCH].

Month	Consumption (kWh)
December	4519
January	6218
February	5860
March	6350
April	5857
May	6252

TABLE II. GREENHOUSE GAS EMISSIONS ASSOCIATED WITH MEETING THE ELECTRICITY DEMANDS OF THE BREWERY [AUTHOR’S RESEARCH].

Photovoltaic solar energy	Greenhouse gas emissions (kg CO_2-eq)
0% (Current situation)	1513
20%	1300
40%	1087
60%	874
80%	661
100%	448

sources, in general, is always beneficial when comparing with the utilization of fossil fuels. These were the same conclusions as [42], who compared GHG emissions associated with electricity generation with diesel and then biomass gas. Lower emissions were also obtained by [43], who verified the carbon footprint associated with the ice cream pasteurization process, where they replaced fuel oil with solar thermal energy. Reference [42] calculated GHG emissions associated with electricity generation from sugarcane bagasse and compared with diesel generation, obtaining considerable environmental advantages with the use of bagasse. Reference [44] studied the supply of electricity to a heat pump, comparing the electric mix with photovoltaic solar electricity and reaching environmental benefits with the latter.

A small brewery that produces about 50 hL per month was used herein as a reference. Considering the overall Brazilian reality, with a production of 12 x 106 hL per month, potential avoided emissions reach 613 x 103 t CO_2-eq per year with only 20% energy substitution. Even the partial replacement of electricity from the Brazilian grid with photovoltaic solar energy has significant potential for mitigating climate change.

V. Final Considerations

This work quantified the carbon footprint associated with the consumption of 1 kWh of electricity to a brewery using electricity from the national electric mix (grid) and then simulated the progressive substitution by photovoltaic electricity generation.

The partial substitution has been demonstrated to be an environmentally viable alternative.

The results can help inform how to diminish the negative effects associated with brewery activities. Applying similar research to food and beverage companies could mitigate the intensification of the greenhouse effect, as the sum of avoided emissions in different sectors is potentially high.

Through such research and paradigm shifts, it will be possible in the near future to establish a low carbon economy.

Acknowledgment

The authors thank the National Council for Scientific and Technological Development (CNPQ, Research Productivity grant, No. 307394/2018-2) and the Coordination for the Improvement of Higher Education Personnel (CAPES) for the MSc. scholarship.

References

[1] Statista. (2018). *Consumption of alcoholic beverages worldwide from 2016 to 2020* (in billion liters). Available at: https://www.statista.com/statistics/726990/alcoholic-beverage-consumption-worldwide/.

[2] CERVBRASIL *Associação Brasileira da Indústria da Cerveja*. (2016). Available at: http://www.cervbrasil.org.br/novo_site/anuarios/CervBrasil-Anuario2016_WEB.pdf.

[3] Cimini, A., & Moresi, M. (2016). Carbon footprint of a pale lager packed in different formats: assessment and sensitivity analysis based on transparent data. *Journal of Cleaner Production*, *112*, 4196-4213.

[4] Russell, S. T., Singh, R. P., & Bamforth, C. W. (2008). Alternative paradigms for the production of beer. *Journal of the Institute of Brewing*, *114*(4), 349-356.

[5] Brewers Association. (2012). *Energy Usage, GHG Reduction, Efficiency, and Load Management Manual*. Boulder, Colorado.

[6] Olajire, A. A. (2020). The brewing industry and environmental challenges. *Journal of Cleaner Production*, *256*, 102817.

[7] Strobl, M. (2019). Continuous Beer Production. In *New Advances on Fermentation Processes*. IntechOpen.

[8] Smil, V. (2015). Energy transitions, renewables and rational energy use: A reality check. *Organisation for Economic Cooperation and Development. The OECD Observer*, (304), 36.

[9] Smil, V. (2016). Examining energy transitions: A dozen insights based on performance. *Energy Research & Social Science*, *22*, 194-197.

[10] Kahn, S. (2016). Caminhos da oferta e demanda de energia ao longo do século XXI. *Boletim de Conjuntura*,*10*, 8-10.

[11] Carvalho, M., & Delgado, D. (2017). Potential of photovoltaic solar energy to reduce the carbon footprint of the Brazilian electricity matrix. *LALCA: Revista Latino-Americana em Avaliação do Ciclo de Vida*, *1*(1), 64-85.

[12] BEN *Balanço Energético Nacional 2019: Ano base 2018.* Available at: http://www.epe.gov.br/sites-pt/publicacoes-dados-abertos/publicacoes/PublicacoesArquivos/publicacao-377/topico-470/Relat%C3%B3rio%20S%C3%ADntese%20BEN%202019%20Ano%20Base%202018.pdf .

[13] ONS - Operador Nacional do Sistema Elétrico, *IPDO Informativo Preliminar Diário de Operação,* Available at:

http://www.ons.org.br/paginas/conhecimento/acervo-digital/documentos-e-publicacoes?categoria=IPDO.

[14] EPE – Empresa de Pesquisa Energética. (2018). *Análise da eficiência energética em segmentos industriais selecionados – alimentos e bebidas* Available at: http://www.epe.gov.br/pt/publicacoes-dados-abertos/publicacoes/projeto-de-assistencia-tecnica-dos-setores-de-energia-e-mineral-projeto-meta.

[15] Amienyo, D., & Azapagic, A. (2016). Life cycle environmental impacts and costs of beer production and consumption in the UK. *The International Journal of Life Cycle Assessment*, *21*(4), 492-509.

[16] BIER - Beverage Industry Environmental Roundtable. (2012). *Research on the carbon footprint of beer. Beverage Industry Environmental Roundtable*, Available at: http://media.wix.com/ugd/49d7a0_70726e8dc94c456caf8a10771fc31625.pdf.

[17] Cimini, A., & Moresi, M. (2018). Mitigation measures to minimize the cradle-to-grave beer carbon footprint as related to the brewery size and primary packaging materials. *Journal of Food Engineering*, *236*, 1-8.

[18] Climate Conservancy. (2008). *The carbon footprint of Fat TireR amber ale*. Available at: www.newbelgium.com/Files/the-carbon-footprint-offat-tire-amber-ale-2008-public-fist-rfs.pdf.

[19] Chicago Manufacturing Center. (2009). *The product carbon footprint of Goose Island brewery 312 beer keg*. Available at: www.glproject.com/filebin/pdf/312_Keg_Footprint_Report.pdf.

[20] EPD. (2010). *EPDR Carlsberg and Tuborg beer. Reg. no S-EP-00264.* Available at: http://www.environdec.com/Detail/?Epd=7819.

[21] EPD. (2011a). *EPDR Tuborg beer. Reg. no S-P-00311*. Available at: http://environdec.com/en/Detail/epd311.

[22] EPD. (2011b). *EPDR BAP Bock chiara and BAP Bock rossa Beer. Reg. no. S-P-00314*. Available at: http://www.environdec.com/en/Detail/epd314.

[23] EPD. (2013). *UN CPC 2431 Beer made from malt. Version 1.01, The International EPDR System.* Available at: http://www.environdec.com/en/PCR/Detail/?show_login=true&error=failure&Pcr=7934.

[24] EPD (2014a). *EPDR Birrificio Angelo Poretti luppoli bockchiara and Birrificio Angelo Poretti luppoli bock rossa Beer. Reg. no. S-P-00314*. Available at: http://gryphon.environdec.com/data/files/6/9938/epd314en_v4.pdf.

[25] EPD (2014b). *EPDR Kronenbourg 1664R Beer. Reg. no. S-P-00533.* Available at: http://www.environdec.com/en/Detail/?Epd=9931.

[26] Koroneos, C., Roumbas, G., Gabari, Z., Papagiannidou, E., & Moussiopoulos, N. (2005). Life cycle assessment of beer production in Greece. *Journal of Cleaner Production*, *13*(4), 433-439.

[27] Lalonde, S., Nicholson, A., & Schenck, R. (2013). *Life cycle assessment of beer in support of an environmental product declaration. Institute for Environmental Research and Education (IERE).* Available at: http://iere.org/wp-content/uploads/2013/10/IERE_Beer_LCA_Final.pdf.

[28] Munoz, E., Riquelme, C., & Cardenas J. P. (November 2012). Carbon Footprint of beer—Analysis of a small scale processing plant in Chile. In *Proceedings of the 2nd LCA Conference*, Lille, France.

[29] Narayanaswamy, V., Altham, W., Van Berkel, R., & McGregor, M. (2005, February). Application of life cycle assessment to enhance eco-efficiency of grains supply chains. In *Proc. Aust. Conf. on Life Cycle Assessment, 4th, Sydney, Australia* (pp. 23-25).

[30] Talve, S. (2001). Life cycle assessment of a basic lager beer. *The International Journal of Life Cycle Assessment*, *6*(5), 293-298.

[31] Williams, A. G., & Mekonen, S. (2014, October). Environmental performance of traditional beer production in a micro-brewery. In *Proceedings of the 9th International Conference on Life Cycle Assessment in the Agri-Food Sector (LCA Food 2014), San Francisco, California, USA, 8-10 October, 2014* (pp. 1535-1540). American Center for Life Cycle Assessment.

[32] Trommer, M. W., & Coutinho, A. R. (2013). ACV do processo de produção da cerveja. *Encontro Nacional de Engenharia de Produção. Anais do ENEGEP*, Salvador, ENEGEP.

[33] CERVBRASIL – Associação Brasileira da Indústria da Cerveja. (2019). *Participação do nordeste na produção nacional de cerveja cresce 1,2% nos últimos cinco anos.* Available at: http://www.cervbrasil.org.br/novo_site/participacao-do-nordeste-na-producao-nacional-de-cerveja-cresce-12-nos-ultimos-cinco-anos/.

[34] International Organization for Standardization – ISO. (2006). ISO 14040:2006: Environmental management - Life cycle assessment - Principles and framework, Genebra.

[35] International Organization for Standardization – ISO. (2006). ISO 14044:2006: Environmental management - Life cycle assessment - Requirements and guidelines, Genebra.

[36] ABNT - Associação Brasileira de Normas TécnicaS. (2009). Gestão Ambiental – Avaliação do Ciclo de Vida - Princípios e estrutura: NBR ISO 14040, Rio de Janeiro, versão corrigida 2014a.

[37] ABNT - Associação brasileira de Normas Técnicas. (2009). Gestão ambiental - Avaliação do ciclo de vida - Requisitos e orientações: NBR ISO 14044, Rio de Janeiro, ABNT – versão corrigida 2014b.

[38] PRÉ CONSULTANTS, SimaPro. (2019). Available at: http://www.simapro.nl

[39] ECOINVENT. (2018). *Database*. Available at: http://www.ecoinvent.ch

[40] IPCC. (2013). *Revised supplementary methods and good practice guidance arising from the Kyoto protocol*. Available at: http://www.ipcc-nggip.iges.or.jp/public/kpsg/

[41] ONS - Operador Nacional do Sistema Elétrico, *Carga e Geração*. Available at: http://www.ons.org.br/paginas/energia-agora/carga-e-geracao.

[42] Carvalho, M., et al. (2019). Carbon footprint of the generation of bioelectricity from sugarcane bagasse in a sugar and ethanol industry. *International Journal of Global Warming*, *17*(3), 235-251.

[43] Melquíades, T. F., et al., (2019). Pegada de carbono associada ao processo de pasteurização de sorvetes. *Revista em Agronegócio e Meio Ambiente*,*12*(2), 609-629.

[44] de Souza Grilo, M. M., Fortes, A. F. C., de Souza, R. P. G., Silva, J. A. M., & Carvalho, M. (2018). Carbon footprints for the supply of electricity to a heat pump: Solar energy vs. electric grid. *Journal of Renewable and Sustainable Energy*, *10*(2), 023701.

Cost Efficiency Analysis of a Solar Energy Integrated Fast Charging Station

Naireeta Deb[1], Rajendra Singh[2]

[1,2]Holcombe Department of Electrical and Computer Engineering, Clemson University, Clemson, SC 29634 USA, ndeb@clemson.edu[1]; srajend@clemson.edu[2]

Abstract—**This paper presents a concept building up to the implementation in a fast charging station integrated with a solar electricity generation system. Using such a system, demand charge can be met, load profile can be improved, and the operational costs of the fast charging station can be minimized heading to cost efficiency. To achieve this, the PV generation system with its limited capacity, will produce electricity that can be used to recharge electric vehicles during on-peak hours. So, it will be possible to shift the EV load from the peak to the valley periods. Therefore, the optimal fast charging station not only reduces the cost of electrical energy, but also improves the network load profile. The detailed analysis of contributing factors and cost calculation of the same is presented in this paper.**

Keywords - charging station, electric vehicles, solar energy, cost function

I. INTRODUCTION

It is no secret that the electric vehicles are the new transport technology that modernizes transportation and contributes to environmental, economic, and humanitarian concerns. It has garnered ever growing attention from industry and consumers alike. However, the development of electric vehicles will automatically point out the necessity of a fast charging infrastructure. The most important factor remains designing a fast charging station that provides the expected demand without breakdown of existing grid. The integration of free fuel resources may eliminate this challenge. Photovoltaic (PV) systems are emerging as a major source of current and future electric power [1]. There are few places on the earth (e.g. Scandinavian countries) where solar intensity is low and there is abundance of wind energy. Implementing free fuel solar and wind generated electrical power and use of batteries for storing electrical power can provide sustainable electric power to all. Photovoltaics has various advantages over wind turbines. The solar panels are cheaper and easier to install. PV power rate per KWh is cheaper than wind. Solar electrical power is also produced as DC power which can directly be used to charge the EV battery or stored in an energy storage unit (ESU) without going through multiple power conversion stages. Thus, reducing energy loss per conversion stage and reducing the installation cost by reducing the necessity of the expensive power electronics converters will reduce system cost and improve energy efficiency.

The integration of a solar and wind generated electrical power with EV charging stations is very well covered in the literature but none of them discuss the economic aspects [2]. This paper proposes to use the power generated from the solar panels to be used during on-peak hours to charge electric vehicles. Thus, the EV charging load on the grid will be shifted from on peak hours to the off-peak hours. The lower tariff rates during off peak hours consolidated with the power generated from solar energy, will give customers cost efficiency. Therefore, the optimal fast charging station not only reduces the cost of electrical energy, but also improves the network load profile. The rest of the paper is arranged as follows. Section II discusses several aspects of electrification with free fuel energy sources. Section III discusses the factors affecting the cost of solar power installation. Section IV shows a business model of practical scenario along with cost efficiency calculations. Finally, the paper is concluded in section V.

II. ELECTRIFICATION WITH FREE FUEL ENERGY SOURCES

The automobile sector consumes one third of world's total energy demand and contributes to one sixth of total greenhouse gas emission [3]. It is also the fastest growing sector for free-fuel energy penetration. Worldwide there are nearly one billion passenger vehicles and 335 million commercial vehicles according to latest statistics. The number has been rising steadily over the past decade like only China almost quadrupling its vehicle sales. Similarly, in USA, transportation contributes to almost 30% of greenhouse gas emission [4]. But the positive news is that passenger vehicles in USA are electrifying at an unparalleled rate. While one million EVs were on the road in 2018, it is predicted by recent studies that the number will be approximately 20 million by 2030. According to International Energy Agency, globally this number could surpass 250 million by 2030 [5]. EVs are 2 to 3 times more energy efficient than gasoline powered vehicles and have almost zero tailpipe emissions. Despite this they might add to the greenhouse gas emission and the air quality degradation depending on the source of electrical power generation that is used by charging stations. Quite evidently it is found that areas heavily populated with fossil fuel generation, even the good intentioned consumer adapting EVs can contribute nothing to the cause of climate change [6]. One study found that in China, EVs contribute two to five times more smog than gasoline-powered vehicles, due to the country's reliance on a coal-fired grid [7].

Acknowledging this, the main focus is now to attract residential and commercial customers to use free-fuel energy for their EV electricity needs, this includes charge scheduling that synchronizes the free fuel energy generation times with the vehicle charging times considering the places with/without adequate storage. For instance day- time charging can be scheduled with peak solar generated power and nighttime charging can often align well with wind generated electrical power.

Several steps have been taken in that direction as mentioned earlier. One can be expressed as network charging which encourages the customers to use a network of stations to charge their EVs which are powered by free fuel energy sources. Austin energy in Texas has constructed an 800-station strong charging network that allows unlimited charging to customers for 4.17$/month [8]. More than one third of the EV owners in that area participate in this program. EVgo has announced that it will power its charging network with 100% solar energy within a couple of years [9]. There is another program called managed charging [10] in which customers synchronize or delay their charging according to the availability of free fuel generated power in favor of lower charging rates.

Charging with onsite free fuel generated energy is another scheme that utilities endorse. The utilities like San Diego gas and electric implemented on site solar canopies and energy storage units that were used in the adjacent charging station [11]. Similar system is employed by google where 750 chargers are installed for their employees which are fully powered by their own PV systems.

Cost efficiency is one of the main reasons for consumers to adopt an emerging technology. As solar energy is cheaper and can be easily stored, its cost can be lower than grid connected power thus making the customers choose the times of the day when solar energy is available.

All these make the cost of ownership very low apart from contributing to undo the effects of climate change.

A. Global Carbon Emission

The Scientists predict catastrophic climate events in near future due the pollutants exerted in the nature by mankind [12]. It is imperative to reduce the emission of anthropogenic green-house gas emission imminently to secure the future of this planet. Efforts to achieve this are being taken by reducing use of fossil fuels for electricity generation, for transport propulsion and by adopting mitigating practices such as reduction of energy consumption and protection of carbon sinks. The internal combustion engines (ICEs) are not only used in transport sector but also for equipment in agriculture and manufacturing industries. Replacement of those engines by electric motors are dependent on a suitable energy alternative that can be stored conveniently as well as being cost effective just as fossil fuel-based electricity.

The transport sector is although the biggest contributor of GHG as the ICES release particles especially those fueled by diesel pollute the air posing a grim developing threat to health problems in largely populated cities [13]. Particle emission is also contributing to soot deposits on the Greenland Ice Sheet, reducing its albedo and accelerating surface melting and Arctic warming [14]. The number of fossil fueled vehicle are still rising with expanding global economy and population and EVs only contribute to 1% of the total vehicle fleet [15]. The hassle of slow charging and the low range of earlier EVs was not making it a lucrative choice for customers which is swiftly improving every passing day. With the development of solid-state batteries which use a solid electrolyte instead of a liquid, the wastage of battery production will come down about 30% thus further reducing the carbon footprint of EV production [16]. Companies like Accuracy Recycling GmbH, Aqua Metals Inc., Exide Technologies and many more, create an evolving battery recycling industry trying to impart a greener future for our environment [17]. In essence, it can be stated that a sharp reduction in the burning of fossil fuels must be achieved over the next decade to avoid catastrophic global warming and climate change within a few decades. A pie chart showing the CO_2 emissions by sector is shown below in Fig. 1 [18].

B. *Autonomous Vehicle will be Electric*

Automation of urban transportation will bring a revolution to electrification of transportation over the next decade [19]. Most self-driving cars seen on road currently are PHEV or BEV. The hybrid technology is projected to slim down in the upcoming years as the electric cars usurp the throne of ICEVs. The reasons autonomous vehicles will be electric are

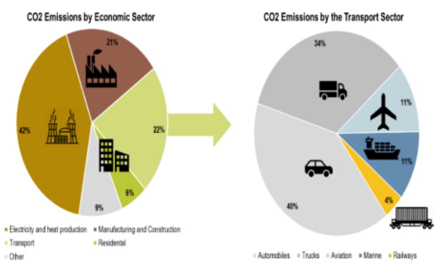

Figure 1. CO2 emissions by sector [18].

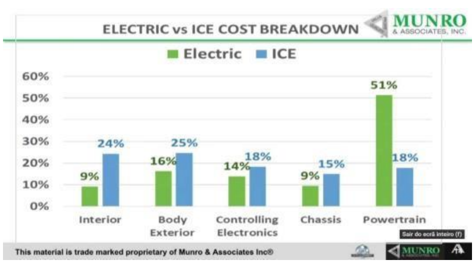

Figure 2. Different parts of EV and ICEV costs compared [23].

numerous, but some important ones are explained below. The regulatory reasons come first in mind which start with the gas mileage requirements [20]. The engineering reasons which make the computers easier to interface with the electric vehicles. The commercial fleet services like Uber or buses will opt for electric vehicle for their unmanned vehicles because it is easier to charge the vehicle than putting fuel in it. Electrification also means less maintenance time required so the commercial autonomous vehicles will opt for the electric option. Last but not the least, the cost effectiveness of EV is always better than ICEV [19].

Most personal transportation vehicles are parked 95% of the time, but even the 5% usage rate requires regular maintenance to avoid breakdown [21]. The human error factor, when eliminated, the artificial intelligence (AI) algorithm correctly calculates every driving movements giving a higher accuracy of driving, thus, less wear and tear leading to less maintenance time. This is especially important as mentioned, to fleet operators. With autonomous vehicle being autonomous and electric, with far fewer moving parts, the maintenance time will drastically be cut short.

EVs are cheaper in fuel cost than ICEV. The overall lifetime of EV vs ICEV [22] and their cost per mile is gradually on the decline with the ongoing development in battery technology. Companies like Tesla are researching on a million-mile battery which will last the entire life cycle of the EV on the road thus eliminating the replacement cost. The cost breakdown [23] of EV and ICEV is given in Fig. 2.

Another interesting push for electrification of transportation overall comes from the grid. As people are getting more dependent on free fuel energy sources, the load on grid is gradually declining. In future electric AVs will become a larger segment of the heavy- duty vehicle fleet. The massive, distributed battery banks in electric AVs and the charging station's free fuel storage will help the utilities to increase demand, support and build a more resilient grid and balance loads [24].

Another advantage as mentioned before is easy charging for unmanned vehicle than fueling gasoline. The electric AVs can charge on their own using wireless charging through inductive charging station thus making charging safer and more easily automated and integrated than gas powered AV.

Last but most important reason for electrification of AVs will pave way to save the climate. The vehicle automation might magnify the vehicle usage and decarbonize the environment rather than exacerbating them via gasoline powered AVs.

C. *Energy Storage*

The energy storage technology has seen massive development in Lithium ion battery modules in terms of cost reduction and increasing energy density. Still, energy storage technology is one of the variable cost factors that needs to be included in the analysis. Companies like Tesla are producing batteries in massive numbers in its Gigafactory in Nevada, Berlin etc. The volume of manufacturing reduces manufacturing [25]. Like Tesla, companies like Panasonic, North Volt, Chem and CATL have set up or are in the process of setting up large scale battery manufacturing units in China, South Korea, Japan, Europe and the USA. Bloomberg news report [26] forecasts large demand growth in manufacturing capacity. The projection tells that the battery pack price will fall as low as 73$/KWh. Fig. 3 shows the gradual decline in battery costs over the years. Based on the trend line, there was a 16% annual decline in the cost of battery packs between 2007 and 2019, and the industry-wide average cost of battery packs in 2019 was US $161 per kWh [27].

D. *Fuel Celled EVs*

Although the fuel cell energy storage research is taking momentum and has several advantages, but it is not feasible to implement right now or soon. The high cost poses the main barrier to its widespread implementation [28]. Traditional fuel sources are far less expensive than fuel cells at this point. Although Hydrogen is abundant in nature, it is hard to store, utilize and fill up the fuel stations with pure Hydrogen.

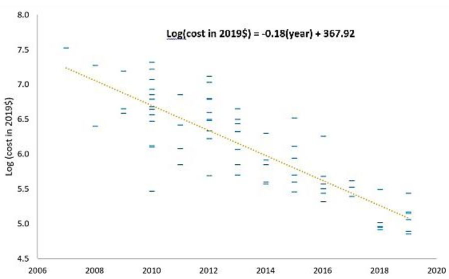

Figure 3. The gradual decline of battery cost over the years [27]

The cost of manufacturing platinum electrodes is quite high. In addition most of the fuel cell technology is in the prototype stage. There is lack of data to validate the various claims made in the media.

III. Factors Affecting Solar Power Installation Cost

A. *Number of Solar Panels Purchased*

The number of solar panels are directly proportional to the power requirement of the charging station. The percentage of power that is supposed to be coming from solar energy is the determining factor of how many solar panels are to be purchased [29]. The larger solar power system, the greater number of panels, the more it will cost. However the companies provide concession to the installer of customer's choice if the purchase is in bulk [30]. Overall this cost factor seems to be a constant in a planning scenario where the capacity of the solar charging station is pre-determined hence the number of panels known.

B. *Ease of Installation*

There are several factors that constitute the cost of installation or labor cost, as discussed in [31]. The ease of installation being one of the major cost factors. If the roof is simple and flat or an angled roof that faces the ideal solar absorbing direction for a particular location, the installation is faster and therefore less costly. Houses with irregular rooflines, skylights, and challenging angles can make installation more complicated.

C. *Type of Solar Panels*

The type of solar panel is the choice of the solar and charging station integration committee or typically the power utility company or the EV manufacturing company. The prospects of choosing type of solar panels and related environment have grown in an industry that has put a lot of effort into developing efficient techniques to generate, use, and store the sun's energy by using different types of solar panels and converting the sunlight into valuable electricity [32]. The Table I shows the top 10 solar panel manufacturing companies with their module/panel efficiency.

Better panel produces more energy more efficiently, thus saving more money for more years. But the primary cost will also be more. For instance, thin film panels can be cited, they cost less than the crystalline ones, but are not as durable or as efficient as bulk silicon modules, the replacement will occur way sooner too. Even within the two categories of thin film and crystalline, there are sub-categories which cost different due to quality and manufacturer brand. The factors that affect the power generated by PV modules are efficiency, irradiance (W/m2), shading, panel orientation, temperature, location (latitude), and time of year, dust, and dirt. Among these, the role of temperature and irradiance are the most important ones to address. Irradiance is influenced by geographical location, time of the year and most importantly temperature. Too high temperature is not applicable for optimum solar power generation efficiency. The example shown in [34] can be discussed here keeping in mind the business models. The paper took a very hot area as a case study and generated solar irradiance data. The observation of the paper was that low intensity sun gave low temperature which means more efficiency from PV panel during these days where sun intensity seems low.

Better panel produces more energy more efficiently, thus saving more money for more years. But the primary cost will also be more. For instance, thin film panels can be cited, they cost less than the crystalline ones, but are not as durable or as efficient as bulk silicon modules, the replacement will occur way sooner too. Even within the two categories of thin film and crystalline, there are sub-categories which cost different due to quality and manufacturer brand. The factors that affect the power generated by PV modules are efficiency, irradiance (W/m2), shading, panel orientation, temperature, location (latitude), and time of year, dust, and dirt. Among these, the role of temperature and irradiance are the most important ones to address. Irradiance is influenced by geographical location, time of the year and most importantly temperature. Too high temperature is not applicable for optimum solar power generation efficiency. The example shown in [34] can be discussed here keeping in mind the business models. The paper took a very hot area as a case study and generated solar irradiance data. The observation of the paper was that low intensity sun gave low temperature which means more efficiency from PV panel during these days where sun intensity seems low.

TABLE I. MARKET DOMINATORS IN SOLAR MANUFACTURING AND THEIR EFFICIENCY [33]

	Make	**Model**	**Power (W)**	**Efficiency (%)**
1	SunPower	Maxeon 3	400	22.6
2	LG	Neon R	380	22
3	REC	Alphs	380	21.7
4	Longi Solar	Hi-Mo 4	375	20.6
5	Trina Solar	Honey M DEO8	375	20.5
6	Solaria	Power XT	370	20.5
7	Jinko Solar	Tiger Pro 6RI3	390	20.4
8	Canadian Solar	HIDM CS1H- MS	345	20.4
9	Phono Solar	TwinPlus-M4-9B-R	375	20.4
10	Q cells	Q.Peak DUO G8+	360	20.3

IV. CASE STUDY

A. Planning the Business Model

Power utilities worldwide are opting for clean energy in favor of economic and technological advancements. Reduced cost and emission are intertwined in the business model that utilities want to choose. Most of the major utilities in USA like Duke Energy, Dominion Energy, South California Gas and Electric are commissioning ambitious free fuel energy integrated projects that give customers the affordability and serves to the clean energy goals.

The customers are also a part of generation now and that is transforming the business models of the utilities. Efficiency and demand response continue to flatten utility demand growth, but a lot is yet to be achieved. Customers providing their own power through customer-side solar and storage exacerbates efficiency-driven flat demand for electricity. In this context of demand response and burden sharing with the utilities the charging stations mainly have two business models to consider as follows:

i. Utility Providing Power from Free Fuel sources
ii. EV Charger Company generates local DC power

When utility is providing the solar power/wind power to be used in the charging station i.e. scenario (i), then, the cost of solar power will be higher as the utility will charge their profit margin in that and then sell the power to the company that has built the charging station. But there is no installation cost or maintenance cost as mentioned in previous sections. So for the companies with lesser capital may choose this option.

For larger companies, they might choose to generate solar power for this specific charging station in a site nearby as mentioned in business model (ii) and store it in battery. Thus, making the power free, not considering, the installation cost.

B. *Example*

To put the cost-efficient model into perspective a practical case needs to be examined. Tesla recently installed 56 numbers of V3 supercharger in a charging station in CA, making it the largest charging station by them, to date. The convenient location near a store and restaurant makes planners think that it will be utilized enough to gain profit. Although by a popular survey report calculates that [35] most of the charging station is not utilized more than 12-18% of its capacity but below the power calculation of such a charging station at 100% occupancy for 24 hours a day is done for the validation of these business models. The 250KW charger being utilized 24 hours a day for 365 days will need 2.190 MWh of power. The on peak times can be given as 12PM to 7PM during the summer months of high temperature and 8AM to 3PM during the colder months. The average per unit cost of electricity in California is 16.67 cents/KWh. Depending on the location and the tiers decided by PG&E the price of electricity can be 30 to 50 cents in peak hours. So for 2190 MW power the cost of the peak hour electricity becomes 191,625 $/year for 30 cents/KWh or 319,375 $/year, for 7 hours a day, 365 days. Solar energy however costs from 6 cents/KWh to 10cents/kWh. Replacing the grid power with solar energy cost, the charge per day, for 7 hours, will be 63.875 $/year or 38,325 $/year for 7 hours a day, for 365 days, for prices 10 C/KWh and 6c/KWh, respectively. Thus giving savings from 153,300$ to 255,500$ per year for different rate and tariff types.

Considering the charging station draws off peak power from the grid and rates remain constant throughout the year for off peak hours.

V. CONCLUSION

In this paper the factors and propose an innovative idea to build a cost-efficient solar power integrated charging station has been analyzed. The solar energy is harnessed and stored to be utilized during the high peak hours of the day to charge the electric vehicle. Therefore the consumer is able to shift the EV charging load from the peak to the valley period and therefore the optimal fast charging station not only reduces the cost of electrical energy for the individual consumer but also improves the network's load profile benefitting the grid. However, the shifting of load effectively during on peak hours and sensing the time effectively remains a challenge. The aspect of intelligent control agents and development of affective algorithms for the fast change in load requirements during the valley and peak period will form the nucleus of our work in the next segment of this research.

REFERENCES

[1] Singh, R., Alapatt, G.F., & Lakhtakia, A. (2013). Making solar cells a reality in every home: Opportunities and challenges for photovoltaic device design. *IEEE Journal of the Electron Devices Society*, *1*(6), 129-144.

[2] Quddus, M.A., Kabli, M., & Marufuzzaman, M. (2019). Modeling electric vehicle charging station expansion with an integration of renewable energy and Vehicle-to-Grid sources. *Transportation Research Part E: Logistics and Transportation Review*, 128, 251-279.

[3] *4 emerging ways to pair electric vehicle and renewable energy*. Available at: https://www.wri.org/blog/2019/11/4-emerging-ways-pair-electric-vehicles-and-renewable-energy

[4] *Car emissions and global warming*. Available at: https://www.ucsusa.org/resources/car-emissions-globalwarming#:~:text=In%20total%2C%20the%20US%20transportation,than%20almost%20any%20other%20s ector.

[5] *World energy outlook 2020*. Available at: https://www.iea.org/reports/world-energy-outlook-2020

[6] *EV are 2 to 3 times more energy efficient than gasoline powered vehicles and have almost zero tailpipe emissions*. Available at: https://afdc.energy.gov/vehicles/electric_emissions.html

[7] *In coal-powered china, electric car surge fuels fear of worsening smog*. Available at: https://www.scientificamerican.com/article/in-coal-powered-china-electric-car-surge-fuels-fear-of-worsening-smog/

[8] *Power up on electric drive*. Available at: https://austinenergy.com/ae/green-power/plug-in-austin/electric-drive

[9] *Evgo goes nation's first renewable*. Available at: https://www.prnewswire.com/news-releases/evgo-goes-100-renewable-to-power-the-nations-largest-public-ev-fast-charging-network-growth-ev-managed-chargingopportunityutilities/20May%207%2C%202019,United%20States%20to%20do%20so.

[10] *Beyond load growth: The EV managed charging opportunity for utilities*. Available at: https://sepapower.org/knowledge/beyond-load-growth-ev-managed-charging-opportunity-utilities/

[11] *What a smart grid means for san diego*. Available at: https://www.sdge.com/more-information/environment/smart-grid/smart-grid-sdge

[12] *EVs: Cruical to reducing CO_2 emissoions*. Available at https://skepticalscience.com/EVs-are- crucial.html

[13] *Global greenhouse gas emissions by the transportation sector*. Available at: https://transportgeography.org/?page_id=15778

[14] *The study of earth as an integrated system*. Available at: https://climate.nasa.gov/nasa_science/science/

[15] *Global EV outlook*. Available at:https://www.iea.org/reports/global-ev-outlook-2020

[16] *Battery breakthrough gives boost to electric flight and long-range electric cars*. Available at: https://www.sciencedaily.com/releases/2020/07/200720102044.html

[17] *Insights into the worldwide battery recycling industry to 2028 - featuring Accurec Recycling, Aqua Metals & Battery Recycling made easy among others* Available at: https://www.businesswire.com/news/home/20200420005653/en/Insights-into-the-Worldwide-Battery-Recycling-Industry-to-2028---Featuring-Accurec-Recycling-Aqua-Metals-Battery-Recycling-Made-Easy-Among-Others---ResearchAndMarkets.com

[18] *Global greenhouse gas emissions by the transportation sector*. Available at: https://transportgeography.org/?page_id=15778

[19] *Will autonomous vehicles be electric*. Available at: https://www.bu.edu/ise/2018/08/27/will- autonomous-vehicles-be-electric/

[20] *6 surprising ways driverless cars will change our world*. Available at: https://www.nbcnews.com/mach/science/6-surprising-ways-driverless-cars-will-change-our-world-ncna867061

[21] *Today's cars are parked 95% of the time*. Available at: https://fortune.com/2016/03/13/cars-parked-95-percent-of-time/

[22] *EV vs ICEV cost breakdown and it's affect on EV adoption.* Available at: https://leandesign.com/ev- vs-ice-cost-breakdown-and-its-effects-on-ev-adoption/

[23] *Why self driving cars will be electric*. Available at: https://www.usatoday.com/story/money/cars/2016/09/19/why-most-self-driving-cars-electric/90614734/

[24] *Electric cars will challenge state power grids*. Available at: https://www.pewtrusts.org/en/research-and- analysis/blogs/stateline/2020/01/09/electric-cars-will- challenge-state-power-grids

[25] *Lithium-ion battery costs and market*. Available at: https://data.bloomberglp.com/bnef/sites/14/2017/07/BNEF-Lithium-ion-battery-costs-and-market.pdf

[26] *Battery pack prices fall as market ramps up with market average at $156/kWh in 2019*. Available at: https://about.bnef.com/blog/battery-pack- prices-fall-as-market-ramps-up-with-market-average- at-156-kwh-in-2019/

[27] *Analysis shows continuious industry wise decline in battery cost*. Available at: https://mackinstitute.wharton.upenn.edu/2020/ electric-vehicle-battery-costs-decline/

[28] *Fuel cell electric vehicles*. Available at: https://afdc.energy.gov/vehicles/fuel_cell.html#:~:text=What%20is%20a%20fuel%20cell,produce%20no%20harmful%20tailpipe%20emissions

[29] *Solar energy costs*. Available at: http://www.alternativeenergyprimer.com/Solar-Energy-Costs.html

[30] *Understanding the cost of commercial solar energy*. Available at: https://telamonenergy.com/blog/cost-of-commercial- solar-energy-solutions

[31] *What factors affect the prices of low-priced u.s. solar PV systems?* Available at: https://www.osti.gov/servlets/purl/1378573/

[32] *Find the right solar panel that fits your home*. Available at: https://www.greenmatch.co.uk/blog/2015/09/types-of-solar-panels

[33] *Most efficient solar panels*. Available at: https://www.cleanenergyreviews.info/blog/most-efficient-solar-panels

[34] Paniyil, P., Powar, V., Singh, R., Hennigan, B., Lule, P., Allison, M., Kimsey, J., Carambia, A., Patel, D., Carrillo, D., & Shriber, Z. (2020). Photovoltaics-and Battery-Based Power Network as Sustainable Source of Electric Power. *Energies*, *13*(19), 5048.

[35] Wolbertus, R., Van den Hoed, R., & Maase, S. (2016). Benchmarking charging infrastructure utilization. *World Electric Vehicle Journal*, *8*(4), 754-771.

Life Cycle Assessment of Different Medical Devices and their Influence on the Environmental Impact of Healthcare Buildings

M Botejara-Antúnez[1], P Garrido-Píriz[2], G Sánchez-Barroso[3], J González-Domínguez[4], J García-Sanz-Calcedo[5]

[1,2,3,4,5]University of Extremadura, Graphical Expression Department, Badajoz, Spain, jgsanz@unex.es[5]

Abstract—**Currently, the optimization of material resources, energy efficiency and the reduction of environmental impact are very important aspects in the selection of a product, process or system. Healthcare buildings are a type of building composed of numerous systems, products and processes, which allows a high margin of improvement in energy efficiency and in the reduction of the environmental impact generated by their construction. The main objective of this work is to test the viability of applying a Life Cycle Assessment (LCA) study to various medical devices, as well as to see the influence of these on the life cycle of a healthcare building. Through the review of the existing literature, a series of characteristics have been defined that allow the construction of scientific knowledge in relation to the application of the methodology to different medical devices. In this way a series of results have been obtained such as the generation of a tool for planning environmental strategies, policies and programmes, the generation of a tool for the evaluation of energy savings, the selection of alternatives for correct waste management and sustainable construction, and the reduction of the total environmental impact generated from the building's construction project. Finally, one of the most important conclusions is the demonstration of the high value that the LCA technique has in the evaluation of environmental impacts. This helps to reduce the total environmental impact generated in the manufacture of a sanitary device, with repercussions on both social and economic benefits. The latter will usually be associated with the reduction of waste and operating costs, and energy savings. In addition, solutions have been proposed for the main drawbacks, such as the creation of a guide for the application of LCA methodology or the provision of training courses.**

Keywords – LCA, medical device, healthcare building, environmental impact

I. INTRODUCTION

Life expectancy is increasing worldwide. From 2000 to 2015, global life expectancy at birth increased by 5.5 years [1]. In parallel to this increase, over the same period, current global health expenditure increased from 5.4 % to 6.3 % of world gross domestic product (World's GDP) [1]. This increase also leads to a growing environmental impact. For example, the US health sector is responsible for 8% of the country's CO_2 equivalent emissions, while hospitals are responsible for 39% of the nation's health sector CO_2 equivalent emissions. [2].

Recent studies have shown that operating rooms are, in addition to the heating, ventilation and air conditioning (HVAC) system, the main driver of the environmental impact of surgical procedures and represent up to 65% of the global warming potential (GWP) [3,4]. Therefore, reducing the environmental impact of surgeries by selecting instruments and implants with a reduced environmental impact throughout their life cycle could contribute to reducing the environmental impact of the total healthcare system.

Life cycle analysis (LCA) is a method used to assess potential environmental and human health impacts over the life of a product, including impacts from: extraction and processing of raw materials, manufacturing, distribution, use, maintenance and repair, and disposal [5]. The LCA attempts to address a range of environmental concerns, including: the compilation of energy and material inputs and outputs; the assessment of potential impacts attributed to the inputs and outputs; and the interpretation of the results to help make a more informed decision [5]. According to International Organization for Standardization (ISO) documents 14040 and 14044, an LCA is defined by four distinct steps, namely: definition of objective and scope, inventory analysis, impact assessment and interpretation [6].

The first step of an LCA, the definition of objective and scope, explicitly sets the context of the study, defines the precise quantities of which product will be analysed and characterises the measure to which the life cycle of a product is analysed (for example, manufacture, use, disposal). After the objective and scope are defined, the second step of the study is the inventory analysis. Inventory analysis documents the exact amounts of emissions, materials and energy to and from the environment. Following the inventory analysis is the impact assessment, which aggregates the inventory data into categories of environmental and human health impact. The final step is interpretation, which is normally carried out iteratively throughout each step of the methodology. Interpretation is carried out in such a way that information from the inventory and impact assessment steps are identified, quantified and evaluated.

The main objective of this study is to evaluate the necessity and feasibility of applying the LCA methodology in medical equipment. The aim is to demonstrate the reduction of the environmental impact generated by this technique throughout the life of a healthcare building, while also favouring other factors such as: reduction of waste, reduction of raw material extraction, economic savings and energy efficiency.

II. METHODOLOGY

To carry out this case study, we used a search of existing bibliography in different scientific databases such as Web of Science (WOS) and Scopus. Firstly, an exhaustive search was carried out for studies based on the LCA of different products in the healthcare field using the following keywords: medical device, LCA and environmental impact. Then, the state of the art was shaped, checking the viability of the work. The bibliography was then analysed in order to obtain the various characteristics provided by the LCA methodology when applied to devices in the healthcare field.

Then, with the different characteristics extracted from this bibliography, an analysis of the results was carried out, adapting the information obtained to the case study of this work, so that a series of advantages and drawbacks of applying this tool to health devices were obtained. To get this, each of the different studies had to be analysed, trying to extract the information that best adapted to this type of healthcare product. With the information obtained from this analysis, the viability of applying the LCA methodology to healthcare devices was evaluated, as well as analysing the impact that it generates on the life cycle of healthcare buildings. In this way, the aim is to visualise the various synergies obtained.

As a summary, a graphic scheme of the methodology followed in this work is presented. This is illustrated in Fig. 1.

III. LITERATURE REVIEW

Firstly, from the review of the scientific and technical literature extracted from various scientific databases, Table I was drawn up.

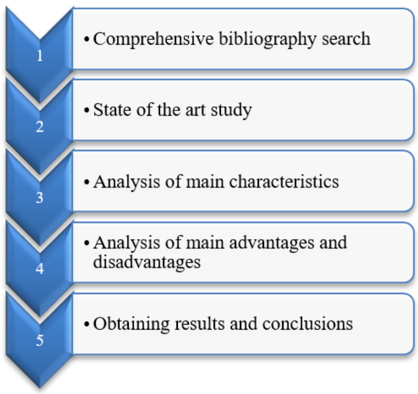

Figure 1. Scheme of the used methodology.

TABLE I. GENERAL DESCRIPTION OF STUDIOS THAT WILL EVALUATE LIFE CYCLE OF PRODUCTS IN THE HEALTHCARE FIELD.

Product	Reference	Journal	Country	Object of study
Medical device	McGain et al. (2017) [7]	British Journal of Anaesthesia	Australia	Anaesthetic equipment
	Unger & Landis (2016) [8]	Journal of Cleaner Production	USA	Several reprocessed medical devices: a deep vein thrombosis compression sleeve, a pulse oximeter, etc.
	Campion et al. (2015) [9]	Journal of Cleaner Production	USA and Thailand	Disposable custom pack
	Sørensen & Wenzel (2014) [10]	Journal of Cleaner Production	Denmark	Bedpans
	Ibbotson et al. (2013) [11]	International Journal of Life Cycle Assessment	Germany	Surgical scissors
	Eckelman et al. (2012) [12]	Anesthesia&Analgesia	USA	Laryngeal mask airways (LMA)
	McGain et al. (2012) [13]	Anesthesia & Analgesia	Australia	Catheter insertion Kit
	Ison & Miller (2000) [14]	Journal of Environmental Assessment Policy and Management	UK	Suction receptable
Compounds	Sherman et al. (2012) [15]	Anesthesia & Analgesia	USA	Anaesthetic drugs
Packaging	Goellner & Sparrow (2014) [16]	International Journal of Life Cycle Assessment	USA	Shipping containers (thermically controlled)
	Grimmond & Reiner (2012) [17]	Waste Management & Research	USA	Sharps containers
	Belboom et al. (2011) [18]	International Journal of Life Cycle Assessment	Belgium	Drug packaging alternatives (glass vs. polymer vials)
	McGain et al. (2010) [19]	Anaesthesia and Intensive Care	Australia	Drug trays

As can be seen in Table I, until now, no study has been carried out to indicate the impact of medical devices on LCA in healthcare buildings.

A careful look at the studies carried out in this area shows that studies based on the stroke of medical devices (study of sheets, surgical scissors, anaesthetic equipment, etc.) predominate. These small observations are of great importance, as they give an idea of the studies that are most probably successful.

Secondly, a check and analysis of the viability of applying LCA methodology to health devices was carried out. To do this, the bibliography in Table I was used again, obtaining a series of advantages and disadvantages in Table II.

TABLE II. ADVANTAGES AND DRAWBACKS OBTAINED ONCE APPLIED THE LCA METHOD IN HEALTHCARE DEVICES.

Advantages	**Drawbacks**
Reduction of the environmental impact generated in the selection of systems, processes, materials, etc	Complexity of the study development
Generation of a tool for planning environmental strategies, policies and programmes	Subjectivity in the study development
Generation of a tool for the evaluation of energy savings (Energy Efficiency)	Limited influence of the specialist's preferences
Selection of alternatives for proper waste management and sustainable construction	Possible renounce to certain technical characteristics, quality, etc, in exchange for the reduction of the environmental impact of the device (Cost of Opportunity)
Comparison between the functionality of products with similar characteristics	
Evaluation of the effects produced by the consumption of resources in the facilities	

As shown in Table II, the advantages of applying LCA methodology to healthcare devices predominate over the disadvantages. This reflects the importance of applying this analysis to this type of healthcare product.

IV. RESULTS AND DISCUSSION

Among the most significant advantages obtained from the analysis of the different studies, works and projects mentioned above, can be found: the generation of a tool for the planning of environmental strategies, policies and programmes, the generation of a tool for the evaluation of energy savings, the selection of alternatives for a correct management of waste and sustainable construction, and the reduction of the total environmental impact generated by the building construction project.

All these advantages have not only an economic benefit, but also considerably reduce the levels of emissions and environmental impact. This translates into sustainable construction materialised as an effort to maintain the planet with sustainable development ethics.

The main drawbacks of this type of study are its high degree of complexity and subjectivity. On the one hand, the subjectivity of the LCA depends mainly on two factors. The first factor is associated with the individual who carries out the analysis or study, since the choice of factors involved is made at the will of the individual. The second factor is associated with the low degree of reliability of the input data of the LCA method, since there are no standardized libraries of life cycle inventory, therefore, this is done at the discretion of the researcher.

On the other hand, the complexity of this type of study is given by the high degree of knowledge required for its elaboration.

Some of the solutions proposed to improve these drawbacks are: creation of a guide for the application of LCA methodology, training courses, use of probability distributions, etc.

A study [20], says that the use of distributions instead of deterministic values for the lifetime of products improves the accuracy of the study and makes the results more objective and comparable. This approach has enormous potential to improve the reliability of the results of LCA methodology by expanding the use of distributions. Aspects such as energy and water use, transport loads and distances, waste reduction, etc. should be assessed using probability density distributions that reflect the effective variability of the parameters in practice.

From this analysis we also observe the great dependence and influence of this type of device on the life cycle of healthcare buildings, in such a way that it generates the following list of benefits:

- Reduction of CO_2 and greenhouse gas levels.
- Reduction of environmental impact.
- Reduction of raw material waste.
- Reduction of plastic consumption.
- Reduction of electrical consumption.
- Promotion, support and performance of R&D.

Throughout the preparation of this study, the importance of this communication has been demonstrated on more than one occasion, since it offers a clear vision of the advantages and drawbacks obtained in the application of the LCA methodology in the procurement of a sanitary device and consequently in the life cycle of a healthcare building. This importance mainly resides in being able to verify that the application of this methodology generates great benefits on an economic, ethical and social level.

It also provides the possibility of developing future studies and lines of research, such as: the generation of environmental impact reduction indicators, the improvement of existing techniques, the quantification of the benefit of applying LCA to health devices, the development of new products, techniques and systems that are more respectful of environmental impact, etc.

V. CONCLUSIONS

This analysis of different case studies indicates a growing attention to sustainability in the health sector. Current regulatory frameworks are being developed to facilitate the implementation of environmental performance assessment. Despite some limitations of the LCA technique, it remains a powerful, science-based tool for assessing environmental impacts.

It can be seen that the application of the LCA study in the procurement of a healthcare device generates a large number of advantages not only in the device itself, but also in the life cycle of a healthcare building. This will not only have a social benefit, as it improves the image of the company in relation to its competitors but will also generate an economic benefit that will normally be associated with the reduction of waste generated and operating costs.

Different solutions have been proposed to reduce the negative impact generated by subjectivity in the application of this methodology. To this end, it is recommended that the LCA methodology be standardised or that a guide be created for applying the methodology to medical devices. Furthermore, to increase the degree of confidence in the results, it is advisable to pay more attention to the use of probability density distributions instead of deterministic values. It should also be noted that, in order to reduce the degree of complexity, solutions such as the following training courses on LCA methodology are proposed.

Finally, there are many advantages to applying LCA methodology to healthcare devices. Among the most important are: the reduction of environmental impact, waste and operating costs, and energy savings. All these advantages translate into sustainable manufacturing, a feature of vital importance, since it contributes, among other things, to energy efficiency and the reduction of emissions, and therefore to the maintenance of the planet.

ACKNOWLEDGMENT

The authors wish to acknowledge the European Regional Development Fund for the financial support provided through Research Projects GR18029 linked to the VI Regional Plan for Research, Technical Development and Innovation from the Regional Government of Extremadura (2017-2020).

REFERENCES

[1] Worl Health Organization, (2018). Global Health Observatory Data Repository.

[2] Chung, J. W., & Meltzer, D. O. (2009). Estimateof the carbon footprint of the US health care sector. *JAMA*, *302*, 1970-1972.

[3] Thiel, C. L., Eckelman, M., Guido, R., Mathew, H., Landis, A. E., Jodi, S., Scott, S. O., Copley-Woods, N., & Bilec, M., M. (2015). Environmental impacts of surgical procedures: life cycle assesment of hysterectomy in the United States. *Environ. Sci. Technol.*, *49*(3), 1779-1786.

[4] Campion, N., Thiel, C. L., DeBlois, J., Woods, N., C., Landis, A. E., & Bilec, M. M. (2012). Life cycle assesment perspectives on delivering an infant in the US. *K. Sci. Total Environ.*, *425*, 191-198.

[5] EPA, (2010). *Life Cycle Assesment (LCA).* Washington, D.C.

[6] Guinée, J. B. (2002). Handbook on life cycle assessment operational guide to the ISO standards. *Int. J. Life Cycle Assess.*, *7*(5), 311-313.

[7] McGain, F., Story, D., Lim, T., & McAlister, S. (2017). Financial and environmental costs of reusable and single-use anaesthetic equipment. *Br. J. Anaesth.*, 118, 862–869.

[8] Unger, S., & Landis, A. (2016). Assessing the environmental, human health, and economic impacts of reprocessed medical devices in a Phoenix hospital's supply chain. *J. Clean. Prod.*, 112, 1995–2003.

[9] Campion, N., Thiel, C. L., Woods, N. C., Swanzy, L., Landis, A. E., & Bilec, M. M. (2015). Sustainable healthcare and environmental life-cycle impacts of disposable supplies: A focus on disposable custom packs. *J. Clean. Prod.*, *94*, 46–55.

[10] Sørensen, B. L., & Wenzel, H. (2014). Life cycle assessment of alternative bedpans - A case of comparing disposable and reusable devices. *J. Clean. Prod.*, 83, 70–79.

[11] Ibbotson, S., Dettmer, T., Kara, S., & Herrmann, C. (2013). Eco-efficiency of disposable and reusable surgical instruments - A scissors case. *Int. J. Life Cycle Assess.*, 18, 1137–1148.

[12] Eckelman, M., Mosher, M., Gonzalez, A., & Sherman, J. (2012). Comparative life cycle assessment of disposable and reusable laryngeal mask airways. *Anaesth. Analg.,* 114, 1067–1072.

[13] McGain, F., McAlister, S., McGavin, A., & Story, D. (2012). A life cycle assessment of reusable and single-use central venous catheter insertion kits. *Anaesth. Analg.,* 114, 1073–1080.

[14] Ison, E., & Miller, A. (2000). The use of LCA to introduce life- cycle thinking into decision-making for the purchase of med- ical devices in the NHS. J. *Environ. Assess. Policy Manag.,* 2, 453– 476.

[15] Sherman, J., Le, C., Lamers, V., & Eckelman, M. (2012). Life cycle greenhouse gas emissions of anesthetic drugs. *Anaesth. Analg.,* 114, 1086–1090.

[16] Goellner, K. N., & Sparrow, E. (2014). An environmental impact comparison of single-use and reusable thermally controlled shipping containers. *Int. J. Life Cycle Assess.,* 19, 611–619.

[17] Grimmond, T., & Reiner, S. (2012). Impact on carbon footprint: A life cycle assessment of disposable versus reusable sharps containers in a large US hospital. *Waste Manag. Res.,* 30, 639–642.

[18] Belboom, S., Renzoni, R., Verjans, B., Léonard, A., & Germain, A. (2011). A life cycle assessment of injectable drug primary packaging: Comparing the traditional process in glass vials with the closed vial technology (polymer vials). *Int. J. Life Cycle Assess.,* 16, 159–167.

[19] McGain, F., McAlister, S., McGavin, A. & Story, D. (2010). The financial and environmental costs of reusable and single-use plastic anaesthetic drug trays. *Anaesth. Intensive Care., 38,* 538–544.

[20] Aktas, C. B., & Bilec, M. M. (2011). Impact of lifetime on US residential building LCA results. *Int. J. Life Cycle Assess.,17*(3),337–49.

Influence on On/Off Switches of Unloaded Transformer on Electricity Quality

Enver Agić[1], Suad Halilčević[2], Damir Šljivac[3], Bakir Agić[4]

[1]PIM University Banja Luka, Bosnia and Herzegovina Organization, enveragic99@gmail.com,
[2,4]Faculty of electricity Tuzla, Tuzla, Bosnia and Herzegovina, suad.halilcevic@untz.ba[2], bakir.agicc@gmail.com[4]
[3]Electrotechnical faculty Osijek, Osijek, Croatia, damir.sljivac@etfos.hr

Abstract—**Distribution power networks contain a greater number of elements with nonlinear characteristics which produce higher order harmonics. These harmonics and other disturbances can cause disorder in the work of the distribution power network, so it is necessary to analyze the electric power quality. Therefore, it is necessary to analyze the quality of electricity. It is theoretically and practically known that in normal conditions of transformer connection at idle, when the voltage at the transformer terminals passes through the maximum value, the magnetizing current is the value of the nominal current. However, the switching on of the transformer at the moment when the voltage of the system passes through the zero value leads to strong electric shocks which are due to the nonlinear character of the transformer of non-sinusoidal size. In conditions of weak systems, ie. systems with relatively low three-pole short-circuit power at the point of observation, connecting a transformer over capacity C, which actually equates to cable or air duct access, filters, resonance can be established with relatively low oscillation frequencies. The analysis of the quality of electricity is not an unjustified cost, but a very important and profitable investment and a step towards optimizing the operation of the network.**

Keywords - transformer, idling, magnetizing current, higher hatmonics

I. INTRODUCTION

The following electrical equipment was used to analyze the above phenomenon of switching on / off the unloaded transformer:

1. MI 7111 power analyzer
2. Control transformer (220/400 V, 1.25 kVA, 5 A)
3. Unloaded transformer (220/24 V, 300 VA)

The MI 7111 power analyzer is a static microprocessor multifunction instrument for accurate and fast power quality analysis [1].

Possibilities are monitoring of all characteristics of three-phase system in real time, memorization, subsequent analysis of stored data, measurement of rms values of voltage, current, power, power factor, energy, detection, recording of voltage disturbances, instrument power interruptions, storing min / medium / max information in certain time intervals, oscilloscopic monitoring of current and voltage waveforms in real time, memorization and analysis of memorized waveforms, analysis of harmonic dystrophy up to the 63 rd harmonic with real-time monitoring and memorization of harmonic components, energy analysis.

The connection diagram of these elements is shown in Fig. 1.

According to the scheme from Fig. 1. The goal is to record the waveforms of the current of the unloaded transformer and the corresponding voltage on the transformer during the transient.

In addition will be determined by the maximum value of the current electricity unloaded transformer, and a comparison with the nominal.

ISBN: 978-86-80616-07-0

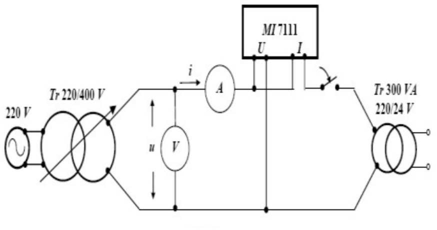

Figure 1. Connection diagram.

It will focus on how long the switching current is greater than the rated current of the unloaded transformer. Measures to reduce the switching current of the unloaded transformer will be proposed.

II. Measurement Analysis

Under normal conditions of transformer connection at idle, when the voltage at the transformer terminals passes through the maximum value, the magnetizing current is the value of the nominal current.

However, the switching on of the transformer at the moment when the voltage of the system passes through the zero value leads to strong electric shocks which are due to the nonlinear character of the transformer of non-sinusoidal size [1].

In conditions of weak systems, i.e. systems with relatively low three-pole short-circuit power at the point of observation, connecting a transformer over a capacity, which actually equates to cable or air duct access, shunt reactors or filters, can lead to resonance with relatively low oscillation frequencies.

Namely, if more harmonic components generated by the transformer current coincide with the resonant frequencies of the system, significant overvoltage can occur at the transformer terminals.

The most important characteristic of these overvoltage is the relatively long duration (over 100 periods, extreme and over 10 seconds). Surge arresters installed with transformers can be heavily thermally loaded with this type of surge.

Initial magnetization during switching is considered to be a very significant transient process in the transformer. When the transformer is disconnected from the power supply (deenergizes), the magnetizing current drops to zero, while the flux follows the hysteresis loop of the core.

This results in the appearance of a certain remanent flux in the nucleus. When the transformer is re-energized by connecting to a sinusoidal voltage, the flux also becomes sinusoidal but increased by the value of the remanent flux, which can be 80-90% of the nominal flux [2].

This reason can lead to displacement above the knee on the flux-current characteristic resulting in large peaks and severe distortion of the magnetizing current. This case is shown in Fig. 2.

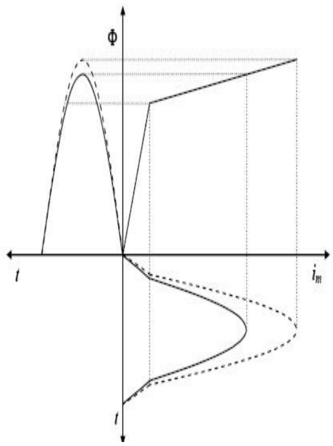

Figure 2. Non-sinusoidal magnetizing current of the transformer.

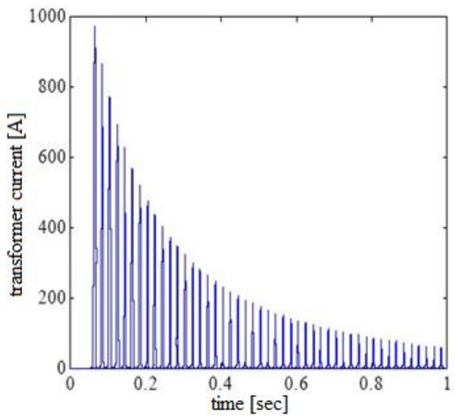

Figure 3. Waveform current of the unloaded transformer.

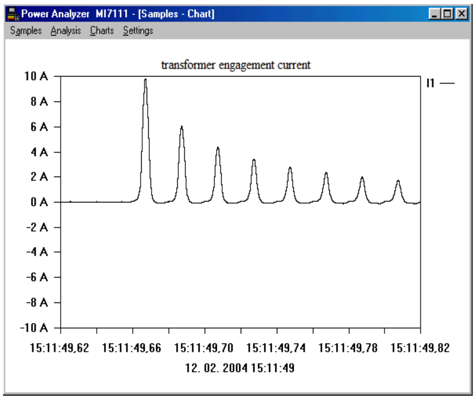

Figure 4. Results form power analyzer MI 7111.

The waveform of the current that occurs then contains a slowly decreasing DC component, a multitude of harmonics, has initially large peaks, and decreasing within a few seconds reaches a nominal value. This waveform is shown in Fig. 3.

Using the power analyzer MI 7111, the following characteristics were obtained (Fig. 4), and after connecting the elements of the electrical circuit as in Fig. 1.

In our analyzed example, we see that the maximum value of the current when the unloaded transformer is switched on is 9.9 (A), which is 5.2 times more than the nominal value IN = 1.9 (A) and that the switching current during 00:00: 00.20h higher than the rated current of the unloaded transformer, Fig. 4.

The peak values of the magnetizing current when the transformer is switched on are higher for smaller transformers, and for larger ones this current has a longer duration. The decay time constant is of the order of 0.1 s for smaller transformers (100 kVA and less) and about 1 s for larger transformers.

Transformers powered from a stronger network have higher switching currents. The resistance between the equivalent source and the observed magnetization branch determines the current attenuation. Therefore, transformers located closer to the generator nodes have a longer switching current duration.

The magnetic shock of a transformer is higher when the saturation flux density or magnetic saturation induction is lower. Designers usually work with magnetic inductions of 1.5-1.75 Tesla. Transformers that work as close as possible to the mentioned values have a lower switching current.

A higher value of the remanent flux causes a higher magnetizing current at start-up. The value of the remanent flux density usually has values of 1.3-1.7 Tesla. The highest values of the switching current occur when the transformer is switched on at the moment when the supply voltage passes through zero and when the newly formed flux has the same direction as the remanent flux of the core. In general, the magnitude of the switching magnetizing current is a random factor and depends on the current value of the sinusoidal voltage to which it is connected as well as on the sign and value residual flux. Usually every 5-6 energizations of transformers result in significantly higher values of switching current.

The cross-section of the area between the transformer core and the energized winding also affects the maximum magnetizing current at switch-on. Namely, it has been noticed that higher values of this current (10-20 times higher than the nominal one) occur when the internal winding, closer to the core, is energized first.

When the external winding is first connected to the power supply, these values are significantly lower (5-10 times higher than the nominal ones). As a lower voltage winding is usually placed closer to the core, energizing the lower voltage side of the transformer causes higher switching currents.

Some transformers can be equipped with a special switch that allows switching over a certain resistance that reduces the magnitude of the switching current and accelerates its decline, which can facilitate the requirements of differential protection and is one way to reduce the switching current of an unloaded transformer.

III. Conclusion

The waveforms and characteristic current values of the individual nonlinear receivers given in these exercises confirm the presence of higher harmonics. Ignoring now the classical sources of harmonics (transformers, induction furnaces, etc.), given the constant increase in the presence of nonlinear receivers in various electrical devices, etc. and with a tendency to increase further, they also become a significant source of higher harmonics in the network.

It can be assumed what are the deviations of the waveforms of the current, the values of the voltage drop, i.e., the presence of harmonics in the low-voltage distribution network (because that is where we have the largest number of these consumers).

With the introduction of normative acts related to the presence of current harmonics, which are similar to the existing international IEEE standard, it will be necessary to review the conditions for connecting individual devices or to consider the possibility of installing harmonic filters in individual transformer stations [3].

In addition, it is necessary to carry out measurements in various places, i.e., transformer stations located in the end nodes of the medium voltage distribution network and those that supply specific nonlinear consumers. The results of these measurements can be used for the purposes of planning and expanding the distribution network.

The questions that arise for further research on the quality of electricity are:

1. What is the status and application of EN50160 in Bosnia and Herzegovina in terms of regulations?
2. Are there electricity quality measurements according to EN 50160 in Bosnia and Herzegovina and how are the possible results applied?
3. Are there similar experiences in the analysis of electricity quality in Bosnia and Herzegovina and which instruments (this or similar).

References

[1] Power Quality Laboratory exercises, PDS Tuzla. (2006). (p. 5; p. 9)

[2] Power Analyzer MI 7111 - User's guide (p. 2)

[3] Gerald Heydt (1994). *Electric power quality*. Second edition. Stars in a Circle Pub. (p. 23).

Effect of Deposition Parameters on Morphology and Optical Properties of Multilayer Selective Solar Surfaces (Mo/Si)

Beatriz Ferreira de Oliveira[1], Camila Rêgo de Andrade[2], Maycon Fagner de Oliveira Meneses[3], Kelly Cristiane Gomes da Silva[4]

[1,2,3,4]Federal University of Paraíba, João Pessoa, Brazil, beatriz.oliveira@cear.ufpb.br[1]; camila.andrade@cear.ufpb.br[2]; maycon.menezes@cear.ufpb.br[3]; gomes@cear.ufpb.br[4]

Abstract—**Energy consumption to meet the needs of society has increased significantly over the years and, consequently, the intensive use of fossil fuels. In this context, the search for clean energy sources has been shown as an alternative to minimize the environmental impacts. One of them is solar energy, which can be used for heating by means of Solar Thermal Systems that have the solar collector as their main component. One of the ways to increase the efficiency of these collectors is with the use of selective solar surfaces (SSS), which are materials with a high capacity for absorbing solar radiation. With this in mind, the present study sought to obtain multilayer SSS based on Molybdenum, with the presence and absence of an anti-reflective layer of Silicon. For this purpose, thin absorbent films were produced on stainless steel substrates that passed through a surface treatment method, and were deposited by the *Sputtering* technique, varying the deposition time parameters, in order to evaluate the influence these parameters in the optical and microstructural properties of these coatings. In order to characterize these films, analyzes of Spectrophotometry in UV-Vis-Infrared and Optical Profilometry were performed and it was found that all of the coatings produced had high absorption averages (above 96%). Therefore, it was realized that the films produced are excellent candidates to be used as SSS in solar collectors, due to their high absorbency, good absorption stability throughout the spectrum and to be microstructurally homogeneous.**

Keywords – selective solar surfaces, *Sputtering*, molybdenum, silicon

I. Introduction

Economic development and high standards of living have led to an increase in energy demand. Energy is an extremely important factor for modern society, since it is an essential resource in the social and economic development of a nation, and its demand increased considerably after the Industrial Revolution, being mainly supplied by the use of fossil fuels, leading to a worsening of environmental degradation and the greenhouse effect [1,2].

In this way, the search for new sources of energy has occurred due to the need to break dependence on fossil fuels and favoritism for non-polluting sources [3,4]. Thus, the use of renewable energies is a high value strategy in the development scenario, being an alternative to conventional energy generating systems [4].

Among the renewable sources of energy, solar stands out, whose use can be made by thermal conversion through the solar collector. An effective method to increase the performance of a collector is to incorporate a selective surface, so that it allows the efficiency of this equipment to increase, enabling it to operate at a higher temperature [5,6]. Selective surfaces are materials that have selective reflectivity, i.e. capable of absorbing the maximum amount of incident solar radiation and minimizing thermal losses due to the emission of infrared radiation [7].

These materials are commonly composed of a thin film superimposed on a thermally conductive substrate, and may be preceded by an antioxidant or anti-diffusion layer and followed by an anti-reflective layer, in contact with the environment [8].

It is necessary that the technique chosen for deposition of the films guarantees a homogeneous solar thermal conversion along the collector, as well as a good adhesion between the metallic substrate and the selective coating. The *Magnetron Sputtering* technique is widely applied industrially for the manufacture of thin films and its advantage is a clean technique compared to the electrochemical processes, which produce a significant portion of waste that must be controlled. This is notoriously important when it comes to solar collectors, since the market is sensitive to ecological issues [7].

Therefore, the objective of this work is to obtain selective surfaces with a single layer of Molybdenum (Mo) and multilayer of Mo and Silicon (Si) using the *Magnetron Sputtering* technique with different deposition parameters and using substrates that have undergone the surface treatment of electropolishing, in order to eliminate scratches and marks present on the surface, ensuring uniformity and a better finish for it.

II. METHODOLOGY

A. *Sub*strate and Surface Treatment choose

The first step was to define the type of substrate used and its surface treatment. AISI 304 stainless steel substrates and electropolishing treatment were chosen. This treatment is a process of improving the finish of a metal surface by applying a positive current in a solution, resulting in improved leveling, brightness and reflectivity due to the reduction of roughness [9]. The samples were electropolished using a solution with 2: 1: 1 volume proportions of phosphoric acid, sulfuric acid and glycerol, so that the final volume of the solution was 300ml, based on the methodology of [10].

After the electropolishing on substrates, they were immersed in isopropyl alcohol and submitted to an ultrasonic bath for 15 minutes, to be taken to the *Sputtering* chamber.

B. *The Deposition Parameters*

Thus, the parameters involved in the deposition process of absorbent films were defined, three of them were fixed in this research: the distance, power and pressure, varying only the time. Regarding the working distance, a target-substrate distance of 105mm was fixed, according to [11].

According to [12], the powers typically used for the deposition of metals are between 10 and 100W, therefore, the power of 60W was adopted for the Molybdenum deposition. For the antireflective layer (AR), the power determined was 200W, based on the work of [13], who deposited cermet layers covered by an AR layer of SiO_2 with this power.

The deposition times were varied in order to obtain different thicknesses and to determine the one that gives the best optical properties to the film. It was found in the works by [9] that the greatest powers and the longest time employed in the study, provided the best absorption results (>90%). Thus, the 10, 20 and 30 min were the times of deposition adopted for this work plan.

The entire process of setting parameters can be seen in Fig. 1.

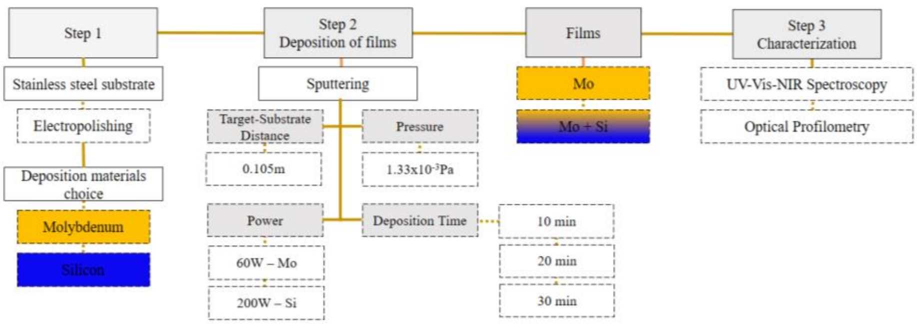

Figure 1. Experimental process flowchart.

C. The Deposition Process

The deposition of the films was performed using a Sputtering RF Orion 5 System, manufactured by AJA International Inc.

To initiate the deposition process, the Mo and Si targets were positioned in the vacuum chamber at the chosen distance. The chamber was evacuated to a pressure of 1.3 x 10^{-3}Pa and then the gas was injected to form the plasma. Was used into the chamber Argon 5.0 gas, causing a new pressure balance to be reached at 0.7Pa. Was supplied to the equipment the desired working power value for each target and the deposition process started. During the process, the substrate rotated at a speed of 20 rpm.

Based on the different parameters adopted in the depositions, 6 conditions were obtained, according to Table I. Then, three samples were produced for each set of conditions, totalizing the production of 18 samples.

D. The Characterization of Films

The main parameter to be evaluated in this research is the film's ability to absorb solar energy. For this purpose, all coatings produced were subjected to characterization by UV-Vis-NIR Spectrophotometry. The equipment used was a Spectrophotometer by Shimadzu, model UV-2600 operating in the region from 220nm to 1400nm with reflectance measurements, using the integration sphere accessory that expands the range of the analyzed spectrum.

The absorptivity is defined as the ratio of the radiation absorbed by the surface to the radiation incident on that surface. Therefore, it is possible to calculate the solar absorptivity of a surface using the (1):

TABLE I. SAMPLES NOMENCLATURE

<table>
<tr><th>Sample</th><th>Treatment</th><th>Composition</th><th>Deposition Time (min)</th></tr>
<tr><td>S1</td><td rowspan="6">Electropolishing</td><td rowspan="3">Mo</td><td>10</td></tr>
<tr><td>S2</td><td>20</td></tr>
<tr><td>S3</td><td>30</td></tr>
<tr><td>S4</td><td rowspan="3">Mo+Si</td><td>10</td></tr>
<tr><td>S5</td><td>20</td></tr>
<tr><td>S6</td><td>30</td></tr>
</table>

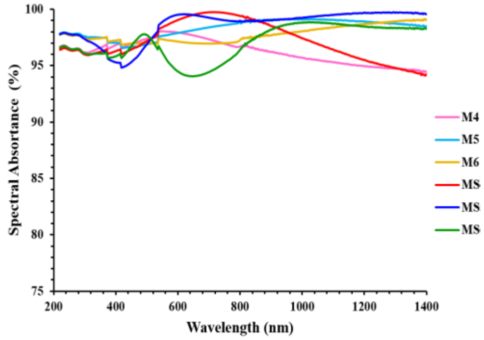

Figure 2. Absorptance spectrum of Mo and Mo/Si films deposited on electropolished substrates.

$$\alpha = \frac{\int_{300}^{2500} \alpha_\lambda I_{sun} d\lambda}{\int_{300}^{2500} I_{sun} d\lambda} , \quad (1)$$

where α_λ is the spectral absorptance of the solid, I_{sun} is the spectral distribution of the solar irradiation and α is the total hemispherical absorptance.

Considering that the samples obtained are opaques (transmittance is zero), the total hemispherical absorptance α can be calculated from (2):

$$\alpha = \frac{\int_{300}^{2500} (1-\rho_\lambda) I_{sun} d\lambda}{\int_{300}^{2500} I_{sun} d\lambda} , \quad (2)$$

where ρ_λ is the solid spectral reflectivity. So, according to (2), the solar absorptivity of the films can be obtained from the spectral reflectance measurements, which are determined in the UV-Vis spectrophotometry.

The topographic profiles of the surfaces were obtained using the optical profiling characterization technique. From the profiles obtained, it is possible to analyze several characteristics of the surfaces such as the roughness and thickness of thin films. The measurements were made by the CCI MP non-contact Optical Profiling device by Taylor Hobson, connected to a computerized unit containing the Talysurf CCI software (Taylor Hobson, England) to obtain and analyze the data.

III. Results and Discussion

E. UV-Vis-NIR Spectrophotometry

The absorber and multilayer films (Mo, Mo/Si) obtained by *Magnetron Sputtering* with different parameters, were subjected to radiation with a wavelength in the range of 220nm to 1400nm (UV-Vis-NIR) in order to determine their spectral absorbances, from the conversion of the reflectance results to absorbance, allowing the plotting of the following curves shown in Fig. 2.

By analyzing the graph in Fig. 2, it can be seen from the spectrum of the MS6 film that it had the lowest spectral absorption, this behavior can be explained by the film having a higher concentration of material in its composition since its deposition time was the longest.

It is also observed that the spectrum of the films shows a very harmonic behavior almost constant throughout the wavelength studied, revealing that the electropolishing on stainless steel substrates provides excellent optical stability to the films produced.

To facilitate the comparison between the different films, the solar absorptivity for each condition was calculated, as well as their respective standard deviation. The addition of the Silicon antireflective layer in the Molybdenum film on the substrate AISI 304 favored the increase in the absorbance of the films that were deposited during 10 and 20 minutes, as can be seen in Fig. 3.

In the case of the film deposited for 30 minutes, there was a reduction in the percentage of absorption, and observing Table II, it is noted that the largest variation of standard deviation of the samples was of the film MS6, although the solar absorbances of the films produced are in a range between 96.51 to 98.41%, with low standard deviations ensuring good optical stability.

It is important to note that the Si layer in the MS6 sample did not hinder the absorptivity of the set, maintaining absorption levels above 96%, as well as preserving the optical stability of the film provided by the electropolishing.

It is noticeable that S5 was the one that presented the best performance, as it obtained the highest solar absorbance (98.41%) and a small standard deviation as well (± 0.51%), which indicates that this condition is reproducible.

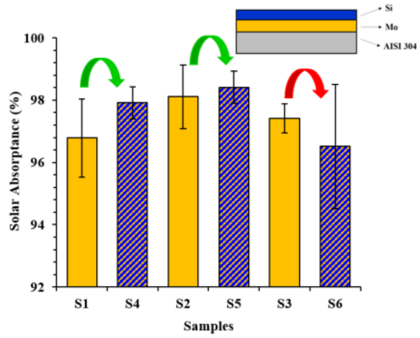

Figure 3. Solar absorptances and their respective standard deviations.

Finally, it is notorious to analyze that all deposited films have average values of solar absorption greater than 85%, which can then be considered as Selective Solar Surfaces (SSS).

F. Optical Profilometry

All films were subjected to optical profilometry analysis, from which the following parameters were obtained: Ra (arithmetic roughness, that is, the mean deviation with respect to the roughness profile) and the thickness values of the films. The data obtained are shown in Table III.

In Fig. 4, it can be seen that the solar absorption of the films slightly rises with the increase in roughness. However, when the surface exhibits Ra values close to or greater than 30 nm, the solar absorptivity starts to decrease, as is the case of the S6 sample that presented the highest Ra (45 nm) with the lowest solar absorption (96.51%). So that films with rougher surfaces (≥30 nm) are likely to exhibit less absorption.

Fig. 5 when correlating the thickness of the films with their respective solar absorbances, shows that, for Molybdenum films, the radiation absorption reaches its maximum for thinner layers of Mo, as in the example of the S2 sample that exhibited 98.11% with 170nm thickness.

TABLE II. Solar Absorptivity and Standard Deviation

Sample	Solar Absorptivity (%)	Standard Deviation (%)
S1	96.78	1.26
S2	98.11	1.03
S3	97.41	0.47
S4	97.92	0.52
S5	98.41	0.51
S6	96.51	2.00

TABLE III. SURFACE ROUGHNESS AND THICKNESS

Sample	Ra (μm)	Thickness (μm)	Solar absorptivity (%)
S1	0.0115	0.191	96.78
S2	0.0279	0.170	98.11
S3	0.0153	0.218	97.41
S4	0.0223	0.272	97.92
S5	0.0268	0.277	98.41
S6	0.0450	0.462	96.51

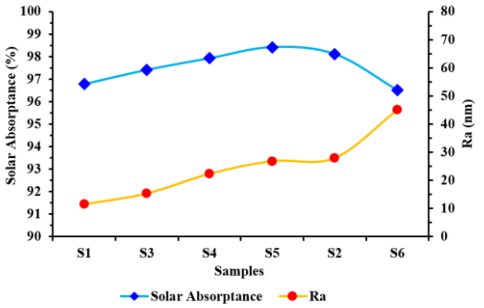

Figure 4. Correlation between the Ra parameter and the solar absorption of the films.

The same is true for multi-layered Mo/Si films, as S5 has excellent solar absorption (98.41%) with a more modest thickness (277nm).

Still in Fig. 5, it is possible to notice that the samples that exhibited the greatest solar absorptions had thicknesses in the range of 170 to 280nm. While the S6 film presented the

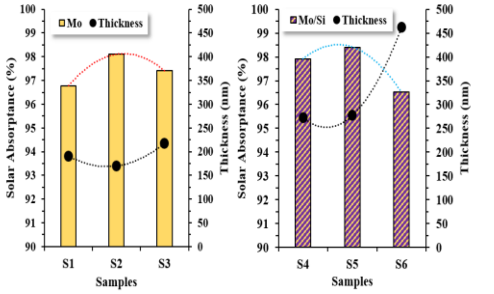

Figure 5. Correlation between solar absorption and film thickness for Mo and Mo/Si.

lowest absorption value (96.51%) and the highest thickness value (462nm).

This suggests that a very thick layer of Silicon is not very favorable for the film's absorptive property, especially when associated with a rougher surface (Ra = 45nm), caused by the longer deposition of this material, which was 30 minutes.

The Fig. 6 shows the 3D morphology of the surfaces of films deposited on substrates subjected to electropolishing, a treatment in which it provided low surface roughness (15 to 45 nm), which reveals its abrasive character.

In addition, it is possible to see that the surface roughness rises with the addition of Si on the Molybdenum layer for most cases, especially when deposited for 30 min, as seen from the S6 profile.

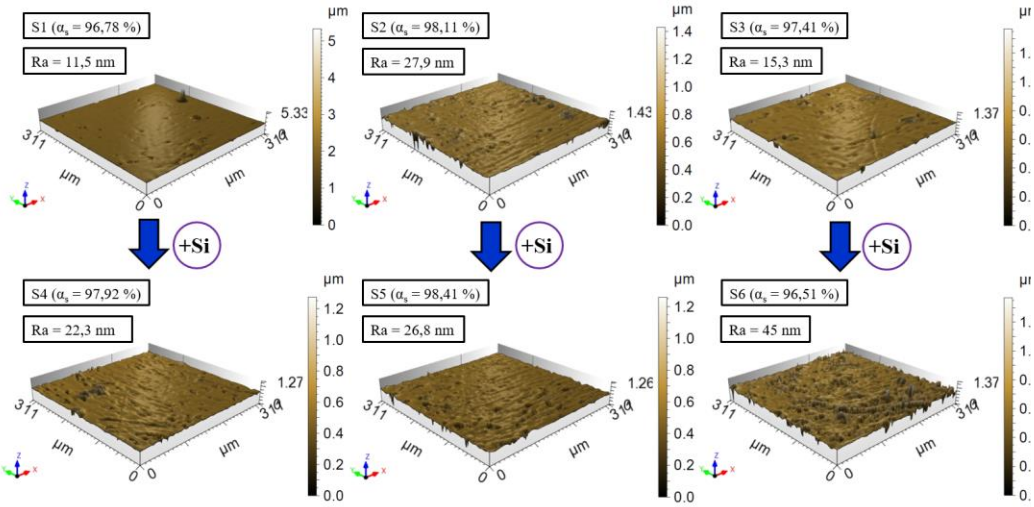

Figure 6. 3D Morphological profiles of films with single layer of Mo and with multilayer of Mo/Si.

IV. CONCLUSIONS

Electropolishing was a very effective surface treatment, as it ensured high levels of solar absorption (96.51% - 98.41%) for all samples with excellent absorption stability through the spectrum.

The films presented homogeneous morphological profiles due to the deposition technique used and the abrasive nature of the electropolishing, which resulted in smoother surfaces and with small Ra values. This may have contributed to the high levels of absorption.

The deposition of the Silicon layer on the molybdenum films caused a greater oscillation in the absorption spectrum, however, in general, it provided an increase in solar absorptivity.

The multilayer film with the deposition time of 20 minutes (S5) obtained the best result, reaching a solar absorption of 98.41%, which characterizes it as an excellent solar absorber.

Therefore, it is observed that the films produced are excellent candidates to be applied as selective solar surfaces, due to the high absorbances, good absorption stability and their surface being microstructurally homogeneous.

ACKNOWLEDGMENT

The authors would like to thank the technical support provided by Integrated Biomaterials Laboratory – LABIO/UFPB, New Materials Technology Laboratory – TECNOMAT/UFPB and Laboratory of Synthesis and Characterization of Thin Films – LABFILM/UFPB, as well the financial support of Coordination for the Improvement of Higher Education Personnel (CAPES), National Council for Scientific and Technological Development (CNPq) and Center for Alternative and Renewable Energies (CEAR/ Federal University of Paraíba).

REFERENCES

[1] Pompelli, M. F., Orozco, A. J., Oliveira, M. T, Rodrigues, B. R. M., Barbosa, M. O., Santos, M. G., Oliveira, A. F. M., & Almeida-Cortez, J. S. (2011). Global energy crisis and the Brazilian role in the biofuels issue. Crise energética mundial e o papel do Brasil na problemática de biocombustíveis. *Agronomía Colombiana*, *29*(2), 231–240.

[2] Meneses, M. F. O. (2019). Evaluation of Film Aging on the Absorptivity of Selective Solar Surfaces. *Relatório Final Projeto de Iniciação Científica*. Universidade Federal da Paraíba. João Pessoa, Brazil. (In Portuguese)

[3] Costa, R. C., & Prates, C. P. T. (2005). The Role of Renewable Energy Sources in the Development of the Energy Sector and barriers to its insertion in the market. *BNDES Setorial*, Rio de Janeiro, Brazil, 21, 5-30. (In Portuguese)

[4] Medeiros, I. D. M. de. (2016). Selective Surfaces based on Inorganic Polymers for Medium and High Temperature Solar Collectors. Dissertação de Mestrado. Universidade Federal da Paraíba. João Pessoa, Brazil. (In Portuguese)

[5] Mihelcic, M., Francetic, V., Kovac, J., Vuk, A. S., Orel, B., Kunic, R., & Peros, D. (2015). Novel sol-gel based selective coatings: from coil absorber coating to high power coating. *Solar Energy Materials and Solar Cells*, *140*, 232-248.

[6] Kennedy, C. E. (2002). Review of Mid- to High-Temperature Solar Selective Absorber Materials. National Renewable Energy Laboratory, Colorado.

[7] Martins, M. (2010). Production of Selective Surfaces by Magnetron Sputtering for Application in Solar Collectors. *Dissertação* (Mestrado em Engenharia Metalúrgica e dos Materiais) – Universidade Federal do Rio de Janeiro, Rio de Janeiro, Brazil. (In Portuguese)

[8] Gomes, C. A. S. (2001). Comparative Study of Selective Surfaces for Solar Collectors. Dissertação (Mestrado em Engenharia e Ciência dos Materiais). Universidade Federal do Ceará, Fortaleza, Brazil. (In Portuguese)

[9] Oliveira, A. S. (2020). Evaluation of the influence of surface treatments on the thermal efficiency of selective surfaces obtained via Sputtering. Relatório de Qualificação (Mestrado em Energias Renováveis), Universidade Federal da Paraíba, João Pessoa, Brazil. (In Portuguese)

[10] Lin, C. C., & Hu, C. C. (2008). Electropolishing of 304 stainless steel: Surface roughness control using experimental design strategies and a summarized electropolishing model. *Elect. Acta*, *53*(8), 3356–3363.

[11] Medeiros, I. D. M. (2020). Obtaining chromium-based solar absorber films: optical and morphological characterization. Tese (Doutorado em Engenharia Mecânica), Universidade Federal da Paraíba. João Pessoa, Brazil. (In Portuguese)

[12] Landi, G. T. (2009). Development of a nanoparticle generator and characterization of cobalt nanoparticles. Dissertação (Mestrado em Ciências) - Universidade de São Paulo, São Paulo, Brazil. (In Portuguese)

[13] Silva Neto, J. F. Da. (2017). Development of Selective Surface for Solar Collectors with Multilayer Deposition of Cr and SiO2. Tese (Doutorado em Engenharia Mecânica), Universidade Federal da Paraíba, João Pessoa, Brazil. (In Portuguese)

Edification Optimization Algorithm for Diminution of Active Power Loss

Lenin Kanagasabai

Prasad V. Potluri Siddhartha Institute of Technology, Department of EEE, Kanuru, Vijayawada, Andhra Pradesh -520007, gklenin@gmail.com

Abstract—**In this paper Edification Optimization (EO) algorithm has been designed for voltage stability enhancement and power loss reduction. Different method's and courses are custom-made to perk up the standard of the learners in the education segment and it has been imitated to formulate the EO algorithm. Most important obstacle of the edificator is to create all the learners to accept the knowledge. Key differentiation amongst the learners is to understand and accepting the knowledge. Consequently a competent outline has to be created by the edificator. An edificator will focus more on the feeble learner (potential is very low in accepting the knowledge) than elevated learner (ability is lofty in gaining the knowledge). For all time there is an opportunity for learner to augment his or her knowledge by self-learning and through communication with other learner's. Perceptibly a competent edificator method or system will perk up the standards of learner's by obtaining additional knowledge. Edification Optimization (EO) algorithm is appraised in 30 bus test systems.**

Keywords – optimal reactive power, transmission loss, edification optimization algorithm

I. INTRODUCTION

Power loss minimization and voltage stability amplification are the most important objectives of this work. Interior point, quadratic programming, Newton's method, [1-6] are applied, and many unable to handle constraints. Then Evolutionary algorithms such latter stages ant colony, wolf search, frog leaping, organism explore algorithms [7-14] are utilized to solve the problem. Edification Optimization (EO) algorithm has been applied to solve the problem. Power loss minimization and voltage stability augmentation is the major objectives of this work. Proposed Edification Optimization (EO) algorithm is based on the learning mechanism. An assortment of strategies and courses are tailored to progress the standard of the learners in the edification area. All the learners will not be similar with reverence to ability, learning, skill and socio-economic conditions. So cluster of edification method is followed to perk up standards of all learners in the learning procedure. Nevertheless practically it's not simple to put into practice the cluster of edification approach with reverence to a variety of differences found between the learners. In the projected design hypothesis has been done to plan the population, fitness value and decision variables with reverence to learner's knowledge, aptitude, learning capacity and dissimilar subjects. The key barrier of the edificator is to make all the learners to comprehend and admit the knowledge. Because the most important dissimilarity among the learners is to comprehend and accommodating the knowledge. Constantly the well-built competence learner will gain knowledge in fast mode and the edificator sketch for the enhancement of all learners. Self learning and through communication with co learners will augment the learner's knowledge. Edification Optimization (EO) algorithm is verified in IEEE 30, bus system. Real power loss has been minimized.

II. PROBLEM FORMULATION

Power loss reduction is defined by:

$$F = P_L = \sum_{k \in Nbr} g_k (V_i^2 + V_j^2 - 2 V_i V_j \cos\theta_{ij}) , \quad (1)$$

$$F = P_L + \omega_v \times VoltageDeviation \ , \quad (2)$$

$$VoltageDeviation = \sum_{i=1}^{Npq} |V_i - 1| \ . \quad (3)$$

Constraint (Equality):

$$P_G = P_D + P_L \ . \quad (4)$$

ISBN: 978-86-80616-07-0

Constraints (Inequality):

$$P_{gslack}^{\min} \le P_{gslack} \le P_{gslack}^{\max} \quad , \tag{5}$$

$$Q_{gi}^{\min} \le Q_{gi} \le Q_{gi}^{\max}, \mathrm{i} \in \mathrm{N}_g \quad , \tag{6}$$

$$\mathrm{V}_i^{\min} \le V_i \le V_i^{\max}, \mathrm{i} \in \mathrm{N}_B \quad , \tag{7}$$

$$Q_c^{\min} \le Q_c \le Q_C^{\max}, \mathrm{i} \in \mathrm{N}_C \quad , \tag{8}$$

$$T_i^{\min} \le T_i \le T_i^{\max}, \mathrm{i} \in \mathrm{N}_T \quad . \tag{9}$$

III. Edification Optimization Algorithm

In this work cluster of Edification Optimization (EO) algorithm is defined to solve the real power loss reduction problem. Various methodologies and courses are adapted to improve the standard of the learners in the education sector. This has been imitated to formulate the algorithm. All the learners will not be same with respect to capability and approach of learning, cleverness and socio-economic conditions. So cluster of edification approach is followed to improve overall standards of all learners in the learning process. But practically it's not easy to implement the cluster of edification approach with respect to various differences found among the learners. In the proposed design assumptions has been done to design the population, fitness value and decision variables with respect to learners knowledge, capability, learning ability and different subjects. The major hurdle of the edificator is to make all the learners to understand and accept the knowledge. Since the major difference among the learners is to understand and accepting the knowledge. So an efficient sketch has to be formulated by the edificator. It's natural that an edificator will concentrate more on the weak learner (whose potential is very low in accepting the knowledge) than high learner (whose capability is high in accepting the knowledge). Always there is a possibility for learner to enhance his or her knowledge by self-learning and by communication with other learner. Obviously an efficient edificator methodology or mechanism will improve the standards of learner's by acquiring more knowledge.

At first capability clustering phase is modelled by assuming that all learners are in the normal distribution state and it defined as:

$$f(x) = \frac{1}{\sqrt{2\pi}\delta} e^{\frac{-(x-u)^2}{\delta^2}} \quad . \tag{10}$$

Always the strong capability learner will learn in fast with accepting knowledge and the edificator plan for the improvement of all learners. Knowledge gaining of most excellent learners is defined by:

$$\begin{aligned} x_{Edificator,i}^{t+1} &= (x_i^t) + O \times \\ \times (E^T - EF \times P \times A^t &+ Q \times x_i^t) \end{aligned} \quad , \tag{11}$$

where x_i^t is the knowledge of the ith learner at time "t", E^T is the knowledge of edificatory at time "t", and EF is the edificatory factor.

In the Edification phase different methodologies will be designed by the edificator based on the learner capability. Separate plan will be formulated for weak capability learner and strong capability learner:

$$Average\_knowledge^t(A) = \frac{1}{NL} \sum_{i=1}^{NL} (x_i^t) \quad , \tag{12}$$

where NL is the number of learners, x_i^t is the knowledge of the ith learner at time "t".

$$P + Q = 1 \quad , \tag{13}$$

O, P, Q are random numbers in the range [0, 1].

Edificator will concentrate more the average learners then excellent learners. The knowledge gained by the average learners is defined by:

$$(x_{Edificator,i}^{t+1}) = (x_i^t) + 2 \times R \times (\mathrm{E}^T - (\mathrm{x}_{Edificator,i}^t)) , \tag{14}$$

where $x_{Edificator,i}^{t+1}$ is the knowledge learned at time "t" from $t+1$, x_i^t is the knowledge of the *i-th* learner at time "t", and R is the random number.

There is possibility of any learner may not learn or gain the knowledge for the Edificator and it mathematically defined as:

$$(x_{Edificator,\mathrm{i}}^{t+1}) = \begin{cases} x_{Edificator,i}^{t+1}, f(x_{Edificator,i}^{t+1}) < f(x_i^t) \\ x_i^t, (x_{Edificator,i}^{t+1}) \ge f(x_i^t) \end{cases} . \tag{15}$$

Self-learning and through communication a learner can enhance his or her knowledge and it defined as:

$$x_{learner,i}^{t+1} = \begin{cases} x_{Edificator,i}^{t+1} + R1 \times (x_{Edificator,i}^{t+1} - x_{Edificator,j}^{t+1}) + \\ +R2 \times (x_{Edificator,i}^{t+1} - x_i^t),\ f(x_{Edificator,i}^{t+1}) < \\ < f(x_{Edificator,j}^{t+1}) \\ x_{Edificator,i}^{t+1} - R1 \times (x_{Edificator,i}^{t+1} - x_{Edificator,j}^{t+1}) + \\ +R2 \times (x_{Edificator,i}^{t+1} - x_i^t),\ f(x_{Edificator,i}^{t+1}) \geq \\ \geq f(x_{Edificator,j}^{t+1}) \end{cases}, \quad (16)$$

where $x_{learner,i}^{t+1}$ is the knowledge of the i-th learner obtained by co-learners communication and self-learning. There is possibility of learner may not gain the know ledge even by self – learning and by communication with co learners after a cycle. This mathematically defined as:

$$x_i^{t+1} = \begin{cases} \{x_{Edificator,i}^{t+1},\ f(x_{Edificator,i}^{t+1}) < f(x_{learner,i}^{t+1}) \\ \{x_{learner,i}^{t+1},\ f(x_{Edificator,i}^{t+1}) \geq f(x_{learner,i}^{t+1}) \end{cases}, \quad (17)$$

where (x_i^{t+1}) is the knowledge of the i-th learner at time t+1.

Then good Edificator allotment system is done based on category of learners (1, 2, 3,..., N) and it defined by:

$$A^t = \begin{cases} x_1^t,\ f(x_1^t) \leq f\left(\frac{x_1^t + x_2^t + x_3^t}{3}\right) \\ \frac{x_1^t + x_2^t + x_3^t}{3},\ f(x_1^t) > f\left(\frac{x_1^t + x_2^t + x_3^t}{3}\right) \end{cases}. \quad (18)$$

a. Start
b. Initialization of parameters (population size, max (UB) and min (LB) bound, max and min evaluation)
c. Engender the population
d. Population $X^t = \left[x_1^t, x_2^t, \ldots, x_N^t\right]^T$

$$x_{i,j}^t = LB_i + (UB_i - LB_i) \times k$$

e. Evaluation of population

$$T_{present} = T_{present} + N.$$

f. End criterion defined
g. Apply good Edificator allotment system phase

$$A^t = \begin{cases} x_1^t,\ f(x_1^t) \leq f\left(\frac{x_1^t + x_2^t + x_3^t}{3}\right) \\ \frac{x_1^t + x_2^t + x_3^t}{3},\ f(x_1^t) > f\left(\frac{x_1^t + x_2^t + x_3^t}{3}\right) \end{cases}$$

h. Cluster the learner's population by average and excellent
i. Apply Edificator and learners phase equations (11-16).
j. Assemble the population based on the fitness value
k. $T_{present} = T_{present} + 2N + 1$
l. apply step "f"
m. End

IV. SIMULATION RESULTS AND DISCUSSION.

Edification Optimization (EO) algorithm verified in IEEE 30 bus test system [15]. Loss comparison is shown in Table I and Fig. 1 gives graphical comparison between the methodologies with reference to power loss.

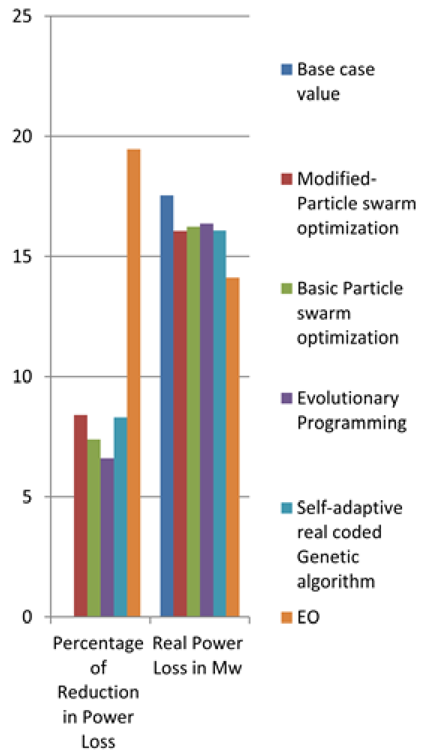

Figure 1. Comparison of Real Power loss.

TABLE I. COMPARISON OF LOSS

Parameter	**Base case value [18]**	**Modified-Particle swarm optimization [18]**	**Basic Particle swarm optimization [17]**	**Evolutionary Programming [16]**	**Self-adaptive real coded Genetic algorithm [16]**	**EO**
Percentage of Reduction in Power Loss	0.0000	8.40000	7.4000	6.60000	8.30000	19.48
Real Power Loss in Mw	17.5500	16.0700	16.2500	16.3800	16.0900	14.13

Table I shows the power loss comparison with other standard techniques - modified particle swarm optimization, particle swarm optimization, canonical genetic algorithm, adaptive genetic algorithm. From the above comparison and analysis it's clear that proposed Edification Optimization (EO) algorithm reduced the power loss effectively when compared to other standard reported algorithms.

V. CONCLUSION

Edification Optimization (EO) algorithm reduced the power loss with augmentation of voltage. Capability of clustering phase is modelled by assuming that all learners are in the normal distribution state. In the Edification phase different methodologies will be designed by the edificator based on the learner capability. Separate plan has been formulated for feeble capability learner and well-built competence learner. Edificator has concentrated more the average learners then brilliant learners. Self learning and through communication a learner augmented the knowledge. Edification Optimization (EO) algorithm verified in IEEE 30- bus test system. EO algorithm effectively reduced the power loss and percentage of real power loss reduction has been improved.

REFERENCES

[1] Lee, K. Y., Park, Y. M., & Ortiz, J. L. (1984, May). Fuel-cost minimisation for both real-and reactive-power dispatches. *IEE proceedings C (generation, transmission and distribution) 131*(3) 85-93.

[2] Deeb, N. I., & Shahidehpour, S. M. (1988). An efficient technique for reactive power dispatch using a revised linear programming approach. *Electric power systems research, 15*(2), 121-134.

[3] Bjelogrlic, M., Calovic, M. S., Ristanovic, P., & Babic, B. S. (1990). Application of Newton's optimal power flow in voltage/reactive power control. *IEEE Transactions on Power Systems, 5*(4), 1447-1454.

[4] Granville, S. (1994). Optimal reactive dispatch through interior point methods. *IEEE Transactions on power systems, 9*(1), 136-146.

[5] Grudinin, N. (1998). Reactive power optimization using successive quadratic programming method. *IEEE Transactions on Power Systems, 13*(4), 1219-1225.

[6] Kamel, S., Abdel-Fatah, S., Ebeed, M., Yu, J., Xie, K., & Zhao, C. (2019, May). Solving optimal reactive power dispatch problem considering load uncertainty. In *2019 IEEE Innovative Smart Grid Technologies-Asia (ISGT Asia)* (pp. 1335-1340). IEEE.

[7] Bhattacharyya, B., & Karmakar, N. (2020). Optimal Reactive Power Management Problem: A Solution Using Evolutionary Algorithms. *IETE Technical Review, 37*(5), 540-548.

[8] Kamel, S., Abdel-Fatah, S., Ebeed, M., Yu, J., Xie, K., & Zhao, C. (2019, May). Solving optimal reactive power dispatch problem considering load uncertainty. In *2019 IEEE Innovative Smart Grid Technologies-Asia (ISGT Asia)* (pp. 1335-1340). IEEE.

[9] Aljohani, T. M., Ebrahim, A. F., & Mohammed, O. (2019). Single and multiobjective optimal reactive power dispatch based on hybrid artificial physics–particle swarm optimization. *Energies, 12*(12), 2333.

[10] Mahate, R. K., & Singh, H. (2019). Multi-objective optimal reactive power dispatch using differential evolution. *International Journal of Engineering Technologies and Management Research, 6*(2), 27-38.

[11] Nguyen, T. T., & Vo, D. N. (2019). Improved social spider optimization algorithm for optimal reactive power dispatch problem with different objectives. *Neural Computing and Applications*, 1-32.

[12] Yang, S., Wang, W., Liu, C., & Huang, Y. (2015). Optimal reactive power dispatch of wind power plant cluster considering static voltage stability for low-carbon power system. *Journal of Modern Power Systems and Clean Energy, 3*(1), 114-122.

[13] Emiroglu, S., Uyaroglu, Y., & Ozdemir, G. (2017). Distributed reactive power control based conservation voltage reduction in active distribution systems. *Advances in Electrical and Computer Engineering, 17*(4), 99-106.

[14] Ghasemi, M., Taghizadeh, M., Ghavidel, S., Aghaei, J., & Abbasian, A. (2015). Solving optimal reactive power dispatch problem using a novel teaching–learning-based optimization algorithm. *Engineering Applications of Artificial Intelligence, 39*, 100-108.

[15] *Illinois Center for a Smarter Electric Grid (ICSEG)*. Available online: https://icseg.iti.illinois.edu/ieee-30-bussystem/ (accessed on 25 February 2019).

[16] Subbaraj, P., & Rajnarayanan, P. N. (2009). Optimal reactive power dispatch using self-adaptive real coded genetic algorithm. *Electric Power Systems Research, 79*(2), 374-381.

[17] Pandya, S., & Roy, R. (2015, March). Particle swarm optimization based optimal reactive power dispatch. In *2015 IEEE International Conference on Electrical, Computer and Communication Technologies (ICECCT)* (pp. 1-5). IEEE.

[18] Hussain, A. N., Abdullah, A. A., & Neda, O. M. (2018). Modified particle swarm optimization for solution of reactive power dispatch. *Research Journal of Applied Sciences, Engineering and Technology, 15*(8), 316-327.

Investigation of Chemically Stored Hydrogen Desorption from Pristine Carbon Based Amine Borane Derivatives: Thermolysis and Hydrothermolysis

Bilge Coşkuner Filiz[1], Aysel Kantürk Figen[2]

[1]Yıldız Technical University, Science and Technology Application and Research Center, İstanbul, Turkey, bilgecoskuner@gmail.com

[2]Yıldız Technical University, Chemical Engineering Department, İstanbul, Turkey, ayselkanturk@gmail.com

Abstract—**In this study, two different carbon derivatives of amine borane as methylamine borane (MeAB, $CH_3BH_3NH_2$) and ethylenediamine bisborane (EDAB, $C_2H_{14}B_2N_2$) were synthesized based on one-pot approach. The structural characterizations were carried out via X-ray diffraction (XRD) and infrared spectroscopy (FT-IR). Thermolyses properties of each component firstly investigated by differential scanning calorimetry (DSC) and then experimental self-thermolysis were performed at various temperatures. Self-hydrothermolyses of pristine compounds were also studied. Hydrothermolyses properties were carried out in presence of limited water and similar trend was observed in both reaction. Methly derivatives of amine borane enable better thermal decomposition properties than diethyl amine derivate one.**

Keywords - ammine borane, thermolysis, hydrothermolysis, hydrogen, production

I. INTRODUCTION

Energy storage have been curial topic for human's daily life. Several alternatives have been testing for improving of innovative, green and applicable technology alternative to conventional fossil based ones [1-3].

Hydrogen become the one the most prominent energy storage medium with its excellent properties such as easy availability, being non-toxic, green by-product, etc. among several hydrogen storage technique, chemical mediums for this aim have been synthesized since 18 century and their hydrogen desorption properties especially ammonia borane based have been actively interested since 2016 [2].

White solid crystal of ammonia borane provides practical use due to its stability under atmospheric conditions. But due to contamination of releases hydrogen during thermolysis reactions such as diborane or borazine made the researchers looking for new components [1,3].

The yield of desorbed hydrogen from chemical compound could be performed via hydrolysis, hydrothermolysis, thermolysis, solvolysis. Besides this, hydrolysis is one of the most studied reaction. Solid state reactions as thermolysis and hydrothermolysis have been spotlighted. During this reactions, by using derivatives of ammonia borane the evolved gas could be obtained pure and obtained by-product include more stable forms [3,4].

Thermolysis is a solid state reaction method by addition of external heat into reaction medium. Hydrothermolysis is a proses that combination of thermolysis and hydrolysis have been considered in the same idea [4].

ISBN: 978-86-80616-07-0

The hydrothermolysis reaction improved the intermolecular interaction, and the oxygen and hydrogen supplied by water vapor promote the dehydrogenation by by-products. This approach is uniquely performed without any catalyst, liquid solvent, or high temperature, and enables a compelling solution for disposable hydrogen source application [5].

Carbon derivatives of ammonia borane as methylamine borane ($BH_3NH_2CH_3$, MeAB) and diethylamine borane ($BH_3NH_2CH_2CH_2NH_2BH_3$, EDAB) provide these advantages. Methylamine borane complex (11.1% hydrogen), and ethylenediamine bisborane complex (11.4% hydrogen) were optimum compounds for these reactions. The low cost of ethylenediamine coupled with similar H_2 storage capacity makes it an attractive reagent for synthesis of ethylenediamine bisborane (ethane 1, 2-diaminoborane, EDAB) as a viable H_2 storage material and contributor to the H_2 economy [6].

In this study, carbon derivatives of amine borane components were synthesized for hydrogen storage. The one-pot synthesized materials were characterized and performed for hydrogen desorption reactions. For this aim, solid state approach thermolysis and hydrothermolysis reactions were carried out for investigation of hydrogen desorption tendency of materials without catalytic material usage.

II. MATERIALS AND METHODS

A. Synthesis of Amine Borane Derivatives

The amine borane derivatives were synthesized via one-pot metathesis reaction. The equivalent molar of sodium borohydride (0.05 mol $NaBH_4$, Sigma Aldrich, >99%) and amine salt (0.05 mol, CH_3NH_2.HCl or Sigma-Aldrich) was mixed in organic solvent tetrahydrofuran (500 ml C_4H_8O, Merck) at room temperature overnight. The obtained mixtures were filtrated and then organic solvent evaporated at 55°C to get white powder. The the powder recrystallized in diethyl ether ($(C_2H_5)_2O$) and characterized after milling.

B. Characterization

The amine borane derivatives were characterized via spectral and crystalline diffraction meter.

The X-ray diffraction (Philips Panalytical X'Pert-Pro diffractometer with CuKα radiation) performed at operating parameters of 40 mA and 45 kV with step size 0.02° and speed of 1°/min. Phase identification of solids was performed by inorganic crystal structure database (ICSD).

The attenuated total reflectance (ATR) of FT-IR spectroscopy (Perkin Elmer Spectrum One) was used in identification of chemical bonds of samples. The IR spectrum was recorded in the spectral range of 4000 to 650 cm^{-1} at ambient temperature and the resolution used was 4 cm^{-1}.

The differential scanning calorimetry was used for thermal characterization of material. The analyses carried out under inert atmosphere (N_2) 30-250°C heating range with 10°Cmin^{-1} heating rate in aluminum crucible.

C. Hydrogen Desorption

The two different approaches as thermolysis and hydrothermolysis were preferred for hydrogen desorption from chemical hydrogen deposition mediums.

The thermolysis experiments were carried out by using 1.2 mmol pristine amine borane derivatives (MeAB or EDAB). The lab-made chemical put into three necked reactor equipped with temperature controlled system and gas collector system to measure evolved gas. The collected volume of gas recorded with time.

The hydrothermolysis experiments were carried out in the identical system. The experimental conditions of thermolysis experiments is addition of 3 droplets of water into reactor.

III. RESULTS AND DISCUSSION

A. Characterization

The white solids were characterized, before the hydrogen desorption studies to ensure the structures were successfully synthesized.

The XRD analysis results proved the crystal structures were methylamineborane ($NH_2(CH_3)(BH_3)$) orthorhombic structure with JCPDS: 01-0178-7313 and ethylenediamine bisborane ($(NH_2)_2(C_2H_4)(B_2H_4)$ orthorhombic structure [7,8] (Fig. 1).

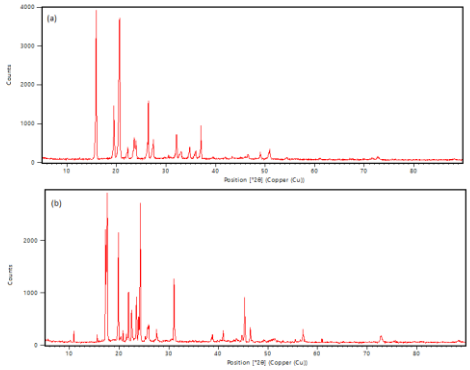

Figure1. XRD patterns of amine borane derivatives: (a) MeAB and (b) EDAB.

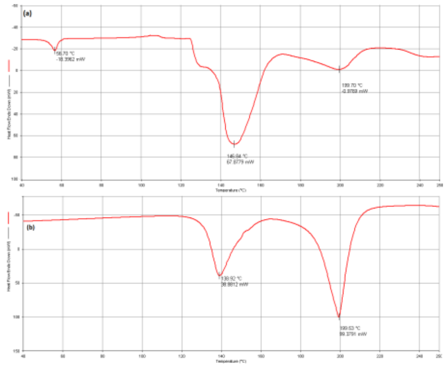

Figure 3. DSC curves of amine borane derivatives: (a) MeAB and (b) EDAB.

Infrared spectroscopy results were given in Fig. 2 to characterized formed bonds. The bands recorded at 3750-3300 cm^{-1}, 3300-3000 cm^{-1}, 2250-2400 cm^{-1}, 1310-1085 cm^{-1} and 1250-600 cm^{-1} were corresponded to N-H, C-H, B-H, C-O and C-H vibrations, respectively [9,10].

The DSC curves of carbon based amine derivatives were given in Fig. 3. The thermolyses properties were firstly examined with DSC. According to DSC curve of MeAB, three endothermic peaks were determined at 56.70°C, 146.84°C and 199.70°C. The first peak was related with the solvent maintained in the structure of MeAB. The other two endothermic peaks were indicated the hydrogen desorption from the chemical structure. Together with this, hydrogen evolution was started at 130°C.

The DSC curve of EDAB showed two main peaks at 138.92°C and 199.53°C that were sign of hydrogen release. Leardini et al. reported that hydrogen evolution just started after melting of EDAB at 119°C [8,10].

The all characterization results were confirmed that obtained white powders were in desired structures.

B. *Hydrogen Desorption Studies*

Carbon derivatives of ammine boranes were used for hydrogen evolution and hydrothermolysis and thermolysis procedures were investigated for both material.

The volume of hydrogen was collected up to 40 ml to make a brief comparison of reactions and components (see Fig. 4 and Fig. 5). The

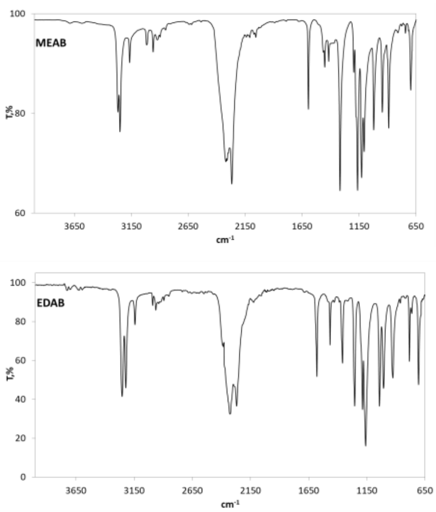

Figure 2. FTIR spectrums of amine borane derivatives: (a) MeAB and (b) EDAB.

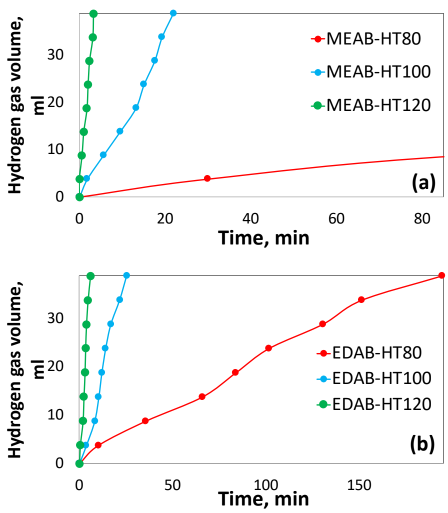

Figure 4. Hydrogen volume generated via hydrothermolysis of MeAB (a) and EDAB (b).

hydrogen desorption from the chemical structure of amine boranes were altered with temperature in hydrothermolyses (Fig. 4). The rising the reaction temperature from 80°C to 120°C had a positive effect on the reaction kinetic. The total time required for the obtaining target volume of hydrogen was shortened for both component. The hydrogen desorption rate from chemical structure of MeAB was two times faster than EDAB at 120°C. Moreover this, rising the temperature from 100°C to 120°C this rate increased almost 7th times.

As could be seen from Fig. 5, similar tendency was obtained for thermolysis reaction. Methyl derivates of amine borane showed short hydrogen releasing time compared to ethyl derivatives one. The positive effect of temperature was also observed thermolyzes reaction. Together with this, at highest temperature the hydrogen collection time was almost same. The rate of hydrogen desorption was obtained higher than the hydrothermolyses as could be seen from Fig. 6. The water addition into the pristine component medium did not significantly change the reaction kinetic.

IV. Conclusion

The identification of hydrogen energy deposition mediums as methyl and diethyl derivatives were showed the target structures were usefully obtained. The two strategy was applied to get deposited hydrogen as thermolysis and hydrothermolysis was successfully desorbed the hydrogen from the structure of amines were performed with application of heat. According to the hydrogen desorption based on

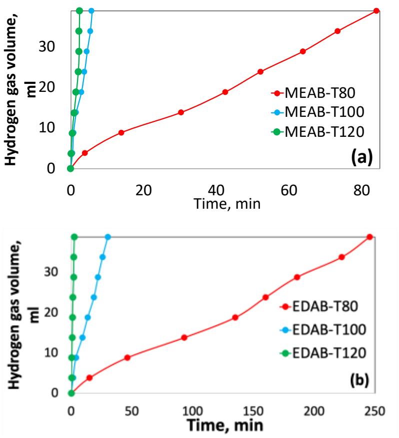

Figure 5. Hydrogen volume generated via hydrothermolysis of MeAB (a) and EDAB (b).

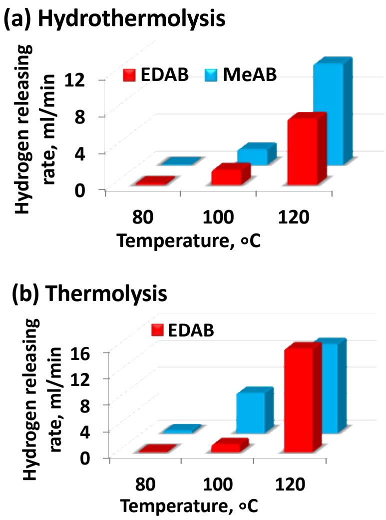

Figure 6. Hydrogen releasing rate via hydrothermolyses (a) and thermolyses (b).

reactions, MeAB releases hydrogen faster than the EDAB and also thermolysis reaction made easier hydrogen production than the hydrothermolysis reaction without stirring the reaction medium.

Acknowledgment

This work was supported by Yildiz Technical University Scientific Research Projects Coordinator's project numbered FBA-2019-3476.

References

[1] Huang, Z., & Autrey, T. (2012). Boron–nitrogen–hydrogen (BNH) compounds: recent developments in hydrogen storage, applications in hydrogenation and catalysis, and new syntheses. *Energy & Environmental Science*, *5*(11), 9257-9268.

[2] Kumar, R., Karkamkar, A., Bowden, M., & Autrey, T. (2019). Solid-state hydrogen rich boron–nitrogen compounds for energy storage. *Chemical Society Reviews*, *48*(21), 5350-5380.

[3] Baitalow, F., Baumann, J., Wolf, G., Jaenicke-Rössler, K., & Leitner, G. (2002). Thermal decomposition of B–N–H compounds investigated by using combined thermoanalytical methods. *Thermochimica Acta*, *391* (1-2), 159-168.

[4] Demirci, U. B., Bernardd, S., Chiriac, R., Toche, F., & Miele, P. (2011). Hydrogen release by thermolysis of ammonia borane NH_3BH_3 and then hydrolysis of its by-product [BNH_x]. *Journal of Power Sources*, *196* (1), 279-286.

[5] Pei, P., Cannon, M., Quan, G., & Kjeang, E. (2020). Effective hydrogen release from ammonia borane and sodium borohydride mixture through homopolar based dehydrocoupling driven by intermolecular interaction

and restrained water supply. *Journal of Materials Chemistry A*, 8(36), 19050-19056.

[6] Ramachandran, P. V., Gagare, P. D., Mistry, H., Biswas, B., & Purdue Research Foundation (2017). Procedures for the synthesis of ethylenediamine bisborane and ammonia borane. U.S. Patent 9,534,002.

[7] Ting, H. Y., Watson, W. H., & Kelly, H. C. (1972). Molecular and crystal structure of ethylenediamine-bisborane, $C_2H_{14}B_2N_3$. *Inorganic Chemistry*, *11*(2), 374-377.

[8] Leardini, F., Valero-Pedraza, M. J., Perez-Mayoral, E., Cantelli, R., & Bañares, M. A. (2014). Thermolytic decomposition of ethane 1, 2-diamineborane investigated by thermoanalytical methods and in situ vibrational spectroscopy. *The Journal of Physical Chemistry C*, *118*(31), 17221-17230.

[9] Coşkuner Filiz, B., & Kantürk Figen, A. (2019). Hydrogen production from sodium borohydride originated compounds: Fabrication of electrospun nano-crystalline Co_3O_4 catalyst and its activity. *International Journal of Hydrogen Energy*, *44*(20), 9883-9895.

[10] Yang, Z., Cheng, F., Tao, Z., Liang, J., & Chen, J. (2012). Decreasing the thermal dehydrogenation temperature of methylamine borane (MeAB) by mixing with poly(methylacrylate) (PMA), *International Journal of Hydrogen Energy*, *37*(76), 38-7644.

The Analysis of the Legal Framework of Energy Management in the Republic of Serbia

Aleksandra Ilić Petković[1], Jelena Malenović Nikolić[2]

[1,2]Faculty of Occupational Safety in Niš, Niš, Serbia, aleksandra.ilic@znrfak.ni.ac.rs[1]; jelena.malenovic@znrfak.ni.ac.rs[2]

Abstract—**In modern political and economic circumstances, the general public, and economic entities in particular, are in need of more detailed information on the concept of energy use from renewable sources and its advantages, despite the obvious pressure on the budgets of these environmental policy entities. In achieving this goal, the state and its national and international environmental policy play a key role. It can be accomplished by the adoption and efficient implementation of regulations in the field of energy, especially energy management. The Republic of Serbia has largely incorporated the acquis communautaire in the field of energy, energy efficiency and energy management into the national legislative framework. What should be especially insisted on is consistent compliance with the adopted regulations and efficient control of their implementation.**

Keywords - energy management, energy efficiency, regulations, the Republic of Serbia

I. Introduction

Some of the burning issues in today's world are global warming and climate change. These phenomena are a direct consequence of greenhouse gas emissions, because the mass construction of power plants has led to the emission of pollutants in concentrations above the prescribed limit values. For this reason, scientists and professionals are fully aware of the need to use renewable energy sources and improve various technologies in order to make energy use as accessible, economical and environmentally friendly as possible [1]. Despite the obvious pressure on the budget, there is an evident need to bring these issues closer to the general public and economic entities, in addition to scientists and professionals.

In achieving this goal, the state plays a key role, as well as its national and international environmental policy. It can be accomplished by the adoption and efficient implementation of regulations in the field of energy, especially energy management. The goal is to reduce energy consumption, while the level of comfort, quality of life and standard of living remain unchanged. Legal regulation of energy efficiency and energy management is important in order to establish a system in which its subjects, their rights and obligations, as well as sanctions in case of non-compliance, are clearly defined. The fact that Serbia has accepted the obligation to harmonize its regulations with the EU regulations, which are highly dedicated to the environment and, consequently, energy policy, speaks in favor of the idea of a complete and comprehensive legal regulation in this area [2].

II. Energy Management in the Legal Framework of The Republic of Serbia

A. *Regulations on Energy in General*

The Republic of Serbia has extensive legal regulation in the field of energy. The two basic laws in the field of energy and energy efficiency are the Law on Energy and the Law on Efficient Use of Energy. The Law on Energy deals with national goals and plans concerning energy policy and the manner of its implementation, conditions for reliable, safe and quality delivery of energy and energy sources, conditions for secure energy supply, protection of energy customers, conditions and manner of performing energy activities, conditions for the construction of new energy facilities, use of renewable energy sources, status and scope of work of the Energy Agency of the Republic of

Serbia, etc. [3]. As can be noticed, this law does not deal with energy management directly; it is more focused on the energy policy of the state in general. On the other hand, the Law on Efficient Use of Energy is a key document which regulates the energy management system in Serbia.

B. *Law on Efficient Use of Energy*

The basic document that regulates the energy management system in Serbia is the Law on Efficient Use of Energy [4]. This law regulates the conditions and manner of efficient use of energy and energy sources in the sector of production, transmission, distribution and consumption of energy, energy efficiency policy, energy management system, level of energy efficiency of products that affect energy consumption, minimum energy efficiency requirements in production, transmission and distribution of electricity and heat and delivery of natural gas, financing, incentives and other measures in this area, etc.

The basic provisions of the Law define some basic terms [4]. Thus, an energy manager is an individual appointed by the obligor of the energy management system to monitor and record the ways of using and the amount of energy used, propose and implement measures for efficient use of energy and perform other tasks determined by this Law. The report of the energy manager is a written report by which he/she reports on the implemented measures and activities defined by the energy efficiency program and plan. The energy management system is a system of organized energy management that includes the widest set of regulatory, organizational, incentive, technical and other measures and activities, as well as organized monitoring and analysis of energy production, transmission, distribution and consumption, which are determined and implemented by state administration, bodies of local self-government units and obligors of the energy management system.

A special chapter of the Law is dedicated to the energy management system [4]. Firstly, it determines the subjects of energy management, which are the Government, the Ministry, the obligors of the energy management system, energy managers and authorized energy advisors. The government is authorized to pass regulations in the field of efficient use of energy, at the proposal of the line ministry. The Ministry organizes, implements and monitors the functioning of the system and the implementation of the goals of the energy management system. The obligors of the energy management system are: companies whose predominant activity is in the production sector, if they use more energy than prescribed by the Government; companies whose predominant activity is in the trade and services sector, if they use more energy than prescribed by the Government; state administration bodies and other bodies of the Republic of Serbia, bodies of the autonomous province, bodies of local self-government units, etc. The obligor of the system is particularly obliged to: implement the energy saving goal prescribed by the Government; appoint the required number of energy managers; adopt an energy efficiency program and plan; implement measures for efficient use of energy specified in the program or plan; submit annual reports on the achievement of the goals contained in the program and plan to the line ministry; ensure that energy audits are conducted at least once every five years, etc.

The energy manager is an individual appointed by the system obligor, who is particularly obliged to: collect and analyze data on the manner of system obligors’ energy use; prepare the stated programs and plans; propose measures that contribute to the efficient energy use and participate in their implementation; ensure the preparation of the annual report, etc. The activities of an energy manager may be performed by a person licensed to perform these activities.

The authorized energy advisor performs energy inspection and energy audit. It is a natural or legal person, entered in the register of authorized energy advisors of the line ministry. After performing energy inspection/audit, he/she is obliged to submit the data on the performed inspection, i.e. energy audit, to the line ministry. The Ministry keeps a database on performed energy inspections, i.e. energy audits. The activities of an energy advisor may be performed by a natural or legal person under the conditions prescribed by law. The authorized energy advisor prepares and signs the report on the conducted energy inspection, with the proposal of measures for efficient energy use, i.e. the report on energy audit. The results of the energy inspection are considered valid if the review was conducted according to the prescribed methodology by an authorized energy advisor and presented according to the prescribed content of the report on the conducted energy inspection.

Energy manager certificate is issued to the person who has passed the exam for energy managers. The exam can be taken by a person who:

- has acquired at least a bachelor’s degree in the field of technical and technological sciences (180 ECTS) and has a certificate of training completion for energy managers; or
- has acquired a master's degree in the field of mechanical engineering, electrical engineering or technology.

Authorized energy advisor certificate is issued to the person who has passed the professional exam for energy advisors. The examination for performing the duties of an authorized energy advisor can be taken by a person who:

- has acquired an energy manager certificate;
- has at least three years of experience in performing energy audits or experience in testing energy or process installations or experience in design or professional construction supervision;
- has a certificate of completion of theoretical and practical training for an authorized energy advisor.

A license to perform the duties of an energy manager may be issued to a person who obtains an energy manager certificate and has three years of work experience in that profession. The license for performing the activities of an authorized energy advisor is issued to a person who: obtains an authorized energy advisor certificate; has acquired a master's degree in the field of technical and technological sciences and has at least three years of work experience in that profession; has not been convicted of any crime against property or the economy. These licenses may be revoked under certain conditions prescribed by law.

Based on the Law on Efficient Use of Energy, a number of bylaws has been passed - one decree and six rulebooks. Together they form a system of regulations on energy management Table I.

TABLE I. REGULATIONS IN THE FIELD OF ENERGY MANAGEMENT

Law on Efficient Use of Energy
Decrees
Decree on determining the limit values of annual energy consumption on the basis of which it is determined which companies are liable for the energy management system, annual energy saving targets and the form of the report on the realized consumption
Rulebooks
Rulebook on the form of the annual report on the achievement of energy saving goals
Rulebook on the conditions for the appointment of energy managers in the bodies of local self-government units
Rulebook on the conditions for the appointment of energy managers in companies whose predominant activity is in the manufacturing sector and companies as public services
Rulebook on the conditions for the appointment of energy managers in companies whose predominant activity is in the trade and services sector, state administration bodies, other bodies of the Republic of Serbia, bodies of the Autonomous Province and institutions
Rulebook on the manner of implementation and content of the training program for energy managers, costs of attending the training, as well as detailed conditions, program and manner of taking the exam for energy managers
Rulebook on conditions regarding personnel, equipment and space of the organization conducting training for energy managers and authorized energy advisors

Source: Ministry of Mining and Energy of the Republic of Serbia

C. Bylawss

Decree on determining the limit values of annual energy consumption on the basis of which it is determined which companies are liable for the energy management system, annual energy saving targets and the form of the report on the realized consumption determines the limit values deciding which companies are liable for energy management system, annual energy saving targets and application form for the realized primary energy consumption of the system payers [5].

Rulebook on the form of the annual report on the achievement of energy saving goals prescribes the form on which the obligor of the energy management system submits an annual report on the achievement of energy saving goals to the ministry [6].

Rulebook on the conditions for the appointment of energy managers in the bodies of local self-government units regulates the conditions for appointing energy managers in the bodies of local self-government units with more than 20,000 inhabitants as obligors of the energy management system [7]. According to this rulebook, the local self-government unit is obliged to appoint at least one energy manager.

Rulebook on the conditions for the appointment of energy managers in companies whose predominant activity is in the manufacturing sector and companies as public services regulates more detailed conditions for the appointment of energy managers with obligors in the energy management system, primarily those companies whose predominant activity is in the manufacturing sector and companies as public services that perform activities in the field of postal traffic, energy, roads, utilities [8].

Rulebook on the conditions for the appointment of energy managers in companies whose predominant activity is in the trade and services sector, state administration bodies, other bodies of the Republic of Serbia, bodies of the Autonomous Province and institutions regulates conditions for the appointment of energy managers with obligors in the energy management system, primarily those companies whose predominant activity is in the trade and services sector, with state administration bodies, other bodies of the Republic of Serbia, bodies of the Autonomous Province and with institutions that perform activities in the field of education, science, culture, healthcare and other areas and which use publicly owned facilities in accordance with law [9]. According to this rulebook, the obligation of the mentioned entities is to appoint at least one energy manager for each location.

Rulebook on the manner of implementation and content of the training program for energy managers, costs of attending the training, as well as detailed conditions, program and manner of taking the exam for energy managers regulates the manner of conducting training, content of theoretical and practical training programs for energy managers, amount and manner of paying training costs, as well as more detailed conditions, program and manner of taking the exam for energy managers [10]. With reference to this rulebook, there is another rulebook in force - Rulebook on conditions regarding personnel, equipment and space of the organization conducting training for energy managers and authorized energy advisors [11]. This Rulebook prescribes more detailed conditions regarding the staff, equipment and space of the organization that conducts theoretical and practical training for energy managers and authorized energy advisors. In terms of the above regulations, the Faculty of Mechanical Engineering of the University of Belgrade, for example, is authorized to perform such training [12].

III. CONCLUSION

It is known that the right to a healthy environment is one of the basic human rights in the theory of environmental law. This right is guaranteed by numerous international documents, as well as the Constitution of the Republic of Serbia. The implementation of this right requires conducting an active state policy in the field of environmental protection in general, and especially in the segment of energy management. The goal is to use renewable energy sources as much as possible and increase energy efficiency. At the same time, the policy requires to maintain the quality of life and living standard at the existing level.

One of the most important instruments for the fulfilment of such requirements is the adoption and active implementation of regulations in the field of energy management. The Republic of Serbia showed its commitment to renewable energy sources as some of the important initial steps towards this commitment were the ratification of the Kyoto Protocol and the signing of the Energy Community Treaty when the country guaranteed to harmonize its laws with EU Directive 2001/77/EC, which promotes electricity produced from renewable sources [13,14]. Energy management should promote the production of energy from renewable energy sources and in accordance with Directive 2003/30/EC [15].

As a result of conducting energy policy, the Law on Efficient Use of Energy was adopted as the basic law in the field of energy management. Based on this law, a number of bylaws was adopted - one decree and six rulebooks. These bylaws mostly regulate the issues of appointing energy managers in various companies, local self-government units, etc. Also, special attention is paid to the requirements for the position of energy managers, their qualifications, program and manner of taking exams, obtaining a license, etc. The issue of appointing an energy advisor is regulated in a similar way. Precisely, European experience shows that we can achieve savings of at least 10% of the total annual energy costs only by establishing an energy management system and appointing a person in charge of energy, [16].

Based on the analysis of legal regulations in the field of energy management in Serbia, it can be concluded that this field, as well as the fields of energy and energy efficiency, are thoroughly regulated by clearly structured documents of different legal force. Their application is still questionable due to certain problems such as lack of financial resources, complex administrative procedures, insufficient number of inspectors, etc. The state faces the same problems in terms of the implementation of other regulations as well. Addressing these challenges will contribute to more efficient implementation of regulations in the field of energy management and, ultimately, the improvement of energy efficiency.

ACKNOWLEDGMENT

This research was funded by the Ministry of Education, Science and Technological Development of the Republic of Serbia.

REFERENCES

[1] Nešić, B. (2016). Origin and development of European Union law in the field of energy. *Foreign Legal Life, 60*(2), 231-241.

[2] Đereg, N., Kalmar Krnajsi Jović, Z., & Apostol, I. (2008). *Renewable energy sources in Serbia - recommendations, potential and criteria*. Subotica: Center for ecology and sustainable development.

[3] Energy Law, "Official Gazette of the Republic of Serbia", No. 145/2014, 95/2018.

[4] Law on Efficient Use of Energy, "Official Gazette of the Republic of Serbia", No. 25/2013.

[5] Decree on determining the limit values of annual energy consumption on the basis of which it is determined which companies are liable for the energy management system, annual energy saving targets and the form of the report on the realized consumption, " "Official Gazette of the Republic of Serbia", No. 18/2016.

[6] Rulebook on the form of the annual report on the achievement of energy saving goals, "Official Gazette of the Republic of Serbia", No. 32/2016, 65/2018.

[7] Rulebook on the conditions for the appointment of energy managers in the bodies of local self-government units, "Official Gazette of the Republic of Serbia", No. 65/2018.

[8] Rulebook on the conditions for the appointment of energy managers in companies whose predominant activity is in the manufacturing sector and companies as public services, "Official Gazette of the Republic of Serbia", No. 98/2016.

[9] Rulebook on the conditions for the appointment of energy managers in companies whose predominant activity is in the trade and services sector, state administration bodies, other bodies of the Republic of Serbia, bodies of the Autonomous Province and institutions, " "Official Gazette of the Republic of Serbia", No. 85/2017.

[10] Rulebook on the manner of implementation and content of the training program for energy managers, costs of attending the training, as well as detailed conditions, program and manner of taking the exam for energy managers, "Official Gazette of the Republic of Serbia", No. 12/2015.

[11] Rulebook on conditions regarding personnel, equipment and space of the organization conducting training for energy managers and authorized energy advisors, "Official Gazette of the Republic of Serbia", No. 12/2015.

[12] Decision authorizing the Faculty of Mechanical Engineering of the University of Belgrade to perform the training of energy managers and authorized energy advisors, "Official Gazette of the Republic of Serbia", No. 84/2019.

[13] Kronja, J. et al. (eds.). (2011). *A guide to the Europe 2020 Strategy*. Belgrade: European movement in Serbia.

[14] Energy Sector Development Strategy of the Republic of Serbia by 2025 with projections until. 2030, "Official Gazette of the Republic of Serbia", No. 101/2015.

[15] Marković, S., Krstić, M., Bojković, R., & Đorđević, Lj. (2009). Management as a factor in intensifying the use of renewable energy sources. *IMK-14 Research and Development, 15*(30-31), 121-128.

[16] Borojević, K., & Milešević, T. (2016). Management in renewable energy sources. *Svarog, 12*, 89-102.

Consideration of Regulating Transformer at Calculate Power Flow

Miloš M. Stevanović[1], Sreten B. Stojanović[2], Dragan S. Tasić[3]

[1,2]University of Nis, Faculty of Technology, Leskovac, Serbia, smilos@tf.ni.ac.rs[1]; sstojanovic@tf.ni.ac.rs[3]

[3]University of Nis, Faculty of Electronic Engineering, Nis, Serbia, e-mail: dragan.tasic@elfak.ni.ac.rs

Abstract—**The paper deals with the calculation of power flows in the electric power system of Serbia 400 kV and 220 kV, where the regulating transformers in the network are modeled by the P replacement scheme.**

Keywords - regulating transformers, power flow, Newton-Raphson method

I. Introduction

Regulation transformers regulate voltages and currents of reactive powers in transmission and distribution networks. Voltage regulation can be performed without load and under load. In the first case, the technical solution is simpler, because the number of coil is changed in the voltage-free state, e.g. the transformer is taken out of operation. When regulating the voltage under load, the change in the number of windings of the multi-voltage winding is implies. Voltage regulation is discontinuous and relatively slow, and is carried out step by step with the help of automatic voltage regulators. Regulation transformers are found in electric power networks as double-winding and three-winding. In three-winding regulation transformers, in some cases the tertiary supplies the consumption or the own consumption of the transformer station, while in some cases the tertiary is idling. A typical regulation transformer encountered in our distribution networks is 110±11×1,5% /36,75/10,5 *kV/kV/kV*, $Y_N y_n 0 d5$. Also, there are regulation transformers at all voltage levels. In our networks at transformers 10/0,4 *kV/kV* voltage regulation is performed without load, while with other transformers (400/220 *kV/kV*, 400/110 *kV/kV*,110/35 *kV/kV*, 35/10 *kV/kV*), regulation is performed under load (consumption is not excluded). Regulation transformers can cause voltage instability, due to increased reactive power in the network [1-3]. Reactive powers lead to an increase in current, and thus to greater voltage drops.

In this paper, the regulation transformer is represented by a P replacement scheme. P replacement scheme is suitable for modeling the elements of the power system, because it does not introduce additional nodes in the replacement scheme of the system being analyzed.

II. „P" Scheme Regulation Transformer

The regulation transformer as an element of the power system acts as a variable impedance. It can be modeled with a P replacement scheme, as shown in Fig. 1.

The corresponding parameters "P" of the replacement scheme from Fig. 1 are:

$$\underline{y}_{pq} = t\underline{Y}_T \ , \tag{1}$$

$$\underline{y}_{p0} = (1-t)\underline{Y}_T \ , \tag{2}$$

$$\underline{y}_{q0} = t(t-1)\underline{Y}_T \ , \tag{3}$$

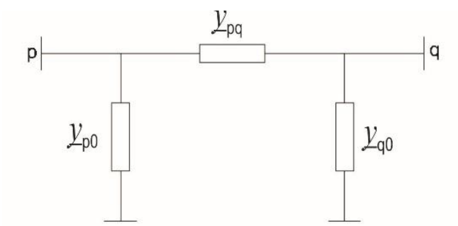

Figure 1. "P" scheme regulation transformer.

ISBN: 978-86-80616-07-0

where are:

$\underline{Y}_T$ – transformer admittance (conductivity), reciprocal value of the transformer impedance Z_T (at the nominal transformation ratio)

t – non-nominal transformation ratio of the regulation transformer:

$$t = 1 + n\Delta t \, . \tag{4}$$

In Eq. (4), n is a positive or negative integer that determines the position of the control switch. Usually n = ± (10÷12) for regulation transformers under load, while n = ± (1 ÷ 2) for control in voltage-free state. A minus sign in front of n indicates a decrease in the number of coils, and a plus sign indicates an increase. $\Delta t = 0,015$ denotes the discrete degree in the relative system of units. For our transformers, it is usually $\Delta t = 0,015$ or $\Delta t = 0,125$ (which for n = 10 gives a regulation range of 15% or 12.5%).

III. Newton – Raphson's Iterative Procedure for Calculate Power Flow when Considering Regulation Transformer

The Newton - Raphson method is a very efficient method for solving nonlinear equations, where the equation is reduced to the form $f\ (x) = 0$. The application of the Newton - Raphson procedure for the calculation of power flows is based on the expressions for active and reactive injection power in hybrid form:

$$P_i(\vec{X}) = U_i^2 G_{ii} + U_i \sum_{\substack{K=1 \\ K \neq i}}^{N} U_k (G_{ik} \cos(\theta_i - \theta_k) + \\ + B_{ik} \sin(\theta_i - \theta_k)) \, , \tag{5}$$

$$Q_i(\vec{X}) = -U_i^2 B_{ii} + U_i \sum_{\substack{K=1 \\ K \neq i}}^{N} U_k (G_{ik} \sin(\theta_i - \theta_k) - \\ - B_{ik} \cos(\theta_i - \theta_k)) \, , \tag{6}$$

$U_i, U_k, \theta_i, \theta_k$ – modules and voltage angles at nodes i and k, respectively.

$$\underline{Y}_{ik} = G_{ik} + jB_{ik} \, , \tag{7}$$

$\underline{Y}_{ik}$ – absolute value of admittance in place *ik* in the admittance matrix (bus matrix).

The admittance matrix gives the relationship between the vector of injected currents into the network nodes and the voltage vector of the nodes. The admittance matrix of nodes is a square matrix. Its diagonal elements $\underline{Y}_{ii}$ are defined as the sum of all admittances encountering in that node, including island admittances, while the non-diagonal elements $\underline{Y}_{ik}$ are negative values of the admittance of the branch connecting the nodes i and k $(\underline{Y}_{ik} = -y_{ik})$. If there is no physical connection between the two nodes then these elements are zero.

Notations to be used in the future:

SL - balance - reference node;

PU - generator (voltage - controlled) node - the active injection power P and the voltage module U are known, and the reactive power Q and the phase position of the voltage phasor are unknown;

PQ - consumer node - the active and reactive injection power P and Q are known, and the voltage module U and the phase position of the voltage phasor are unknown;

N_{PU} - number of generator nodes;

N_{PQ} - number of consumer nodes;

N_{rt} - number of control transformers.

Based on equations (5) and (6) and the fact that the active injection power is known in all PU and PQ nodes, and the reactive injection power in all PQ nodes comes to a system of $N - 1 + N_{PQ}$ equations, which is given in matrix form by the following relation:

$$\vec{f}(\vec{X}) = \begin{bmatrix} P_i^{sp} - P_i(\vec{X}) \\ ------ \\ Q_i^{sp} - Q_i(\vec{X}) \end{bmatrix} = \vec{0} \, ,$$

$\vec{P}^{sp} = \begin{bmatrix} P_2^{sp} & P_3^{sp} & \cdots & P_N^{sp} \end{bmatrix}^T$ – vector of (known) specified active powers injected into the network nodes,

$\vec{P}(\vec{X}) = \begin{bmatrix} P_2(\vec{X}) & P_3(\vec{X}) & \cdots & P_N(\vec{X}) \end{bmatrix}^T$ – vector of active powers injected in network nodes as a function of vectors of unknown variables $\vec{X}$,

$\vec{Q}^{sp} = \left[Q^{sp}_{N-N_{PQ+1}} \quad Q^{sp}_{N-N_{PQ+2}} \quad \cdots \quad Q^{sp}_{N} \right]^T$ – vector of (known) specified active powers injected into the network nodes,

$\vec{Q}(\vec{X}) = \left[Q_{N-N_{PQ+1}}(\vec{X}) \quad Q_{N-N_{PQ+2}}(\vec{X}) \quad \cdots \quad Q_N(\vec{X}) \right]^T$ – vector of reactive powers injected into network nodes as a function of vectors of unknown variables $\vec{X}$.

Based on the P scheme of the regulation transformer from Fig. 1, it is concluded that by changing the gear ratio, the values of the elements in the admittance matrix of nodes $\left[Y_{čv}\right]$ that correspond to nodes p and q, i.e. at positions pp, pq, qp, qq, change. Therefore, it is concluded that the corresponding elements of the node admittance matrix depend on the non-nominal transformation ratio t. The injection forces depend on the elements of the node admittance matrix, so it can be concluded that they also depend on the non-nominal transformation ratio t. Therefore, a vector of transmission ratios of regulation transformers $\vec{t}$ whose dimension is equal to the number of control transformers is introduced. For the vector of unknown variables $\vec{X}$ the following is obtained:

$$\vec{X} = \begin{bmatrix} \vec{\theta} \\ \vec{U} \\ \vec{t} \end{bmatrix}, \tag{8}$$

$\vec{\theta} = \left[\theta_2 \quad \theta_3 \quad \cdots \quad \theta_N\right]^T$ - vector of unknown node voltage phasor angles,

$\vec{U} = \left[U_{N-N_{PQ+1}} \quad U_{N-N_{PQ+2}} \quad \cdots \quad U_N \right]^T$ - vector of unknown node voltage phasor modules,

$\vec{t} = \left[t_1 \quad t_2 \quad \cdots \quad t_{Nrt}\right]^T$ - vector of unknown gear ratios of regulation transformers.

For a vector of unknown variables $\vec{X}$ defined in this way, the Jacobian matrix is:

$$\left[J\right] = -\begin{bmatrix} \dfrac{\partial P}{\partial \theta} & | & \dfrac{\partial P}{\partial U} & | & \dfrac{\partial P}{\partial t} \\ - & & - & & - \\ \dfrac{\partial Q}{\partial \theta} & | & \dfrac{\partial Q}{\partial U} & | & \dfrac{\partial Q}{\partial t} \end{bmatrix}, \tag{9}$$

and the increment of unknown variables is:

$$\begin{bmatrix} \Delta\vec{\theta} \\ \Delta\vec{U} \\ \Delta\vec{t} \end{bmatrix} = \begin{bmatrix} \dfrac{\partial P}{\partial \theta} & | & \dfrac{\partial P}{\partial U} & | & \dfrac{\partial P}{\partial t} \\ - & & - & & - \\ \dfrac{\partial Q}{\partial \theta} & | & \dfrac{\partial Q}{\partial U} & | & \dfrac{\partial Q}{\partial t} \end{bmatrix}^{-1} \begin{bmatrix} \Delta\vec{P} \\ \Delta\vec{Q} \end{bmatrix}. \tag{10}$$

If the voltage regulator in some iteration reaches its limit position, the derivatives of active and reactive powers on the variable t in that node are equal to zero, so in the next iteration the third column in the Jacobian matrix for that node is excluded:

$$\vec{X}^{(\nu+1)} = \vec{X}^{(\nu)} + \Delta\vec{X}^{(\nu)}, \tag{11}$$

where is:

$$\Delta\vec{X}^{(\nu)} = -\left[J(\vec{X}^{(\nu)})\right]^{-1} \vec{f}(\vec{X}^{(\nu)}). \tag{12}$$

In equations (11) and (12) is:

$\vec{X}^{(\nu)}$ - vector of unknown variable states in ν-th iteration;

$J(\vec{X}^{(\nu)})$ – Jacobi's matrix of the first derive in ν-th iteration;

$\Delta\vec{X}^{(\nu)}$ - growth vector of unknown variable states in ν-th iteration;

$\vec{X}^{(\nu+1)}$ - vector of unknown variable states in $\nu+1$ - th iteration;

The iterative procedure is terminated when the following conditions are met:

$$\left|P_i^{sp} - P_i(\vec{X})\right| \le \varepsilon, \quad i = 2, \cdots N, \tag{13}$$

and

$$\left|Q_i^{sp} - Q_i(\vec{X})\right| \le \varepsilon, \quad i = N + N_{PQ} - 1, \cdots, N. \tag{14}$$

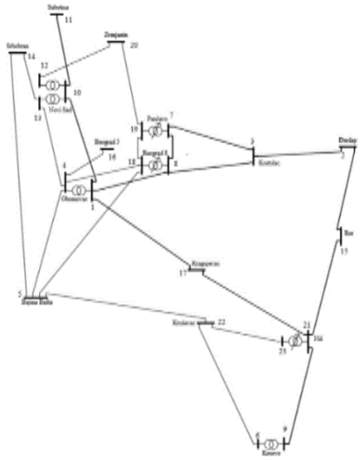

Figure 2. Schematic representation of the simplified power system of 400 kV and 220. kV EPS.

IV. APLICATION OF POWER FLOW CALCULATION

Newton - Raphson's method for calculating power flows with respect to regulation transformers, was applied to a simplified power system of 400 kV and 220 kV EPS, which is schematically shown in Fig. 2. Regulation transformers are modeled „P” replacement scheme.

This system includes all 400 kV nodes (11 in total) and 12 nodes of 220 kV real EPS system, while all nodes of lower voltage levels are neglected, as well as all connecting lines with neighboring power systems.

The generating powers in the nodes of the considered network correspond to the equivalent generators, formed on the basis of data of all generators connected in those nodes, as well as generators connected to nodes of the corresponding part of the low voltage network, thus considering all EPS system generators. The power consumption in the nodes of the low voltage network is joined by the power consumption in the nodes of the considered part of the system. The connections of the system with the neighboring systems are modeled by constant active and reactive injections in the boundary nodes of the EPS system. All data on generation and consumption forces in individual nodes of the considered simplified system, calculated on the basis of the real situation on March 18, 1997 at 4 pm, as well as the corresponding data on the specified voltages and desired voltages behind the control transformers are given in Table II.15a. ([4], p. 169). The desired voltages behind the control transformers are nodes Belgrade 8 (220), Pancevo 220 and Nis. Data for lines and transformers are expressed in relative units and are shown in Table II.15b and II.15c, respectively, ([4], page 170). The base power is SB = 100 MVA, and the base voltage UB = 400 kV. These parameters of the EPS power system represent the real parameters of the existing elements.

The control transformers have a transmission ratio of 400 ± 12 × 1.25% / 220 kV/kV, ie the transmission ratio in relative units is in the interval (0.85-1.15).

It is necessary to determine the voltages of individual nodes, the transmission ratios of the transformation of regulation transformers, generator power, as well as power flows on individual lines and transformers for a given stationary state of the system from Table I.

By applying the Newton - Raphson's method for the calculation of power flows when considering regulation transformers, solutions were obtained on the power system of Serbia after 31 iterations, with a given accuracy 10^{-4}. The criterion for exiting the iteration is that the absolute values of the differences of the injected active powers of all generator and consumer nodes, as well as the absolute values of the differences of the injected reactive powers of all consumer nodes, are less than the specified accuracy. By executing the program code, the calculated transmission ratios of the control transformers are obtained, which are given in Table I.

Based on the calculated transmission ratios of the control transformers, the actual transmission ratios of the control transformers are determined by selecting the appropriate position of the voltage regulator for which the actual transmission ratio of the regulation transformer is closest to the calculated transmission ratio. Given that one discrete step of these control transformers 1.25% (0.0125 relative units, abbreviated r.j.), the actual transmission ratios are obtained, which are given in Table IV.

$$\text{Nis:}\ 1 - K\Delta t = 1 - 1 \cdot 0.0125 = 0.9875$$

$$\text{Pancevo:}\ 1 - K\Delta t = 1 - 4 \cdot 0.0125 = 0.95$$

$$\text{Beograd 8:}\ 1 - K\Delta t = 1 - 8 \cdot 0.0125 = 0.9$$

Based on the actual transmission ratios of the regulation transformers, the values of voltage, active and reactive injection forces are obtained by executing a computer code.

The calculated values of node voltage, power generation and consumption by the Newton - Raphson method for the calculation of power flows with respect to regulation transformers are given in Table II.

TABLE I. CALCULATED VALUES OF TRANSMISSIONS RELATIONSHIPS OF REGULATION TRANSFORMERS WITH SET PRECISION.

Node	**Name node**	**$U_{with\ RT}$**	**$U_{without\ RT}$**
18	Beograd 8 (220)	1	0.9489
19	Pancevo 220	1	0.9563
23	Nis 220	1	0.9899

TABLE II. CALCULATED VALUES OF NODE VOLTAGE, INJECTION OF POWER IN SL NODES AND REACTIVE POWERS IN PU NODES BY NEWTON-RAPHSON PROCEDURE WITH A SET PRECISION OF 10^{-4}.

Node	**Name node**	**$U_{desired}$[r.j]**	**U_{realy} [r.j.]**	**θ [°]**	**P_G [r.j.]**	**Q_G [r.j.]**	**P_p [r.j.]**	**Q_p [r.j.]**
1	Obrenovac 400	1.0075	1.0075	0	12.0483	5.8759	0.000	0.000
2	Đerdap	1.05	1.05	3.352	6.75	1.8737	1.000	0.300
3	Kostolac	1.005	1.005	-0.3373	3.49	2.4808	2.398	0,980
4	Obrenovac 220	0.975	0.975	-2.5453	5.53	0.3919	2.735	1.210
5	Bajina Bašta	0.97	0.97	1.4647	11.11	-0.2303	4.760	1.570
6	Kosovo 220	0.975	0.975	-4.4673	4.36	0.8742	4.330	1.690
7	Pančevo 400	-	0.9822	-1.5147	0	0	0.240	0.070
8	Beograd 8 (400)	-	0.9779	-1.4428	0	0	0.000	0.000
9	Kosovo 400	-	0.9891	-4.238	0	0	1.080	0.120
10	Novi Sad 400	-	0.9824	-2.6803	0	0	0.910	0.310
11	Subotica	-	0.9727	-4.5122	0	0	1.825	0.565
12	Novi Sad 220A	-	0.9719	-5.438	0	0	0.783	0.277
13	Novi Sad 220B	-	0.9341	-3.9466	0	0	1.242	0.490
14	Srbobran	-	0.8923	-3.1385	0	0	2.400	0.766
15	Bor	-	1.0304	0.1028	0	0	1.377	0.500
16	Beograd 5	-	0.9631	-4.171	0	0	5.586	1.430
17	Kragujevac	-	1.0148	-1.7814	0	0	1.080	0.100
18	Beograd 8 (220)	1	0.9969	-5.0056	0	0	5.400	3.320
19	Pančevo 220	1	0.9965	-5.3389	0	0	1.670	0.650
20	Zrenjanin	-	0.9668	-7.0438	0	0	1.305	0.470
21	Niš 400	-	1.0119	-2.3352	0	0	0.468	0.290
22	Kruševac	-	0.9532	-5.9773	0	0	2.140	0.905
23	Niš 220	1	0.9979	-3.9796	0	0	0.000	0.000

TABLE III. CALCULATED VALUES OF TRANSMISSIONS RELATIONSHIPS OF REGULATION TRANSFORMERS WITH SET PRECISION.

Regulation transformers					
Node *p*	Node *q*	Name TS	Computational transmission ratio	Actual transmission ratio	Voltage regulator position
21	23	Nis	0.9842	0.9875	-1
7	19	Pancevo	0.9447	0.95	-4
8	18	Beograd 8	0.894	0.9	-8

It can be seen from Table II that the actual voltages behind the regulation transformers differ slightly from the desired voltages behind the control transformers. This difference is of the order of 10^{-3} in relative units. This is due to the fact that the actual transmission ratios of control transformers differ slightly from the calculated transmission ratios (Table I).

Table II shows that the regulation of voltage in the nodes behind the control transformers (Belgrade 8 (220), Pancevo 220 and Nis 220) was largely achieved. If regulation would not be performed in these nodes, by executing the program code, voltages are obtained in these nodes without control transformers. These voltages are given in Table III.

Power flows on lines and transformers calculated on the basis of complex values of voltage of nodes (modules of voltage phasors and angles of voltage phasors from Table II) are given in Table IV- VI and VII, respectively.

TABLE IV. VALUES OF POWER FLOWS PER 400 KV SYSTEM LINES OBTAINED ON THE BASIS OF VALUES OF NODE VOLTAGE PHASERS FROM TABLE II.

Node i	Node j	P_{ij} [r.j.]	Q_{ij} [r.j.]	S_{ij} [r.j.]
400 kV				
15	2	-3.5485	-0.9793	3.6812
2	15	3.5675	0.7134	3.6381
2	3	2.1825	0.8602	2.3459
3	2	-2.1659	-1.544	2.6599
3	7	2.0962	1.881	2.8164
7	3	-2.0887	-2.0501	2.9267
3	8	1.1616	1.1639	1.6444
8	3	-1.1564	-1.5644	1.9454
7	8	-0.1691	0.8183	0.8356
8	7	0.1695	-0.9283	0.9436
1	8	2.6194	2.5424	3.6503
8	1	-2.6071	-2.6578	3.723
17	21	0.3555	-0.311	0.4723
21	17	-0.3552	-0.443	0.5678
1	17	1.4397	-0.7199	1.6097
17	1	-1.4355	0.211	1.4509
21	9	1.3569	0.4482	1.429
9	21	-1.3513	-1.0565	1.7153
21	15	-2.1625	-0.9299	2.354
15	21	2.1715	0.4793	2.2238
1	10	5.0179	1.8112	5.3348
10	1	-4.9926	-2.4855	5.5771
10	11	1.8306	0.2129	1.8429
11	10	-1.825	-0.565	1.9105

TABLE V. VALUES OF POWER FLOWS PER 220 KV SYSTEM LINES OBTAINED ON THE BASIS OF VALUES OF NODE VOLTAGE PHASERS FROM TABLE II.

Node *i*	Node *j*	P_{ij} [r.j.]	Q_{ij} [r.j.]	S_{ij} [r.j.]
220 kV				
13	14	-0.1664	1.5035	1.5127
14	13	0.1795	-1.4747	1.4856
13	4	-0.3756	-0.4899	0.6173
4	13	0.3808	0.3997	0.5521
12	20	0.767	0.0103	0.7671
20	12	-0.7638	-0.0511	0.7655
19	20	0.5462	0.3458	0.6465
20	19	-0.5412	-0.4189	0.6844
18	19	0.2011	-0.0414	0.2053
19	18	-0.2009	-0.0081	0.2011
4	18	1.1902	-0.9043	1.4948
18	4	-1.1777	0.9016	1.4832
4	5	-1.4212	0.2807	1.4487
5	4	1.4399	-0.462	1.5122
14	5	-2.5795	0.7087	2.6751
5	14	2.8669	-0.8033	2.9773
5	18	0.8583	-0.4196	0.9554
18	5	-0.8389	0.331	0.9018
4	16	5.6141	1.4459	5.7973
16	4	-5.586	-1.43	5.7661
5	22	1.1848	-0.1154	1.1904
22	5	-1.1588	-0.0255	1.1591
22	23	-0.6823	-0.6406	0.9359
23	22	0.6921	0.5985	0.9150
6	22	0.3011	0.1064	0.3193
22	6	-0.2989	-0.2389	0.3826

TABLE VI. VALUES OF POWER FLOWS TROUGH TRANSFORMERS OF SYSTEM OBTAINED ON THE BASIS OF VALUES OF NODE VOLTAGE PHASERS FROM TABLE II.

Node *i*	Node *j*	P_{ij} [r.j.]	Q_{ij} [r.j.]	S_{ij} [r.j.]
10	12	1.5509	0.3654	1.5934
12	10	-1.55	-0.2873	1.5764
10	13	0.7011	1.5973	1.7444
13	10	-0.7	-1.5036	1.6586
1	4	2.9713	2.2423	3.7224
4	1	-2.969	-2.0401	3.6024
9	6	0.2713	0.9365	0.9750
6	9	-0.271	-0.9221	0.9611

TABLE VII. VALUES OF POWER FLOWS TROUGH REGULATION TRANSFORMERS OF SYSTEM OBTAINED ON THE BASIS OF VALUES OF NODE VOLTAGE PHASERS FROM TABLE II.

Node *i*	Node *j*	P_{ij} [r.j.]	Q_{ij} [r.j.]	S_{ij} [r.j.]
Regulation transformers				
21	23	0.6928	0.6347	0.9396
23	21	-0.6921	-0.5985	0.915
7	19	2.0179	1.1619	2.3285
19	7	-2.0153	-0.9877	2.2443
8	18	3.594	5.1505	6.2805
18	8	-3.5845	-4.5112	5.7619

V. APLICATION OF POWER FLOW CALCULATION

In this paper, the regulation transformer is represented by a P replacement scheme. This introduces certain changes in the Newton - Raphson's iterative procedure for the calculation of power flows because the injection powers into the nodes between the regulation transformers depend on the nonnominal transformation ratio t. Therefore, the transmission vector of control transformers $\vec{t}$ is introduced. Also, the elements in the admittance matrix of nodes [Y_node] that correspond to the nodes between which there are regulation transformers, depend on the transmission ratios of the corresponding regulation transformers.

The power losses in the network are (0.5593-j4.7463) pj, which means that the active power losses are 0.5593 pj, ie 55.93 MW, and the reactive power losses are -4.7463 pj, ie -474.63 MVAr. A minus sign at reactive power means that 474.63 MVAr of reactive power is generated in the network. This generation of reactive power in the network is a consequence of low-load lines, i.e. the lines are generally loaded below the natural transmission power.

VI. APPENDIX

The part of the program code used to calculate the power flows is given below.

```
                %Creation Ybus matrix

for k=1:n
    for l=k+1:n
        if Zgr(k,l)~=0
        Ygr(k,l)=1/(Zgr(k,l));
        Bot(k,l)=0.5*bot(k,l);
    end
    end
end
for k=1:n
    for l=1:n
        if k~=l
        Ygr(l,k)=Ygr(k,l);
        Bot(l,k)=Bot(k,l);
        else
            Ygr(k,l)=0;
            Bot(k,l)=0;
        end
    end
end

for k=1:n
    for l=1:n
        if k~=l
        Ybus(k,l)=-Ygr(k,l);
else
Ypom(k,l)=0;
for m=1:n
Ybus(k,l)=Ypom(k,l)+Ygr(k,m)+Bot(k,m);
Ypom(k,l)=Ybus(k,l);
end
end
end
end
Ybus_bez_RT=Ybus;
for k=1:nrt
Ybus(p(k),p(k))=Ybus_bez_RT(p(k),p(k))+Yt(k);
Ybus(p(k),q(k))=Ybus_bez_RT(p(k),q(k))-
t(k)*Yt(k);
Ybus(q(k),p(k))=Ybus(p(k),q(k));
Ybus(q(k),q(k))=Ybus_bez_RT(q(k),q(k))+t(k)*t
(k)*Yt(k);
end
Ybus
```


ACKNOWLEDGMENT

This work was supported in part by the Ministry of Science and Technological Development of Republic of Serbia under Grant ON174001.

REFERENCES

[1] Ćalović, M. S., & Sarić, A. T. (2004). *Osnovi analize elektroenergetskih mreža i sistema*. Akademska misao, Beograd, Tehnički fakultet, Čačak.

[2] Ćalović, M. S. (1997). *Regulacija elektroenergetskih sistema; Tom 2 - Regulacija napona i reaktivnih snaga*. Elektrotehnički fakultet, Beograd.

[3] Tasić, D., & Rajaković, N. (2000). *Uticaj potrošnje na naponsku nestabilnost elektroenergetskog sistema*. Edicija Monografije, Elektronski fakultet, Niš.

[4] Rajaković, N., Ćalović, M., Stefanov, P., & Savić, A. (2002). 100 rešenih zadataka iz analize elektroenergetskih sistema. Akademska misao, Beograd.

Author Index

Bul. Nikole Tesle 63/5, 18000 Niš
Tel. 018 293 920; Fax: 018 293 921
e-mail: office@alfatec.rs; http://www.alfatec.rs
PIB: 104099234; m.b. 20090219; š.d. 73102
t.r.: 165-4863-06; 275-0010220587184-85

R&DC "ALFATEC" was founded in November 2005, with the purpose of enabling placement of innovative products and services developed by a group of researchers, who have worked as a part of the Section of Electric Machinery, at the Department of Energetics of the Faculty of Electronics in Nis.

R&DC "ALFATEC", upon being founded, worked in the field of measurement and control systems, where it has developed a substantial number of innovative products for the needs of various users.

In February 2008, R&DC "ALFATEC" became registered as a research and development centre by the Ministry of Science and Technological Development of the Republic of Serbia.

R&DC "ALFATEC" is currently the leader in:

- the number of realised innovative products and services which are successfully administered on the market of Serbia;
- the diversity of realised projects;
- the projecting and realisation of complex measurement and information systems, as well as measurement and control systems;
- savings of electric energy achieved by various users;
- innovative investment models for electric energy consumption reduction in small and medium-sized enterprises;
- software for decision support in emergency situations;
- design of electrical installations according to international standards.

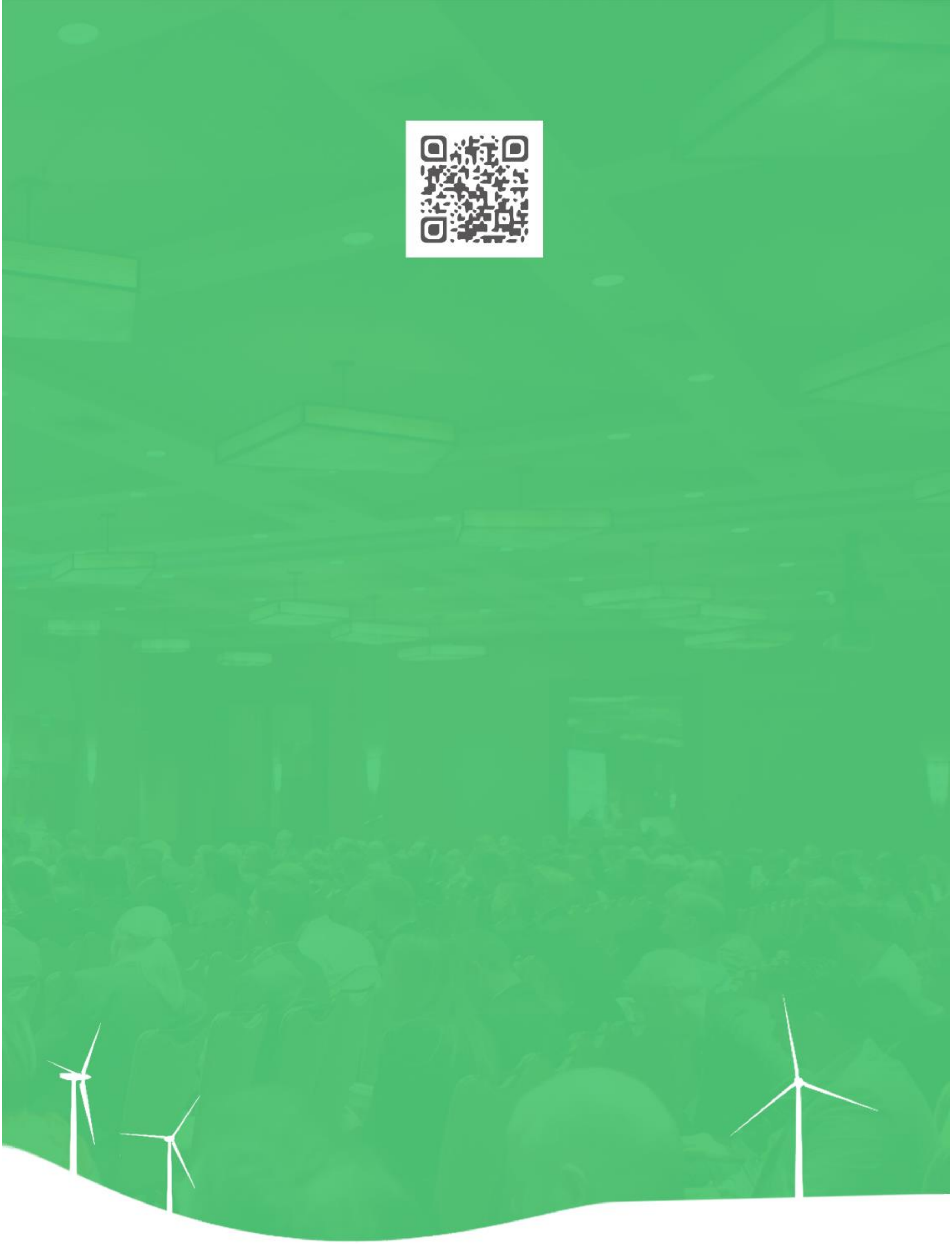

www.energetics.cosrec.org

ISBN: 978-86-80616-07-0